Jochen Hoefs

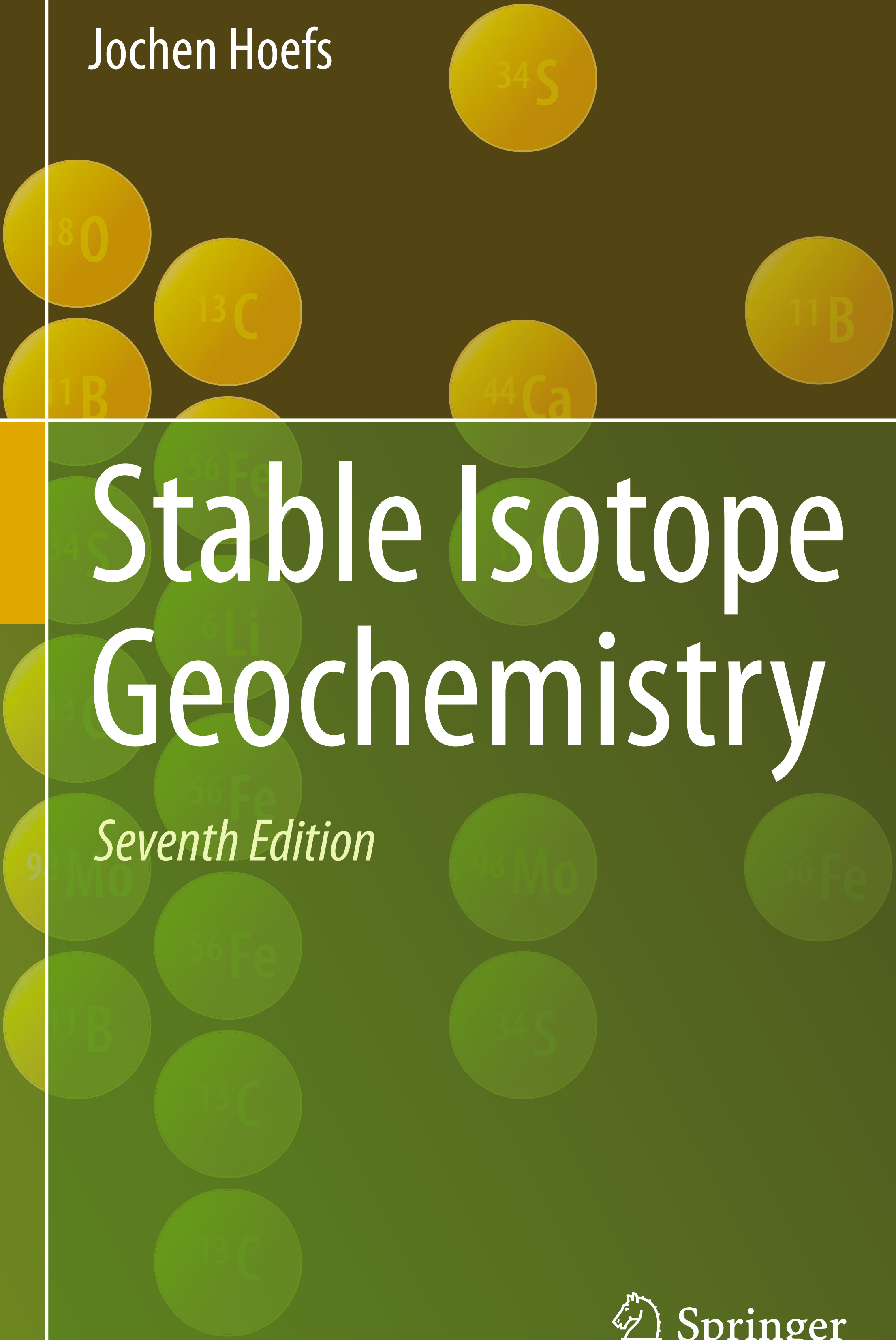

Stable Isotope Geochemistry

Seventh Edition

Springer

Stable Isotope Geochemistry

Jochen Hoefs

Stable Isotope Geochemistry

Seventh Edition

Springer

Jochen Hoefs
Abt. Isotopengeologie
Geowissenschaftliches Zentrum der
Universität Göttingen
Göttingen
Germany

ISBN 978-3-319-19715-9 ISBN 978-3-319-19716-6 (eBook)
DOI 10.1007/978-3-319-19716-6

Library of Congress Control Number: 2015941341

Springer Cham Heidelberg New York Dordrecht London

Printed on acid-free paper

Springer International Publishing AG Switzerland is part of Springer Science+Business Media
(www.springer.com)

Preface

Studies in stable isotope geochemistry have been since its beginning a strong and vital branch of earth sciences, but in the past decade, growth has occurred at an ever-increasing pace as a consequence of major advances in mass spectrometry, in micro-analytical techniques, and in calculating equilibrium isotope fractionations using ab initio methods. In specific, the application of multicollector-ICP-mass spectrometry now enables investigations of stable isotope compositions with adequate precisions for a wide range of transition and heavy elements that could not be measured before. Precise ion-microprobe measurements on the micrometer scale allow the detection of isotope heterogeneities in individual minerals. Analysis of multiple rare isotopes of elements permit the detection and distinction of mass-dependent and mass-independent processes. These major advances in analytical tools make substantial major revisions and extensions of the last edition necessary.

The structure of the book has been retained. New topics are presented that range from the isotope composition of plants to the isotope composition of the earth's core. The first part gives a general introduction to the theoretical and experimental principles. In the second part, natural isotope variations and fractionation processes of 30 elements are discussed. By adding 25 "non-traditional" elements, including Sr and U, this part has been substantially enlarged, although the backbone of this chapter is still the classic elements H, C, O, N and S. Conclusions from the newly added elements rely sometimes on a very limited data base; future studies have to strengthen some of the inferences.

As in earlier editions, the third part discusses natural variations of isotope compositions in the context of the classic geochemical "spheres". New findings from non-traditional isotope systems have been incorporated. A very long list of references with many new citations enables a quick access to the exponentially growing recent literature. Nevertheless, I have neglected a number of recent references, because the citation list encompasses already about 30 % of the book.

Again, I have tried to provide a contemporary overview of the entire field of stable isotope geochemistry. I hope I am presenting a well-balanced discussion, although I am fully aware of omissions and shortcomings.

Michael Böttcher is thanked for reviewing the manuscript, Klaus Simon has been of great help during the preparation of the manuscript.

Contents

1 Theoretical and Experimental Principles 1
- 1.1 General Characteristics of Isotopes 1
- 1.2 Isotope Effects 3
- 1.3 Isotope Fractionation Processes 5
  - 1.3.1 Isotope Exchange 5
    - 1.3.1.1 Fractionation Factor (α) 7
    - 1.3.1.2 The Delta Value (δ) 8
    - 1.3.1.3 Evaporation-Condensation Processes 9
  - 1.3.2 Kinetic Effects 10
  - 1.3.3 Mass-Dependent and Mass-Independent Isotope Effects 12
    - 1.3.3.1 Mass Dependent Effects 12
    - 1.3.3.2 Mass Independent Effects 13
  - 1.3.4 Nuclear Volume and Magnetic Isotope Effects 14
    - 1.3.4.1 Nuclear Volume Effects 14
    - 1.3.4.2 Magnetic Isotope Effects 14
  - 1.3.5 Multiply Substituted Isotopologues 14
    - 1.3.5.1 Position or Site-Specific Isotope Fractionations. 17
  - 1.3.6 Diffusion 18
  - 1.3.7 Other Factors Influencing Isotopic Fractionations 20
  - 1.3.8 Isotope Geothermometers. 22
- 1.4 Basic Principles of Mass Spectrometry 27
  - 1.4.1 Continuous Flow—Isotope Ratio Monitoring Mass Spectrometers. 30
  - 1.4.2 General Remarks on Sample Preparation Methods for Gases 31
- 1.5 Standards 33
- 1.6 Microanalytical Techniques 36
  - 1.6.1 Laser Microprobe 37
  - 1.6.2 Secondary Ion Mass Spectrometry (SIMS) 37
  - 1.6.3 Multicollector-ICP-Mass Spectrometry. 38

1.7 Stable Isotope Variations of Metal Elements 38
References 40

2 Isotope Fractionation Processes of Selected Elements 47
2.1 Hydrogen 48
2.1.1 Methods 48
2.1.2 Standards 50
2.1.3 Fractionation Processes 50
2.1.3.1 Water Fractionations 50
2.1.3.2 Equilibrium Reactions 52
2.1.3.3 Fractionations During Biosynthesis 54
2.1.3.4 Other Fractionations 55
2.2 Lithium 55
2.2.1 Methods 56
2.2.2 Diffusion 56
2.2.3 Magmatic Rocks 57
2.2.4 Weathering 58
2.2.5 Ocean Water 59
2.3 Boron 59
2.3.1 Methods 60
2.3.2 Isotope Fractionation Mechanism 61
2.3.3 Fractionations at High Temperatures 63
2.3.4 Tourmaline 63
2.3.5 Tracer for Anthropogenic Pollution 64
2.4 Carbon 64
2.4.1 Analytical Methods 65
2.4.1.1 Standards 65
2.4.2 Fractionation Processes 65
2.4.2.1 Carbonate System 66
2.4.2.2 Organic Carbon System 66
2.4.2.3 Interactions Between Carbonate-Carbon and Organic Carbon 69
2.5 Nitrogen 70
2.5.1 Analytical Methods 70
2.5.2 Biological Nitrogen Isotope Fractionations 71
2.5.3 Nitrogen Isotope Distribution in the Earth 73
2.5.4 Nitrogen in the Ocean 74
2.5.5 Anthropogenic Nitrogen Sources 75
2.6 Oxygen 76
2.6.1 Analytical Methods 76
2.6.1.1 Water 76
2.6.1.2 Carbonates 77
2.6.1.3 Silicates 78
2.6.1.4 Phosphates 78

2.6.1.5 Sulfates 79
2.6.1.6 Nitrates 79
2.6.2 Standards 79
2.6.3 Fractionation Processes 80
2.6.3.1 Fractionation of Water 80
2.6.3.2 CO_2–H_2O System 82
2.6.3.3 Mineral Fractionations 83
2.6.4 Triple Oxygen Isotope Compositions 85
2.6.5 Fluid-Rock Interactions 86
2.7 Magnesium 88
2.7.1 High-Temperature Fractionations 89
2.7.2 Fractionations During Weathering 90
2.7.3 Ocean Water 91
2.7.4 Carbonates 91
2.7.4.1 Cave Carbonates 92
2.7.5 Plants 92
2.8 Silicon 93
2.8.1 High-Temperature Fractionations 94
2.8.2 Cherts 94
2.8.3 Chemical Weathering and Mineral Precipitation 95
2.8.4 Fractionations in Ocean Water 95
2.8.5 Plants 96
2.9 Sulfur 96
2.9.1 Methods 97
2.9.2 Fractionation Mechanisms 98
2.9.2.1 Equilibrium Reactions 98
2.9.2.2 Dissimilatory Sulfate Reduction 99
2.9.2.3 Thermochemical Reduction of Sulfate 103
2.9.3 Quadruple Sulfur Isotopes 103
2.10 Chlorine 105
2.10.1 Methods 105
2.10.2 Hydrosphere 106
2.10.3 Mantle-Derived Rocks 107
2.10.4 Applications in the Environment 107
2.11 Calcium 108
2.11.1 Analytical Techniques 108
2.11.2 High Temperature Fractionations 109
2.11.3 Weathering 110
2.11.4 Fractionations During Carbonate Precipitation 111
2.11.5 Variations with Geologic Time 111
2.11.6 Ca in Plants, Animals and Humans 112
2.12 Vanadium 113

2.13 Chromium 113
  2.13.1 Mantle Rocks 114
  2.13.2 Low-Temperature Fractionations 115
  2.13.3 Anthropogenic Cr in the Environment 115
2.14 Iron 116
  2.14.1 Analytical Methods 116
  2.14.2 Isotope Equilibrium Studies 117
  2.14.3 Meteorites 118
  2.14.4 Igneous Rocks 119
  2.14.5 Sediments 120
  2.14.6 Ocean and River Water 121
  2.14.7 Plants 121
2.15 Nickel 122
  2.15.1 Meteorites and Mantle Derived Rocks 122
  2.15.2 Water and Organisms 123
2.16 Copper 123
  2.16.1 Low-Temperature Fractionations 124
  2.16.2 Variations in Ore Deposits 125
  2.16.3 Variations in Plants 126
2.17 Zinc 126
  2.17.1 Fractionations During Evaporation 127
  2.17.2 Variations in Mantle Derived Rocks 127
  2.17.3 Ore Deposits 128
  2.17.4 Variations in the Ocean 128
  2.17.5 Anthropogenic Contamination 128
  2.17.6 Variations in Plants 129
2.18 Germanium 129
2.19 Selenium 130
  2.19.1 Fractionation Processes 131
  2.19.2 Natural Variations 131
2.20 Bromine 132
2.21 Strontium 133
  2.21.1 Silicates 133
  2.21.2 Carbonates 134
  2.21.3 Rivers and Plants 134
2.22 Molybdenum 135
  2.22.1 Molybdenites 135
  2.22.2 Sediments 136
  2.22.3 Palaeoredox Proxy 137
  2.22.4 Carbonates 137
2.23 Cadmium 138
  2.23.1 Extraterrestrial Materials 139
  2.23.2 Marine Environment 139
  2.23.3 Pollution Indicator 140

2.24 Tin . . . 140
2.25 Antimony . . . 141
2.26 Tellurium . . . 141
2.27 Barium . . . 142
2.28 Mercury . . . 143
  2.28.1 MDF and MIF Fractionation Processes . . . 144
  2.28.2 Variations in Rocks . . . 145
  2.28.3 Environmental Pollutant . . . 146
2.29 Thallium . . . 147
  2.29.1 Igneous Rocks . . . 147
  2.29.2 Fractionations in the Ocean . . . 148
2.30 Uranium . . . 149
  2.30.1 Fractionation Processes . . . 149
  2.30.2 Characteristic U Signatures . . . 150
References . . . 151

3 Variations of Stable Isotope Ratios in Nature . . . 191
3.1 Extraterrestrial Materials . . . 191
  3.1.1 Chondrites . . . 192
    3.1.1.1 Oxygen . . . 192
    3.1.1.2 Hydrogen . . . 194
    3.1.1.3 Carbon . . . 195
    3.1.1.4 Nitrogen . . . 196
    3.1.1.5 Sulfur . . . 196
    3.1.1.6 Metal Isotopes . . . 197
  3.1.2 The Moon . . . 198
    3.1.2.1 Oxygen . . . 198
    3.1.2.2 Hydrogen . . . 199
  3.1.3 Mars . . . 200
    3.1.3.1 Oxygen . . . 200
    3.1.3.2 Hydrogen . . . 200
    3.1.3.3 Carbon . . . 201
    3.1.3.4 Sulfur . . . 202
  3.1.4 Venus . . . 202
3.2 The Isotopic Composition of the Earth's Upper Mantle . . . 203
  3.2.1 Oxygen . . . 204
  3.2.2 Hydrogen . . . 205
  3.2.3 Carbon . . . 207
  3.2.4 Nitrogen . . . 208
  3.2.5 Sulfur . . . 209
  3.2.6 Lithium and Boron . . . 210
  3.2.7 Stable Isotope Composition of the Core . . . 211
  3.2.8 Magmatic Rocks . . . 212
  3.2.9 Fractional Crystallization . . . 212

3.2.10 Differences Between Volcanic and Plutonic Rocks . . . 212
3.2.11 Low Temperature Alteration Processes 213
3.2.12 Assimilation of Crustal Rocks 213
3.2.13 Glasses from Different Tectonic Settings 214
    3.2.13.1 Oxygen 214
    3.2.13.2 Hydrogen 215
    3.2.13.3 Carbon 216
    3.2.13.4 Nitrogen 217
    3.2.13.5 Sulfur 217
    3.2.13.6 Ocean Water/Basaltic Crust Interactions . . . 218
3.2.14 Granitic Rocks 219
    3.2.14.1 Zircon 219
3.3 Volatiles in Magmatic Systems 220
3.3.1 Volcanic Gases and Hot Springs 221
    3.3.1.1 Water 222
    3.3.1.2 Carbon 223
    3.3.1.3 Nitrogen 224
    3.3.1.4 Sulfur 224
3.3.2 Isotope Thermometers in Geothermal Systems 226
3.4 Ore Deposits and Hydrothermal Systems 226
3.4.1 Origin of Ore Fluids 228
    3.4.1.1 Magmatic Water 229
    3.4.1.2 Metamorphic Water 230
    3.4.1.3 Formation Waters 230
3.4.2 Wall-Rock Alteration 230
3.4.3 Fossil Hydrothermal Systems 231
3.4.4 Hydrothermal Carbonates 232
3.4.5 Sulfur Isotope Composition of Ore Deposits 233
    3.4.5.1 The Importance of FO_2 and pH 233
    3.4.5.2 Magmatic Ore Deposits 235
    3.4.5.3 Magmatic Hydrothermal Deposits 235
    3.4.5.4 Epithermal Deposits 235
    3.4.5.5 Recent and Fossil Sulfide Deposits at Mid-Ocean Ridges 236
    3.4.5.6 Mississippi-Valley-Type (MVT) Deposits 237
    3.4.5.7 Biogenic Deposits 237
    3.4.5.8 Metamorphosed Deposits 238
3.4.6 Metal Isotopes 238
3.5 Hydrosphere 239
3.5.1 Meteoric Water—General Considerations 239
    3.5.1.1 δD - $\delta^{18}O$ Relationship, Deuterium (D) - Excess 242

3.5.1.2 $\delta^{17}O$-$\delta^{18}O$ Relationships, ^{17}O Excess 243
3.5.1.3 Meteoric Waters in the Past 244
3.5.2 Ice Cores 244
3.5.3 Groundwater 245
3.5.4 Isotope Fractionations During Evaporation 247
3.5.5 Ocean Water 248
3.5.6 Pore Waters 250
3.5.7 Formation Water. 250
3.5.8 Water in Hydrated Salt Minerals. 253
3.6 The Isotopic Composition of Dissolved and Particulate Compounds in Ocean and Fresh Waters 253
3.6.1 Carbon Species in Water 254
3.6.1.1 Bicarbonate in Ocean Water. 254
3.6.1.2 Particulate Organic Matter (POM). 255
3.6.1.3 Carbon Isotope Composition of Pore Waters 255
3.6.1.4 Carbon in Fresh Waters. 256
3.6.2 Silicon. 257
3.6.3 Nitrogen 258
3.6.4 Oxygen 258
3.6.5 Sulfate. 259
3.6.6 Phosphate 261
3.7 Isotopic Composition of the Ocean During Geologic History . . . 261
3.7.1 Oxygen 262
3.7.2 Carbon 264
3.7.3 Sulfur 266
3.7.4 Lithium 268
3.7.5 Boron 268
3.7.6 Calcium. 268
3.8 Atmosphere. 269
3.8.1 Atmospheric Water Vapour 270
3.8.2 Nitrogen 271
3.8.2.1 Nitrous Oxide 271
3.8.3 Oxygen 272
3.8.3.1 Evolution of Atmospheric Oxygen 273
3.8.4 Carbon Dioxide 274
3.8.4.1 Carbon 274
3.8.4.2 Oxygen 276
3.8.4.3 Long Term Variations in the CO_2 Concentration. 278
3.8.5 Carbon Monoxide. 280
3.8.6 Methane 280
3.8.7 Hydrogen. 281
3.8.8 Sulfur 282

3.8.9 Sulfate and Nitrate in Ice Cores 283
3.8.10 Perchlorate 284
3.9 Biosphere 284
3.9.1 Living Organic Matter 284
3.9.1.1 Bulk Carbon 284
3.9.1.2 Position Specific Isotope Composition of Organic Constituents 287
3.9.1.3 Hydrogen 287
3.9.1.4 Oxygen 288
3.9.1.5 Nitrogen 289
3.9.1.6 Sulfur 289
3.9.1.7 Metal Isotopes 289
3.9.2 Indicators of Diet and Metabolism 290
3.9.3 Tracing Anthropogenic Organic Contaminant Sources 291
3.9.4 Marine Versus Terrestrial Organic Matter 292
3.9.5 Fossil Organic Matter 293
3.9.6 Oil 294
3.9.7 Coal 296
3.9.7.1 Black Carbon 296
3.9.8 Natural Gas 297
3.9.8.1 Biogenic Gas 298
3.9.8.2 Thermogenic Gas 299
3.9.8.3 Isotope Clumping in Methane 300
3.9.8.4 Abiogenic Methane 300
3.9.8.5 Nitrogen in Natural Gas 300
3.10 Sedimentary Rocks 301
3.10.1 Clay Minerals 301
3.10.2 Clastic Sedimentary Rocks 303
3.10.3 Biogenic Silica and Cherts 305
3.10.3.1 Biogenic Silica 305
3.10.3.2 Cherts 305
3.10.4 Marine Carbonates 306
3.10.4.1 Oxygen 306
3.10.4.2 Carbon 310
3.10.5 Diagenesis 312
3.10.5.1 Burial Pathway 312
3.10.5.2 Meteoric Pathway 312
3.10.6 Limestones 313
3.10.7 Dolomites 313
3.10.8 Freshwater Carbonates 314
3.10.9 Phosphates 316
3.10.10 Iron Oxides 317

3.10.10.1 Oxygen 317
3.10.10.2 Iron 318
3.10.11 Sedimentary Sulfur and Pyrite 318
3.10.11.1 Sulfur 318
3.10.11.2 Pyrite 320
3.11 Palaeoclimatology 321
3.11.1 Continental Records 321
3.11.1.1 Tree Rings. 322
3.11.1.2 Organic Matter. 322
3.11.1.3 Hydroxyl-Bearing Minerals 322
3.11.1.4 Lake Sediments 323
3.11.1.5 Speleothems. 323
3.11.1.6 Phosphates. 324
3.11.2 Ice Cores 324
3.11.2.1 Correlations of Ice-Core Records 325
3.11.2.2 Gas-Inclusions in Ice Cores 326
3.11.3 Marine Records 327
3.11.3.1 Corals 329
3.11.3.2 Conodonts 329
3.11.3.3 Characteristic Climatic Events 329
3.12 Metamorphic Rocks 331
3.12.1 Contact Metamorphism 334
3.12.2 Regional Metamorphism 335
3.12.3 Lower Crustal Rocks. 336
3.12.4 Thermometry 337
References 340

Index 385

Theoretical and Experimental Principles

1

1.1 General Characteristics of Isotopes

Isotopes are atoms whose nuclei contain the same number of protons but a different number of neutrons. The term “isotopes” is derived from Greek (meaning equal places) and indicates that isotopes occupy the same position in the periodic table.

It is convenient to denote isotopes in the form $^{m}_{n}E$, where the super-script “m” denotes the mass number (i.e., sum of the number of protons and neutrons in the nucleus) and the subscript “n” denotes the atomic number of an element E. For example, $^{12}_{6}C$ is the isotope of carbon which has six protons and six neutrons in its nucleus. The atomic weight of each naturally occurring element is the average of the weights contributed by its various isotopes.

Isotopes can be divided into two fundamental kinds, stable and unstable (radioactive) species. The number of stable isotopes is about 300; whilst over 1200 unstable ones have been discovered so far. The term “stable” is relative, depend-ing on the detection limits of radioactive decay times. In the range of atomic numbers from 1 (H) to 83 (Bi), stable nuclides of all masses except 5 and 8 are known. Only 21 elements are pure elements, in the sense that they have only one stable isotope. All other elements are mixtures of at least two isotopes. The relative abundance of different isotopes of an element may vary substantially. In copper, for example, ^{63}Cu accounts for 69 % and ^{65}Cu for 31 % of all copper nuclei. For the light elements, however, one isotope is predominant, the others being present only in trace amounts.

The stability of nuclides is characterized by several important rules, two of which are briefly discussed here. The first is the so-called symmetry rule, which states that in a stable nuclide with low atomic number, the number of protons is approximately equal to the number of neutrons, or the neutron-to-proton ratio, N/Z, is approximately equal to unity. In stable nuclei with more than 20 protons or neutrons, the N/Z ratio is always greater than unity, with a maximum value of about 1.5 for the heaviest stable nuclei. The electrostatic Coulomb repulsion of the positively charged protons grows rapidly with increasing Z. To maintain the

J. Hoefs, *Stable Isotope Geochemistry*, DOI 10.1007/978-3-319-19716-6_1

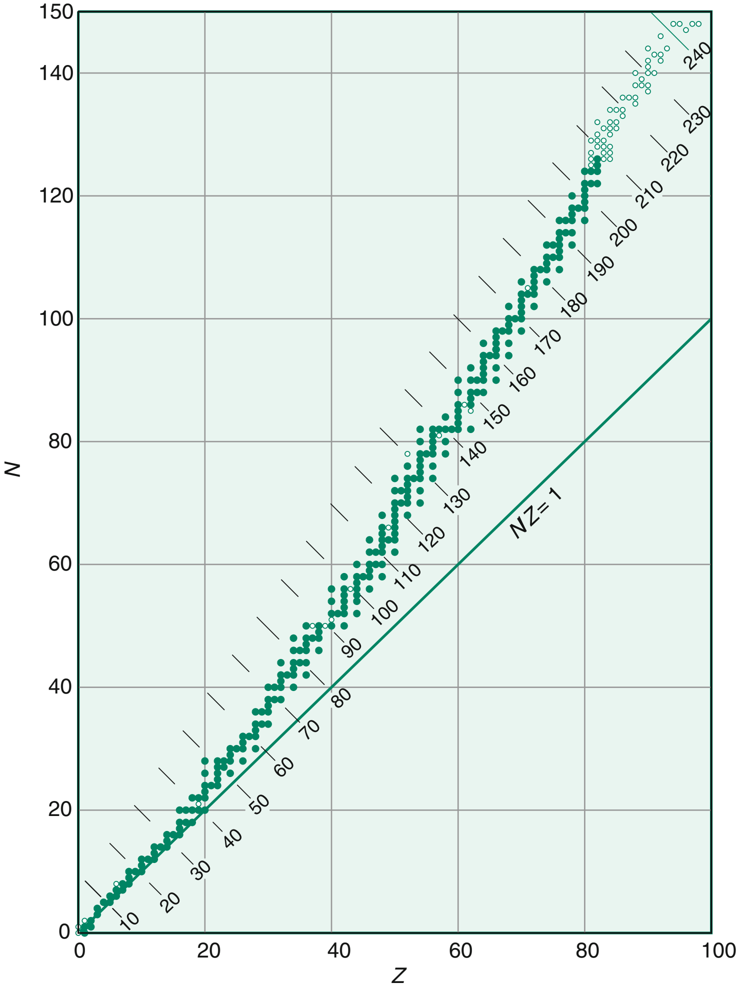

Fig. 1.1 Plot of number of protons (Z) and number of neutrons (N) in stable (*filled circles*) and unstable (*open circles*) nuclides (Fig. 1.1, 6th edition, p. 2)

stability in the nuclei more neutrons (which are electrically neutral) than protons are incorporated into the nucleus (see Fig. 1.1).

The second rule is the so-called “Oddo-Harkins” rule, which states that nuclides of even atomic numbers are more abundant than those with odd numbers. As shown in Table 1.1, the most common of the four possible combinations is even-even, the least common odd-odd.

The same relationship is demonstrated in Fig. 1.2, which shows that there are more stable isotopes with even than with odd proton numbers.

Table 1.1 Types of atomic nuclei and their frequency of occurrence

Z–N combination	Number of stable nuclides
Even–even	160
even–odd	50
Odd–even 50	56
Odd–odd	5

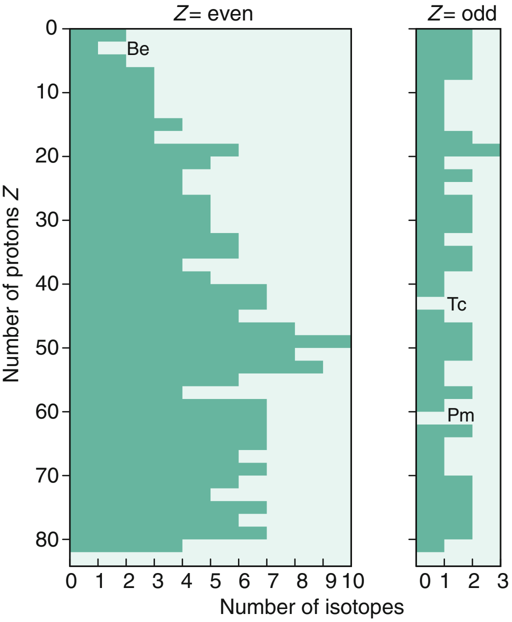

Fig. 1.2 Number of stable isotopes of elements with even and odd number of protons (radioactive isotopes with half-lives greater than 10^9 years are included) (Fig. 1.2, 6th edition, p. 3)

Radioactive isotopes can be classified as being either artificial or natural. Only the latter are of interest in geology, because they are the basis for radiometric dating methods. Radioactive decay processes are spontaneous nuclear reactions and may be characterized by the radiation emitted, i.e. α, β and/or γ-emission. Decay processes may also involve electron capture.

Radioactive decay is one process that produces variations in isotope abundance. A second cause of differences in isotope abundance is isotope fractionation caused by small chemical and physical differences between the isotopes of an element. It is exclusively this important process that will be discussed in the following chapters.

1.2 Isotope Effects

Differences in chemical and physical properties arising from variations in atomic mass of an element are called “isotope effects”. It is well known that the electronic structure of an element essentially determines its chemical behaviour, whereas the

Table 1.2 Characteristic physical properties of $H_2^{16}O$, $D_2^{16}O$, and $H_2^{18}O$

Property	$H_2^{16}O$	$D_2^{16}O$	$H_2^{18}O$
Density (20 °C, in g cm^{-3})	0.997	1.1051	1.1106
Temperature of greatest density (°C)	3.98	11.24	4.30
Melting point (760 Torr, in °C)	0.00	3.81	0.28
Boiling point (760 Torr, in °C)	100.00	101.42	100.14
Vapor pressure (at 100 °C, in Torr)	760.00	721.60	
Viscosity (at 20 °C, in centipoise)	1.002	1.247	1 .056

nucleus is more or less responsible for its physical properties. Because all isotopes of a given element contain the same number and arrangement of electrons, a far-reaching similarity in chemical behaviour is the logical consequence. But this similarity is not unlimited; certain differences exist in physicochemical properties due to mass differences. The replacement of any atom in a molecule by one of its isotopes produces a very small change in chemical behaviour. The addition of one neutron can, for instance, depress the rate of chemical reaction considerably. Furthermore, it leads, for example, to a shift of the lines in the Raman and IR spectra. Such mass differences are most pronounced among the lightest elements. For example, some differences in physicochemical properties of $H_2^{16}O$, $D_2^{16}O$, $H_2^{18}O$ are listed in Table 1.2. To summarize, the properties of molecules differing only in isotopic substitution are qualitatively the same, but quantitatively different.

Differences in the chemical properties of the isotopes of H, C, N, O, S, and other elements have been calculated by the methods of statistical mechanics and also determined experimentally. These differences can lead to considerable separation of the isotopes during chemical reactions.

The theory of isotope effects and a related isotope fractionation mechanism will be discussed very briefly. For a more detailed introduction to the theoretical background, see Bigeleisen and Mayer (1947), Urey (1947), Melander (1960), Bigeleisen (1965), Richet et al. (1977), O'Neil (1986), Criss (1999), Chacko et al. (2001), Schauble (2004) and others.

Differences in the physicochemical properties of isotopes arise as a result of quantum mechanical effects. Figure 1.3 shows schematically the energy of a diatomic molecule as a function of the distance between the two atoms. According to the quantum theory, the energy of a molecule is restricted to certain discrete energy levels. The lowest level is not at the minimum of the energy curve, but above it by an amount 1/2 hν, where h is Planck's constant and ν is the frequency with which the atoms in the molecule vibrate with respect to one another. Thus, even in the ground state at a temperature of absolute zero, the vibrating molecule would possess a certain zero point energy above the minimum of the potential energy curve of the molecule. It vibrates with its fundamental frequency, which depends on the mass of the isotopes. In this context, it is important to note that vibrational motions dominate chemical isotope effects; rotational and translational motions either have no effect on isotope separations or are subordinate. Therefore, molecules of the same

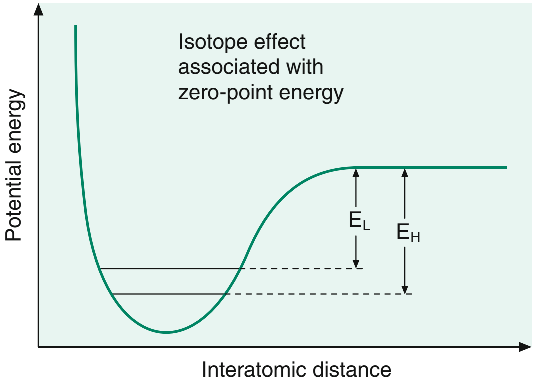

Fig. 1.3 Schematic potential energy *curve* for the interaction of two atoms in a stable molecule or between two molecules in a liquid or solid (after Bigeleisen 1965) (Fig. 1.3, 6th edition, p. 5)

chemical formula that have different isotopic species will have different zero-point energies: the molecule of the heavy isotope will have a lower zero-point energy than the molecule of the light isotope, because it has a lower vibrational frequency. This is shown schematically in Fig. 1.3, where the upper horizontal line (EL) represents the dissociation energy of the light molecule and the lower line (EH), that of the heavy one. EL is actually not a line, but an energy interval between the zero-point energy level and the "continuous" level. This means that the bonds formed by the light isotope are weaker than bonds involving the heavy isotope. Thus, during a chemical reaction, molecules bearing the light isotope will, in general, react slightly more readily than those with the heavy isotope.

1.3 Isotope Fractionation Processes

The partitioning of isotopes between two substances or two phases of the same substance with different isotope ratios is called "isotope fractionation". The main phenomena producing isotope fractionations are

1. isotope exchange reactions (equilibrium isotope distribution),
2. kinetic processes, which depend primarily on differences in reaction rates of isotopic molecules

1.3.1 Isotope Exchange

Isotope exchange includes processes with very different physico-chemical mechanisms. Here, the term "isotope exchange" is used for all situations in which there is no net reaction, but in which the isotope distribution changes between different chemical substances, between different phases, or between individual molecules.

Isotope exchange reactions are a special case of general chemical equilibrium and can be written

$$aA_1 + bB_2 = aA_2 + bB_1 \tag{1.1}$$

where the subscripts indicate that species A and B contain either the light or heavy isotope 1 or 2, respectively. For this reaction the equilibrium constant is expressed by

$$K = \frac{\left(\frac{A_2}{A_1}\right)^a}{\left(\frac{B_2}{B_1}\right)^b} \tag{1.2}$$

where the terms in parentheses may be, for example, the molar ratios of any species. Using the methods of statistical mechanics, the isotopic equilibrium constant may be expressed in terms of the partition functions Q of the various species

$$k = \left(\frac{Q_{A2}}{Q_{A1}}\right) \Big/ \left(\frac{Q_{B2}}{Q_{B1}}\right) \tag{1.3}$$

Thus, the equilibrium constant then is simply the quotient of two partition function ratios, one for the two isotopic species of A, the other for B.

The partition function is defined by

$$Q = \sum\nolimits_i (g_i \exp(-E_i/kT)) \tag{1.4}$$

where the summation is over all the allowed energy levels, E_i, of the molecules and g_i is the degeneracy or statistical weight of the ith level [of E_i], k is the Boltzmann constant and T is the temperature. Urey (1947) has shown that for the purpose of calculating partition function ratios of isotopic molecules, it is very convenient to introduce, for any chemical species, the ratio of its partition function to that of the corresponding isolated atom, which is called the reduced partition function. This reduced partition function ratio can be manipulated in exactly the same way as the normal partition function ratio. The partition function of a molecule can be separated into factors corresponding to each type of energy: translation, rotation, and vibration

$$Q_2/Q_1 = (Q_2/Q_1)_{\text{trans}} \times (Q_2/Q_1)_{\text{rot}} \times (Q_2/Q_1)_{\text{vib}} \tag{1.5}$$

The difference of the translation and rotation energy is more or less the same among the compounds appearing at the left and right hand side of the exchange reaction equation, except for hydrogen, where rotation must be taken into account. This leaves differences in vibrational energy as the predominant source of isotope effects. The vibrational energy term can be separated into two components. The first is related to the zero-point energy difference and accounts for most of the variation with temperature. The second term represents the contributions of all the other bound states and is not very different from unity. The complications which may occur relative to this simple model are mainly that the oscillator is not perfectly harmonic, so an "anharmonic" correction has to be added.

For geologic purposes the dependence of the equilibrium constant K on temperature is the most important property (Eq. 1.4). In principle, isotope fractionation factors for isotope exchange reactions are also slightly pressure-dependent because isotopic substitution makes a minute change in the molar volume of solids and liquids. Experimental studies up to 20 kbar by Clayton et al. (1975) have shown that the pressure dependence for oxygen is, however, less than the limit of analytical detection. Thus, as far as it is known today, the pressure dependence seems with the exception of hydrogen to be of no importance for crustal and upper mantle environments (but see Polyakov and Kharlashina 1994).

Isotope fractionations tend to become zero at very high temperatures. However, isotope fractionations do not decrease to zero monotonically with increasing temperatures. At higher temperatures, fractionations may change sign (called crossover) and may increase in magnitude, but they must approach zero at very high temperatures. Such crossover phenomena are due to the complex manner by which thermal excitation of the vibration of atoms contributes to an isotope effect (Stern et al. 1968).

For ideal gas reactions, there are two temperature regions where the behavior of the equilibrium constant is simple: at low temperatures (generally much below room temperature) the natural logarithm of K (ln K) follows $\sim 1/T$ where T is the absolute temperature and at high temperatures the approximation becomes $\ln K \sim 1/T^2$

The temperature ranges at which these simple behaviors are approximated depend on the vibrational frequencies of the molecules involved in the reaction. For the calculation of a partition function ratio for a pair of isotopic molecules, the vibrational frequencies of each molecule must be known. When solid materials are considered, the evaluation of partition function ratios becomes even more complicated, because it is necessary to consider not only the independent internal vibrations of each molecule, but also the lattice vibrations.

1.3.1.1 Fractionation Factor (α)

For isotope exchange reactions in geochemistry, the equilibrium constant K is often replaced by the fractionation factor α. The fractionation factor is defined as the ratio of the numbers of any two isotopes in one chemical compound A divided by the corresponding ratio for another chemical compound B:

$$\alpha_{A-B} = \frac{R_A}{R_B} \tag{1.6}$$

If the isotopes are randomly distributed over all possible positions in the compounds A and B, then α is related to the equilibrium constant K by

$$\alpha = \mathrm{K}^{1/\mathrm{n}} \tag{1.7}$$

where "n" is the number of atoms exchanged. For simplicity, isotope exchange reactions are written such that only one atom is exchanged. In these cases, the equilibrium constant is identical to the fractionation factor. For example, the fractionation factor for the exchange of ^{18}O and ^{16}O between water and $CaCO_3$ is expressed as follows:

$$\mathrm{H_2^{18}O} + \frac{1}{3}\mathrm{CaC^{16}O_3} \Leftrightarrow \mathrm{H_2^{16}O} + \frac{1}{3}\mathrm{CaC^{18}O_3} \tag{1.8}$$

with the fractionation factor $\alpha_{\mathrm{CaCO_3-H_2O}}$ defined as:

$$\alpha_{\mathrm{CaCo_3-H_2O}} = \frac{\left(\frac{^{18}\mathrm{O}}{^{16}\mathrm{O}}\right)_{\mathrm{CaCo_3}}}{\left(\frac{^{18}\mathrm{O}}{^{16}\mathrm{O}}\right)_{\mathrm{H_2o}}} = 1.031\,\mathrm{at}\,25^{\circ}\mathrm{C} \tag{1.9a}$$

It has become common practice in recent years to replace the fractionation factor α by the ε-value (or isotope enrichment factor) which is defined as

$$\varepsilon = \alpha - 1 \tag{1.9b}$$

because ε × 1000 approximates the fractionation in parts per thousand, similar to the δ-value (see below).

1.3.1.2 The Delta Value (δ)

In isotope geochemistry, it is common practice to express isotopic composition in terms of "delta"–(δ) values. For two compounds "A" and "B" whose isotopic compositions have been measured in the laboratory by conventional mass spectrometry:

$$\delta_{\mathrm{A}} = \left(\frac{\mathrm{R_A}}{\mathrm{R_{St}}} - 1\right) \cdot 10^3 (\text{‰}) \tag{1.10}$$

and

$$\delta_{\mathrm{B}} = \left(\frac{\mathrm{R_B}}{\mathrm{R_{St}}} - 1\right) \cdot 10^3 (\text{‰}) \tag{1.11}$$

where R_A and R_B are the respective isotope ratio measurements for the two compounds and R_{St} is the defined isotope ratio of a standard sample.

Table 1.3 Comparison between δ, α, and 10^3 ln α_{A-B}

$^{\delta}$A	$^{\delta}$B	$^{\Delta}$A-B	$^{\alpha}$A-B	103 lnα_{A-B}
1.00	0	1.00	1.001	1.00
5.00	0	5.00	1.005	4.99
10.00	0	10.00	1.01	9.95
15.00	0	15.00	1.015	14.98
20.00	0	20.00	1.02	19.80
10.00	5.00	5.00	1.00498	4.96
20.00	15.00	5.00	1.00493	4.91
30.00	15.00	15.00	1.01478	14.67
30.00	20.00	10.00	1.00980	9.76
30.00	10.00	20.00	1.01980	19.61

For the two compounds A and B, the δ-values and fractionation factor α are related by:

$$\delta_A - \delta_B = \Delta_{A-B} \approx 10^3 \ln \alpha_{A-B} \qquad (1.12)$$

Table 1.3 illustrates the closeness of the approximation. Considering experimental uncertainties in isotope ratio determinations (typically ≥0.1 ‰), these approximations are excellent for differences in δ-values of less than about 10 and for δ-values that are relatively small in magnitude.

1.3.1.3 Evaporation-Condensation Processes

Of special interest in stable isotope geochemistry are evaporation-condensation processes, because differences in the vapor pressures of isotopic compounds lead to significant isotope fractionations. For example, from the vapor pressure data for water given in Table 1.2, it is evident that the lighter molecular species are preferentially enriched in the vapor phase, the extent depending upon the temperature. Such an isotopic separation process can be treated theoretically in terms of fractional distillation or condensation under equilibrium conditions as is expressed by the Rayleigh (1896) equation. For a condensation process this equation is

$$\frac{R_V}{R_{V_0}} = f^{\alpha-1} \qquad (1.13)$$

where "R_{vo}" is the isotope ratio of the initial bulk composition and "R_v" is the instantaneous ratio of the remaining vapour (v); "f" is the fraction of the residual vapour, and the fractionation factor α is given by R_l/R_V (l = liquid). Similarly, the instantaneous isotope ratio of the condensate (R_l) leaving the vapour is given by

$$\frac{R_l}{R_{V_0}} = \alpha f^{\alpha-1} \qquad (1.14)$$

and the average isotope ratio of the separated and accumulated condensate (R_l) at any time of condensation is expressed by

$$\frac{\bar{R}_1}{R_{v_o}} = \frac{1 - f^{\alpha}}{1 - f} \tag{1.15}$$

For a distillation process the instantaneous isotope ratios of the remaining liquid and the vapor leaving the liquid are given by

$$\frac{R_l}{R_{l_0}} = f^{\left(\frac{1}{\alpha}-1\right)} \tag{1.16}$$

and

$$\frac{\bar{R}_v}{R_{l_0}} = \frac{1}{\alpha} f^{\left(\frac{1}{\alpha}-1\right)} \tag{1.17}$$

The average isotope ratio of the separated and accumulated vapor is expressed by

$$\frac{\bar{R}_v}{R_{l_0}} = \frac{1 - f^{\frac{1}{\alpha}}}{1 - f} \ (\mathrm{f} \ = \ \text{fraction of residual liquid}) \tag{1.18}$$

Any isotope fractionation occuring in such a way that the products are isolated from the reactants immediately after formation will show a characteristic trend in isotopic composition. As condensation or distillation proceeds the residual vapor or liquid will become progressively depleted or enriched with respect to the heavy isotope. A natural example is the fractionation between oxygen isotopes in the water vapor of a cloud and the raindrops released from the cloud. The resulting decrease of the $^{18}O/^{16}O$ ratio in the residual vapor and the instantaneous isotopic composition of the raindrops released from the cloud are shown in Fig. 1.4 as a function of the fraction of vapor remaining in the cloud.

1.3.2 Kinetic Effects

The second main phenomena producing fractionations are kinetic isotope effects, which are associated with incomplete and unidirectional processes like evaporation, dissociation reactions, biologically mediated reactions, and diffusion. The latter process is of special significance for geological purposes, which warrants separate treatment (1.3.3.). A kinetic isotope effect also occurs when the rate of a chemical reaction is sensitive to atomic mass at a particular position in one of the reacting species.

The theory of kinetic isotope fractionations has been discussed by Bigeleisen and Wolfsberg (1958), Melander (1960), and Melander and Saunders (1980). Knowledge of kinetic isotope effects is very important, because it can provide unique informations about details of reaction pathways.

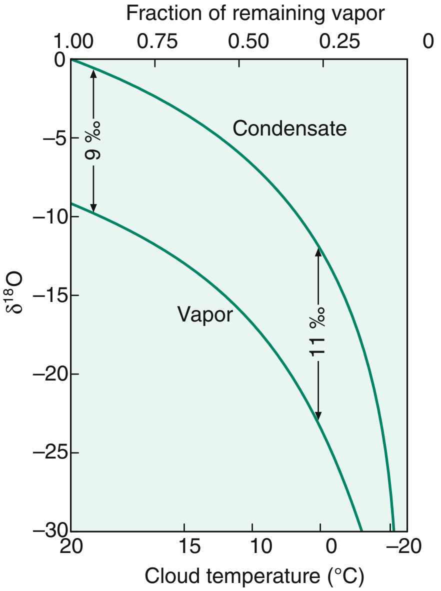

Fig. 1.4 $\delta^{18}O$ in a cloud vapor and condensate plotted as a function of a fraction of remaining vapour in a cloud for a Rayleigh process. The temperature of the cloud is shown on the lower axis. The increase in fractionation with decreasing temperature is taken into account (after Dansgaard 1964) (Fig. 1.4, 6th edition, p. 10)

Quantitatively, many observed deviations from simple equilibrium processes can be interpreted as consequences of the various isotopic components having different rates of reaction. Isotope measurements taken during unidirectional chemical reactions always show a preferential enrichment of the lighter isotope in the reaction products. The isotope fractionation introduced during the course of a unidirectional reaction may be considered in terms of the ratio of rate constants for the isotopic substances. Thus, for two competing isotopic reactions

$$\begin{aligned} \mathrm{k1} &\rightarrow \mathrm{k2}, \\ \mathrm{A1} \rightarrow \mathrm{B1}, \quad \text{and } \mathrm{A2} &\rightarrow \mathrm{B2} \end{aligned} \tag{1.19}$$

the ratio of rate constants for the reaction of light and heavy isotope species k_1 / k_2, as in the case of equilibrium constants, is expressed in terms of two partition function ratios, one for the two reactant isotopic species, and one for the two isotopic species of the activated complex or transition state A^X:

$$\frac{k_1}{k_2} = \left[\frac{Q^*_{(A_2)}}{Q^*_{(A_1)}} \Big/ \frac{Q^*_{(A_2^X)}}{Q^*_{(A_1^X)}} \right] \frac{v_1}{v_2} \tag{1.20}$$

The factor v_1/v_2 in the expression is a mass term ratio for the two isotopic species. The determination of the ratio of rate constants is, therefore, principally the same as the determination of an equilibrium constant, although the calculations are not so precise because of the need for detailed knowledge of the transition state. The term “transition state” refers to the molecular configuration that is most difficult to attain along the path between the reactants and the products. This theory follows the concept that a chemical reaction proceeds from some initial state to a final configuration by a continuous change, and that there is some critical intermediate configuration called the activated species or transition state. There are a small number of activated molecules in equilibrium with the reacting species and the rate of reaction is controlled by the rate of decomposition of these activated species.

1.3.3 Mass-Dependent and Mass-Independent Isotope Effects

1.3.3.1 Mass Dependent Effects

At thermodynamic equilibrium isotope distributions are strictly governed by relative mass differences among different isotopes of an element. Mass dependent relationships hold for many kinetic processes as well. Thus it has been a common belief that for most natural reactions isotope effects arise solely because of isotopic mass differences. This means that for an element with more than two isotopes, such as oxygen or sulfur, the enrichment of ^{18}O relative to ^{16}O or ^{34}S relative to ^{32}S is expected to be approximately twice as large as the enrichment of ^{17}O relative to ^{16}O or as the enrichment of ^{33}S relative to ^{32}S. Therefore, for many years interest in measuring more than one isotope ratio of a specific element was limited. Recent analytical improvements of multiple isotope elements have demonstrated, however, that different mass-dependent processes (e.g. diffusion, metabolism, high-temperature equilibrium processes) can deviate by a few percent and follow slightly different mass-dependent fractionation laws (Young et al. 2002; Miller 2002; Farquhar et al. 2003). These very small differences are measurable and have been documented for oxygen (Luz et al. 1999), for magnesium (Young et al. 2002), for sulfur (Farquhar et al. 2003) and for mercury (Blum 2011). As shown by Young et al. (2002) mass dependent fractionation laws for three or more isotopes are different for equilibrium and kinetic processes, the latter having shallower slopes than those produced by equilibrium exchange.

It is common practice to describe mass dependent isotope fractionation processes by a single linear curve on a three-isotope-plot (Matsuhisa et al. 1978). The resulting straight lines are referred to as terrestrial mass fractionation lines and deviations from it are used as indicating non-mass dependent isotope effects. The three-isotope plot is based on the approximation of a power law function to linear format. To describe how far a sample plots off the mass dependent fractionation line, a new term has been defined: $\Delta^{17}O$, $\Delta^{25}Mg$, $\Delta^{33}S$ etc. Several definitions of Δ have been introduced in the literature, that have been discussed by Assonov and Brenninkmeijer (2005). The simpliest definition is given by:

$$\Delta^{17}\mathrm{O} = \delta^{17}\mathrm{O} - \lambda\delta^{18}\mathrm{O}$$

$$\Delta^{25}\mathrm{Mg} = \delta^{25}\mathrm{Mg} - \lambda\delta^{26}\mathrm{Mg} \text{ or}$$

$$\Delta^{33}\mathrm{S} = \delta^{33}\mathrm{S} - \lambda\delta^{34}S,$$

where λ is the main parameter that characterizes the mass-dependent fractionation. The value of the coefficient λ depends on the molecular mass, which for oxygen may range from 0.53 for atomic oxygen to 0.500 for species with high molecular weight. Recent progress in high-precision measurement of isotope ratios allows to distinguish λ-values in the third decimal, which has obscured the difference between mass-dependent and mass-independent fractionations at small Δ-values (Farquhar et al. 2003).

1.3.3.2 Mass Independent Effects

A few processes in nature do not follow the above mass-dependent fractionations. Deviations from mass-dependent fractionations were first observed for oxygen in meteorites (Clayton et al. 1973) and in ozone (Thiemens and Heidenreich 1983) and for sulfur in sulfides older than 2.45 Ga (Farquhar et al. 2000). These Mass Independent Fractionations (MIF) describe relationships that violate the mass-dependent rules $\delta^{17}O \approx 0.5\ \delta^{18}O$ or $\delta^{33}S \approx 0.5\ \delta^{34}S$ and produce isotopic compositions with nonzero $\Delta^{17}O$ and $\Delta^{33}S$.

A number of experimental and theoretical studies have focused on the causes of mass-independent fractionation effects, but as summarized by Thiemens (1999) the mechanism for mass independent fractionations remains uncertain. The best studied reaction is the formation of ozone in the stratosphere. Mauersberger et al. (1999) demonstrated experimentally that it is not the symmetry of a molecule that determines the magnitude of ^{17}O enrichment, but it is the difference in the geometry of the molecule. Gao and Marcus (2001) presented an advanced model, which has lead to a better understanding of non-mass dependent isotope effects.

Mass-independent isotopic fractionations are widespread in the earth's atmosphere and have been observed in O_3, CO_2, N_2O and CO, which are all linked to reactions involving stratospheric ozone (Thiemens 1999). For oxygen this is a characteristic marker in the atmosphere (see Sect. 3.9). These processes probably also play a role in the atmosphere of Mars and in the presolar nebula (Thiemens 1999). The discovery of chemically produced mass-independent oxygen isotope composition in ozone opened the view to investigate multi-isotope fractionation in other natural systems as summarized by Thiemens et al. (2012).

Oxygen isotope measurements in meteorites by Clayton et al. (1973) (Sect. 3.1) first demonstrated that the effect is of significance in the formation of the solar system. There are numerous terrestrial solid reservoirs where mass independent isotope variations have been observed. For instance, Farquhar et al. (2000c) and Bao et al. (2000) reported mass-independent oxygen isotope fractionations in terrestrial sulfates. A positive ^{17}O-excess in sulfate has been found to be almost ubiquitous in desert environments (Bao et al. 2001).

Significant mass independent sulfur isotope fractionations have been reported first by Farquhar et al. (2000c) in sulfides older than 2.4 Ga, whereas these fractionations do not occur in measurable amounts in sulfides younger than 2.4 Ga (see Fig. 2.24). Smaller, but clearly resolvable MIFs have been measured in volcanic aerosol sulfates in polar ice (Baroni et al. 2007). Photolysis of SO_2 to sulfuric acid is thought to be the source reaction for these sulfur MIFs. These findings indicate that non-mass dependent isotope fractionations are more abundant than originally thought and constitute a novel form of isotopic fingerprint.

1.3.4 Nuclear Volume and Magnetic Isotope Effects

1.3.4.1 Nuclear Volume Effects

For heavy elements, mass-independent isotope fractionations are considered to be due to nuclear volume fractionations (Fujii et al. 2009). Bigeleisen (1996), Schauble (2007, 2013), Estrade et al. (2009), and others demonstrated that isotope variations of very heavy elements (i.e. Hg, U) are driven by differences in nuclear volumes and shapes which affect the electronic structure of atoms and molecules. Nuclear volume fractionations may be estimated using first principles quantum mechanical calculations (Schauble 2007). The magnitude of nuclear volume fractionations is very small for the light elements, but increases with nuclear weight.

The binding energy between electrons and nuclei depend on the distribution of protons inside the nucleus. Nuclear volume increases with the number of neutrons, but the increase caused by an odd isotope is slightly smaller than for an isotope with an even number (Bigeleisen 1996). Thus, nuclear volume effects are expected to generate odd-even isotope fractionation patterns (Schauble 2007; Fujii et al. 2009).

1.3.4.2 Magnetic Isotope Effects

In contrast to nuclear volume effects that select isotopes due to their different masses, magnetic isotope effects sparate isotopes by spin and magnetic moment (Bucharenko 2001; Epov et al. 2011). The magnetic isotope effect separates isotopes with and without unpaired nuclear spin due to coupling between nuclear spin and electronic spin. Thus magnetic isotope effects distinguish between isotopes with odd and even numbers.

1.3.5 Multiply Substituted Isotopologues

In stable isotope geochemistry generally bulk isotopic compositions of natural samples are given (e.g. $\delta^{13}C$, $\delta^{18}O$…). In measured gases, bulk compositions depend only on abundances of molecules containing one rare isotope (e.g. $^{13}C^{16}O^{16}O$ or $^{12}C^{18}O^{16}O$). However, there also exist in very low concentration, molecules having more than one rare isotope such as $^{13}C^{18}O^{16}O$ or $^{12}C^{18}O^{17}O$. These socalled isotopologues are molecules that differ from one another only in

Table 1.4 Stochastic abundances of CO_2 isotopologues (Eiler 2007)

Mass	Isotopologue	Relative abundance
44	$^{12}C^{16}O_2$	98.40 %
45	$^{13}C^{16}O_2$	1.11 %
	$^{12}C^{17}O^{16}O$	748 ppm
46	$^{12}C^{18}O^{16}O$	0.040 %
	$^{13}C^{17}O^{16}O$	8.4 ppm
	$^{12}C^{17}O_2$	0.142 ppm
47	$^{13}C^{18}O^{16}O$	44.4 ppm
	$^{12}C^{17}O^{18}O$	1.50 ppm
	$^{13}C^{17}O_2$	1.60 ppb
48	$^{12}C^{18}O_2$	3.96 ppm
	$^{13}C^{17}O^{18}O$	16.8 ppb
49	$^{13}C^{18}O_2$	44.5 ppb

isotopic composition. Table 1.4 gives the stochastic abundances of isotopologues of CO_2.

Already Urey (1947) and Bigeleisen and Mayer (1947) recognized that multiply substituted isotopologues have unique thermodynamic properties different from singly substituted isotopologues of the same molecule. Natural distributions of multiply substituted isotopologues can thus provide unique constraints on geological, geochemical and cosmochemical processes (Wang et al. 2004).

"Normal" gas-source mass spectrometers do not allow meaningful abundance measurements of these very rare species. However, if some demands on high abundance sensitivity, high precision and high mass resolving power are met, John Eiler and his group (e.g. Eiler and Schauble 2004; Affek and Eiler 2006; Eiler 2007) have reported precise (< 0.1 ‰) measurements of CO_2 with mass 47 (Δ_{47}-values) with an especially modified, but normal gas-source mass-spectrometer. The Δ_{47}-values are defined as ‰ differences between the measured abundance of all molecules with mass 47 relative to the abundance of 47 expected for the stochastic distribution. Huntington et al. (2009) described the technical details of the method and discussed potential errors and precisions. The main limitation of the analytical method for its wide application is the need for a relatively large amount (5–10 mg) of pure sample necessary for a precise measurement.

This new technique is termed "clumped isotope geochemistry" (Eiler 2007) because the respective species are produced by clumping two rare isotopes together. "Clumping" results in a statistical overabundance of multiply substituted isotopologues relative to a purely random distribution of all isotopes. Deviations from stochastic distributions are generally within 1 % and may result from all processes of isotope fractionation observed in nature. Thus, processes that lead to isotope fractionations of bulk compositions also lead to fractionations of multiply substituted isotopologues (Eiler 2007). So far the most used application is a carbonate thermometer based on isotope exchange reactions inside the carbonate group, where the equilibrium constant does not depend on the isotopic composition of parental water.

Schauble et al. (2006) calculated an ~0.4 ‰ excess of $^{13}C^{18}O^{16}O$ groups in carbonate groups at room temperature relative to what would be expected in a stochastic mixture of carbonate isotopologues with the same bulk $^{13}C/^{12}C$, $^{18}O/^{16}O$ and $^{17}O/^{16}O$ ratios. The excess amount of $^{13}C^{18}O^{16}O$ decreases with increasing temperature (Ghosh et al. 2006). Figure 1.5 shows an empirical calibration of the clumped isotope thermometer as summarized by Wacker et al. (2014).

The advantage of this thermometer is the potential to determine formation temperatures of carbonates without knowing the isotope composition of the fluid. The latter can be deduced from a combination with the major isotope ratios.

Although clumped isotope thermometry has already made important strides from its infancy, clumped isotope measurements are still restricted to a few laboratories around the world. Thus far the clumped isotope technique has been contributing to palaeoclimatology, (temperatures of foraminifera and other marine organisms, Tripati et al. 2010 and others), to estimate temperatures of paleosol carbonates (Quade et al. 2011), of speleothems (Affek et al. 2008), and to constrain the diagenetic history of calcite (Huntington et al. 2010) and of dolomite.

Tripati et al. (2010) presented a global dataset for foraminifera and coccolliths and demonstrated that the clumped isotope thermometer is applicable as a temperature proxy. In the case of speleothems and surface corals, however, calculated

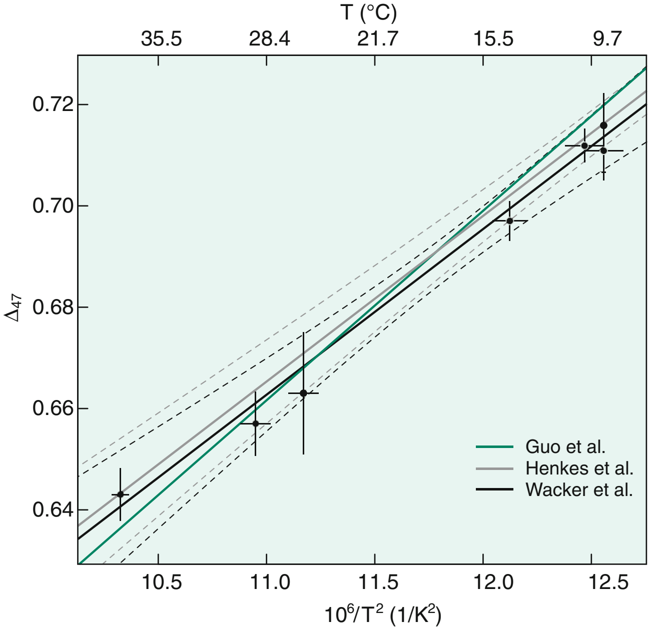

Fig. 1.5 Empirical calibrations of the clumped isotope thermometer (after Wacker et al. 2014)

clumped temperatures markedly differ from known temperatures (Saenger et al. 2012; Eiler et al. 2014). For speleothems, derived clumped temperatures are significantly higher than known growth temperatures. Deviations for corals may depend on growth rates, implying the impact of kinetic effects on clumped isotope signals.

By analyzing ^{13}C–^{18}O bonds in the carbonate component of apatite of vertebrates, Eagle et al. (2010) showed that it is possible to deduce body temperatures of extinct vertebrates.

The clumped isotope geothermometer may be applicable in the 50–300 °C range (Passey and Henkes 2012), relevant to processes such as dolomitization (Ferry et al. 2011) and burial diagenesis (Huntington et al. 2011). Dennis and Schrag (2010) have used carbonatites to test the isotope integrity of the clumped isotope composition over long timescales and concluded reordering of C-and O-atoms is sufficiently slow to enable the use of clumped paleothermometry on timescales of 10^8 years. Henkes et al. (2014) argued that calcites being exposed to temperatures of about 100 °C for 10^6–10^8 years will not be affected by solid state C–O reordering.

The key question in using clumped temperatures of deeply buried carbonates is the closure temperature for isotopic redistribution by lattice diffusion. Studies of marbles and carbonatites indicate closure temperatures in the order of 200 °C for calcite and somewhat higher for dolomite (Dennis and Schrag 2010; Ferry et al. 2011).

Methane is another gas, in which clumped isotopes have been investigated (Stolper et al. 2014). Besides the 3 most abundant isotopologues, $^{12}CH_4$, $^{13}CH_4$ and $^{12}CH_3D$, there are 7 more isotopologues with the heaviest mass 21 for $^{13}CD_4$. In a first attempt Stolper et al. (2014) presented data for the isotologues $^{13}CH_3D$ and $^{12}CH_2D_2$ which for equilibrated systems can be used as a geothermometer. Clumped isotopes yield consistent temperatures of formation for low-temperature biogenic and high-temperature thermogenic methane.

1.3.5.1 Position or Site-Specific Isotope Fractionations

Site-specific isotope fractionations describe differences between the isotope composition of a site in a molecule and the isotope composition it would have if the molecule had randomly distributed isotopes (Galimov 2006; Eiler 2013). Examples are the distribution of ^{15}N in the central position and the terminal position in N_2O. Nitrifying bacteria enrich ^{15}N in the central position, whereas N_2O from denitrifying bacteria and other natural sources of N_2O do not show site-specific fractionations.

Other characteristic site-specific fractionations are ^{13}C and D fractionations occurring during the synthesis of organic molecules. Abelson and Hoering (1961) were the first to analyse the $\delta^{13}C$-value of isolated amino acids separately and showed that the terminal carboxyl groups on most amino acids where significantly enriched in ^{13}C relative to other C positions. Blair et al. (1985) demonstrated that in acetate (CH_3COOH), the methyl group (CH_3) and the carboxyl group (COOH) differ by up to 20 ‰ in ^{13}C. It can be expected that with further advances in analytical techniques many more applications of site-specific isotope fractionations will arise.

1.3.6 Diffusion

Ordinary diffusion can cause significant isotope fractionations. In general, light isotopes are more mobile and hence diffusion can lead to a separation of light from heavy isotopes. For gases, the ratio of diffusion coefficients is equivalent to the inverse square root of their masses. Consider the isotopic molecules of carbon in CO_2 with masses $^{12}C^{16}O^{16}O$ and $^{13}C^{16}O^{16}O$ having molecular weights of 44 and 45. Solving the expression equating the kinetic energies (1/2 m v^2) of both species, the ratio of velocities is equivalent to the square root of 45/44 or 1.01. That is regardless of temperature, the average velocity of $^{12}C^{16}O^{16}O$ molecules is about 1 % higher than the average velocity of $^{13}C^{16}O^{16}O$ molecules in the same system. This isotope effect, however, is more or less limited to ideal gases, where collisions between molecules are infrequent and intermolecular forces negligible. The carbon isotope fractionation of soil-CO_2 due to diffusional movement, for instance, has been estimated to be around 4 ‰ (Cerling 1984; Hesterberg and Siegenthaler 1991).

Distinctly different from ordinary diffusion is the process of thermal diffusion where a temperature gradient results in a mass transport. The greater the mass difference the more pronounced is the tendency of the two species to separate by thermal diffusion. A natural example of thermal diffusion has been presented by Severinghaus et al. (1996) who observed a small isotope depletion of ^{15}N and ^{18}O in air from a sand dune relative to the free atmosphere. This observation is contrary to the expectation that heavier isotopes in unsaturated zones of soils would be enriched by gravitational settling. Such thermally driven diffusional isotope effects have also been described in air bubbles from ice cores (Severinghaus et al. 1998; Severinghaus and Brook 1999; Grachiev and Severinghaus 2003).

In solutions and solids the relationships are much more complicated than in gases. The term "solid state diffusion" generally includes volume diffusion and diffusion mechanisms where the atoms move along paths of easy diffusion such as grain boundaries and surfaces. Diffusive-penetration experiments indicate a marked enhancement of diffusion rates along grain boundaries which are orders of magnitude faster than for volume diffusion. Thus, grain boundaries can act as pathways of rapid exchange. Volume diffusion is driven by the random temperature dependent motion of an element or isotope within a crystal lattice, and it depends on the presence of point defects, such as vacancies or interstitial atoms within the lattice.

The flux F of elements or isotopes diffusing through a medium is proportional to the concentration gradient (dc/dx) such that:

$$F = -D(dc/dx) \quad \text{(Fick, s first law)} \tag{1.21}$$

where “D” represents the diffusion coefficient, and the minus sign denotes that the concentration gradient has a negative slope, i.e. elements or isotopes move from points of high concentration towards points of low concentration. The diffusion coefficient “D” varies with temperature according to the Arrhenius relation

$$D = D_o e^{(-E_a/RT)} \tag{1.22}$$

where “D_o” is a temperature-independent factor, “E_a” is the activation energy, “R” is the gas constant and T is in Kelvins.

In recent years there have been several attempts to determine diffusion coefficients, mostly utilizing Secondary Ion Mass Spectrometry (SIMS), where isotope compositions have been measured as a function of depth below a crystal surface after exposing the crystal to solutions or gases greatly enriched in the heavy isotopic species.

A plot of the logarithm of the diffusion coefficient versus reciprocal temperature yields a linear relationship over a significant range of temperature for most minerals. Such an Arrhenius plot for various minerals is shown in Fig. 1.6, which illustrates the variability in diffusion coefficients for different minerals. The practical application of this fact is that the different minerals in a rock will exchange oxygen at different rates and become closed systems to isotopic exchange at different temperatures. As a rock cools from the peak of a thermal event, the magnitude of isotope fractionations between exchanging minerals will increase. The rate at which the coexisting minerals can approach equilibrium at the lower temperature is limited by the volume diffusion rates of the respective minerals.

Several models for diffusive transport in and among minerals have been discussed in the literature, one is the “Fast Grain Boundary/FGB) model” of Eiler et al. (1992, 1993). The FGB model considers the effects of diffusion between non-adjacent grains and shows that, when mass balance terms are included, closure temperatures become a strong function of both the modal abundances of constituent minerals and the differences in diffusion coefficients among all coexisting minerals.

Surprisingly large fractionations by chemical and thermal diffusion at very high temperatures have been reported by Richter et al. (1999, 2003, 2007, 2009) and others observing large isotope variations of Mg, Ca, Fe, Si and O in silicate melts subjected to thermal gradients Diffusion experiments between molten basalt and rhyolite also demonstrated considerable isotope fractionations of Li, Ca and Ge (the latter used as a Si analogue). Especially for Li, diffusion processes occuring at high temperatures seem to be of first order importance (see p. 56). Thus the notion that isotope fractionations above 1000 °C appear to be negligible has to be reconsidered, although the physical mechanisms are not clear.

Dominguez et al. (2011) presented a model of diffusion in solid phases that explains both thermal and mass transport in silicate melts. Thermal and chemical mass transport rely on the same diffusion mechanism. The model in conjunction

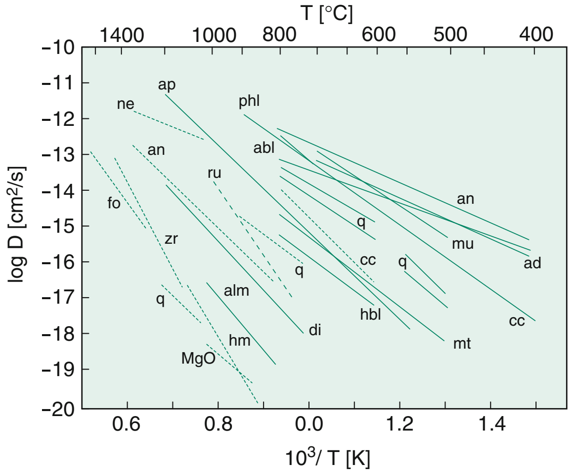

Fig. 1.6 Arrhenius plot of diffusion coefficients versus reciprocal temperatures for various minerals. Data from phases reacted under *wet conditions* are given as *solid lines*, whereas *dry conditions* are represented by *dashed lines*. Note that the rates for dry systems are generally lower and have higher activation energies (steeper slopes) (after Cole and Chakraborty 2011) (Fig. 1.5 6th edition, p. 17)

with measured isotope ratios in zoned minerals can be also used to reconstruct cooling histories.

Diffusion of dissolved species was also used as a process to explain the precipitation-rate dependence of isotope fractionation of earth alkaline elements during low-temperature carbonate formation (Fietzke and Eisenhauer 2006).

1.3.7 Other Factors Influencing Isotopic Fractionations

(a) Pressure

It is commonly assumed that temperature is the main variable determining the isotopic fractionation and that the effect of pressure is negligible, because molar volumes do not change with isotopic substitution. This assumption is generally fulfilled, except for hydrogen. Driesner (1997), Horita et al. (1999, 2002) and Polyakov et al. (2006) have shown, however, that for isotope exchange reactions involving water, changes of pressure can influence isotope fractionations. Driesner (1997) calculated hydrogen isotope fractionations between epidote and water and observed at 400 °C a change from –90 ‰ at 1 bar to –30 ‰ at 4000 bars. Horita et al. (1999, 2002) presented experimental evidence for a pressure effect in the system brucite ($Mg(OH)_2$—water. Theoretical calculations indicate that pressure effects largely result on water rather than effects on brucite. Thus it is likely that D/H fractionations of any hydrous mineral is subject to similar pressure effects (Horita et al. 2002). These pressure effects have to be taken into account when calculating the hydrogen isotope composition of the fluid from the mineral composition.

(b) Chemical composition
Qualitatively, the isotopic composition of a mineral depends to a very high degree upon the nature of the chemical bonds within the mineral and to a smaller degree upon the atomic mass of the respective elements. In general, bonds to ions with a high ionic potential and small size are associated with high vibrational frequencies and have a tendency to incorporate preferentially the heavy isotope. This relationship can be demonstrated by considering the bonding of oxygen to the small highly charged Si^{4+} ion compared to the relatively large Fe^{2+} ion of the common rock-forming minerals. In natural mineral assemblages: quartz is the most ^{18}O-rich mineral and magnetite is the most ^{18}O-deficient given equilibration in the system. Furthermore, carbonates are always enriched in ^{18}O relative to most other mineral groups because oxygen is bonded to the small, highly charged C^{4+} ion. The mass of the divalent cation is of secondary importance to the C–O bonding. However, the mass effect is apparent in ^{34}S distributions among sulfides, where, for example, ZnS always concentrates ^{34}S relative to coexisting PbS.
Compositional effects in silicates are complex and difficult to deduce, because of the very diverse substitution mechanisms in silicate minerals (Kohn and Valley 1988). The largest fractionation effect is clearly related to the NaSi=-CaAl substitution in plagioclases which is due to the higher Si to Al ratio of albite and the greater bond strength of the Si–O bond relative to the Al–O bond. In pyroxenes, the jadeite ($NaAlSi_2O_6$)—diopside ($CaMgSi_2O_6$) substitution also involves Al, but Al in this case replaces an octahedral rather than tetrahedral site. Chacko et al. (2001) estimate that at high temperatures the Al-substitution in pyroxenes is about 0.4 ‰ per mole Al substitution in the tetrahedral site. The other very common substitutions, the Fe–Mg and the Ca–Mg substitutions, do not generate any significant difference in oxygen isotope fractionation (Chacko et al. 2001).

(c) Crystal structure
Structural effects are secondary in importance to those arising from the primary chemical bonding: the heavy isotope being concentrated in the more closely-packed or well-ordered structures. The ^{18}O and D fractionations between ice and liquid water arise mainly from differences in the degree of hydrogen bonding (order). A relatively large isotope effect associated with structure is observed between graphite and diamond (Bottinga 1969). With a modified increment method, Zheng (1993a) has calculated this structural effect for the SiO_2 and Al_2SiO_5 polymorphs and demonstrated that ^{18}O will be enriched in the high-pressure forms. In this connection it should be mentioned, however, that Sharp (1995) by analyzing natural Al_2SiO_5 minerals observed no differences for kyanite versus sillimanite. Other examples of structural effects on isotope fractionations are carbonate minerals (Zheng and Böttcher 2015).

(d) Sorption

The term “sorption” is used to indicate the uptake of dissolved species by solids irrespective of the mechanism. Isotope fractionations during sorption depend on mineral surface chemistry and on compositions of the solution. During physical sorption, when the element in question is not structurally incorporated, isotope fractionations should be small, whereas during chemical sorption, when the element is incorporated by stronger bonds, isotope fractionations are larger.

Considering the large range of possible sorbents (oxide/hydroxides, phyllosilicates, biologic surfaces etc.), knowledge of isotope fractionations on solid/water interfaces are of crucial importance to understand the isotope geochemistry of metals. Experimental determinations on the fractionation of metal isotopes during absorption onto metal oxide phases have been presented by a number of studies (i.e. Teutsch et al. 2005; Gelabert et al. 2006, and others). Most studies show small (less than 1 ‰) isotope fractionations as metal ions are removed from solution onto oxide surfaces, except Mo where absorption on oxides causes about 2 ‰ fractionation in ^{98}Mo/^{95}Mo ratios. Generally, elements that are present as cations in a solution (Fe, Cu, Zn) exhibit enrichment of the heavier isotope on the surface of solids, which is consistent with shorter metal-oxide bonds and lower coordination numbers for the metal at the surface relative to the aqueous ion. Thus the heavier isotope should concentrate in the species in which it is most strongly bound, for example, enrichment of absorbed tetrahedral metal with shorter metal-oxygen bonds compared to octahedral metal in solution.

Metal cations in solution that form soluble oxyanions such as Ge, Se, Mo, and U enrich the lighter isotope on Fe/Mn oxide surfaces. The molecular mechanism responsible for the sign and size of metal isotope fractionation between solids and aqueous phases remain poorly understood. Wasylenki et al. (2011) postulated that largest isotope effects occur when a trace solution species with different coordination than the major solution species absorb. Kashiwabara et al. (2011) argued similarly by stating that small isotope fractionations are associated with little changes in local structures during absorption.

1.3.8 Isotope Geothermometers

Isotope thermometry has become well established since the classic paper of Urey (1947) on the thermodynamic properties of isotopic substances. The partitioning of two stable isotopes of an element between two mineral phases can be viewed as a special case of element partitioning between two minerals. The most important difference between the two exchange reactions is the pressure-insensitivity of isotope partitioning due to the negligible ΔV of reaction for isotope exchange. This represents a considerable advantage relative to the numerous types of other geothermometers, all of which exhibit a pressure dependence.

The necessary condition to apply an isotope geothermometer is isotope equilibrium, which is most readily achieved at high temperatures, where isotope geothermometers are, however, less sensitive that at low temperatures. Isotope exchange equilibrium should be established during reactions whose products are in **chemical** and **mineralogical** equilibrium. Demonstration that the minerals in a rock are in oxygen isotope equilibrium is strong evidence that the rock is in chemical equilibrium. To break Al–O and Si–O bonds and allow re-arrangement towards oxygen isotope equilibrium needs sufficient energy to effect chemical equilibrium as well.

Theoretical studies show that the fractionation factor α for isotope exchange between minerals is a linear function of $1/T^2$, where "T" is temperature in degrees Kelvin. Bottinga and Javoy (1973) demonstrated that O-isotopic fractionation between anhydrous mineral pairs can be expressed in terms of a relationship of the form:

$$1000 \ln \alpha = A/T^2 + B/T + C,$$

One drawback to isotope thermometry in slowly cooled metamorphic and magmatic rocks is that, temperature estimates are often significantly lower than those from other geothermometers. This results from isotopic resetting associated with retrograde isotope exchange between coexisting phases or with transient fluids. During cooling in closed systems, volume diffusion may be the principal mechanism by which isotope exchange occurs between coexisting minerals.

Giletti (1986) proposed a model in which experimentally-derived diffusion data can be used in conjunction with measured isotope ratios to explain disequilibrium isotope fractionations in slowly-cooled, closed-system mineral assemblages. This approach describes diffusional exchange between a mineral and an infinite reservoir whose bulk isotopic composition is constant during exchange. However, mass balance requires that loss or gain of an isotope from one mineral must be balanced by a change in the other minerals still subject to isotopic exchange. Numerical modeling by Eiler et al. (1992) has shown that closed-system exchange depends not only on modal proportions of all of the minerals in a rock, but also on oxygen diffusivity in minerals, grain size, grain shape and cooling rate. As shown by Kohn and Valley (1998) there is an important water fugacity dependence as well. In the presence of fluids further complications may arise because isotope exchange may also occur by solution-reprecipitation or chemical reaction rather than solely by diffusion.

Three different methods have been used to determine the equilibrium fractionations for isotope exchange reactions:

(a) theoretical calculations
(b) experimental determinations in the laboratory, and
(c) empirical or semi-empirical calibrations.

Method (c) is based on the idea that the calculated "formation temperature" of a rock (calculated from other geothermometers) serves as a calibration to the measured isotopic fractionations, assuming that all minerals were at equilibrium. However, because there is evidence that equilibrium is not always attained or retained in nature, such empirical calibrations should be regarded with caution.

Nevertheless, rigorous applications of equilibrium criteria to rock-type and the minerals investigated can provide important information on mineral fractionations (Kohn and Valley 1998; Sharp 1995; Kitchen and Valley 1995).

(A). Theoretical calculations

Calculations of equilibrium isotope fractionation factors have been particularly successful for gases. Richet et al. (1977) calculated the partition function ratios for a large number of gaseous molecules. They demonstrated that the main source of error in the calculation is the uncertainty in the vibrational molecular constants.

The theory developed for perfect gases could be extended to solids if the partition functions of crystals could be expressed in terms of a set of vibrational frequencies that correspond to its various fundamental modes of vibration (O'Neil 1986). By estimating thermodynamic properties from elastic, structural and spectroscopic data, Kieffer (1982) and subsequently Clayton and Kieffer (1991) calculated oxygen isotope partition function ratios and from these calculations derived a set of fractionation factors for silicate minerals. The calculations have no inherent temperature limitations and can be applied to any phase for which adequate spectroscopic and mechanical data are available. They are, however, limited in accuracy as a consequence of the approximations needed to carry out the calculations and the limited accuracy of the spectroscopic data.

Isotope fractionations in solids depend on the nature of the bonds between atoms of an element and the nearest atoms in the crystal structure (O'Neil 1986). The correlation between bond strength and oxygen isotope fractionation was investigated by Schütze (1980), who developed an "increment" method for predicting oxygen isotope fractionations in silicate minerals. Richter and Hoernes (1988) applied this method to the calculation of oxygen isotope fractionations between silicate minerals and water. Zheng (1991, 1993 b, c) extended the increment method by using parameters of crystal chemistry with no empirical factor. The fractionation factors calculated using these methods over the temperature range 0–1200 °C are in relatively good agreement with experimental calibrations.

Ongoing advances in computer capacity and new development of software, have opened the possibility to calculate equilibrium isotope fractionations using first principles (or ab initio) methods on the base of density functional theory (Meheut et al. 2007; Schauble et al. 2009; Schauble 2011; Kowalski and Jahn 2011; Kowalski et al. 2013 and others). Calculations of equilibrium isotope fractionations can be carried out for fluids and solids at high P and T conditions with a reasonable precision (i.e. Kowalski and Jahn 2011; Kowalski et al. 2013). Although different approaches have been used in these calculations, all methods require knowledge of the vibrational spectrum of a system.

(B) Experimental calibrations

In general, experimental calibrations of isotope geothermometers have been performed between 250 and 800 °C. The upper temperature limit is usually determined by the stability of the mineral being studied or by limitations of the experimental apparatus, whereas the lower temperature limit is determined by the decreasing rate of exchange.

Various experimental approaches have been used to determine fractionation factors. The three most common techniques are described below.

(a) Two-direction approach

This method is analogous to reversing reactions in experimental petrology and is the only method by which the attainment of equilibrium can be convincingly demonstrated. Equilibrium fractionations are achieved by starting on opposite sides of the equilibrium distribution.

(b) Partial-exchange technique

The partial exchange technique is used when rates of isotopic exchange are relatively low and is based on the assumption that the rates of isotope exchange for companion exchange experiments are identical. Experimental runs have to be the same in every respect except in the isotopic compositions of the starting materials. Rates of isotope exchange reactions in heterogeneous systems are relatively high at first (surface control) and then become progressively lower with time (diffusion control). Four sets of experiments are shown in Fig. 1.7 for the CO_2—graphite system (after Scheele and Hoefs 1992). Northrop and Clayton (1966) presented a set of equations to describe the kinetics of isotope exchange reactions and developed a general equation for the partial exchange technique. At low degrees of exchange the fractionations determined by the partial exchange technique are often larger than the equilibrium fractionations (O'Neil 1986).

(c) Three-isotope method

This method, introduced by Matsuhisa et al. (1978) and later modified by Matthews et al. (1983), uses the measurement of both $^{17}O/^{16}O$ and $^{18}O/^{16}O$ fractionations in a single experiment that has gone to equilibrium. The initial $^{18}O/^{16}O$ fractionation for the mineral—fluid system is selected to be close to the assumed equilibrium, while the initial $^{17}O/^{16}O$ fractionation is chosen to be very different from the equilibrium value. In this way the change in the $^{17}O/^{16}O$ fractionations monitor the extent of isotopic exchange and the $^{18}O/^{16}O$ fractionations reflect the equilibrium value. Figure 1.8 gives a schematic diagram of the three-isotope exchange method.

Most of the published data on mineral fractionations have been determined by exchange of single minerals with water. This approach is limited by two

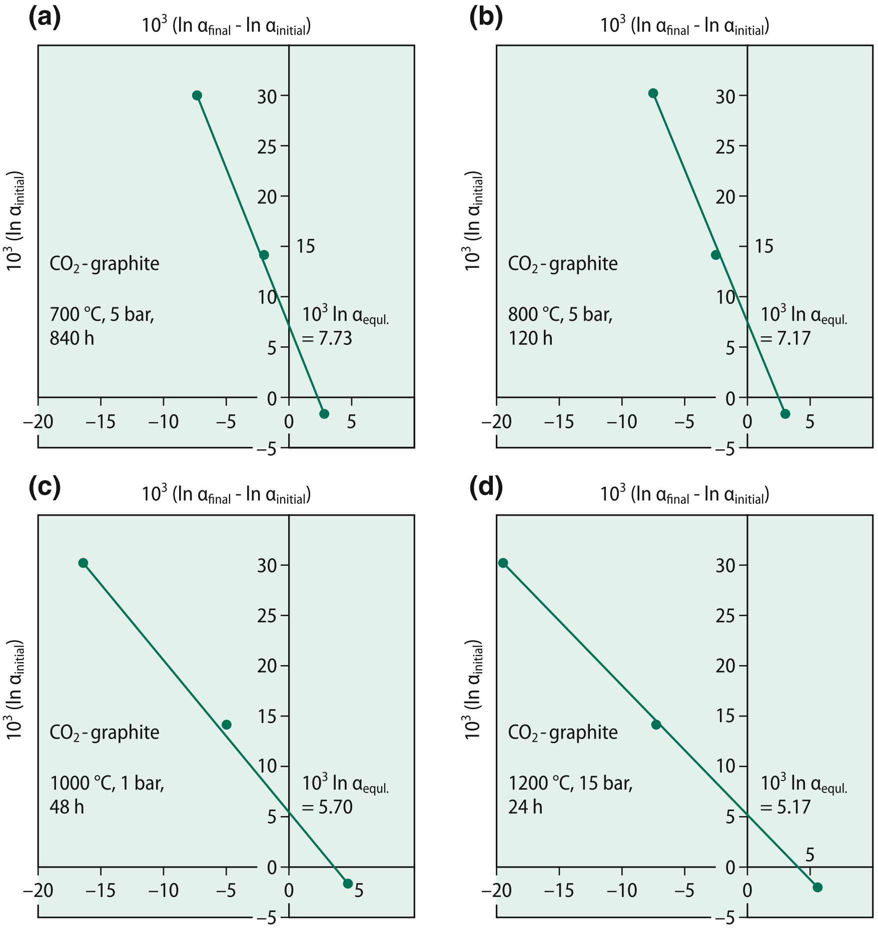

Fig. 1.7 CO_2-graphite partial exchange experiments in a Northrop and Clayton plot at 700, 800, 1000 and 1200 °C. The connecting line in experiment at 1200 °C has a plain slope and defines the intercept more precisely than the experiment at 700 °C (after Scheele and Hoefs 1992) (Fig. 1.6, 6th edition, p. 22)

factors: (i) many minerals are unstable, melt, or dissolve in the presence of water and (ii) the temperature dependence of the fractionation factor for aqueous systems is complicated as a consequence of the high vibrational frequencies of the water molecule. An alternative approach to the experimental determination of isotope fractionation between minerals was first employed by Clayton et al. (1989) and Chiba et al. (1989) who demonstrated that both limitations can be avoided by using $CaCO_3$, instead of H_2O, as the common exchange medium. These studies showed that most common silicates undergo rapid oxygen isotope exchange with $CaCO_3$ at temperatures above 600 °C and pressures of 15 kbars.

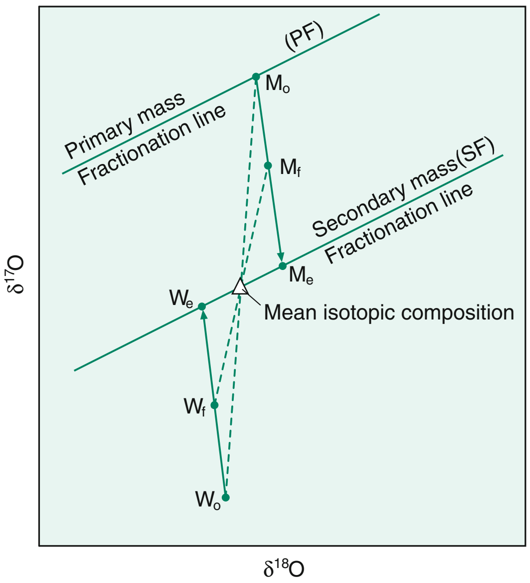

Fig. 1.8 Schematic representation of the three-isotope exchange method. Natural samples plotted on the primary mass fractionation line (PF). Initial isotopic composition are mineral (M_0) and water (W_0) which is well removed from equilibrium with M_0 in δ^{17}O, but very close to equilibrium with M_0 in δ^{18}O. Complete isotopic equilibrium is defined by a secondary mass fractionation line (SF) parallel to PF and passing through the bulk isotopic composition of the mineral plus water system. Isotopic composition of partially equilibrated samples M_f and W_f and completely equilibrated samples are M_e and W_e. Values for M_e and W_e can be determined by extrapolation from the measured values M_0, M_f, W_0 and W_f (after Matthews et al. 1983) (Fig. 1.7, 6th edition, p. 23)

Advantages of the carbonate-exchange technique are: (i) experiments up to 1400 °C, (ii) no problems associated with mineral solubility and (iii) ease of mineral separation (reaction of carbonate with acid). Mineral fractionations derived from hydrothermal and carbonate exchange techniques are generally in good agreement except for fractionations involving quartz and calcite. A possible explanation is a salt effect in the quartz-water system, but no salt effect has been observed in the calcite-water system (Hu and Clayton 2003).

1.4 Basic Principles of Mass Spectrometry

Mass spectrometric methods are by far the most effective means of measuring isotope abundances. A mass spectrometer separates charged atoms and molecules on the basis of their masses and their motions in magnetic and/or electrical fields. The design and applications of the many types of mass spectrometers are too broad to cover here. Therefore, only the principles of mass analysis will be discussed briefly (for a more detailed review see Brand 2002).

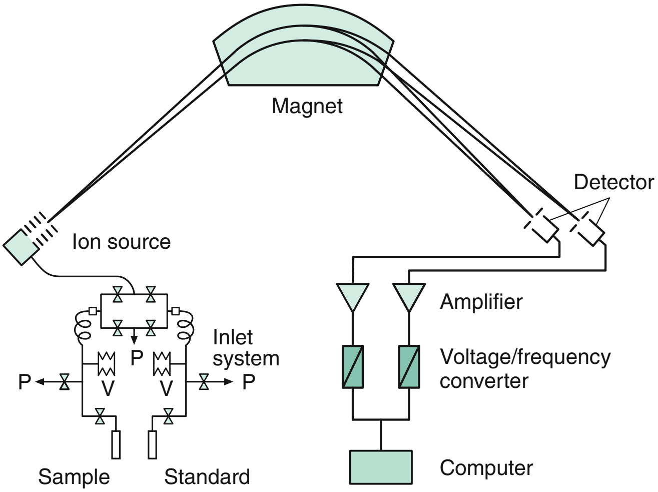

Fig. 1.9 Schematic representation of a gas-source mass spectrometer for stable isotope measurements during the 1960s and 70s. P denotes pumping system, V denotes a variable volume (Fig. 1.8 6th edition, p. 24)

In principle, a mass spectrometer may be divided into four different central constituent parts: (1) the inlet system, (2) the ion source, (3) the mass analyzer, and (4) the ion detector (see Fig. 1.9).

1. Special arrangements for the *inlet system* include a changeover valve. This allows rapid, consecutive analysis between two gas samples (sample and standard gas) within a couple of seconds. The two gases are fed from reservoirs by capillaries of around 0.1 mm in diameter and about 1 m in length. While one gas flows to the ion source the other flows to a waste pump so that flow through the capillaries remains uninterrupted. To avoid a mass discrimination, isotope abundance measurements of gaseous substances are carried out utilizing viscous gas flow. During viscous gas flow, the free path length of molecules is small, molecule collisions are frequent (causing the gas to be well mixed), and no mass separation takes place. At the end of the viscous-flow inlet system, there is a "leak", a constriction in the flow line.
   The smallest amount of sample that can be analyzed with high precision using the dual inlet system is limited by the maintenance of viscous flow conditions. This is generally in the order of 15–20 mbar (Brand 2002). When trying to reduce sample size, it is necessary to concentrate the gas into a small volume in front of the capillary.
2. The *ion source* is that part of the mass spectrometer where ions are formed, accelerated, and focused into a narrow beam. In the ion source, the gas flow is always molecular. Ions of gaseous samples are most reliably produced by electron bombardment. A beam of electrons is emitted by a heated filament, usually tungsten or rhenium, and is accelerated by electrostatic potentials to an

energy between 50 and 150 eV before entering the ionization chamber, which maximizes the efficiency of single ionization. Following ionization any charged molecule can be further fragmented into several pieces depending on the energy the ion has acquired, producing a mass spectrum of a specific compound.

To increase the ionization probability, a homogeneous weak magnetic field is used to keep the electrons on a spiral path. At the end of the ionization chamber, electrons are collected in a positively charged trap, where the electron current is measured and kept constant by the emission regulator circuitry.

The ionized molecules are drawn out of the electron beam by action of an electric field, subsequently accelerated by up to several kV and their path shaped into a beam which passes through an exit slit into the analyzer. Thus, the positive ions entering the magnetic field are essentially monoenergetic, i.e., they will possess the same kinetic energy, given by the equation:

$$1/2\mathrm{Mv}^2 = \mathrm{eV}. \tag{1.24}$$

The efficiency of the ionization process determines the sensitivity of the mass spectrometer which generally is on the order of 1000–2000 molecules per ion (Brand 2002).

3. The *mass analyzer* separates the ion beams emerging from the ion source according to their m/e (mass/charge) ratios. As the ion beam passes through the magnetic field, the ions are deflected into circular paths, the radii of which are proportional to the square root of m/e. Thus, the ions are separated into beams, each characterized by a particular value of m/e.

   In 1940, Nier introduced the sector magnetic analyzer. In this type of analyzer, deflection takes place in a wedge-shaped magnetic field. The ion beam enters and leaves the field at right angles to the boundary, so the deflection angle is equal to the wedge angle, for instance, 60°. The sector instrument has the advantage of its source and detector being comparatively free from the mass-discriminating influence of the analyzer field.
4. After passing through the magnetic field, the separated ions are collected in *ion detectors*, where the input is converted into an electrical impulse, which is then fed into an amplifier. The use of multiple detectors to simultaneously integrate the ion currents was introduced by Nier et al. (1947). The advantage of the simultaneous measurement with two separate amplifiers is that relative fluctuations of the ion currents as a function of time are the same for all m/e beams. Each detector channel is fitted with a high ohmic resistor appropriate for the mean natural abundance of the ion current of interest.

   Modern isotope ratio mass spectrometers have at least three Faraday collectors, which are positioned along the focal plane of the mass spectrometer. Because the spacing between adjacent peaks changes with mass and because the scale is not linear, each set of isotopes often requires its own set of Faraday cups.

1.4.1 Continuous Flow—Isotope Ratio Monitoring Mass Spectrometers

Between the early 1950s, when the dual viscous flow mass spectrometer was introduced by A. Nier, until the mid 80s only minor modifications have been made on the hardware of commercial mass spectrometers. Special efforts had been undertaken to reduce the sample size for isotope measurements. This has led to a modification of the classic dual inlet technique to the continuous-flow isotope ratio monitoring mass spectrometer in which the gas to be analyzed is a trace gas in a stream of carrier gas which achieves viscous flow conditions. Today the majority of gas mass spectrometers is sold with the continuous flow system instead of the dual inlet system.

The classical off-line procedures for sample preparations are time consuming and analytical precision depends on the skill of the investigator. With on-line techniques using a combination of an elemental analyzer directly coupled to the mass spectrometer many problems of the off-line preparation can be overcome and minimized. Differences in both techniques are summarized in Table 1.5.

This new generation of mass-spectrometers is often combined with chromatographic techniques. The sample size required for an isotope measurement has been drastically reduced to the nano–or even picomolar range (Merritt and Hayes 1994). Important features of the GC-IRMS technique are (Brand 2002):

i. ion currents are measured in the order in which molecules emerge from a GC column without significant capability of modifying their intensity relative to the reference gas. Chromotagraphy separates not only different chemical species, but also the different isotope species, which means that the isotope composition of a compound varies across the peak of the chemical species after elution. Therefore, each peak must be integrated over its entire width to obtain the true isotope ratio

Table 1.5 Differences between the offline and online techniques

Offline method (dual inlet)	Online method (continuous flow)
Offline sample preparation	Online sample preparation
Offline purification of gases	Purification of gases by GC column
Large sample size (mg)	Small sample size (micrograms)
Direct inlet of sample gas	Sample gas inlet via carrier gas
Pressure adjust of both gases	No pressure adjust, linearity and stability of the system are necessary conditions
Sample/standard changes (>6 times)	One peak per sample
δ-value calculated from statistical mean	δ-value calculated by peak integration and reference gas
System calibration on a monthly basis	System calibration on a daily basis and during the run
Little problems with homogeneity of sample	Problems with homogeneity of sample

ii. the time for measurement of the isotope signals is restricted by the width of the chromatographic peak. For sharply defined peaks this can mean less than 5s.
iii. absolute sensitivity is much more important than with the dual inlet system. Because sample sizes required for chromatography are significantly smaller, it is often important to use a significantly large set of samples in order to obtain a statistically sound data base.

Standardization has to be accomplished through the use of an added internal standard whose isotopic composition has been determined using conventional techniques.

The development of this technique has proceeded along several independent paths with two principal lines being elemental analyzer-IRMS and capillary gas chromatography-IRMS. In elemental analyzers, samples are combusted to CO_2, N_2, SO_2 and H_2O, which are either chemically trapped or separated on GC columns. There are two types of elemental analyzer: for carbon, nitrogen and sulfur, the sample is combusted in an oxygen containing atmosphere, for hydrogen and oxygen, the sample undergoes high temperature thermal conversion. The advantages of these techniques are an automated preparation with low costs per sample and a large sample through-put at comparable or even better precisions. Figure 1.10 shows a schematic diagram of an elemental analyser-IRMS.

1.4.2 General Remarks on Sample Preparation Methods for Gases

Isotopic differences between samples to be measured are often extremely small. Therefore, great care has to be taken to avoid any isotope fractionation during chemical or physical treatment of the sample. The quality of a stable isotope

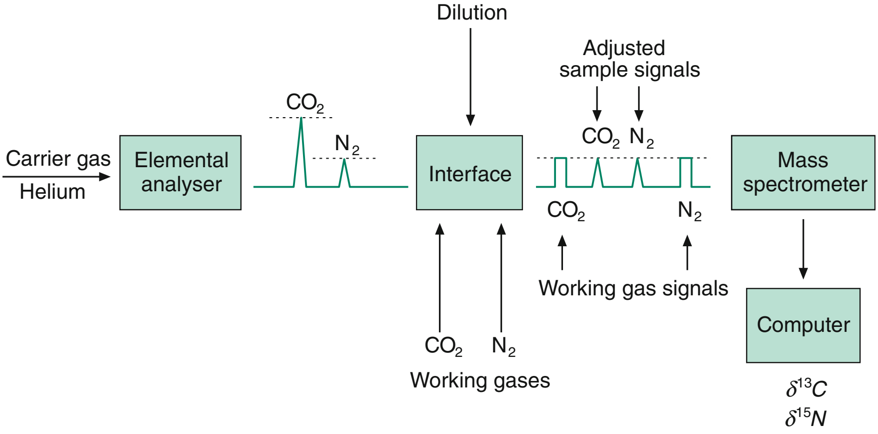

Fig. 1.10 Schematic diagram of an elemental analyser-isotope ratio-mass spectrometer for the determination of carbon and nitrogen isotopes

analysis is determined by the purity of the gas prepared from the sample, quantitative yield, blank and memory effects.

To convert geologic samples to a suitable form for analysis, many different chemical preparation techniques must be used. These techniques all have one general feature in common: any preparation procedure providing a yield of less than 100 % may produce a reaction product that is isotopically different from the original specimen because the different isotopic species have different reaction rates.

A quantitative yield of a pure gas is usually necessary for the mass spectrometric measurement in order to prevent not only isotope fractionation during sample preparation, but also interference in the mass spectrometer. Contamination with gases having the same molecular masses and having similar physical properties may be a serious problem. This is especially critical with CO_2 and N_2O, (Craig and Keeling 1963), and N_2 and CO. When CO_2 is used, interference by hydrocarbons and a CS + ion may also pose a problem.

Contamination may result from incomplete evacuation of the vacuum system and/or from degassing of the sample. The system blank should be normally less than 1 % of the amount of gas prepared from a sample for analysis. For very small sample sizes, the blank may ultimately limit the analysis. Memory effects result from samples that have previously been analyzed. They will become noticeable when samples having widely different isotopic compositions are analyzed consecutively.

How gases are transferred, distilled, or otherwise processed in vacuum lines is briefly discussed under the different elements. A more detailed description can be found in the recently published “Handbook of stable isotope analytical techniques” edited by de Groot (2004).

All errors due to chemical preparation limit the overall precision of an isotope ratio measurement to usually 0.1–0.2 ‰, while modern mass spectrometer instrumentation enables a precision better than 0.02 ‰ for light elements other than hydrogen. Larger uncertainties are expected when elements present in a sample at very low concentration are extracted by chemical methods (e.g., carbon and sulfur from igneous rocks).

Commercial combustion elemental analyzers perform a “flash combustion” converting samples to CO_2, H_2O, N_2 and SO_2 simultaneously. These different gases are then chemically trapped, converted or separated on GC columns and measured in a continuous flow mass-spectrometer. This technique allows the determination of several isotope ratios from the same component, increasing the possibilities of isotope fingerprinting of organic and inorganic compounds containing isotopes of more than one element of interest. Because of very high combustion temperatures, the quantitative conversion of the sample material is guaranteed.

By coupling chromatographic techniques with isotope ratio mass spectrometers mixtures of organic compounds can be analysed separately (compound-specific stable isotope analysis). This method has been first introduced for carbon by Matthews and Hayes (1978) and later modified for the separate analysis of hydrogen, nitrogen, chlorine and oxygen compounds. A recent review of the technique has been published by Elsner et al. (2012).

1.5 Standards

The accuracy with which *absolute* isotope abundances can be measured is substantially poorer than the precision with which *relative* differences in isotope abundances between two samples can be determined. Nevertheless, the determination of absolute isotope ratios is very important, because these numbers form the basis for the calculation of the relative differences, the δ-values. Table 1.6 summarizes absolute isotope ratios of primary standards used by the international stable isotope community.

To compare isotope data from different laboratories an internationally accepted set of standards is necessary. Irregularities and problems concerning standards have been evaluated by Friedman and O'Neil (1977), Gonfiantini (1978, 1984), Coplen et al. (1983), Coplen (1996) and Coplen et al. (2006). The accepted unit of isotope ratio measurements is the delta value (δ) given in per mil (‰). The δ-value is defined as

$$\delta \text{ in } ‰ = \frac{R_{(\text{Sample})} - R_{(\text{Standard})}}{R_{(\text{Standard})}} \cdot 1000 \tag{1.25}$$

where "R" represents the measured isotope ratio. If $\delta_A > \delta_B$, it is convenient to speak of A being enriched in the rare or "heavy" isotope compared to B. Unfortunately, not all of the δ-values cited in the literature are given relative to a single universal standard, so that often several standards of one element are in use. To convert δ-values from one standard to another, the following equation may be used

$$\delta_{X-A} = \left[\left(\frac{\delta_{B-A}}{10^3} + 1\right)\left(\frac{\delta_{X-B}}{10^3} + 1\right) - 1\right] \cdot 10^3 \tag{1.26}$$

Table 1.6 Absolute isotope ratios of international standards (After Hayes 1983)

Standard	Ratio source	Accepted value ($\times 10^6$) (with 95 % confidence interval)	
SMOW	D/H	155.76 ± 0.10	Hagemann et al. (1970)
	$^{18}O/^{16}O$	2,005.20 ± 0.43	Baertschi (1976)
	$^{17}O/^{16}O$	373 ± 15	Nier (1950) by Hayes (1983)
PDB	$^{13}C/^{12}C$	11,237.2 ± 2.9	Craig (1957)
	$^{18}O/^{16}O$	2 067.1 ± 2.1	
	$^{17}O/^{16}O$	379 ± 15	
Air nitrogen	$^{15}N/^{14}N$	3,676.5 ± 8.1	Junk and Svec (1958)
Canyon Diablo Troilite (CDT)	$^{34}S/^{32}S$	45,004.5 ± 9.3	Jensen and Nakai (1962)

Fig. 1.11 Relationship between ^{18}O (^{16}O) content in per cent and $\delta^{18}O$ in per mill (Fig. 1.9, 6th edition, p. 28)

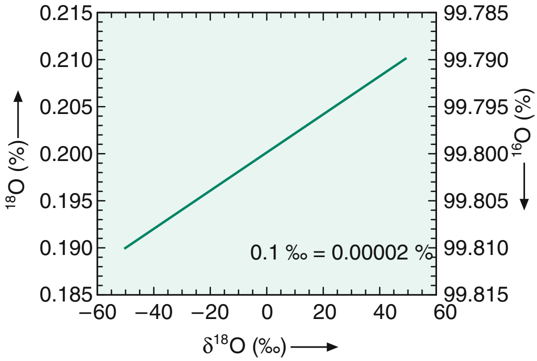

where X represents the sample, A and B different standards.

For different elements a convenient "working standard" is used in each laboratory. However, all values measured relative to the respective "working standard" are reported in the literature relative to a universal standard.

As an example for the relationship between the content of an isotope in % and the δ-value in ‰, Fig. 1.11 demonstrates that large changes in the δ-value only involve very small changes in the heavy isotope content (in this case the ^{18}O content). An ideal standard used worldwide as the "zero-point" on a δ-scale should satisfy the following requirements:

1. be homogeneous in composition,
2. be available in relatively large amounts,
3. be easy to handle for chemical preparation and isotopic measurement, and
4. have an isotope ratio near the middle of the natural range of variation.

Among the reference samples now used, relatively few meet all of these requirements. For instance, the situation for the SMOW standard is rather confusing. The SMOW standard was originally a hypothetical water sample with an isotopic composition very similar to average untreated ocean water (Craig 1961), but being defined in terms of a water sample distributed by the National Bureau of Standards (NBS-1). Later, the IAEA distributed a distilled water sample named V-SMOW (Vienna-SMOW) which is very close to but not identical in isotope composition to the original SMOW standard. The worldwide standards now in general use are given in Table 1.7.

The problems related to standards are discussed by an IAEA advisory group, which meet from time to time. As a result of these meetings the quality and availibility of the existing standards and the need of new standards have been discussed and agreed on.

A further advancement comes from interlaboratory comparison of two standards having different isotopic composition that can be used for a normalization procedure correcting for all proportional errors due to mass spectrometry and to sample preparation. Ideally, the two standard samples should have isotope ratios as

Table 1.7 Worldwide standards in use for the isotopic composition of hydrogen, boron, carbon, nitrogen, oxygen, silicium, sulfur, chlorine and of selected metals (Möller et al. 2012)

Element	Standard	Standard
H	Standard Mean Ocean Water	V-SMOW
B	Boric acid (NBS)	SRM 951
C	Belemnitella americana from the Cretaceous, Peedee formation, South Carolina	V-PDB
N	Air nitrogen	N_2 (atm.)
O	Standard Mean Ocean Water	V-SMOW
Si	Quartz sand	NBS-28
S	Troilite (FeS) from the Canyon Diablo iron meteorite	V-CDT
Cl	Seawater chloride	SMOC
Mg		DSM-3 NIST SRM 980
Ca		NIST SRM 915a
Cr		NIST SRM 979
Fe		IRMM-014
Cu		NIST SRM 976
Zn		JMC3-0749
Mo		NIST 3134
Tl		NIST SRM 997
U		NIST SRM 950a

different as possible, but still within the range of natural variations. There are, however, some problems connected with data normalization, which are still under debate. For example, the CO_2 equilibration of waters and the acid extraction of CO_2 from carbonates are indirect analytical procedures, involving temperature-dependent fractionation factors (whose values are not beyond experimental uncertainties) with respect to the original samples and which might be reevaluated on the normalized scale.

For metal isotopes, standards generally come from two institutions: the Institute for Reference Materials and Mesurements (IRMM) in Belgium and from the National Institute for Standards and Technology (NIST) in the USA. IRMM and NIST mostly supply standard materials in the form of a purified metal or a salt that are easy to dissolve. Some laboratories use natural samples as standards, which has the advantage that samples and standards have to follow the same chemical purification steps. So far, for some elements, there is no consensus on one wordwide used standard, which complicates direct comparison of datasets. Vogl and Pritzkow (2010) have listed currently available reference materials that will be presented under the specific elements.

Table 1.8 summarizes which gases are used for mass-spectrometric analysis of the various elements.

Table 1.8 Gases most commonly used in isotope ratio in mass spectrometry

Element	Gas
H	H_2
C	CO_2, CO
N	N_2, N_2O
O	CO_2, CO, O_2
S	SO_2, SF_6
Si	SiF_4

1.6 Microanalytical Techniques

In recent years microanalytical techniques, which permit relatively precise isotopic determinations on a variety of samples that are orders of magnitude smaller than those used in conventional techniques, have become increasingly important. Different approaches have been used in this connection, which generally reveal greater isotope heterogeneity than conventional analytical approaches. As a rule of thumb: the smaller the scale of measurement the larger the sample heterogeneity.

Figure 1.12 demonstrates the improvement in analytical techniques involving lasers and ion microprobes and the enormous reduction in sample sizes. There is of course a reduction in precision with decreasing sample sizes, which is fortunately surprisingly small.

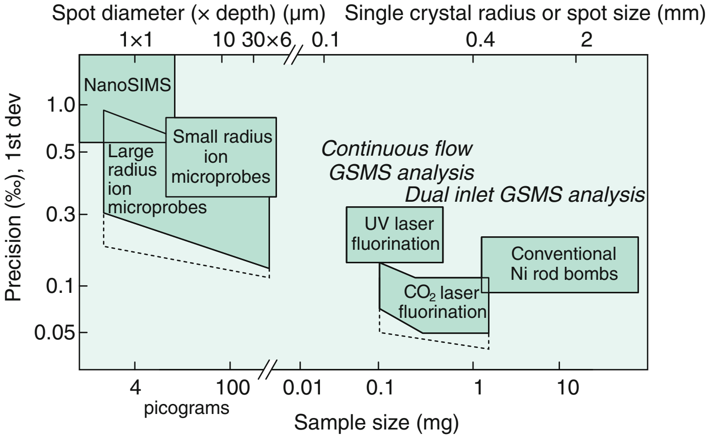

Fig. 1.12 Precision of various oxygen isotope methods as a function of sample weight or size (from Bindeman 2008)

1.6.1 Laser Microprobe

Laser assisted extraction is based on the fact that the energy of the laser beam is absorbed efficiently by a number of natural substances of interest. The absorption characteristics depends on the structure, composition, and crystallinity of the sample. High-energy, finely-focussed laser beams have been used for some years for Ar isotope analysis, the first well-documented preparation techniques with CO_2 and Nd:YAG laser systems for stable isotope determinations have been described by Crowe et al. (1990), Kelley and Fallick (1990) and Sharp (1990). Their results show that sub-milligram quantities of mineral can be analyzed for oxygen, sulfur and carbon. In order to achieve precise and accurate measurements, the samples have to be evaporated completely because steep thermal gradients during laser heating induce isotopic fractionations (Elsenheimer and Valley 1992). The thermal effects of CO_2 and Nd-YAG laser assisted preparation techniques require that sample sections be cut into small pieces before total evaporation. The spatial resolution of this technique is limited to about 500 µm.

Thermal effects can be overcome by vaporizing samples with ultraviolet (UV) KrF and ArF lasers, thus making possible in situ oxygen isotope analysis of silicates (Wiechert and Hoefs 1995; Fiebig et al. 1999; Wiechert et al. 2002).

1.6.2 Secondary Ion Mass Spectrometry (SIMS)

Two different types of SIMS are generally used: the Cameca f-series and the SHRIMP (Sensitive High mass Resolution Ion MicroProbe) series (Valley and Graham 1993; Valley et al. 1998; McKibben and Riciputi 1998). Analysis in the ionmicroprobe is accomplished by sputtering a sample surface using a finely focused primary ion beam producing secondary ions which are extracted and analyzed in the secondary mass spectrometer. The main advantages of this technique are its high sensitivity, high spatial resolution and its small sample size. Sputter pits for a typical 30 min SIMS analyses have a diameter of 10–30 µm and a depth of 1–6 µm, a spatial resolution that is an order of magnitude better than laser techniques. Disadvantages are that the sputtering process produces a large variety of molecular secondary ions along with atomic ions which interfere with the atomic ions of interest and that the ionization efficiencies of different elements vary by many orders of magnitude and strongly depend on the chemical composition of the sample. This “matrix” effect is one of the major problems of quantitative analysis. The two instruments (Cameca and SHRIMP) have technical features, such as high resolving power and energy filtering, which help to overcome the problems of the presence of molecular isobaric interferences and the matrix dependence of secondary ion yields.

Fitzsimons et al. (2000) and Kita et al. (2010) and others have reviewed the factors that influence the precision of SIMS stable isotope data. The latest version of ion microprobe is the Cameca-IMS-1280 type, allowing further reduction in sample and spot size may achieve at the 10 μm scale precise precisions for O, S and Fe isotope ratios at the ≤0.3 ‰ level (Huberty et al. 2010; Kita et al. 2010)

In some minerals like magnetite, hematite, sphalerite and galena the authors recognized analytical artefacts related to crystal orientation effects.

1.6.3 Multicollector-ICP-Mass Spectrometry

Advances in TIMS-techniques and the introduction of multiple collector-ICP-MS (MC-ICP-MS) techniques have enabled the research on natural variations of a wide range of transition and heavy metal systems for the first time which so far could not have been measured with the necessary precision. The technique combines the strength of the ICP technique (high ionization efficiency for nearly all elements) with the high precision of thermal ion source mass-spectrometry equipped with an array of Faraday collectors (Becker 2005; Vanhaecke et al. 2009). The ICP source allows the analysis of samples introduced either as an solution or as an aerosol produced by laser ablation.

Accuracy and precision of MC-ICP-MS mainly depends on 2 factors: (i) quantitative removal of molecular interferences. All MC-ICP-MS instruments need Ar as the plasma support gas in a similar manner to that commonly used in conventional ICP-MS. Mass interferences are thus an inherent feature of this technique, which have to be circumvented by using desolvating nebulisers and other techniques, (ii) corrections for isobaric elemental interferences and for instrumental mass bias depending on the purity and the matrix of the sample. The uptake of elements from solution and ionisation in a plasma allows correction for instrument-dependent mass fractionations by addition of external spikes or the comparison of standards with samples under identical operating conditions.

1.7 Stable Isotope Variations of Metal Elements

Maréchal et al. (1999) and Zhu et al. (2000) first described techniques for the determination of Cu- and Zn-isotope ratios. Observed variations at low temperatures are on the order of several ‰, much more than originally expected on the basis of the relatively small mass differences among isotopes of heavier elements. The magnitude of fractionations depends on several factors such as the participation of redox reactions and biologically mediated reactions.

Equilibrium fractionations of metal isotopes depend primarely on vibration frequencies. As a complete set of frequencies is generally not availiable, advances in computer capacity have allowed to calculate vibrational frequencies of simple molecules and crystalline compounds using first-principles electronic structure theory, which have the advantage that isotope effects can be calculated self-consistent and errors cancel out when calculating isotope frequency shifts (Schauble et al. 2009). Another advantage of first principles vibrational models is that output data can be compared with measured data and thus can test the accuracy of the model (e.g. Polyakov et al. 2007). First calculations applying equilibrium fractionations derived by ab initio methods have been published by Blanchard et al. (2009) for Fe and by Rustad et al. (2010) for Mg and Ca.

Although equilibrium fractionations have been documented for some transition metal (i.e. Fe), they should be small and may be overwhelmed by kinetic fractionations in low-temperature and biological systems (Schauble 2004). Kinetic fractionations have been observed for instance during diffusive mass transfer for elements like Li, Mg and Fe, which in the case of Li can be large and which occur an spatial scales from µm to m. Kinetic isotope fractionations are also observed during the precipitation of solid metal compounds (i.e. carbonates), opposite to equilibrium isotope fractionation which depend on bond energies (Hofmann et al. 2013).

Of special importance are redox reactions, either inorganic or microbially mediated. Like the light elements C and S, the reduced species of the metal is generally isotopically lighter than the oxidized species. Thus the isotope composition of redox sensitive metals may help to understand redox systematics in the environment.

Another important fractionation mechanism for metal isotopes is sorption of metals on particle surfaces. The direction and magnitude of isotope fractionation is, however, highly metal specific. For example, sorption of isotopically light Mo on Fe–Mn oxides can be regarded as the most important fractionation mechanism of Mo (Wasylenki et al. 2008). In contrast Fe (II) sorbed on goethite particles is isotopically heavy compared to dissolved Fe (II) (Beard et al. 2010). For Cr, a negligible isotope fractionation is reported (Ellis et al. 2004).

Coordination numbers of metals in liquids and solids are an additional parameter governing isotope fractionations. Schauble (2004) pointed out that differences in coordination numbers among coexisting phases control isotope fractionation of cations. The lighter isotope preferentially occupies the higher coordinated site. As an example, hematite is isotopically lighter than magnetite, because hematite is in octahedral coordination, whereas magnetite is in octahedral and tetrahedral coordination. Thus differences in isotope composition of lithophile elements such as Fe, Mg, Ca and Li are likely to reflect changes in coordination numbers.

Another characteristic feature of metal isotopes is their fractionation in plants and animals that can be used to understand transport mechanism. Generally, heavy metal isotopes are depleted in plants relatively to the soil in which they grew. Weiss et al. (2005) first showed that plants are generally depleted in heavy metal isotopes compared to their growth solution and that shoots of plants are isotopically lighter than roots.

The uptake and transformation of metals within the organisms can lead to further characteristic isotope fractionations that depend on the specific metal, its chemical speciation and on the type of organisms. Metal isotope fractionations induced by physiological processes in the human body have great potential to be used in medical research. First applications have used Ca isotopes in urine as an indicator of Ca metabolism (Skulan et al. 2007; Heuser and Eisenhauer 2009) and Fe isotopes in human blood (Walczyk and von Blanckenburg 2002).

References

Abelson PH, Hoering TC (1961) Carbon isotope fractionation in formation of amino acids by photosynthetic organisms. Proc Natl Acad Sci USA 47:623

Affek HP, Bar-Matthews M, Ayalon A, Matthews A, Eiler JM (2008) Glacial/interglacial temperature variations in Soreq cave speleothems as recorded by "clumped isotope" thermometry. Geochim Cosmochim Acta 72:5351–5360

Affek HP, Eiler JM (2006) Abundance of mass 47 CO_2 in urban air, car exhaust and human breath. Geochim Cosmochim Acta 70:1–12

Assonov SS, Brenninkmeijer CA (2005) Reporting small $\Delta^{17}O$ values: existing definitions and concepts. Rapid Commun Mass Spectrom 19:627–636

Baertschi P (1976) Absolute 18O content of standard mean ocean water. Earth Planet Sci Lett 31:341–344

Bao H, Thiemens MH, Farquahar J, Campbell DA, Lee CC, Heine K, Loope DB (2000) Anomalous 17O compositions in massive sulphate deposits on the Earth. Nature 406:176–178

Bao H, Thiemens MH, Heine K (2001) Oxygen-17 excesses of the Central Namib gypcretes: spatial distribution. Earth Planet Sci Letters 192:125–135

Baroni M, Thiemens MH, Delmas RJ, Savarino J (2007) Mass-independent sulfur isotopic composition in stratospheric volcanic eruptions. Science 315:84–87

Beard BL, Handler RM, Scherer MM, Wu L, Czaja AD, Heimann A, Johnson CM (2010) Iron isotope fractionationbetween aqueous ferrous iron and goethite. Earth Planet Sci Lett 295:241–250

Becker JS (2005) Recent developments in isotopic analysis by advancedmass spectrometric techniques. J Anal At Spectrom 20:1173–1184

Bigeleisen J (1965) Chemistry of isotopes. Science 147:463–471

Bigeleisen J (1996) Nuclear size and shape effects in chemical reactions. Isotope chemistry of heavy elements. J Am Chem Soc 118:3676–3680

Bigeleisen J, Mayer MG (1947) Calculation of equilibrium constants for isotopic exchange reactions. J Chem Phys 15:261–267

Bigeleisen J, Wolfsberg M (1958) Theoretical and experimental aspects of isotope effects in chemical kinetics. Adv Chem Phys 1:15–76

Bindeman I (2008) Oxygen isotopes in mantle and crustal magmas as revealed by single crystal analysis. Rev Miner Geochem 69:445–478

Blair N, Leu A, Munoz E, Olsen J, Kwong E, Desmarais D (1985) Carbon isotopic fractionation in heterotrophic microbial metabolism. Appl Environ Microbiol 50:996–1001

Blanchard M, Poitrasson F, Meheut M, Lazzari M, Mauri F, Balan E (2009) Iron isotope fractionation between pyrite (FeS_2), hematite (Fe_2O_3) and siderite ($FeCO_3$): a first-principles density functional theory study. Geochim Cosmochim Acta 73:6565–6578

Blum JD (2011) Applications of stable mercury isotopes to biogeochemistry. In: Baskaran M (Ed) Handbook of environmental isotope geochemistry, Springer, pp 229–246

Bottinga Y (1969) Carbon isotope fractionation between graphite, diamond and carbon dioxide. Earth Planet Sci Lett 5:301–307

Bottinga Y, Javoy M (1973) Comments on oxygen isotope geothermometry. Earth Planet Sci Lett 20:250–265

Brand W (2002) Mass spectrometer hardware for analyzing stable isotope ratios. In: de Groot P (ed) Handbook of stable isotope analytical techniques. Elsevier, New York

Bucharenko AI (2001) Magnetic isotope effect: nuclear spin control of chemical reactions. J Phys Chem A 105:9995–10011

Cerling TE (1984) The stable isotopic composition of modern soil carbonate and its relationship to climate. Earth Planet Sci Lett 71:229–240

Chacko T, Cole DR, Horita J (2001) Equilibrium oxygen, hydrogen and carbon fractionation factors applicable to geologic systems. Rev Miner Geochem 43:1–81

Chiba H, Chacko T, Clayton RN, Goldsmith JR (1989) Oxygen isotope fractionations involving diopside, forsterite, magnetite and calcite: application to geothermometry. Geochim Cosmochim Acta 53:2985–2995

Clayton RN, Goldsmith JR, Karel KJ, Mayeda TK, Newton RP (1975) Limits on the effect of pressure in isotopic fractionation. Geochim Cosmochim Acta 39:1197–1201

Clayton RN, Goldsmith JR, Mayeda TK (1989) Oxygen isotope fractionation in quartz, albite, anorthite and calcite. Geochim Cosmochim Acta 53:725–733

Clayton RN, Grossman L, Mayeda TK (1973) A component of primitive nuclear composition in carbonaceous meteorites. Science 182:485–488

Clayton RN, Kieffer SW (1991) Oxygen isotope thermometer calibrations. In: Taylor HP, O'Neil JR, Kaplan IR (ed) Stable Isotope Geochemistry: a tribute to Sam Epstein. Geochem Soc Spec Publ 3:3–10

Cole DR, Chakraborty S (2011) Rates and mechanisms of isotopic exchange. In: Stable isotope geochemistry. Rev Mineral Geochem 43:83–223

Coplen TB (1996) New guidelines for the reporting of stable hydrogen, carbon and oxygen isotope ratio data. Geochim Cosmochim Acta 60:3359–3360

Coplen TB, Kendall C, Hopple J (1983) Comparison of stable isotope reference samples. Nature 302:236–238

Coplen TB, Wa Brand, Gehre M, Gröning M, Meijer HA, Toman B, Verkouteren RM (2006) New guidelines for $\delta^{13}C$ measurements. Anal Chem 78:2439–2441

Craig H (1957) Isotopic standards for carbon and oxygen and correction factors for mass-spectrometric analysis of carbon dioxide. Geochim Cosmochim Acta 12:133–149

Craig H (1961) Standard for reporting concentrations of deuterium and oxygen-18 in natural waters. Science 133:1833–1834

Craig H, Keeling CD (1963) The effects of atmospheric N20 on the measured isotopic composition of atmospheric CO_2. Geochim Cosmochim Acta 27: 549–551

Criss RE (1999) Principles of stable isotope distribution. Oxford University Press

Crowe DE, Valley JW, Baker KL (1990) Micro-analysis of sulfur isotope ratios and zonation by laser microprobe. Geochim Cosmochim Acta 54:2075–2092

Dansgaard W (1964) Stable isotope in precipitation. Tellus 16:436–468

De Groot PA (2004) Handbook of stable isotope analytical techniques. Elsevier Amsterdam, Europe

Dennis KJ, Schrag DP (2010) Clumped isotope thermometry of carbonatites as an indicator of diagenetic alteration. Geochim Cosmochim Acta 74:4110–4122

Dominguez G, Wilikins G, Thiemens MH (2011) The Soret effect and isotope fractionation in high-temperature silicate melts. Nature 473:70–73

Driesner T (1997) The effect of pressure on deuterium-hydrogen fractionation in high-temperature water. Science 277:791–794

Eagle RA, Schauble EA, Tripati AK, Tütken T, Hulbert RC, Eiler JM (2010) Body temperatures of modern and extinct vertebrates from ^{13}C–^{18}O bond abundances in bioapatite. PNAS 107:10377–10382

Eiler JM (2007) The study of naturally-occuring multiply-substituted isotopologues. Earth Planet Sci Lett 262:309–327

Eiler JM (2013) The isotopic anatomies of molecules and minerals. Ann Rev Earth Planet Sci 41:411–441

Eiler JM, Baumgartner LP, Valley JW (1992) Intercrystalline stable isotope diffusion: a fast grain boundary model. Contr Mineral Petrol 112:543–557

Eiler JM, Schauble E (2004) $^{18}O^{13}C^{16}O$ in earth, s atmosphere. Geochim Cosmochim Acta 68:4767–4777

Eiler JM, Valley JW, Baumgartner LP (1993) A new look at stable isotope thermometry. Geochim Cosmochim Acta 57:2571–2583

Eiler JM et al (2014) Frontiers of stable isotope geoscience. Chem Geol 372: 119–143

Ellis AS, Johnson TM, Bullen TD (2004) Using chromium stable isotope ratios to quantify Cr(VI) reduction: lack of sorption effects. Environ Sci Techn 38:3604–3607

Elsenheimer D, Valley JW (1992) In situ oxygen isotope analysis of feldspar and quartz by Nd-YAG laser microprobe. Chem Geol 101:21–42

Elsner M, Jochmann MA, Hofstetter TB, Hunkeler D, Bernstein A, Schmidt T, Schimmelmann A (2012) Current challenges in compound-specific stable isotope analysis of environmental organic contaminants. Anal Bioanal Chem 403:2471–2491

Epov VN, Malinovskiy D, Vanhaecke F, Begue D, Donard OF (2011) Modern mass spectrometry for studying mass-independent fractionation of heavy stable isotopes in environmental and biological sciences. J Anal At Spectrom 26:1142–1156

Estrade N, Carignan J, Sonke JE, Donard O (2009) Mercury isotope fractionation during liquid-vapor evaporation experiments. Geochim Cosmochim Acta 73:2693–2711

Farquhar J, Bao H, Thiemens M (2000) Atmospheric influence of Earth's earliest sulfur cycle. Science 289:756–759

Farquhar J, Johnston DT, Wing BA, Habicht KS, Canfield DE, Airieau S, Thiemens MH (2003) Multiple sulphur isotope interpretations for biosynthetic pathways: implications for biological signatures in the sulphur isotope record. Geobiology 1:27–36

Ferry JM, Passey BH, Vasconcelos C, Eiler JM (2011) Formation of dolomite at 40–80°C in the Latemar carbonate buildup, Dolomites, Italy from clumped isotope thermometry. Geology 39:571–574

Fiebig J, Wiechert U, Rumble D, Hoefs J (1999) High-precision in-situ oxygen isotope analysis of quartz using an ArF laser. Geochim Cosmochim Acta 63:687–702

Fietzke J, Eisenhauer A (2006) Determination of temperature-dependent stable strontium isotope (^{88}Sr/^{86}Sr) fractionation via bracketing standard MC-ICP-MS. Geochem Geophys Geosys 7, p 8. doi: 10.1029/2006GC001243

Fitzsimons ICW, Harte B, Clark RM (2000) SIMS stable isotope measurement: counting statistics and analytical precision. Min Mag 64:59–83

Friedman I, O'Neil JR (1977) Compilation of stable isotope fractionation factors of geochemical interest. In: Data of geochemistry, 6th edn. Geological States Geological Survey Professional Paper 440-KK

Fujii T, Moynier F, Albarede F (2009) The nuclear field shift effect in chemical exchange reactions. Chem Geol 267:139–156

Galimov EM (2006) Isotope organic geochemistry. Org Geochem 37:1200–1262

Gao YQ, Marcus RA (2001) Strange and unconventional isotope effects in ozone formation. Science 293:259–263

Gelabert A, Pokrovsky OS, Viers J, Schott J, Boudou A, Feurtet-Mazel A (2006) Interaction between zinc and marine diatom species: surface complexation and Zn isotope fractionation. Geochim Cosmochim Acta 70:839–857

Ghosh P et al. (2006) ^{13}C–^{18}O bonds in carbonate minerals: a new kind of paleothermometer. Geochim Cosmochim Acta 70: 1439–1456

Giletti BJ (1986) Diffusion effect on oxygen isotope temperatures of slowly cooled igneous and metamorphic rocks. Earth Planet Sci Lett 77:218–228

Gonfiantini R (1978) Standards for stable isotope measurements in natural compounds. Nature 271:534–536

Gonfiantini R (1984) Advisory group meeting on stable isotope reference samples for geochemical and hydrological investigations. Report Director General IAEA Vienna

Grachev AM, Severinghaus JP (2003) Laboratory determination of thermal diffusion constants for ^{29}N/^{28}N$_2$ in air at temperatures from –60 to 0 °C for reconstruction of magnitudes of abrupt climate changes using the ice core fossil-air paleothermometer. Geochim Cosmochim Acta 67:345–360

Hagemann R, Nief G, Roth E (1970) Absolute isotopic scale for deuterium analysis of natural waters. Absolute D/H ratio for SMOW. Tellus 22:712–715

Hayes JM (1983) Practice and principles of isotopic measurements in organic geochemistry. In: Organic geochemistry of contemporaneous and ancient sediments, Great Lakes Section, SEPM, Bloomington, Ind, pp 5-1–5-31

Henkes GA, Passey BH, Grossman EL, Shenton BJ, Perez-Huerta A, Yancey TE (2014) Temperature limits of preservation of primary calcite clumped isotope paleotemperatures. Geochim Cosmochim Acta 139:362–382

Hesterberg R, Siegenthaler U (1991) Production and stable isotopic composition of CO2 in a soil near Bern, Switzerland. Tellus 43B:197–205

Heuser A, Eisenhauer A (2009) A pilot study on the use of natural calcium isotope (^{44}Ca/^{40}Ca) fractionation in urine as a proxy for the human body calcium balance. Bone. doi:10.1016/j.bone.2009.11037

Hofmann AE, Bourg IC, DePaolo DJ (2013) Ion desolvation as a mechanism for kinetic isotope fractionation in aqueous systems. PNAS (in press)

Horita J, Cole DR, Polyakov VB, Driesner T (2002) Experimental and theoretical study of pressure effects on hydrous isotope fractionation in the system brucite-water at elevated temperatures. Geochim Cosmochim Acta 66:3769–3788

Horita J, Driesner T, Cole DR (1999) Pressure effect on hydrogen isotope fractionation between brucite and water at elevated temperatures. Science 286:1545–1547

Hu G, Clayton RN (2003) Oxygen isotope salt effects at high pressure and high temperature and the calibration of oxygen isotope thermometers. Geochim Cosmochim Acta 67:3227–3246

Huberty JM, Kita NT, Kozdon R et al (2010) Crystal orientation effects in δ^{18}O for magnetite and hematite by SIMS. Chem Geol 276:269–283

Huntington KW, Budd DA, Wernicke BP, Eiler JM (2011) Use of clumped-isotope thermometry to constrain the crystallization temperature of diagenetic calcite. J Sediment Res 81:656–669

Huntington KW, Wernicke BP, Eiler JM (2010) Influence of climate change and uplift on Colorado Plateau paleotemperatures from carbonate clumped isotope thermometry. Tectonics 29 TC3005. doi:10.1029/2009TC002449

Huntington KW, Eiler JM et al. (2009) Methods and limitations of “clumped” CO_2 isotope (Δ_{47}) analysis by gas-source isotope ratio mass spectrometry. J Mass Spectrom 44:1318–1329

Jensen ML, Nakai N (1962) Sulfur isotope meteorite standards, results and recommendations. In: Jensen ML (ed) Biogeochemistry of sulfur isotopes. NSF Symp Vol, p 31

Junk G, Svec H (1958) The absolute abundance of the nitrogen isotopes in the atmosphere and compressed gas from various sources. Geochim Cosmochim Acta 14:234–243

Kashiwabara T, Takahashi Y, Tanimizu M, Usui A (2011) Molecular-scale mechanisms of distribution and isotopic fractionation of molybdenum between seawater and ferromanganese oxides. Geochim Cosmochim Acta 75:5762–5784

Kelley SP, Fallick AE (1990) High precision spatially resolved analysis of δ34S in sulphides using a laser extraction technique. Geochim Cosmochim Acta 54:883–888

Kieffer SW (1982) Thermodynamic and lattice vibrations of minerals: 5. Application to phase equilibria, isotopic fractionation and high-pressure thermodynamic properties. Rev Geophys Space Phys 20:827–849

Kita NT, Hyberty JM, Kozdon R, Beard BL, Valley JW (2010) High-precision SIMS oxygen, sulfur and iron stable isotope analyses of geological materials: accuracy, surface topography and crystal orientation. Surf Interface Anal 43:427–431

Kitchen NE, Valley JW (1995) Carbon isotope thermometry in marbles of the Adirondack Mountains, New York. J metamorphic Geol 13:577–594

Kohn MJ, Valley JW (1998) Obtaining equilibrium oxygen isotope fractionations from rocks: theory and examples. Contr Mineral Petrol 132:209–224

Kowalski PM, Jahn S (2011) Prediction of equilibrium Li isotope fractionation between minerals and aqueous solutions at high P and T: an efficient ab initio approach. Geochim Cosmochim Acta 75:6112–6123

Kowalski PM, Wunder B, Jahn S (2013) Ab initio prediction of equilibrium boron isotope fractionation between minerals and aqueous fluids at high P and T. Geochim Cosmochim Acta 101:285–301

Luz B, Barkan E, Bender ML, Thiemens MH, Boering KA (1999) Triple-isotope composition of atmospheric oxygen as a tracer of biosphere productivity. Nature 400:547–550

Maréchal CN, Télouk P, Albarède F (1999) Precise analysis of copper and zinc isotopic compositions by plasma-source mass spectrometry. Chem Geol 156:251–273

Matsuhisa Y, Goldsmith JR, Clayton RN (1978) Mechanisms of hydrothermal crystallization of quartz at 250 °C and 15 kbar. Geochim Cosmochim Acta 42:173–182

Matthews A, Goldsmith JR, Clayton RN (1983) Oxygen isotope fractionation involving pyroxenes: the calibration of mineral-pair geothermometers. Geochim Cosmochim Acta 47:631–644

Matthews DE, Hayes JM (1978) Isotope-ratio-monitoring gas chromatography-mass spectrometry. Anal Chem 50:1465–1473

Mauersberger K, Erbacher B, Krankowsky D, Günther J, Nickel R (1999) Ozone isotope enrichment: isotopomer-specific rate coefficients. Science 283:370–372

McKibben MA, Riciputi LR (1998) Sulfur isotopes by ion microprobe. In: applications of microanalytical techniques to understanding mineralizing processes. Rev Econ Geol 7: 121–140

Meheut M, Lazzari M, Balan E, Mauri F (2007) Equilibrium isotopic fractionation in the kaolinite, quartz, water system: prediction from first principles calculations density-functional theory. Geochim Cosmochim Acta 71:3170–3181

Melander L (1960) Isotope effects on reaction rates. Ronald, New York

Melander L, Saunders WH (1980) Reaction rates of isotopic molecules. Wiley, New York

Merritt DA, Hayes JM (1994) Nitrogen isotopic analyses of individual amino acids by isotope-ratio-monitoring gas chromatography/mass spectrometry. J Am Soc Mass Spectrom 5:387–397

Miller MF (2002) Isotopic fractionation and the quantification of 17O anomalies in the oxygen three-isotope system: an appraisal and geochemical significance. Geochim Cosmochim Acta 66:1881–1889

Möller K, Schoenberg R, Pedersen RB, Weiss D, Dong S (2012) Calibration of new certified reference materials ERM-AE633 and ERM-AE647 for copper and IRMM-3702 for zinc isotope amount ratio determinations. Geostand Geoanal Res 36:177–199

Nier AO (1950) A redetermination of the relative abundances of the isotopes of carbon, nitrogen, oxygen, argon and potassium. Phys Rev 77:789

Nier AO, Ney EP, Inghram MG (1947) A null method for the comparison of two ion currents in a mass spectrometer. Rev Sci Instrum 18:294

Northrop DA, Clayton RN (1966) Oxygen isotope fractionations in systems containing dolomite. J Geol 74:174–196

O'Neil JR (1986) Theoretical and experimental aspects of isotopic fractionation. In: Stable isotopes in high temperature geological processes. Rev Mineral 16:1–40

Passey BJ, Henkes GA (2012) Carbonate clumped isotope bond reordering and geospeeedometry. Earth Planet Sci Lett 351-352:223–236

Polyakov VB, Clayton RN, Horita J, Mineev SD (2007) Equilibrium iron isotope fractionation factors of minerals: reevaluation from the data of nuclear inelastic resonant X-ray scattering and Mossbauer spectroscopy. Geochim Cosmochim Acta 71:3833–3846

Polyakov VB, Horita J, Cole DR (2006) Pressure effects on the reduced partition function ratio for hydrogen isotopes in water. Geochim Cosmochim Acta 70:1904–1913

Polyakov VB, Kharlashina NN (1994) Effect of pressure on equilibrium isotope fractionation. Geochim Cosmochim Acta 58:4739–4750

Quade J, Breecker DO, Daeron M, Eiler J (2011) The paleoaltimetry of Tibet: an isotopic perspective. Am J Sci 311:77–115

Rayleigh JWS (1896) Theoretical considerations respecting the separation of gases by diffusion and similar processes. Philos Mag 42:493

Richet P, Bottinga Y, Javoy M (1977) A review of H, C, N, O, S, and Cl stable isotope fractionation among gaseous molecules. Ann Rev Earth Planet Sci 5:65–110

Richter FM (2007) Isotopic fingerprints of mass transport processes. Geochim Cosmochim Acta 71:A839

Richter FM, Dauphas N, Teng FZ (2009) Non-traditional fractionation of non-traditional isotopes: evaporation, chemical diffusion and Soret diffusion. Chem Geol 258:92–103

Richter FM, Davis AM, DePaolo D, Watson BE (2003) Isotope fractionation by chemical diffusion between molten basalt and rhyolite. Geochim Cosmochim Acta 67:3905–3923

Richter R, Hoernes S (1988) The application of the increment method in comparison with experimentally derived and calculated O-isotope fractionations. Chem Erde 48:1–18

Richter FM, Liang Y, Davis AM (1999) Isotope fractionation by diffusion in molten oxides. Geochim Cosmochim Acta 63:2853–2861

Rustad JR, Casey WH, Yin QZ, Bylaska EJ, Felmy AR, Bogatko SA, Jackson VE, Dixon DA (2010) Isotopic fractionation of $Mg^{2+}(aq)$, $Ca^{2+}(aq)$ and $Fe^{2+}(aq)$ with carbonate minerals. Geochim Cosmochim Acta 74: 6301–6323

Saenger C, Affek HP, Felis T, Thiagarajan N, Lough JM, Holcomb M (2012) Carbonate clumped isotope variability in shallow water corals: temperature dependence and growth-related vital effects. Geochim Cosmochim Acta 99:224–242

Schauble EA (2004) Applying stable isotope fractionation theory to new systems. Rev Mineral Geochem 55:65–111

Schauble EA (2007) Role of nuclear volume in driving equilibrium stable isotope fractionation of mercury, thallium and other very heavy elements. Geochim Cosmochim Acta 71:2170–2189

Schauble EA (2011) First principles estimates of equilibrium magnesium isotope fractionation in silicate, oxide, carbonate and hexaaquamagnesium(2+) crystals. Geochim Cosmochim Acta 75:844–869

Schauble EA (2013) Modeling nuclear volume isotope effects in crystals. PNAS 110:17714–17719

Schauble EA, Ghosh P, Eiler JM (2006) Preferential formation of ^{13}C-^{18}O bonds in carbonate minerals, estimated using first-principles lattice dynamics. Geochim Cosmochim Acta 70:2510–2519

Schauble E, Meheut M, Hill PS (2009) Combining metal stable isotope fractionation theory with experiments. Elements 5:369–374

Scheele N, Hoefs J (1992) Carbon isotope fractionation between calcite, graphite and CO2. Contr Mineral Petrol 112:35–45

Schütze H (1980) Der Isotopenindex—eine Inkrementmethode zur näherungsweisen Berechnung von Isotopenaustauschgleichgewichten zwischen kristallinen Substanzen. Chemie Erde 39:321–334

Severinghaus JP, Bender ML, Keeling RF, Broecker WS (1996) Fractionation of soil gases by diffusion of water vapor, gravitational settling and thermal diffusion. Geochim Cosmochim Acta 60:1005–1018

Severinghaus JP, Brook EJ (1999) Abrupt climate change at the end of the last glacial period inferred from trapped air in polar ice. Science 286:930–934

Severinghaus JP, Sowers T, Brook EJ, Alley RB, Bender ML (1998) Timing of abrupt climate change at the end of the Younger Dryas interval from thermally fractionated gases in polar ice. Nature 391:141–146

Sharp ZD (1990) A laser-based microanalytical method for the in situ determination of oxygen isotope ratios of silicates and oxides. Geochim Cosmochim Acta 54:1353–1357

Sharp ZD (1995) Oxygen isotope geochemistry of the Al_2SiO_5 polymorphs. Am J Sci 295:1058–1076

Skulan JL, Bullen TD, Anbar AD, Puzas JE, Shackelford L, LeBlanc A, Smith SM (2007) Natural calcium isotope composition of urine as a marker of bone mineral balance. Clin Chem 53:1155–1158

Stern MJ, Spindel W, Monse EU (1968) Temperature dependence of isotope effects. J Chem Phys 48:2908

Stolper DA, Sessions AL, Ferreira AA, Santos Neto EV, Schimmelmann A, Shusta SS, Valentine DL, Eiler JM (2014) Combined ^{13}C–D and D–D clumping in methane: methods and preliminary results. Geochim Cosmochim Acta 126:169–191

Teutsch N, von Gunten U, Hofstetter TB, Halliday AN (2005) Adsorption as a cause for isotope fractionation in reduced groundwater. Geochim Cosmochim Acta 69:4175–4185

Thiemens MH (1999) Mass-independent isotope effects in planetary atmospheres and the early solar system. Science 283:341–345

Thiemens MH, Chakraborty S, Dominguez G (2012) The physical chemistry of mass-independent isotope effects and their observation in nature. Ann Rev Phys Chem 63:155–177

Thiemens MH, Heidenreich JE (1983) The mass independent fractionation of oxygen—a novel isotope effect and its cosmochemical implications. Science 219:1073–1075

Tripati AK, Eagle RA, Thiagarajan N, Gagnon AC, Bauch H, Halloran PR, Eiler JM (2010) ^{13}C–^{18}O isotope signaturesand "clumped isotope" thermometry in foraminifera and coccoliths. Geochim Cosmochim Acta 74:5697–5717

Urey HC (1947) The thermodynamic properties of isotopic substances. J Chem Soc 1947:562

Valley JW, Graham C (1993) Cryptic grain-scale heterogeneity of oxygen isotope ratios in metamorphic magnetite. Science 259:1729–1733

Valley J, Graham CM, Harte B, Eiler JM, Kinney PD (1998) Ion microprobe analysis of oxygen, carbon and hydrogen isotope ratios. In: applications of microanalytical techniques to understanding mineralizing processes. Rev Econ Geol 7:73–98

Vanhaecke F, Balcaen L, Malinovsky D (2009) Use of single-collector and multi-collector ICP-mass spectrometry for isotope analysis. J Anal At Spectrom 24:863–886

Vogl J, Pritzkow W (2010) Isotope reference materials for present and future isotope research. J Anal At Spectrom 25:923–932

Wacker U, Fiebig J, Tödter J, Schöne BR, Bahr A, Friedrich O, Tütken T, Gischler E, Joachimski MM (2014) Emperical calibration of the clumped isotope paleothermometer using calcites of various origins. Geochim Cosmochim Acta 141:127–144

Walczyk T, von Blanckenburg F (2002) Natural iron isotope variation in human blood. Science 295:2065–2066

Wang Z, Schauble EA, Eiler JM (2004) Equilibrium thermodynamics of multiply substituted isotopologues of molecular gas. Geochim Cosmochim Acta 68:4779–4797

Wasylenki LE, Rolfe BA, Weeks CL, Spiro TB, Anbar AD (2008) Experimental investigation of the effects of temperature and ionic strength on Mo isotope fractionation during adsorption to manganese oxides. Geochim Cosmochim Acta 72:5997–6005

Wasylenki LE, Weeks CL, Bargar JR, Spiro TG, Hein JD, Anbar AD (2011) The molecular mechanism of Mo isotope fractionation during adsorption to birnessite. Geochim Cosmochim Acta 75:5019–5031

Weiss DJ, Mason TFD, Zhao FJ, Kirk GJD, Coles BJ, Horstwood MSA (2005) Isotopic discriminationof zinc in higher plants. New Phytol 165:703–710

Wiechert U, Fiebig J, Przybilla R, Xiao Y, Hoefs J (2002) Excimer laser isotope-ratio-monitoring mass spectrometry for in situ oxygen isotope analysis. Chem Geol 182:179–194

Wiechert U, Hoefs J (1995) An excimer laser-based microanalytical preparation technique for in-situ oxygen isotope analysis of silicate and oxide minerals. Geochim Cosmochim Acta 59:4093–4101

Young ED, Galy A, Nagahara H (2002) Kinetic and equilibrium mass-dependent isotope fractionation laws in nature and their geochemical and cosmochemical significance. Geochim Cosmochim Acta 66:1095–1104

Zheng YF (1991) Calculation of oxygen isotope fractionation in metal oxides. Geochim Cosmochim Acta 55:2299–2307

Zheng YF (1993a) Oxygen isotope fractionation in SiO_2 and Al_2SiO_5 polymorphs: effect of crystal structure. Eur J Mineral 5:651–658

Zheng YF (1993b) Calculation of oxygen isotope fractionation in anhydrous silicate minerals. Geochim Cosmochim Acta 57:1079–1091

Zheng YF (1993c) Calculation of oxygen isotope fractionation in hydroxyl-bearing minerals. Earth Planet Sci Lett 120:247–263

Zheng YF, Böttcher ME (2015) Oxygen isotope fractionation in double carbonates. Isoto Environ Health Stud (in press)

Zhu XK, O'Nions RK, Guo Y, Belshaw NS, Rickard D (2000) Determination of natural Cu-isotope variations by plasma-source mass spectrometry: implications for use as geochemical tracers. Chem Geol 163:139–149

Isotope Fractionation Processes of Selected Elements

2

The foundations of stable isotope geochemistry were laid in 1947 by Urey's classic paper on the thermodynamic properties of isotopic substances and by Nier's development of the ratio mass spectrometer. Before discussing details of the naturally occurring variations in stable isotope ratios, it is useful to describe some generalities that are pertinent to the field of non-radiogenic isotope geochemistry as a whole.

1. Isotope fractionation is pronounced when the mass differences between the isotopes of a specific element are large relative to the mass of the element. Therefore, isotope fractionations are especially large for the light elements. Recent developments in analytical techniques have opened the possibility to detect small variations in elements with much higher mass numbers. The heaviest element for which natural variations have been reported is uranium.
2. All elements that form solid, liquid, and gaseous compounds stable over a wide temperature range are likely to have variations in isotopic composition. Generally, the heavy isotope is concentrated in the solid phase in which it is more tightly bound. Heavier isotopes tend to concentrate in molecules in which they are present in the highest oxidation state.
3. Mass balance effects can cause isotope fractionations because modal proportions of substances can change during a chemical reaction. They are especially important for elements in situations where these coexist in molecules of reduced and oxidized compounds. Conservation of mass in an n component system can be described by

$$\delta_{(\text{system})} = \Sigma\, x_i\, \delta_i \tag{2.1}$$

where "x_i" is the mole fraction of the element in question for each of n phases within the system.

4. Isotopic variations in most biological systems are mostly caused by kinetic effects. During biological reactions (e.g. photosynthesis, bacterial processes) the lighter isotope is very often enriched in the reaction product relative to the

J. Hoefs, *Stable Isotope Geochemistry*, DOI 10.1007/978-3-319-19716-6_2

substrate. Most of the fractionations in biological reactions generally take place during the so-called rate determining step, which is the slowest step. It commonly involves a large reservoir, where the material actually used is small compared to the size of the reservoir.

2.1 Hydrogen

Until 1931 it was assumed that hydrogen consists of only one isotope. Urey et al. (1932) detected the presence of a second stable isotope, which was called deuterium. (In addition to these two stable isotopes there is a third naturally occurring but radioactive isotope, ^{3}H, tritium, with a half-life of approximately 12.5 years.) Rosman and Taylor (1998) gave the following average abundances of the stable hydrogen isotopes:

$$^{1}\text{H:}\quad 99.9885\,\%$$
$$^{2}\text{D:}\quad 0.0115\,\%$$

The isotope geochemistry of hydrogen is particular interesting, for two reasons:

(1) Hydrogen is omnipresent in terrestrial environments occurring in different oxidation states in the forms of H_2O, H_3O^+, OH^-, H_2 and CH_4, even at great depths within the Earth. Therefore, hydrogen is envisaged to play a major role, directly or indirectly, in a wide variety of naturally occurring geological processes.
(2) Hydrogen has by far the largest mass difference relative to the mass of the element between its two stable isotopes. Consequently hydrogen exhibits the largest variations in stable isotope ratios of all elements.

The ranges of hydrogen isotope compositions of some geologically important reservoirs are given in Fig. 2.1. It is noteworthy that all rocks on Earth have somewhat similar hydrogen isotope compositions, which is a characteristic feature of hydrogen, but not of the other elements. The reason for this overlap in isotope composition for rocks is likely due to the enormous amounts of water that have been cycled through the outer shell of the Earth.

2.1.1 Methods

Determination of the D/H ratio of water is performed on H_2-gas. There are two different preparation techniques: (i) equilibration of milliliter-sized samples with gaseous hydrogen gas, followed by mass-spectrometric measurement and back calculation of the D/H of the equilibrated H_2 (Horita 1988). Due to the very large fractionation factor (0.2625 at 25 °C) the measured H_2 is very much depleted in D, which complicates the mass-spectrometric measurement. (ii) water is converted to

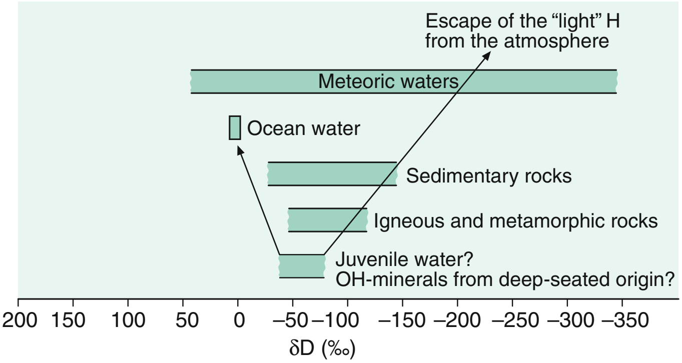

Fig. 2.1 δD variation ranges of geologically important reservoirs (Fig. 2.1, 6th edition, p. 37)

hydrogen by passage over hot metals (uranium: Bigeleisen et al. 1952; Friedman 1953 and Godfrey 1962, zinc: Coleman et al. 1982, chromium: Gehre et al. 1996). This is still the classic method and commonly used.

A difficulty in measuring D/H isotope ratios is that, along with the H_2^+ and HD^+ formation in the ion source, H_3^+ is produced as a by-product of ion-molecule collisions. Therefore, a H_3^+ correction has to be made. The amount of H_3^+ formed is directly proportional to the number of H_2 molecules and H^+ ions. Generally the H_3^+ current measured for hydrogen from ocean water is on the order of 16 % of the total mass 3. The relevant procedures for correction have been evaluated by Brand (2002).

Analytical uncertainty for hydrogen isotope measurements is usually in the range ±0.5 to ±3 ‰ depending on different sample materials, preparation techniques and laboratories.

Burgoyne and Hayes (1998) and Sessions et al. (1999) introduced the continuous flow technique for the D/H measurement of individual organic compounds. Quantitative conversion to H_2 is achieved at high temperatures (>1400 °C). The precise measurement of D/H ratios in a He carrier poses a number of analytical problems, related to the tailing from the abundant $^4He^+$ onto the minor HD^+ peak as well as on reactions occurring in the ion source that produce H_3^+; these problems have been overcome, however, and precise D/H measurements of individual organic compounds are possible.

An alternative to mass-spectrometry represents the direct measurement of D/H, $^{17}O/^{16}O$ and $^{18}O/^{16}O$ isotope compositions of water vapour by laser absorption spectroscopy, also called Cavity Ring-Down Spectroscopy (CRDS) (Kerstel et al. 2002; Brand et al. 2009a, b; Schmidt et al. 2010 and others). The CRDS technique is fast and easy in operation and allows the direct analysis of water vapour with high precisions comparable to the classic continuous flow techniques (Brand et al. 2009a, b).

Table 2.1 Hydrogen isotope standards

Standards	Description	δ-value
V-SMOW	Vienna standard mean Ocean water	0
GISP	Greenland ice sheet Precipitation	−189.9
V-SLAP	Vienna standard light Antarctic precipitation	−428
NBS-30	Biotite	65

2.1.2 Standards

There is a range of standards for hydrogen isotopes. The primary reference standard, the zero point of the δ-scale, is V-SMOW, which is virtually identical in isotopic composition with the earlier defined SMOW, being a hypothetical water sample orginally defined by Craig (1961b).

V-SMOW has a D/H ratio that is higher than most natural samples on Earth, thus δD-values in the literature are generally negative. The other standards, listed in Table 2.1, are generally used to verify the accuracy of sample preparation and mass spectrometry.

2.1.3 Fractionation Processes

2.1.3.1 Water Fractionations

The most effective processes in the generation of hydrogen isotope variations in the terrestrial environment are phase transitions of water between vapor, liquid, and ice through evaporation/precipitation and/or boiling/condensation in the atmosphere, at the Earth's surface, and in the upper part of the crust. Differences in H-isotopic composition arise due to vapor pressure differences of water and, to a smaller degree, to differences in freezing points. Because the vapor pressure of HDO is slightly lower than that of H_2O, the concentration of D is lower in the vapor than in the liquid phase. In a simple, but elegant experiment Ingraham and Criss (1998) have monitored the effect of vapor pressure on the rate of isotope exchange between water and vapor, which is shown in Fig. 2.1. Two beakers with isotopically differing waters were juxtaposed in a sealed box to monitor the exchange process at different temperatures (in this case 21 and 52 °C). As shown in Fig. 2.1 in the 52 °C experiment the isotopic composition of the water changes rapidly and nearly reaches equilibrium in only 27 days.

Horita and Wesolowski (1994) have summarized experimental results for the hydrogen isotope fractionation between liquid water and water vapor in the temperature range 0–350 °C (see Fig. 2.2). Hydrogen isotope fractionations decrease rapidly with increasing temperatures and become zero at 220–230 °C. Above the

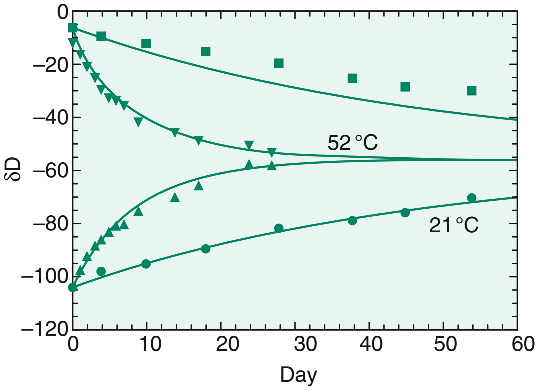

Fig. 2.2 δD-values versus time for two beakers that have equal surface areas and equal volumes undergoing isotopic exchange in sealed systems. In both experiments at 21 and 52 °C isotope ratios progress toward an average value of −56 ‰ via exchange with ambient vapour: *solid curves* are calculated, *points* are experimental data (after Criss 1999) (Fig. 2.2, 6th edition, p. 39)

crossover temperature, water vapor is more enriched in deuterium than liquid water. Fractionations again approach zero at the critical temperature of water (Fig. 2.2).

From experiments, Lehmann and Siegenthaler (1991) determined the equilibrium H-isotope fractionation between ice and water to be +21.2 ‰. Under natural conditions, however, ice will not necessarily be formed in isotopic equilibrium with the bulk water, depending mainly on the freezing rate.

In all processes concerning the evaporation and condensation of water, hydrogen isotopes are fractionated in a similar fashion to those of oxygen isotopes, albeit with a different magnitude, because a corresponding difference in vapor pressures exists between H_2O and HDO in one case and $H_2^{16}O$ and $H_2^{18}O$ in the other.

Therefore, the hydrogen and oxygen isotope distributions are correlated for meteoric waters. Craig (1961a) first defined the generalized relationship:

$$\delta D \ = 8\delta^{18}O + 10,$$

which describes the interdependence of H- and O-isotope ratios in meteoric waters on a global scale.

This relationship, shown in Fig. 2.3, is described in the literature as the “Global Meteoric Water Line (GMWL)”.

Neither the numerical coefficient 8 nor the constant 10, also called the deuterium excess d, are constant in nature. Both may vary depending on the conditions of evaporation, vapor transport and precipitation and, as a result, offer insight into climatic processes. The deuterium excess d is a valuable tool to derive information on relative humidities (see discussion on p. 242).

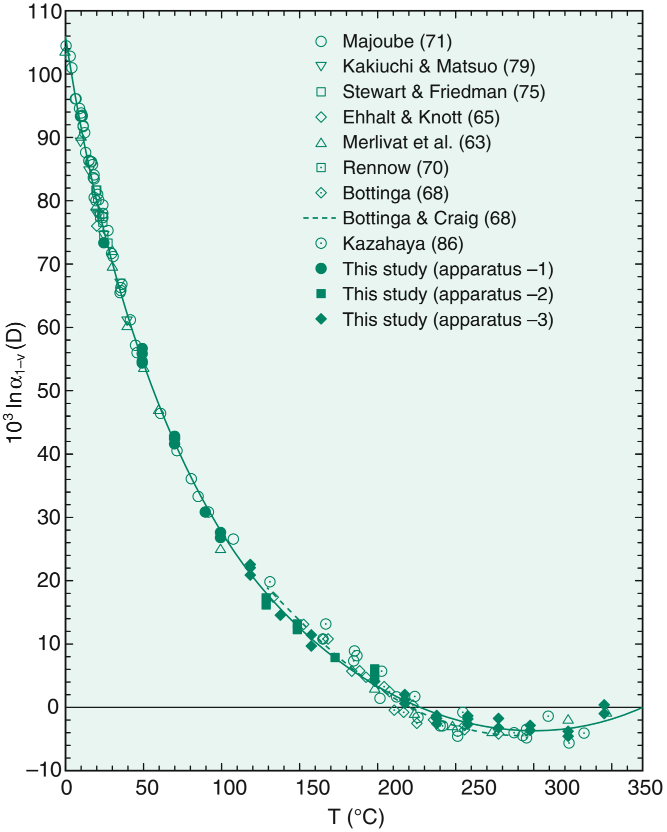

Fig. 2.3 Experimentally determined fractionation factors between liquid water and water vapour from 1 to 350 °C (after Horita and Wesolowski 1994) (Fig. 2.3, 6th edition, p. 39)

2.1.3.2 Equilibrium Reactions

D/H fractionations among gases are extraordinarily large, as calculated by Bottinga (1969) and Richet et al. (1977) and plotted in Fig. 2.4. Even in magmatic systems, fractionation factors are sufficiently large to affect the δD-value of dissolved water in melts during degassing of H_2, H_2S or CH_4. The oxidation of H_2 or CH_4 to H_2O and CO_2 may also have an effect on the isotopic composition of water dissolved in melts due to the large fractionation factors (Fig. 2.5).

With respect to mineral-water systems, different experimental studies obtained widely different results for the common hydrous minerals with respect to the absolute magnitude and the temperature dependence of D/H fractionations (Suzuoki and Epstein 1976; Graham et al. 1980; Vennemann and O'Neil 1996; Saccocia et al. 2009). Suzuoki and Epstein (1976) first demonstrated the importance of the chemical composition of the octahedral sites in crystal lattices to the mineral H-isotope composition. Subsequently, isotope exchange experiments by Graham

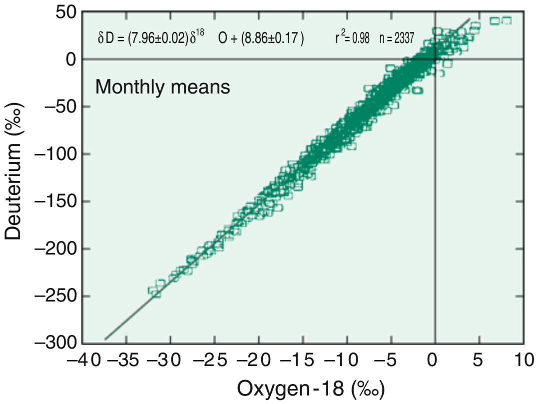

Fig. 2.4 Global relationship between monthly means of δD and $\delta^{18}O$ in precipitation, derived for all stations of the IAEA global network. *Line* indicates the global Meteoric Water Line (MWL) (after Rozanski et al. 1993) (Fig. 2.4, 6th edition, p. 40)

Fig. 2.5 D/H fractionations between H_2O–H_2, H_2O–H_2S and H_2O–CH_4 (from calculated data of Richet et al. 1977) (Fig. 2.5, 6th edition, p. 41)

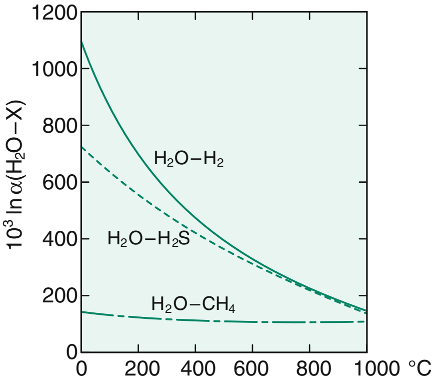

et al. (1980, 1984) suggested that the chemical composition of sites other than the octahedral sites can also affect hydrogen isotope compositions. These authors postulate a qualitative relationship between hydrogen-bond distances and hydrogen isotope fractionations: the shorter the hydrogen bond, the more depleted the mineral is in deuterium.

On the basis of theoretical calculations, Driesner (1997) proposed that many of the discrepancies between the experimental studies were due to pressure differences at which the experiments were carried out. Thus for hydrogen, pressure is a variable that must be taken into account in fluid-bearing systems. Later, Horita et al. (1999) presented experimental evidence for a pressure effect between brucite and water.

Chacko et al. (1999) developed an alternative method for the experimental determination of hydrogen isotope fractionation factors. Instead of using powdered minerals as starting materials, these authors carried out exchange experiments with large single crystals and then analyzed the exchanged rims with the ion probe. Although the precision of the analytical data is less than that for conventional bulk techniques, the advantage of this technique is that it allows the determination of fractionation factors in experiments in which isotopic exchange occurs by a diffusional process rather than by a combination of diffusion and recrystallization.

In summary, as discussed by Vennemann and O’Neil (1996), discrepancies between published experimental calibrations in individual mineral-water systems are difficult to resolve, which limits the application of D/H fractionations in mineral-water systems to estimate δD-values of coexisting fluids. As shown by Méheut et al. (2010) first-principles calculations of D/H fractionations may reproduce experimental calculations within a range of about 15 ‰. These authors also demonstrated that internal fractionations between inner-surface and inner hydroxyl groups may be large and even opposite in sign.

2.1.3.3 Fractionations During Biosynthesis

Water is the ultimate source of hydrogen in all naturally organic compounds produced by photosynthesis. Thus D/H ratios in organic matter contain information about climate (see Sect. 3.11). During biosynthetic hydrogen conversion of water to organic matter, large H-isotope fractionations with δD-values between −400 and +200 ‰ have been observed (Sachse et al. 2012).

δD-variations in individual compounds within a single plant or organism can be related to differences in biosynthesis. Accurate isotope fractionation factors among organic molecules and water are difficult to be determined, although tremendous progress has been achieved through the introduction of the compound specific hydrogen isotope analysis (Sessions et al. 1999; Sauer et al. 2001; Schimmelmann et al. 2006), which allows the δD analysis of individual biochemical compound. Further details are discussed in Sect. 3.10.1.2.

Using a combination of experimental calibration and theoretical calculation Wang et al. (2009a, b) estimated equilibrium factors for various H positions in molecules such as alkanes, ketones, carboxyl acids and alcoholes. By summing over individual H positions, equilibrium fractionations relative to water are −90 to −70 ‰ for n-alkanes and about −100 ‰ for pristane and phytane. Wang et al. (2013a, b) extended his approach to cyclic compounds and observed total equilibrium fractionations of −100 to −65 ‰ for typical cyclic paraffins being similar to linear hydrocarbons. These numbers, however, are very different to typical biosynthetic fractionations that are between −300 and −150 ‰ due to kinetic isotope fractionations.

The biosynthesis of lipids as one of the most common group of organic material involves complex enzymatic reactions in which hydrogen may be added, removed or exchanged, all potentially leading to H isotope fractionations. Lipids with the smallest D depletion relative to water are n-alkyl lipids. Isoprenoid lipids show depletions by 200–250 ‰ and phytol and related compounds have the largest D-depletion.

2.1.3.4 Other Fractionations

In salt solutions, isotopic fractionations can occur between water in the “hydration sphere” and free water (Truesdell 1974). The effects of dissolved salts on hydrogen isotope activity ratios in salt solutions can be qualitatively interpreted in terms of interactions between ions and water molecules, which appear to be primarily related to their charge and radius. Hydrogen isotope activity ratios of all salt solutions studied so far are appreciably higher than H-isotope composition ratios. As shown by Horita et al. (1993), the D/H ratio of water vapor in isotope equilibrium with a solution increases as salt is added to the solution. Magnitudes of the hydrogen isotope effects are in the order $CaCl_2 > MgCl_2 > MgSO_4 > KCl \sim NaCl > NaSO_4$ at the same molality.

Isotope effects of this kind are relevant for an understanding of the isotope composition of clay minerals and absorption of water on mineral surfaces. The tendency for clays and shales to act as semipermeable membranes is well known. This effect is also known as “ultrafiltration”. Coplen and Hanshaw (1973) postulated that hydrogen isotope fractionations may occur during ultrafiltration in such a way that the residual water is enriched in deuterium due to its preferential adsorption on the clay minerals and its lower diffusivity.

2.2 Lithium

Lithium has two stable isotopes with the following abundances (Rosman and Taylor 1998):

$$^{6}\mathrm{Li} \quad 7.59\,\%$$

$$^{7}\mathrm{Li} \quad 92.41\,\%$$

Lithium is one of the rare elements where the lighter isotope is less abundant than the heavier one. In order to be consistent with the other isotope systems lithium isotope ratios are reported as δ^7Li-values.

The large relative mass difference between ^{6}Li and ^{7}Li of about 16 % is a favorable condition for their fractionation in nature. Taylor and Urey (1938) found a change of 25 % in the Li-isotope ratio when Li-solutions percolate through a zeolite column. Thus, fractionation of Li-isotopes might be expected in geochemical settings in which cation exchange processes are involved. Li is only present in the +1 valence state, so redox reactions do not influence its isotope composition. A recent review about natural Li isotope variations has been given by Burton and Vigier (2011).

Lithium isotope geochemistry is characterized by a difference close to 30 ‰ between ocean water (δ^7Li +31 ‰) and bulk silicate earth with a δ^7Li-value of 3.2 ‰ (Seitz et al. 2007). In this respect lithium isotope geochemistry is very similar to that of boron (see p. 59). The isotopic difference between the mantle and the ocean

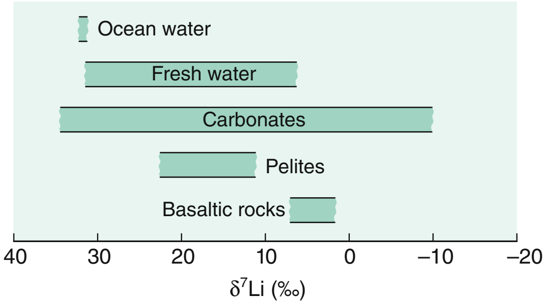

Fig. 2.6 Lithium isotope variations in major geological reservoirs (Fig. 2.6, 6th edition, p. 43)

can be used as a powerful tracer to constrain water/rock interactions (Tomaszak 2004). Figure 2.6 gives an overview of Li-isotope variations in major geological reservoirs.

2.2.1 Methods

Early workers had to struggle with serious lithium fractionation effects during mass spectrometric analysis. Li isotopes have been analysed with TIMS (James and Palmer 2000) and ion microprobe (Kasemann et al. 2005a, b). Most workers use the multicollector sector ICP-MS technique first described by Tomascak et al. (1999), modified by Millot et al. (2004) and Jeffcoate et al. (2004). In order to avoid interferences and matrix effects, Li has to be separated from the rest of the sample. During elution, a 100 % yield is necessary, even a small loss of Li may shift the δ^7Li value by several ‰.

Unfortunately, there are no internationally accepted Li isotope values for rocks or waters. James and Palmer (2000) have determined nine international rock standards ranging from basalt to shale relative to the so-called NIST L-SVEC standard. In addition, Jeffcoate et al. (2004) and Gao and Casey (2011) presented δ^7Li values for other reference materials.

2.2.2 Diffusion

Li isotope variations have been interpreted—like other isotope systems—in terms of isotope equilibrium between minerals and fluids, however, the analysis of natural samples and experimental studies have shown that Li isotope variations may be very often kinetically controlled due to the large differences in ^{6}Li and ^{7}Li diffusivities that may far exceed Li isotope variations produced by equilibrium processes. Diffusive Li isotope fractionation has been reported to occur on a meter to micrometer scale during cooling processes (Lundstrom et al. 2005; Teng et al. 2006; Jeffcoate et al. 2007; Parkinson et al. 2007). In silicate minerals ^{6}Li diffuses 3 % faster than ^{7}Li, consistent with experiments by Richter et al. (2003). Dohmen et al. (2010) measured Li diffusion rates in olivine and observed a complex diffusion behaviour, that can be described by a model that partitions Li between two sites: an octahedral and an interstitial site. Published Li isotope data indicate that the interstitial mechanism is unlikely to be the dominant system (Seitz et al. 2004; Jeffcoate et al. 2007).

In summary, diffusion at magmatic temperatures is a very effective mechanism for generating large variations in ^{7}Li/^{6}Li ratios (Lundstrom et al. 2005; Teng et al. 2006; Rudnick and Ionov 2007). Although diffusion profiles will relax with time, the existence of sharp δ^7Li-profiles suggest diffusional Li isotope fractionation over short timescales (days to a few months) and therefore diffusion profiles in mantle minerals may be used as geospeedometers (Parkinson et al. 2007). At the same time diffusion may obliterate primary mantle signatures.

2.2.3 Magmatic Rocks

High temperature equilibrium Li isotope fractionations have been investigated experimentally (Wunder et al. 2006, 2007) and theoretically (Kowalski and Jahn 2011). Calculated fractionation factors between staurolite, spodumene, mica and aqueous fluids are in good agreement with experimentally derived fractionation factors.

Mantle-derived basalts have a relatively uniform composition with δ^7Li values of 4 ± 2 ‰ (Tomaszak 2004; Elliott et al. 2004), close to undepleted upper mantle (Jeffcoate et al. 2007). The δ^7Li range for MORB is relatively narrow, but larger than for mantle peridotites. On the other hand, some peridotites have a wide range in δ^7Li values from values as low as −17 ‰ (Nishio et al. 2004) to values as high as +10 ‰ (Brooker et al. 2004). This large range might be explained by diffusion controlled Li exchange.

Mantle minerals show a typical order of ^{7}Li enrichment: olivines and orthopyroxenes have ± the same isotope composition, whereas clinopyroxenes are enriched in ^{7}Li and more variable. Olivines generally keep the mantle signatures whereas clinopyroxenes are more sensitive to metasomatic overprint leading to isotope variations, which can be explained by diffusion processes that may affect clinopyroxenes during melt migration (Parkinson et al. 2007).

Because Li isotopes may be used as a tracer to identify the existence of recycled material in the mantle, systematic studies of arc lavas have been undertaken (Moriguti and Nakamura 1998; Tomascak et al. 2000; Leeman et al. 2004 and others). However, most arc lavas have δ^7Li values that are indistinguishable from those of MORB. Thus Li seems to be decoupled from other fluid mobile elements, because Li can partition into the Mg-silicates, pyroxene, olivine (Tomascak et al. 2002).

Granites of various origin display an average δ^7Li value slightly lighter than the mantle (Teng et al. 2004, 2009). Considering the small Li isotope fractionation at high temperature during igneous differentiation processes (Tomaszak 2004), pristine continental crust should not be too different in Li isotope composition from the mantle. Because this is not the case, the isotopically light crust must have been modified by secondary processes, such as weathering, hydrothermal alteration and prograde metamorphism (Teng et al. 2007a, b).

Li isotope distribution through the oceanic crust reflects the varying conditions of seawater alteration with depth (Chan et al. 2002; Gao et al. 2012). At low temperatures, altered volcanic rocks have heavier Li isotope compositions than MORB whereas at higher temperatures in deeper parts of the oceanic crust δ^7Li-values become similar to MORB. Gao et al. (2012) concluded that the Li isotope pattern in drilled oceanic sections reflects variations in water/rock ratios in combination with increasing downhole temperatures.

During fluid-rock interaction, Li as a fluid-mobile element will enrich in aqueous fluids. It might therefore be expected that δ^7Li enriched seawater incorporated into altered oceanic crust should be removed during subduction zone metamorphism. Continuous dehydration of pelagic sediments and altered oceanic crust results in ^{7}Li-depleted rocks and in ^{7}Li enriched fluids. A subducting slab therefore should introduce large amounts of ^{7}Li into the mantle wedge. To quantitatively understand this process Li isotope fractionation factors between minerals and coexisting fluids must be known (Wunder et al. 2006, 2007).

2.2.4 Weathering

Li is relatively mobile during weathering. The best evidence for Li isotope fractionation during weathering is the systematic ^{7}Li enrichment of natural waters relative to their source rocks (Burton and Vigier 2011). During weathering ^{7}Li is preferentially mobilized, whereas ^{6}Li becomes enriched in the weathering residue. The range of δ^7Li values in river waters can be quite large (from +6 to +33 ‰, Huh et al. 1998, 2004). The major control of Li isotopic composition is the balance between primary mineral dissolution and secondary mineral formation, where ^{6}Li is preferentially taken up by the solid, driving the fluid to heavy values (Wimpenny et al. 2010). The magnitude of fractionation seems to depend on the extent of weathering: large Li isotope fractionations seem to occur during superficial weathering while little fractionation is observed during prolonged weathering in stable environments (Millot et al. 2010a, b). Rudnick et al. (2004) have demonstrated that Li isotope fractionation correlates directly with the degree of weathering leading to very light δ^7Li-values in soils.

Preferential weathering of primary minerals does not generate significant Li isotope fractionations. Wimpenny et al. (2010) demonstrated that dissolution of basaltic glass and olivine does not result in measurable Li isotope fractionation. Secondary mineral formation and adsorption on mineral surfaces are regarded to be the major process responsible for the high δ^7Li values in waters. Considerable Li isotope fractionations, for instance, have been observed during chemical sorption of

Li on the surface of gibbsite (Pistiner and Henderson 2003) or on clay minerals (Zhang et al. 1998; Millot et al. 2010a, b).

2.2.5 Ocean Water

Lithium is a conservative element in the ocean with a residence time of about one million year. Its isotope composition (δ^7Li: 31 ‰) is maintained by inputs of dissolved Li from rivers (average δ^7Li +23 ‰, Huh et al. 1998) and high-temperature hydrothermal fluids at ocean ridges at one hand and low temperature removal of Li into oceanic basalts and marine sediments at the other. Precipitation of carbonates does not play a major role due to the low Li-concentrations of carbonates. This fractionation pattern explains, why the Li isotope composition of seawater is heavier than its primary sources (continental weathering: 23 ‰; Huh et al. 1998) and high-temperature hydrothermal fluids (6–10 ‰, Chan et al. 1993).

In this connection it is interesting to note that ocean water is not the major Li supplier in rainwater (Millot et al. 2010a, b). Rainwater has low Li concentrations, but very variable Li isotope compositions. High δ^7Li values have been explained by anthropogenic contamination from fertilizers in agriculture (Millot et al. 2010a, b).

Any variance in Li sources and sinks during geologic history should cause secular variations in the isotope composition of oceanic Li. And indeed Misra and Froelich (2012) reconstructed the Li isotope composition of ocean water for the last 68 Ma and observed an 9 ‰ increase from the Paleocene to the present requiring changes in continental weathering and/or low temperature ocean crust alteration (see p. 268). By extending this approach, Wanner et al. (2014) presented a model that revealed a close relationship between δ^7Li and CO_2 consumption by silicate weathering.

2.3 Boron

Boron has two stable isotopes with the following abundances (Rosman and Taylor 1998).

$$^{10}\mathrm{B} \quad 19.9\,\%$$
$$^{11}\mathrm{B} \quad 80.1\,\%$$

The large mass difference between ^{10}B and ^{11}B and large chemical isotope effects between different species (Bigeleisen 1965) make boron a very promising element to study for isotope variations. The utility of boron isotopes as a geochemical tracer stems from the high mobility of boron during high- and low-temperature fluid-related processes, showing a strong affinity for silicate melts

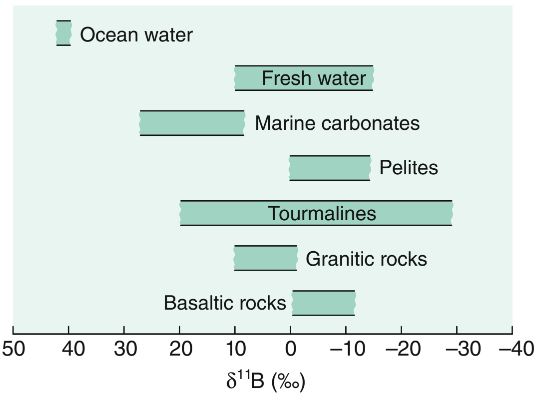

Fig. 2.7 Boron isotope variations in geologically important reservoirs (Fig. 2.7, 6th edition, p. 45)

and aqueous fluids. B is preferentially hosted in phyllosilicates; common mantle and crustal minerals except tourmaline have low B concentrations.

Boron isotope geochemistry is characterized by distinct isotope signatures:

(i) strong enrichment of ^{11}B in seawater (+39.6 ‰, Foster et al. 2010).
(ii) depletion of ^{11}B in the continental crust and marine sediments
(iii) slight depletion of ^{11}B in the upper mantle (Chaussidon and Marty 1995)

The lowest $\delta^{11}B$-values of around −70 ‰ have been observed for certain coals (Williams and Hervig 2004), whereas the most enriched ^{11}B-reservoir has been found in brines from Australia and Israel (Dead Sea) which have $\delta^{11}B$-values of up to 60 ‰ (Vengosh et al. 1991a, b). A very characteristic feature of boron geochemistry is the isotopic composition of ocean water with a constant $\delta^{11}B$-value of 39.6 ‰ (Foster et al. 2010), which is about 50 ‰ heavier than the average continental crust of −10 ± 2 ‰ (Chaussidon and Albarede 1992). Isotope variations of boron in some geological reservoirs are shown in Fig. 2.7.

2.3.1 Methods

In recent years 3 different methods have been used for boron isotope analysis: (i) thermal ionisation mass-spectrometry (TIMS), either with positively charged (P-TIMS) or negatively charged (N-TIMS) ions, (ii) multi-collector-ICP mass spectrometry and (iii) secondary ion mass spectrometry (SIMS).

(i) Two different methods have been developed for TIMS. The positive thermal ionization technique uses $Na_2BO_2^+$ ions (McMullen et al. 1961). Subsequently, Spivack and Edmond (1986) modified this technique by using $Cs_2BO_2^+$ ions (measurement of the masses 308 and 309). The substitution of ^{133}Cs for ^{23}Na increases the molecular mass and reduces the relative mass difference of its isotopic species, which limits the thermally induced mass dependent isotopic fractionation. This latter method has a precision of about ±0.25 ‰, which is better by a factor of 10 than the $Na_2BO_2^+$ method. In negative ion mode (N-TIMS), boron isotopes are analysed as BO_2^- (masses 42 and 43). N-TIMS has the advantage that no chemical separation of boron from the sample matrix is required.

(ii) Lecuyer et al. (2002) first described the use of MC-ICP-MS for B isotopic measurements of waters, carbonates, phosphates and silicates with an external reproducibilty of ±0.3 ‰, improvement in reproducibility has been achieved by Guerrot et al. (2011) and Louvat et al. (2011). Le Roux et al. (2004) introduced an in situ laser ablation ICP-MS method at the nanogram level. The amount of boron measured are two orders of magnitude lower than P-TIMS and acid solution ICP-MS methods.

(iii) Chaussidon and Albarede (1992), performed boron isotope determinations with an ion-microprobe having an analytical uncertainty of about ±2 ‰. Significant improvements with SIMS analysis have been described by Rollion and Erez (2010).

As analytical techniques have been consistently improved in recent years, the number of boron isotope studies has increased rapidly. $\delta^{11}B$-values are generally given relative NBS boric acid SRM 951, which is prepared from a Searles Lake borax. This standard has a $^{11}B/^{10}B$ ratio of 4.04558 (Palmer and Slack 1989).

2.3.2 Isotope Fractionation Mechanism

(a) pH dependence of isotope fractionations

Boron is generally bound to oxygen or hydroxyl groups in either triangular (e.g., BO_3) or tetrahedral (e.g., $B(OH)_4^-$) coordination. The dominant isotope fractionation process occurs in aqueous systems via an equilibrium exchange process between boric acid ($B(OH)_3$) and coexisting borate anion ($B(OH)_4^-$). At low pH-values trigonal $B(OH)_3$ predominates, at high pH-values tetrahedral $B(OH)_4^-$ is the primary anion. The pH-dependence of the two boron species and their related isotope fractionation is shown in Fig. 2.8 (after Hemming and Hanson 1992). The pH dependence has been used reconstructing past ocean pH-values by measuring the boron isotope composition of carbonates e.g. foraminifera. This relies on the fact that mainly the charged species $B(OH)_4^-$ is incorporated into carbonate minerals with small to insignificant fractionations (Hemming and Hanson 1992; Sanyal et al. 2000). In corals, Rollion-Bard et al. (2011), however, observed both coordination species in the coral microstructure.

Because of the inability to quantitatively separate the two species in solution, a theoretically calculated fractionation factor of about 1.0194 at 25 °C has been widely used for p_H estimates (Kakihana et al. 1977). As recently shown by Zeebe

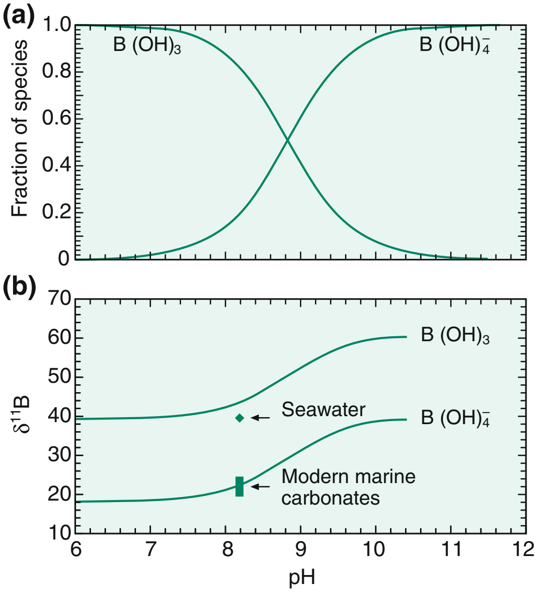

Fig. 2.8 **a** Distribution of aqueous boron species versus pH; **b** δ^{11}B of the two dominant species $B(OH)_3$ and $B(OH)_4^-$ versus pH (after Hemming and Hanson 1992)

(2005) and Klochko et al. (2006), the equilibrium fractionation factor appears to be significantly larger than the theoretical value of Kakihana et al. (1977) used in paleo-pH studies. Klochko et al. (2006), for instance, reported a fractionation factor of 1.0272. Furthermore, it has to be assumed that no "vital effect" occurs during incorporation of borate into the carbonate lattice or the species-specific fractionation effect is known and can be corrected for.

This approach has been not only used to indirectly estimate the seawater pH from δ^{11}B of foraminifera, but to estimate from the p_H proxy the past atmospheric CO_2 concentrations (i.e. Pearson and Palmer 1999, 2000; Pagani et al. 2005). An increase in atmospheric CO_2 results in increased dissolved CO_2 in ocean water, which in turn causes a reduction in oceanic $p_{H,}$ well known as ocean acidification. A note of caution was presented by Lemarchand et al. (2000), who suggested that boron isotope variations in foraminifera depend at least in part on variations in the supply of riverine boron to the ocean during the geologic past. And indeed the boron isotope composition of rivers can be extremely variable (Rose et al. 2000; Lemarchand et al. 2002).

(b) Adsorption

Significant isotope fractionations may occur when aqueous boric acid absorbs on solid surfaces, as shown by Lemarchand et al. (2005) and others. Boron isotopic compositions are controlled by ion exchange rates at the mineral/water interface. The extent of B isotope fractionation depends on B aqueous speciation and on the structure of surface complexes. High values of B isotope fractionation are observed at low pH, lower values are observed at high pH, which is due to the change in coordination from trigonal to tetrahedral.

2.3.3 Fractionations at High Temperatures

Experimental studies of boron isotope fractionation between hydrous fluids, melts and minerals have shown that ^{11}B preferentially partitions into the fluid relative to minerals or melts (Palmer et al. 1987; Williams et al. 2001; Wunder et al. 2005; Liebscher et al. 2005), ranging from about 33 ‰ for fluid-clay (Palmer et al. 1987), to about 6 ‰ for fluid-muscovite at 700 °C (Wunder et al. 2005) and to a few ‰ for fluid-melt above 1000 °C (Hervig et al. 2002). The main fractionation effect seems to be due to the change from trigonal boron in neutral pH hydrous fluid to tetrahedrally coordinated boron in most rock forming minerals.

At high temperatures, B isotope fractionations during crystal fractionation and melting are small. Boron like lithium are useful tracers for mass transfer in subduction zones. Both elements are mobilized by fluids and melts and display considerable isotope fractionation during dehydration reactions. Concentrations of B are low in mantle derived materials, whereas they are high in sediments and altered oceanic crust. Any input of fluid and melt from the subducting slab into the overlying mantle has a strong impact on the isotope composition of the mantle wedge and on magmas generated there. Recycled marine boron, for instance, may lead to an enrichment of ^{11}B in sources for arc volcanic rocks (Tonarini et al. 2011).

2.3.4 Tourmaline

Tourmaline is the most abundant reservoir of boron in metamorphic and magmatic rocks. Tourmaline is stable over a very large p-T range and forms where crustal rocks interact with fluids or melts. Thus, its isotope composition provides a record of fluids and melts from which it crystallized. Swihart and Moore (1989), Palmer and Slack (1989), Slack et al. (1993), Smith and Yardley (1996) and Jiang and Palmer (1998) analyzed tourmaline from various geological settings and observed a large range in $\delta^{11}B$-values which reflects the different origins of boron and its high mobility during fluid related processes.

Boron isotope compositions of tourmalines vary from about +30 ‰ to values below −20 ‰ (Marschall and Jiang 2011). High $\delta^{11}B$-values can be related to seawater, whereas low $\delta^{11}B$-values are either derived from nonmarine evaporites or produced by interaction between rocks and fluids during metamorphic dehydration. Tourmalines in most granites and pegmatites show $\delta^{11}B$-values around −10 ‰ close to the average composition of the continental crust (Marschall and Jiang 2011).

Since volume diffusion of B isotopes is insignificant in tourmalines (Nakano and Nakamura 2001), isotopic heterogeneities of zoned tourmalines should be preserved up to at least 600 °C. By using the SIMS method, Marschall et al. (2008) demonstrated that boron isotopes in zoned tourmalines, indeed, may reflect different stages of tourmaline growth. Besides, the large chemical variability of tourmaline can be used as a fingerprint for a large number of other isotope systems including O, H, Si, Mg and Li (Marschall and Jiang 2011).

2.3.5 Tracer for Anthropogenic Pollution

Boron is widely used in industry; most commonly in the form of sodium perborate as an oxidative bleaching agent in cleaning products. The abundant use results in boron accumulation in waste effluents. Borate minerals and synthetic borate products are characterized by a narrow range in δ^{11}B-values that are distinctly different from boron isotope values in unpolluted groundwater (Vengosh et al. 1994; Barth 1998). Thus, boron isotopes may identify or even quantify contamination of surface waters.

Although the concentration of B in rain water is low, improved analytical techniques have allowed the determination of very precise B isotope data (Chetelat et al. 2009; Millot et al. 2010a, b). δ^{11}B values in rain show a large variation depending on the sampling site (coastal vs. inland). Near coastal stations reflect the marine origin of boron, variably influenced by evaporation-condensation fractionation processes, For inland stations, crustal, anthropogenic and biogenic boron sources have to be included.

2.4 Carbon

Carbon occurs in a wide variety of compounds on Earth, from reduced organic compounds in the biosphere to oxidized inorganic compounds like CO_2 and carbonates. The broad spectrum of carbon-bearing compounds involved in low- and high-temperature geological settings can be assessed on the basis of carbon isotope fractionations.

Carbon has two stable isotopes (Rosman and Taylor 1998)

$$^{12}\mathrm{C} = 98.93\,\%\,(\text{reference mass for atomic weight scale})$$
$$^{13}\mathrm{C} = 1.07\,\%$$

The naturally occurring variations in carbon isotope composition are greater than 120 ‰, neglecting extraterrestrial materials. Heavy carbonates with δ^{13}C-values > +20 ‰ and light methane of <−100 ‰ have been reported in the literature.

Table 2.2 $\delta^{13}C$-values of NBS-reference samples relative to V-PDB

NBS-18	Carbonatite	−5.00
NBS-19	Marble	+1.95
NBS-20	Limestone	−1.06
NBS-21	Graphite	−28.10
NBS-22	Oil	−30.03

2.4.1 Analytical Methods

The gases used in $^{13}C/^{12}C$ measurements are CO_2 or CO obtained during pyrolysis. For CO_2 the following preparation methods exist:

(a) Carbonates are reacted with 100 % phosphoric acid at temperatures between 20 and 90 °C (depending on the type of carbonate) to liberate CO_2 (see also “oxygen”).

(b) Organic compounds are generally oxidized at high temperatures (850–1000 °C) in a stream of oxygen or by an oxidizing agent like CuO. For the analysis of individual compounds in complex organic mixtures, a gas chromatography—combustion—isotope ratio mass-spectrometry (GC-C-IRMS) system is used, first described by Matthews and Hayes (1978). This device can measure individual carbon compounds in mixtures of sub-nanogram samples with a precision of better than ±0.5 ‰.

2.4.1.1 Standards

As the commonly used international reference standard PDB has been exhausted for several decades, there is a need for introducing new standards. Even though several different standards are in use today, the international standard the δ-values are referred to remains to be the V-PDB-standard (Table 2.2).

2.4.2 Fractionation Processes

The two main terrestrial carbon reservoirs, organic matter and sedimentary carbonates, have distinctly different isotopic characteristics because of the operation of two different reaction mechanisms:

1. Isotope equilibrium exchange reactions within the inorganic carbon system “atmospheric CO_2—dissolved bicarbonate—solid carbonate” lead to an enrichment of ^{13}C in carbonates.
2. Kinetic isotope effects during photosynthesis concentrate the light isotope ^{12}C in the synthesized organic material.

2.4.2.1 Carbonate System

The inorganic carbonate system is comprised of multiple chemical species linked by a series of equilibria:

$$CO_{2(aq)} + H_2O \leftrightarrow H_2CO_3 \tag{2.2}$$

$$H_2CO_3 \leftrightarrow H^+ + HCO_3{}^- \tag{2.3}$$

$$HCO_3^- \leftrightarrow H^+ + CO_3{}^{2-} \tag{2.4}$$

The carbonate ($CO_3{}^{2-}$) ion can combine with divalent cations to form solid minerals, calcite and aragonite being the most common

$$Ca^{2+} + CO_3{}^{2-} = CaCO_3 \tag{2.5}$$

An isotope fractionation is associated with each of these equilibria, the ^{13}C-differences between the species depend only on temperature, although the relative abundances of the species are strongly dependent on pH. Several authors have reported isotope fractionation factors for the system dissolved inorganic carbon (DIC)—gaseous CO_2 (Vogel et al. 1970; Mook et al. 1974; Zhang et al. 1995). The major problem in the experimental determination of the fractionation factor is the separation of the dissolved carbon phases (CO_{2aq}, $HCO_3{}^-$, $CO_3{}^-$) because isotope equilibrium among these phases is reached within seconds. The generally accepted carbon isotope equilibrium values between calcium carbonate and dissolved bicarbonate are derived from inorganic precipitate data of Rubinson and Clayton (1969), Emrich et al. (1970), and Turner (1982). What is often not adequately recognized is the fact that systematic C-isotope differences exist between calcite and aragonite. Rubinson and Clayton (1969) and Romanek et al. (1992) found calcite and aragonite to be 0.9 and 2.7 ‰ enriched in ^{13}C relative to bicarbonate at 25 °C. Another complicating factor is that shell carbonate—precipitated by marine organisms—is frequently not in isotopic equilibrium with the ambient dissolved bicarbonate. Such so-called “vital” effects can be as large as a few permil (see discussion on p. 307).

Carbon isotope fractionations under equilibrium conditions are important not only at low-temperature, but also at high temperatures within the system carbonate, CO_2, graphite, and CH_4. Of these, the calcite-graphite fractionation has become a useful geothermometer (e.g., Valley and O’Neil 1981; Scheele and Hoefs 1992; Kitchen and Valley 1995) (see discussion on p. 339).

Figure 2.9 summarizes carbon isotope fractionations between various geologic materials and gaseous CO_2 (after Chacko et al. 2001).

2.4.2.2 Organic Carbon System

Early reviews by O’Leary (1981) and Farquhar et al. (1989) have provided the biochemical background of carbon isotope fractionations during photosynthesis,

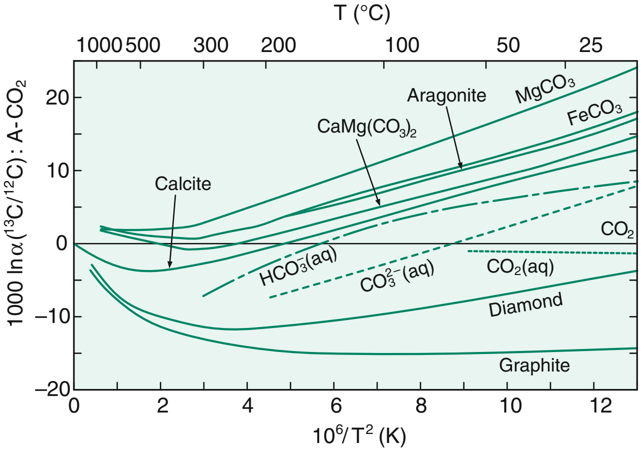

Fig. 2.9 Carbon isotope fractionation between various geologic compounds and CO_2 (after Chacko et al. 2001) (Fig. 2.9, 6th edition, p. 50)

with more recent accounts by Hayes (2001), Freeman (2001) and Galimov (2006). The main isotope-discriminating steps during biological carbon fixation are (i) the uptake and intracellular diffusion of CO_2 and (ii) the biosynthesis of cellular components. Such a two-step model was first proposed by Park and Epstein (1960):

$$CO_{2(\text{external})} \leftrightarrow CO_{2(\text{internal})} \rightarrow \text{organic molecule}$$

From this simplified scheme, it follows that the diffusional process is reversible, whereas the enzymatic carbon fixation is irreversible. The two-step model of carbon fixation clearly suggests that isotope fractionation is dependent on the partial pressure of CO_2 of the system. With an unlimited amount of CO_2 available to a plant, the enzymatic fractionation will determine the isotopic difference between the inorganic carbon source and the final bioproduct. Under these conditions, ^{13}C fractionations may vary from −17 to −40 ‰ (O'Leary 1981). When the concentration of CO_2 is the limiting factor, the diffusion of CO_2 into the plant is the slow step in the reaction and carbon isotope fractionation of the plant decreases.

Atmospheric CO_2 first moves through the stomata, dissolves into leaf water and enters the outer layer of photosynthetic cells, the mesophyll cell. Mesophyll CO_2 is directly converted by the enzyme ribulose biphosphate carboxylase/oxygenase ("Rubisco") to a 6 carbon molecule, that is then cleaved into 2 molecules of phosphoglycerate (PGA), each with 3 carbon atoms (plants using this photosynthetic pathway are therefore called C_3 plants). Most PGA is recycled to make ribulose biphosphate, but some is used to make carbohydrates. Free exchange between external and mesophyll CO_2 makes the carbon fixation process less efficient, which causes the observed large ^{13}C-depletions of C_3 plants.

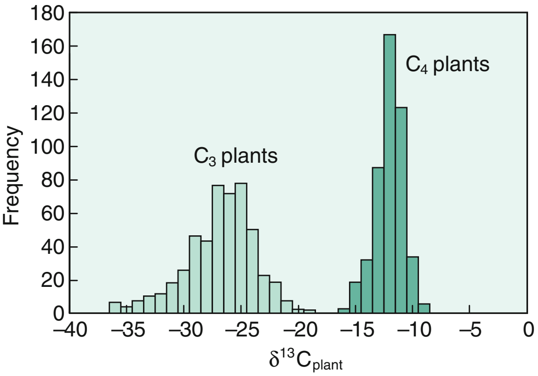

Fig. 2.10 Histogram of $\delta^{13}C$ values of C_3 and C_4 plants (after Cerling and Harris 1999) (Fig. 2.10, eth edition, p. 52)

C_4 plants incorporate CO_2 by the carboxylation of phosphoenolpyruvate (PEP) via the enzyme PEP carboxylase to make the molecule oxaloacetate which has 4 carbon atoms (hence C_4). The carboxylation product is transported from the outer layer of mesophyll cells to the inner layer of bundle sheath cells, which are able to concentrate CO_2, so that most of the CO_2 is fixed with relatively little carbon fractionation.

In conclusion, the main controls on carbon fractionation in plants are the action of a particular enzyme and the “leakiness” of cells. Because mesophyll cells are permeable and bundle sheath cells are less permeable, C_3 versus C_4 plants have ^{13}C-depletions of −18 ‰ versus –4 ‰ relative to atmospheric CO_2 (see Fig. 2.10).

The final carbon isotope composition of naturally synthesized organic matter depends on a complex set of parameters. (i) the ^{13}C-content of the carbon source, (ii) isotope effects associated with the assimilation of carbon, (iii) isotope effects associated with metabolism and biosynthesis and (iv) cellular carbon budgets (Hayes 1993, 2001).

Even more complex is C-isotope fractionation in aquatic plants. Factors that control the $\delta^{13}C$ of phytoplankton include temperature, availability of $CO_{2(aq)}$, light intensity, nutrient availability, pH and physiological factors such as cell size and growth rate (Laws et al. 1995, 1997; Bidigare et al. 1997; Popp et al. 1998 and others). In particular the relationship between C-isotope composition of phytoplankton and concentration of oceanic dissolved CO_2 has been subject of considerable debate because of its potential as a palaeo-CO_2 barometer (see discussion p. 278).

Since the pioneering work of Park and Epstein (1960) and Abelson and Hoering (1961), it is well known that ^{13}C is not uniformly distributed among the total organic matter of plant material, but varies between carbohydrates, proteins and lipids. The latter class of compounds is considerably depleted in ^{13}C relative to the other products of biosynthesis. Although the causes of these ^{13}C-differences are not entirely clear, kinetic isotope effects seem to be more plausible (De Niro and Epstein 1977; Monson and Hayes 1982) than thermodynamic equilibrium effects (Galimov 1985a, 2006). The latter author argued that ^{13}C-concentrations at individual carbon positions within organic molecules are principally controlled by structural factors. Approximate calculations suggested that reduced C–H bonded positions are systematically depleted in ^{13}C, while oxidized C–O bonded positions are enriched in ^{13}C. Many of the observed relationships are qualitatively consistent with that concept. However, it is difficult to identify any general mechanism by which thermodynamic factors should be able to control chemical equilibrium within a complex organic structure. Experimental evidence presented by Monson and Hayes (1982) suggests that kinetic effects will be dominant in most biological systems.

2.4.2.3 Interactions Between Carbonate-Carbon and Organic Carbon

Variations in ^{13}C content of some important carbon compounds are schematically demonstrated in Fig. 2.11: The two most important carbon reservoirs on Earth, marine carbonates and the biogenic organic matter, are characterized by very different isotopic compositions: the carbonates being isotopically heavy with a mean δ^{13}C-value around 0 ‰ and organic matter being isotopically light with a mean δ^{13}C-value around −25 ‰. For these two sedimentary carbon reservoirs an isotope mass balance must exist such that:

$$\delta^{13}\mathrm{C}_{\mathrm{input}} = \mathrm{f}_{\mathrm{org}}\,\delta^{13}\mathrm{C}_{\mathrm{org}} + \left(1 - \mathrm{f}_{\mathrm{org}}\right)\delta^{13}\mathrm{C}_{\mathrm{carb}} \tag{2.6}$$

If δ_{input}, δ_{org}, δ_{carb} can be determined for a specific geologic time, $\mathrm{f}_{\mathrm{org}}$ can be calculated, where $\mathrm{f}_{\mathrm{org}}$ is the fraction of organic carbon entering the sediments. It should be noted that $\mathrm{f}_{\mathrm{org}}$ is defined in terms of the global mass balance and is independent of biological productivity referring to the burial rather than the synthesis of organic material. That means that large $\mathrm{f}_{\mathrm{org}}$ values might be a result of high productivity and average levels of preservation of organic material or of low levels of productivity and high levels of preservation.

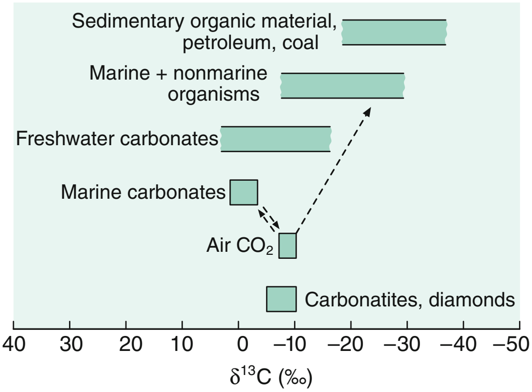

Fig. 2.11 δ^{13}C-values of important geological reservoirs (Fig. 2.11, 6th edition, p. 53)

The $\delta^{13}C$-value for the input carbon cannot be measured precisely but can be estimated with a high degree of certainty. As will be shown later, mantle carbon has an isotopic composition around −5 ‰ and estimates of the global average isotope composition for crustal carbon also fall in that range. Assigning −5 ‰ to $\delta^{13}C$-input, a modern value for f_{org} is calculated as 0.2 or expressed as the ratio of C_{org}/C_{carb} = 20/80. As will be shown later (Chap. 3.7.2) f_{org} has obviously changed during specific periods of the Earth's history (e.g. Hayes et al. 1999). With each molecule of organic carbon being buried, a mole of oxygen is released to the atmosphere. Hence, knowledge of f_{org} is of great value in reconstructing the crustal redox budget.

2.5 Nitrogen

More than 99 % of the known nitrogen on or near the Earth's surface is present as atmospheric N_2 or as dissolved N_2 in the ocean. Only a minor amount is combined with other elements, mainly C, O, and H. Nevertheless, this small part plays a decisive role in the biological realm. Since nitrogen occurs in various oxidation states and in gaseous, dissolved, and solid forms (N_2, NO_3^-, NO_2^-, NH_3, NH_4^+), it is a highly suitable element for the search of natural variations in its isotopic composition. Schoenheimer and Rittenberg (1939) were the first to report nitrogen isotopic variations in biological materials. Today, the range of reported $\delta^{15}N$-values covers 100 ‰, from about −50 to +50 ‰. However, most δ-values fall within the much narrower spread from −10 to +20 ‰, as described in more recent reviews of the exogenic nitrogen cycle by Heaton (1986), Owens (1987), Peterson and Fry (1987) and Kendall (1998).

Nitrogen consists of two stable isotopes, ^{14}N and ^{15}N. Atmospheric nitrogen, given by Rosman and Taylor (1998) has the following composition:

$$^{14}N:\quad 99.63\,\%$$

$$^{15}N:\quad 0.37\,\%.$$

2.5.1 Analytical Methods

N_2 is used for $^{15}N/^{14}N$ isotope ratio measurements, the standard is atmospheric N_2. Various preparation procedures have been described for the different nitrogen compounds (Bremner and Keeney 1966; Owens 1987; Velensky et al. 1989; Kendall and Grim 1990, and others). In the early days of nitrogen isotope investigations, the extraction and combustion techniques potentially involved chemical treatments that could have introduced isotopic fractionations. More recently, simplified techniques for combustion have come into routine use, so that a precision of 0.1–0.2 ‰ for $\delta^{15}N$ determinations can be achieved. Organic nitrogen-compounds are combusted to CO_2, H_2O and N_2 in an elemental analyzer. The cryogenically purified N_2 is trapped on molecular sieves for analysis.

More recently methods have been described that are based on the isotope analysis of N_2O. Measurements of bulk δ^{15}N-values yield qualitative rather quantitative information on the nitrogen cycle, special techniques are necessary for a separate analysis of nitrate and nitrite in samples containing both species. Sigman et al. (2001) measured N_2O generated by denitrifying bacteria lacking N_2O reductase. McIlvin and Altabet (2005) introduced an alternative approach of the bacteria method. Nitrate is first reduced with a Cd catalyst to nitrite followed by sodium azide treatment to reduce nitrite to N_2O. This method allows sequential analysis of nitrate and nitrite, but azide is toxic and has to be handled with great care.

Compound-specific analysis of amino acids has been described by McClelland and Montoya (2002) studying 16 amino acids in planktonic consumers and their food sources. Some amino acids, like glutamate and aspartate, show ^{15}N-enrichments with increased trophic level, while others like phenylamine, serine and threonine record the N-isotope composition of the system in which organism exist. ^{15}N differences between the two groups can be attributed to differences in metabolic pathways.

Even different preparation techniques have been used for nitrogen in mantle derived samples with N-concentrations being too low to be analysed by conventional techniques. For these samples, static mass spectrometry, in which the gas is left under static conditions in the ion source, a method developed for noble gas analysis and adopted for nitrogen, has been used. As an alternative, Bebout et al. (2007) described a continuous flow technique for nanomole quantities of nitrogen.

2.5.2 Biological Nitrogen Isotope Fractionations

To understand the processes leading to the nitrogen isotope distribution in the geological environment, a short discussion of the biological nitrogen cycle is required. Atmospheric nitrogen, the most abundant form of nitrogen, is the least reactive species of nitrogen. It can, however, be converted to “fixed” nitrogen by bacteria and algae, which, in turn, can be used by biota for degradation to simple nitrogen compounds such as ammonium and nitrate. Thus, microorganisms are responsible for all major conversions in the biological nitrogen cycle, which generally is divided into fixation, nitrification, and denitrification. Other bacteria return nitrogen to the atmosphere as N_2.

The term *fixation* is used for processes that convert unreactive atmospheric N_2 into reactive nitrogen such as ammonium, usually involving bacteria. Fixation commonly produces organic materials with δ^{15}N-values slightly less than 0 ‰ ranging from –3 to +1 (Fogel and Cifuentes 1993) and occurs in the roots of plants by many bacteria. The large amount of energy needed to break the molecular nitrogen bond makes nitrogen fixation a very inefficient process with little associated N-isotope fractionation.

Nitrification is a multi-step oxidation process mediated by several different autotrophic organisms. Nitrate is not the only product of nitrification, different reactions produce various nitrogen oxides as intermediate species. Nitrification can be described as two partial oxidation reactions, each of which proceeds separately: oxidation by Nitrosomas ($NH_4 \rightarrow NO_2^-$) followed by oxidation by Nitrobacter ($NO_2 \rightarrow NO_3$). Because the oxidation of nitrite to nitrate is generally rapid, most of the N-isotope fractionations is caused by the slow oxidation of ammonium by Nitrosomas. However, as shown by Casciotti (2009) the second oxidation step from nitrite to nitrate is accompanied by an inverse kinetic isotope fractionation, such that nitrite becomes progressively depleted in ^{15}N as the oxidation reaction proceeds.

Denitrification (reduction of more oxidized forms to more reduced forms of nitrogen) is a multi-step process with various nitrogen oxides as intermediate compounds resulting from biologically mediated reduction of nitrate. Denitrification takes place in poorly aerated soil and in suboxic water bodies, especially in oxygen minimum zones of the ocean. There is debate about the relative contributions of denitrification in sediments versus in the ocean. Denitrification supposedly balances the natural fixation of nitrogen, if it did not occur, then atmospheric nitrogen would be exhausted in less than 100 million years. Denitrification causes the $\delta^{15}N$-values of the residual nitrate to increase exponentially as nitrate concentrations decrease. Experimental investigations have demonstrated that fractionation factors may change from 10 to 30 ‰, with the largest values obtained under lowest reduction rates. Nitrogen isotope fractionations during denitrification in the ocean involves a greater fractionation than in sediments. Table 2.3, which gives a summary of observed N-isotope fractionations.

Noteworthy is the inverse kinetic fractionation during nitrite oxidation, which is different from all other microbial processes in which N-isotope fractionation is involved. Casciotti (2009) argued that the inverse fractionation effect is due to reverse reaction at the enzyme level.

Table 2.3 Nitrogen isotope fractionations for microbial cultures (after Casciotti 2009)

N_2 fixation	$N_2 \rightarrow N_{org}$	−2 to +2 ‰
NH_4^+ assimilation	$NH_4^+ \rightarrow N_{org}$	+14 to +27 ‰
NH4$^+$ oxidation (nitrification)	$NH_4^+ \rightarrow NO_2^-$	+14 to 38 ‰
Nitrite oxidation (nitrification)	$NO_2^- \rightarrow NO_3^-$	−12.8 ‰
Nitrate reduction (denitrification)	$NO_3^- \rightarrow NO_2^-$	+13 to +30 ‰
Nitrite reduction (denitrification)	$NO_2^- \rightarrow NO$	+5 to +10 ‰
Nitrous oxide reduction (denitrification)	$N_2O \rightarrow N_2$	+4 to +13 ‰
Nitrate reduction (nitrate assimilation)	$NO_3^- \rightarrow NO_2^-$	+5 to +10

One very important recent finding in the nitrogen cycle is the discovery of anaerobic ammonium oxidation, briefly called anammox, a dissimilatory process involving the reaction of ammonia with nitrite

$$NH_4^+ + NO_2^- \rightarrow N_2 + 2\ H_2O$$

which first has been demonstrated using sediment incubations (Thamdrup and Dalsgaard 2002) and later shown to be the major N-loss process in oxygen minimum zone waters.

So far, only kinetic isotope effects have been considered, but isotopic fractionations associated with equilibrium exchange reactions have been demonstrated for the common inorganic nitrogen compounds (Letolle 1980). Of special importance in this respect is the ammonia volatilization reaction:

$$NH_{3gas} \leftrightarrow NH_4^+aq$$

for which isotope fractionation factors of 1.025–1.035 have been determined (Kirshenbaum et al. 1947; Mariotti et al. 1981). Experimental data by Nitzsche and Stiehl (1984) indicate fractionation factors of 1.0143 at 250 °C and of 1.0126 at 350 °C. During the solution of atmospheric N_2 in ocean water, a very small ^{15}N-enrichment of about 0.1 ‰ occurs (Benson and Parker 1961).

2.5.3 Nitrogen Isotope Distribution in the Earth

Nitrogen is generally regarded as a volatile element with chemical similarities to noble gases. Common belief restricts the dominant nitrogen reservoir to the atmosphere, which is true, if only the earth's surface is considered. Budget estimates of N for the earth as a whole indicate, however, that the dominant reservoir is in the mantle. The average content and speciation of nitrogen in the mantle is poorly constrained. Estimates for average concentrations vary between 0.3 and 36 ppm (Busigny and Bebout 2013).

Mantle nitrogen extracted from MORB glasses (Marty and Humbert 1997; Marty and Zimmermann 1999) and from diamonds (Javoy et al. 1986; Cartigny et al. 1997, 2005; Cartigny and Marty 2013) has an average $\delta^{15}N$-value of around −5 ‰ with considerable scatter. Nitrogen isotope values extracted from peridotie xenoliths and mineral separates show large variations with phlogopites being depleted and clinopyroxene and olivine being enriched in ^{15}N (Yokochi et al. 2009). Positive $\delta^{15}N$ values measured in some MORB samples may reflect the occurrence of subducted nitrogen.

In the crust, during metamorphism of sediments, there is a significant loss of ammonium during devolatilisation, which is associated with a nitrogen fractionation, leaving behind ^{15}N residues (Haendel et al. 1986; Bebout and Fogel 1992; Jia 2006; Plessen et al. 2010). Thus high-grade metamorphic rocks and granites are relatively enriched in ^{15}N and typically have $\delta^{15}N$-values between 8 and 10 ‰.

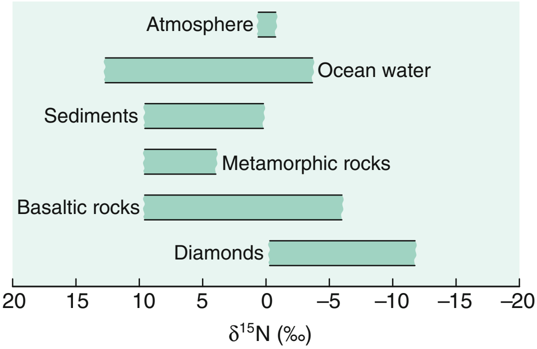

Fig. 2.12 δ^{15}N-values of important geological reservoirs (Fig. 2.12, 6th edition, p. 57)

Sadofsky and Bebout (2000) have examined the nitrogen isotope fractionation among coexisting micas, but could not find any characteristic difference between biotite and white mica.

In summary, nitrogen in sediments and crustal rocks exhibits positive δ^{15}N-values around 6 ‰, whereas in mantle-derived rocks δ^{15}N-values are around −5 ‰.

Figure 2.12 gives an overview about the nitrogen isotope variations in some important reservoirs.

2.5.4 Nitrogen in the Ocean

Nitrogen isotope studies may evaluate the source and fate of nitrogen in the ocean. Nitrogen in the ocean is present in different redox states (nitrate, nitrite, ammonium). Biological processes in the water column may transform one nitrogen compound to the other which is associated with N-isotope fractionations. Nitrogen fixation is regarded as the dominant process for primary production that causes little N isotope fractionation. Thus, nitrogen produced by this process should have a δ^{15}N-value close to zero. However, average oceanic δ^{15}N is close to 5 ‰ as measured in nitrate, the N-isotope enrichment resulting from denitrification. Denitrification occurring in oxygen depleted zones preferentially reduces ^{14}N, the remaining nitrate thus becomes progressively enriched in ^{15}N. Upwelling of such ^{15}N enriched water masses causes the production of relatively ^{15}N-rich phytoplankton particles that sink to the seafloor. The nitrogen isotope composition of sedimentary organic material, thus, can serve as an indicator of water column nitrogen reactions and of nutrient dynamics (e.g. Farrell et al. 1995).

Nitrogen isotopes in particulate organic nitrogen depends on (i) the isotopic composition of dissolved nitrate, and on (ii) isotope fractionation that occurs during nitrogen uptake by phytoplankton. In the photic zone phytoplankton preferentially incorporates ^{14}N, which results in a corresponding ^{15}N-enrichment in the residual nitrate. The N-isotope composition of settling organic detritus, thus varies depending on the extent of nitrogen utilization: low ^{15}N contents indicate low relative utilisation, high ^{15}N contents indicate a high utilization.

Denitrification is believed to be enhanced in interglacial times compared to glacial times. Ganeshram et al. (2000) showed that $\delta^{15}N$ values during interglacials are about 2–3 ‰ heavier than $\delta^{15}N$ values during glacial times. This relationship has been used as a recorder of paleoproductivity.

Nitrogen isotopes in marine sediments, thus, may reflect nutrient cycles of ancient oceans. However, diagenetic reactions on the seafloor and deeper in the sediments may alter the primary nitrogen isotope signal. Nevertheless, Tesdall et al. (2013) argue that although diagenetic effects have to be taken into account, diagenesis is a secondary effect and therefore bulk sedimentary nitrogen isotope records from the seafloor and subseafloor sediments monitor past changes of the marine nitrogen cycle. They presented a global database of more than 2300 bulk sediment $\delta^{15}N$ measurements and demonstrated that $\delta^{15}N$-values range from 2.5 to 16.6 ‰ with a mean value of 6.7 ‰ which is higher than the average 5 ‰ of nitrate in the ocean (http://www.ncdc.noaa.gov/paleo/pubs/nicopp/nicopp.html).

For long, denitrification was believed to be the only mechanism that reduces nitrate to N_2, however, as found more recently the anaerobic oxidation of ammonia, called anammox reaction, is another mechanism in which bacteria use ammonium to convert nitrite to N_2. Brunner et al. (2013) demonstrated that N isotope fractionation associated with the anammox reaction fall in the same range as denitrification. They further showed that anammox may be responsible for the large fractionations between nitrate and nitrite in oxygen minimum zones.

In sediments, with increasing thermal degradation of the organic matter, ammonium (NH_4) is liberated which can replace potassium in clay minerals. The nitrogen in the crystal lattice of clay minerals and micas, thus, is derived from decomposing organic matter reflecting the N-isotope composition of organic matter (Scholten 1991; Williams et al. 1995).

2.5.5 Anthropogenic Nitrogen Sources

The nitrogen cycle has been influenced considerably by human activities including agriculture and fossil fuel burning, adding reactive nitrogen to the environment on a local and a global scale. As demonstrated by Hastings et al. (2009, 2013), nitrogen isotopes of reactive nitrogen can be used to trace its origin. For example, Hastings et al. (2009) analysed N isotopes in a 100 m long ice core and observed a decrease from pre-industrial $\delta^{15}N$-values of +11 ‰ to present day values of −1 ‰. Other studies have shown that fertilizer, animal wastes or sewage are the main sources of nitrate pollution in the hydrosphere. Under favorable conditions, these N-bearing compounds can be isotopically distinguished from each other (Heaton 1986). Anthropogenic fertilizers have $\delta^{15}N$-values in the range −4 to +4 ‰ reflecting their atmospheric source, whereas animal waste typically has δ^{15}N-values >5 ‰. Soil-derived nitrate and fertilizer nitrate commonly have overlapping δ^{15}N-values. In another example, Redling et al. (2013) documented foliar uptake and fertilization effects of car nitrogen oxides on vegetation.

2.6 Oxygen

Oxygen is the most abundant element on Earth. It occurs in gaseous, liquid and solid compounds, most of which are thermally stable over large temperature ranges. These facts make oxygen one of the most interesting elements in isotope geochemistry.

Oxygen has three stable isotopes with the following abundances (Rosman and Taylor 1998)

$$^{16}\mathrm{O}:\quad 99.757\,\%$$

$$^{17}\mathrm{O}:\quad 0.038\,\%$$

$$^{18}\mathrm{O}:\quad 0.205\,\%$$

Because of the higher abundance and the greater mass difference, the ^{18}O/^{16}O ratio is normally determined, which may vary in natural samples by about 10 % or in absolute numbers from about 1 : 475 to 1 : 525. More recently, with improved analytical techniques, the precise measurement of the ^{17}O/^{16}O ratio also became of interest (see p. 85).

2.6.1 Analytical Methods

CO_2 is the gas generally used for mass-spectrometric analysis. CO and O_2 have also been used in high temperature conversion of organic material and in laser probe preparation techniques. A wide variety of methods have been described to liberate oxygen from the various oxygen-containing compounds.

2.6.1.1 Water

The ^{18}O/^{16}O ratio of water is usually determined by equilibration of a small amount of CO_2 with a surplus of water at a constant temperature. For this technique, the exact value of the fractionation for the CO_2/H_2O equilibrium at a given temperature is of crucial importance. A number of authors have experimentally determined this fractionation at 25 °C with variable results. A value of 1.0412 was proposed at the 1985 IAEA Consultants Group Meeting to be the best estimate.

It is also possible to quantitatively convert all water oxygen directly to CO_2 by reaction with guanidine hydrochloride (Dugan et al. 1985) which has the advantage that it is not necessary to assume a value for the H_2O–CO_2 isotope fractionation in order to obtain the $^{18}O/^{16}O$ ratio. Sharp et al. (2001) described a technique reducing H_2O by reaction with glassy carbon at 1450 °C. O'Neil and Epstein (1966) first described the reduction of water with Br_5F. For the precise measurement of ^{17}O and ^{18}O the method later was modified using CoF_3 (Baker et al. 2002; Barkan and Luz 2005).

As mentioned under Sect. 2.1.1, an alternative method to mass spectrometry is the direct determination of oxygen isotope ratios by laser absorption spectroscopy (Brand et al. 2009a, b and others).

2.6.1.2 Carbonates

The standard procedure for the isotope analysis of carbonates is the reaction with 100 % phosphoric acid at 25 °C first described by McCrea (1950). The following reaction equation:

$$\mathrm{MeCO_3 + H_3PO_4 \rightarrow MeHPO_4 + CO_2 + H_2O}$$

where Me is a divalent cation, shows that only two-thirds of the carbonate oxygen present in the product CO_2 is liberated, which carries a significant isotope effect being on the order of 10 ‰, but varies up to a few ‰ depending on the cation, the reaction temperature and the preparation procedure. The so-called acid fractionation factor must be precisely known to obtain the oxygen isotope ratio of the carbonate. This can be done by measuring the $\delta^{18}O$-value of the carbonate by fluorination with BrF_5, first described by Sharma and Clayton (1965).

Experimental details of the phosphoric acid method vary significantly among different laboratories. The two most common varieties are the "sealed vessel" and the "acid bath" methods. In the latter method the CO_2 generated is continuously removed, while in the former it is not. Swart et al. (1991) demonstrated that the two methods exhibit a systematic ^{18}O difference between 0.2 and 0.4 ‰ over the temperature range 25 to 90 °C. Of these the "acid-bath" method probably provides the more accurate results. A further modification of this technique is referred to as the "individual acid bath", in which contaminations from the acid delivery system are minimized. Wachter and Hayes (1985) demonstrated that careful attention must be given to the phosphoric acid. In their experiments best results were obtained by using a 105 % phosphoric acid and a reaction temperature of 75 °C. This high reaction temperature should not be used when attempting to discriminate between mineralogically distinct carbonates by means of differential carbonate reaction rates.

Because some carbonates like magnesite or siderite react very sluggishly at 25 °C, higher reaction temperatures are necessary to extract CO_2 from these minerals. Reaction temperatures have varied up to 90 or even 150 °C (Rosenbaum and Sheppard 1986; Böttcher 1996), but there still exist considerable differences in the fractionation factors determined by various workers. Crowley (2010) showed that for minerals of the $CaCO_3$–$MgCO_3$ group the oxygen isotope composition of CO_2 is a linear function of the reciprocal of reaction temperature. Deviations from this

Table 2.4 Acid fractionation factors for various carbonates determined at 25 °C (modified after Kim et al. 2007)

Mineral	α	References
Calcite	10.30	Kim et al. (2007)
Aragonite	10.63	Kim et al. (2007)
	11.14	Gilg et al. (2007)
Dolomite	11.75	Rosenbaum and Sheppard (1986)
Magnesite	10.79 (50 °C)	Das Sharma et al. (2002)
Siderite	11.63	Carothers et al. (1988)
Witherite	10.57	Kim and O'Neil (1997)

relationship may be attributed to structural state and differences in chemical composition.

Another uncertainty exists for fractionations between aragonite and calcite. Different workers have reported fractionations from negative to positive. Nevertheless there seems to be a general agreement that the fractionation factor for aragonite is about 0.6 ‰ higher than for calcite (Tarutani et al. 1969; Kim and O'Neil 1997), although Grossman and Ku (1986) have reported a value of up to 1.2 ‰. The dolomite-calcite fractionation may vary depending on specific composition (Land 1980). Table 2.4 reports acid fractionation factors for various carbonates.

2.6.1.3 Silicates

Oxygen in silicates and oxides is usually liberated through fluorination with F_2, BrF_5 or ClF_3 in nickel-tubes at 500 to 650 °C (Taylor and Epstein 1962; Clayton and Mayeda 1963; and Borthwick and Harmon 1982) or by heating with a laser (Sharp 1990). Decomposition by carbon reduction at 1000–2000 °C may be suitable for quartz and iron oxides but not for all silicates (Clayton and Epstein 1958). The oxygen is converted to CO_2 over heated graphite or diamond. For an analysis of the three isotope (^{16}O, ^{17}O, ^{18}O) O_2 has to be the analyte gas. Care must be taken to ensure quantitative oxygen yields, which can be a problem in the case of highly refractive minerals like olivine and garnet. Low yields may result in anomalous $^{18}O/^{16}O$ ratios, high yields are often due to excess moisture in the vacuum extraction line.

Today, infrared-laser fluorination, first described by Sharp (1990), most commonly is used for mineral analysis. Alternatively, UV lasers have been used by Wiechert and Hoefs (1995) and Wiechert et al. (2002). A precise SIMS method with a reproducibility of 0.3 ‰ from 15 μm mineral spots has been described by Kita et al. (2009).

2.6.1.4 Phosphates

Phosphates are first dissolved, then precipitated as silver phosphate (Crowson et al. 1991). Ag_3PO_4 is preferred because it is non-hydroscopic and can be precipitated rapidly without numerous chemical purification steps (O'Neil et al. 1994). This

Ag_3PO_4 is then fluorinated (Crowson et al. 1991), reduced with C either in a furnace (O'Neil et al. 1994) or with a laser (Wenzel et al. 2000) or pyrolyzed (Vennemann et al. 2002). Because PO_4 does not exchange oxygen with water at room temperature (Kolodny et al. 1983), the isotopic composition of the Ag_3PO_4 is that of the PO_4 component of the natural phosphate. As summarized by Vennemann et al. (2002) conventional fluorination remains the most precise and accurate analytical technique for Ag_3PO_4. Laser techniques on bulk materials have also been attempted (Cerling and Sharp 1996; Kohn et al. 1996; Wenzel et al. 2000), but because fossil phosphates invariably contain diagenetic contaminants, chemical processing and analysis of a specific component (CO_3 or PO_4) is ordinarily performed.

2.6.1.5 Sulfates

Sulfates are precipitated as $BaSO_4$, and then reduced with carbon at 1000 °C to produce CO_2 and CO. The CO is either measured directly or converted to CO_2 by electrical discharge between platinum electrodes (Longinelli and Craig 1967). Total pyrolysis by continuous flow methods has made the analysis of sulfate oxygen more precise and less time-consuming than the off-line methods. Bao and Thiemens (2000) have used a CO_2-laser fluorination system to liberate oxygen from barium sulfate.

2.6.1.6 Nitrates

Oxygen isotopes in nitrate may be measured by high-temperature combustion with graphite (Revesz et al. 1997). Since this method is labour-intensive, Sigman et al. (2001) used cultured denitryfing bacteria for the reduction of nitrate. In the analyzed N_2O only one of six oxygen atoms present in the initial nitrate will be measured, therefore potential oxygen isotope fractionations must be adequately taken into account (Casciotti et al. 2002).

2.6.2 Standards

Two different δ-scales are in use: $\delta^{18}O_{(VSMOW)}$ and $\delta^{18}O_{(VPDB)}$, because of two different categories of users, who have traditionally been engaged in O-isotope studies. The VPDB scale is used in low-temperature studies of carbonate. The original PDB standard was prepared from a Cretaceous belemnite from the Pee Dee Formation and was the laboratory working standard used at the University of Chicago in the early 1950s when the paleotemperature scale was developed. The original supply of this standard has long been exhausted, therefore secondary standards have been introduced (see Table 2.5), whose isotopic compositions have been calibrated relative to PDB. All other oxygen isotope analyses (waters, silicates, phosphates, sulfates, high-temperature carbonates) are given relative to SMOW.

Table 2.5 $\delta^{18}O$-values of commonly used O-isotope standards (data for sulfate and nitrate are from Brand et al. 2009a, b)

Standard	Material	VPDB scale	VSMOW scale
NBS-19	Marble	−2.20	
NBS-20	Limestone	−4.14	
NBS-18	Carbonatite	−23.00	
NBS-28	Quartz		9.60
NBS-30	Biotite		5.10
GISP	Water		−24.75
SLAP	Water		−55.50
NBS-127	Ba sulfate		8.59
USGS 35	Na nitrate		56.81

The conversion equations of $\delta^{18}O_{(VPDB)}$ versus $\delta^{18}O_{(VSMOW)}$ and vice versa (Coplen et al. 1983) are:

$$\delta^{18}O(VSMOW) = 1.03091\,\delta^{18}O(PDB) + 30.91$$

and

$$\delta^{18}O(VPDB) = 0.97002\,\delta^{18}O(VSMOW) - 29.98$$

Table 2.5 gives the $\delta^{18}O$-values of commonly used oxygen isotope standards on both scales.

2.6.3 Fractionation Processes

Out of the numerous possibilities to fractionate oxygen isotopes in nature, the following are of special significance.

2.6.3.1 Fractionation of Water

Knowledge of the oxygen isotope fractionation between liquid water and water vapor is essential for the interpretation of the isotope composition of different water types. Fractionation factors experimentally determined in the temperature range from 0 to 350 °C have been summarized by Horita and Wesolowski (1994). This is shown in Fig. 2.13.

Addition of salts to water also affects isotope fractionations. The presence of ionic salts in solution changes the local structure of water around dissolved ions. Taube (1954) first demonstrated that the $^{18}O/^{16}O$ ratio of CO_2 equilibrated with pure H_2O decreased upon the addition of $MgCl_2$, $AlCl_3$ and HCl, remained more or less unchanged for NaCl, and increased upon the addition of $CaCl_2$. The changes vary roughly linearly with the molality of the solute (see Fig. 2.14).

To explain this different fractionation behavior, Taube (1954) postulated different isotope effects between the isotopic properties of water in the hydration

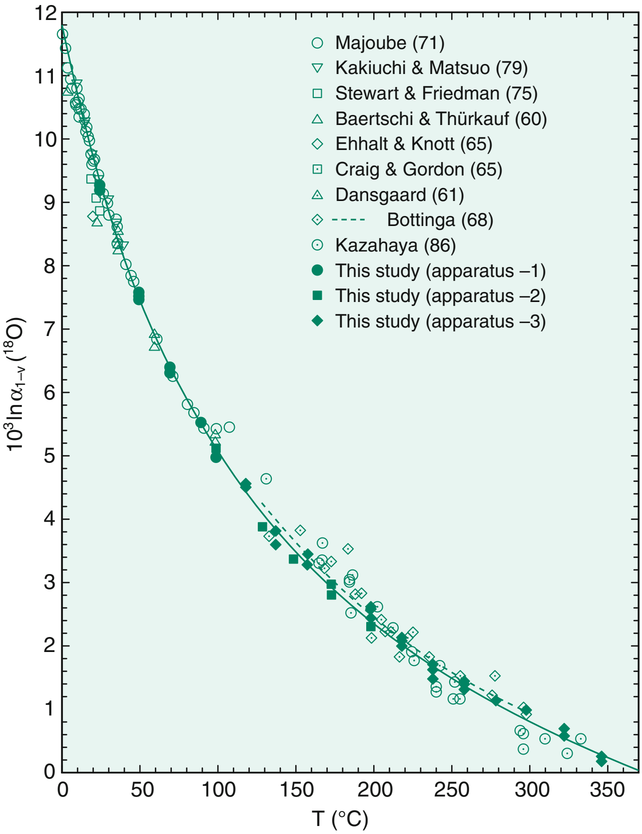

Fig. 2.13 Oxygen isotope fractionation factors between liquid water and water vapour in the temperature range 0–350 °C (after Horita and Wesolowski 1994) (Fig. 2.13, 6th edition p. 62)

sphere of the cation and the remaining bulk water. The hydration sphere is highly ordered, whereas the outer layer is poorly ordered. The relative sizes of the two layers are dependent upon the magnitude of the electric field around the dissolved ions. The strength of the interaction between the dissolved ion and water molecules is also dependent upon the atomic mass of the atom to which the ion is bonded. O'Neil and Truesdell (1991) have introduced the concept of "structure-making" and "structure-breaking" solutes: structure makers yield more positive isotope fractionations relative to pure water whereas structure breakers produce negative isotope fractionations. Any solute that results in a positive isotope fractionation is one that causes the solution to be more structured as is the case for ice structure, when compared to solutes that lead to less structured forms, in which cation–H_2O bonds are weaker than H_2O–H_2O bonds.

As already treated in Sect. 2.1, isotope fractionations, the hydration of ions may play a significant role in hydrothermal solutions and volcanic vapors (Driesner and

Fig. 2.14 Oxygen isotope fractionation between pure water and solutions of various ions (after O'Neil and Truesdell 1991) (Fig. 2.14, 6th edition, p. 63)

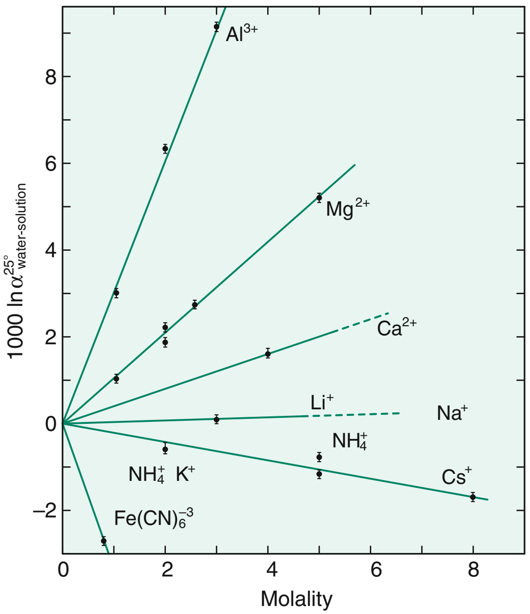

Table 2.6 Experimentally determined oxygen isotope fractionation factors relative to water for the aqueous system CO_2–H_2O between 5 and 40 °C according to $10^3 \ln \alpha = A(10^6/T^{-2}) + B$ (Beck et al. 2005)

	A	B
HCO_3^-	2.59	1.89
CO_3^{2-}	2.39	−2.70
$CO_{2(aq)}$	2.52	12.12

Seward 2000). Such isotope salt effects may change the oxygen isotope fractionation between water and other phases by several permil.

2.6.3.2 CO_2–H_2O System

Of equal importance is the oxygen isotope fractionation in the CO_2–H_2O system. Early work concentrated on the oxygen isotope partitioning between gaseous CO_2 and water (Brenninkmeijer et al. 1983). In more recent work by Usdowski et al. (1991), Beck et al. (2005) and Zeebe (2007), it has been demonstrated that the oxygen isotope composition of the individual carbonate species are isotopically different, which is consistent with experimental work of McCrea (1950) and Usdowski and Hoefs (1993). Table 2.6 summarizes the equations for the temperature dependence between 5 and 40 °C (Beck et al. 2005).

The oxygen isotope fractionation (1000 lnα) between aqueous CO_2 and water at 25 °C is 41.6, dropping to 24.7 at high pH values when CO_3^{2-} is the dominant species (see Fig. 2.15). The pH dependence of the oxygen isotope composition in

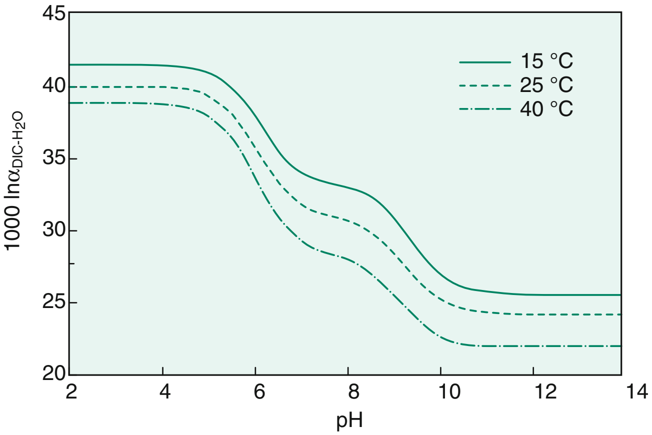

Fig. 2.15 Oxygen isotope fractionations between dissolved inorganic carbon (DIC) and water as function of pH and temperatures (after Beck et al. 2005) (Fig. 2.15, 6th edition, p. 64)

the carbonate-water system has important implications in the derivation of oxygen isotope temperatures.

2.6.3.3 Mineral Fractionations

The oxygen isotope composition of a rock depends on the ^{18}O contents of the constituent minerals and the mineral proportions. Garlick (1966) and Taylor (1968) arranged coexisting minerals according to their relative tendencies to concentrate ^{18}O. The list given in Table 2.7 has been augmented by data from Kohn et al. (1998a, b, c).

This order of decreasing ^{18}O-contents has been explained in terms of the bond-type and strength in the crystal structure. Semi-empirical bond-type calculations have been developed by Garlick (1966) and Savin and Lee (1988) by

Table 2.7 Sequence of minerals in the order (bottom to top) of their increasing tendency to concentrate ^{18}O

Quartz
Dolomite
K-feldspar, albite
Calcite
Na-rich plagioclase
Ca-rich plagioclase
Muscovite, paragonite, kyanite, glaucophane
Orthopyroxene, biotite
Clinopyroxene, hornblende, garnet, zircon
Olivine
Ilmenite
Magnetite, hematite

assuming that oxygen in a chemical bond has similar isotopic behavior regardless of the mineral in which the bond is located. This approach is useful for estimating fractionation factors. The accuracy of this approach is limited due to the assumption that the isotope fractionation depends only upon the atoms to which oxygen is bonded and not upon the structure of the mineral, which is not strictly true. Kohn and Valley (1998a, b) determined empirically the effects of cation substitutions in complex minerals such as amphiboles and garnets spanning a large range in chemical compositions. Although isotope effects of cation exchange are generally less than 1 ‰ at $T > 500$ °C, they increase considerably at lower temperatures. Thus; use of amphiboles and garnets for thermometry requires exact knowledge of chemical compositions.

On the basis of these systematic tendencies of ^{18}O enrichment found in nature, significant temperature information can be obtained up to temperatures of 1000 °C, and even higher, if calibration curves can be worked out for the various mineral pairs. The published literature contains many calibrations of oxygen isotope geothermometers, most are determined by laboratory experiments, although some are based on theoretical calculations.

Although much effort has been directed toward the experimental determination of oxygen isotope fractionation factors in mineral—water systems, the use of water as an oxygen isotope exchange medium has several disadvantages. Some minerals become unstable in contact with water at elevated temperatures and pressures, leading to melting, breakdown and hydration reactions. Incongruent solubility and ill-defined quench products may introduce additional uncertainties. Most of the disadvantages of water can be circumvented by using calcite as an exchange medium (Clayton et al. 1989; Chiba et al. 1989). Mineral-mineral fractionations—determined by these authors (Table 2.8)—give internally consistent geothermometric information that generally is in accord with independent estimates, such as the theoretical calibrations of Kieffer (1982).

A more recent summary has been given by Chacko et al. (2001) (see Fig. 2.16).

Many isotopic fractionations between low-temperature minerals and water have been estimated by assuming that their temperature of formation and the isotopic composition of the water in which they formed (for example, ocean water) are well known. This is sometimes the only approach available in cases in which the rates of isotope exchange reactions are slow and in which minerals cannot be synthesized in the laboratory at appropriate temperatures.

Table 2.8 Coefficients A for silicate—pair fractionations ($1000 \ln \alpha_{X-Y} = A/T^2$) 10^6 (after Chiba et al. 1989)

	Cc	Ab	An	Di	Fo	Mt
Qtz	0.38	0.94	1.99	2.75	3.67	6.29
Cc		0.56	1.61	2.37	3.29	5.91
Ab			1.05	1.81	2.73	5.35
An				0.76	1.68	4.30
Di					0.92	3.54
Fo						2.62

Fig. 2.16 Oxygen isotope fractionations between various minerals and calcite (after Chacko et al. 2001) (Fig. 2.16, 6th edition, p. 66)

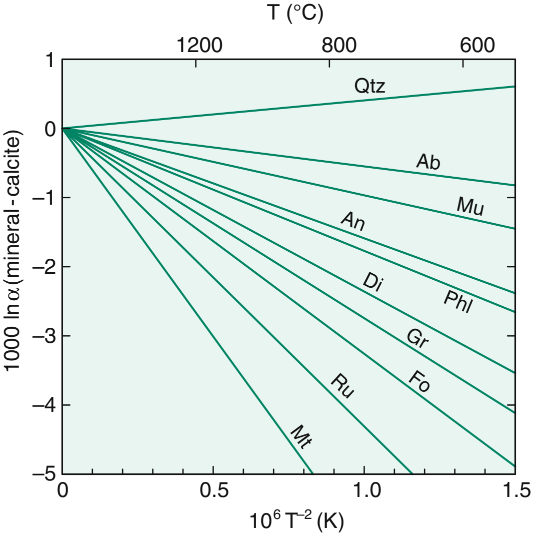

2.6.4 Triple Oxygen Isotope Compositions

Measurements of $^{17}O/^{16}O$ ratios potentially expand the utility of $^{18}O/^{16}O$ studies, the latter being hampered by difficulties to differentiate between temperature and water composition. Since the natural oxygen isotope ratio of $^{17}O/^{16}O$ is close to one half of the $^{18}O/^{16}O$ ratio, in the past it was generally assumed that there was no need to measure the rare ^{17}O. However, with improvements in analytical techniques, it became clear that the precise measurement of ^{17}O contents may give additional informations on fractionation processes in the earth's reservoirs. In a diagram $\delta^{17}O$ versus $\delta^{18}O$ values; all terrestrial rocks and minerals plot on a line with a coefficient λ 0.52× which was called the Terrestrial Fractionation Line (TFL). Deviations from the TFL reference line are given as $\Delta^{17}O$ and are termed oxygen isotope anomalies. The coefficient λ differs for equilibrium and kinetic fractionation processes and varies between 0.509 which is the lower limit for kinetic fractionations and 0.530 which is the equilibrium high temperature limit (Young et al. 2002).

For water, for instance, the triple oxygen isotope composition is characterized by an equilibrium fractionation exponent λ between liquid water and water vapour of 0.529 compared to a value of 0.518 for diffusion of water vapour. The global meteoric water line has a slope of 0.528 (Luz and Barkan 2010) (analogous to a slope of 8 of the δD-$\delta^{18}O$ meteoric water line). For rocks and minerals the slope λ is between 0524 and 0.526 (Miller et al. 1999; Rumble et al. 2007) and for meteoric waters the slope is 0.528 (Luz and Barkan 2010).

With further analytical improvements, Pack and Herwartz (2014) demonstrated that the concept of a single TFL is invalid and that different reservoirs on Earth are characterized by individual mass fractionation lines with individual slopes and intercepts. Similar conclusions have been reached by Levin et al. (2014) and Passey et al. (2014).

2.6.5 Fluid-Rock Interactions

Oxygen isotope ratio analysis provides a powerful tool for the study of water/rock interaction. The geochemical effect of such an interaction between water and rock or mineral is a shift of the oxygen isotope ratios of the rock and/or the water away from their initial values, given that their compositions are not in equilibrium.

Detailed studies of the kinetics and mechanisms of oxygen isotope exchange between minerals and fluids show that there are three possible exchange mechanisms (Matthews et al. 1983a, b; Giletti 1985).

(1) Solution-precipitation. During a solution-precipitation process, larger grains grow at the expense of smaller grains. Smaller grains dissolve and recrystallize on the surface of larger grains which decreases the overall surface area and lowers the total free energy of the system. Isotopic exchange with the fluid occurs while material is in solution.

(2) Chemical reaction. The chemical activity of one component of both fluid and solid is so different in the two phases that a chemical reaction occurs. The breakdown of a finite portion of the original crystal and the formation of new crystals is implied. The new crystals would form at or near isotopic equilibrium with the fluid.

(3) Diffusion. During a diffusion process isotopic exchange takes place at the interface between the crystal and the fluid with little or no change in morphology of the reactant grains. The driving force is the random thermal motion of the atoms within a concentration or activity gradient.

In the presence of a fluid phase coupled dissolution—reprecipitation is known to be a much more effective process than diffusion. This has been first demonstrated experimentally by O'Neil and Taylor (1967) and later re-emphasized by Cole (2000) and Fiebig and Hoefs (2002).

The first attempts to quantify isotope exchange processes between water and rocks were made by Sheppard et al. (1971) and Taylor (1974). By using a simple closed-system material balance equation these authors were able to calculate cumulative fluid/rock ratios.

$$\mathrm{W/R} = \frac{\delta_{\mathrm{rock_f}} - \delta_{\mathrm{rock_i}}}{\delta_{\mathrm{H_2O_i}} - (\delta_{\mathrm{rock_f}} - \Delta)}, \tag{2.7}$$

where $\Delta = \delta_{\mathrm{rock_f}} - \delta\mathrm{H_2O_f}$

The equation requires adequate knowledge of both the initial (i) and final (f) isotopic states of the system and describes the interaction of one finite volume of rock with a fluid. The utility of such "zero-dimensional" equations has been questioned by Baumgartner and Rumble (1988), Blattner and Lassey (1989), Nabelek (1991), Bowman et al. (1994) and others. Only under special conditions do one-box models yield information on the amount of fluid that actually flowed through the rocks. If the rock and the infiltrating fluid were not far out of isotopic equilibrium, then the calculated fluid/rock ratios rapidly approach infinity. Therefore, the equations are sensitive only to small fluid/rock ratios. Nevertheless, the equations can constrain fluid sources. More sophisticated one-dimensional models like the chromatographic or continuum mechanics models (i.e. Baumgartner and Rumble 1988) are physically more plausible and can describe how the isotopic composition of the rock and of the fluid change with time and space. The mathematical models are complex and are based on partial differential equations that must be solved numerically. Examples of fluid-rock interactions in contact metamorphic environments have been presented by Nabelek and Labotka (1993), Bowman et al. (1994) and application to contrasting lithologies by Bickle and Baker (1990) and Cartwright and Valley (1991).

Criss et al. (1987) and Gregory et al. (1989) developed a theoretical framework that describes the kinetics of oxygen isotope exchange between minerals and coexisting fluids. Figure 2.17 shows characteristic patterns in δ–δ plots for some hydrothermally altered granitic and gabbroic rocks. The $^{18}O/^{16}O$ arrays displayed on Fig. 2.17 cut across the 45° equilibrium lines at a steep angle as a result of the much faster oxygen isotope exchange of feldspar compared to that of quartz and pyroxene. If a low-^{18}O fluid such as meteoric or ocean water is involved in the exchange process, the slopes of the disequilibrium arrays can be regarded as "isochrons" where, with continued exchange through time the slopes become less

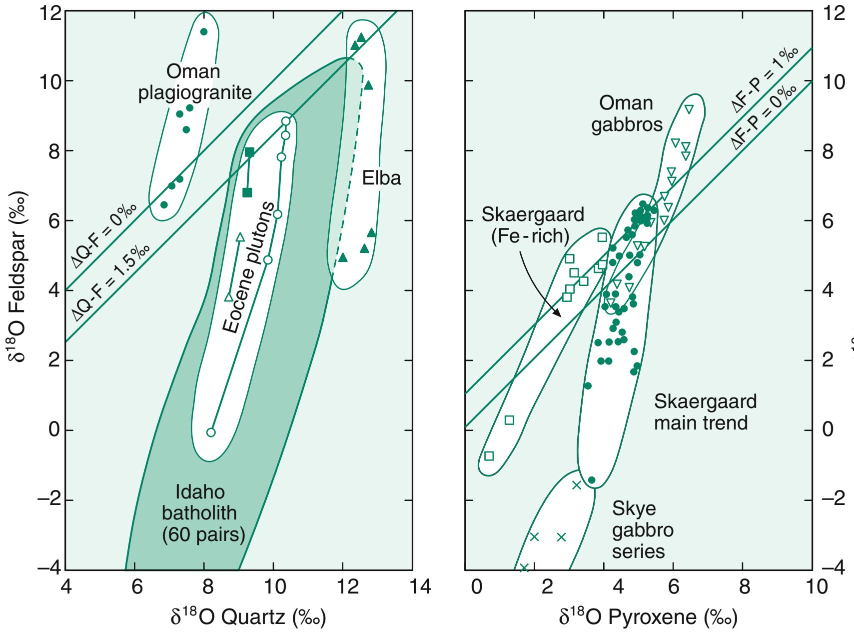

Fig. 2.17 $\delta^{18}O_{(feldspar)}$ versus $\delta^{18}O_{(quartz)}$ and versus $\delta^{18}O_{(pyroxene)}$ plots of disequilibrium mineral pair arrays in granitic and gabbroic rocks. The arrays indicate open-system conditions from circulation of hydrothermal meteoric fluids (after Gregory et al. 1989) (Fig. 2.17, 6th edition, p. 68)

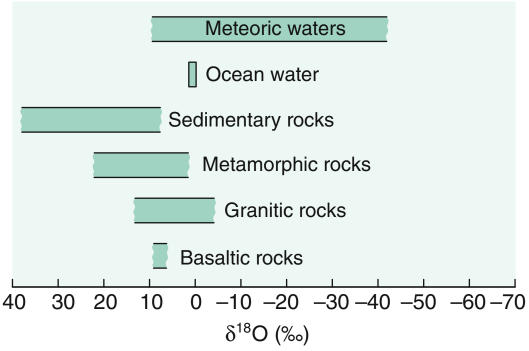

Fig. 2.18 $\delta^{18}O$ values of important geological reservoirs (Fig. 2.18, 6th edition, p. 68)

steep and approach the 45° equilibrium line. These "times" represent the duration of a particular hydrothermal event.

Figure 2.18 summarizes the naturally observed oxygen isotope variations in important geological reservoirs.

2.7 Magnesium

The oxidation state of magnesium in natural compounds always is two, thus it might be expected that the natural range of Mg isotope composition is comparably small. On the other hand, Mg is incorporated during growth of biogenic $CaCO_3$ and plays an essential role during photosynthesis indicating that biological fractionations may play an important role for Mg isotopes.

Magnesium is composed of three isotopes (Rosman and Taylor 1998)

$$^{24}\mathrm{Mg}\quad 78.99\,\%$$

$$^{25}\mathrm{Mg}\quad 10.00\,\%$$

$$^{26}\mathrm{Mg}\quad 11.01\,\%$$

Early investigations on Mg isotope variations have been limited by an uncertainty of 1–2 ‰. Catanzaro and Murphy (1966) for instance concluded that terrestrial Mg isotope variations are restricted to a few ‰. The introduction of multicollector-inductively coupled-plasma mass spectrometry (MC-ICP-MS) increased the precision by one order of magnitude and has initiated a new search of natural isotope variations (Galy et al. 2001, 2002). Factors affecting the accuracy of Mg isotopes measured by MC-ICP-MS have been summarized by Teng and Yang (2013). δ^{25}Mg and δ^{26}Mg values are reported relative to the DSM-3 standard (Galy et al. 2003; Oeser et al. 2014; Teng et al. 2014). Teng et al. (2014) published Mg isotope compositions for 24 reference materials, the long-term reproducibility for δ^{25}Mg was 0.05 ‰ and for δ^{26}Mg 0.07 ‰. One of the advantages of the

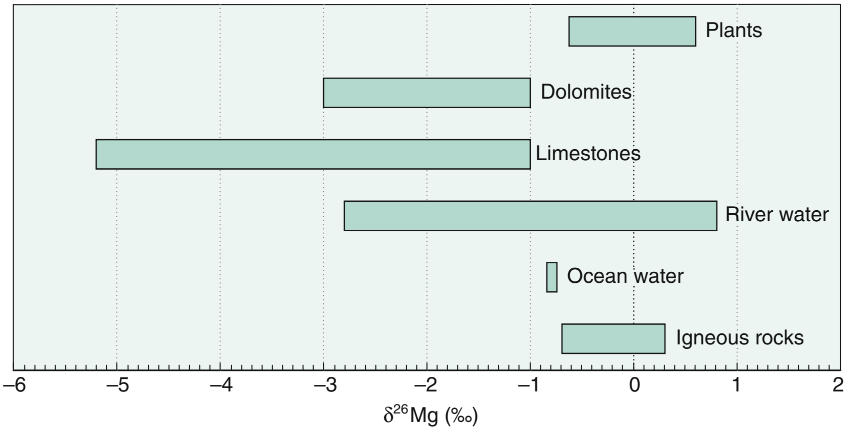

Fig. 2.19 δ^{26}Mg values of important geological reservoirs

MC-ICPMS technique is the ability to measure ^{25}Mg/^{24}Mg and ^{26}Mg/^{24}Mg ratios independently many times smaller than the magnitude of the natural variations. The relationship between ^{25}Mg/^{24}Mg and ^{26}Mg/^{24}Mg ratios is diagnostic of kinetic versus equilibrium fractionations: for equilibrium processes the slope on a three-isotope diagram should be close to 0.521, for kinetic processes the slope should be 0.511 (Young and Galy 2004).

Figure 2.19 summarizes the natural δ^{26}Mg isotope variations relative to DSM-3.

2.7.1 High-Temperature Fractionations

Calculations by Schauble (2011) yield systematic ^{26}Mg isotope fractionations among silicates, carbonates and oxides ín the order magnesite, dolomite, forsterite, orthoenstatite, diopside, periclase and spinel. Fractionations correlate with coordination numbers, tetrahedral sites tend to have higher ^{26}Mg/^{24}Mg ratios than octahedral sites: thus, pyrope in which Mg is in eightfold coordination is depleted in heavy Mg isotopes relative to pyroxenes and olivine, in which Mg is in sixfold coordination. Experimentally determined equilibrium isotope fractionations between spinel, forsterite and magnesite by Macris et al. (2013) are consistent with the postulated dependence on coordination numbers. In the temperature range from 600 to 800 °C, Mg isotope fractionations between spinel and forsterite vary from 1.3 to 0.86 ‰ indicating isotope equilibrium. It is still unclear whether small intermineral fractionations among olivine and pyroxenes in mantle rocks represent equilibrium conditions or are products of melt-rock interactions (Xiao et al. 2013). Studies by Teng et al. (2007), Wiechert and Halliday (2007), Young et al. (2009), Handler et al. (2009) and Bourdon et al. (2010) have demonstrated slight differences between basalts and peridotite. Mineral Mg isotope fractionations among olivine and pyroxene are very small (Handler et al. 2009; Wiechert and Halliday 2007; Yang et al. 2009; Liu et al. 2011), clinopyroxene and phlogopite are more variable and slightly heavier than olivine suggesting that inter-mineral fractionations are controlled by Mg–O bond strengths (Liu et al. 2011). Furthermore, as pointed out by Young et al. (2015), the effects of mineral chemistry are crucial to understand high-temperature mineral Mg isotope distributions.

The Mg isotope composition of the Moon and chondrites are indistinguishable from Earth, suggesting a homogenous Mg-isotope distribution in the solar system and no Mg isotope fractionation during the Moon-forming event (Sedaghatpour et al. 2013). In contrast to the mantle, the upper and lower continental crust is heterogeneous in Mg isotope composition and on average slightly heavier than the mantle (Shen et al. 2009; Li et al. 2010; Liu et al. 2010a, b; Teng et al. 2013). Li et al. (2010) concluded that compared to granites, sediments are heavier and more variable. Such larger variations may result from chemical weathering during which light isotopes are lost to the hydrosphere, leaving ^{26}Mg enriched sedimentary rocks.

Clastic sediments are generally enriched in heavy Mg isotopes with δ^{26}Mg values up to 0.92 ‰ (Li et al. 2010). During subduction, clastic sediments generally retain their Mg isotope composition (Li et al. 2014), thus recycling of clastic sediments will introduce Mg enriched in heavy isotopes into the mantle. Carbonates on the hand are significantly depleted in heavy Mg isotopes. Light isotope values in basalts from the North China Craton have been interpreted to indicate recycling of carbonates derived from oceanic crust (Yang et al. 2012a, b).

2.7.2 Fractionations During Weathering

The behaviour of Mg isotopes during weathering is rather complex (Wimpenny et al. 2010; Huang et al. 2012). Mg is soluble and mobile during weathering potentially inducing small fractionations during dissolution and precipitation of minerals. Wimpenny et al. (2010) and Huang et al. (2012) observed that light Mg isotopes are preferentially released during dissolution of basalt leading to enriched residues. Ryu et al. (2011), however, reported little fractionation during dissolution of granite. The different behaviour of Mg isotopes during weathering may reflect crystallographic differences of Mg-sites in minerals.

Compared to dissolution, the behaviour of Mg isotopes during secondary formation of Mg minerals may be even more complex (Huang et al. 2012). Soil and clays are generally heavier than their parent rocks (Tipper et al. 2006a, b, 2010; Opfergelt et al. 2012; Pogge von Strandmann et al. 2014) suggesting that heavy Mg isotopes are preferentially incorporated into the structure of clay minerals or absorbed in soils.

The complex behaviour of Mg during weathering results in large Mg isotope variations of river waters. As summarized by Li et al. (2012) δ^{26}Mg values range from −3.80 to +0.75 ‰ reflecting differences of catchment lithologies particularly in the proportions of carbonate to silicate rocks. Tipper et al. (2006a) on the other hand observed a total variation in ^{26}Mg of 2.5 ‰ and concluded that the lithology in the drainage area is of limited significance, instead the major part of the variability has to be attributed to fractionations in the weathering environment.

2.7.3 Ocean Water

The dominant Mg source to the ocean is riverine input, major sinks are removal by hydrothermal fluids, dolomite formation and low-temperature clay formation during alteration of the oceanic crust. The average δ^{26}Mg-value of riverine input is −1.09 ‰ (Tipper et al. 2006b).

Because of its relatively long mean residence time, ocean water has a constant isotope composition of −0.80 ‰ that is slightly heavier than average river water resulting from Mg uptake into silicate minerals during weathering. Mg removal from seawater by hydrothermal interaction with the oceanic crust forming smectites and at higher temperatures chlorite does not cause a measurable Mg isotope fractionation. Dolomitisation, however, affects the ocean water, driving seawater to heavier values.

By analyzing pore waters from a large range of oceanographic settings, Higgins and Schrag (2010) demonstrated, that although Mg concentrations in pore waters are very similar in many deep-sea sediments, profiles of δ^{26}Mg values are very different, which is best explained by precipitation of Mg-minerals in sediments or underlying crust.

2.7.4 Carbonates

Dolomite is one of the major Mg carbonate that forms under specific environmental conditions. Geske et al. (2015) reported Mg isotope compositions of dolomite from various environments having a total range from −2.49 to −0.45 ‰ and argued that Mg isotope ratios are affected by a variety of factors, making the application of Mg isotopes as a proxy for their depositional and diagenetic environment problematic. On the hand, as observed by Azmy et al. (2013), early diagenetic dolomite inherits its isotope signature from precursor carbonates and diagenetic fluids. Later formed diagenetic dolomite phases may be slightly enriched in ^{26}Mg suggesting that temperature is not the decisive factor, but instead the Mg-isotope composition of the diagenetic fluid.

Mg is present in $CaCO_3$ in the form of high Mg calcite (4 to ≈30 mol%), as low Mg calcite (≤4 mol%) and to a minor extent as aragonite (≤0.6 mol%). Marine organisms produce a wide range of δ^{26}Mg values from −5 to −1 ‰ that are species dependent (Hippler et al. 2009; Li et al. 2012). Since the extent of Mg substitution in $CaCO_3$ is temperature dependant, Mg/Ca ratios are used as a thermometer for oceanic temperatures. The Mg/Ca temperature dependence, however, does not play a major play in determining Mg isotope ratios, the observed variability can instead be attributed to mineralogy (Hippler et al. 2009). Mg isotope fractionations between carbonates and water follows the sequence aragonite < dolomite < magnesite < calcite (Saenger and Wang 2014).

Vital effects in low-Mg calcite organisms exhibit no clear temperature dependence affecting the Mg isotope composition (Wang et al. 2013a, b). Most recent benthic and planktonic foraminifera show nearly identical δ^{26}Mg ratios (Pogge von Strandmann 2008), making them suitable for investigating past isotopic variations of ocean water. Pogge von Strandmann et al. (2014) measured Mg isotopes from single-species planktonic foraminifera of the past 40 Ma and concluded that seawater Mg has changed from δ^{26}Mg of −0.83 ‰ at present to 0 ‰ at 15 Ma.

2.7.4.1 Cave Carbonates

Evidence for near equilibrium fractionation has been presented for low-Mg calcite speleothems (Galy et al. 2002). Mg isotope fractionation between speleothems and associated drip waters give a characteristic difference between both phases, which might indicate near equilibrium conditions. Buhl et al. (2007) argued that isotope equilibrium alone cannot explain the Mg isotope data from speleothems. Immenhauser et al. (2010) presented a complete data set of Mg isotopes on solid and liquid phases from a cave. They demonstrated that Mg isotope fractionations depend on a complex interplay of solution residence times, precipitation rates and adsorption effects.

2.7.5 Plants

Magnesium is an essential plant nutrient that is central to photosynthesis. Black et al. (2008) investigated the Mg isotope distribution in wheat and observed a slight enrichment of the whole plant in ^{25}Mg and ^{26}Mg relative to the nutrient solution. These results have been confirmed by Boulou-Bi et al. (2010). Most of the plant Mg is bound in leaves, but the decisive process for the enrichment of ^{26}Mg occurs at the root level. From roots to leaves or shoots a slight ^{26}Mg depletion is observed (Boulou-Bi et al. 2010).

Mg plays a fundamental role in the formation of chlorophyll, in which it is the central ion. The biological process linked to the incorporation of Mg into the chlorophyll molecule induces Mg isotope fractionation, the sign and size of isotope fractionations depend on species and environmental conditions (Black et al. 2006; Ra and Kitagawa 2007; Ra 2010). Ra (2010) observed a 2.4 ‰ ^{26}Mg variation in phytoplankton from different regions in the northwestern Pacific and related them to different growth rates and phytoplankton heterogeneities.

2.8 Silicon

Silicon has three stable isotopes with the following abundances (Rosman and Taylor 1998):

^{28}Si	92.23 %
^{29}Si	4.68 %
^{30}Si	3.09 %

Because of its high abundance on Earth, silicon is a very interesting element to be investigated for isotope variations. However, because there is no redox reaction, silicon is always bound to oxygen, relatively small isotope fractionations are to be expected in nature. Early investigations by Douthitt (1982) and more recent ones by Ding (1996) observed a total range of δ^{30}Si values in the order of 6 ‰. This range has extended to about 12 ‰ with the lowest δ^{30}Si value of −5.7 ‰ in siliceous cements (Basile-Doelsch et al. 2005) and the highest of +6.1 ‰ for rice grains (Ding et al. 2006).

Silicon isotope ratios have been generally measured by fluorination (Douthitt 1982; Ding 1996). However, the method is time consuming and potentially hazardous, therefore, more recently MC-ICP-MS techniques have been introduced (Cardinal et al. 2003; Engstrom 2006). Chmeleff et al. (2008) have shown that a UV-femtosecond laser ablation system coupled with MC-ICP-MS gives δ^{29}Si- and δ^{30}Si-values with very high precision. Determinations with SIMS have been carried out by Robert and Chaussidon (2006), Heck et al. (2011) and others. Independent of the method used, the standard generally is NBS-28 quartz. Figure 2.20 summarizes the naturally occurring silicon isotope variations.

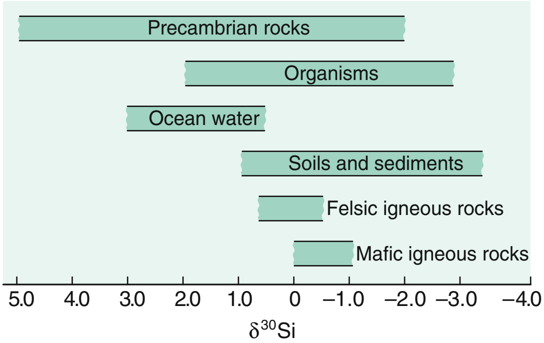

Fig. 2.20 δ^{30}Si-values of important geological reservoirs

2.8.1 High-Temperature Fractionations

A number of studies have estimated the δ^{30}Si-value of the bulk silicate earth as to be −0.29 ‰ (Fitoussi et al. 2009; Savage et al. 2010, 2014; Armytage et al. 2011; Zambardi et al. 2013). This value is identical with the Moon, but isotopically heavier than all types of meteorites. The difference is best explained by Si fractionation during earth's core formation. High pressure, high temperature experiments by Shahar et al. (2009) indicated a 2 ‰ fractionation between metal and silicate melts (see discussion on p. 211). Similar findings have been reported by Ziegler et al. (2010) by measuring silicon isotope fractionations between Si in metal and silicates in enstatite achondrites. Using a continuous accretion model, the Si isotope fractionation can be used to constrain the amount of Si that entered the Earth's core (Chakrabarti and Jacobsen 2010; Zambardi et al. 2013). Estimated percentages vary somewhat depending on model assumptions, but generally are between 6 and 12 %. However, as demonstrated by Huang et al. (2014), Si isotope fractionations decrease with increasing pressure, thus silicon isotope fractionations obtained experimentally at relatively low pressures may not be applicable to the high pressure conditions of core formation.

Huang et al. (2014) furthermore showed that equilibrium isotope fractionations among mantle minerals are negligible, but may become significant between minerals with different Si coordination numbers, such as Mg-perovskite in 6-coordination and olivine in 4-coordination.

No differences in Si isotope composition are observed between ultramafic rocks and basalts indicating no isotope fractionation during partial melting (Savage et al. 2014). As shown on rocks from the Hekla volcano, Iceland, magmatic differentiation may cause Si isotope fractionation (Savage et al. 2011). δ^{30}Si-values become progressively enriched with increasing SiO_2 contents.

Felsic rocks and minerals exhibit small, but systematic ^{30}Si variations increasing with the silicon contents of igneous rocks and minerals. The order of ^{30}Si enrichment in minerals is quartz, feldspar, muscovite and biotite, which is consistent with the order of ^{18}O enrichment. Thus felsic igneous rocks are slightly heavier than mafic igneous rocks.

2.8.2 Cherts

Silicon isotope ratios of quartzites and sandstones are in the range of felsic magmatic and metamorphic rocks reflecting their detrital derivation (Andre et al. 2006). In contrast, microcrystalline quartz from silcretes and clay minerals formed by weathering processes incorporate preferentially light Si isotopes relative to igneous minerals. A wide range of δ^{30}Si values from −0.8 to +5.0 ‰ have been reported for Precambrian cherts (Robert and Chaussidon 2006), much larger than for Phanerozoic cherts. These authors observed a positive correlation of δ^{18}O with δ^{30}Si values, which they interpreted as reflecting temperature changes in the ocean from about 70 °C

3.5 Ga to about 20 °C 0.8 Ga years ago. In contrast, cherts within BIFs exhibit largely negative δ^{30}Si-values from −2.5 to −0.5 ‰ (Andre et al. 2006; Van den Boorn et al. 2010; Steinhöfel et al. 2010) reflecting different sources of silica. These authors argued that variations in δ^{30}Si are best explained by mixing between hydrothermal fluids and seawater. Lamina-scale Si isotope heterogeneity within individual chert layers up to 2.2 ‰ may reflect the dynamics of hydrothermal systems.

2.8.3 Chemical Weathering and Mineral Precipitation

Considerable Si isotope fractionation takes place during chemical weathering (Ziegler et al. 2005; Basile-Doelsch et al. 2005; Georg et al. 2006; Cardinal et al. 2010; Opfergelt et al. 2012; Pogge von Strandmann et al. 2014). During dissolution of primary silicate minerals, silicon partitions in about equal proportions into the dissolved phase that is isotopically enriched and into solid secondary phases that are isotopically depleted (Ziegler et al. 2005a, b; Georg et al. 2007). Oelze et al. (2014) demonstrated that preferential adsorption of ^{28}Si on Al-hydroxides may be the cause for the light isotope signature of clay minerals.

Soil-clay mineral formation is, thus, responsible for high δ^{30}Si values of continental surface waters and ocean water. For the Yangtze river, Ding et al. (2004) measured a δ^{30}Si range from 0.7 to 3.4 ‰, whereas the suspended matter has a more constant composition from 0 to −0.7 ‰. For the Congo, Cardinal et al. (2010) measured low δ^{30}Si values close to zero ‰ for small tributaries rich in organic carbon ("black water") and high δ^{30}Si values close to 1 ‰ in large tributaries.

Georg et al. (2009) presented δ^{30}Si values of dissolved Si in groundwaters. Of special interest is the observation that δ^{30}Si decreases by about 2 ‰ along the groundwater flow path of 100 km deciphering complex Si-cycling, weathering and diagenetic reactions. Thus weathering processes can be regarded as one of the main fractionation mechanism separating silicon isotopes into an isotopically heavy dissolved phase and an isotopically light residue.

2.8.4 Fractionations in Ocean Water

Silicic acid is an important nutrient in the ocean that is required for the growth of mainly diatoms and radiolaria. Silicon incorporation into siliceous organisms is associated with Si isotope fractionation, because ^{28}Si is preferentially removed as the organisms form biogenic silica (de la Rocha et al. 1998, 2003, 2006; Reynolds et al. 2006; Hendry et al. 2010; Egan et al. 2012).

De la Rocha et al. (1997, 1998) observed a 1 ‰ fractionation between dissolved and biogenic silica during opal formation by marine diatoms that does not vary with temperature, at least not among the three species of diatoms investigated by de la Rocha. Varela et al. (2004) observed depletions in ^{30}Si between 1.1 and 1.9 ‰ independent of temperature, pCO_2 or species. Recent culture experiments on polar diatom species by Sutton et al. (2013), however, yielded species dependent fractionation with silicon isotope values from −0.5 to −2.1 ‰. An increase in opal formation by diatoms results in more positive δ^{30}Si-values, whereas a decrease results in more negative δ-values. In this manner variations in ^{30}Si contents of diatoms may provide information on changes of oceanic silicon cycling (De la Rocha et al. 1998).

In early studies it was assumed that dissolution of diatoms—the majority of biogenic silica produced in surface water dissolves before the particles have reached the ocean floor—does not fractionate Si isotopes. However, as shown by Demarest et al. (2009) dissolved silicon is ca 0.55 ‰ depleted in ^{30}Si relative to biogenic SiO_2. Thus dissolution acts in the opposite sense to production and reduces the net silicon fractionation considerably.

Diatoms as surface dwellers give a surface water signal only. Sponges, however, can be found throughout the water column. The δ^{30}Si of sponges is thus a potential proxy to quantify changes in oceanic Si concentrations (Hendry et al. 2010; Wille et al. 2010). As shown by these authors ^{30}Si fractionations during biosilification of sponges depends on silica concentrations in sea water with larger ^{30}Si depletions as silica concentrations increase. Thus, δ^{30}Si values of fossil silicified sponges may be used as a proxy for the reconstruction of palaeo Si-concentrations during the past (Hendry et al. 2010; Wille et al. 2010).

2.8.5 Plants

Silicon is an important element for vascular plants favouring growth. Silicon is taken up by terrestrial plants from soil solution, transported into the xylem and deposited as hydrated amorphous silica to form phytoliths that are restored to the soil by decomposition of plant material. Already Douthitt (1982) noted that Si uptake by plants leads to Si isotope fractionation. Plants preferentially incorporate the light Si isotopes; Si concentrations and δ^{30}Si-values increase from soil and roots through the stem and leaves. δ^{30}Si values range from 1.3 to 6.1 ‰ (Ding et al. 2005, 2008) with large interplant fractionations of 3.5 ‰ between low values in roots and high values in leaves and corn.

2.9 Sulfur

Sulfur has four stable isotopes with the following abundances (De Laeter et al. 2003).

$$
\begin{aligned}
{}^{32}\mathrm{S}: &\quad 95.04\,\% \\
{}^{33}\mathrm{S}: &\quad 0.75\,\% \\
{}^{34}\mathrm{S}: &\quad 4.20\,\% \\
{}^{36}\mathrm{S}: &\quad 0.01\,\%
\end{aligned}
$$

Fig. 2.21 δ^{34}S-values of important geological reservoirs (Fig. 2.20, 6th edition, p. 72)

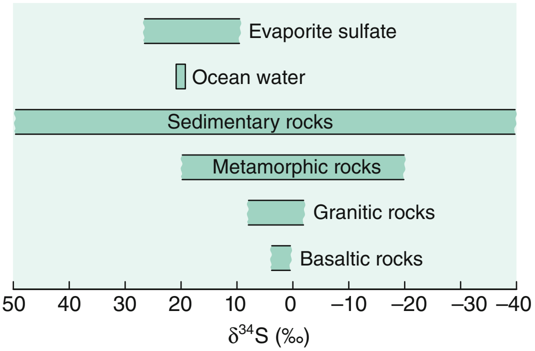

Sulfur is present in nearly all natural environments. It may be a major component in ore deposits, where sulfur is the dominant nonmetal, and as sulfates in evaporites. It occurs as a minor component in igneous and metamorphic rocks, throughout the biosphere in organic substances, in marine waters and sediments as both sulfide and sulfate. These occurrences cover the whole temperature range of geological interest. Thus, it is quite clear that sulfur is of special interest in stable isotope geochemistry.

Thode et al. (1949) and Trofimov (1949) were the first to observe wide variations in the abundances of sulfur isotopes. Variations on the order of 180 ‰ have been documented with the "heaviest" sulfates having δ^{34}S-values of greater than +120 ‰ (Hoefs, unpublished results), and the "lightest" sulfides having δ^{34}S-values of around −65 ‰. Some of the naturally occurring S-isotope variations are summarized in Fig. 2.21. Reviews of the isotope geochemistry of sulfur have been published by Rye and Ohmoto (1974), Nielsen (1979), Ohmoto and Rye (1979), Ohmoto (1986), Ohmoto and Goldhaber (1997), Seal et al. (2000), Canfield (2001a) and Seal (2006).

For many years the reference standard commonly referred to is sulfur from troilite of the Canyon Diablo iron meteorite (CDT). As Beaudoin et al. (1994) have pointed out, the original CDT is not homogeneous and may display variations in ^{34}S up to 0.4 ‰. Therefore a new reference scale, Vienna-CDT (V-CDT) has been introduced by an advisory committee of IAEA in 1993, recommending an artificially prepared Ag_2S (IAEA-S-1) with a $\delta^{34}S_{VCDT}$ of −0.3 ‰ as the new international standard reference material.

2.9.1 Methods

The gas conventionally used for gas-source mass-spectrometric measurement is SO_2. The introduction of on-line combustion methods (Giesemann et al. 1994) has reduced multistep off-line preparations to one single preparation step, namely the combustion in an elemental analyzer. Sample preparations have become less dependent on possibly fractionating wet-chemical extraction steps and less time-consuming, thereby reducing minimum sample gas to less than 1 mg.

Puchelt et al. (1971) and Rees (1978) first described a method using SF_6 instead of SO_2 which has some distinct advantages: it has no mass spectrometer memory effect and because fluorine is monoisotopic, no corrections of the raw data of measured isotope ratios are necessary. Comparison of δ^{34}S-values obtained using the conventional SO_2 and the laser SF_6 technique has raised serious questions about the reliability of the SO_2 correction for oxygen isobaric interferences (Beaudoin and Taylor 1994). Therefore the SF_6 technique has been revitalized (Hu et al. 2003), demonstrating that SF_6 is an ideal gas for measuring $^{33}S/^{32}S$, $^{34}S/^{32}S$ and $^{36}S/^{32}S$ ratios.

Microanalytical techniques such as laser microprobe (Kelley and Fallick 1990; Crowe et al. 1990; Hu et al. 2003; Ono et al. 2006) and ion microprobe (Chaussidon et al. 1987, 1989; Eldridge et al. 1988, 1993; Kozdon et al. 2010) have become promising tools for determining sulfur isotope ratios.

More recently the use of MC-ICP-MS techniques has been described by Craddock et al. (2008) and Paris et al. (2013). Amrani et al. (2009) developed a MC-ICP-MS method for the analysis of individual sulfur organic compounds. Due to low detection limits, sample sizes are orders of magnitude smaller than for SO_2 and SF_6. MC-ICP-MS requires no chemical pretreatment and allows for simultaneous collection of the individual 4 sulfur isotopes.

2.9.2 Fractionation Mechanisms

Two types of fractionation mechanisms are responsible for the naturally occurring sulfur isotope variations:

(a) Kinetic isotope effects during microbial processes. Micro-organisms have long been known to fractionate isotopes during their sulfur metabolism, particularly during dissimilatory sulfate reduction, which produces the largest fractionations in the sulfur cycle,

(b) Various chemical exchange reactions between both sulfate and sulfides and the different sulfides themselves.

2.9.2.1 Equilibrium Reactions

There have been a number of theoretical and experimental determinations of sulfur isotope fractionations between coexisting sulfide phases as a function of temperature. Theoretical studies of fractionations among sulfides have been undertaken by Sakai (1968) and Bachinski (1969), who reported reduced partition function ratios and bond strengths of sulfide minerals and described the relationship of these parameters to isotope fractionation. In a manner similar to that for oxygen in silicates, there is a relative ordering of ^{34}S-enrichment among coexisting sulfide minerals (Table 2.9). Considering the three most common sulfides (pyrite,

Table 2.9 Equilibrium isotope fractionation factors of sulfides with respect to H_2S

Mineral	Chemical composition	A
Pyrite	FeS_2	0.40
Sphalerite	ZnS	0.10
Pyrrhotite	FeS	0.10
Chalcopyrite	$CuFeS_2$	−0.05
Covellite	CuS	−0.40
Galena	PbS	−0.63
Chalcosite	Cu_2S	−0.75
Argentite	Ag_2S	−0.80

The temperature dependence is given by A/T^2 (after Ohmoto and Rye 1979)

sphalerite and galena) under conditions of isotope equilibrium, pyrite is always the most ^{34}S enriched mineral and galena the most ^{34}S depleted, sphalerite displays an intermediate enrichment in ^{34}S.

The experimental determinations of sulfur isotope fractionations between various sulfides do not exhibit good agreement. The most suitable mineral pair for temperature determination is the sphalerite—galena pair. Rye (1974) has argued that the Czamanske and Rye (1974) fractionation curve gives the best agreement with filling temperatures of fluid inclusions over the temperature range from 370 to 125 °C. By contrast, pyrite—galena pairs do not appear to be suitable for a temperature determination, because pyrite tends to precipitate over larger intervals of ore deposition than galena, implying that these two minerals may frequently not be contemporaneous. The equilibrium isotope fractionations for other sulfide pairs are generally so small that they are not useful as geothermometers. Ohmoto and Rye (1979) critically examined the available experimental data and presented a summary of what they believe to be the best S-isotope fractionation data. These S-isotope fractionations relative to H_2S are shown in Fig. 2.22.

Sulfur isotope temperatures from ore deposits often have been controversial; one of the reasons are strong ^{34}S zonations in sulfide minerals that have been observed by laser probe and ion probe measurements (McKibben and Riciputi 1998).

2.9.2.2 Dissimilatory Sulfate Reduction

Dissimilatory sulfate reduction is conducted by a large group of organisms (over 100 species are known so far, Canfield 2001a), that gain energy for their growth by reducing sulfate while oxidizing organic carbon (or H_2). Sulfate reducers are widely distributed in anoxic environments. They can tolerate temperatures from −1.5 to over 100 °C and salinities from fresh water to brines.

Since the early work with living cultures (Harrison and Thode 1957a, b; Kaplan and Rittenberg 1964) it is well known that sulfate reducing bacteria produce ^{32}S-depleted sulfide. Despite decades of intense research the factors that determine the magnitude of sulfur isotope fractionation during bacterial sulfate reduction are

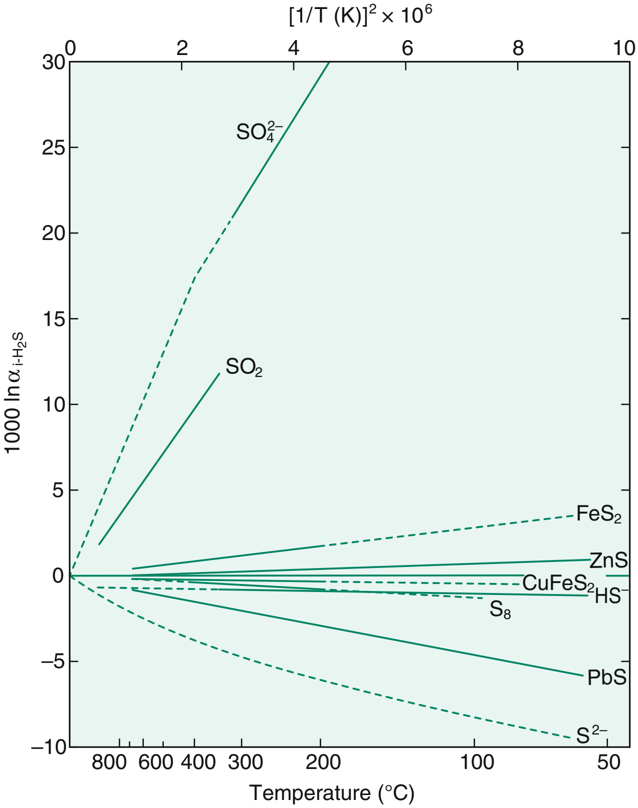

Fig. 2.22 Equilibrium fractionations among sulfur compounds relative to H_2S (*solid lines* experimentally determined, *dashed lines* extrapolated or theoretically calculated (after Ohmoto and Rye 1979) (Fig. 2.22, 6th edition, p. 78)

still under debate. The magnitude of isotope fractionation depends on the rate of sulfate reduction with the highest fractionation at low rates and the lowest fractionation at high rates. Kaplan and Rittenberg (1964) and Habicht and Canfield (1997) suggested that fractionations depend on the specific rate (cell^{-1} time$^{-1)}$ and not so much on absolute rates (volume^{-1} time $^{-1}$). What is clear, however, is that the rates of sulfate reduction are controlled by the availability of dissolved organic compounds. One parameter which remains unclear is sulfate concentration. While for instance Boudreau and Westrich (1984) argued that the concentration of sulfate becomes important at rather low concentrations (less than 15 % of the seawater value), Canfield (2001b) observed no influence of isotope fractionations on sulfate concentrations for natural populations. Another parameter, that has been assumed to be important is temperature insofar as it regulates in natural populations the sulfate-reducing community (Kaplan and Rittenberg 1964; Brüchert et al. 2001). Furthermore differences in fractionation with temperature relate to differences in the specific temperature response to internal enzyme kinetics as well as cellular properties and corresponding exchange rates of sulfate in and out of the cell of mesophilic sulfate reducing bacteria. Considering different types (including thermophilic) of sulfate-reducers, Canfield et al. (2006), however, found in contrast to earlier belief high fractionations in the low and high temperature range, but lowest fractionations in the intermediate temperature range.

The reaction chain during anaerobic sulfate reduction has been described in detail by Goldhaber and Kaplan (1974). In general, the rate-limiting step is the breaking of the first S–O bond, namely the reduction of sulfate to sulfite. Early laboratory studies with pure cultures of mesophilic sulfate reducing bacteria produced sulfide depleted in ^{34}S by 4 up to 47 ‰ (Harrison and Thode 1957a, b; Kaplan and Rittenberg 1964; Kemp and Thode 1968; McCready et al. 1974; McCready 1975; Bolliger et al. 2001) and for decades this maximum value was considered to be a possible limit for the microbial dissimilatory process (e.g. Canfield and Teske 1996). More recently, sulfur isotope fractionations have been determined from incubations with sediments containing natural populations covering a wide spectrum of environments (from rapidly metabolizing microbial mats to slowly metabolizing coastal sediments; Habicht and Canfield 1997, 2001; Canfield 2001a). Sim et al. (2011) found that the type of organic electron donor is essential in controlling the magnitude of sulfur isotope fractionations of pure culture sulfate reducing bacteria, with complex substrates leading to sulfur isotope discrimination exceeding 47 ‰.

Naturally occurring sulfides in sediments and euxinic waters are commonly depleted in ^{34}S by up to 70 ‰ (Jørgensen et al. 2004), covering the range of experiments with sulfate reducing bacteria (Sim et al. 2011). Recent studies have demonstrated that natural populations are able to fractionate S-isotopes by up to more than 70 ‰ under in situ conditions (Wortmann et al. 2001; Rudnicki et al. 2001; Canfield et al. 2010).

In marine sediments typically 90 % of the sulfide produced during sulfate reduction is reoxidized (Canfield and Teske 1996). The pathways of sulfide oxidation are poorly known, but include biological and abiological oxidation to sulfate, elemental sulfur and other intermediate compounds (Fry et al. 1988). Reoxidation of sulfide often occurs via compounds in which sulfur has intermediate oxidation states (sulfite, thiosulfate, elemental sulfur, polythionates) that do not accumulate, but are readily transformed and can be anaerobically disproportionated by bacteria. Therefore, Canfield and Thamdrup (1994) suggested that through a repeated cycle of sulfide oxidation to sulfur intermediates like elemental sulfur and subsequent disproportionation, bacteria can additionally generate ^{34}S depletions that may add on the isotopic composition of marine sulfides.

Another factor that is of great importance for the preserved sulfur isotope signatures of natural sulfides is whether sulfate reduction took place in a system open or closed with respect to dissolved sulfate. An “open” system has an infinite reservoir of sulfate in which continuous removal from the source produces no detectable loss of material. Typical examples are the Black Sea and local oceanic deeps. In such cases, H_2S is extremely depleted in ^{34}S while consumption and

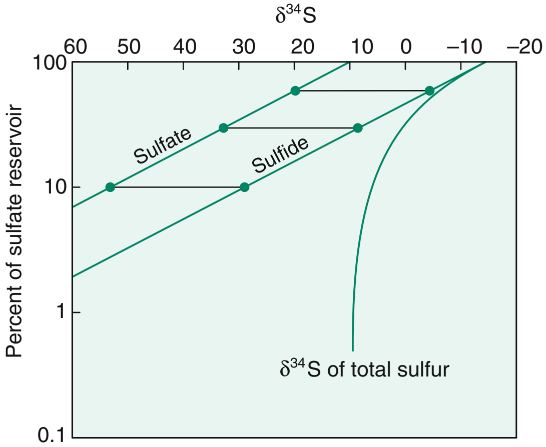

Fig. 2.23 Rayleigh plot for sulfur isotope fractionations during reduction of sulfate in a closed system. Assumed fractionation factor 1.025, assumed composition of initial sulfate: +10 ‰) (Fig. 2.21, 6th edition, p. 75)

change in ^{34}S remain negligible for the sulfate (Neretin et al. 2003). In a "closed" system, the preferential loss of the lighter isotope from the reservoir has a feedback on the isotopic composition of the unreacted source material. The changes in the ^{34}S-content of residual sulfate and of the H_2S are modeled in Fig. 2.23, which shows that $\delta^{34}S$-values of the residual sulfate steadily increase with sulfate consumption (a linear relationship on the log-normal plot). The curve for the derivative H_2S is parallel to the sulfate curve at a distance which depends on the magnitude of the fractionation factor. As shown in Fig. 2.23, H_2S may become isotopically heavier than the original sulfate when about 2/3 of the reservoir has been consumed. The $\delta^{34}S$-curve for "total" sulfide asymptotically approaches the initial value of the original sulfate. It should be noted, however, that apparent "closed-system" behavior of covarying sulfate and sulfide $\delta^{34}S$-values might be also explained by "open-system" differential diffusion of the different sulfur isotope species (Jǿrgensen et al. 2004).

Finally it should be mentioned that sulfate is labeled with two biogeochemical isotope systems, sulfur and oxygen. Coupled isotope fractionations of both sulfur and oxygen isotopes have been investigated in experiments (Mizutani and Rafter 1973; Böttcher et al. 2001) and in naturally occurring sediments and aquifers (Fritz et al. 1989; Böttcher et al. 1989; Ku et al. 1999; Aharon and Fu 2000; Wortmann et al. 2001). Böttcher et al. (1998) and Brunner et al. (2005) argued that a characteristic $\delta^{34}S$–$\delta^{18}O$ fractionation slope does not exist, but that the isotope covariations depend on cell-specific sulfate reduction rates and associated oxygen isotope exchange rates with cellular water. Despite the extremely slow oxygen isotope exchange of sulfate with ambient water, $\delta^{18}O$ in sulfate obviously depend on the $\delta^{18}O$ of water via an exchange of sulfite with water. Böttcher et al. (1998) and Antler et al. (2013) demonstrated how the fractionation slopes depend on the net sulfate reduction rate: higher rates result in a lower slope meaning that sulfur isotopes increase faster relative to oxygen isotopes. The critical parameter for the evolution of oxygen and sulfur isotopes in sulfate is the relative difference in rates of sulfate reduction and of intracellular sulfite oxidation.

Recently, Bao (2015) has discussed the triple oxygen isotope composition of sedimentary sulfates, demonstrating that sulfate carries direct signals of ancient atmospheric O_2 and O_3.

2.9.2.3 Thermochemical Reduction of Sulfate

In contrast to bacterial reduction, thermochemical sulfate reduction is an abiotic process with sulfate being reduced to sulfide under the influence of heat rather than bacteria (Trudinger et al. 1985; Krouse et al. 1988). The crucial question, which has been the subject of a controversial debate, is whether thermochemical sulfate reduction can proceed at temperatures as low as about 100 °C, just above the limit of microbiological reduction (Trudinger et al. 1985). There is increasing evidence from natural occurrences that the reduction of aqueous sulfates by organic compounds can occur at temperatures as low as 100 °C, given enough time for the reduction to proceed (Krouse et al. 1988; Machel et al. 1995). S isotope fractionations during thermochemical reduction generally should be smaller than during bacterial sulfate reduction, although experiments by Kiyosu and Krouse (1990) have indicated S-isotope fractionations of 10–20 ‰ in the temperature range of 200–100 °C.

To summarize, bacterial sulfate reduction is characterized by large and heterogeneous ^{34}S-depletions over very small spatial scales, whereas thermogenic sulfate reduction leads to smaller and “more homogeneous” ^{34}S-depletions.

2.9.3 Quadruple Sulfur Isotopes

With respect to quadruple S isotope investigations, a distinction has to be made between large mass-independent S isotope fractionations observed in Archean sulfides and sulfates (Farquhar et al. 2000 and following papers) and much smaller mass-dependent S fractionations being characteristic for biosynthetic pathways. (Farquhar et al. 2003; Johnston 2011; Johnston et al. 2005; Ono et al. 2006, 2007). For long it was thought δ^{33}S and δ^{36}S values carry no additional information, because sulfur isotope fractionations follow strictly mass-dependent fractionation laws. By studying all sulfur isotopes with very high precision, it was demonstrated that bacterial sulfate reduction follows a mass-dependent relationship that is slightly different from that expected by equilibrium fractionations. On plots Δ^{33}S versus δ^{34}S, mixing of two sulfur reservoirs is non-linear in these coordinates (Young et al. 2002). As a result samples with the same δ^{34}S-value can have different Δ^{33}S and Δ^{36}S values. This opens the possibility to distinguish between different fractionation mechanisms and biosynthetic pathways, even when δ^{34}S fractionations are identical (Ono et al. 2006, 2007). Bacterial sulfate reduction shows slightly different fractionation relationships compared to sulfur disproportionation reactions. For instance, multiple S-isotope measurements of 1.8 Ga sulfates indicate the earliest initiation of microbial S disproportionation (Johnston et al. 2005). In another example, Canfield et al. (2010) demonstrated that S-isotope systematics in an euxinic lake in Switzerland clearly favour microbial reduction as the only reduction pathway. Thus multiple sulfur isotope analyses have great potential in identifying the presence or absence of specific metabolisms in modern environment or may represent a proxy when a particular sulfur metabolism develops in the geologic record.

Large independent S isotope fractionations observed in Archean sulfides and sulfates are a distinctive feature of sedimentary rocks older than 2.4 Ga. It is generally agreed that they indicate the near absence of O_2 and the presence of a reducing gas (likely CH_4 and/or H_2) in the Archean atmosphere. The geologic record of $\Delta^{33}S$ is shown in Fig. 2.24, which is characterized by time dependent magnitudes and signs of MIF-S indicating a temporal structure: ≤4 ‰ $\Delta^{33}S$ anomalies in early Archean sulfides, even smaller variations in the mid Archean and very large (≈12 ‰) variations in late Archean (see Fig. 2.24). The record of large magnitude $\Delta^{33}S$ values for sulfides terminates abruptly at approximately 2.4 Ga. Besides $\Delta^{33}S$, $\Delta^{36}S$ records also have received a great deal of attention, demonstrating that $\Delta^{36}S$ is preferentially negative down to values lower than −8 ‰.

Experiments that have verified the large $\Delta^{33}S$ and $\Delta^{36}S$ values in the Archean geologic record involve gaseous SO_2 (Farquhar et al. 2000; Claire et al. 2014). The specific chemical reaction that produced the effect observed in Archean samples is unknown, but gas phase reactions involving SO_2 are likely candidates. Farquhar and Wing (2003) and others demonstrated that photolysis of atmospheric SO_2 produces mass-independent S isotope fractionations, if atmospheric O_2 concentrations are very

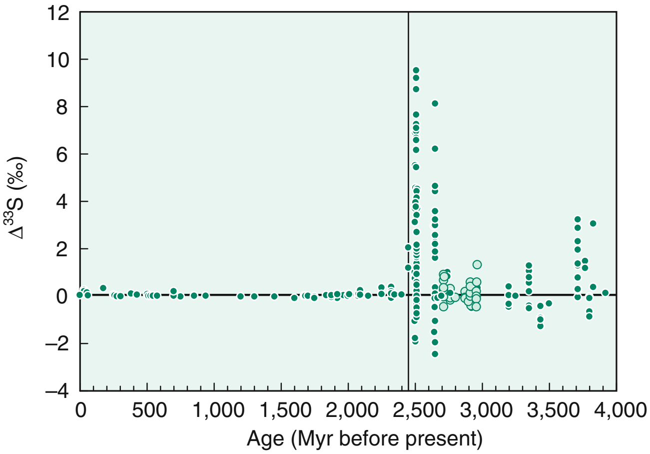

Fig. 2.24 Compilation of $\Delta^{33}S$ versus age for rock samples. Note large $\Delta^{33}S$ before 2.45 Ga, indicated by *vertical line*, small but measurable $\Delta^{33}S$ after 2.45 Ga (Farquahar et al. 2007) (Fig. 3.29, 6th edition, p. 167)

low. The majority of $\Delta^{33}S$ and $\Delta^{36}S$ values scatter around zero, but displays greater variability when $\Delta^{33}S$ and $\Delta^{36}S$ are large. Farquhar et al. (2007) and Halevy et al. (2010) attributed these variations to changes in the composition and oxidation state of volcanic sulfur gases. $\Delta^{33}S/\Delta^{36}S$ ratios in Archean samples and in products of laboratory photochemical experiments yield characteristic slopes which may be used as fingerprints (Farquhar et al. 2013).

2.10 Chlorine

Chlorine has two stable isotopes with the following abundances (Coplen et al. 2002):

^{35}Cl 75.78 %
^{37}Cl 24.22 %

Natural isotope variations in chlorine isotope ratios might be expected due to the mass difference between ^{35}Cl and ^{37}Cl as well as to variations in coordination of chlorine in the vapor, aqueous and solid phases. Schauble et al. (2003) calculated equilibrium fractionation factors for some geochemically important species. They showed that the magnitude of fractionations systematically varies with the oxidation state of Cl, but also depends on the oxidation state of elements to which Cl is bound with larger fractionations for 2+ cations than for 1+ cations. Chlorine in silicates appears to be enriched compared to coexisting brines; organic molecules are enriched relative to dissolved Cl^-.

2.10.1 Methods

Measurements of Cl-isotope abundances have been made by different techniques. The first measurements by Hoering and Parker (1961) used gaseous chlorine in the form of HCl. The 81 samples measured exhibited no significant variations relative to the standard ocean chloride. In the early eighties a new technique has been developed by Kaufmann et al. (1984), that uses methylchloride (CH_3Cl). The chloride-containing sample is precipitated as AgCl, reacted with excess methyliodide, and separated by gas chromatography. The total analytical precision reported is near ±0.1 ‰ (Long et al. 1993; Eggenkamp 1994; Sharp et al. 2007). The technique requires relatively large quantities of chlorine (>1 mg), which precludes the analysis of materials with low chlorine concentrations. Magenheim et al. (1994) described a method involving the thermal ionization of Cs_2Cl^+, which, as argued by Sharp et al. (2007), is very sensitive to analytical artefacts and therefore might lead to erroneous results. In any case both methods are laborintensive and rely on offline chemical conversion reactions. Recent attempts use continuous flow mass-spectrometry (Shouakar-Stash et al. 2005) or use MC-ICPMS techniques (Van Acker et al. 2006).

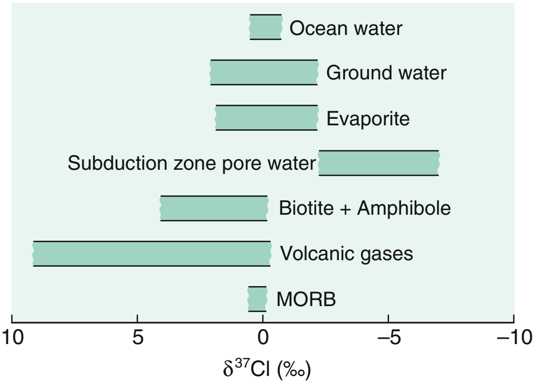

Fig. 2.25 δ^{37}Cl values of important geological reservoirs

δ-values are generally given relative to seawater chloride termed SMOC (Standard Mean Ocean Chloride). Knowledge about chlorine isotope geochemistry has been summarized in a recent book by Eggenkamp (2014). A summary of the observed natural chlorine isotope variations is presented in Fig. 2.25. Ransom et al. (1995) gave a natural variation range in chlorine isotope composition of about 15 ‰ with subduction zone pore waters having δ^{37}Cl values as low as −8 ‰ whereas minerals in which Cl substitutes OH have δ^{37}Cl values as high as 7 ‰.

2.10.2 Hydrosphere

Chloride (Cl^-) is the major anion in surface- and mantle-derived fluids. It is the most abundant anion in ocean water and in hydrothermal solutions and is the dominant metal complexing agent in ore forming environments (Banks et al. 2000). Despite its variable occurrence, chlorine isotope variations in natural waters commonly are small and close to the chlorine isotope composition of the ocean. This is also true for chlorine from fluid inclusions in hydrothermal minerals which indicate no significant differences between different types of ore deposits such as Mississippi-Valley and Porphyry Copper type deposits (Eastoe et al. 1989; Eastoe and Gilbert 1992).

Relatively large isotopic differences have been found in slow flowing groundwater, where Cl-isotope fractionation is attributed to a diffusion process (Kaufmann et al. 1984; Desaulniers et al. 1986; Kaufmann et al. 1986). Desaulniers et al. (1986) for instance investigated a ground water system, in which chloride diffused upward from saline into fresh water deposits by demonstrating that ^{35}Cl moved about 1.2 ‰ faster than ^{37}Cl.

Cl isotope fractionations between salt minerals and brine have been determined by Eggenkamp et al. (1995), Eastoe et al. (1999, 2007). Halites are enriched by 0.3 ‰ relative to the brine, whereas potassium and magnesium chloride show more or less no fractionation relative to the brine. ^{37}Cl depletions detected in some pore waters have been attributed to processes such as ion filtration, alteration and dehydration reactions and clay mineral formation (Long et al. 1993; Eggenkamp 1994; Eastoe et al. 2001; Hesse et al. 2006). A pronounced downward depletion of −4 ‰ in pore waters has been presented by Hesse et al. (2006). Even lower δ^{37}Cl-values have been reported in pore waters from subduction-zone environments (Ransom et al. 1995; Spivack et al. 2002). The downward depletion trend might be explained by mixing of shallow ocean water with a deep low ^{37}Cl fluid of unknown origin.

2.10.3 Mantle-Derived Rocks

Controversial results have been reported for chlorine isotopes in mantle-derived rocks. According to Magenheim et al. (1995) δ^{37}Cl-values for MORB glasses show a surprisingly large range. By questioning the findings of Magenheim et al. (1995), Sharp et al. (2007) argued that the mantle and the crust have very similar isotopic composition. A possible explanation for this apparent discrepancy might be related to analytical artifacts of the TIMS technique (Sharp et al. 2007). Bonifacie et al. (2008) also observed small Cl-isotope variations only in mantle derived rocks. They demonstrated that δ^{37}Cl values correlate with chlorine concentrations: Cl-poor basalts have low δ^{37}Cl values representing the composition of uncontaminated mantle derived magmas, whereas Cl-rich basalts are enriched in ^{37}Cl being contaminated by ocean water. In contrast to MORB, John et al. (2010) observed with the SIMS technique larger δ^{37}Cl variations in OIB glasses which they interpreted as being due to subducting sediments that have developed high δ^{37}Cl-values by expelling ^{37}Cl depleted pore fluids.

Barnes et al. (2009) have investigated the serpentinization process in the oceanic lithosphere and interpreted chlorine isotope data to reflect a record of multiple fluid events. Slightly positive δ^{37}Cl-values represent typical seawater-hydration conditions under low temperature conditions, negative δ^{37}Cl-values result from interaction with porefluids from overlying sediments.

Volcanic gases and associated hydrothermal waters have a large range in δ^{37}Cl-values from –2 to +12 ‰ (Barnes et al. 2006). To evaluate chlorine isotope fractionations in volcanic systems, HCl liquid-vapor experiments performed by Sharp (2006) yield large isotope fractionations of dilute HCl at 100 °C. ^{37}Cl enrichments in fumaroles seem to be due to isotope fractionations between between Cl^- in aquatic solution and HCl gas.

Very interesting results have been reported by Sharp et al. (2010) on lunar basalts showing a very large range in δ^{37}Cl-values from −1 to +24 ‰ that have been interpreted to reflect conditions or processes on Moon that do not exist on Earth.

2.10.4 Applications in the Environment

Chlorine isotope studies have been performed to understand the environmental chemistry of anthropogenic organic compounds, such as chlorinated organic solvents or biphenyls. The primary goal of such studies is to identify and quantify sources and biodegradation processes in the environment. To do this successfully, chorine isotope values should differ among compounds and manufacturers and indeed the range of reported δ^{37}Cl-values is from about –5 to +6 ‰ with distinct signatures from different suppliers (van Warmerdam et al. 1995; Jendrzewski et al. 2001).

Perchlorate is another anthropogenic compound, which may contaminate surface and ground waters. The widespread occurrence of perchlorate in the environment makes it necessary to distinguish between a synthetic or a natural origin (Böhlke et al. 2005). The occurrence of natural perchlorate is limited to extremely dry environments, such as the Atacama desert. Synthetic perchlorate is produced by electrolyte oxidation reactions, whereas natural perchlorate is formed by photochemical reactions involving atmospheric ozone. Böhlke et al. (2005) showed that natural perchlorate have the lowest δ^{37}Cl-values on Earth, whereas synthetic perchlorate has more "normal" δ^{37}Cl-values. During microbial reduction of perchlorate, large kinetic isotope effects have been observed by Sturchio et al. (2003) and Ader et al. (2008), which may document in situ bioremediation.

2.11 Calcium

Calcium has six stable isotopes in the mass range of 40–48 with the following abundances (Taylor and Rosman 1998).

$$
\begin{aligned}
{}^{40}\mathrm{Ca}: &\quad 96.94\,\% \\
{}^{42}\mathrm{Ca}: &\quad 0.647\,\% \\
{}^{43}\mathrm{Ca}: &\quad 0.135\,\% \\
{}^{44}\mathrm{Ca}: &\quad 2.08\,\% \\
{}^{46}\mathrm{Ca}: &\quad 0.004\,\% \\
{}^{48}\mathrm{Ca}: &\quad 0.187\,\%
\end{aligned}
$$

Calcium plays an essential role in biological processes such as the calcification of organisms, and the formation of bones. Its wide natural distribution and the large relative mass difference suggest a large isotope fractionation, which may be caused by mass-dependent fractionations and by radiogenic growth (radioactive decay of ^{40}K to ^{40}Ca, half life of about 1.3 Ga). Felsic Archean rocks with high K/Ca ratios, thus, should show a relative enrichment of ^{40}Ca and, indeed, as demonstrated by Caro et al. (2010), Archean K-rich, Ca-poor rocks show enlarged ^{44}Ca/^{40}Ca variations.

2.11.1 Analytical Techniques

Early studies on natural Ca isotope variations found no differences or ambigous results. By using a double-spike technique and by using a mass-dependent law for

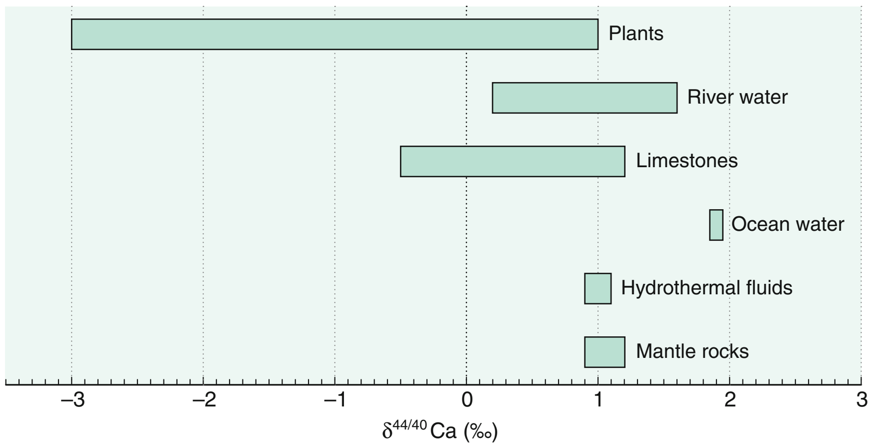

Fig. 2.26 $\delta^{44/40}$Ca-values of important geological reservoirs

correction of instrumental mass fractionation, Russell et al. (1978) were the first to demonstrate that differences in the ^{44}Ca/^{40}Ca ratio are clearly resolvable to a level of 0.5 ‰. More recent investigations by Skulan et al. (1997) and by Zhu and MacDougall (1998), also using the TIMS technique, have improved the precision to about 0.1–0.15 ‰.

MC-ICP-MS techniques have been described by Halicz et al. (1999) using a “hot plasma” and by Fietzke et al. (2004) using a “cool plasma”. SIMS techniques with high spatial resolution and uncertainties of about 0.3 ‰ have been developed by Rollion-Bard et al. (2007) and Kasemann et al. (2008).

Comparing data obtained with different methods and from different laboratories, complications may arise from the use of different δ-values, either $\delta^{44/40}$ or $\delta^{44/42}$, and from the use of different standards. By initiating a laboratory exchange of internal standards, Eisenhauer et al. (2004) have suggested to use NIST SRM 915a as international standard. As the original SRM 915a is not any more available, SRM 915a has been replaced by SRM 915b which is 0.72 ‰ heavier than SRM 915a (Heuser and Eisenhauer 2008). In the following all data are given as $\delta^{44/40}$Ca-values. As shown in reviews by DePaolo (2004), Nielsen et al. (2011a, b, c) and Fantle and Tipper (2014), the natural variation range in $\delta^{44/40}$Ca-values is about 5 ‰. Figure 2.26 shows natural Ca-isotope variations of important geological reservoirs.

2.11.2 High Temperature Fractionations

Calcium as a lithophile element does not partition into planetary cores, therefore Ca isotopes may reveal genetic links between Earth and meteorites. According to Simon and de Paolo, (2010) and Valdes et al. (2014), Earth, Moon, Mars and differentiated asteroids are indistinguishable from ordinary chondrites, whereas enstatite chondrites are slightly enriched in heavier Ca isotopes and carbonaceous chondrites are variably depleted in heavier Ca isotopes. Ca isotopes, thus suggest that ordinary chondrites are representative for the material that formed the terrestrial planets.

Huang et al. (2010) and Chen et al. (2014) analysed a suite of terrestrial mantle xenoliths, ocean island basalts, komatiites and carbonatites. Mantle xenoliths vary by about 0.5 ‰ indicating that the mantle is heterogeneous in Ca isotope composition. Ocean island basalts are on average 0.2 ‰ lighter than mantle xenoliths suggesting Ca isotope fractionation during partial melting. During fractional crystallization very limited Ca isotope fractionation seems to occur.

Huang et al. (2010) measured the Ca isotope composition of coexisting clino- and orthopyroxene in mantle peridotites. δ^{44}Ca-values of orthopyroxene are about 0.5 ‰ heavier than clinopyroxene. First principles calculations by Feng et al. (2014) reached very similar conclusions. Combined with data from low-temperature Ca-minerals, Huang et al. (2010) inferred that inter-mineral fractionations are controlled by Ca–O bond strengths. Thus, the Ca-mineral with a shorter Ca–O bond yields a heavier δ^{44}Ca-value. Furthermore, these authors estimated that the upper mantle has an average Ca isotope composition slightly higher than the average for basalts. In Hawaiian tholeiites, Huang et al. (2011) observed a 0.3 ‰ variation in ^{44}Ca/^{40}Ca ratios, which they attributed to recycling of carbonates into the mantle. Besides inter-mineral equilibrium fractionations, high temperature diffusion processes may also affect Ca-isotope fractionations (Richter et al. 2003).

2.11.3 Weathering

Chemical weathering of silicates controls long-term atmospheric CO_2 concentrations coupling the cycles of carbon and calcium. Dissolution of silicates and carbonates does not strongly fractionate Ca isotopes (Fantle and Tipper 2014). Ca ions released during dissolution may be taken up by vegetation, may precipitate as secondary minerals or can be absorbed by clays, oxyhydroxides and humic acids. As shown by Ockert et al. (2013), the absorption of Ca^{2+} on clay minerals favors light Ca isotopes over heavy ones. The largest Ca isotope fractionation in the weathering environment, however, is the uptake by plants.

Ca isotope analysis of rivers represents another approach to identify weathering processes (Tipper et al. 2008, 2010; Fantle and Tipper 2014). From an extensive data compilation, Fantle and Tipper (2014) concluded that the average Ca isotope value of carbonates is 0.60 ‰, whereas average river water has a value of 0.88 ‰ and silicates a value of 0.94 ‰. Since most of the Ca in river water originates from the the dissolution of carbonates and not from silicates, the Ca isotope difference between carbonates and rivers remain unexplained.

2.11.4 Fractionations During Carbonate Precipitation

Calcium carbonates that precipitate from aqueos solutions do not form at isotope equilibrium (DePaolo 2011). Marine carbonates are isotopically depleted in ^{44}Ca relative to seawater (Skulan et al. 1997; Zhu and MacDougall 1998). Experiments on inorganic precipitation of calcite and aragonite (Marriott et al. 2004; Gussone et al. 2003) have demonstrated that Ca isotope fractionation correlates with temperature with an offset of aragonite of about −0.5 ‰ relative to calcite. During biogenic precipitation, the Ca isotope composition of shells depend on the chemistry of the solution, in which the organisms live and on the process by which Ca is precipitated (Griffith et al. 2008a, b, c). Calcification processes differ among different types of organisms: foraminifera precipitate carbonate in vacuoles from pH-modified seawater, corals pump seawater through various tissues to the site of precipitation. Each step in these processes may cause differences in Ca isotope fractionation.

The magnitude of Ca isotope fractionation during biogenic carbonate precipitation as well as the mechanism—either isotope equilibrium or kinetic effects—remain a matter of debate. Studies by Nägler et al. (2000), Gussone et al. (2005) and Hippler et al. (2006) reported temperature dependent Ca isotope fractionations precipitated in natural environments or under cultured laboratory conditions with a slope of about 0.02 ‰/°C. Temperature dependent fractionations, however, have not been found in all shell secreting organisms (Lemarchand et al. 2004; Sime et al. 2005). Sime et al. (2005) analyzed 12 species of foraminifera and found negligible temperature dependence for all 12 species. These contradictory results indicate a complex physiological control on Ca uptake by calcifying organisms (Eisenhauer et al. 2009).

In the case of dolomite, Holmden (2009) observed a 0.6 ‰ difference between dolomite and its precursor limestone. Gypsum also preferentially incorporates light Ca compared to dissolved Ca (Harouaka et al. 2014).

2.11.5 Variations with Geologic Time

Zhu and MacDougall (1998) have made the first attempt to investigate the global Ca cycle. They found a homogeneous isotope composition of the ocean, but distinct isotope differences of the sources and sinks and suggested that the ocean is not in steady state. The marine Ca-cycle is characterized by inputs from hydrothermal fluids at oceanic ridge systems and from dissolved Ca delivered by continental weathering and by output through $CaCO_3$ precipitation, the latter causing the main Ca isotope fractionation. Dissolution of silicate and carbonate rocks during weathering does not strongly fractionate Ca isotopes (Hindshaw et al. 2011). Ca dissolved in rivers shows a very narrow range in Ca isotope composition that is close to the average Ca isotope composition of limestones (Tipper et al. 2010). Hydrothermal solutions to the ocean at ocean ridges are about 1 ‰ depleted in $\delta^{44/40}$Ca values relative to seawater (Amini et al. 2008).

Since the first study of Zhu and MacDougall (1998), several studies have investigated secular changes in the Ca isotope composition of the ocean: De La Rocha and de Paolo (2000b), Fantle and de Paolo (2005) and Fantle (2010) for the Neogene, Steuber and Buhl (2006) for the Cretaceous; Farkas et al. (2007) for the late Mesozoic; and Kasemann et al. (2005a, b) for the Neoproterozoic. Model simulations of the Ca cycle by Farkas et al. (2007) indicated that the observed Ca isotope variations can be produced by variable Ca input fluxes to the oceans. Maximum measured temporal variations in selected age periods are around 1 ‰ in $^{44/40}$Ca isotope ratios (see also p. 268 about ocean water history).

High resolution records with 0.3 ‰ excursions for the Permian-Triassic boundary from southern China have been reported by Payne et al. (2010) and by Hinojosa et al. (2012). Shifts in isotope composition could be due to changes in mineralogy (i.e. calcite/aragonite) or to a change in ocean pH-values. By comparing δ^{44}Ca-values of conodont apatite with coexisting carbonates, Hinojosa et al. (2012) found a comparable shift in apatite, which argues against a shift in mineralogy, but favors an episode of ocean acidification.

In this context, it is interesting to note, that Griffith et al. (2008a, b, c, 2011) proposed that pelagic barite, containing about 400 ppm Ca, might be an additional recorder of Ca seawater isotope composition through time showing an offset of about 2 ‰ from seawater.

2.11.6 Ca in Plants, Animals and Humans

Vegetation shows the widest range in Ca isotope values, which is larger than variations caused by carbonate precipitation. Studies on higher plants by Page et al. (2008), Wiegand et al. (2005) and Holmden and Belanger (2010) demonstrated systematic Ca isotope fractionations between roots, stemwood and leaves: fine roots yield the lowest δ^{44}Ca-values, stemwood are intermediate and leaves have the highest δ-values. Overall variation in ^{44}Ca values from bottom to top in trees is about 0.8 ‰ (Cenki-Tok et al. 2009; Holmden and Belanger 2010). The magnitude of Ca isotope fractionation depends on species and on season (Hindshaw et al. 2013). The preferential uptake of light Ca-isotopes into plants results in an enrichment of Ca in soil solutions. Thus vegetation controls the Ca isotope composition of soil pools (Cenki-Tok et al. 2009).

Experiments under controlled plant growth conditions allow the identification of 3 different Ca isotope fractionation steps (Cobert et al. 2011; Schmitt et al. 2013): (i) preferential ^{40}Ca uptake in the roots, (ii) preferential adsorption of ^{40}Ca on the cell walls during transfer from the roots to the leaves, (iii) additional ^{40}Ca fractionation in the storage organs, which seems to be controlled by the physiology of the plant.

Ca isotope measurements of diet, soft tissues and bone show that bone is considerably lighter than soft tissue and diet. As much as 4 ‰ variation in ^{44}Ca/^{40}Ca ratios is observed in single organisms (Skulan and DePaolo 1999). Ca isotopes of bone apatite in animals suggest that Ca isotope composition gets increasingly light as trophic levels increases. Reynard et al. (2010) reported Ca isotope data of modern and archaeological animal and human bones. Sheep at the same location show higher Ca isotope ratios in females than in males which is attributed to lactation by females. Reynard et al. (2010) further demonstrated that human bones are lighter than the local fauna.

2.12 Vanadium

Vanadium has two stable isotopes

^{50}V	0.24 %
^{51}V	99.76 %

Since vanadium exists in four valence states (2^+, 3^+, 4^+, 5^+), it is highly sensitive to reduction-oxidation reactions potentially inducing isotope fractionations.

Nielsen et al. (2011a, b, c) and Prytulak et al. (2011) described a precise MC-ICP-MS technique and reported a δ^{51}V isotope variation of 1.2 ‰ for various reference samples. Nielsen et al. (2014) demonstrated that V in the silicate earth is 0.8 ‰ enriched relative to carbonaceous and ordinary chondrites. Although the cause for the enrichment is unknown, Nielsen et al. (2014) postulated that bulk Earth cannot be entirely reconstructed by mixing chondritic meteorites in various proportions. Prytulak et al. (2013) observed a 1 ‰ variation in mafic and ultramafic rocks. Secondary alteration reactions do not appear to induce V isotope fractionations, therefore, V isotopes have the potential to indicate the oxidation state of ancient mantle.

V is enriched in organic matter, especially in crude oils. The analysis of V isotopes in crude oils potentially should be an interesting tool for petroleum geologists. Future vanadium isotope studies certainly will give a more detailed picture of V isotope fractionations.

2.13 Chromium

Chromium has 4 stable isotopes with the following abundances (Rosman and Taylor 1998)

^{50}Cr	4.35 %
^{52}Cr	83.79 %
^{53}Cr	9.50 %
^{54}Cr	2.36 %

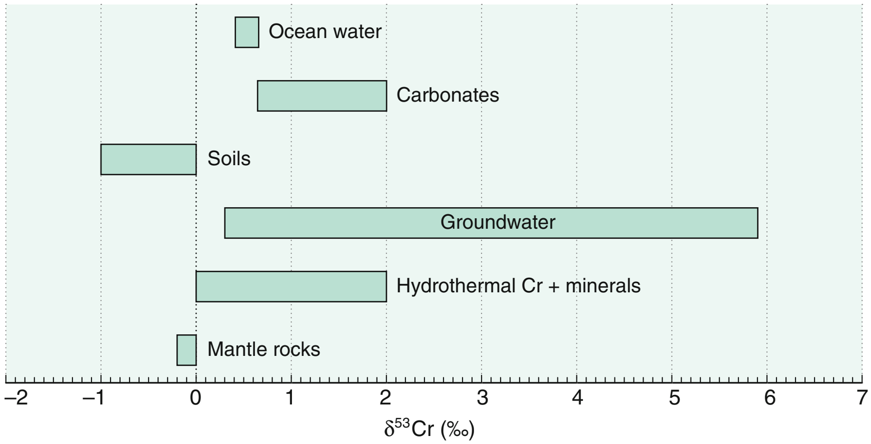

Fig. 2.27 δ^{53}Cr-values of important geological reservoirs

Chromium exists in two oxidation states, Cr(III) as a cation Cr^{3+}, and Cr(VI), as an oxyanion (CrO_4^{2-} or $HCrO_4^{-}$) having different chemical behaviors: Cr^{3+} is the dominant form in most minerals and in water under reducing conditions, whereas Cr(VI) is stable under oxidizing conditions. Cr(VI) in chromate is highly soluble, mobile and toxic, whereas trivalent chromium, existing as a cation, is largely insoluble and immobile. These properties make Cr isotope investigations very suitable to detect and quantify redox changes in different geochemical reservoirs.

Equilibrium isotope fractionations between Cr(VI) and Cr (III) have been estimated by Schauble et al. (2004), who predicted Cr isotope fractionations >1 ‰ between Cr species with different oxidation states. At 0 °C, Cr isotope fractionations between CrO_4^{2-} and $Cr(H_2O)_6^{3+}$ complexes have been calculated to be 7 ‰ with chromate being enriched in ^{53}Cr. However, since isotope equilibration between Cr(VI) and Cr(III) species at low temperatures is slow (Zink et al. 2010), it appears that isotope disequilibrium between Cr-species is common and, therefore, natural Cr isotope fractionations probably are kinetically controlled. Cr isotope variations are measured generally with MC-ICP-MS techniques (Halicz et al. 2008a, b; Schoenberg et al. 2008), $\delta^{53/52}$Cr-values are given relative to the NIST SRM 979 standard. Figure 2.27 summarizes average Cr-isotope compositions in important reservoirs.

2.13.1 Mantle Rocks

Mantle xenoliths and ultramafic cumulates have, as first shown by Schoenberg et al. (2008), a δ^{53}Cr-value of −0.12 ‰ relative to the certified Cr standard NIST SRM 979 being 0.4 ‰ heavier than various chondritic meteorites (Moynier et al. 2011). The enrichment of the Earth relative to meteorites may be explained by preferential partitioning of light Cr isotopes into the Earth's core, leaving the mantle enriched in ^{53}Cr. For mantle derived chromites, Farkas et al. (2013) observed a mean δ^{53}Cr-value of 0.08 ‰, slightly heavier than for mantle xenoliths possibly suggesting slight Cr fractionations during partial melting. Hydrothermal chromates (crocoites) are considerable enriched with ^{53}Cr contents of up to 2 ‰. During serpentinization of ultramafic rocks, ^{53}Cr will become enriched (Farkas et al. 2013). Thus, oxidative secondary aqueous alteration of ultramafic rocks shifts the primary mantle composition towards heavier ^{53}Cr-values.

2.13.2 Low-Temperature Fractionations

During weathering, oxidation of Cr(III) leads to a ^{53}Cr enrichment in the resulting Cr(VI), leaving soils depleted in ^{53}Cr. Thus, river and ocean water is enriched in heavy Cr-isotopes relative to mantle and crustal rocks indicating Cr isotope fractionation during weathering and transport to the ocean (Bonnand et al. 2013; Frei et al. 2014). Coastal waters are heavier than open ocean waters possible reflecting in situ reduction of Cr(VI) to Cr(III).

Carbonates encompass the range of Cr-isotopes in seawater (Bonnand et al. 2013). Cr isotopes in marine carbonates, thus, may be a sensitive tracer of weathering of the continental crust as well as of variations of hydrothermal input (Frei et al. 2011).

Frei et al. (2009) used Cr-isotopes to deduce the oxygenation history of the Earth's hydro- and atmosphere. They suggested that the Great Oxidation Event did not lead to a unidirectional increase of oxygen, but instead is better characterized by punctuated fine-scale fluctuations. This view was challenged by Konhauser et al. (2011) argueing that Cr was largely immobile on land till the GOE, but was solubilized in the period that followed. Frei and Polat (2013) interpreted Cr isotope fractionations in 2.0 Ga soils as indicating oxidative weathering on land.

2.13.3 Anthropogenic Cr in the Environment

Extensive industrial use of hexavalent chromate has led to a widespread Cr contamination of soils and groundwater. Reduction of Cr(VI) to Cr(III) may proceed by a variety of abiogenic and microbial processes. All reduction mechanisms induce Cr isotope fractionations with the lighter isotope enriched in the product (Dossing et al. 2011; Sikora et al. 2008). Kitchen et al. (2012) determined experimentally Cr isotope fractionations for Cr-reduction by dissolved Fe(II) up to 4.2 ‰.

Since isotope fractionation during Cr(VI) reduction is little affected by adsorption (Ellis et al. 2004), ^{53}Cr/^{52}Cr ratios in soils and groundwaters can be used as an indicator of Cr(VI) reduction and pollution. Groundwaters have δ^{53}Cr-values ranging from 0.3 to 5.9 ‰ (Ellis et al. 2002, 2004; Berna et al. 2010 and Zink et al. 2010; Izbicki et al. 2012). These authors observed an increase up to 6 ‰ in

$^{53}Cr/^{52}Cr$ ratios during the reduction of chromate. In experiments with *Shewanella*, Sikora et al. (2008) observed a Cr isotope fractionation of about 4 ‰ during dissimilatory Cr(VI) reduction. There are other genera of anaerobic and aerobic bacteria that produce comparable isotope fractionations during Cr(VI) reduction (Han et al. 2012). These findings can be applied to quantify Cr(VI) reduction at sites undergoing active remediation.

2.14 Iron

Iron has 4 stable isotopes with the following abundances (Beard and Johnson 1999)

^{54}Fe	5.84 %
^{56}Fe	91.76 %
^{57}Fe	2.12 %
^{58}Fe	0.28 %

Iron is the third most abundant element on Earth that participates in a wide range of biotically- and abiotically-controlled redox processes in low- and high-temperature environments. Iron has a variety of important bonding partners and ligands, forming sulfide, oxide and silicate minerals as well as complexes with water. As is well known, bacteria can use Fe during both dissimilatory and assimilatory redox processes. Because of its high abundance and its important role in high and low temperature processes, isotope studies of iron have received the most attention of the transition elements. Since the first investigations on Fe isotope variations by Beard and Johnson (1999), the number of studies on Fe isotope variations has increased exponentially. Reviews on Fe-isotope geochemistry have been given by Anbar (2004a, b), Beard and Johnson (2004), Johnson and Beard (1999), Dauphas and Rouxel (2006) and Anbar and Rouxel (2007). Figure 2.28 summarizes Fe-isotope variations in important geological reservoirs.

2.14.1 Analytical Methods

By using the double-spike SIMS technique, Johnson and Beard (1999) described an analytical procedure with very good precision. Nevertheless, with the introduction of MC-ICP-MS techniques and their ability to measure Fe isotope ratios with little drift, most researchers have concentrated on MC-ICP-MS (Weyer and Schwieters 2003; Arnold et al. 2004a, b; Schoenberg and von Blanckenburg 2005; Dauphas et al. 2009; Craddock and Dauphas 2010; Millet et al. 2012). Fe isotope analysis is highly challenging, because of interferences from $^{40}Ar^{14}N^+$, $^{40}Ar^{16}O^+$ and $^{40}Ar^{16}OH^+$ at masses 54, 56 and 57 respectively. Nevertheless δ-values can be measured routinely with a precision of ±0.05 ‰ or better (Craddock and Dauphas 2010).

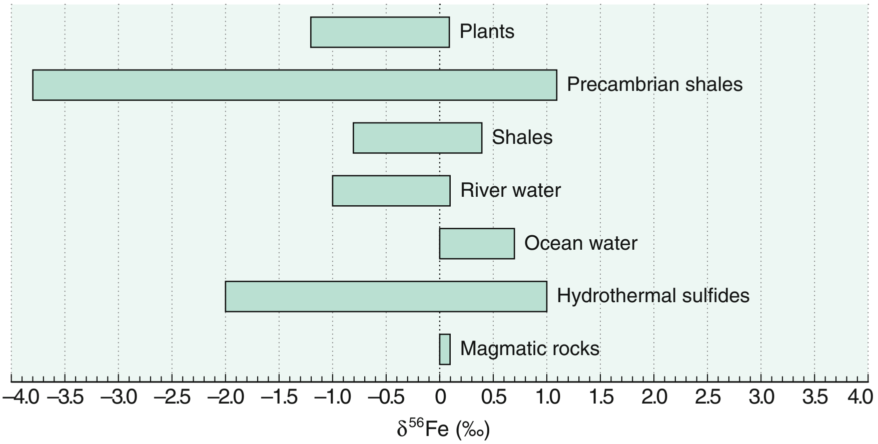

Fig. 2.28 δ^{56}Fe-values of important geological reservoirs

Literature data have been presented either in the form of ^{57}Fe/^{54}Fe or as ^{56}Fe/^{54}Fe ratios. In the following all data are given as δ^{56}Fe values. δ^{57}Fe values would be 1.5 times greater than δ^{56}Fe values, because only mass-dependent fractionations are expected. Fe isotope ratios are generally reported relative to the IRMM-14 standard, an ultra-pure synthetic Fe metal, or are given to the average composition of various rock types (Beard et al. 2003; Craddock and Dauphas 2010; He et al. 2015). Relative to IRMM-14, igneous rocks have an average composition of δ^{56}Fe of 0.09 ‰. The maximum range in δ^{56}Fe-values is more than 5 ‰, with low values for sedimentary pyrite and high values in iron oxides from banded iron formations.

2.14.2 Isotope Equilibrium Studies

Equilibrium Fe isotope fractionations for mineral-mineral and mineral-fluid systems have been determined by 3 different approaches: (i) calculations of β-factors based on density functional theory (DFT) (Schauble et al. 2001; Anbar et al. 2005; Blanchard et al. 2009; Rustad and Dixon 2009; Rustad et al. 2010) and (ii) calculations based on Mössbauer spectroscopy and inelastic nuclear resonant X-ray scattering measurements (Polyakov 2007; Polyakov and Soultanov 2011; Dauphas et al. 2012) and (iii) isotope exchange experiments (Skulan et al. 2002; Welch et al. 2003; Shahar et al. 2008; Beard et al. 2010; Saunier et al. 2011; Wu et al. 2011; Frierdich et al. 2014).

Fe isotope fractionations obtained from density functional theory (Blanchard et al. 2009) and from Mossbauer or Inelastic Nuclear Resonant Xray scattering spectroscopic data (Polyakov et al. 2007; Polyakov and Soultanov 2011) exhibit significant discrepancies. Large discrepancies also exist between calculated and experimentally determined fractionation factors, especially for mineral-fluid systems. Rustad et al. (2010) achieved better agreement by considering the second hydration shell of Fe dissolved complexes. In a multi direction 3-isotope experimental approach for the $Fe^{2+}{}_{aq}$—magnetite system, Frierdrich et al. (2014) achieved good agreement with calculated Fe fractionations of Rustad et al. (2010).

First experimental studies at magmatic temperatures, conducted by Schüßler et al. (2007) for equilibrium isotope fractionations between iron sulfide (pyrrhotite) and silicate melt and by Shahar et al. (2008) for fayalite and magnetite demonstrate that Fe isotope fractionations are relatively large at magmatic temperatures and potentially can be used as a geothermometer. Under equilibrium conditions common igneous and metamorphic Fe-minerals should show an order of ^{56}Fe depletion from hematite to magnetite to olivine/pyroxene to ilmenite. For instance, at 800 °C Fe isotope fractionation between magnetite-ilmenite should be around 0.5 ‰ becoming larger with decreasing temperatures. Thus, the pair magnetite-ilmenite potentially may be used as a geothermometer.

Mechanism governing Fe isotope fractionation include precipitation of Fe bearing minerals (Skulan et al. 2002; Butler et al. 2005), isotope exchange between different ligand species (Hill and Schauble 2008; Dideriksen et al. 2008; Wiederhold et al. 2006) and adsorption of dissolved Fe(II) to Fe(III) surfaces (Icopini et al. 2004; Crosby et al. 2007; Jang et al. 2008). Changes in bond partners and/or coordination number also have an effect on isotope fractionation (Hill et al. 2009, 2010), implying that Fe isotope compositions reflect both the redox state and the solution chemistry.

Theoretical calculations and experimental determinations show that Fe(III) bearing phases tend to be enriched in heavy Fe isotopes compared to Fe(II) bearing phases. The largest Fe isotope fractionations have been attributed to redox effects (Johnson et al. 2008). For example, Fe isotope fractionations between Fe(II) and Fe (III) species at 25 °C yield a 2.5–3 ‰ ^{54}Fe depletion in the Fe(II) species. As discussed by Crosby et al. (2005), Fe isotope fractionation results from isotope exchange between Fe(II) and Fe(III) at oxide surfaces explaining why Fe isotope fractionations are very similar for microbial dissimilatory Fe(III) reduction, microbial Fe(II) oxidation and equilibrium between dissolved Fe(II) and Fe(III) species in abiotic systems. This hampers the assertion of Fe isotopes as biosignatures.

2.14.3 Meteorites

Carbonaceous and ordinary chondrites have a uniform bulk Fe isotope composition close to zero ‰ (Craddock and Dauphas 2010; Wang et al. 2013b), whereas the individual Fe components in meteorites are isotopically variable. Chondrules display the largest variation, metals and sulphides show smaller variations (Needham et al. 2009). As shown by Williams et al. (2006) Fe isotope differences between metal and troilite are in the range of 0.5 ‰—the metal phase being heavier than the sulfide phase troilite, potentially reflecting equilibrium fractionations.

Fe isotopes in meteorites have been used to investigate processes associated with core formation. Iron meteorites are considered to represent remnants of metallic cores of differentiated planetary bodies. Whether core formation fractionates Fe isotopes or not is a matter of debate. Poitrasson et al. (2009) and Hin et al. (2012) experimentally determined no Fe isotope fractionation between Fe–Ni alloy and silicate liquid at temperatures up to 2000 °C.

For the Moon, the bulk iron isotope composition is not well constrained. As shown by Liu et al. (2010a, b), low Ti-basalts have δ^{56}Fe values that are 0.1 ‰ lower than high Ti basalts, possibly reflecting differences in mantle sources.

2.14.4 Igneous Rocks

Early studies demonstrated that all terrestrial igneous rocks have homogeneous Fe isotope compositions (Beard and Johnson 1999, 2004). Later studies suggested that igneous processes such as partial melting and crystal fractionation may lead to measurable Fe isotope variations. Weyer et al. (2005) and Weyer and Ionov (2007) found that the Fe isotope composition in mantle peridotites is about 0.1 ‰ lighter than in basalts. Because Fe^{3+} is more incompatible than Fe^{2+} during partial melting and given the fact that Fe^{3+} has higher δ^{56}Fe values than Fe^{2+}, liquids should become enriched relative to the solid residue. Dauphas et al. (2009) presented a quantitative model that relates the iron isotope composition of basalts to the degree of partial melting.

Small Fe isotope variations between MORB and OIB have been reported by Teng et al. (2013) that can be explained by fractional crystallization of OIBs. Teng et al. (2008) demonstrated that Fe isotopes fractionate during magmatic differentiation on whole-rock and on crystal scales. They observed that iron in basalts becomes isotopically heavier as more olivine crystallizes, implying that differences in the redox state of Fe play a decisive role. Zoned olivine crystals yield ^{56}Fe isotope fractionations of up to 1.6 ‰, which they interpreted as being due to diffusion between olivines and evolving melt (Teng et al. 2011).

Metasomatism and/or metamorphic/hydrothermal alterations are additional processes that can modify the Fe isotope composition of mantle material (Williams et al. 2005; Weyer and Ionov 2007; Dziony et al. 2014).

In granitic rocks δ^{56}Fe values are generally positively correlated with SiO_2 contents (Poitrasson and Freydier 2005; Heimann et al. 2008). These authors suggested that exsolution of fluids has removed light Fe isotopes causing the enrichment of SiO_2-rich granitoids. Telus et al. (2012) argued that exsolution alone cannot explain the high δ^{56}Fe values in all granitoids, instead fractional crystallization seems to be the major cause of ^{56}Fe enrichment.

2.14.5 Sediments

Marine sediments reflect the average Fe isotope composition of the continental crust, deviations from the mean value are due to biogeochemical processes in the sediments. Under low-temperature conditions the observed natural Fe isotope variations of around 5 ‰ have been attributed to a large number of processes, which can be divided into inorganic reactions and into processes initiated by micro-organisms. Up to 1 ‰ fractionation can result from precipitation of Fe-containing minerals (oxides, carbonates, sulfides) (Anbar and Rouxel 2007). Larger Fe isotope fractionations occur during biogeochemical redox processes, which include dissimilatory Fe(III) reduction (Beard et al. 1999; Icopini et al. 2004; Crosby et al. 2007), anaerobic photosynthetic Fe(II) oxidation (Croal et al. 2004), abiotic Fe (II) oxidation (Bullen et al. 2001) and sorption of aqueous Fe(II) on Fe (III) hydroxides (Balci et al. 2006). Controversy exists whether iron isotope variations observed are controlled by kinetic or equilibrium factors and/or by abiological or microbiological fractionations. This complicates the ability to use iron isotopes to identify microbiological processing in the rock record (Balci et al. 2006). As argued by Johnson et al. (2008) microbiological reduction of Fe^{3+} produces much larger quantities of iron with distinct δ^{56}Fe values than abiological processes. Thus a number of studies have interpreted negative δ^{56}Fe values in sediments to reflect dissimilatory iron reduction (DIR) (e.g. Bergquist and Boyle 2006; Severmann et al. 2006, 2008, 2010; Teutsch et al. 2009). Coupled Fe and S isotope intergrain variations in pyrite have been used as a proxy for microbial dissimilatory Fe(III) and sulfate reduction (Archer and Vance 2006).

During weathering, Fe is dissolved by ligands and/or bacteria. Fe isotope fractionation may occur during Fe mobilization by Fe reduction or ligand-promoted dissolution or during immobilization of Fe oxy/hydroxides (Fantle and de Paolo 2005; Yesavage et al. 2012 and others). δ^{56}Fe values of bulk and HCl-extractable Fe become isotopically lighter as the extent of weathering proceeds; exchangeable Fe is more depleted in ^{56}Fe than Fe in ironhydroxides.

In summary, negative δ^{56}Fe-values in sedimentary rocks may reflect ancient DIR (Yamaguchi et al. 2005; Johnson et al. 2008), other studies have, however, favored abiological processes for the occurrence of negative Fe isotope values (Rouxel et al. 2005; Anbar and Rouxel 2007; Guilbaud et al. 2011). Especially large iron isotope fractionations have been found in Proterozoic and Archean banded iron formations (BIFs) and shales (Rouxel et al. 2005; Yamaguch et al. 2005). In particular BIFs have been used to reconstruct Fe cycling through Archean oceans and the rise of $O_{2\,(atm)}$ during the Proterozoic (see discussion under Sect. 3.8.4 and Fig. 3.30). The pattern shown in Fig. 3.30 distinguishes three stages of Fe isotope evolution, which might reflect redox changes in the Fe cycle (Rouxel et al. 2005). Interplays of the Fe-cycle with the C- and S-record might reflect changing microbial metabolims during the Earth's history (Johnson et al. 2008).

2.14.6 Ocean and River Water

Dissolved and particulate iron in water occur not only in two oxidation states but in a wide range of chemical species that interact by adorption/desorption, precipitation/dissolution processes. All these processes potentially fractionate Fe isotopes that may modify the iron isotope composition of waters.

Iron in the ocean is an important micronutrient; the growth of phytoplankton is often limited by low Fe concentrations. Because of its very low concentration, the Fe isotope composition of ocean water is not easily determined. Radic et al. (2011) and John and Adkins (2012) were among the first presenting dissolved and particulate Fe isotope data in depth profiles from the Pacific and Atlantic. Water profiles characterized by positive δ^{56}Fe values mainly reflect the continental input with slight transformations in the water column. John and Adkins (2012) demonstrated that dissolved iron in the upper 1500 m is homogeneous with δ^{56}Fe values between 0.30 and 0.45 ‰, whereas in the deeper ocean δ^{56}Fe-values increase to 0.70 ‰.

Rivers rich in clastic suspended detrital material, like the white waters of the Amazon have a Fe isotope composition close to the continental crust (Poitrasson et al. 2014). Rivers rich in organic material contain a large portion in dissolved Fe form and are depleted in heavy Fe isotopes with significant annual variations (Dos Santos Pinheiro et al. 2014).

Fluids in diagenetic systems are variable in Fe isotope composition with a preferential depletion in ^{56}Fe (Severmann et al. 2006) reflecting the interaction of Fe^{3+} with Fe^{2+} during bacterial iron and sulfate reduction. Processes dominated by sulfate reduction produce high δ^{56}Fe values in porewaters, whereas the opposite occurs when dissimilatory iron reduction is the major pathway (Severmann et al. 2006). Fe isotope compositions of pore fluids may reflect the extent of Fe recycling during early diagenesis (Homoky et al. 2011). Fe(II) in pore waters, formed by bacterial Fe(III) reduction, may be reoxidized during sediment suspension events. The resulting fine grained isotopically light FeOOH may be transported back to the deep ocean, a process that has been termed “benthic iron shuttle” (Severmann et al. 2008).

2.14.7 Plants

Although sufficient supply of Fe is essential for all living organisms, iron is one of the most limiting nutrients, because iron in soils exists predominantly in the nearly insoluble Fe (III) form. Therefore, higher plants developed different strategies to make iron available. Guelke and von Blanckenburg (2007) presented evidence that Fe isotope signatures in plants reflect two different strategies that plants have developed to incorporate Fe from the soil. Group I plants induce chemical reactions in the rhizosphere and reduce iron before uptake by incorporating light isotopes in the roots with further depletion during transport to leaves and seeds. Group II plants transport Fe(III) complexes into plant roots via a specific membrane transport system that do not fractionate Fe relative to Fe in soils (Guelke et al. 2010; Guelke-Stelling and von Blanckenburg 2012). As shown by Kiczka et al. (2010) Fe isotopes may fractionate during remobilization of Fe from old into new plant tissues which may change the Fe isotope composition of leaves and flowers over the season.

2.15 Nickel

Nickel can occur in oxidation states from 4+ to 0, but the 2+ state is essentially the only natural oxidation state. Thus, redox controlled reactions do not play an important role, but instead chemical precipitation, adsorption in aqueous systems and crystallization of Ni-sulfides in magmatic systems might induce fractionations. Since nickel is a bioessential trace element, playing vital roles in enzymes, biological processes also might cause isotope fractionations.

Ni has five stable isotopes

^{58}Ni	68.08
^{60}Ni	26.22
^{61}Ni	1.14
^{62}Ni	3.63
^{64}Ni	0.93

Ni isotopes generally are reported as $\delta^{60/58}$Ni values, Gueguen et al. (2013) described an analytical procedure for Ni isotope determinations and determined Ni isotope ratios for various geological reference materials.

2.15.1 Meteorites and Mantle Derived Rocks

The amount of published Ni isotope data is small. First measurements by Cameron et al. (2009) indicated that Ni isotope variations in the mantle and the continental crust are negligible. More recently, Gueguen et al. (2013) and Hofmann et al. (2014) reported Ni isotope fractionations up to 1 ‰ among komatiites and associated Ni-sulfide mineralisations, the latter being depleted in heavy Ni isotopes.

In the metal phase of meteorites, Ni isotopes fractionate between kamacite (Fe-rich phase) and taenite (Ni rich phase), the former being isotopically heavier than the latter (Cook et al. 2007). To investigate potential Ni isotope fractionation between core and mantle, Lazar et al. (2012) determined Ni isotope fractionations between Ni metal and Ni talc silicate. Since the metal has been found to be enriched in the light Ni isotopes, they suggested that Ni isotope fractionations might have occurred during Earth's core segregation.

2.15.2 Water and Organisms

Large fractionations have been observed in the ocean and in organisms. Fujii et al. (2011) investigated theoretically and experimentally Ni isotopes fractionations between inorganic Ni-species and organic ligands and observed Ni isotope fractionations up to 2.5 ‰ controlled by organic ligands.

Dissolved Ni compounds in rivers vary by about 1 ‰ (Cameron and Vance 2014), and are heavier than average continental rocks. Ni dissolved in the ocean has a mean δ^{60}Ni-value of 1.44 ‰ (Cameron and Vance 2014) being heavier than riverine Ni. No Ni isotope difference between surface and deep ocean water has been observed.

Gall et al. (2013) observed Ni isotope enrichment of Fe/Mn crusts relative to continental crust and concluded that weathering is accompanied by Ni isotope fractionation resulting in rivers and oceans being isotopically heavy. A depth profile through a sediment core displays large Ni isotope fractionations which might indicate variations in ocean water composition. In another example, Porter et al. (2014) reported Ni isotope variations between 0.15 and 2.5 ‰ in sediments rich in organic carbon.They argued that variable Ni isotope values are controlled by differences in oceanic sources.

Ni plays an essential role in the metabolism of methanogenic archaea. Biological uptake during methanogenic growth produces substantial Ni isotope fractionations resulting in isotopically light cells and heavy residual media (Cameron et al. 2009). As postulated by these authors biological fractionations of Ni may provide a tracer for elucidating the nature of early life.

2.16 Copper

Copper occurs in two oxidation states, Cu^{+} and Cu^{++} and rarely in the form of elemental copper. The major Cu-containing minerals are sulfides (chalcopyrite, bornite, chalcosite and others), and, under oxidizing conditions, secondary copper minerals in the form of oxides and carbonates. Cu(I) is the common form in sulfide minerals, whereas Cu(II) is dominant in aqueous solution. Copper is a nutrient element, although toxic for all aquatic photosynthetic microorganisms. Copper may form a great variety of complexes with very different coordinations such as square, trigonal and tetragonal complexes. These properties are ideal prerequisites for relatively large isotope fractionations.

Copper has two stable isotopes

$$^{63}\mathrm{Cu} \quad 69.1\,\%$$
$$^{65}\mathrm{Cu} \quad 30.9\,\%.$$

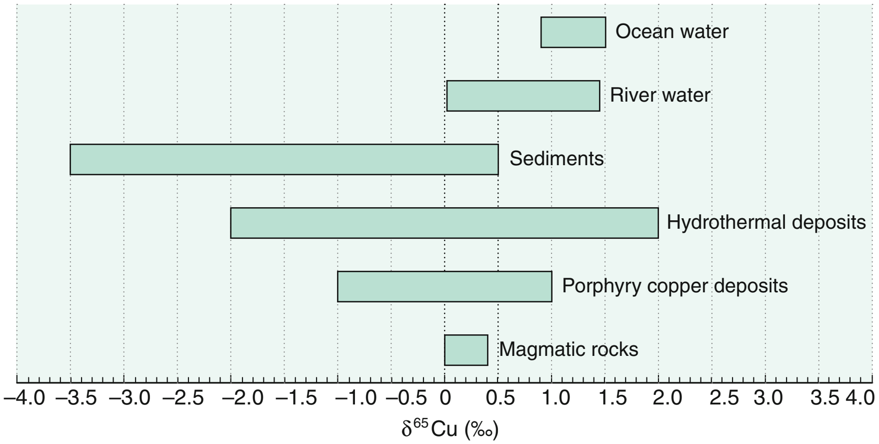

Fig. 2.29 δ^{65}Cu-values of important geological reservoirs

Early work of Shields et al. (1965) using the TIMS technique has indicated a total variation of ~12 ‰ with the largest variations in low temperature secondary minerals. Later studies using laser-ICP-MS techniques, by Maréchal et al. (1999), Maréchal and Albarede (2002), Zhu et al. (2002), Ruiz et al. (2002), observed a variation range of nearly 10 ‰, which is larger than for Fe. Most samples so far analysed, however, vary between δ^{65}Cu values from +2 to −2 ‰ (see Fig. 2.29). The commonly used Cu standard NIST SRM 976 is no longer available, new certified reference materials are ERM-AE633 and ERM-AE647 (Möller et al. 2012).

2.16.1 Low-Temperature Fractionations

Low-temperature processes are the major source of Cu isotope variations; the main processes are: (i) variation of redox conditions, (ii) adsorption on mineral surfaces and organic matter (Pokrovsky et al. 2008; Balistrieri et al. 2008), (iii) inorganic and organic complexation to ligands (Pokrovsky et al. 2008), (iv) biological fractionation by plants and micro-organisms (Weinstein et al. 2011).

Experimental investigations have demonstrated that redox reactions between Cu (I) and Cu(II) species are the principal process that fractionates Cu isotopes (Ehrlich et al. 2004; Zhu et al. 2002). During precipitation of copper without redox change the heavier Cu isotope is preferentially incorporated, however, during Cu(II) reduction precipitated Cu(I) species are 3–5 ‰ lighter than dissolved Cu(II) species. Pokrovsky et al. (2008) observed experimentally a change in sign of Cu isotope fractionations during adsorption from aqueous solutions depending on the kind of surface, either organic or inorganic: on biological cell surfaces a depletion of ^{65}Cu, whereas on hydroxide surfaces an enrichment of ^{65}Cu is observed. In contrast to abiotic reactions, bacteria preferentially incorporate the lighter Cu isotope into their cells, regardless of experimentally conditions (Navarette et al. 2011).

During oxidative weathering of copper rich sulphides, soils become isotopically depleted in ^{65}Cu while porewaters are isotopically enriched (Mathur et al. 2012). Cu isotopes in rivers and seawater indicate that particle-bound Cu are isotopically lighter than dissolved Cu species (Vance et al. 2008). Dissolved Cu in ocean water is heavier than the dissolved riverine input which may be caused by scavenging of light Cu to particulate material, preferentially to Fe–Mn oxides (Vance et al. 2008; Little et al. 2014).

2.16.2 Variations in Ore Deposits

Cu isotopic fractionations at magmatic temperatures appear to be negligible. By analysing native copper grains and whole rock copper in peridotite, Ikehata and Hirata (2012) reported Cu isotope values close to zero ‰ with no differences between Cu metal grains and whole rock copper; thus the Cu isotope composition of mantle and crust appear to be close to zero ‰ (Li et al. 2009a, b).

Various types of Cu-ore deposits have been investigated (Larson et al. 2003; Rouxel et al. 2004a, b; Mathur et al. 2005, 2010; Markl et al. 2006; Li et al. 2010). Early studies showed very limited Cu-isotope variations at high temperatures, but later studies by Maher and Larson (2007) and Li et al. (2010) demonstrated that variations of up to 4 ‰ may occur in porphyry copper deposits. Individual deposits show characteristic Cu isotope zonations that may be caused by fractionations between sulfide, brine and vapour during copper precipitation.

The magnitude of isotope fractionation in copper sulfides increases with secondary alteration and reworking processes (i.e. Markl et al. 2006). Thus copper isotope ratios may be used to decipher details of natural redox processes, but hardly can be used as reliable fingerprints for the source of copper because the variation caused by redox processes within a single deposit is usually much larger than the inter-deposit variation. Experiments by Maher et al. (2011) indicated that the magnitude of Cu-isotope fractionation depend on the pH of the mineralizing fluid and the partitioning of Cu between vapor and liquid. This means that Cu isotope fractionation depend on the physico-chemical conditions during Cu-precipitation. Heavier isotope compositions in supergene Cu minerals and a lighter isotope signature in the leach cap and oxidation zone of an ore deposit can be used as a tool for exploration.

On sites contaminated by acid mine drainage, Borrok et al. (2008) and Kimball et al. (2009) demonstrated systematic copper isotope fractionations between ore minerals and stream water that may be used for ore-prospecting.

2.16.3 Variations in Plants

Copper is an essential micronutrient for plant growth. Cu isotopes may be used to elucidate Cu uptake. Studies by Weinstein et al. (2011), Jouvin et al. (2012) and Ryan et al. (2013) demonstrated that different uptake strategies lead to different Cu isotope fractionations in plants. Tomatoe and oat grown under controlled solution cultures yield Cu isotope fractionations which support previous findings for Fe uptake in strategy 1 and 2 plants (Ryan et al. 2013). Tomatoes preferentially fractionate light ^{63}Cu by about 1 ‰, which is attributed to Cu reduction whereas oat shows minimal Cu fractionation suggesting that Cu uptake and transport is not redox selective.

2.17 Zinc

Zinc has 5 stable isotopes of mass 64, 66, 67, 68 and 70 with the following abundances:

^{64}Zn	48.63 %
^{66}Zn	27.90 %
^{67}Zn	4.10 %
^{68}Zn	18.75 %
^{70}Zn	0.62 %

The JMC-Lyon standard has been the commonly used Zn isotope standard in the past, which however is not longer available. Möller et al. (2012) calibrated IRMM-3702 as the new certified Zn standard, which has a δ^{66}Zn-value of 0.29 ‰ relative to the JMC-Lyon standard. In Fig. 2.30 natural Zn isotope variations given as ^{66}Zn/^{64}Zn ratios are summarized.

The main processes fractionating zinc isotopes are (i) evaporation-condensation processes in which the vapor phase is depleted in the heavier isotopes relative to the solid phase and (ii) sorption processes (Cloquet et al. 2008). Zn isotope fractionation during sorption on Fe hydroxides has been determined by Juillot et al. (2008), Zn-sorption on organic matter has been investigated by Jouvin et al. (2009). The magnitude of isotope fractionation depends on the structure of Zn-complexes on the surface of the solid.

In water, Zn isotope fractionation depends on the ligands present, especially on dissolved phosphate and carbonate. Ab initio calculations of Zn isotope fractionations between aqueous sulfide, chloride and carbonate species by Black et al. (2011) and Fujii et al. (2011) indicate that Zn sulfide complexes are isotopically depleted in heavy Zn isotopes relative to Zn^{2+} and Zn chlorides, whereas carbonates are more enriched than chlorides.

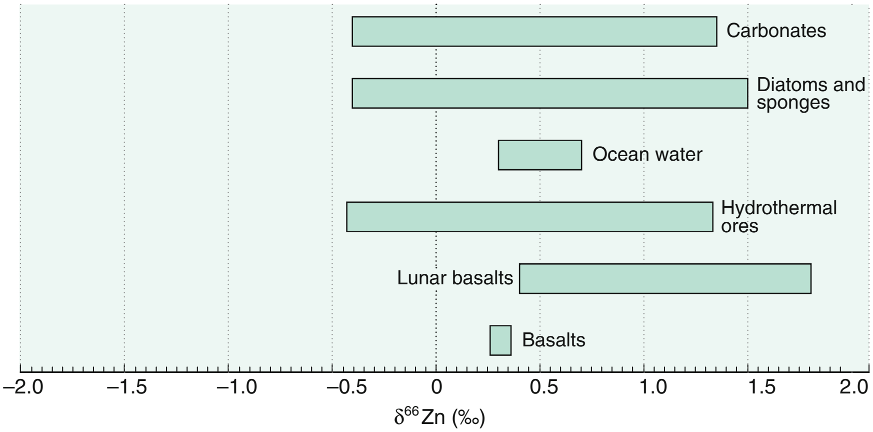

Fig. 2.30 δ^{66}Zn-values of important geological reservoirs

2.17.1 Fractionations During Evaporation

Evaporation-condensation processes may cause large fractionations in meteorites (Luck et al. 2005; Wombacher et al. 2008); Paniello et al. (2012) postulated that loss of volatiles in lunar magmatic rocks has lead to an enrichment of heavy Zn isotopes on the Moon relative to Earth.

Significant amounts of Zn may be emitted by degassing from volcanoes. Fumarolic gases and condensates from the Merapi volcano have a relatively large range in Zn isotope compositions. Gaseous Zn samples are enriched in lighter Zn isotopes whereas condensates are enriched in the heavier isotopes (Toutain et al. 2008).

2.17.2 Variations in Mantle Derived Rocks

Early measurements of the ^{66}Zn/^{64}Zn ratio in mantle—and crustal derived rocks yielded a small variation of about 1 ‰ (Maréchal et al. 1999, 2000; Maréchal and Albarede 2002). One of the main reasons for this small variability appears to be that Zn in natural environments does not participate in redox reactions. It occurs as Zn^{2+}, except, in rare cases, as Zn(0) metal which is an anthropogenic contaminant.

Recent measurements by Chen et al. (2013a, b) indicate small Zn isotope variations induced by high-temperature igneous processes. By studying two chemically diverse suites of volcanic rocks from Hawaii and Iceland, Chen et al. (2013a, b) concluded that the Earth's mantle is homogeneous in Zn isotope composition and that the bulk silicate earth has a δ^{66}Zn-value of 0.28 ‰. Kilauea basalts show small, but systematic Zn isotope enrichment with increasing degree of differentiation.

2.17.3 Ore Deposits

By analyzing sphalerites from ore deposits, Mason et al. (2005), Wilkinson et al. (2005), Kelley et al. (2009), Gagnevin et al. (2012) and Zhou et al. (2014) observed Zn isotope variations of about 1.5 ‰. These studies indicate that early precipitated sphalerites have higher ^{64}Zn-values than late precipitates. The variations have been related to kinetic fractionations during rapid sphalerite precipitation. Gagnevin et al. (2012) explained relatively large Zn-isotope variations at the millimetre scale by mixing of hot hydrothermal fluids with cool brines containing bacterial sulfide. John et al. (2008) reported relatively large Zn isotope fractionation in hydrothermal vent fluids. Low-temperature fluids have heavier δ^{66}Zn-values than high temperature fluids. Cooling of vent fluids leads to precipitation of isotopically light sphalerite causing enrichments of the fluid.

2.17.4 Variations in the Ocean

Zinc is an essential micronutrient for phytoplankton, its concentration is controlled by phytoplankton uptake and remineralization. Light Zn isotopes are preferentially incorporated into phytoplankton organic matter, leaving residual Zn in surface water enriched in Zn isotopes (John et al. 2007; Andersen et al. 2011; Hendry and Andersen 2013). Surface waters have a lighter δ^{66}Zn signature than deep waters suggesting that absorption of Zn on particle carries heavy Zn out of surface waters (John et al. 2007a). Thus, biological usage and adsorption onto particles are likely to cause isotope fractionations (Gelabert et al. 2006).

In a depth profile of the upper 400 m of Pacific seawater, Bermin et al. (2006) observed small isotope variations which they interpreted as being due to biological recycling. The bulk isotope composition of dissolved Zn in the ocean below 1000 m is around 0.5 ‰, which is heavier than the input from river water (Little et al. 2014; Balistrieri et al. 2008; Chen et al. 2008; Borrok et al. 2009).

Variations of Zn isotopes in marine carbonates have been interpreted to reflect changes in nutrient availability (Pichat et al. 2003; Kunzmann et al. 2013).

2.17.5 Anthropogenic Contamination

Due to anthropogenic activities, many environmental systems are polluted with zinc. The potential of using zinc isotopes to trace Zn contaminations and atmospheric transport was demonstrated by Cloquet et al. (2008), Sonke et al. (2008), Chen et al. (2008) and Weiss et al. (2007). John et al. (2007) measured the Zn isotope composition of various man-made Zn products. They showed that the range of δ^{66}Zn values of industrial products is smaller than of Zn ores indicating Zn isotope homogenezation during processing and ore purification.

Chen et al. (2008) measured Zn isotope variations along a transsect of the Seine. Variations along the river transect showed an increase in Zn concentrations with highest values in the region of Paris. Less polluted waters have higher δ^{66}Zn-values than polluted ones. Roof leaching in the Paris area is a major Zn source.

By analyzing peat profiles, Weiss et al. (2007) concluded that Zn isotopes have the potential to identify atmospheric sources such as zinc derived from mining and smelting. Biogeochemical processes within peat profiles, however, may complicate the interpretation of the record.

2.17.6 Variations in Plants

Zinc is a vital element for most organisms, it plays an essential role in various biochemical processes. The largest variation of Zn isotopes have been found in land plants (Viers et al. 2007; Weiss et al. 2005). As shown by Moynier et al. (2008) and Viers et al. (2007), Zn isotopes fractionate during incorporation of Zn into roots and during transport within plants. The size of the fractionation is species dependent (Viers et al. 2007) and may depend on the height of the plant. The mechanisms of Zn isotope fractionations are not well understood, but may depend on surface absorption, solution speciation and membrane-controlled uptake.

2.18 Germanium

Because of nearly identical ionic radii, Ge may replace Si in minerals and thus may show isotope fractionation behaviour similar to silicon. However, Ge is generally associated to sulfides where it may substitute Zn and Cu at concentrations of more than 1000 ppm, whereas the average concentrations in the earth's crust is around 1 ppm.

Ge has 5 stable isotopes with the following abundances (Rosman and Taylor 1998):

^{70}Ge	20.84 %
^{72}Ge	27.54 %
^{73}Ge	7.73 %
^{74}Ge	36.28 %
^{76}Ge	7.61 %

Early investigations using the TIMS method had an uncertainty of several ‰. Over the past few years advances have been made with the MC-ICP-MS technique with a long term external reproducibility of 0.2–0.4 ‰ (Rouxel et al. 2006; Siebert et al. 2006a). Even better reproducibility has been performed by Luais (2012).

Li et al. (2009a, b) and Li and Liu (2010) estimated isotope fractionation factors among Ge-bearing phases and predicted that sulfides will be depleted in heavy Ge isotopes relative to Ge-oxides. Based on a few measurements of basalts and granites

Rouxel et al. (2006) concluded that the bulk silicate earth has a homogeneous isotope composition. However, chemical sediments like sponges and authigenic glauconites are enriched in δ^{74}Ge by about 2 ‰. This suggests that Ge in seawater —similar to silicon—is isotopically enriched in ^{74}Ge relative to the bulk earth. Ge isotopes thus might offer new insights into the biogeochemistry of the present and past ocean, but more data are needed.

Relatively high Ge concentrations have been reported in coal seams. Qi et al. (2011) observed δ^{74}Ge variations of more than 7 ‰ in coals and their combustion products. They showed that coal combustion fractionates Ge isotopes, with soot being more depleted in ^{74}Ge than slags.

2.19 Selenium

Selenium is an essential trace element for animals and humans having a narrow concentration range between sufficiency and toxicity (Schilling et al. 2011). It occurs in four oxidation states that differ in their nutritional and toxic behaviour. Selenium to some extent is chemically similar to sulfur, therefore, one might expect relatively large fractionations of selenium isotopes in nature. Six stable selenium isotopes are known with the following abundances (Coplen et al. 2002)

^{74}Se	0.89 %
^{76}Se	9.37 %
^{77}Se	7.63 %
^{78}Se	23.77 %
^{80}Se	49.61 %
^{82}Se	8.73 %

In general ^{82}Se/^{76}Se ratios have been measured. Because of the 7 % mass difference between ^{76}Se and ^{82}Se and numerous microbial and inorganic Se redox transformations, interest in selenium isotope studies has grown in recent years.

An early study by Krouse and Thode (1962), using SeF_6 gas, required relatively large quantities of Se, limiting the applications of selenium isotopes. Johnson et al. (1999) developed a double-spike solid-source technique that corrects for fractionations during sample preparation and mass spectrometry, yielding an overall reproducibility of ±0.2 ‰. This technique brings sample requirements down to submicrogram levels. Even lower Se amounts (10 ng) are required for measurements with the MC-ICP-MS technique (Rouxel et al. 2002) using a commercial Se solution as standard. Carignan and Wen (2007) published δ^{82}Se-values relative to the NIST SRM 3149 standard. Figure 2.31 summarizes Se isotope variations in specific reservoirs.

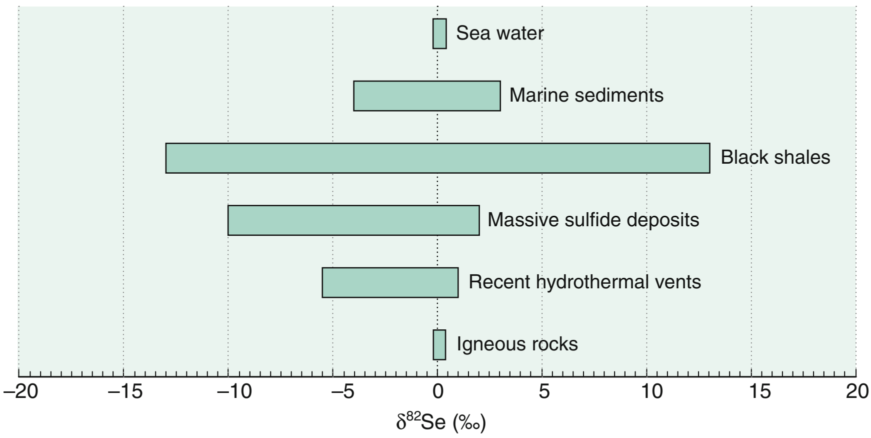

Fig. 2.31 δ^{82}Se-values of important geological reservoirs

2.19.1 Fractionation Processes

Selenium oxyanions can be reduced by certain microbes. Reduction proceeds in 3 steps with Se(IV) and Se(0) species as stable intermediates (Johnson 2004). Se isotope fractionation experiments by Herbel et al. (2000) indicate about 5 ‰ fractionations during reduction of selenate to selenite. Little or no fractionation has been observed during selenite sorption, oxidation of reduced Se in soils, or Se volatilization by algae.

Johnson and Bullen (2003) investigated Se isotope fractionations induced by inorganic reduction of selenate by Fe(II)-Fe(III) hydroxide sulfate ("green rust"). The overall fractionation is 7.4 ‰, which is larger than during bacterial selenate reduction. This indicates that the magnitude of Se isotope fractionations depends on the specific reaction mechanism. Mitchell et al. (2013) determined Se isotope fractionations during sorption to iron oxides and to iron sulfides: fractionations to iron oxides are generally very small, whereas fractionations to sulfides are much larger.

2.19.2 Natural Variations

Mantle-derived rocks have a δ^{82}Se composition close to zero. Rouxel et al. (2002) measured several igneous rocks and a few iron meteorites, which all lie within 0.6 ‰ of the NIST-SRM 3149 standard. Selenium may become enriched in recent hydrothermal vent sulfides, in which Se may be derived from leaching of igneous rocks or of Se-rich organic sediments. Layton-Matthews et al. (2013) reported a wide range of δ^{82}Se values in ancient seafloor hydrothermal deposits. Very negative values are probably due to Se loss from carbonaceous shales during hydrothermal activity.

Although Se and S share similar geochemical behaviour; in the oceanic environment, Se behaves different to S, where it exists as Se VI and Se IV oxyanions and—most important—as dissolved organic Se. Mitchell et al. (2012) observed in marine shales with low organic carbon content a small range in δ^{82}Se values, whereas in black shales with high Se concentrations larger Se isotope variations occur (Wen and Carigman 2011). In a profile of very Se-rich carbonaceous shales, Zhu et al. (2014) observed a range in $^{82/76}$Se-values from −14.2 to +11.4 ‰, suggesting multiple cycles of oxidation and reduction.

2.20 Bromine

Bromine has two stable isotopes with nearly equal abundances (Berglund and Wieser 2011).

$$^{79}\text{Br} \quad 50.69\,\%$$

$$^{81}\text{Br} \quad 49.31\,\%$$

The most common natural form of bromine is the bromide anion (Br^-). Although higher oxidation states of bromine exist in nature, little is known about the Br isotope composition of bromine oxyanions.

Eggenkamp and Coleman (2000) measured Br isotope values in the form of gaseous CH_3Br. Xiao et al. (1993) used positive thermal ionization mass spectrometry for the measurement of Cs_2Br^+. Bromine in organic compounds have been analysed with MC-ICP-MS techniques (Hitzfeld et al. 2011; Holmstrand et al. 2010). The standard in use is SMOB (Standard Mean Ocean Bromine).

Bromide concentrations in most geological settings are too low for a precise isotope measurement, a notable exception are sedimentary formation waters. Although no direct Br isotope measurements of salt minerals are known, indirect evidence from porewaters suggest that evaporites have δ^{81}Br-values between 0.5 and 1.0 ‰ (Eggenkamp 2014).

Of special interest are high bromine concentrations in very saline deep groundwaters from old crystalline shields. Shouakar-Stash et al. (2007) and Stotler et al. (2010), observed very large Br-isotope variations from −0.80 to +3.35 ‰ that do not indicate a simple marine origin, but favor complex water/rock interactions.

Another interesting aspect of bromine isotope geochemistry is that of all brominated organic compounds in the stratosphere, methyl bromide is the most important contributor to stratospheric ozone depletion. CH_3Br may originate from natural and anthropogenic sources. Horst et al. (2013) determined the Br isotope composition of methyl bromide at two locations in Sweden. Subarctic samples in northern Sweden were more negative than samples in the Stockholm area. The CH_3Br concentration in northern Sweden was 2–3 times lower than in the Stockholm area, possibly indicating industrial contamination of the latter area. CH_3Br emissions from plants are about 2 ‰ depleted in ^{81}Br relative to bromine in the plant (Horst et al. 2014).

2.21 Strontium

Sr has 4 stable isotopes.

^{84}Sr	0.56 %
^{86}Sr	9.86 %
^{87}Sr	7.00 %
^{88}Sr	82.58 %

In the past, isotopes of Sr mainly have been used as a geochronometer. Due to radioactive decay of ^{87}Rb to ^{87}Sr, the ^{87}Sr/^{86}Sr ratio of a sample together with the Rb/Sr concentration ratio carries geochronologic information. Conventional ^{87}Sr/^{86}Sr measurements by thermal ionisation mass-spectrometry (TIMS) use the ^{88}Sr/^{86}Sr ratio for internal instrumental mass fractionations. Normalization to a fixed ^{88}Sr/^{86}Sr ratio assumes that this ratio is constant for natural samples. However, as shown by Fietzke and Eisenhauer (2006), this is not the case. MC-ICP-MS and double spike TIMS methods document ^{88}Sr/^{86}Sr variations in terrestrial and meteoritic samples (Fietzke and Eisenhauer 2006; Krabbenhöft et al. 2009; Neymark et al. 2014). Figure 2.32 demonstrates the range of natural variations of $\delta^{88/86}$Sr-values relative to the SrCO$_3$ standard SRM987.

2.21.1 Silicates

Earth, Mars and Moon have indistinguishable bulk Sr isotope compositions, exceptions are some carbonaceous chondrites being depleted in heavy Sr isotopes (Moynier et al. 2010). The bulk Earth has a δ^{88}Sr-value of 0.27 ‰. With respect to magmatic rocks, first measurements by Halicz et al. (2008a, b) and Charlier et al.

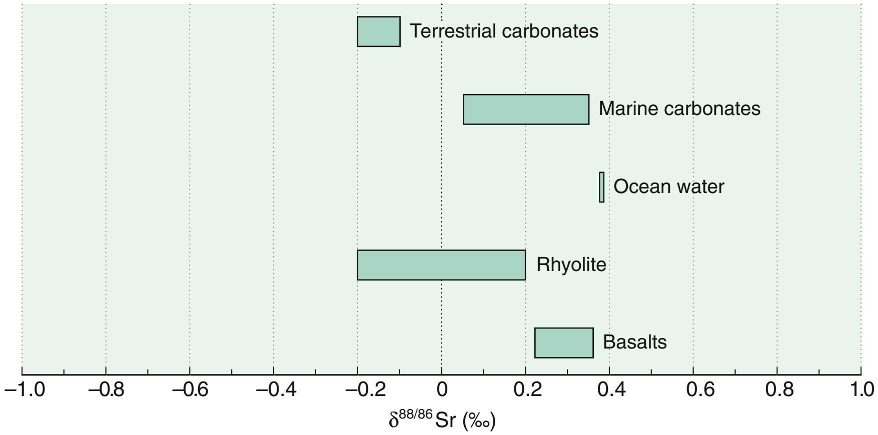

Fig. 2.32 $\delta^{88/86}$Sr-values of important geological reservoirs

(2012) indicated that basaltic rocks have a rather uniform value of +0.3 ‰ whereas more evolved rocks—andesites to rhyolites—have lighter values from −0.2 to +0.2 ‰. Charlier et al. (2012) interpreted the observed Sr isotope variations as resulting from isotope fractionations during fractional crystallization in which ^{88}Sr becomes enriched in plagioclase and K-feldspar.

2.21.2 Carbonates

One of the main Sr isotope fractionation processes is the preferential uptake of lighter Sr isotopes during carbonate precipitation. Sr isotope fractionations during inorganic precipitation of calcite depend primarily on precipitation rates resulting in larger fractionations at higher rates (Böhm et al. 2012). Carbonate precipitating organisms generally fractionate ^{88}Sr/^{86}Sr ratios by 0.1–0.2 ‰ relative to ocean water; the magnitude of Sr isotope fractionation is species dependent. Larger depletions in heavy isotopes have been observed in planktonic foraminifera (Böhm et al. 2012; Stevenson et al. 2014). For tropical corals, Fietzke and Eisenhauer (2006) and Rüggeburg et al. (2008) used ^{88}Sr/^{86}Sr ratios to reconstruct oceanic surface temperatures. For cold-water corals, however, Raddatz et al. (2013) observed no temperature dependence, instead Sr isotope ratios reflect sea water composition with an offset of −0.2 ‰.

Knowledge of the magnitude of Sr fractionations during carbonate precipitation opens the possibility to quantify the output carbonate flux from the ocean (Krabbenhöft et al. 2010), which is not possible on the basis of ^{87}Sr/^{86}Sr ratios because ocean water and carbonates are very similar in ^{87}S/^{86}Sr ratios.

By analysing biogenic fossil carbonates, mostly brachiopods, Vollstädt et al. (2014) concluded that seawater throughout the Phanerozoic has varied in $\delta^{88/86}$Sr values by 0.25–0.60 ‰, which they interpreted to result from varying amounts of buried carbonates.

In contrast to marine carbonates, terrestrial carbonates, i.e. speleothems, display negative ^{88}Sr/^{86}Sr ratios from −0.1 to −0.2 ‰ (Halicz et al. 2008a, b).

2.21.3 Rivers and Plants

By analysing Sr dissolved in rivers, the behaviour of $^{88/86}$Sr during weathering has been investigated (Krabbenhöft et al. 2010; de Souza et al. 2010; Wei et al. 2013). Krabbenhöft et al. (2010) demonstrated that large rivers are quite variable in δ^{88}Sr. De Souza et al. (2010) concluded that Sr released during weathering of silicate rocks does not indicate any Sr-isotope fractionation. By analyzing a river from South China, large seasonal Sr-isotope differences depend on the amount of precipitation (Wei et al. 2013).

Plants are isotopically lighter by 0.2–0.5 ‰ than corresponding soils (De Souza et al. 2010). δ^{88}Sr values of foliar tissues (leaves, flowers) are isotopically depleted relative to roots and stem which is opposite to the trend observed for Ca isotopes (Wiegand et al. 2005; Page et al. 2008).

2.22 Molybdenum

Mo consists of 7 stable isotopes that have the following abundances:

^{92}Mo	15.86 %,
^{94}Mo	9.12 %,
^{95}Mo	15.70 %,
^{96}Mo	16.50 %,
^{97}Mo	9.45 %,
^{98}Mo	23.75 %,
^{100}Mo	9.62 %.

Either ^{97}Mo/^{95}Mo or ^{98}Mo/^{95}Mo ratios have been reported in the literature. Therefore care has to be taken when comparing Mo isotope values. Mo isotope data, given in the following as δ^{98}Mo values, are generally reported relative to internal laboratory standards calibrated against ocean water (Mean Ocean Molybdenum (MOMo), Barling et al. 2001; Siebert et al. 2003). More recently, Nägler et al. (2014) proposed that NIST SRM 3134 should be accepted as international standard with a δ^{98}Mo value of +0.25 ‰ relative to MOMo.

What makes Mo particular interesting, is its use as a potential proxy for the redox history of the oceans and the atmosphere (Barling et al. 2001; Siebert et al. 2003; Wille et al. 2007; Dahl et al. 2010a, b; Herrrmann et al. 2012; Scott and Lyons 2012 besides others). Figure 2.33 summarizes natural Mo isotope variations.

2.22.1 Molybdenites

Limited data from igneous and clastic sedimentary rocks show very small isotope variations (Siebert et al. 2003). Larger variations have been found in molybdenites (MoS_2), an accessory mineral in many magmatic rocks (Hannah et al. 2007; Mathur et al. 2010a, b). According to Mathur et al. (2010a, b) Mo isotope variations depend on the type of ore deposit; molybdenites from porphyry coppers have lighter Mo isotope composition relative to other ore deposits. Greber et al. (2011) observed isotope variations of 1.35 ‰ in a single molybdenite deposit which is larger than the overall Mo isotope variation in igneous rocks. By analysing molybdenites from the well-known porphyry copper deposit of Questa, New Mexico, Greber et al. (2014) subdivided three stages during which Mo isotope fractionations may occur, all lead to molybdenites being heavier than the magmatic source. This implies that Mo isotope compositions of molydenites are not necessarily representative of the average isotope composition of igneous rocks.

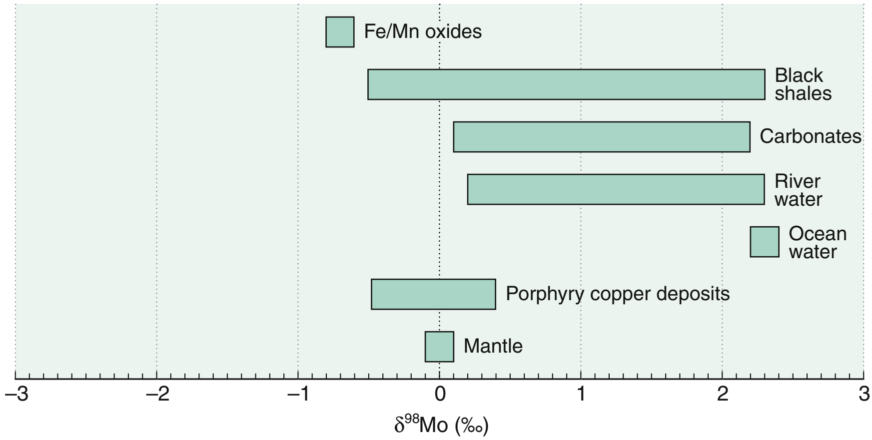

Fig. 2.33 $\delta^{98/95}$Mo-values of important geological reservoirs

2.22.2 Sediments

Marine sediments show a large range in isotope composition (Siebert et al. 2006a, b; Poulson et al. 2006). As summarized by Poulsen Brucker et al. (2009) Mo in sediments originates from 3 different sources:

(1) A small riverine fraction. The isotope composition of Mo input from rivers has been investigated by Archer and Vance (2008) and Neubert et al. (2011). They found a large range of δ^{98}Mo values from 0.2 to 2.3 ‰ that are heavier than the average continental crust. Along streams no significant modification of Mo isotope signatures is observed (Neubert et al. 2011). Thus catchment lithology probably controls the delivery of Mo to the ocean. Pearce et al. (2010), on the other hand, argued that Mo isotope differences might be explained by retention of light Mo isotopes in soils.

(2) Mo associated with biological material that is delivered to the seafloor. The relationship between organic matter and Mo is complex, because Mo is not only incorporated into cells, but is also absorbed to organic material in the water column (Poulson Brucker et al. 2009; Kowalski et al. 2013). As demonstrated by Kowalski et al. (2013), Mo isotope fractionations in tidal systems of the North Sea are caused by biological activity. Zerkle et al. (2011) reported cyanobacterial assimilation of Mo that produce considerable isotope fractionations comparable to those in sedimentary organic matter.

(3) Mo absorbed to Fe/Mn oxides under oxic conditions and Mo bounded through complexation with sulfides under anoxic conditions. Absorbed Mo has a light composition (δ^{98}Mo −0.7 ‰) being 3 ‰ depleted relative to seawater (Barling et al. 2001; Siebert et al. 2003, Anbar 2004b; Anbar and Rouxel 2007 and others). In euxinic waters, i.e. below 400 m in the Black Sea, molybdate is converted to MoS_4^{2-} that is completely removed to the sediment thus resulting

in a sediment isotope signature of seawater (Neubert et al. 2008; Nägler et al. 2011). Black shales in general formed in an anoxic environment have a Mo isotope composition nearly identical to ocean water (Barling et al. 2001; Arnold et al. 2004a, b; Nägler et al. 2005). In suboxic and weakly euxinic waters, the removal of Mo is not quantitative leading to isotope fractionations that are superimposed by effects associated with particle scavenging yielding Mo-isotope values intermediate between Fe–Mn crusts and euxinic black shales (McManus et al. 2002, 2006; Nägler et al. 2005; Poulson et al. 2006; Siebert et al. 2003, 2006b). Thus, the Mo isotope composition of black shales only reflects the seawater composition when a critical sulfidity is reached.

2.22.3 Palaeoredox Proxy

Because of its long residence time, Mo in ocean water has a uniform isotope composition with a δ^{98}Mo value of 2.3 ‰ (Anbar 2004b; Anbar and Rouxel 2007). The Mo isotope composition of ancient oceans has been inferred from black shales assuming that the C-org rich sediments accumulated in euxinic settings (Gordon et al. 2009). However, not all black shales represent euxinic conditions. In recent Black Sea sediments, incomplete removal of Mo from seawater may lead to a Mo isotope depletion of ^{98}Mo in anoxic sediments (Neubert et al. 2008). Therefore when reconstructing paleoenvironments it is important to distinguish between euxinic and non-euxinic black shales.

Nevertheless, variations in the Mo isotope compositions of black shales, have been used as a palaeoredox proxy showing changes of reducing marine conditions throughout periods of Earth's history (Arnold et al. 2004a, b; Siebert et al. 2005; Wille et al. 2007; Pearce et al. 2008; Gordon et al. 2009; Dahl et al. 2010a, b, 2011). In a compilation of Mo-isotope values from black shales, Dahl et al. (2010a, b) postulated two episodes of global ocean oxygenation: the emergence of the Ediacaran fauna at around 550 Ma, and the diversification of vascular plants at around 400 Ma. However, as shown by Gordon et al. (2009) the reconstruction of the Mo isotope composition of ancient oceans from organic rich-shales requires independent evidence of local euxinia.

2.22.4 Carbonates

As an alternative tool for the reconstruction of past ocean chemistry, Voegelin et al. (2009, 2010) analyzed the Mo isotopic composition of carbonates. They observed a large spread in δ^{98}Mo-values of biogenic carbonates, which they attributed to vital effects. In contrast inorganic carbonates closely approach modern ocean Mo-values and are not controlled by local redox conditions. Voegelin et al. (2009) concluded that the Mo-isotopic composition of inorganic carbonates may be used to characterize the Mo isotopic composition of past oceanic water masses.

2.23 Cadmium

Cadmium has 8 stable isotopes:

^{106}Cd	1.25 %
^{108}Cd	0.89
^{110}Cd	12.49
^{111}Cd	12.80
^{112}Cd	24.13
^{113}Cd	12.22
^{114}Cd	28.73
^{116}Cd	7.49

Either ^{114}Cd/^{110}Cd or ^{112}Cd/^{110}Cd ratios have been reported in the literature, analytical techniques are MC-ICP-MS or double-spike TIMS (Schmitt et al. 2009). Comparing datasets from different laboratories is difficult, because no generally agreed standard exists. Different laboratories have used different commercially available Cd-solutions. Recently, Rehkämper et al. (2011) and Abouchami et al. (2013) suggested NIST SRM 3108 as certified reference material. δ-values reported here are $^{114/110}$Cd ratios given relative to SRM 3108 (see Fig. 2.34). A recent review of Cd isotope variations has been published by Rehkämper et al. (2011).

Cd isotope variations are generated mainly by two fractionation processes: (i) partial evaporation/condensation processes in planetary objects and during refining of ore minerals, and (ii) biological utilization of Cd in the oceanic water column. Rocks and minerals show rather constant Cd isotope compositions

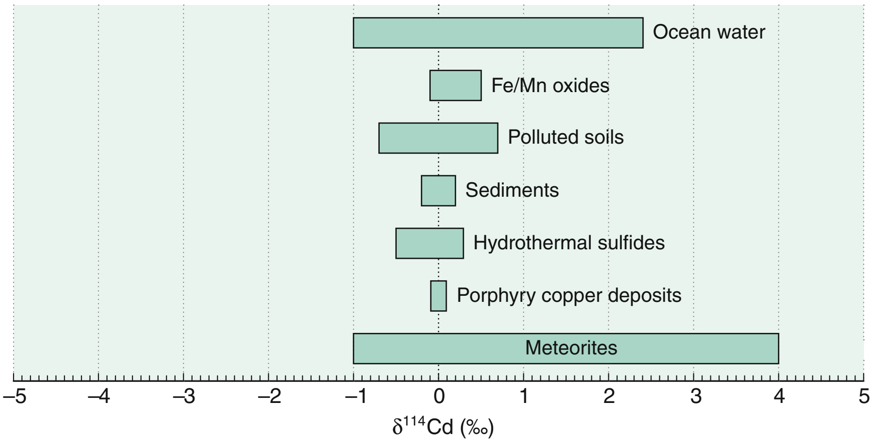

Fig. 2.34 $\delta^{114/110}$Cd-values of important geological reservoirs

(Wombacher et al. 2003, 2008). Schmitt et al. (2009) observed in basalts and loess very small differences, suggesting small Cd isotope differences in mantle and crustal rocks.

2.23.1 Extraterrestrial Materials

Cd isotope variations in extraterrestrial material may be caused by kinetic fractionations during evaporation/condensation processes. Carbonaceous chondrites have relative constant Cd isotope compositions (Rehkämper et al. 2011). In contrast, ordinary chondrites and many enstatite chondrites show very large Cd isotope variations with a range in δ^{114}Cd values from −8 to +16 ‰ (Wombacher et al. 2008). The large range of Cd isotopes in ordinary chondrites obviously obviously results from evaporation/condensation processes, which has been supported by experiments evaporating Cd in vacuo (Wombacher et al. 2004).

The Moon seems to have the same Cd isotope composition as the Earth. Lunar soils are enriched in heavy Cd isotopes, indicating kinetically controlled cadmium loss from the soils.

2.23.2 Marine Environment

Rivers are thought to be the most important source of marine Cd. Rivers in Siberia, analyzed by Lambelet et al. (2013), show a Cd isotope composition close to the continental crust implying that weathering does not produce a measurable Cd isotope fractionation.

Cd in the ocean is a micronutrient, its distribution resembles that of phosphate. Large Cd isotope variations are observed in oceanic surface waters, the most ^{114}Cd enriched values, up to 4 ‰, correlate with waters most depleted in Cd concentration. Rather uniform δ^{114}Cd values of 0.3 ‰ were determined for waters below 1000 m water depth (Lacan et al. 2006; Rippberger et al. 2007; Horner et al. 2010; Abouchami et al. 2011; Yang et al. 2012a, b; Gault-Ringold et al. 2012; Xue et al. 2013).

Phytoplankton in surface waters preferentially incorporates isotopically light Cd making the surface ocean isotopically heavy. On the other hand, Yang et al. (2012a, b) observed no net biological fractionation between phytoplankton and ocean water, and suggested that mixing of different water masses might be an important process. Abouchami et al. (2011) observed distinct Cd isotope boundaries in southern Ocean water masses, thereby tracing surface ocean circulation regimes.

Carbonates precipitated from ocean water show very little Cd isotope fractionation and therefore might be used as a tracer for the Cd isotope composition of oceans in the past (Horner et al. 2011). Schmitt et al. (2009) and Horner et al. (2010) reported Cd isotopes for Fe–Mn crusts and demonstrated that nearly all samples were indistinguishable from oceanic deep waters. Thus, Fe–Mn crusts might potentially be used as a proxy of ancient deep-water Cd isotope composition (Wasylenki et al. 2014).

2.23.3 Pollution Indicator

Soils sampled near ore refineries may be enriched in Cd concentration exhibiting characteristic δ-values (Cloquet et al. 2006). Since Cd isotopes fractionate during evaporation, measurable Cd isotope fractionations should occur during coal burning and sulfide smelting and refining, and indeed, Shiel et al. (2010) observed a 1 ‰ fractionation in δ^{114}Cd values during smelting of Zn and Pb ores. Thus, Cd isotope ratios can be used to identify their anthropogenic origin.

2.24 Tin

Tin has 10 stable isotopes, more than any other element, covering the mass range from 112 to 124.

^{112}Sn	0.97
^{114}Sn	0.66
^{115}Sn	0.34
^{116}Sn	14.54
^{117}Sn	7.68
^{118}Sn	24.22
^{119}Sn	8.59
^{120}Sn	32.58
^{122}Sn	4.63
^{124}Sn	5.79

Tin has two oxidation states, Sn(II) and Sn(IV). Cassiterite (SnO_2) is the major tin mineral, but tin also occurs in complex sulfide minerals. Organotin compounds are used in industry, most prominently in the production of polyvinyl chloride as heat and light stabilizer. Due to their widespread use, large amounts of organotin compounds have entered the environment.

Early studies using TIMS could not detect measurable Sn isotope fractionations due to the high ionization potential of Sn. However, with the introduction of MC-ICP-MS, precise Sn isotope measurements become possible (Clayton et al. 2002; Haustein et al. 2010; Yamazaki et al. 2013). These authors demonstrated that cassiterites from ore deposits in Europe and Asia exhibit relatively large Sn isotope variations. Haustein et al. (2010) used Sn isotope signatures in cassiterites for the provenance of ancient tin.

Polyakov et al. (2005) concluded from synchrotron radiation experiments that large tin isotope fractionations should be found between tin compounds of different oxidation states. Investigating Sn isotope fractionations during methylation reactions, Malinovskiy et al. (2009) demonstrated that under irradiation of UV light, synthesis and decomposition of methyltin is accompanied by mass-dependent and mass-independent tin isotope fractionations. In summary, although the data base is poor, future Sn isotope studies appear to be promising.

2.25 Antimony

Antimony has two stable isotopes with high abundances

^{121}Sb	57.21
^{123}Sb	42.79

In nature, antimony occurs mainly as sulfide, particularly as stibnite, Sb_2S_3; oxides are far less common, although the main industrial use is as Sb_2O_3. Antimony is moderately volatile and occurs in two oxidation states, Sb(V) and Sb(III).

The most extensive study about Sb isotope variations has been presented by Rouxel et al. (2003) using a MC-ICP-MS technique. More recently, modified MC-ICP techniques have been published by Tanimizu et al. (2011) and Lobo et al. (2013).

By analysing water samples and a suite of sedimentary and magmatic rocks including hydrothermal sulfides from deep-sea vents, Rouxel et al. (2003) observed a total range in ^{123}Sb/^{121}Sb ratios of 1.6 ‰ with the largest variations occurring in hydrothermal sulfides. Redox changes from Sb being reduced in vent fluids to oxidized Sb in seawater may cause the Sb fractionations, which have been confirmed experimentally during the reduction of Sb(V) to Sb(III).

An interesting aspect of Sb isotope geochemistry is its potential use of provenancing ancient pre-Roman and Roman glass. Sb had been added to obtain colour and opacity in glass. Lobo et al. (2013) demonstrated that different Sb sources had been used for glass production in the Roman era.

2.26 Tellurium

Tellurium occurs in nature in four oxidation states: as two oxyanions, tellurate and tellurite, and in two reduced forms, as native tellurium and as metal telluride. As a chalcophile element, tellurium might show similar behaviour in isotope fractionation with sulfur.

Tellurium has 8 stable isotopes with the following abundances

^{120}Te	0.10 %
^{122}Te	2.60
^{123}Te	0.91
^{124}Te	4.82
^{125}Te	7.14
^{126}Te	19.0
^{128}Te	31.6
^{130}Te	33.7

By measuring $^{130/122}$Te ratios in gaseous TeF$_6$, Smithers and Krouse (1968) first demonstrated that inorganic and microbiological reductions of tellurite to elemental tellurium causes isotope fractionations with depletions in the heavy isotope in the reaction product. Due to considerable memory effects and other chemical disadvantages, the method has been abandoned. Fehr et al. (2004) introduced a MC-ICP-MS method for tellurium. They found no differences in isotope composition between meteorites and terrestrial tellurides. By measuring ^{130}Te/^{125}Te ratios with a modified MC-ICP-MS technique, Fornadel et al. (2014) demonstrated that tellurides and native tellurium in ore deposits reveal isotope differences up to 1.64 ‰ with significant variations within individual deposits.

2.27 Barium

Barium consists of 7 naturally occurring isotopes:

^{130}Ba	0.11
^{132}Ba	0.10
^{134}Ba	2.42
^{135}Ba	6.59
^{136}Ba	7.85
^{137}Ba	11.23
^{138}Ba	71.70

Since barium belongs to the earth alkaline elements, its chemical and isotopic behaviour should be closely related to Ca and Sr isotopes. Barium in nature occurs as discrete minerals such as barite and witherite (BaCO$_3$), but also may substitute potassium in common minerals, especially feldspars. In the ocean, Ba shows a nutrient-type behaviour being associated with organic matter. The wide occurrence of Ba in low- and high-temperature environments makes Ba an interesting element to look for isotope variations.

Early studies on Ba isotopes concentrated on meteorites (Eugster et al. 1969). More recently, by measuring ^{137}Ba/^{134}Ba ratios with a MC-ICP-MS technique, von Allmen et al. (2010), Böttcher et al. (2012) and Pretet et al. (2015) reported that Ba minerals and standards vary by up to 0.5 ‰. Distinct differences in Ba-isotope compositions have been reported for barites of different origins (von Allemen et al. 2010).

Besides biological reactions, mineral precipitation and sorption-desorption processes may induce Ba isotope fractionations. Pretet et al. (2015) demonstrated that during inorganic and organic precipitation of carbonates light Ba isotopes are preferentially incorporated, similar to Ca and Sr isotopes. Corals from different oceanic localities show considerable Ba isotope variations which may suggest a heterogeneous Ba isotope composition of seawater. Future Ba isotope measurements may provide a better understanding of the biogeochemical Ba cycle.

2.28 Mercury

Mercury has seven stable isotopes with the following abundances (Rosman and Taylor 1998)

^{196}Hg	0.15
^{198}Hg	9.97
^{199}Hg	16.87
^{200}Hg	23.10
^{201}Hg	13.18
^{202}Hg	29.86
^{204}Hg	6.87

Due to the relative uniform isotope abundances in the mass range ^{198}Hg to ^{204}Hg, several possibilities exist for the measurement of Hg isotope ratios; in most studies δ-values are given as ^{202}Hg/^{198}Hg ratios. Since the first description of a precise MC-ICP-MS technique (Lauretta et al. 2001), the number of Hg-isotope studies has grown exponentially. Reviews have been presented by Bergquist and Blum (2009), Yin et al. (2010), Blum (2011) and Blum et al. (2014). The large interest in Hg isotopes relies on two factors: (i) due to its ability to be transported over long distances in the atmosphere, mercury is a global pollutant and (ii) large mass independent isotope fractionations have been observed besides mass-dependent fractionations (Sonke 2011 and others).

The biogeochemical cycle of Hg is complex including different redox states and various chemical speciations affecting its mobility and toxicity. Mercury can exist as stable HgS (cinnabar) and in the form of Hg–S complexes, in methylated form (methylmercury) and in gaseous and aerosol phases in the atmosphere. Emissions are dominated by anthropogenic activity (coal combustion), but inputs from volcanic and hydrothermal emissions are also significant. Atmospheric Hg can be converted into methylmercury by bacteria that may accumulate in aquatic food webs potentially causing severe health problems.

Large $\delta^{202/198}$Hg-isotope fractionations have been observed in natural samples (Bergquist and Blum 2009 and others), far larger than anticipated. The natural Hg isotope variation encompasses 7 ‰, from δ^{202}Hg −4.5 to +2.5 ‰ relative to NIST 3133 (Zambardi et al. 2009).

Bucharenko (2001) and Schauble (2007) demonstrated that isotope variations are controlled by nuclear volume and magnetic shift isotope effects being negligible for the light elements.

2.28.1 MDF and MIF Fractionation Processes

Most equilibrium and kinetic processes for Hg are mass dependent fractionations (MDF), i.e. Hg reacting during microbial transformations (Kritee et al. 2007, 2009); as for other elements, MDF depend on the type of organism, temperature, growth rate etc. On the other hand, experiments during abiotic photoreduction show MDF and mass independent fractionations, MIF, that have been observed for the odd isotopes ^{199}Hg and ^{201}Hg (Bergquist and Blum 2009). Experiments identified photoreduction of aquatic inorganic Hg^{2+} and photodegradation of monomethylmercury as MIF inducing reactions (Sonke 2011).

The magnitude of the observed MIF due to the nuclear volume effect is generally small. As predicted by Bucharenko et al. (2004) and Schauble (2007) and confirmed in experiments by Zheng and Hintelmann (2010), nuclear volume effects have been reported for the Hg liquid-vapor transition (Estrade et al. 2009; Ghosh et al. 2013), in which a small enrichment of the odd over the even isotopes takes place (Sonke and Blum 2013) (<0.2 ‰ for Δ^{199}Hg and Δ^{201}Hg) resulting in Δ^{199}Hg/Δ^{201}Hg ratios of 1.5–2 (Estrade et al. 2009; Zheng and Hintelmann 2010). Larger MIFs have been observed during photochemical reduction of Hg (Bergquist and Blum 2009), in which magnetic isotope effects are the major fractionation process. The largest positive MIF of Hg isotopes (odd mass excess) probably is caused by photochemical degradation of methylmercury in water, which is transferred to the biosphere, in specific to fish (Bergquist and Blum 2009; Blum and Bergquist 2007, 2009). The largest negative MIF (odd mass deficit) is caused by photochemical reduction of inorganic Hg.

MIF reactions may yield a characteristic signature insofar that only odd isotopes (^{199}Hg, ^{201}Hg) deviate significantly from MDF. The ratio Δ^{199}Hg/Δ^{201}Hg seems to be diagnostic of the process causing the MIF (Bergquist and Blum 2009). Recent

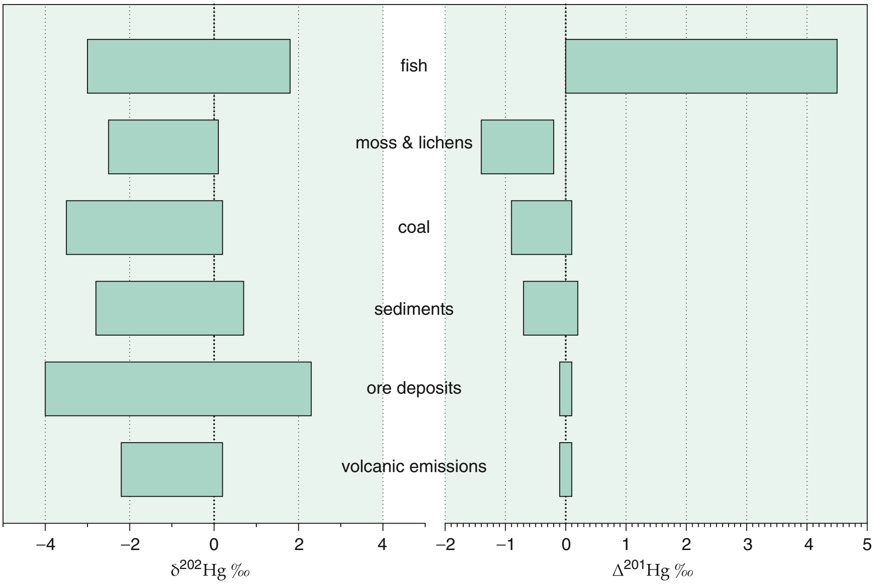

Fig. 2.35 $\delta^{202/198}$ Hg and Δ^{201}Hg values of important geological reservoirs

studies of atmospheric Hg samples show, however, that even isotopes of Hg may also show small non-mass dependent fractionations (Chen et al. 2012; Rolison et al. 2013). The mechanism for the even isotope mass independent fractionations remain, however, unclear.

For the calculation of odd and even numbered MIF values, Blum and Bergquist (2007) gave the following definitions.

$$\Delta^{199}\mathrm{Hg} = \delta^{199}\mathrm{Hg} - (\delta^{202}\mathrm{Hg} \times 0.2520)$$
$$\Delta^{200}\mathrm{Hg} = \delta^{200}\mathrm{Hg} - (\delta^{202}\mathrm{Hg} \times 0.5024)$$
$$\Delta^{201}\mathrm{Hg} = \delta^{201}\mathrm{Hg} - (\delta^{202}\mathrm{Hg} \times 0.7520)$$
$$\Delta^{204}\mathrm{Hg} = \delta^{204}\mathrm{Hg} - (\delta^{202}\mathrm{Hg} \times 1.4930)$$

Figure 2.35 summarizes MDF and MIF Hg isotope variations in important reservoirs (modified from Bergquist and Blum 2009).

2.28.2 Variations in Rocks

Hg has two common oxidation states: Hg(0) exists primarily in gaseous form and Hg(II) exists as highly particle-reactive gaseous, aqueous and solid species. Dissolved Hg(II) has affinities for sulfides and organic matter.

Isotope variations of mercury in common magmatic rocks are very small. A larger range does occur in Hg ore deposits and in hydrothermal springs (Smith et al. 2008). Smith et al. (2008) postulated that boiling of hydrothermal fluids and separation of a Hg-bearing vapour phase are responsible for the observed isotope variations. Sherman et al. (2009) investigated the Guaymas and Yellowstone hydrothermal systems. They reported considerable isotope fractionations, in the Guyamas system solely being mass-dependent, whereas at Yellowstone small mass-independent fractionations occur which may be due to the presence of light facilitating photochemical reactions.

Sapropels—sediments deposited during periods of high primary productivity—may record the Hg isotopic composition of the ocean by quantitative sequestration of Hg by organic matter. Sapropels from the Mediterranean gave δ^{202}Hg values from −1.0 to −0.6 ‰ (Gehrke et al. 2009).

Mosses and lichens are passive filters of atmospheric particulates, which may monitor atmospheric Hg emissions. Carignan et al. (2009) demonstrated that they are characterized by negative MIF. Snow samples also may be regarded as good collectors of atmospheric Hg particulates (Sherman et al. 2010).

2.28.3 Environmental Pollutant

The geochemical cycle of mercury is characterized by atmospheric transport over long distances. Mercury exists in 3 species in the atmosphere: (i) elemental Hg (Hg^0) having a residence time of about 1 year in the atmosphere, (ii) divalent reactive gaseous Hg^{2+} and (iii) Hg bound to particles. These species are linked together by abundant oxidation and reduction processes. Hg^0 comprises more than 90 % of total atmospheric Hg and is relatively stable allowing large scale mixing, whereas the other two species are much more reactive and deposit readily.

Besides natural inputs from volcanic and hydrothermal emissions, anthropogenic sources dominate Hg emissions with coal combustion being the largest contributor. Because elementary Hg is extremely volatile, mercury easily exchanges between water and air and between land and air, resulting in global dispersion.

Hg MDF and MIF signatures in moss, peat, coal and soils demonstrate that a large part of the Hg surface reservoir has been affected by anthropogenic activities offering the possibility to use Hg isotopes as a fingerprint (Sonke 2011) and to quantify the relative contributions of Hg deposition from local, regional and global sources. As suggested by Kritee et al. (2007, 2009), Hg isotopes may distinguish between different sources of mercury emissions based on the magnitude of isotope fractionations. Sonke et al. (2010) investigated mercury pollution from two European metal refiniries and showed that heavy Hg isotopes are preferentially retained in slag residues. Ma et al. (2013) investigated Hg emissions from a heavy metal smelter in Manitoba. Hg isotope variations observed in sediment cores can be explained by mixing of a natural endmember (δ^{202}Hg −2.4 ‰) and an anthropogenic endmember emitted from the smelter (δ^{202}Hg −0.9). Sediment cores 5 and 73 km away from the smelter reveal decreasing Hg concentrations and characteristic shifts in Hg isotope values. Even at the distance of 73 km 70 % of the Hg in the sediments originated from the smelter. In comparable studies, Stetson et al. (2009)

and Yin et al. (2013) have reached similar conclusions by investigating Hg pollution and Hg isotope fractionation in the vicinity of Ag, Au and Hg mines.

At the global scale, anthropogenic emissions are dominated by coal fired power plants. Biswas et al. (2008) demonstrated that coal deposits in the United States, China and Kazakhstan have characteristic Hg isotope values that can be used to discriminate among Hg sources. δ^{202}Hg in coal vary by 3 ‰ and Δ^{201}Hg by 0.9 ‰. Combining the two variables may result in a characteristic fingerprint for coal deposits.

2.29 Thallium

The geochemical behaviour of thallium is largely controlled by its large ionic radius, which makes it highly incompatible during magmatic processes. Tl exists in two valence states as Tl^+ and Tl^{3+}. Because of its high redox potential, the oxidized form is uncommon in natural environments, but seems to play an important role during adsorption processes. Furthermore Tl is a highly volatile element favoring kinetic fractionations during degassing processes.

Thallium has two stable isotopes with masses 203 and 205.

^{203}Tl	29.52
^{205}Tl	70.48

The small relative mass difference between the two Tl isotopes predicts little Tl isotope fractionations. However, the so far observed Tl isotope variation is larger than 3 ‰ (Rehkämper et al. 2002; Nielsen et al. 2006). Responsible for the large variation are Tl isotope fractionations between seawater and Fe–Mn oxyhydroxides and fractionations during low temperature alterations of the oceanic crust.

The generally used standard is NIST 997 Tl metal. It is important to note that Tl isotope ratios are generally given in the ε-notation (variations in parts per 10,000), in the following Tl isotope ratios are given, however, as δ-values. A recent review about the Tl isotope geochemistry has been published by Nielsen and Rehkämper (2011). Figure 2.36 summarizes natural Tl isotope variations

2.29.1 Igneous Rocks

During magmatic processes (crystal fractionation, crustal assimilation etc.) little fractionations seem to occur. Nielsen et al. (2005, 2006, 2007) demonstrated that the continental crust does not differ from the mantle. By analysing igneous rocks in the vicinity of porphyry copper deposits, Baker et al. (2010) reported a variation range of about 0.6 ‰ due to hydrothermal alteration processes.

Because Tl is a volatile trace element, it becomes enriched in volcanic condensates. As shown by Baker et al. (2009) gaseous volcanic emissions are more variable in Tl isotope composition than igneous rocks, but have a mean value being indistinguishable from the estimated mantle composition. The larger variability may

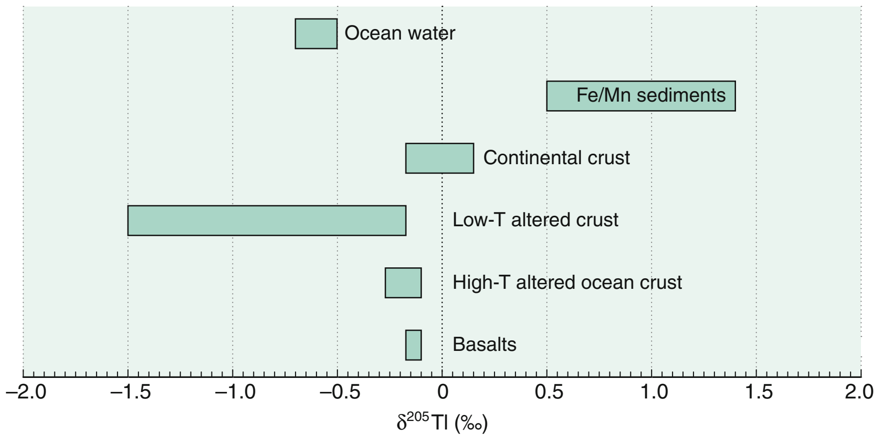

Fig. 2.36 δ^{205}Tl-values of important geological reservoirs

result from partial evaporation during mantle degassing. As indicated in late magmatic/hydrothermal veins, Hettmann et al. (2014) demonstrated that fluids released during degassing are enriched in ^{205}Tl.

Since most geochemical reservoirs except Fe–Mn marine sediments and low temperature seawater altered basalts are more or less invariant in Tl isotope composition, admixing of small amounts of Fe–Mn sediments or low-temperature altered oceanic crust into the mantle should induce small Tl isotope fractionations in mantle derived rocks (Nielsen et al. 2006, 2007). Thus, Tl isotopes may have potential to distinguish between different admixtures to arc lavas. Lavas from the Mariana arc, however, overlap with MORB basalts in Tl isotope composition (Prytulak et al. 2013a, b); thus, no external input can be detected.

2.29.2 Fractionations in the Ocean

No significant Tl isotope fractionations occur during weathering. Dissolved and particulate components in river water do not differ from those of the continental crust (Nielsen et al. 2005). The oceans, however, are depleted in ^{203}Tl compared to the continental crust. A systematic 2 ‰ difference between Fe–Mn crusts enriched in ^{205}Tl and seawater has been observed by Rehkämper et al. (2002), which seems to be due to a fractionation effect during adsorption of Tl onto Fe–Mn particles (Rehkämper et al. 2004).

Variations of Tl concentrations and isotope compositions of seawater over time may depend on different rates of Tl removal via scavenging on Fe–Mn oxyhydoxides and via uptake during low temperature alteration of oceanic crust (Nielsen et al. 2009, 2011a, b, c). Nielsen et al. (2009) observed that growth layers of two Fe–Mn crusts from the Pacific Ocean show a systematic change Tl isotope composition with age, which they explained by time-dependent changes in Tl-isotope composition of seawater. Low Tl isotope ratios during the age range between 55 and 45 Ma might be explained by a fourfold increase of Fe–Mn oxide precipitation compared to present day.

The potential to use Tl isotopes as a paleoredox proxy has been shown by Nielsen et al. (2011a, b, c). Early diagenetic pyrite deposited in an oxic water column display Tl isotope ratios heavier than seawater, whereas pyrite deposited under euxinic conditions have a Tl isotope composition close to seawater, due to reduced precipitation of Fe/Mn oxides in a sulfidic water column.

2.30 Uranium

Natural uranium is mainly composed of two long-lived radioactive isotopes:

$$^{235}\mathrm{U} \quad 0.72\,\%$$
$$^{238}\mathrm{U} \quad 99.27\,\%$$

In the past uranium isotopes have been widely used as a chronological tool. Present day isotope fractionation between ^{235}U and ^{238}U has been considered to be insignificant. The ratio ^{238}U/^{235}U has been assumed to be a constant with a value of 137.88. However, precise measurements by Hiess et al. (2012) on a suite of uranium-bearing minerals commonly used for U-Pb geochronology, e.g. zircons, exhibit isotope variations in δ^{238}U values larger than 5 ‰.

Uranium exists in two oxidation states having different solubilities. Under oxidizing conditions, U is typically present as soluble hexavalent uranyl ion UO_2^{2+}, under reducing conditions U occurs in the tetravalent state, forming relatively insoluble complexes. These properties favor natural isotope variations. Fractionations occur due to mass-independent nuclear volume fractionations, resulting from the differences in nuclear size and shape (Schauble 2007; Abe et al. 2008). Schauble (2007) showed that as a function of oxidation state enriched δ^{238}U values occur in reduced species, opposite to fractionations generally observed.

Using MC-ICP-MS techniques, Stirling et al. (2007), Weyer et al. (2008), Bopp et al. (2009), Montoya-Pino et al. (2010) reported δ^{238}U variations of more than 1 ‰ in various rock types (see Fig. 2.37). Several standards are in use, δ-values measured with a precision better than 0.1 ‰ are given relative to the SRM 950a standard.

2.30.1 Fractionation Processes

Uranium isotope fractionations mainly are attributed to biogenic or abiogenic reduction of U(VI) to U(IV). Basu et al. (2014) determined experimentally uranium isotope fractionations of up to 1 ‰ during microbial U(VI) reduction. Diverse

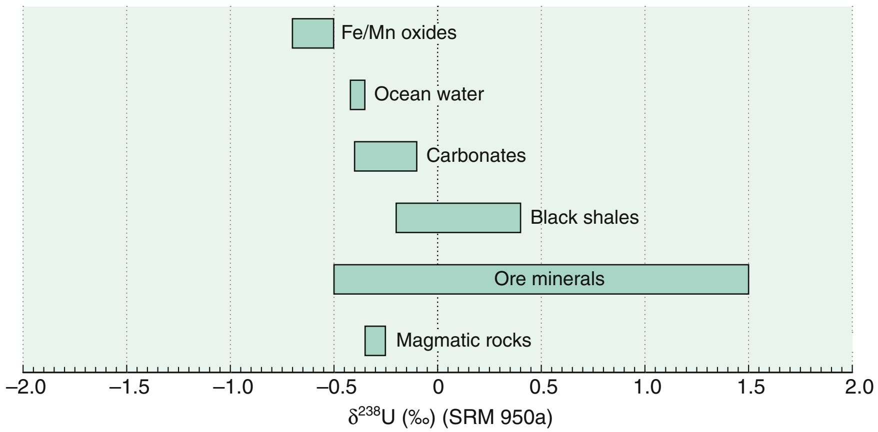

Fig. 2.37 δ^{238}U-values of important geological reservoirs

microorganisms are capable of reducing U(VI) to U(IV) inducing isotope fractionations that is opposite in direction observed during reduction of nitrate, sulphate and chromate: ^{238}U preferentially partitions into U(IV) phases, whereas ^{235}U is enriched in U(VI) phases. Thus, heavy δ^{238}U values are observed for black shales, which contain the reduced form of U, and light isotope values are observed for Fe/Mn oxides.

Another process causing significant U isotope fractionation occurs between seawater and Fe–Mn oxides. Brennacka et al. (2013) postulated that U fractionation is due to coordination changes during absorption. As the redox change of U does not change during absorption, a difference in the coordination environment between dissolved and absorbed U is obviously responsible for the isotope fractionation.

2.30.2 Characteristic U Signatures

Uranium in the ocean occurs mainly in the soluble U(VI) form with a δ^{238}U-value of −0.4 ‰ (Weyer et al. 2008). Under oxic conditions U may be removed through adsorption on Fe/Mn oxides depleted in ^{238}U, shifting oceanic U to heavier values. Under anoxic conditions, sediments enrich ^{238}U shifting ocean water to lighter U isotope values.

The potential of uranium isotopes as a paleo-redox tracer has been investigated by Montoya-Pino et al. (2010), Brennecka et al. (2011), Kendall et al. (2013) and Noordmann et al. (2015). Montoya-Pino et al. (2010) demonstrated that U isotope variations in black shales can be used to quantify the extent of marine anoxia. Black shales from the Cretaceous (Oceanic Anoxic Event 2) are systematically lighter in ^{238}U than modern Black Sea shales which corresponds to a threefold increase of oceanic anoxia relative to the present ocean.

Measurements by Stirling et al. (2007) and Weyer et al. (2008) on recent and fossil corals suggested that carbonates might record the isotope composition of seawater of the geologic past. On the other hand, as argued by Romaniello et al. (2013), $\delta^{238}U$ values of ancient carbonates, affected by diagenetic processes, may be enriched in ^{238}U due to U accumulation under anoxic pore water conditions.

Large differences of nearly 2 ‰ have been observed between uranium ores formed at low and at high temperatures (Bopp et al. 2009; Uvarova et al. 2015; Murphy et al. 2014): magmatic ores vary from −0.7 to −0.3 ‰ whereas sandstone-type low temperature ores have $\delta^{238}U$-values around +0.4 ‰. Isotope variations seem to be controlled by the isotope composition of the U source and the efficiency of U reduction. Up to 5 ‰ fractionations have been observed in U mineralised sediment—groundwater systems (Murphy et al. 2014). ^{238}U preferentially enriches in the sediment, leading to depletions in the groundwater.

References

Abe M, Suzuki T, Fujii Y, Hada M, Hirao K (2008) An ab initio molecular orbital study oft he nuclear volume effects in uranium isotope fractionations. J Chem Phys 129:164309

Abelson PH, Hoering TC (1961) Carbon isotope fractionation in formation of amino acids by photosynthetic organisms. Proc Natl Acad Sci USA 47:623

Abouchami W, Galer S et al (2013) A common reference material for cadmium isotope studies—NIST SRM 3108. Geostand Geoanal Res 37:5–17

Abouchami W, Galer S, de Baar H, Alderkamp A, Middag R, Laan P, Feldmann H, Andreae M (2011) Modulation of the southern ocean cadmium isotope signature by ocean circulation and primary productivity. Earth Planet Sci Lett 305:83–91

Ader M, Chaudhuri S, Coates JD, Coleman M (2008) Microbial perchlorate reduction: a precise laboratory determination of the chlorine isotope fractionation and its possible biochemical basis. Earth Planet Sci Lett 269:604–612

Aharon P, Fu B (2000) Microbial sulfate reduction rates and sulfur and oxygen isotope fractionation at oil and gas seeps in deepwater Gulf of Mexico. Geochim Cosmochim Acta 64:233–246

Amini M, Eisenhauer A, Böhm F, Fietzke J, Bach W, Garbe-Schoenberg D, Rosner M, Bock B, Lackschewitz K, Hauff F (2008) Calcium isotope ($\delta^{44/40}Ca$) fractionation along hydrothermal pathways, Logatchev field (Mid-Atlantic Ridge, 14°45′N). Geochim Cosmochim Acta 72:4107–4122

Amrani A, Sessions AL, Adkins JF (2009) Compound-specific $\delta^{34}S$ analysis of volatile organics by coupled GC/Multicollector-ICPMS. Anal Chem 81:9027–9034

Anbar AD (2004a) Iron stable isotopes: beyond biosignatures. Earth Planet Sci Lett 217:223–236

Anbar AD (2004b) Molybdenum stable isotopes: observations, interpretations and directions. Rev Mineral Geochem 55:429–454

Anbar AD, Jarzecki AA, Spiro TG (2005) Theoretical investigation of iron isotope fractionation between $Fe(H_2O)_6^{3+}$ and $Fe(H_2O)_6^{2+}$: implications for iron stable isotope geochemistry. Geochim Cosmochim Acta 69:825–837

Anbar AD, Rouxel O (2007) Metal stable isotopes in paleoceanography. Ann Rev Earth Planet Sci 35:717–746

Andersen MB, Vance D, Archer C, Anderson RF, Ellwood MJ, Allen CS (2011) The Zn abundance and isotopic composition of diatom frustules, a proxy for Zn availability in ocean surface seawater. Earth Planet Sci Lett 301:137–145

Andre L, Cardinal D, Alleman LY, Moorbath S (2006) Silicon isotopes in 3.8 Ga west Greenland rocks as clues to the Eoarchaean supracrustal Si cycle. Earth Planet Sci Lett 245:162–173

Antler G, Turchyn AV, Rennie V, Herut B, Sivan O (2013) Coupled sulphur and oxygen isotope insight into bacterial sulphate reduction in the natural environment. Geochim Cosmochim Acta 118:98–117

Archer C, Vance D (2006) Coupled Fe and S isotope evidence for Archean microbial Fe(III) and sulphate reduction. Geology 34:153–156

Archer C, Vance D (2008) The isotopic signature of the global riverine molybdenum flux and anoxia in the ancient oceans. Nat Geosci 1:597–600

Arnold GL, Anbar AD, Barling J, Lyons TW (2004a) Molybdenum isotope evidence for widespread anoxia in Mid-Proterozoic oceans. Science 304:87–90

Arnold GL, Weyer S, Anbar AD (2004b) Fe isotope variations in natural materials measured using high mass resolution multiple collector ICPMS. Anal Chem 76:322–327

Azmy K, Lavoie D, Wang Z, Brand U, Al-Aasm I, Jackson S, Girard I (2013) Magnesium-isotope and REE compositions of Lower Ordovician carbonates from eastern Laurentia: implications for the origin of dolomites and limestones. Chem Geol 356:64–75

Bachinski DJ (1969) Bond strength and sulfur isotope fractionation in coexisting sulfides. Econ Geol 64:56–65

Baker L, Franchi IA, Maynard J, Wright IP, Pillinger CT (2002) A technique for the determination of $^{18}O/^{16}O$ and $^{17}O/^{16}O$ isotopic ratios in water from small liquid and solid samples. Anal Chem 74:1665–1673

Baker RG, Rehkämper M, Hinkley TK, Nielsen SG, Poutain JP (2009) Investigation of thallium fluxes from subaerial volcanism- implications for the present and past mass balance of thallium in the oceans. Geochim Cosmochim Acta 73:6340–6359

Baker RG, Rehkämper M, Ihlenfeld C, Oates CJ, Coggon R (2010) Thallium isotope variations in an ore-bearing continental igneous setting: Collahuasi Formation, northern Chile. Geochim Cosmochim Acta 74:4405–4416

Balci N, Bullen TD, Witte-Lien K, Shanks WC, Motelica M, Mandernack KW (2006) Iron isotope fractionation during microbially simulated Fe(II) oxidation and Fe(III) precipitation. Geochim Cosmochim Acta 70:622–639

Balistrieri L, Borrok DM, Wanty RB, Ridley WI (2008) Fractionation of Cu and Zn isotopes during adsorption onto amorphous Fe(III) oxyhydroxide: experimental mixing of acid rock drainage and ambient river water. Geochim Cosmochim Acta 72:311–328

Banks DA, Green R, Cliff RA, Yardley BWD (2000) Chlorine isotopes in fluid inclusions: determination of the origins of salinity in magmatic fluids. Geochim Cosmochim Acta 64:1785–1789

Bao H (2015) Sulfate: a time capsule for bEarth's O2, O3 and H2O. Chem Geol 395:108–118

Bao H, Thiemens MH (2000) Generation of O_2 from $BaSO_4$ using a CO_2-laser fluorination system for simultaneous $\delta^{18}O$ and $\delta^{17}O$ analysis. Anal Chem 72:4029–4032

Barkan E, Luz B (2005) High precision measurements of $^{17}O/^{16}O$ and $^{18}O/^{16}O$ ratios in H_2O. Rapid Commun Mass Spectr 19:3737–3742

Barling J, Arnold GL, Anbar AD (2001) Natural mass-dependent variations in the isotopic composition of molybdenum. Earth Planet Sci Lett 193:447–457

Barnes JD, Paulick H, Sharp ZD, Bach W, Beaudoin G (2009) Stable isotope ($\delta^{18}O$, δD, $\delta^{37}Cl$) evidence for multiple fluid histories in mid-Atlantic abyssal peridotites (ODP Leg 209). Lithos 110:83–94

Barnes JD, Sharp ZD, Fischer TP (2006) Chlorine stable isotope systematics and geochemistry along the Central American and Izu-Bonin-Mariana volcanic arc. Eos Trans AGU 87(52), Fall Meet Suppl V52B-08

Barth S (1998) Application of boron isotopes for tracing source of anthropogenic contamination in groundwater. Water Res 32:685–690

Basile-Doelsch I, Meunier JD, Parron C (2005) Another continental pool in the terrestrial silicon cycle. Nature 433:399–402

Basu A, Sanford RA, Johnson TM, Lundstrom CC, Löffler FE (2014) Uranium isotopic fractionation factors during U(VI) reduction by bacterial isolates. Geochim Cosmochim Acta 136:100–113

Baumgartner LP, Rumble D (1988) Transport of stable isotopes. I. Development of a kinetic continuum theory for stable isotope transport. Contr Mineral Petrol 98:417–430

Beard BL, Handler RM, Scherer MM, Wu L, Czaja AD, Heimann A, Johnson CM (2010) Iron isotope fractionationbetween aqueous ferrous iron and goethite. Earth Planet Sci Lett 295:241–250

Beard BL, Johnson CM (1999) High-precision iron isotope measurements of terrestrial and lunar materials. Geochim Cosmochim Acta 63:1653–1660

Beard BL, Johnson CM (2004) Fe isotope variations in the modern and ancient Earth and other planetary bodies. Rev Mineral Geoch 55:319–357

Beard BL, Johnson CM, Cox L, Sun H, Nealson KH, Aguilar C (1999) Iron isotope biosphere. Science 285:1889–1892

Beard BL, Johnson CM, Skulan JL, Nealson KH, Cox L, Sun H (2003) Application of Fe isotopes to tracing the geochemical and biological cycling of Fe. Chem Geol 195:87–117

Beaudoin G, Taylor BE (1994) High precision and spatial resolution sulfur-isotope analysis using MILES laser microprobe. Geochim Cosmochim Acta 58:5055–5063

Beaudoin G, Taylor BE, Rumble D, Thiemens M (1994) Variations in the sulfur isotope composition of troilite from the Canyon Diablo iron meteorite. Geochim Cosmochim Acta 58:4253–4255

Bebout GE, Fogel ML (1992) Nitrogen isotope compositions of metasedimentary rocks in the Catalina Schist, California: implications for metamorphic devolatilization history. Geochim Cosmochim Acta 56:2839–2849

Bebout GE, Idleman BD, Li L, Hilkert A (2007) Isotope-ratio-monitoring gas chromatography methods for high-precision isotopic analysis of nanomole quantities of silicate nitrogen. Chem Geol 240:1–10

Beck WC, Grossman EL, Morse JW (2005) Experimental studies of oxygen isotope fractionation in the carbonic acid system at 15°, 25°, and 40 °C. Geochim Cosmochim Acta 69:3493–3503

Benson BB, Parker PDM (1961) Nitrogen/argon and nitrogen isotope ratios in aerobic sea water. Deep Sea Res 7:237–253

Berglund M, Wieser ME (2011) Isotopic compositions of the elements 2009 (IUPAC Technical Report). Pure Appl Chem 83:397–410

Bergquist BA, Blum JD (2009) The odds and evens of mercury isotopes: applications of mass-dependent and mass-independent isotope fractionation. Elements 5:353–357

Bergquist BA, Boyle EA (2006) Iron isotopes in the Amazon River system:weathering and transport signatures. Earth Planet Sci Lett 248:54–68

Bermin J, Vance D, Archer C, Statham PJ (2006) The determination of the isotopic composition of Cu and Zn in seawater. Chem Geol 226:280–297

Berna EC, Johnson TM, Makdisi RS, Basu A (2010) Cr stable isotopes as indicators of Cr (VI) reduction in groundwater: a detailed time-series study of a point-source plume. Environ Sci Technol 44:1043–1048

Bickle MJ, Baker J (1990) Migration of reaction and isotopic fronts in infiltration zones: assessments of fluid flux in metamorphic terrains. Earth Planet Sci Lett 98:1–13

Bidigare RR et al (1997) Consistent fractionation of ^{13}C in nature and in the laboratory: growth-rate effects in some haptophyte algae. Global Biogeochem Cycles 11:279–292

Bigeleisen J (1965) Chemistry of isotopes. Science 147:463–471

Bigeleisen J, Perlman ML, Prosser HC (1952) Conversion of hydrogenic materials for isotopic analysis. Anal Chem 24:1356

Biswas A, Blum JD, Bergquist BA, Keeler GJ, Xie Z (2008) Natural mercury isotope variation in coal deposits and organic soils. Environ Sci Technol 42:8303–8309

Black JR, Epstein E, Rains WD, Yin Q-Z, Casey WD (2008) Magnesium isotope fractionation during plant growth. Environ Sci Tech 42:7831–7836

Black JR, Kavner A, Schauble EA (2011) Calculation of equilibrium stable isotope partition function ratios for aqueous zinc complexes and metallic zinc. Geochim Copsmochim Acta 75:769–783

Blanchard M, Poitrasson F, Meheut M, Lazzari M, Mauri F, Balan E (2009) Iron isotope fractionation between pyrite (FeS_2), hematite (Fe_2O_3) and siderite ($FeCO_3$): a first-principles density functional theory study. Geochim Cosmochim Acta 73:6565–6578

Blattner P, Lassey KR (1989) Stable isotope exchange fronts, Damköhler numbers and fluid to rock ratios. Chem Geol 78:381–392

Blum JD, Sherman LS, Johnson MW (2014) Mercury isotopes in earth and environmental sciences. Ann Rev Earth Planet Sci 42:249–269

Blum JD (2011) Applications of stable mercury isotopes to biogeochemistry. In: Baskaran M (Ed) Handbook of environmental isotope geochemistry. Springer, New York, pp 229–246

Bolliger C, Schroth MH, Bernasconi SM, Kleikemper J, Zeyer J (2001) Sulfur isotope fractionation during microbial reduction by toluene-degrading bacteria. Geochim Cosmochim Acta 65:3289–3299

Bonifacie M, Jendrzejewski N, Agrinier P, Humler E, Coleman M, Javoy M (2008) The chlorine isotope composition of the Earth's mantle. Science 319:1518–1520

Bonnand P, James RH, Parkinson IJ, Connelly DP, Fairchild IJ (2013) The chromium isotopic composition of seawater and marine carbonates. Earth Planet Sci Lett 382:10–20

Bopp CJ, Lundstrom CC, Johnson TM, Glessner JJ (2009) Variations in $^{238}U/^{235}U$ in uranium ore deposits: isotopic signatures of the U reduction process? Geology 37:611–614

Borrok DM, Nimick DA, Wanty RB, Ridley WI (2008) Isotope variations of dissolved copper and zinc in stream water affected by historical mining. Geochim Cosmochim Acta 72:329–344

Borrok DM, Wanty RB, Ridley WI, Lamothe PJ, Kimball BA, Verplanck PL, Runkel RL (2009) Application of iron and zinc isotopes to track the sources and mechanisms of metal loading in a mountain watershed. Appl Geochem 24:1270–1277

Borthwick J, Harmon RS (1982) A note regarding ClF3 as an alternative to Br F5 for oxygen isotope analysis. Geochim Cosmochim Acta 46:1665–1668

Bottinga Y (1969) Calculated fractionation factors for carbon and hydrogen isotope exchange in the system calcite-carbon dioxide-graphite-methane-hydrogen-water-vapor. Geochim Cosmochim Acta 33:49–64

Boudreau BP, Westrich JT (1984) The dependence of bacterial sulfate reduction on sulfate concentration in marine sediments. Geochim Cosmochim Acta 48:2503–2516

Boulou-Bi EB, Poszwa A, Leyval C, Vigier N (2010) Experimental determination of magnesium isotope fractionation during higher plant growth. Geochim Cosmochim Acta 74:2523–2537

Bourdon B, Tipper ET, Fitoussi C, Stracke A (2010) Chondritic Mg isotope composition of the Earth. Geochim Cosmochim Acta 74:5069–5083

Bowman JR, Willett SD, Cook SJ (1994) Oxygen isotope transport and exchange during fluid flow. Am J Sci 294:1–55

Brand W, Coplen TB et al (2009a) Comprehensive inter-laboratory calibration of reference materials for $\delta^{18}O$ versus VSMOW using various on-line high-temperature conversion techniques. Rapid Comm Mass Spectrom 23:999–1019

Brand W, Geilmann H, Crosson ER, Rella CW (2009b) Cavity ring-down spectroscopy versus high-temperature conversion isotope ratio mass spectrometry: a case study on δ^2H and $\delta^{18}O$ of pure water samples and alcohol/water mixtures. Rapid Comm Mass Spectrom 23:1879–1884

Brand W (2002) Mass spectrometer hardware for analyzing stable isotope ratios. In: de Groot P (ed) Handbook of stable isotope analytical techniques. Elsevier, New York

Bremner JM, Keeney DR (1966) Determination and isotope ratio analysis of different forms of nitrogen in soils, III. Soil Sci Soc Am Proc 30:577–582

Brennecka GA, Wasylenki LE, Bargar JR, Weyer S, Anbar AD (2011) Uranium isotope fractionation during adsorption to Mn-oxyhydroxides. Environ Sci Technol 45:1370–1375

Brennikmeijer CAM, Kraft MP, Mook WG (1983) Oxygen isotope fractionation between CO_2 and H_2O. Isotope Geosci 1:181–190

Brooker R, Blundy J, James R (2004) Trace element and Li isotope systematics in zabargad peridotites: evidence of ancient subduction processes in the Red Sea mantle. Chem Geol 212:179–204

Brunner B, Bernasconi SM, Kleikemper J, Schroth MH (2005) A model of oxygen and sulfur isotope fractionation in sulfate during bacterial sulfate reduction. Geochim Cosmochim Acta 69:4773–4785

Brunner B, Contreras S and 9 others (2013) Nitrogen isotope effects induced by anammox bacteria. PNAS 1310488110

Brüchert V, Knoblauch C, Jörgensen BB (2001) Controls on stable sulfur isotope fractionation during bacterial sulfate reduction in Arctic sediments. Geochim Cosmochim Acta 65:763–776

Bucharenko AI (2001) Magnetic isotope effect: nuclear spin control of chemical reactions. J Phys Chem A105:9995–10011

Buhl D, Immenhauser A, Smeulders G, Kabiri L, Richter DK (2007) Time series δ^{26}Mg analysis in speleothem calcite: kinetic versus equilibrium fractionation, comparison with other proxies and implications for palaeoclimate research. Chem Geol 244:715–729

Burgoyne TW, Hayes JM (1998) Quantitative production of H_2 by pyrolysis of gas chromatographic effluents. Anal Chem 70:5136–5141

Burton KW, Vigier N (2011) Lithium isotopes as tracers in marine and terrestrial environments. In: Baskaran M (ed) Handbook environment isotope geochemistry. Springer, New York, pp 41–59

Busigny V, Bebout GE (2013) Nitrogen in the silicate earth: speciation and isotopic behavior during mineral-fluid interactions. Elements 9:353–358

Butler IB, Archer C, Vance D, Oldroyd A, Rickard D (2005) Fe isotope fractionation on FeS formation in ambient aqueous solution. Earth Planet Sci Lett 236:430–442

Böhlke JK, Sturchio NC, Gu B, Horita J, Brown GM, Jackson WA, Batista J, Hatzinger PB (2005) Perchlorate isotope forensics. Anal Chem 77:7838–7842

Böhm F, Eisenhauer A, Tang J, Dietzel M, Krabbenhöft A, Kisakürek B, Horn C (2012) Strontium isotope fractionation of planktic foraminifera and inorganic calcite. Geochim Cosmochim Acta 93:300–314

Böttcher ME (1996) $^{18}O/^{16}O$ and $^{13}C/^{12}C$ fractionation during the reaction of carbonates with phosphoric acid: effects of cationic substitution and reaction temperature. Isotopes Environ Health Stud 32:299–305

Böttcher ME, Brumsack HJ, Lange GJ (1998) Sulfate reduction and related stable isotope (^{34}S, ^{18}O) variations in interstitial waters from the eastern Mediterranean. Proc Ocean Drill Progr, Scientific Res 160:365–373

Böttcher ME, Thamdrup B, Vennemann TW (2001) Oxygen and sulfur isotope fractionation during anaerobic bacterial disproportionation of elemental sulfur. Geochim Cosmochim Acta 65:1601–1609

Böttcher M, Geprägs P, Neubert N, von Allmen K, Pretet C, Samankassou E, Nägler Tf (2012) Barium isotope fractionation during experimental formation of the double carbonate BaMn $(CO_3)_2$ at ambient temperature. Isotopes in environmental and health studies. doi:10.1080/10256016.2012.673489

Cameron V, Vance D, Archer C, House CH (2009) A biomarker based on the stable isotopes of nickel. PNAS 106:10944–10948

Cameron V, Vance D (2014) Heavy nickel isotope compositions in rivers and oceans. Geochim Cosmochim Acta (in press)

Canfield DE (2001a) Biogeochemistry of sulfur isotopes. Rev Mineral 43:607–636

Canfield DE (2001b) Isotope fractionation by natural populations of sulfate-reducing bacteria. Geochim Cosmochim Acta 65:1117–1124

Canfield DE, Farquhar J, Zerkle AL (2010) High isotope fractionations during sulfate reduction in a low-sulfate euxinic ocean analog. Geology 38:415–418

Canfield DE, Olsen CA, Cox RP (2006) Temperature and ist control of isotope fractionation by a sulfate reducing bacterium. Geochim Cosmochim Acta 70:548–561

Canfield DE, Teske A (1996) Late Proterozoic rise in atmospheric oxygen concentration inferred from phylogenetic and sulphur-isotope studies. Nature 382:127–132

Canfield DE, Thamdrup B (1994) The production of ^{34}S depleted sulfide during bacterial disproportion to elemental sulfur. Science 266:1973–1975

Cardinal D, Gaillardet J, Hughes HJ, Opfergelt S, Andre L (2010) Contrasting silicon isotope signetures in rivers from the Congo Basin and the specific behaviour of organic-rich waters. Geophys Res Lett 37:L12403

Carignan J, Estrade N, Sonke J, Donard O (2009) Odd isotope deficit in atmospheric Hg measured in lichens. Environ Sci Technol 43:5660–5664

Carignan J, Wen H (2007) Scaling NIST SRM 3149 for Se isotope analysis and isotopic variations of natural samples. Chem Geol 242:347–350

Caro G, Papanastassiou DA, Wasserburg GJ (2010) ^{40}K/^{40}Ca isotopic constraints on the oceanic calcium cycle. Earth Planet Sci Lett 296:124–132

Cartigny P (2005) Stable isotopes and the origin of diamond. Elements 1:79–84

Cartigny P, Boyd SR, Harris JW, Javoy M (1997) Nitrogen isotopes in peridotitic diamonds from Fuxian, China: the mantle signature. Terra Nova 9:175–179

Cartigny P, Marty B (2013) Nitrogen isotopes and mantle geodynamics: the emergence of life and the atmosphere-crust-mantle connection. Elements 9:359–366

Cartwright I, Valley JW (1991) Steep oxygen isotope gradients at marble-metagranite contacts in the NW Adirondacks Mountains, N.Y. Earth Planet Sci Lett 107:148–163

Casciotti KL (2009) Inverse kinetic isotope fractionation during bacterial nitrite oxidation. Geochim Cosmochim Acta 73:2061–2076

Casciotti KL, Sigman DM, Galanter Hastings M, Böhlke JK, Hilkert A (2002) Measurement of the oxygen isotopic composition of nitrate in seawater and freshwater using the denitrifier method. Anal Chem 74:4905–4912

Catanzaro EJ, Murphy TJ (1966) Magnesium isotope ratios in natural samples. J Geophys Res 71:1271

Cenki-Tok B, Chabaux F, Lemarchand D, Schmitt A, Pierret M, Viville D, Bagard M, Stille P (2009) The impact of water-rock interaction and vegetation on calcium isotope fractionation in soil- and stream waters of a small, forested catchment (the Strengbach case). Geochim Cosmochim Acta 73:2215–2228

Cerling TE, Sharp ZD (1996) Stable carbon and oxygen isotope analyses of fossil tooth enamel using laser ablation. Palaeo Palaeo Palaeoecol 126:173–186

Cerling TE, Harris JM (1999) Carbon isotope fractionation between diet and bioapatite in ungulate mammals and implications for ecological and paleocogical studies. Oecologia 120:347–363

Chacko T, Cole DR, Horita J (2001) Equilibrium oxygen, hydrogen and carbon fractionation factors applicable to geologic systems. Rev Mineral Geochem 43:1–81

Chacko T, Riciputi LR, Cole DR, Horita J (1999) A new technique for determining equilibrium hydrogen isotope fractionation factors using the ion microprobe: application to the epidote-water system. Geochim Cosmochim Acta 63:1–10

Chakrabarti B, Jacobsen S (2010) Silicon isotopes in the inner solar system: implications for core formation, solar nebula processes and partial melting. Geochim Cosmochim Acta 74:6921–6933

Chan LH, Alt JC, Teagle DAH (2002) Lithium and lithium isotope profiles through the upper oceanic crust: a study of seawater-basalt exchange at ODP Sites 504B and 896A. Earth Planet Sci Lett 201:187–201

Chan LH, Edmond JM, Thompson G (1993) A lithium isotope study of hot-springs and metabasalts from midocean ridge hydrothermal systems. J Geophys Res 98:9653–9659

Charlier BL, Nowell GM, Parkinson IJ, Kelley SP, Pearson DG, Burton KW (2012) High temperature strontium stable isotope behaviour in the early solar system and planetary bodies. Earth Planet Sci Lett 329–330:31–40

Chaussidon M, Albarede F (1992) Secular boron isotope variations in the continental crust: an ion microprobe study. Earth Planet Sci Lett 108:229–241

Chaussidon M, Albarede F, Sheppard SMF (1987) Sulphur isotope heterogeneity in the mantle from ion microprobe measurements of sulphide inclusions in diamonds. Nature 330:242–244

Chaussidon M, Albarede F, Sheppard SMF (1989) Sulphur isotope variations in the mantle from ion microprobe analysis of microsulphide inclusions. Earth Planet Sci Lett 92:144–156

Chaussidon M, Marty B (1995) Primitive boron isotope composition of the mantle. Science 269:383–386

Chen JB, Gaillardet J, Louvat P (2008) Zinc isotopes in the Seine river waters, France: a probe of anthropogenic contamination. Environ Sci Technol 42:6494–6501

Chen JB, Hintelmann H, Feng XB, Dimcock B (2012) Unusual fractionation of both odd and even mercury isotopes in precipitation from Peterborough, ON, Canada. Geochim Cosmochim Acta 90:33–46

Chen H, Nguyen BM, Moynier F (2013b) Zinc isotopic composition of iron meteorites: absence of isotope anomalies and origin of the volatile element depletion. Meteor Panet Sci 48:2441–2450

Chen H, Savage PS, Teng FZ, Helz RT, Moynier F (2013a) Zinc isotopic fractionation during magmatic differentiation and the isotopic composition of bulk Earth. Earth Planet Sci Lett 369–370:34–42

Chen H, Savage PS, Valdes M, Puchtel IS, Day JM, Moreira M, Jackson M, Moynier F (2014) Heterogeneity of calcium isotopes in Earth's mantle. Goldschmidt 2014 Abstracts, p 400

Chetelat B, Gaillardet J, Freydier F (2009) Use of B isotopes as a tracer of anthropogenic emissions in the atmosphere of Paris, France. Appl Geochem 24:810–820

Chiba H, Chacko T, Clayton RN, Goldsmith JR (1989) Oxygen isotope fractionations involving diopside, forsterite, magnetite and calcite: application to geothermometry. Geochim Cosmochim Acta 53:2985–2995

Chmeleff J, Horn I, Steinhöfel G, von Blanckenburg F (2008) In situ determination of precise stable Si isotope ratios by UV-femtosecond laser ablation high-resolution multi-collector ICP-MS. Chem Geol 249:155–160

Claire MW, Kasting JF, Domagal-Goldman SD, Stueken EE, Buick R, Meadows VS (2014) Modeling the signature of sulphur mass-independent fractionation produced in the Archean atmosphere. Geochim Cosmochim Acta 141:365–380

Clayton RN, Anderson P, Gale NH, Gills G, Whitehouse MJ (2002) Precise determination of the isotopic composition of Sn using MC-ICP-MS. J Anal At Spectrom 17:1248–1256

Clayton RN, Epstein S (1958) The relationship between $^{18}O/^{16}O$ ratios in coexisting quartz, carbonate and iron oxides from various geological deposits. J Geol 66:352–373

Clayton RN, Goldsmith JR, Mayeda TK (1989) Oxygen isotope fractionation in quartz, albite, anorthite and calcite. Geochim Cosmochim Acta 53:725–733

Clayton RN, Mayeda TK (1963) The use of bromine pentafluoride in the extraction of oxygen from oxides and silicates for isotopic analysis. Geochim Cosmochim Acta 27:43–52

Cloquet C, Carignan J, Lehmann MF, Vanhaecke F (2008) Variation in the isotopic composition of zinc in the natural environment and the use of zinc isotopes in biogeosciences: a review. Anal Bioanal Chem 390:451–463

Cloquet C, Carignan J, Libourel G, Sterckeman T, Perdrix E (2006) Tracing source pollution in soils using cadmium and lead isotopes. Environ Sci Technol 40:2525–2530

Cobert F, Schmitt AD, Bourgeade P, Labolle F, Badot PM, Chabaux F, Stille P (2011) Experimental identification of Ca isotopic fractionations in higher plants. Geochim Cosmochim Acta 75:5467–5482

Cole DR (2000) Isotopic exchange in mineral-fluid systems IV: the crystal chemical controls on oxygen isotope exchange rates in carbonate-H_2O and layer silicate-H_2O systems. Geochim Cosmochim Acta 64:921–933

Coleman ML, Sheppard TJ, Durham JJ, Rouse JE, Moore GR (1982) Reduction of water with zinc for hydrogen isotope analysis. Anal Chem 54:993–995

Cook DL, Wadhwa M, Clayton RN, Dauphas N, Janney PE, Davis AM (2007) Mass-dependent fractionation of nickel isotopes in meteoritic metal. Meteorit Planet Sci 42:2067–2077

Coplen TB et al (2002) Isotope abundance variations of selected elements. Pure Appl Chem 74:1987–2017

Coplen TB, Hanshaw BB (1973) Ultrafiltration by a compacted clay membrane. I. Oxygen and hydrogen isotopic fractionation. Geochim Cosmochim Acta 37:2295–2310

Coplen TB, Kendall C, Hopple J (1983) Comparison of stable isotope reference samples. Nature 302:236–238

Craddock PR, Dauphas N (2010) Iron isotopic compositions of geological reference materials and chondrites. Geostand Geoanal Res 35:101–123

Craddock PR, Rouxel OJ, Ball LA, Bach W (2008) Sulfur isotope measurement of sulfate and sulfide by high-resolution MC-ICP-MS. Chem Geol 253:102–113

Craig H (1961a) Isotopic variations in meteoric waters. Science 133:1702–1703

Craig H (1961b) Standard for reporting concentrations of deuterium and oxygen-18 in natural waters. Science 133:1833–1834

Criss RE, Gregory RT, Taylor HP (1987) Kinetic theory of oxygen isotopic exchange between minerals and water. Geochim Cosmochim Acta 51:1099–1108

Criss RE (1999) Principles of stable isotope distribution. Oxford University Press, Oxford

Croal LR, Johnson CM, Beard BL, Newman DK (2004) Iron isotope fractionation by Fe(II)-oxidizing photoautotrophic bacteria. Geochim Cosmochim Acta 68:1227–1242

Crosby HA, Johnson CM, Roden EE, Beard BL (2005) Fe(II)-Fe(III) electron/atom exchange as a mechanism for Fe isotope fractionation during dissimilatory iron oxide reduction. Environ Sci Tech 39:6698–6704

Crosby HA, Roden EE, Johnson CE, Beard BL (2007) The mechanisms of iron isotope fractionation produced during dissimilatory Fe(III) reduction by *Shewanella putrefaciens* and *Geobacter sulfurreducens*. Geobiology 5:169–189

Crowe DE, Valley JW, Baker KL (1990) Micro-analysis of sulfur isotope ratios and zonation by laser microprobe. Geochim Cosmochim Acta 54:2075–2092

Crowley SF (2010) Effect of temperature on the oxygen isotope composition of carbon dioxide ($\delta^{18}_{CO2}O$) prepared from carbonate minerals by reaction with polyphosphoric acid: an example of the rhombohedral $CaCO_3$-$MgCO_3$ group minerals. Geochim Cosmochim Acta 74:6406–6421

Crowson RA, Showers WJ, Wright EK, Hoering TC (1991) Preparation of phosphate samples for oxygen isotope analysis. Anal Chem 63:2397–2400

Czamanske GK, Rye RO (1974) Experimentally determined sulfur isotope fractionations between sphalerite and galena in the temperature range 600 °C to 275 °C. Econ Geol 69:17–25

Dahl TW, Anbar AD, Gordon GW, Rosing MT, Frei R, Canfield DE (2010a) The behavior of molybdenum and its isotopes across the chemocline and in the sediments of sulfidic Lake Cadagno, Switzerland. Geochim Cosmochim Acta 74:144–163

Dahl TW, Canfield DE, Rosing MT, Frei RE, Gordon GW, Knoll AH, Anbar AD (2011) Molybdenum evidence for expansive sulfidic water masses in ≈ 750 Ma oceans. Earth Planet Sci Lett 311:264–274

Dahl TW, Hammarlund EU et al (2010b) Devonian rise in atmospheric oxygen correlated to the radiations of terrestrial plants and large predatory fish. PNAS 107:17911–17915

Dauphas N, Craddock PR, Asimov PD, Bennett VC, Nutman A, Ohnenstetter D (2009a) Iron isotopes may reveal the redox conditions of mantle melting from Archean to Present. Earth Planet Sci Lett 288:255–267

Dauphas N, Pourmand A, Teng FZ (2009b) Routine isotopic analysis of iron by HR-MC-ICPMS: how precise and how accurate? Chem Geol 267:175–184

Dauphas N, Roskosz M et al (2012) A general moment NRIXS approach to the determination of equilibrium Fe isotope fractionation factors: application to goethite and jarosite. Geochim Cosmochim Acta 94:254–275

Dauphas N, Rouxel O (2006) Mass spectrometry and natural variations in iron isotopes. Mass Spectrom Rev 25:515–550

De Laeter JR, Böhlke JK, De Bièvre P, Hidaka H, Peiser HS, Rosman KJR, Taylor PD (2003) Atomic weights of the elements: review 2000 (IUPAC Technical Report). Pure Appl Chem 75:683–2000

De La Rocha C (2003) Silicon isotope fractionation by marine sponges and the reconstruction of the silicon isotope composition of ancient deep water. Geology 31:423–426

De La Rocha CL, Brzezinski MA, De Niro MJ (1997) Fractionation of silicon isotopes by marine diatoms during biogenic silica formation. Geochim Cosmochim Acta 61:5051–5056

De La Rocha CL, Brzezinski MA, De Niro MJ, Shemesh A (1998) Silicon-isotope composition of diatoms as an indicator of past oceanic change. Nature 395:680–683

De La Rocha CL, De Paolo DJ (2000) Isotopic evidence for variations in the marine calcium cycle over the Cenozoic. Science 289:1176–1178

De Souza GF, Reynolds B, Kiczka M, Bourdon B (2010) Evidence for mass-dependent isotopic fractionation of strontium in a glaciated granitic watershed. Geochim Cosmochim Acta 74:2596–2614

DeNiro MJ, Epstein S (1977) Mechanism of carbon isotope fractionation associated with lipid synthesis. Science 197:261–263

DePaolo D (2004) Calcium isotope variationsproduced by biological, kinetic, radiogenic and nucleosynthetic processes. Rev Mineral Geochem 55:255–288

DePaolo D (2011) Surface kinetic model for isotopic and trace element fractionation during precipitation of calcite from aqueous solution. Geochim Cosmochim Acta 75:1039–1056

Demarest MS, Brzezinski MA, Beucher CP (2009) Fractionation of silicon isotopes during biogenic silica dissolution. Geochim Cosmochim Acta 73:5572–5583

Desaulniers DE, Kaufmann RS, Cherry JO, Bentley HW (1986) ^{37}Cl-^{35}Cl variations in a diffusion-controlled groundwater system. Geochim Cosmochim Acta 50:1757–1764

Dideriksen K, Baker JA, Stipp SLS (2008) Equilibrium Fe isotope fractionaqtion between inorganic aqueous Fe(III) and the siderophore complex, Fe(III)-desferrioxamine B. Earth Planet Sci Lett 269:280–290

Ding T, Ma GR, Shui MX, Wan DF, Li RH (2005) Silicon isotope study on rice plants from the Zhejiang province, China. Chem Geol 218:41–50

Ding T, Wan D, Wang C, Zhang F (2004) Silicon isotope compositions of dissolved silicon and suspended matter in the Yangtze River, China. Geochim Cosmochim Acta 68:205–216

Ding TP, Zhou JX, Wan DF, Chen ZY, Wang CY, Zhang F (2008) Silicon isotope fractionation in bamboo and ist significance tot he biogeochemical cycle of silicon. Geochim Cosmochim Acta 72:1381–1395

Ding T et al (1996) Silicon isotope geochemistry. Geological Publishing House, Beijing

Dohmen R, Kasemann SA, Coogan L, Chakraborty S (2010) Diffusion of Li in olivine. Part !: Experimental observations and a multi species diffusion model. Geochim Cosmochim Acta 74:274–292

Dos Santos Pinheiro GM, Poitraason F, Sondag F, Cochonneau G, Cruz Vieira L (2014) Contrasting iron isotopic compositions in river suspended particulate matter: the Negro and the Amazon annual river cycles. Earth Planet Sci Lett 394:168–178

Dossing LN, Dideriksen K, Stipp SL, Frei R (2011) Reduction of hexavalent chromium by ferrous iron: a process of chromium isotope fractionation and its relevance to natural environments. Chem Geol

Douthitt CB (1982) The geochemistry of the stable isotopes of silicon. Geochim Cosmochim Acta 46:1449–1458

Driesner T (1997) The effect of pressure on deuterium-hydrogen fractionation in high-temperature water. Science 277:791–794

Driesner T, Seward TM (2000) Experimental and simulation study of salt effects and pressure/density effects on oxygen and hydrogen stable isotope liquid-vapor fractionation for 4–5 molal aqueous NaCl and KCl solutions to 400° C. Geochim Cosmochim Acta 64:1773–1784

Dugan JP, Borthwick J, Harmon RS, Gagnier MA, Glahn JE, Kinsel EP, McLeod S, Viglino JA (1985) Guadinine hydrochloride method for determination of water oxygen isotope ratios and the oxygen-18 fractionation between carbon dioxide and water at 25 °C. Anal Chem 57:1734–1736

Dziony W, Horn I, Lattard D, Koepke J, Steinhoefel G, Schuessler J, Holtz F (2014) In-situ Fe isotope ratio determination in Fe-Ti oxides and sulphides from drilled gabbros and basalt from the IODP Hole 1256D in the eastern equatorial Pacific. Chem Geol 363:101–113

Eastoe CJ, Gilbert JM, Kaufmann RS (1989) Preliminary evidence for fractionation of stable chlorine isotopes in ore-forming hydrothermal deposits. Geology 17:285–288

Eastoe CJ, Guilbert JM (1992) Stable chlorine isotopes in hydrothermal processes. Geochim Cosmochim Acta 56:4247–4255

Eastoe CJ, Long A, Knauth LP (1999) Stable chlorine isotopes in the Palo Duro basin, Texas: evidence for preservation of Permian evaporate brines. Geochim Cosmochim Acta 63:1375–1382

Eastoe CJ, Long A, Land LS, Kyle JR (2001) Stable chlorine isotopes in halite and brine from the Gulf Coast Basin: brine genesis and evolution. Chem Geol 176:343–360

Eastoe CJ, Peryt TM, Petrychenko OY, Geisler-Cussey D (2007) Stable chlorine isotopes in Phanerozoic evaporates. Appl Geochem 22:575–588

Egan KE, Rickaby RE, Leng H, Hendry KE, Hemoso M, Sloane HJ, Bostock H, Halliday RN (2012) Diatom silicon isotopes as a proxy for silicic acid utilisation: a southern ocean core top calibration. Geochim Cosmochim Acta 96: 174–192

Eggenkamp HGM, Coleman M (2000) Rediscovery of classical methods and their application to the measurement of stable bromine isotopes in natural samples. Chem Geol 167:393–402

Eggenkamp HGM, Kreulen R, Koster van Groos AF (1995) Chlorine stable isotope fractionation in evaporates. Geochim Cosmochim Acta 59:5169–5175

Eggenkamp HGM (1994) δ^{37}Cl: the geochemistry of chlorine isotopes. Thesis, University of Utrecht

Eggenkamp HGM (2014) The geochemistry of stable chlorine and bromine isotopes. Springer, New York

Ehrlich S, Butler I, Halicz L, Rickard D, Oldroyd A, Matthews A (2004) Experimental study of the copper isotope fractionation between aqueous Cu(II) and covellite, CuS. Chem Geol 209:259–269

Eisenhauer A et al (2004) Proposal for an international agreement on Ca notation as result of the discussion from the workshops on stable isotope measurements in Davos (Goldschmidt 2002) and Nice (EUG 2003). Geostand Geoanal Res 28:149–151

Eisenhauer A, Kisakürek B, Böhm F (2009) Marine calcification: an alkali earth metal isotope perspective. Elements 5:365–368

Eldridge CS, Compston W, Williams IS, Both RA, Walshe JL, Ohmoto H (1988) Sulfur isotope variability in sediment hosted massive sulfide deposits as determined using the ion microprobe SHRIMP. I. An example from the Rammelsberg ore body. Econ Geol 83:443–449

Eldridge CS, Williams IS, Walshe JL (1993) Sulfur isotope variability in sediment hosted massive sulfide deposits as determined using the ion microprobe SHRIMP. II. A study of the H.Y.C. deposit at McArthur River, Northern Territory. Australia. Econ Geol. 88:1–26

Elliott T, Jeffcoate AB, Bouman C (2004) The terrestrial Li isotope cycle: light-weight constraints on mantle convection. Earth Planet Sci Lett 220:231–245

Ellis AS, Johnson TM, Bullen TD (2002) Chromium isotopes and the fate of hexavalent chromium in the environment. Science 295:2060–2062

Ellis AS, Johnson TM, Bullen TD (2004) Using chromium stable isotope ratios to quantify Cr(VI) reduction: lack of sorption effects. Environ Sci Technol 38:3604–3607

Emrich K, Ehhalt DH, Vogel JC (1970) Carbon isotope fractionation during the precipitation of calcium carbonate. Earth Planet Sci Lett 8:363–371

Engstrom E, Rodushkin I, Baxter DC, Ohlander B (2006) Chromatographic purification for the determination of dissolved silicon isotopic compositions in natural waters by high-resolution multicollector inductively coupled mass spectrometry. Anal Chem 78:250–257

Estrade N, Carignan J, Sonke JE, Donard O (2009) Mercury isotope fractionation during liquid-vapor evaporation experiments. Geochim Cosmochim Acta 73:2693–2711

Eugster O, Tera F, Wasserburg GJ (1969) Isotopic analyses of barium in meteorites and in terrestrial samples. J Geophys Res 74:3897–3908

Fantle MS (2010) Evaluating the Ca isotope proxy. Am J Sci 310:194–210

Fantle MS, de Paolo DJ (2005) Variations in the marine Ca cycle over the past 20 million years. Earth Planet Sci Lett 237:102–117

Fantle MS, Tipper ET (2014) Calcium isotopes in the global biogeochemical Ca cycle: implications for development of a Ca isotope proxy. Earth Sci Rev 129:148–177

Farkas J, Buhl D, Blenkinsop J, Veizer J (2007) Evolution of the oceanic calcium cycle during the late Mesozoic: evidence from $\delta^{44/40}$ Ca of marine skeletal carbonates. Earth Planet Sci Lett 253:96–111

Farkas J, Chrastny V, Novak M, Cadkova E, Pasava J, Chakrabarti R, Jacobsen S, Ackerman L, Bullen TD (2013) Chromium isotope variations (d53/52Cr) in mantle-derived sources and their weathering products: implications for environmental studies and the evolution of d53/52Cr in the Earth's mantle over geologic time. Geochim Cosmochim Acta 123:74–92

Farquhar J, Bao H, Thiemens M (2000) Atmospheric influence of Earth's earliest sulfur cycle. Science 289:756–759

Farquhar J, Day JM, Hauri EH (2013) Anomaleous sulphur isotopes in plume lavas reveal deep mantle storage of Archaean crust. Nature 496:490–493

Farquhar GD, Ehleringer JR, Hubick KT (1989) Carbon isotope discrimination and photosynthesis. Ann Rev Plant Physiol Plant Mol Biol 40:503–537

Farquhar J, Johnston DT, Wing BA, Habicht KS, Canfield DE, Airieau S, Thiemens MH (2003) Multiple sulphur isotope interpretations for biosynthetic pathways: implications for biological signatures in the sulphur isotope record. Geobiology 1:27–36

Farquhar J, Kim ST, Masterson A (2007) Implications from sulfur isotopes of the Nakhla meteorite for the origin of sulfate on Mars. Earth Planet Sci Lett 264:1–8

Farrell JW, Pedersen TF, Calvert SE, Nielsen B (1995) Glacial-interglacial changes in nutrient utilization in the equatorial Pacific Ocean. Nature 377:514–517

Fehr MA, Rehkämper M, Halliday AN (2004) Application of MC-ICP-MS to the precise determination of tellurium isotope compositions in chondrites, iron meteorites and sulphides. Inter J Mass Spectr 232:83–94

Feng C, Qin T, Huang S, Wu Z, Huang F (2014) First principles investigations of equilibrium calcium isotope fractionation between clinopyroxene and Ca-doped orthopyroxene. Geochim Cosmochim Acta 143:132–142

Fiebig J, Hoefs J (2002) Hydrothermal alteration of biotite and plagioclase as inferred from intragranular oxygen isotope- and cation-distribution patterns. Eur J Mineral 14:49–60

Fietzke J, Eisenhauer A et al (2004) Direct measurement of 44Ca/40Ca ratios nby MC-ICP-MS using the cool plasma technique. Chem Geol 206:11–20

Fietzke J, Eisenhauer A (2006) Determination of temperature-dependent stable strontium isotope (^{88}Sr/^{86}Sr) fractionation via bracketing standard MC-ICP-MS. Geochem Geophys Geosys 7(8). doi:10.1029/2006GC001243

Fogel ML, Cifuentes LA (1993) Isotope fractionation during primary production. In: Engel MH, Macko SA (eds) Organic geochemistry. Plenum Press, New York, pp 73–98

Fornadel AP, Spry GP, Jackson SE, Mathur RD, Chapman JB, Girard I (2014) Methods for the determination of stable Te isotopes of minerals in the system Au-Ag-Te by MC-ICP-MS. J Anal At Spectrom 29:623–637

Foster GI, Pogge von Strandmann PA, Rae JW (2010) Boron and magnesium isotopic compositions of seawater. Geochem Geophys Geosys 11. doi:10.1029/2010GC003201

Freeman KH (2001) Isotopic biogeochemistry of marine organic carbon. Rev Mineral Geochem 43:579–605

Frei R, Gaucher C, Dossing LN, Sial AN (2011) Chromium isotopes in carbonates—a tracer for climate change and for reconstructing the redox state of ancient seawater. Earth Planet Sci Lett 312:114–125

Frei R, Gaucher C, Poulton SW, Canfield DE (2009) Fluctuations in Precambrian atmospheric oxygenation recorded by chromium isotopes. Nature 461:250–253

Frei R, Poiret D, Frei KM (2014) Weathering on land and transport of chromium to the ocean in a subtropical region (Misiones, NW Argentina): a chromium stable isotope perspective. Chem Geol 381:110–124

Frei R, Polat A (2013) Chromium isotope fractionation during oxidative weathering—implications from the study of a paleoproterozoic (ca. 1.9 Ga) paleosol, Schreiber Beach, Ontario, Canada. Precam Res 224:434–453

Friedman I (1953) Deuterium content of natural waters and other substances. Geochim Cosmochim Acta 4:89–103

Friedrich AJ, Beard BL, Scherer MM, Johnson CM (2014) Determination of the Fe(II) aq-magnetite equilibrium iron isotope fractionation factor using the three-isotope method and a multi-direction approach to equilibrium. Earth Planet Sci Lett 391:77–86

Fritz P, Basharmel GM, Drimmie RJ, Ibsen J, Qureshi RM (1989) Oxygen isotope exchange between sulphate and water during bacterial reduction of sulphate. Chem Geol 79:99–105

Fry B, Ruf W, Gest H, Hayes JM (1988) Sulphur isotope effects associated with oxidation of sulfide by O_2 in aqueous solution. Chem Geol 73:205–210

Fujii T, Moynier F, Dauphas N, Abe M (2011b) Theoretical and experimental investigation of nickel isotope fractionation in species relevant to modern and ancient oceans. Geochim Cosmochim Acta 75:469–482

Fujii T, Moynier F, Pons ML, Albarede F (2011a) The origin of Zn isotope fractionation in sulfides. Geochim Cosmochim Acta 75:7632–7643

Gagnevin D, Boyce AJ, Barrie CD, Menuge JF, Blakeman RJ (2012) Zn, Fe, and S isotope fractionation in a large hydrothermal system. Geochim Cosmochim Acta 88:183–198

Galimov EM (2006) Isotope organic geochemistry. Org Geochem 37:1200–1262

Galimov EM (1985a) The biological fractionation of isotopes. Academic Press Inc, Orlando

Gall L, Williams HM, Siebert C, Halliday AN, Herrington RJ, Hein JR (2013) Nickel isotopic compositions of ferromanganese crusts and the constancy of deep ocean inputs and continental weathering effects. Earth Planet Sci Lett

Galy A et al (2003) Magnesium isotope heterogeneity of the isotopic standard SRM980 and new reference materials for magnesium-isotope-ratio measurements. J Anal At Spectr 18:1352–1356

Galy A, Bar-Matthews M, Halicz L, O'Nions RK (2002) Mg isotopic composition of carbonate: insight from speleothem formation. Earth Planet Sci Lett 201:105–115

Galy A, Belshaw NS, Halicz L, O'Nions RK (2001) High-precision measurement of magnesium isotopes by multiple-collector inductively coupled plasma mass spectrometry. Inter J Mass Spectr 208:89–98

Ganeshram RS, Pedersen TF, Calvert SE, McNeill GW, Fontugue MR (2000) Glacial-interglacial variability in denitrification in the world's oceans: causes and consequences. Paleoceanography 15:361–376

Gao Y, Casey JF (2011) Lithium isotope composition of ultramafic geological reference materials JP-1 and DTS-2. Geostand Geoanal Res 36:75–81

Gao Y, Vils F et al (2012) Downhole variation of lithium and oxygen isotopic compositions of oceanic crust at East Pacific Rise, ODP Site 1256. Geochem Geophys Geosystems 13. doi:10.1029/2012GC004207

Garlick GD (1966) Oxygen isotope fractionation in igneous rocks. Earth Planet Sci Lett 1:361–368

Gault-Ringold M, Adu T, Stirling C, Frew RD, Hunter KA (2012) Anomalous biogeochemical behaviour of cadmium in subantarctic surface waters: mechanistic constraints from cadmium isotopes. Earth Planet Sci Lett 341–344:94–103

Gehre M, Hoefling R, Kowski P, Strauch G (1996) Sample preparation device for quantitative hydrogen isotope analysis using chromium metal. Anal Chem 68:4414–4417

Gehrke GE, Blum JD, Meyers PA (2009) The geochemical behaviour and isotope composition of Hg in a mid-Pleistocene western Mediterranean sapropel. Geochim Cosmochim Acta 73:1651–1665

Gelabert A, Pokrovsky OS, Viers J, Schott J, Boudou A, Feurtet-Mazel A (2006) Interaction between zinc and marine diatom species: surface complexation and Zn isotope fractionation. Geochim Cosmochim Acta 70:839–857

Georg RB, Halliday AN, Schauble EA, Reynolds BC (2007) Silicon in the Earth's core. Nature 447:1102–1106

Georg RB, Reynolds BC, Frank M, Halliday AN (2006) Mechanisms controlling the silicon isotopic compositions of river water. Earth Planet Sci Lett 249:290–306

Georg RB, Zhu C, Reynolds BC, Halliday AN (2009) Stable silicon isotopes of groundwater, feldspars and clay coating in the Navajo sandstone aquifer, Black Mesa, Arizona, USA. Geochim Cosmochim Acta 73:2229–2241

Geske A, Goldstein RH, Mavromatis V, Richter DK, Buhl D, Kluge T, John CM, Immenhauser A (2015) The magnesium isotope (δ^{26}Mg) signature of dolomites. Geochim Cosmochim Acta 149:131–151

Ghosh S, Schauble EA, Lacrampe Coulome G, Blum JD, Bergquist BA (2013) Estimation of nuclear volume dependent fractionation of mercury isotopes in equilibrium liquid-vapor evaporation experiment. Chem Geol 366:5–12

Giesemann A, Jäger HA, Norman AL, Krouse HR, Brand WA (1994) On-line sulphur isotope determination using an elemental analyzer coupled to a mass spectrometer. Anal Chem 66:2816–2819

Giletti BJ (1985) The nature of oxygen transport within minerals in the presence of hydrothermal water and the role of diffusion. Chem Geol 53:197–206

Godfrey JD (1962) The deuterium content of hydrous minerals from the East Central Sierra Nevada and Yosemite National Park. Geochim Cosmochim Acta 26:1215–1245

Goldhaber MB, Kaplan IR (1974) The sedimentary sulfur cycle. In: Goldberg EB (ed) The sea, vol IV. Wiley and Sons, New York

Gordon GW, Lyons TW, Arnold GL, Roe J, Sageman BB, Anbar AD (2009) When do black shales tell molybdenum isotope tales? Geology 37:535–538

Graham CM, Harmon RS, Sheppard SMF (1984) Experimental hydrogen isotope studies: hydrogen isotope exchange between amphibole and water. Am Mineral 69:128–138

Graham CM, Sheppard SMF, Heaton THE (1980) Experimental hydrogen isotope studies. I. Systematics of hydrogen isotope fractionation in the systems epidote-H_2O, zoisite-H_2O and AlO(OH)-H_2O. Geochim Cosmochim Acta 44:353–364

Greber ND, Hofmann BD, Voegelin AR, Villa IM, Nägler TF (2011) Mo isotope compositions in Mo-rich high- und low-T hydrothermal systems from the Swiss Alps. Geochim Cosmochim Acta 75:6600–6609

Greber ND, Pettke T, Nägler TF (2014) Magmatic-hydrothermal molybdenum isotope fractionation and its relevance to the igneous crustal signature. Lithos 190–191:104–110

Gregory RT, Criss RE, Taylor HP (1989) Oxygen isotope exchange kinetics of mineral pairs in closed and open systems: applications to problems of hydrothermal alteration of igneous rocks and Precambrian iron formations. Chem Geol 75:1–42

Griffith EM, Paytan A, Eisenhauer A, Bullen TD, Thomas E (2011) Seawater calcium isotope ratios across the Eocene-Oligocene transition. Geology 39:683–686

Griffith EM, Paytan A, Kozdon R, Eisenhauer A, Ravelo AC (2008a) Influences on the fractionation of calcium isotopes in planktonic foraminifera. Earth Planet Sci Lett 268:124–136

Griffith EM, Payton A, Caldeira K, Bullen TD, Thomas E (2008c) A dynamic marine calcium cycle during the past 28 million years. Science 322:1671–1674

Griffith EM, Schauble EA, Bullen TD, Paytan A (2008b) Characterization of calcium isotopes in natural and synthetic barite. Geochim Cosmochim Acta 72:5641–5658

Grossman EL, Ku T-L (1986) Oxygen and carbon isotope fractionation in biogenic aragonite: temperature effects. Chem Geol 59:59–74

Gueguen B, Rouxel O, Ponzevera E, Bekker A, Fouquet Y (2013) Nickel isotope variations in terrestrial silicate rocks and geological reference materials measured by MC-ICP-MS. Geostand Geoanal Res 37:297–317

Guelke M, von Blanckenburg F (2007) Fractionation of stable iron isotopes in higher plants. Environ Sci Technol 41:1896–1901

Guelke M, von Blanckenburg F, Schoenberg R, Staubwasser M, Stuetzel H (2010) Determining the stable Fe isotope signature of plant-available iron in soils. Chem Geol 277:269–280

Guelke-Stelling M, von Blanckenburg F (2012) Fe isotope fractionation caused by translocation of iron during growth of bean and oat as models of strategy I and II plants. Plant Soil 352:217–231

Guerrot C, Millot R, Robert M, Negrel P (2011) Accurate and high-precision determination of boron isotopic ratios at low concentration by MC-ICP-MS (Neptune). Geostand Geoanal Res 35:275–284

Guilbaud R, Butler IB, Ellam RM (2011) Abiotic pyrite formation produces a large Fe isotope fractionation. Science 332:1548–1551

Gussone N et al (2003) Model for kinetic effects on calcium isotope fractionations ($\delta^{44}Ca$) in inorganic aragonite and cultured planktonic foraminifera. Geochim Cosmochim Acta 67:1375–1382

Gussone N et al (2005) Calcium isotope fractionation in calcite and aragonite. Geochim Cosmochim Acta 69:4485–4494

Habicht KS, Canfield DE (1997) Sulfur isotope fractionation during bacterial sulfate reduction in organic-rich sediments. Geochim Cosmochim Acta 61:5351–5361

Habicht KS, Canfield DE (2001) Isotope fractionation by sulfate-reducing natural populations and the isotopic composition of sulfide in marine sediments. Geology 29:555–558

Haendel D, Mühle K, Nitzsche HIM, Stiehl G, Wand U (1986) Isotopic variations of the fixed nitrogen in metamorphic rocks. Geochim Cosmochim Acta 50:749–758

Halevy I, Johnston DT, Schrag DP (2010) Explaining the structure of the Archean mass-independent sulfur isotope record. Science 329:204–207

Halicz L, Galy A, Belshaw N et al (1999) High-precision measurement of calcium isotopes in carbonates and related materials by multiple collector inductively coupled plasma mass spectrometry (MC-ICP-MS). J Anal At Spectr 14:1835–1838

Halicz L, Segal I, Fruchter N, Stein M, Lazar B (2008b) Strontium stable isotopes fractionate in the soil environment? Earth Planet Sci Lett 272:405–411

Halicz L, Yang L, Teplyakov N, Burg A, Sturgeon R, Kolodny Y (2008a) High precision determination of chromium isotope ratios in geological samples by MC-ICP-MS. J Anal At Spectrom 23:1622–1627

Han R, Qin L, Brown ST, Christensen JN, Beller HR (2012) Differential isotopic fractionation during Cr(VI) reduction by an aquifer-derived bacterium under aerobic versus denitrifying conditions. Appl Environ Microbiol 78:2462–2464

Handler MR, Baker JA, Schiller M, Bennett VC, Yaxley GM (2009) Magnesium stable isotope composition of Earth's upper mantle. Earth Planet Sci Lett 282:306–313

Hannah JL, Stein HJ, Wieser ME, de Laeter JR, Varner MD (2007) Molybdenum isotope variations in molybdenite: vapor transport and Rayleigh fractionation of Mo. Geology 35:703–706

Harouaka K, Eisenhauer A, Fantle MS (2014) Experimental investigation of Ca isotopic fractionation during abiotic gypsum precipitation. Geochim Cosmochim Acta 129:157–176

Harrison AG, Thode HG (1957a) Kinetic isotope effect in chemical reduction of sulphate. Faraday Soc Trans 53:1648–1651

Harrison AG, Thode HG (1957b) Mechanism of the bacterial reduction of sulphate from isotope fractionation studies. Faraday Soc Trans 54:84–92

Hastings MG, Jarvis JC, Steig EJ (2009) Anthropogenic impacts on nitrogen isotopes of ice-core nitrate. Science 324:1238

Hastings MG, Casciotti KL, Elliott EM (2013) Stable isotopes as tracers of anthropogenic nitrogen sources, deposition, and impacts. Elements 9: 339–34

Haustein M, Gillis C, Pernicka E (2010) Tin isotopy – a new method for solving old questions. Archaeometry 52:816–832

Hayes JM (1993) Factors controlling 13C contents of sedimentary organic compounds: principle and evidence. Mar Geol 113:111–125

Hayes JM, Strauss H, Kaufman AJ (1999) The abundance of ^{13}C in marine organic matter and isotopic fractionation in the global biogeochemical cycle of carbon during the past 800 Ma. Chem Geol 161:103–125

Hayes JM (2001) Fractionation of carbon and hydrogen isotopes in biosynthetic processes. In: Valley JW, Cole DR (eds) Stable isotope geochemistry. Rev Mineral Geochem 43:225–277

He Y, Ke S, Teng FZ, Wang T, Wu H, Lu Y, Li S (2015) High precision iron isotope analysis of geological standards by high resolution MC-ICPMS. Geostand Geoanal Res (in press)

Heaton THE (1986) Isotopic studies of nitrogen pollution in the hydrosphere and atmosphere: a review. Chem Geol 59:87–102

Heck PR, Huberty JM, Kita NT, Ushikubo T, Kozdon R, Valley JW (2011) SIMS analysis of silicon and oxygen isotope ratios for quartz from Archean and Paleoproterozoic banded iron formations. Geochim Cosmochim Acta 75:5879–5891

Heimann A, Beard BL, Johnson CM (2008) The role of volatile exsolution and sub-solidus fluid/rock interactions in producing high ^{56}Fe/^{54}Fe ratios in siliceous igneous rocks. Geochim Cosmochim Acta 72:4379–4396

Hemming NG, Hanson GN (1992) Boron isotopic composition in modern marine carbonates. Geochim Cosmochim Acta 56:537–543

Hendry KR, Andersen MB (2013) The zinc isotopic composition of siliceous marine sponges: investigating nature's sediment traps. Chem Geol 354:33–41

Hendry KR, Georg RB, Rickaby R, Robinson LR, Halliday AN (2010) Deep ocean nutrients during the last glacial maximum deduced from sponge silicon isotopic compositions. Earth Planet Sci Lett 292:290–300

Herbel MJ, Johnson TM, Oremland RS, Bullen TD (2000) Fractionation of selenium isotopes during bacterial respiratory reduction of selenium oxyanions. Geochim Cosmochim Acta 64:3701–3710

Herrmann AD, Kendall B, Algeo TJ, Gordon GW, Wasylenki LE, Anbar AD (2012) Anomalous molybdenum isotope trends in Upper Pennsylvanian euxinic facies: significance for the use of δ^{98}Mo as a global marine redox proxys. Chem Geol 324–325:87–98

Hervig RL, Moore GM, Williams LB, Peacock SM, Holloway JR, Roggensack K (2002) Isotopic and elemental partitioning of boron between hydrous fluid and silicate melt. Am Mineral 87:769–774

Hesse R, Egeberg PK, Frape SK (2006) Chlorine stable isotope ratios as tracer for pore-water advection rates in a submarine gas-hydrate field: implication for hydrate concentration. Geofluids 6:1–7

Hettmann K, Marks MA, Kreissig K, Zack T, Wenzel T. Rehkämper M, Jacob DE, Markl G (2014) The geochemistry of Tl and its isotopes during magmatic and hydrothermal processes: the peralkaline Ilimaussaq complex. southwest Greenland. Chem Geol

Heuser A, Eisenhauer A (2008) The calcium isotope composition (d$^{44/40}$Ca) of NIST SRM 915a and NIST SRM 1486. Geostand Newslett J Geostand Geoanal 32:311–315

Hiess J, Condon DJ, McLean N, Noble SR (2012) ^{238}U/^{235}U systematics in terrestrial uranium-bearing minerals. Science 335:1610–1614

Higgins JA, Schrag DP (2010) Constraining magnesium cycling in marine sediments using magnesium isotopes. Geochim Cosmochim Acta 74:5039–5053

Hill P, Schauble E (2008) Modeling the effects of bond environment on equilibrium iron isotope fractionation in ferric aquo-chloro complexes. Geochim Cosmochim Acta 72:1939–1958

Hill P, Schauble E, Shahar A, Tonui E, Young ED (2009) Experimental studies of equilibrium iron isotope fractionation in ferric aquo-chloro complexes. Geochim Cosmochim Acta 73:2366–2381

Hill P, Schauble E, Young ED (2010) Effects of changing solution chemistry on Fe^{3+}/Fe^{2+} isotope fractionation in aqueous Fe-Cl solution. Geochim Cosmochim Acta 74:6669–6705

Hin RC, Schmidt MW, Bourdon B (2012) Experimental evidence for the absence of iron isotope fractionation between metal and silicate liquids at 1GPA and 1250-1300 °C and its cosmochemical consequences. Geochim Cosmochim Acta 93:164–181

Hindshaw RS, Reynolds BC, Wiederhold JG, Kiczka M, Kretzschmar R, Bourdon B (2013) Calcium isotope fractionation in alpine plants. Biogeochemistry 112:373–388

Hindshaw RS, Reynolds BC, Wiederhold JG, Kretzschmar R, Bourdon B (2011) Calcium isotopes in a proglacial weathering environment: Damma glacier, Switzerland. Geochim Cosmochim Acta 75:106–118

Hinojosa JL, Brown ST, Chen J, DePaolo DJ, Paytan A, Shen SZ, Payne J (2012) Evidence for end-Permian ocean acidification from calcium isotopes in biogenic apatite. Geology

Hippler D, Buhl D, Witbaard R, Richter DK, Immenhauser A (2009) Towards a better understanding of magnesium-isotope ratios from marine skeletal carbonates. Geochim Cosmochim Acta 73:6134–6146

Hippler D, Eisenhauer A, Nägler TF (2006) Tropical Atlantic SST history inferred from Ca isotope thermometry over the last 140 ka. Geochim Cosmochim Acta 70:90–100

Hitzfeld KL, Gehre M, Richnow HH (2011) A novel online approach to the determination of isotope ratios for organically bound chlorine, bromine and sulphur. Rapid Commun Mass Spectr 25:3114–3122

Hoering T, Parker PL (1961) The geochemistry of the stable isotopes of chlorine. Geochim Cosmochim Acta 23:186–199

Hofmann A, Bekker A, Dirks P, Gueguen B, Rumble D, Rouxel O (2014) Comparing orthomagmatic and hydrothermal mineralization models for komatiite-hosted nickel deposits in Zimbabwe using multiple-sulfur, iron and nickel isotope data. Miner Deposita 49:75–100

Holmden C (2009) Ca isotope study of Ordovician dolomite, limestone, and anhydrite in the Williston basin: Implications for subsurface dolomitization and local Ca cycling. Chem Geol 268:180–188

Holmden C, Belanger N (2010) Ca isotope cycling in a forested ecosystem. Geochim Cosmochim Acta 74:995–1015

Holmstrand H, Unger M, Carrizo D, Andersson P, Gustafsson Ö (2010) Compound specific bromine isotope analysis of brominated diphenyl ethers using GC-ICP-MC-MS. Rapid Commun Mass Spectr 24:2135–2142

Homoky WB, Severmann S, Mills RA, Statham PJ, Fones GR (2011) Pore-fluid Fe isotopes reflect the extent of benthic Fe redox recycling: evidence from continental shelf and deep-sea sediments. Geology 37:751–754

Horita J (1988) Hydrogen isotope analysis of natural waters using an H_2-water equilibration method: a special implication to brines. Chem Geol 72:89–94

Horita J, Driesner T, Cole DR (1999) Pressure effect on hydrogen isotope fractionation between brucite and water at elevated temperatures. Science 286:1545–1547

Horita J, Wesolowski DJ (1994) Liquid-vapor fractionation of oxygen and hydrogen isotopes of water from the freezing to the critical temperature. Geochim Cosmochim Acta 58:3425–3437

Horita J, Wesolowski DJ, Cole DR (1993) The activity-composition relationship of oxygen and hydrogen isotopes in aqueous salt solutions. I. Vapor-liquid water equilibration of single salt solutions from 50 to 100 °C. Geochim Cosmochim Acta 57:2797–2817

Horner TJ, Schönbächler M, Rehkämper M et al (2010) Ferromanganese crusts as archives of deep water Cd isotope composition. Geochem Geophys Geosyst 11:Q04001

Horner T, Rickaby R, Henderson G (2011) Isotopic fractionation of cadmium into calcite. Earth Planet Sci Lett 312:243–253

Horst A, Andersson P, Thornton BJ, Holmstrand H, Wishkerman A, Keppler F, Gustafsson Ö (2014) Stable bromine isotope composition of methyl bromide released from plant matter. Geochim Cosmochim Acta 125:186–195

Horst A, Thornton BJ, Holmstrand H, Andersson P, Crill PM, Gustafsson Ö (2013) Stable bromine isotopic composition of atmospheric CH_3Br. Tellus Ser B Chem Phys Meteor 65:21040

Hu GX, Rumble D, Wang PL (2003) An ultraviolet laser microprobe for the in-situ analysis of multisulfur isotopes and its use in measuring Archean sulphur isotope mass-independent anomalies. Geochim Cosmochim Acta 67:3101–3118

Huang S, Farkas J, Jacobsen SB (2010) Calcium isotopic fractionation between clinopyroxene and orthopyroxene from mantle peridotites. Earth Planet Sci Lett 292:337–344

Huang S, Farkas J, Jacobsen S (2011) Stable calcium isotopic compositions of Hawaiian shield lavas: evidence for recycling of ancient marine carbonates into the mantle. Geochim Cosmochim Acta 75:4987–4997

Huang KJ, Teng FZ, Wei GJ, Ma JL, Bao ZY (2012) Adsorption- and desorption-controlled magnesium isotope fractionation during extreme weathering of basalt in Hainan Island, China. Earth Planet Sci Lett 359–360:73–83

Huang F, Wu Z, Huang S, Wu F (2014) First-principles calculations of equilibrium silicon isotope fractionation among mantle minerals. Geochim Cosmochim Acta 140:509–520

Huh Y, Chan L-H, Zhang L, Edmond JM (1998) Lithium and its isotopes in major world rivers; implications for weathering and the oceanic budget. Geochim Cosmochim Acta 62:2039–2051

Icopini GA, Anbar AD, Ruebush SS, Tien M, Brantley SL (2004) Iron isotope fractionation during microbial reduction of iron: the importance of adsorption. Geology 32:205–208

Ikehata K, Hirata T (2012) Copper isotope characteristics of copper-rich minerals from the Horoman peridotite complex, Hokkaido, Northern Japan. Econ Geol 107:1489–1497

Immenhauser A, Buhl D, Richter D, Niedermayer A, Riechelmann D, Dietzel M, Schulte U (2010) Magnesium isotope fractionation during low-Mg calcite precipitation in a limestone cave – field study and experiments. Geochim Cosmochim Acta 74:4346–4364

Ingraham NL, Criss RE (1998) The effect of vapor pressure on the rate of isotopic exchange between water and vapour. Chem Geol 150:287–292

Izbicki JA, Bullen TD, Martin P, Schroth B (2012) Delta chromium-53/52 isotopic composition of native and contaminated groundwater, Mojave Desert, USA. Appl Geochem 27:841–853

James RH, Palmer MR (2000) The lithium isotope composition of international rock standards. Chem Geol 166:319–326

Jang JH, Mathur R, LiermannLJ Ruebush S, Brantley SL (2008) An iron isotope signature related to electron transfer between aqueous ferrous iron and goethite. Chem Geol 250:40–48

Javoy M, Pineau F, Delorme H (1986) Carbon and nitrogen isotopes in the mantle. Chem Geol 57:41–62

Jeffcoate AB, Elliott T, Kasemann SA, Ionov D, Cooper K, Brooker R (2007) Li isotope fractionation in peridotites and mafic melts. Geochim Cosmochim Acta 71:202–218

Jeffcoate AB, Elliott T, Thomas A, Bouman C (2004) Precise, small sample size determination of lithium isotope isotopic compositions of geological reference materials and moders seawater by MC-ICP-MS. Geostand Geoanal Res 28:161–172

Jendrzejewski N, Eggenkamp HGM, Coleman ML (2001) Characterisation of chlorinated hydrocarbons from chlorine and carbon isotopic compositions: scope of application to environmental problems. Appl Geochem 16:1021–1031

Jia Y (2006) Nitrogen isotope fractionations during progressive metamorphism: A case study from the Paleozoic Cooma metasedimentary complex, southeastern Australia. Geochim Cosmochim Acta 70:5201–5214

Jiang SY, Palmer MR (1998) Boron isotope systematics of tourmaline from granites and tourmalines: a synthesis. Eur J Mineral 10:1253–1265

John SG, Geis RW, Saito MA, Boyle EA (2007a) Zinc isotope fractionation during high-affinity and low-affinity ziinc transport by the marine diatom *Thalassiosira oceanica*. Limnol Oceanogr 52:2710–2714

John SG, Park JG, Zhang Z, Boyle EA (2007b) The isotopic composition of some common forms of anthropogenic zinc. Chem Geol 245:61–69

John SG, Rouxel OJ, Craddock PR, Engwall AM, Boyle EA (2008) Zinc stable isotopes in seafloor hydrothermal vent fluids and chimneys. Earth Planet Sci Lett 269:17–28

John SG, Adkins J (2012) The vertical distribution of iron stable isotopes in the North Atlantic near Bermuda. Global Biogeochem Cycles 26:GB2034

John T, Layne GD, Haase KM, Barnes JD (2010) Chlorine isotope evidence for crustal recycling into the Earth's mantle. Earth Planet Sci Lett

Johnson TM (2004) A review of mass-dependent fractionation of selenium isotopes and implications for other heavy stable isotopes. Chem Geol 204:201–214

Johnson CM, Beard BL (1999) Correction of instrumentally produced mass fractionation during isotopic analysis of Fe by thermal ionization mass spectrometry. Int J Mass Spectr 193:87–99

Johnson CM, Beard BL, Roden EE (2008) The iron isotope fingerprints of redox and biogeochemical cycling in modern and ancient Earth. Ann Rev Earth Planet Sci 36:457–493

Johnson TM, Bullen TD (2003) Selenium isotope fractionation during reduction by Fe(II)-Fe(III) hydroxide-sulfate (green rust). Geochim Cosmochim Acta 67:413–419

Johnson TM, Herbel MJ, Bullen TD, Zawislanski PT (1999) Selenium isotope ratios as indicators of selenium sources and oxyanion reduction. Geochim Cosmochim Acta 63:2775–2783

Johnston DT (2011) Multiple sulphur isotopes and the evolution of the Earth's sulphur cycle. Earth Sci Rev 106:161–183

Johnston DT, Farquhar J, Wing BA, Kaufman AJ, Canfield DE, Habicht KS (2005) Multiple sulphur isotope fractionations in biological systems: a case study with sulphate reducers and sulphur disproportionators. Am J Sci 305:645–660

Jouvin D, Louvat P, Juillot F, Marechal CN, Benedetti MF (2009) Zinc isotopic fractionation: why organic matters. Environ Sci Tech 43:5747–5754

Jouvin D, Weiss DJ, Mason TF, Bravin MN, Louvat P, Zhao F, Ferec F, Hinsinger P, Benedetti MF (2012) Stable isotopes of Cu and Zn in higher plants: evidence for Cu reduction at the root surface and two conceptional models for isotopic fractionation processes. Environ Sci Technol 46:2652–2660

Juillot F, Marechal C, Ponthieu M, Cacaly S, Morin G, Benedetti M, Hazemann JL, Proux O, Guyot F (2008) Zn isotopic fractionation caused by sorption on goethite and 2-Lines ferrihydrite. Geochim Cosmochim Acta 72:4886–4900

Jǿrgensen BB, Böttcher MA, Lüschen H, Neretin LN, Volkov II (2004) Anaerobic methane oxidation and a deep H_2S sink generate isotopically heavy sulfides in Black Sea sediments. Geochim Cosmochim Acta 68:2095–2118

Kakihana H, Kotaka M, Shohei S, Nomura M, Okamoto N (1977) Fundamental studies on the ion-exchange separation of boron isotopes. Bull Chem Soc Japan 50:158–163

Kaplan IR, Rittenberg SC (1964) Microbiological fractionation of sulphur isotopes. J Gen Microbiol 34:195–212

Kasemann SA, Jeffcoate AB, Elliott T (2005a) Lithium isotope composition of basalt glass reference material. Ann Chem 77:5251–5257

Kasemann S, Schmidt D, Pearson P et al (2008) Biological and ecological insights into Ca isotopes in planktic foraminifera as a paleotemperature proxy. Earth Planet Sci Lett 271:292–302

Kasemann SA, Hawkesworth CJ, Prave AR, Fallick AE, Pearson PN (2005b) Boron and calcium isotope composition in Neproterozoic carbonate rocks from Namibia: evidence for extreme environmental change. Earth Planet Sci Lett 231:73–86

Kaufmann RS, Long A, Bentley H, Campbell DJ (1986) Chlorine isotope distribution of formation water in Texas and Louisiana. Bull Am Assoc Petrol Geol 72:839–844

Kaufmann RS, Long A, Bentley H, Davis S (1984) Natural chlorine isotope variations. Nature 309:338–340

Kelley SP, Fallick AE (1990) High precision spatially resolved analysis of $\delta^{34}S$ in sulphides using a laser extraction technique. Geochim Cosmochim Acta 54:883–888

Kelley KD, Wilkinson JJ, Chapman JB, Crowther HL, Weiss DJ (2009) Zinc isotopes in sphalerite from base metal deposits in the Red Dog district, northern Alaska. Econ Geol 104:767–773

Kemp ALW, Thode HG (1968) The mechanism of the bacterial reduction of sulphate and of sulphite from isotopic fractionation studies. Geochim Cosmochim Acta 32:71–91

Kendall B, Brennecka GA, Weyer S, Anbar AD (2013) Uranium isotope fractionation suggests oxidative uranium mobilization at 2.50 Ga. Chem Geol 362:105–114

Kendall C, Grim E (1990) Combustion tube method for measurement of nitrogen isotope ratios using calcium oxide for total removal of carbon dioxide and water. Anal Chem 62:526–529

Kendall C (1998) Tracing nitrogen sources and cycling in catchments. In: Kendall C, McDonnell JJ (eds) Isotope tracers in catchment hydrology. Elsevier Science, Amsterdam, pp 519–576

Kerstel ER, Gagliardi G, Gianfrani L, Meijer HA, van Trigt R, Ramaker R (2002) Determination of the $^{2}H/^{1}H$, $^{17}O/^{16}O$ and $^{18}O/^{16}O$ isotope ratios in water by means of tunable diode laser spectroscopy at 1.39 μ. Spectrochim Acta A 58:2389–2396

Kiczka M, Wiederhold JG, Kraemer SM, Bourdon B, Kretzschmar R (2010) Iron isotope fractionation during Fe uptake and translocation in Alpine plants. Environ Sci Techn 44:6144–6150

Kieffer SW (1982) Thermodynamic and lattice vibrations of minerals: 5. Application to phase equilibria, isotopic fractionation and high-pressure thermodynamic properties. Rev Geophys Space Phys 20:827–849

Kim S-T, Mucci A, Taylor BE (2007) Phosphoric acid fractionation factors for calcite and aragonite between 25 and 75 °C. Chem Geol 246:135–146

Kim S-T, O’Neil JR (1997) Equilibrium and nonequilibrium oxygen isotope effects in synthetic carbonates. Geochim Cosmochim Acta 61:3461–3475

Kimball BE, Mathur R, Dohnalkova AC, Wall AJ, Runkel RL, Brantley SL (2009) Copper isotope fractionation in acid mine drainage. Geochim Cosmochim Acta 73:1247–1263

Kirshenbaum I, Smith JS, Crowell T, Graff J, McKee R (1947) Separation of the nitrogen isotopes by the exchange reaction between ammonia and solutions of ammonium nitrate. J Chem Phys 15:440–446

Kita NT, Ushikubo T, Fu B, Valley JW (2009) High precision SIMS oxygen isotope analysis and the effect of sample topography. Chem Geol 264:43–57

Kitchen JW, Johnson TM, Bullen TD, Zhu J, Raddatz A (2012) Chromium isotope fractionation factors for reduction of Cr(VI) by aqueous Fe(II) and organic molecules. Geochim Cosmochim Acta 89:190–201

Kitchen NE, Valley JW (1995) Carbon isotope thermometry in marbles of the Adirondack Mountains, New York. J Metamorph Geol 13:577–594

Kiyosu Y, Krouse HR (1990) The role of organic acid in the abiogenic reduction of sulfate and the sulfur isotope effect. Geochemical J 24:21–27

Klochko K, Kaufman AJ, Yao W, Byrne RH, Tossell JA (2006) Experimental measurement of boron isotope fractionation in seawater. Earth Planet Sci Lett 248:276–285

Kohn MJ, Schoeninger MJ, Valley JW (1996) Herbivore tooth oxygen isotope compositions: effects of diet and physiology. Geochim Cosmochim Acta 60:3889–3896

Kohn MJ, Valley JW (1998a) Oxygen isotope geochemistry of amphiboles: isotope effects of cation substitutions in minerals. Geochim Cosmochim Acta 62:1947–1958

Kohn MJ, Valley JW (1998b) Effects of cation substitutions in garnet and pyroxene on equilibrium oxygen isotope fractionations. J Metam Geol 16:625–639

Kohn MJ, Valley JW (1998c) Obtaining equilibrium oxygen isotope fractionations from rocks: theory and examples. Contr Mineral Petrol 132:209–224

Kolodny Y, Luz B, Navon O (1983) Oxygen isotope variations in phosphate of biogenic apatites, I. Fish bone apatite—rechecking the rules of the game. Earth Planet Sci Lett 64:393–404

Konhauser KO, Lalonde SV et al (2011) Aerobic bacterial pyrite oxidation and acid rock drainage during the great oxidation event. Nature 478:369–374

Kowalski N, Dellwig O et al (2013) Pelagic molybdenum concentration anomalies and the impact of sediment resuspension on the molybdenum budget in two tidal systems of the North Sea. Geochim Cosmochim Acta 119:198–211

Kowalski PM, Jahn S (2011) Prediction of equilibrium Li isotope fractionation between minerals and aqueous solutions at high p and T: an efficient ab initio approach. Geochim Cosmochim Acta 75:6112–6123

Kozdon R, Kita RN, Huberty JM, Fournelle JH, Johnson CA, Valley JW (2010) In situ sulfur isotope analysis of sulfide minerals by SIMS: precision and accuracy with application to thermometry of similar to 3.5 Ga Pilbara cherts. Chem Geol 275:243–253

Krabbenhöft A, Eisenhauer A et al (2010) Constraining the marine strontium budget with natural isotope fractionations ($^{87}Sr/^{86}Sr$, $\delta^{88/86}Sr$) of carbonates, hydrothermal solutions and river waters. Geochim Cosmochim Acta 74:4097–4109

Krabbenhöft A, Fietzke J, Eisenhauer A, Liebetrau V, Böhm F, Vollstaedt H (2009) Determination of radiogenic and stable strontium isotope ratios ($^{87}Sr/^{86}Sr$; $\delta^{88/86}Sr$) by thermal ionization mass spectrometry applying an $^{87}Sr/^{84}Sr$ double spike. J Anal At Spectr 24:1267–1271

Kritee K, Barkay T, Blum JD (2009) Mass-dependent stable isotope fractionation of mercury during *mer* mediated microbial degradation of monoethylmercury. Geochim Cosmochim Acta 73:1285–1296

Kritee K, Blum JD, Johnson MW, Bergquist BA, Barkay T (2007) Mercury stable isotope fractionation during reduction of Hg(II) to Hg(0) by mercury resistant microorganisms. Environ Sci Technol 41:1889–1895

Krouse HR, Thode HG (1962) Thermodynamicproperties and geochemistry of isotopic compounds of selenium. Can J Chem 40:367–375

Krouse HR, Viau CA, Eliuk LS, Ueda A, Halas S (1988) Chemical and isotopic evidence of thermochemical sulfate reduction by light hydrocarbon gases in deep carbonate reservoirs. Nature 333:415–419

Ku TCW, Walter LM, Coleman ML, Blake RE, Martini AM (1999) Coupling between sulfur recycling and syndepositional carbonate dissolution: evidence from oxygen and sulfur isotope composition of pore water sulfate, South Florida Platform, USA. Geochim Cosmochim Acta 63:2529–2546

Kunzmann M, Halverson GP, Sossi PA, Raub TD, Payne JL, Kirby J (2013) Zn isotope evidence for immediate resumption of primary productivity after snowball Earth. Geology 41:27–30

Lacan F, Francois R, Ji Y, Sherrell RM (2006) Cadmium isotopic composition in the ocean. Geochim Cosmochim Acta 70:5104–5118

Lambelet M, Rehkämper M, van de Flierdt T, Xue Z, Kreissig K, Coles B, Porecelli D, Andersson P (2013) Isotopic analysis of Cd in the mixing zone of Siberian rivers with the Arctic Ocean—new constraints on marine Cd cycling and the isotopic composition of riverine Cd. Earth Planet Sci Lett 361:64–73

Land LS (1980) The isotopic and trace element geochemistry of dolomite: the state of the art. In: Concepts and models of dolomitization. Soc Econ Paleontol Min Spec Publ 28:87–110

Larson PB, Maher K, Ramos FC, Chang Z, Gaspar M, Meinert LD (2003) Copper isotope ratios in magmatic and hydrothermal ore-forming processes. Chem Geol 201:337–350

Lauretta DS, Klaue B, Blum JD, Buseck PR (2001) Mercury abundances and isotopic compositions in the Murchison (CM) and Allende (CV) carbonaceous chondrites. Geochim Cosmochim Acta 65:2807–2816

Laws EA, Bidigare RR, Popp BN (1997) Effect of growth rate and CO_2 concentration on carbon isotope fractionation by the marine diatom *Phaeodactylum tricornutum*. Limnol Oceanogr 42:1552–1560

Laws EA, Popp BN, Bidigare RR, Kennicutt MC, Macko SA (1995) Dependence of phytoplankton carbon isotopic composition on growth rate and CO_{2aq}: theoretical considerations and experimental results. Geochim Cosmochim Acta 59:1131–1138

Layton-Matthews D, Leybourne M, Peter JM, Scott SD, Cousens B, Eglington BM (2013) Multiple sources of selenium in ancient seafloor hydrothermal systems: compositional and Se, S and Pb isotopic evidence from volcanic-hosted and volcanic-sediment hosted massive sulphide deposits of the Finlayson Lake district, Yukon, Canada. Geochim Cosmochim Acta 117:313–331

Lazar C, Young ED, Manning CE (2012) Experimental determination of equilibrium nickel isotope fractionation between metal and silicate from 500 °C to 950 °C. Geochim Cosmochim Acta 86:276–295

Le Roux PJ, Shirey SB, Benton L, Hauri EH, Mock TD (2004) In situ, multiple-multiplier, laser ablation ICP-MS measurement of boron isotopic composition ($\delta^{11}B$) at the nanogram level. Chem Geol 203:123–138

Leeman WP, Tonarini S, Chan LH, Borg LE (2004) Boron and lithium isotopic variations in a hot subduction zone—the southern Washington Cascades. Chem Geol 212:101–124

Lehmann M, Siegenthaler U (1991) Equilibrium oxygen- and hydrogen-isotope fractionation between ice and water. J Glaciol 37:23–26

Lemarchand D, Gaillardet J, Lewin E, Allegre CJ (2000) The influence of rivers on marine boron isotopes and implications for reconstructing past ocean p_H. Nature 408:951–954

Lemarchand D, Gaillardet J, Lewin E, Allègre CJ (2002) Boron isotope systematics in large rivers: implications for the marine boron budget and paleo-pH reconstruction over the Cenozoic. Chem Geol 190:123–140

Lemarchand E, Schott J, Gaillardet J (2005) Boron isotopic fractionation related to boron sorption on humic acid and the structure of surface complexes formed. Geochim Cosmochim Acta 69:3519–3533

Lemarchand E, Schott J, Gaillardet J (2007) How surface complexes impact boron isotopic fractionation: evidence from Fe and Mn oxides sorption experiments. Earth Planet Sci Lett 260:277–296

Lemarchand D, Wasserburg GJ, Papanastassiou DA (2004) Rate-controlled calcium isotope fractionation in synthetic calcite. Geochim Cosmochim Acta 68:4665–4678

Letolle R (1980) Nitrogen-15 in the natural environment. In: Fritz P, Fontes JCh (eds) Handbook of environmental isotope geochemistry. Elsevier, Amsterdam, pp 407–433

Levin NE, Raub TD, Dauphas N, Eiler JM (2014) Triple-oxygen-isotope variations in sedimentary rocks. Geochim Cosmochim Acta 139:173–189

Li W, Chakraborty S, Beard BL, Romanek CS, Johnson CM (2012) Magnesium isotope fractionation during precipitation of inorganic calcite under laboratory conditions. Earth Planet Sci Lett 333–314:304–316

Li W, Jackson SE, Pearson NJ, Alard O, Chappell BW (2009a) The Cu isotope signature of granites from the Lachlan Fold Belt, SE Australia. Chem Geol 258:38–49

Li X, Liu Y (2010) First principles study of Ge isotopic fractionation during adsorption onto Fe (III)-oxyhydroxidessurfaces. Chem Geol 278:15–22

Li W-Y, Teng F-Z, Ke S, Rudnick R, Gao S, Wu F-Y, Chappell B (2010) Heterogeneous magnesium isotopic composition of the upper continental crust. Geochim Cosmochim Acta 74:6867–6884

Li X, Zhao H, Tang M, Liu Y (2009b) Theoretical prediction for several important equilibrium Ge isotope fractionation factors and geological implications. Earth Planet Sci Lett 287:1–11

Li W-Y, Teng FZ, Wing BA, Xiao Y (2014) Limited magnesium isotope fractionation during metamorphic dehydration in metapelites from the Onawa contact aureole, Maine. Geochem Geophys Geosys 15(10). doi:10.1002/2013GC004992

Liebscher A, Meixner A, Romer R, Heinrich W (2005) Liquid-vapor fractionation of boron and boron isotopes: experimental calibration at 400 °C/23 Mpa to 450 °C/42Mpa. Geochim Cosmochim Acta 69:5693–5704

Little SH, Vance D, Walker-Brown C, Landing WM (2014) The oceanic mass balance of copper and zinc isotopes, investigated by analysis of their inputs, and outputs to ferromanganese oxide sediments. Geochim Cosmochim Acta 125:653–672

Liu Y, Spicuzza MJ, Craddock PR, Day JM, Valley JW, Dauphas N, Taylor LA (2010a) Oxygen and iron isotope constraints on near-surface fractionation effects and the composition of lunar mare basalt source regions. Geochim Cosmochim Acta 74:6249–6262

Liu SA, Teng FZ, He Y, Ke S, Li S (2010b) Investigation of magnesium isotope fractionation during granite differentiation: implication for Mg isotopic composition of the continental crust. Earth Planet Sci Lett 297:646–654

Liu SA, Teng FZ, Yang W, Wu FY (2011) High-temperature inter-mineral magnesium isotope fractionation in mantle xenoliths from the North China craton. Earth Planet Sci Lett 308:131–140

Lobo L, Degryse P, Shortland A, Vanhaeke F (2013) Isotopic analysis of antimony using multi-collector ICP-mass spectrometry for provenance determination of Roman glass. J Anal At Spectrom 28: 1213–129

Long A, Eastoe CJ, Kaufmann RS, Martin JG, Wirt L, Fincey JB (1993) High precision measurement of chlorine stable isotope ratios. Geochim Cosmochim Acta 57:2907–2912

Longinelli A, Craig H (1967) Oxygen-18 variations in sulfate ions in sea-water and saline lakes. Science 156:56–59

Louvat P, Bouchez J, Paris G (2011) MC-ICP-MS isotope measurements with direct injection nebulisation (d-DIHEN): optimisation and application to boron in seawater and carbonate samples. Geostand Geoanal Res 35:75–88

Luais B (2012) Germanium chemistry and MC-ICPMS isotopic measurements of Fe-Ni, Zn alloys and silicate matrices: insights into deep Earth processes. Chem Geol

Luck JM, Ben Othman D, Albarede F (2005) Zn and Cu isotopic variations in chondrites and iron meteorites: early solar nebula reservoirs and parent-body processes. Geochim Cosmochim Acta 69:5351–5363

Lundstrom CC, Chaussidon M, Hsui AT, Keleman P, Zimmermann M (2005) Observations of Li isotope variations in the Trinity ophiolite: evidence for isotope fractionation by diffusion during mantle melting. Geochim Cosmochim Acta 69:735–751

Luz B, Barkan E (2010) Variations of $^{17}O/^{16}O$ and $^{18}O/^{16}O$ in meteoric waters. Geochim Cosmochim Acta 74:6276–6286

Lécuyer C, Grandjean P, Reynard B, Albarede F, Telouk P (2002) $^{11}B/^{10}B$ analysis of geological materials by ICP-MS Plasma 54: application to bron fractionation between brachiopod calcite and seawater. Chem Geol 186:45–55

Ma J, Hintelmann H, Kirk JL, Muir DC (2013) Mercury concentrations and mercury isotope compositionin lake sediment cores Chem Geol. 336:96–102

Machel HG, Krouse HR, Sassen P (1995) Products and distinguishing criteria of bacterial and thermochemical sulfate reduction. Appl Geochemistry 10:373–389

MacrisCA Young ED, Manning CE (2013) Experimental determination of equilibrium magnesium isotope fractionation between spinel, forsterite and magnesite from 600 to 800 °C. Geochim Cosmochim Acta 118:18–32

Magenheim AJ, Spivack AJ, Michael PJ, Gieskes JM (1995) Chlorine stable isotope composition of the oceanic crust: implications for earth's distribution of chlorine. Earth Planet Sci Lett 131:427–432

Magenheim AJ, Spivack AJ, Volpe C, Ranson B (1994) Precise determination of stable chlorine isotope ratios in low-concentration natural samples. Geochim Cosmochim Acta 58:3117–3121

Maher K, Jackson S, Mountain B (2011) Experimental evaluation of the fluid-mineral fractionation of Cu isotopes at 250 °C and 300 °C. Chem Geol 286:229–239

Maher K, Larson P (2007) Variation in copper isotope ratios and controls on fractionation in hypogene skarn mineralization at Coroccohuayco and Tintaya, Peru. Econ Geol 102:225–237

Malinovskiy D, Moens L, Vanhaecke F (2009) Isotopic fractionation of Sn during methylation and demethylation in aqueous solution. Environ Sci Tech 43: 4399–4404

Mariotti A, Germon JC, Hubert P, Kaiser P, Letolle R, Tardieux P (1981) Experimental determination of nitrogen kinetic isotope fractionation: some principles, illustration for the denitrification and nitrification processes. Plant Soil 62:413–430

Markl G, von Blanckenburg F, Wagner T (2006b) Iron isotope fractionation during hydrothermal ore deposition and alteration. Geochim Cosmochim Acta 70:3011–3030

Markl G, Lahaye Y, Schwinn G (2006a) Copper isotopes as monitors of redox processes in hydrothermal mineralization. Geochim Cosmochim Acta 70:4215–4228

Marriott CS, Henderson GM, Belshaw NS, Tudhope AW (2004) Temperature dependence of δ^7Li, δ^{44}Ca and Li/Ca during growth of calcium carbonate. Earth Planet Sci Lett 222:615–624

Marschall HR, Altherr R, Kalt A, Ludwig T (2008) Detrital, metamorphic and metasomatic tourmaline in high-pressure metasediments from Syros (Greece): intra-grain boron isotope patterns determined by secondary-ion mass spectrometry. Contr Mineral Petrol 155:703–717

Marschall HR, Jiang SY (2011) Tourmaline isotopes: no element left behind. Elements 7:313–319

Marty B, Humbert F (1997) Nitrogen and argon isotopes in oceanic basalts. Earth Planet Sci Lett 152:101–112

Marty B, Zimmermann L (1999) Volatiles (He, C, N, Ar) in mid-ocean ridge basalts: assesment of shallow-level fractionation and characterization of source composition. Geochim Cosmochim Acta 63:3619–3633

Maréchal CN, Albarede F (2002) Ion-exchange fractionation of copper and zinc isotopes. Geochim Cosmochim Acta 66:1499–1509

Maréchal CN, Télouk P, Albarède F (1999) Precise analysis of copper and zinc isotopic compositions by plasma-source mass spectrometry. Chem Geol 156:251–273

Maréchal CN, Nicolas E, Douchet C, Alabarède F (2000) Abundance of zinc isotopes as a marine biogeochemical tracer. Geochem Geophys Geosys G^3 1:1999GC000029

Mason TFD et al (2005) Zn and Cu isotopic variability in the Alexandrinka volcanic-hosted massive sulphide (VHMS) ore deposit, Urals, Russia. Chem Geol 221:170–187

Mathur R, Brantley S, Anbar A, Munizaga F, Maksaev R, Vervoort J, Hart G (2010a) Variations of Mo isotopes from molybdenite in high-temperature hydrothermal ore deposits. Mineral Deposita 45:43–50

Mathur R, Dendas M, Titley S, Phillips A (2010b) Patterns in the copper isotope composition of minerals in porphyry copper deposits in southwestern United States. Econ Geol 105:1457–1467

Mathur R, Jin L, Prush V, Paul J, Ebersole C, Fornadel A, Williams JZ, Brantley S (2012) Cu isotopes and concentrations during weathering of black shale of the Marcellus Formation, Huntington County, Pennsylvania (USA). Chem Geol 304–305:175–184

Mathur R, Ruiz J, Titley S, Liermann L, Buss H, Brantley S (2005) Cu isotopic fractionation in the supergene environment with and without bacteria. Geochim Cosmochim Acta 69:5233–5246

Matthews A, Goldsmith JR, Clayton RN (1983a) Oxygen isotope fractionation between zoisite and water. Geochim Cosmochim Acta 47:645–654

Matthews A, Goldsmith JR, Clayton RN (1983b) On the mechanics and kinetics of oxygen isotope exchange in quartz and feldspars at elevated temperatures and pressures. Geol Soc Am Bull 94:396–412

Matthews DE, Hayes JM (1978) Isotope-ratio-monitoring gas chromatography-mass spectrometry. Anal Chem 50:1465–1473

McClelland JW, Montoya JP (2002) Trophic relationships and the nitrogen isotope composition of amino acids in plankton. Ecology 83:2173–2180

McCrea JM (1950) On the isotopic chemistry of carbonates and a paleotemperature scale. J Chem Phys 18:849–857

McCready RGL (1975) Sulphur isotope fractionation by Desulfovibrio and Desulfotomaculum species. Geochim Cosmochim Acta 39:1395–1401

McCready RGL, Kaplan IR, Din GA (1974) Fractionation of sulfur isotopes by the yeast Saccharomyces cerevisiae. Geochim Cosmochim Acta 38:1239–1253

McIlivin MR, Altabet MA (2005) Chemical conversion of nitrate and nitrite to nitrous oxide for nitrogen and oxygen isotopic analysis in freshwater and seawater. Anal Chem 77:5589–5595

McKibben MA, Riciputi LR (1998) Sulfur isotopes by ion microprobe. In: Applications of microanalytical techniques to understanding mineralizing processes. Rev Econ Geol 7:121–140

McManus J et al (2006) Molybdenum and uranium geochemistry in continental margin sediments: palaeoproxy potential. Geochim Cosmochim Acta 70:4643–4662

McManus J, Nägler T, Siebert C, Wheat CG, Hammond D (2002) Oceanic molybdenum isotope fractionation: diagenesis and hydrothermal ridge flank alteration. Geochem Geophys Geosyst 3:1078. doi:10.1029/2002GC000356

McMullen CC, Cragg CG, Thode HG (1961) Absolute ratio of $^{11}B/^{10}B$ in Searles Lake borax. Geochim Cosmochim Acta 23:147

Miller MF, Franchi IA, Sexton AS, Pillinger CT (1999) High precision $\delta^{17}O$ isotope measurements of oxygen from silicates and other oxides: method and applications. Rapid Commun Mass Spect 13:1211–1217

Millet MA, Baker JA, Payne CE (2012) Ultra-precise stable Fe isotope measurements by high resolution multi-collector inductively coupled mass spectrometry with a ^{57}Fe-^{58}Fe double spike. Chem Geol 304–305:18–25

Millot R, Guerrot C, Vigier N (2004) Accurate and high-precision measurement of lithium isotopes in two reference materials by MC-ICP-MS. Geostand Geoanal Res 28:153–159

Millot R, Petelet-Giraud E, Guerrot C, Negrel P (2010b) Multi-isotopic composition ($\delta^{7}Li$-$\delta^{11}B$-δD-$\delta^{18}O$) of rainwaters in France: origin and spatio-temporal characterization. Appl Geochem 25:1510–1524

Millot R, Vigier N, Gaillardet J (2010a) Behaviour of lithium and its isotopes during weathering in the Mackenzie Basin, Canada. Geochim Cosmochim Acta 74:3897–3912

Misra S, Froelich PN (2012) Lithium isotope history of Cenozoic seawater: changes in silicate weathering and reverse weathering. Science 335:818–823

Mitchell K, Couture RM, Johnson TM, Mason PRD, Van Cappellen P (2013) Selenium sorption and isotope fractionation: iron(III) oxides versus iron (II) sulfides. Chem Geol 342:21–28

Mitchell K, Mason P, Van Cappellen P, Johnson TM, Gill BC, Owens JD, Diaz J, Ingall E, Reichart GJ, Lyons T (2012) Selenium as paleo-oceanographic proxy: a first assessment. Geochim Cosmochim Acta 89:302–317

Mizutani Y, Rafter TA (1973) Isotopic behavior of sulfate oxygen in the bacterial reduction of sulfate. Geochem J 6:183–191

Monson KD, Hayes JM (1982) Carbon isotopic fractionation in the biosynthesis of bacterial fatty acids. Ozonolysis of unsaturated fatty acids as a means of determining the intramolecular distribution of carbon isotopes. Geochim Cosmochim Acta 46:139–149

Montoya-Pino C, Weyer S, Anbar AD, Pross J, Oschmann J, van de Schootbrugge B, Arz HW (2010) Global enhancement of ocean anoxia during Oceanic Anoxic Event 2: a quantitative approach using U isotopes. Geology 38:315–318

Mook WG, Bommerson JC, Stavermann WH (1974) Carbon isotope fractionation between dissolved bicarbonate and gaseous carbon dioxide. Earth Planet Sci Lett 22:169–174

Moriguti T, Nakamura E (1998) Across-arc variation of Li-isotopes in lavas and implications for crust /mantle recycling at subduction zones. Earth Planet Sci Lett 163:167–174

Moynier F, Agranier A, Hezel DC, Bouvier A (2010) Sr stable isotope composition of Earth, the Moon, Mars, Vesta and meteorites. Earth Planet Sci Lett 300:359–366

Moynier F, Yin QZ, Schauble E (2011) Isotopic evidence of Cr partitioning into Earth's core. Science 331:1417–1420

Moynier F, Pichat S, Pons ML, Fike D, Balter V, Albarède F (2008) Isotope fractionation and transport mechanisms of Zn in plants. Chem Geol 267:125–130

Murphy MJ, Stirling CH, Kaltenbach A, Turner SP, Schaefer BF (2014) Fractionation of $^{238}U/^{235}U$ by reduction during low temperature uranium mineralization processes. Earth Planet Sci Lett 388:306–317

Méheut M, Lazzeri M, Balan E, Mauri F (2010) First-principles calculation of H/D isotopic fractionation between hydrous minerals and water. Geochim Cosmochim Acta 74:3874–3882

Möller K, Schoenberg R, Pedersen RB, Weiss D, Dong S (2012) Calibration of the new certified reference materials ERM-AE633 and ERM-AE647 for copper and IRMM-3702 for zinc isotope amount ratio determinations. Geostand Geoanal Res 36:177–199

Nabelek PI, Labotka TC (1993) Implications of geochemical fronts in the Notch Peak contact-metamorphic aureole, Utah, USA. Earth Placet Sci Lett 119:539–559

Nabelek PI (1991) Stable isotope monitors. In: Contact metamorphism. Rev Mineral 26:395–435

Nakano T, Nakamura E (2001) Boron isotope geochemistry of metasedimentary rocks and tourmalines in a subduction zone metamorphic suite. Phys Earth Planet Inter 127:233–252

Navarette JU, Borrok DM, Viveros M, Elzey JT (2011) Copper isotope fractionation during surface adsorption and intracellular incorporation by bacteria. Geochim Cosmochim Acta 75:784–799

Needham AW, Porcelli D, Russell SS (2009) An Fe isotope study of ordinary chondrites. Geochim Cosmochim Acta 73:7399–7413

Neretin LN, Böttcher ME, Grinenko VA (2003) Sulfur isotope geochemistry of the Black Sea water column. Chem Geol 200:59–69

Neubert N, Heri AR, Voegelin AR, Schlunegger F, Villa IM (2011) The molybdenum isotopic composition in river water; constraints from small catchments. Earth Planet Sci Lett 304:180–190

Neubert N, Nägler TF, Böttcher ME (2008) Sulfidity controls molybdenum isotope fractionation into euxinic sediments: evidence from the modern Black Sea. Geology 36:775–778

Neymark LA, Premo WR, Mel'nikov NN, Emsbo P (2014) Precise determination of δ^{88}Sr in rocks, minerals and waters by double-spike TIMS: a powerful tool in the study of geological, hydrological and biological processes. J Anal At Spectr 29:65–75

Nielsen SG et al (2005) Thallium isotope composition of the upper continental crust and rivers—an investigation of the continental sources of dissolved marine thallium. Geochim Cosmochim Acta 69:2007–2019

Nielsen SG, Goff M, Hesselbo SP, Jenkyns HC, LaRowe DE, Lee CT (2011b) Thallium isotopes in early diagentic pyrite—a paleoredox proxy? Geochim Cosmochim Acta 75:6690–6704

Nielsen H (1979) Sulfur isotopes. In: Jager E, Hunziker J (eds) Lectures in isotope geology. Springer, Berlin, pp 283–312

Nielsen SG, Mar-Gerrison S, Gannoun A, LaRowe D, Klemm V, Halliday A, Burton KW, Hein JR (2009) Thallium isotope evidence for a permanent increase in marine organic carbon export in the early Eocene. Earth Planet Sci Lett 278:297–307

Nielsen SG, Prytulak J, Halliday AN (2011c) Determination of precise and accurate ^{51}V/^{50}V isotope ratios by MC-ICP-MS, Part 1: Chemical separation of vanadium and mass spectrometric protocols. Geostand Geoanal Res 35:293–306

Nielsen SG, Prytulak J, Wood BJ, Halliday AN (2014) Vanadium isotopic difference between the silicate Earth and meteorites. Earth Planet Sci Lett 389:167–175

Nielsen SG, Rehkämper M, Brandon AD, Norman MD, Turner S, O'Reilly SY (2007) Thallium isotopes in Iceland and Azores lavas—implications for the role of altered crust and mantle geochemistry. Earth Planet Sci Lett 264:332–345

Nielsen SG, Rehkämper M, Norman MD, Halliday AN, Harrison D (2006) Thallium isotopic evidence for ferromanganese sediments in the mantle source of Hawaiian basalts. Nature 439:314–317

Nielsen SG, Rehkämper M (2011) Thallium isotopes and their application to problems in earth and environmental science. In: Baskaran M (ed) Handbook of environmental isotope geochemistry, vol 1. Springer, New York, pp 247–269

Nielsen LC, Druhan JL, Yang W, Brown ST, DePaolo DJ (2011) Calcium isotopes as tracers of biogeochemical processes. In: Handbook of environmental isotope geochemistry. Springer, New York, pp 105–124

Nishio Y, Nakai S, Yamamoto J, Sumino H, Matsumoto T, Prikhod'ko VS, Arai S (2004) Lithium isotope systematics of the mantle derived ultramafic xenoliths: implications for EM1 origin. Earth Planet Sci Letters 217:245–261

Nitzsche HM, Stiehl G (1984) Untersuchungen zur Isotopenfraktionierung des Stickstoffs in den Systemen Ammonium/Ammoniak und Nitrid/Stickstoff. ZFI Mitt 84:283–291

Noordmann J, Weyer S, Montoya-Pino C, Dellwig O, Neubert N, Eckert S, Paetzel M, Böttcher ME (2015) Uranium and molybdenum isotope systematics in modern euxinic basins: case studies from the central Baltic Sea and the Kyllaren fjord (Norway). Chem Geol (in press)

Nägler TF et al (2014) Proposal for an international molybdenum isotope reference standard and data representation. Geostand Geoanal Res 38:149–151

Nägler TF, Neubert N, Böttcher ME, Dellwig O, Schnetger B (2011) Molybedenum isotope fractionation in pelagic euxinia: evidence from the modern Black and Baltic Seas. Chem Geol 289:1–11

Nägler TF, Siebert C, Lüschen H, Böttcher ME (2005) Sedimentary Mo isotope records across the Holocene fresh-brackish water transition of the Black Sea. Chem Geol 219:283–295

Nägler TF, Eisenhauer A, Müller A, Hemleben C, Kramers J (2000) The δ^{44}Ca-temperature calibration on fossil and cultured *Globigerinoides sacculifer*: new tool for reconstruction ofpast sea surface temperatures. Geochem Geophys Geosyst G^3 1(2000GC000091)

Ockert C, Gussone N, Kaufhold S, Teichert BM (2013) Isotope fractionation during Ca exchange on clay minerals in a marine environment. Geochim Cosmochim Acta 112:374–388

Oelze M, von Blanckenburg F, Hoellen D, Dietzel M, Bouchez J (2014) Si stable isotope fractionation during adsorption and the competition between kinetic and equilibrium isotope fractionation: implications for weathering systems. Chem Geol (in press)

Oeser M, Weyer S, Horn I, Schuth S (2014) High-precision Fe and Mg isotope ratios of silicate reference glasses determined in situ by femtosecond LA-MC-ICP-MS and by solution nebulisation MC-ICP-MS. Geostand Geoanal Res 38:311–328

Ohmoto H (1986) Stable isotope geochemistry of ore deposits. Rev Mineral 16:491–559

Ohmoto H, Goldhaber MB (1997) Sulfur and carbon isotopes. In: Barnes HL (ed) Geochemistry of hydrothermal ore deposits, 3rd edn. Wiley Interscience, New York, pp 435–486

Ohmoto H, Rye RO (1979) Isotopes of sulfur and carbon. In: Geochemistry of hydrothermal ore deposits, 2nd edn. Holt Rinehart and Winston, New York

Ono S, Shanks WC, Rouxel OJ, Rumble D (2007) S-33 constraints on the seawater sulphate contribution in modern seafloor hydrothermal vent sulfides. Geochim Cosmochim Acta 71:1170–1182

Ono S, Wing BA, Johnston D, Farquhar J, Rumble D (2006) Mass-dependent fractionation of quadruple sulphur isotope system as a new tracer of sulphur biogeochemical cycles. Geochim Cosmochim Acta 70:2238–2252

Opfergelt S, Georg RB, Delvaux B, Cabidoche YM, Burton KW, Halliday AN (2012) Mechanism of magnesium isotope fractionation in volcanicsoil weathering sequences, Guadeloupe. Earth Planet Sci Lett 341–344:176–185

Owens NJP (1987) Natural variations in^{15}N in the marine environment. Adv Mar Biol 24:390–451

O'Leary MH (1981) Carbon isotope fractionation in plants. Phytochemistry 20:553–567

O'Neil JR, Epstein S (1966) A method for oxygen isotope analysis of milligram quantities of water and some of its applications. J Geophys Res 71:4955–4961

O'Neil JR, Roe LJ, Reinhard E, Blake RE (1994) A rapid and precise method of oxygen isotope analysis of biogenic phosphate. Isr J Earth Sci 43:203–212

O'Neil JR, Taylor HP (1967) The oxygen isotope and cation exchange chemistry of feldspars. Am Mineral 52:1414–1437

O'Neil JR, Truesdell AH (1991) Oxygen isotope fractionation studies of solute-water interactions. In: Stable isotope geochemistry: a tribute to Samuel Epstein. Geochemical Soc Spec Publ 3:17–25

Pack A, Herwartz D (2014) The triple oxygen isotope composition of the Earth mantle and Δ^{17}O variations in terrestrial rocks. Earth Planet Sci Lett (inpress)

Pagani M, Lemarchand D, Spivack A, Gaillardet j (2005) A critical evaluation of the boron isotope-p_H proxy: the accuracy of ancient ocean p_H estimates. Geochim Cosmochim Acta 69:953–961

Page B, Bullen T, Mitchell M (2008) Influences of calcium availability and tree species on Ca isotope fractionation in soil and vegetation. Biogeochemistry 88:1–13

Palmer MR, Slack JF (1989) Boron isotopic composition of tourmaline from massive sulfide deposits and tourmalinites. Contr Mineral Petrol 103:434–451

Palmer MR, Spivack AJ, Edmond JM (1987) Temperature and pH controls over isotopic fractionation during the absorption of boron on marine clays. Geochim Cosmochim Acta 51:2319–2323

Paniello RC, Day JM, Moynier F (2012) Zinc isotopic evidence for the origin of the Moon. Nature 490:376–379

Paris G, Sessions A, Subhas AV, Adkins JF (2013) MC-ICP-MS measurement of $d^{34}S$ and $D^{33}S$ in small amounts of dissolved sulphate. Chem Geol 345:50–61

Park R, Epstein S (1960) Carbon isotope fractionation during photosynthesis. Geochim Cosmochim Acta 21:110–126

Parkinson IJ, Hammond SJ, James RH, Rogers NW (2007) High-temperature lithium isotope fractionation: insights from lithium isotope diffusion in magmatic systems. Earth Planet Sci Lett 257:609–621

Passey BH, Hu H, Ji H, Montanari S, Li G, Henkes GA, Levin NE (2014) Triple oxygen isotopes in biogenic and sedimentary carbonates. Geochim Cosmochim Acta 141:1–25

Payne JL, Turchyn AV, Paytan A, DePaolo DJ, Lehrmann DJ, Yu M, Wei J (2010) Calcium isotope constraints on the end-Permian mass exttinction. PNAS 107:8543–8548

Pearce CR, Burton KW, Pogge von Strandmann PA, James RH, Gislason SR (2010) Molybdenum isotope behaviour accompanying weathering and riverine transport in a basaltic terrain. Earth Planet Sci Lett 295:104–114

Pearce CR, Cohen AS, Coe AL, Burton KW (2008) Molybdenum isotope evidence for global ocean anoxia coupled with perturbationsto the carbon cycle during the Early Jurassic. Geology 36:231–234

Pearson PN, Palmer MR (1999) Middle Eocene seawater pH and atmospheric carbon dioxide. Science 284:1824–1826

Pearson PN, Palmer MR (2000) Atmospheric carbon dioxide concentrations over the past 60 million years. Nature 406:695–699

Peterson BJ, Fry B (1987) Stable isotopes in ecosystem studies. Ann Rev Ecol Syst 18:293–320

Pichat S, Douchet C, Albarede F (2003) Zinc isotope variations in deep-sea carbonates from the eastern equatorial Pacific over the last 175 ka. Earth Planet Sci Lett 210:167–178

Pistiner JS, Henderson GM (2003) Lithium-isotope fractionation during continental weathering processes. Earth Planet Sci Lett 214:327–339

Plessen B, Harlov DE, Henry D, Guidotti CV (2010) Ammonium loss and nitrogen isotopic fractionation in biotite as a function of metamorphic grade in metapelites from western Main, USA. Geochim Cosmochim Acta 74:4759–4771

Pogge von Strandmann PA, Forshaw J, Schmidt DN (2014) Modern and Cenozoic records of magnesium behaviour from foraminiferal Mg isotopes. Biogeosci Discuss 11:7451–7464

Pogge von Strandmann PA, Burton KW, James RH, van Calsteren P, Gislason SR, Sigfusson B (2008) The influence of weathering processes on riverine magnesium isotopes in a basaltic terrain. Earth Planet Sci Lett 276:187–197

Poitrasson F, Cruz Vieira L et al (2014) Iron isotope composition of the bulk waters and sediments from the Amazon River basin. Chem Geol 377:1–11

Poitrasson F, Freydier R (2005) Heavy iron isotope composition of granites determined by high resolution MC-ICP-MS. Chem Geol 222:132–147

Poitrasson F, Roskosz M, Corgne A (2009) No iron isotope fractionation between molten alloys and silicate melt to 2000 °C and 7.7 GPa: experimental evidence and implications for planery differentiation and accretion. Earth Planet Sci Lett 278:376–385

Pokrovsky OS, Viers J, Emnova EE, Kompantseva EI, Freydier R (2008) Copper isotope fractionation during its interaction with soil and aquatic microorganisms and metal oxy(hydr) oxides: possible structural control. Geochim Cosmochim Acta 72:1742–1757

Polyakov VB, Clayton RN, Horita J, Mineev SD (2007) Equilibrium iron isotope fractionation factors of minerals:reevaluation from the data of nuclear inelastic resonant X-ray scattering and Mossbauer spectroscopy. Geochim Cosmochim Acta 71:3833–3846

Polyakov VB, Mineev SD, Clayton RN, Hu G, Mineev KS (2005) Determination of tin equilibrium fractionation factors from synchrotron radiation experiments. Geochim Cosmochim Acta 69:5531–5536

Polyakov VB, Soultanov DM (2011) New data on equilibrium iron isotope fractionation among sulfides: constraints on mechanisms of sulfide formation in hydrothermal and igneous systems. Geochim Cosmochim Acta 75:1957–1974

Popp BN, Laws EA, Bidigare RR, Dore JE, Hanson KL, Wakeham SG (1998) Effect of phytoplankton cell geometry on carbon isotope fractionation. Geochim Cosmochim Acta 62:69–77

Porter SJ, Selby D, Cameron V (2014) Characterising the nickel isotopic composition of organic-rich marine sediments. Chem Geol 387:12–21

Poulson RL, Siebert C, McManus J, Berelson WM (2006) Authigenic molybdenum isotope signatures in marine sediments. Geology 34:617–620

Poulson-Brucker RL, McManus J, Severmann S, Berelson WM (2009) Molybdenum behaviour during early diagenesis: insights from Mo isotopes. Geochem Geophys Geosys 10(Q06010):1–25

Pretet C, van Zuilen K, Nägler TF, Reynaud S, Immenhauser A, Böttcher ME, Samankassou E (2015) The barium isotope composition of corals: a potential proxy for seaweater? Chem Geol (in press)

Prytulak J, Nielsen SG et al (2013b) The stable vanadium isotope composition of the mantle and mafic lavas. Earth Planet Sci Lett 365:177–189

Prytulak J, Nielsen RG, Halliday AN (2011) Determination of precise and accurate $^{51}V/^{50}V$ isotope ratios by multi-collector ICP-MS, Part 2: Isotope composition of six reference materials plus the Allende chondrite and verification tests. Geostand Geoanal Res 35:307–318

Prytulak J, Nielsen SG, Plank T, Barker M, Elliott T (2013a) Assessing the utility of thallium and thallium isotopes for tracing subduction zone inputs to the Mariana arc. Chem Geol 345:139–149

Puchelt H, Sabels BR, Hoering TC (1971) Preparation of sulfur hexafluoride for isotope geochemical analysis. Geochim Cosmochim Acta 35:625–628

Qi HW, Rouxel O, Hu RZ, Bi XW, Wen HJ (2011) Germanium isotopic systematics in Ge-rich coal from the Lincang Ge deposit, Yunnan, Southwestern China. Chem Geol. 286:252–265

Ra K (2010) Determination of Mg isotopes in chlorophyll *a* for marine bulk phytoplankton from the northwestern Pacific ocean. Geochem Geophys Geosys 11(12):Q12011. doi:10.1029/2010GC003350

Ra K, Kitagawa H (2007) Magnesium isotope analysis of different chlorophyll forms in marine phytoplankton using multi-collector ICP-MS. J Anal At Spectrom 22:817–821

Raddatz J, Liebetrau V et al (2013) Stable Sr-isotope, Sr/Ca, Mg/Ca, Li/Ca and Mg/Li ratios in the scleractinian cold-water coral *Lophelia pertusa*. Chem Geol 352:143–152

Radic A, Lacan F, Murray JW (2011) Iron isotopes in the seawater of the equatorial Pacific Ocean: new constraints for the oceanic iron cycle. Earth Planet Sci Lett 306:1–10

Ransom B, Spivack AJ, Kastner M (1995) Stable Cl isotopes in subduction-zone pore waters: implications for fluid-rock reactions and the cycling of chlorine. Geology 23:715–718

Redling K, Elliott E, Bain D, Sherwell J (2013) Highway contributions to reactive nitrogen deposition: tracingthe fate of vehicular NOx using stable isotopes and plant biomonitors. Biogeochemistry 116:261–274

Rees CE (1978) Sulphur isotope measurements using SO_2 and SF_6. Geochim Cosmochim Acta 42:383–389

Rehkämper M, Frank M, Hein JR, Halliday A (2004) Cenozoic marine geochemistry of thallium deduced from isotopic studies of feromanganese crusts and pelagic sediments. Earth Planet Sci Lett 219:77–91

Rehkämper M, Frank M, Hein JR, Porcelli D, Halliday A, Ingri J, Libetrau V (2002) Thallium isotope variations in seawater and hydrogenetic, diagenetic and hydrothermal ferromanganese deposits. Earth Planet Sci Lett 197:65–81

Rehkämper M, Wombacher F, Horner TJ, Xue Z (2011) Natural and anthropogenic Cd isotope variations. In: Baskaran M (ed) Handbook of environmental isotope geochemistry. Springer, New York, pp 125–154

Revesz K, Böhlke JK, Yoshinari T (1997) Determination of ^{18}O and ^{15}N in nitrate. Anal Chem 69:4375–4380

Reynard LM, Henderson GM, Hedges RE (2010) Calcium isotope ratios in animal and human bone. Geochim Cosmochim Acta 74:3735–3750

Reynolds BC, Frank M, Halliday AN (2006) Silicon isotope fractionation during nutrient utilization in the North Pacific. Earth Planet Sci Letters 244:431–443

Richet P, Bottinga Y, Javoy M (1977) A review of H, C, N, O, S, and Cl stable isotope fractionation among gaseous molecules. Ann Rev Earth Planet Sci 5:65–110

Richter FM, Davis AM, DePaolo D, Watson BE (2003) Isotope fractionation by chemical diffusion between molten basalt and rhyolite. Geochim Cosmochim Acta 67:3905–3923

Rippberger S, Rehkämper VM, Porcelli D, Halliday AN (2007) Cadmium isotope fractionation in seawater – a signature of biological activity. Earth Planet Sci Lett 261:670–684

Robert F, Chaussidon M (2006) A paleotemperature curve for the Precambrian oceans based on silicon isotopes in cherts. Nature 443:969–972

Rolison JM, Landing WM, Luke W, Cohen M, Salters VJ (2013) Isotopic composition of species-specific atmospheric Hg in a coastal environment. Chem Geol 336:37–49

Rollion-Bard C, Blamart D, Trebosc J, Tricot G, Mussi A, Cuif JP (2011) Boron isotopes as pH proxy: a new look at boron speciation in deep-sea corals using ^{11}B MAS NMR and EELS. Geochim Cosmochim Acta 75:1003–1012

Rollion-Bard C, Erez J (2010) Intra-shell boron isotope ratios in the symbiont-bearing benthic foraminifera *Amphistegina lobifera*: implications for d^{11}B vital effects and paleo-pH reconstructions. Geochim Cosmochim Acta 74:1530–1536

Rollion-Bard C, Vigier N, Spezzaferri S (2007) In-situ measurements of calcium isotopes by ion microprobe in carbonates and application to foraminifera. Chem Geol 244:679–690

Romanek CS, Grossman EL, Morse JW (1992) Carbon isotope fractionation in synthetic aragonite and calcite: effects of temperature and precipitation rate. Geochim Cosmochim Acta 56:419–430

Romaniello SJ, Herrmann AD, Anbar AD (2013) Uranium concentrations and ^{238}U/^{235}U isotope ratios in modern carbonates from the Bahamas: assessing a novel paleoredox proxy. Chem Geol 362:305–316

Rose EF, Chaussidon M, France-Lanord C (2000) Fractionation of boron isotopes during erosion processes: the example of Himalayan rivers. Geochim Cosmochim Acta 64:397–408

Rosenbaum J, Sheppard SMF (1986) An isotopic study of siderites, dolomites and ankerites at high temperatures. Geochim Cosmochim Acta 50:1147–1150

Rosman JR, Taylor PD (1998) Isotopic compositions of the elements (technical report): commission on atomic weights and isotopic abundances. Pure Appl Chem 70:217–235

Rouxel O, Bekker A, Edwards KJ (2005) Iron isotope constraints on the Archean and Proterozoic ocean redox state. Science 307:1088–1091

Rouxel O, Fouquet Y, Ludden JN (2004a) Copper isotope systematics of the Lucky Strike, Rainbow and Logatschev seafloor hydrothermal fields on the Mi-Atlantic Ridge. Econ Geol 99:585–600

Rouxel O, Fouquet Y, Ludden JN (2004b) Subsurface processes at the Lucky Strike hydrothermal field, Mid-Atlantic Ridge: evidence from sulfur, selenium and iron isotopes. Geochim Cosmochim Acta 68:2295–2311

Rouxel O, Galy A, Elderfield H (2006) Germanium isotope variations in igneous rocks and marine sediments. Geochim Cosmochim Acta 70:3387–3400

Rouxel O, Ludden J, Carignan J, Marin L, Fouquet Y (2002) Natural variations in Se isotopic composition detemined by hydride generation multiple collector inductively coupled plasma mass spectrometry. Geochim Cosmochim Acta 66:3191–3199

Rouxel O, Ludden J, Fouquet Y (2003) Antimony isotope variations in natural sytems and implications for their use as geochemical tracers. Chem Geol 200:25–40

Rozanski K, Araguas-Araguas L, Gonfiantini R (1993) Isotopic patterns in modern global precipitation. In: Climate change in continental isotopic records. Geophys Monograph 78:1–36

Rubinson M, Clayton RN (1969) Carbon-13 fractionation between aragonite and calcite. Geochim Cosmochim Acta 33:997–1002

Rudnick RL, Ionov DA (2007) Lithium elemental and isotopic disequilibrium in minerals from peridotite xenoliths from far-east Russia: product of recent melt/fluid-rock interaction. Earth Planet Sci Lett 256:278–293

Rudnick RL, Tomascak PB, Njo HB, Gardner LR (2004) Extreme lithium isotopic fractionation during continental weathering revealed in saprolites from South Carolina. Chem Geol 212:45–57

Rudnicki MD, Elderfield H, Spiro B (2001) Fractionation of sulfur isotopes during bacterial sulfate reduction in deep ocean sediments at elevated temperatures. Geochim Cosmochim Acta 65:777–789

Ruiz J, Mathur R, Young S, Brantley S (2002) Controls of copper isotope fractionation. Geochim Cosmochim Acta Spec Suppl 66:A654

Rumble D, Miller MF, Franchi IA, Greenwood RC (2007) Oxygen three-isotope fractionation lines in terrestrial silicate minerals: an inter-laboratory comparison of hydrothermal quartz and eclogitic garnet. Geochim Cosmochim Acta 71:3592–3600

Russell WA, Papanastassiou DA, Tombrello TA (1978) Ca isotope fractionation on the Earth and other solar system materials. Geochim Cosmochim Acta 42:1075–1090

Rustad JR, Casey WH, Yin QZ, Bylaska EJ, Felmy AR, Bogatko SA, Jackson VE, Dixon DA (2010) Isotopic fractionation of $Mg^{2+}_{(aq)}$, $Ca^{2+}_{(aq)}$ and $Fe^{2+}_{(aq)}$ with carbonate minerals. Geochim Cosmochim Acta 74:6301–6323

Rustad JR, Dixon DA (2009) Prediction of iron-isotope fractionation between nematite (α-Fe_2O_3) and ferric and ferrous iron in aqueous solution from density functional theory. J Phys Chem 113:12249–12255

Ryan BM, Kirby JK, Degryse F, Harris H, McLaughlin MJ, Scheiderich K (2013) Copper speciation and isotopic fractionation in plants: uptake and translocation mechanism. New Phytol 199:367–378

Rye RO (1974) A comparison of sphalerite-galena sulfur isotope temperatures with filling-temperatures of fluid inclusions. Econ Geol 69:26–32

Ryu JS, Jacobson AD, Holmden C, Lundstrom C, Zhang Z (2011) The major ion, $\delta^{44/40}$Ca, $\delta^{44/42}$Ca and $\delta^{26/24}$Mg geochemistry of granite weathering at pH = 1 and T = 25 °C: power-law processes and the relative reactivity of minerals. Geochim Cosmochim Acta 75:6004–6026

Rüggeburg A, Fietzke J, Liebetrau V, Eisenhauer A, Dullo WC, Freiwald A (2008) Stable strontium isotopes (d$^{88/86}$Sr) in cold-water corals—a new proxy for reconstruction of intermediate ocean water temperatures. Earth Planet Sci Lett 269:570–575

Saccocia PJ, Seewald JS, Shanks WC (2009) Oxygen and hydrogen isotope fractionation in serpentine-water and talc-water systems from 250 to 450 °C, 50 MPa. Geochim Cosmochim Acta 73:6789–6804

Sachse D, Billault I et al (2012) Molecular paleohydrology: interpreting the hydrogen-isotopic composition of lipid biomarkers from photosynthesizing organisms. Ann Rev Earth Planet Sci 40:221–249

Sadofsky SJ, Bebout GE (2000) Ammonium partitioning and nitrogen isotope fractionation among coexisting micas during high-temperature fluid-rock interaction. Examples from the New England Appalachians. Geochim Cosmochim Acta 64:2835–2849

Saenger C, Wang Z (2014) Magnesium isotope fractionation in biogenic and abiogenic carbonates: implications for paleoenvironmental proxies. Quarter Sci Rev 90:1–21

Sakai H (1968) Isotopic properties of sulfur compounds in hydrothermal processes. Geochem J 2:29–49

Sanyal A, Nugent M, Reeder RJ, Bijma J (2000) Seawater p_H control on the boron isotopic composition of calcite: evidence from inorganic calcite precipitation experiments. Geochim Cosmochim Acta 64:1551–1555

Sauer PE, Eglinton TI, Hayes JM, Schimmelmann A, Sessions AL (2001) Compound-specific D/H ratios of lipid biomarkers from sediments as a proxy for environmental and climatic conditions. Geochim Cosmochim Acta 65:213–222

Saunier G, Pokrovski GS, Poitrasson F (2011) First experimental determination of iron isotope fractionation between hematite and aqueous solution at hydrothermal conditions. Geochim Cosmochim Acta 75:6629–6654

Savage PS, Armytage R, Georg RB, Halliday AN (2014) High temperature silicon isotope geochemistry. Lithos 190–191:500–519

Savage PS, Georg RB, Williams HM, Burton KW, Halliday AN (2011) Silicon isotope fractionation during magmatic differentiation. Geochim Cosmochim Acta 75:6124–6139

Savin SM, Lee M (1988) Isotopic studies of phyllosilicates. Rev Mineral 19:189–223

Schauble EA (2007) Role of nuclear volume in driving equilibrium stable isotope fractionation of mercury, thallium and other very heavy elements. Geochim Cosmochim Acta 71:2170–2189

Schauble EA (2011) First principles estimates of equilibrium magnesium isotope fractionation in silicate, oxide, carbonate and hexaaquamagnesium(2 +) crystals. Geochim Cosmochim Acta 75:844–869

Schauble EA, Rossman GR, Taylor HP (2001) Theoretical estimates of equilibrium Fe isotope fractionations from vibrational spectroscopy. Geochim Cosmochim Acta 65:2487–2498

Schauble ES, Rossman GR, Taylor HP (2003) Theoretical estimates of equilibrium chlorine-isotope fractionations. Geochim Cosmochim Acta 67:3267–3281

Schauble EA, Rossman GR, Taylor HP (2004) Theoretical estimates of equilibrium chromium isotope fractionations. Chem Geol 205:99–114

Scheele N, Hoefs J (1992) Carbon isotope fractionation between calcite, graphite and CO_2. Contr Mineral Petrol 112:35–45

Schilling K, Johnson TM, Wilcke W (2011) isotope fractionation of selenium during fungal biomethylation by *Alternaria alternata*. Environ Sci Technol 45:2670–2676

Schimmelmann A, Sessions AL, Mastalerz M (2006) Hydrogen isotopic (D/H) composition of organic matter during diagenesis and thermal maturation. Ann Rev Earth Planet Sci 34:501–533

Schmidt M, Maseyk K, Lett C, Biron P, Richard P, Bariac T, Seibt U (2010) Concentration effects on laser based $\delta^{18}O$ and δ^2H measurements and implications for the calibration of vapour measurements with liquid standards. Rapid Comm Mass Spectrom 24:3553–3561

Schmitt AD, Galer SJ, Abouchami W (2009) Mass-dependent cadmium isotopic variations in nature with emphasis on the marine environment. Earth Planet Sci Lett 277:262–272

Schmitt AD, Cobert F, Bourgeade P et al (2013) Calcium isotope fractionation during plant growth under a limited nutrient supply. Geochim Cosmochim Acta

Schoenberg R, von Blanckenburg F (2005) An assessment of the accuracy of stable Fe isotope ratio measurements on samples with organic and inorganic matrices by high-resolution multicollector ICP-MS. Int J Mass Spectr 242:257–272

Schoenberg R, Zink S, Staubwasser M, von Blanckenburg F (2008) The stable Cr isotope inventory of solid Earth reservoirs determined by double-spike MC-ICP-MS. Chem Geol 249:294–306

Schoenheimer R, Rittenberg D (1939) Studies in protein metabolism: I. General considerations in the application of isotopes to the study of protein metabolism. The normal abundance of nitrogen isotopes in amino acids. J Biol Chem 127:285–290

Schüßler JA, Schoenberg R, Behrens H, von Blanckenburg F (2007) The experimental calibration of iron isotope fractionation factor between pyrrhotite and peralkaline rhyolitic melt. Geochim Cosmochim Acta 71:417–433

Scott C, Lyons TW (2012) Contrasting molybdenum cycling and isotopic properties in euxinix versus non-euxinic sediments and sedimentary rocks: refining the paleoproxies. Chem Geol

Seal RR (2006) Sulfur isotope geochemistry of sulfide minerals. Rev Mineral Geochem 61:633–677

Seal RR, Alpers CN, Rye RO (2000) Stable isotope systematics of sulfate minerals. Rev Mineral 40:541–602

Sedaghatpour F, Teng FZ, Liu Y, Sears DW, Taylor LA (2013) Magnesium isotope composition of the Moon. Geochim Cosmochim Acta 120:1–16

Seitz HM, Brey GP, Lahaye Y, Durali S, Weyer S (2004) Lithium isotope signatures of peridotite xenoliths and isotope fractionation at high temperature between olivine and pyroxene. Chem Geol 212:163–177

Seitz HM, Brey GP, Zipfel J, Ott U, Weyer S, Durali S, Weinbruch S (2007) Lithium isotope composition of ordinary and carbonaceous chondrites and differentiated planetary bodies: bulk solar system and solar reservoirs. Earth Planet Sci Lett 260:582–596

Sessions AL, Burgoyne TW, Schimmelmann A, Hayes JM (1999) Fractionation of hydrogen isotopes in lipid biosynthesis. Org Geochem 30:1193–1200

Severmann S, Johnson CM, Beard BL, McManus J (2006) The effect of early diagenesis on the Fe isotope composition of porewaters and authigenic minerals in continental margin sediments. Geochim Cosmochim Acta 70:2006–2022

Severmann S, Lyons TW, Anbar A, McManus J, Gordon G (2008) Modern iron isotope perspective on the benthic iron shuttle and the redox evolution of ancient oceans. Geology 36:487–490

Severmann S, McManus J, Berelson WM, Hammond DE (2010) The continental shelf benthic flux and its isotope composition. Geochim Cosmochim Acta 74:3984–4004

Shahar A, Young ED, Manning CE (2008) Equilibrium high-temperature Fe isotope fractionation between fayalite and magnetite: an experimental calibration. Earth Planet Sci Lett 268:330–338

Shahar A, Ziegler K, Young ED, Ricollaeu A, Schauble E, Fei Y (2009) Experimentally determined Si isotope fractionation between silcate and Fe metal and implications for the Earth's core formation. Earth Planet Sci Lett 288:228–234

Sharma T, Clayton RN (1965) Measurement of 18O/16O ratios of total oxygen of carbonates. Geochim Cosmochim Acta 29:1347–1353

Sharp ZD (1990) A laser-based microanalytical method for the in situ determination of oxygen isotope ratios of silicates and oxides. Geochim Cosmochim Acta 54:1353–1357

Sharp ZD, Atudorei V, Durakiewicz T (2001) A rapid method for determination of hydrogen and oxygen isotope ratios from water and hydrous minerals. Chem Geol 178:197–210

Sharp ZD, Barnes JD, Brearley AJ, Chaussidon M, Fischer TP, Kamenetsky VS (2007) Chlorine isotope homogeneity of the mantle, crust and carbonaceous chondrites. Nature 446:1062–1065

Sharp ZD, Shearer CK, McKeegan KD, Barnes JD, Wang YD (2010) The chlorine isotope composition of the Moon and implications for an anhydrous mantle. Science 239:1050–1053

Shen B, Jacobson B, Lee CT, Yin QZ, Mourton DM (2009) The Mg isotopic systematics of granitoids in continental arcs and implications for the role of chemical weathering in crust formation. PNAS 106:20652–20657

Sheppard SMF, Nielsen RL, Taylor HP (1971) Hydrogen and oxygen isotope ratios in minerals from Porphyry Copper Deposits. Econ Geol 66:515–542

Sherman LS, Blum JD, Johnson KP, Keeler GJ, Barres JA, Douglas TA (2010) Mass-independent fractionation of mercury isotopes in Arctic snow driven by sunlight. Nat Geosci 3:173–177

Sherman LS, Blum JD, Nordstrom DK, McCleskey RB, Barkay T, Vetriani C (2009) Mercury isotope composition of hydrothermal systems in the Yellowstone Plateau volcanic field and Guaymas Basin sea-floor rift. Earth Planet. Sci Lett 279:86–96

Shiel AE, Weis D, Orians KJ (2010) Evaluation of zinc, cadmium and lead isotope fractionation during smelting and refining. Sci Tot Environ 408:2357–2368

Shields WR, Goldich SS, Garner EI, Murphy TJ (1965) Natural variations in the abundance ratio and the atomic weight of copper. J Geophys Res 70:479–491

Shouakar-Stash O, Alexeev SV, Frape SK, Alexeeva LP, Drimmie RJ (2007) Geochemistry and stable isotope signatures including chlorine and bromine isotopes of the deep groundwaters of the Siberian Platform, Russia. Appl Geochem 22:589–605

Shouakar-Stash O, Drimmie RJ, Frape SK (2005) Determination of inorganic chlorine stable isotopes by continuous flow isotope mass spectrometry. Rapid Commun Mass Spectr 19:121–127

Siebert C, Kramers JD, Meisel T, Morel P, Nägler TF (2005) PGE, Re-Os and Mo isotope systematics in Archean and early Proterozoic sedimentary systems as proxies for redox conditions of the early Earth. Geochim Cosmochim Acta 69:1787–1801

Siebert C, McManus J, Bice A, Poulson R, Berelson WM (2006b) Molybdenum isotope signatures in continental margin sediments. Earth Planet Sci Lett 241:723–733

Siebert C, Nägler TF, von Blanckenburg F, Kramers JD (2003) Molybdenum isotope records as potential proxy for paleoceanography. Earth Planet Sci Lett 211:159–171

Siebert C, Ross A, McManus J (2006a) Germanium isotope measurements of high-temperature geothermal fluids using double-spike hydride generation MC-ICP-MS. Geochim Cosmochim Acta 70:3986–3995

Sigman DM, Casciotti KL, Andreani M, Barford C, Galanter M, Böhlke JK (2001) A bacterial method for the nitrogen isotopic analysis of nitrate in seawater and freshwater. Anal Chem 73:4145–4153

Sikora ER, Johnson TM, Bullen TD (2008) Microbial mass-dependent fractionation of chromium isotopes. Geochim Cosmochim Acta 72:3631–3641

Sim MS, Bosak T, Ono S (2011) Large sulfur isotope fractionation does not require disproportionnation. Science 333:74–77

Sime NG, De la Rocha C, Galy A (2005) Negligible temperature dependence of calcium isotope fractionation in 12 species of planktonic foraminifera. Earth Planet Sci Lett 232:51–66

Simon JI, dePaolo DJ (2010) Stable calcium isotopic composition of meteorites and rocky planets. Earth Planet Sci Lett 289:457–466

Skulan JL, Beard BL, Johnson CM (2002) Kinetic and equilibrium isotope fractionation between aqueous Fe(III) and hematite. Geochim Cosmochim Acta 66:2505–2510

Skulan JL, DePaolo DJ, Owens TL (1997) Biological control of calcium isotopic abundances in the global calcium cycle. Geochim Cosmochim Acta 61:2505–2510

SkulanJL DePaolo DJ (1999) Calcium isotope fractionation between soft and mineralised tissues as a monitor of calcium use in vertebrates. PNAS 96:13709–13713

Slack JF, Palmer MR, Stevens BPJ, Barnes RG (1993) Origin and significance of tourmaline-rich rocks in the Broken Hill district, Australia. Econ Geol 88:505–541

Smith CN, Kesler SE, Blum JD, Rytuba JR (2008) Isotope geochemistry of mercury in source rocks, mineral deposits and spring deposits of the California Coast Ranges, USA. Earth Planet Sci Lett 269:398–406

Smith MP, Yardley BWD (1996) The boron isotopic composition of tourmaline as a guide to fluid processes in the southwestern England orefield: an ion microprobe study. Geochim Cosmochim Acta 60:1415–1427

Smithers RM, Krouse HR (1968) Tellurium isotope fractionation study. Can J Chem 46:583–591

Sonke JE (2011) A global model of mass independent mercury stable isotope fractionation. Geochim Cosmochim Acta 75:4577–4590

Sonke JE, Blum JD (2013) Advances in mercury stable isotope geochemistry. Chem Geol 366:1–4

Sonke JE, Schäfer J et al (2010) Sedimentary mercury stable isotope records of atmospheric and riverine pollution from two major European heavy metal refineries. Chem Geol 279:90–100

Sonke JE, Sivry Y et al (2008) Historical variations in the isotopic composition of atmospheric zinc deposition from a zinc smelter. Chem Geol 252:145–157

Spivack AJ, Edmond JM (1986) Determination of boron isotope ratios by thermal ionization mass spectrometry of the dicesium metaborate cation. Anal Chem 58:31–35

Spivack AJ, Kastner M, Ransom B (2002) Elemental and isotopic chloride geochemistry in the Nankai trough. Geophysical Res Lett 29:1661. doi:10.1029/2001GL014122

Stetson SJ, Gray JE, Wanty RB, MacLady DL (2009) Isotope variability of mercury in ore, mine-waste calcine, and leachates of mine-waste calcine from areas mined for mercury. Environ Sci Technol 43:7331–7336

Steuber T, Buhl D (2006) Calcium-isotope fractionation in selected modern and ancient marine carbonates. Geochim Cosmochim Acta 70:5507–5521

Stevenson EI, Hermoso M, Rickaby RE, Tyler JJ, Minoletti F, Parkinson IJ, Mokadem F, Burton KW (2014) Controls on stable strontium isotope fractionation in coccolithophores with implications for the marine Sr cycle. Geochim Cosmochim Acta 128:225–235

Stirling CH, Andersen MB, Potter EK, Halliday AN (2007) Low-temperature isotopic fractionation of uranium. Earth Planet Sci Lett 264:208–225

Stotler RL, Frape SK, Shouakar-Stash O (2010) An isotopic survey of d^{81}Br and d^{37}Cl of dissolved halides in the Canadian and Fennoscandian shields. Chem Geol 274:38–55

Sturchio NC, Hatzinger PB, Atkins MD, Suh C, Heraty LJ (2003) Chlorine isotope fractionation during microbial reduction of perchlorate. Environ Sci Technol 37:3859–3863

Sutton JN, Varela DE, Brzezinski MA, Beucher CP (2013) Species-dependent silicon isotope fractionationby marine diatoms. Geochim Cosmochim Acta 104:300–309

Suzuoki T, Epstein S (1976) Hydrogen isotope fractionation between OH-bearing minerals and water. Geochim Cosmochim Acta 40:1229–1240

Swart PK, Burns SJ, Leder JJ (1991) Fractionation of the stable isotopes of oxygen and carbon in carbon dioxide during the reaction of calcite with phosphoric acid as a function of temperature and technique. Chem Geol 86:89–96

Swihart GH, Moore PB (1989) A reconnaissance of the boron isotopic composition of tourmaline. Geochim Cosmochim Acta 53:911–916

Tanimizu M, Araki Y, Asaoka S, Takahashi Y (2011) Determination of natural isotopic variation in antimony using inductively coupled plasma mass spectrometry for an uncertainty estimation of the standard atomic weight of antimony. Geochem J 45:27–32

Tarutani T, Clayton RN, Mayeda TK (1969) The effect of polymorphism and magnesium substitution on oxygen isotope fractionation between calcium carbonate and water. Geochim Cosmochim Acta 33:987–996

Taube H (1954) Use of oxygen isotope effects in the study of hydration ions. J Phys Chem 58:523

Taylor HP (1968) The oxygen isotope geochemistry of igneous rocks. Contr Mineral Petrol 19:1–71

Taylor HP (1974) The application of oxygen and hydrogen isotope studies to problems of hydrothermal alteration and ore deposition. Econ Geol 69:843–883

Taylor HP, Epstein S (1962) Relation between ^{18}O/^{16}O ratios in coexisting minerals of igneous and metamorphic rocks. I Principles and experimental results. Geol Soc Am Bull 73:461–480

Taylor TI, Urey HC (1938) Fractionation of the lithium and potassium isotopes by chemical exchange with zeolites. J Chem Phys 6:429–438

Telus M, Dauphas N, Moynier F, Tissot F, Teng FZ, Nabelek PI, Craddock PR, Groat LA (2012) Iron, zinc, magnesium and uranium isotopic fractionation during continental crust differentiation: the tale from migmatites, granitoids and pegmatites. Geochim Cosmochim Acta 97:247–265

Teng FZ et al (2004) Lithium isotope composition and concentration of the upper continental crust. Geochim Cosmochim Acta 68:4167–4178

Teng FZ, Dauphas N, Helz R (2008) Iron isotope fractionation during magmatic differentiation in Kilauea Iki lava lake. Science 320:1620–1622

Teng FZ, Dauphas N, Helz RT, Gao S, Huang S (2011) Diffusion-driven magnesium and iron isotope fractionation in Hawaiian olivine. Earth Planet Sci Lett 308:317–324

Teng FZ, Dauphas N, Huang S, Marty B (2013) Iron isotope systematics of oceanic basalts. Geochim Cosmochim Acta 107:12–26

Teng FZ, McDonough WF, Rudnick RL, Walker RJ (2006) Diffusion-driven extreme lithium isotopic fractionation in country rocks of the Tin Mountain pegmatite. Earth Planet Sci Lett 243:701–710

Teng FZ, McDonough WF, Rudnick RL, Wing BA (2007a) Limited lithium isotopic fractionation during progressive metamorphic dehydration in metapelites: a case study from the Onawa contact aureole, Maine. Chem Geol 239:1–12

Teng FZ, Rudnick RL, McDonough WF, Wu FY (2009) Lithium isotope systematics of A-type granites and their mafic enclaves: further constraints on the Li isotopic composition of the continental crust. Chem Geol 262:415–424

Teng FZ, Wadhwa M, Helz RT (2007b) Investigation of magnesium isotope fractionation during basalt differentiation: implications for a chondritic composition of the terrrestrial mantle. Earth Planet Sci Lett 261:84–92

Teng FZ, Yang W (2013) Comparison of factors affecting the accuracy of high-precision magnesium isotope analysis by multi-collector inductively coupled plasma mass spectrometry. Rapid Commun Mass Spectrom 28:19–24

Teng FZ et al. (2014) Magnesium isotopic compositions of international geological refrence materials. Geostand Geoanal Res (in press)

Tesdal JE, Galbraith ED, Kienast M (2013) Nitrogen isotopes in bulk marine sediments: linking seafloor observations with subseafloor records. Biogeosciences 10:101–118

Teutsch N, Schmid M, Muller B, Halliday AN, Burgmann H, Wehrli B (2009) Large iron isotope fractionation at the oxic-anoxic boundary in lake Nyos. Earth Planet Sci Lett 285:52–60

Thamdrup B, Dalsgaard T (2002) Production of N_2 through anaerobic ammonium oxidation coupled to nitrate reduction in marine sediments. Appl Environ Microbiol 68:1312–1318

Thode HG, Macnamara J, Collins CB (1949) Natural variations in the isotopic content of sulphur and their significance. Can J Res 27B:361

Tipper ET, Galy A, Bickle MJ (2006a) Riverine evidence for a fractionated reservoir of Ca and Mg on the continents: implications for the oceanic Ca cycle. Earth Planet Sci Lett 247:267–279

Tipper ET, Galy A, Bickle MJ (2008) Calcium and magnesium isotope systematics in rivers draining the Himalaya-Tibetan–Plateau region: lithological or fractionation control? Geochim Cosmochim Acta 72:1057–1075

Tipper ET, Galy A, Gaillardet J, Bickle MJ, Elderfield H, Carder EA (2006b) The magnesium isotope budget of the modern ocean: constraints from riverine magnesium isotope ratios. Earth Planet Sci Lett 250:241–253

Tipper ET, Gaillardet J, Galy A, Louvat P, Bickle MJ, Capmas F (2010) Calcium isotope ratios in the world´s largest rivers: a constraint on the maximum imbalance of oceanic calcium fluxes. Global Biogeochemical Cycles 24:10.1029/2009GB003574

Tomascak PB, Ryan JG, Defant MJ (2000) Lithium isotope evidence for light element decoupling in the Panama subarc mantle. Geology 28:507–510

Tomascak PB, Tera F, Helz RT, Walker RJ (1999) The absence of lithium isotope fractionation during basalt differentiation: new measurements by multicollector sector ICP-MS. Geochim Cosmochim Acta 63:907–910

Tomascak PB, Widom E, Benton LD, Goldstein SL, Ryan JG (2002) The control of lithium budgets in island arcs. Earth Planet Sci Lett 196:227–238

Tomaszak PB (2004) Lithium isotopes in earth and planetary sciences. Rev Mineral Geochem

Tonarini S, Leeman WP, Leat PT (2011) Subduction erosion of forearc mantle wedge implicated in the genesis of the South Sandwich Island (SSI) arc: evidence from boron isotope systematics. Earth Planet Sci Lett 301:275–284

Toutain JP, Sonke J et al (2008) Evidence for Zn isotopic fractionation at Merapi volcano. Chem Geol 253:74–82

Trofimov A (1949) Isotopic constitution of sulfur in meteorites and in terrestrial objects. Dokl Akad Nauk SSSR 66:181 (in Russian)

Trudinger PA, Chambers LA, Smith JW (1985) Low temperature sulphate reduction: biological versus abiological. Can J Earth Sci 22:1910–1918

Truesdell AH (1974) Oxygen isotope activities and concentrations in aqueous salt solution at elevated temperatures: Consequences for isotope geochemistry. Earth Planet Sci Lett 23:387–396

Turner JV (1982) Kinetic fractionation of carbon-13 during calcium carbonate precipitation. Geochim Cosmochim Acta 46:1183–1192

Urey HC, Brickwedde FG, Murphy GM (1932) A hydrogen isotope of mass 2 and its concentration. Phys Rev 40:1

Usdowski E, Hoefs J (1993) Oxygen isotope exchange between carbonic acid, bicarbonate, carbonate, and water: a re-examination of the data of McCrea (1950) and an expression for the overall partitioning of oxygen isotopes between the carbonate species and water. Geochim Cosmochim Acta 57:3815–3818

Usdowski E, Michaelis J, Böttcher MB, Hoefs J (1991) Factors for the oxygen isotope equilibrium fractionation between aqueous CO_2, carbonic acid, bicarbonate, carbonate, and water. Z Phys Chem 170:237–249

Uvarova YA, Kyser TK, Geagea ML, Chipley D (2015) Variations in the uranium isotopic composition of uranium ores from different types of uranium deposits. Geochim Cosmochim Acta (in press)

Valdes MC, Moreira M, Foriel J, Moynier F (2014) The nature of Earth's building blocks as revealed by calcium isotopes. Earth Planet Sci Lett 394:135–145

Valley JW, O'Neil JR (1981) $^{13}C/^{12}C$ exchange between calcite and graphite: a possible thermometer in Greville marbles. Geochim Cosmochim Acta 45:411–419

Van Acker M, Shahar A, Young ED, Cöleman ML (2006) GC/Multiple Collector-ICPMS method for chlorine stable isotope analysis of chlorinated aliphatic hydrocarbons. Anal Chem 78:4663–4667

Van den Boorn SH, van Bergen MJ, Vroon PZ, de Vries ST, Nijman W (2010) Silicon isotope and trace element constraints on the origin of ≈ 3.5 Ga cherts: implications for Early Archaean marine environments. Geochim Cosmochim Acta 74:1077–1103

Van Warmerdam EM, Frape SK, Aravena R, Drimmie RJ, Flatt H, Cherry JA (1995) Stable chlorine and carbon isotope measurements of selected chlorinated organic solvents. Appl Geochem 10:547–552

Vance D, Archer C, Bermin J, Perkins J, Statham PC, Lohan MC, Ellwood MJ, Mills RA (2008) The copper isotope geochemistry of rivers and oceans. Earth Planet Sci Lett 274:204–213

Varela DE, Pride CJ, Brzezinski MA (2004) Biological fractionation of silicon isotopes in southern ocean surface waters. Glob Biogeochem Cycles 18. doi:10/1029/2003GB002140

Velinsky DJ, Pennock JR, Sharp JH, Cifuentes LA, Fogel ML (1989) Determination of the isotopic composition of ammonium-nitrogen at the natural abundance level from estuarine waters. Mar Chem 26:351–361

Vengosh A, Chivas AR, McCulloch M, Starinsly A, Kolodny Y (1991a) Boron isotope geochemistry of Australian salt lakes. Geochim Cosmochim Acta 55:2591–2606

Vengosh A, Heumann KG, Juraske S, Kasher R (1994) Boron isotope application for tracing sources of contamination in groundwater. Environ Sci Tech 28:1968–1974

Vengosh A, Starinsky A, Kolodny Y, Chivas AR (1991b) Boron isotope geochemistry as a tracer for the evolution of brines and associated hot springs from the Dead Sea, Israel. Geochim Cosmochim Acta 55:1689–1695

Vennemann TW, Fricke HC, Blake RE, O'Neil JR, Colman A (2002) Oxygen isotope analysis of phosphates: a comparison of techniques for analysis of Ag_3PO_4. Chem Geol 185:321–336

Vennemann T, O'Neil JR (1996) Hydrogen isotope exchange reactions between hydrous minerals and hydrogen: I. A new approach for the determination of hydrogen isotope fractionation at moderate temperatures. Geochim Cosmochim Acta 60:2437–2451

Viers J et al (2007) Evidence of Zn isotope fractionation in a soil-plant system of a pristine tropical watershed (Nsimi, Cameroon). Chem Geol 239:124–137

Voegelin AR, Nägler TF, Beukes NJ, Lacassie JP (2010) Molybdenum isotopes in late Archean carbonate rocks: implications for early Earth oxygenation. Precambr Res 182:70–82

Voegelin AR, Nägler TF, Samankassou E, Villa IM (2009) Molybdenum isotopic composition of modern and Carboniferous carbonates. Chem Geol 265:488–498

Vogel JC, Grootes PM, Mook WG (1970) Isotopic fractionation between gaseous and dissolved carbon dioxide. Z Physik 230:225–238

Vollstädt H, Eisenhauer A et al. (2014) The Phanerozoic $\delta^{88/86}$Sr record of seawater: new constraints on past changes in oceanic carbonate fluxes. Geochim Cosmochim Acta 128:249–265

Von Allmen K, Böttcher ME, Samankassou E, Nägler TF (2010) Barium isotope fractionation in the global barium cycle: first evidence from barium minerals and precipitation experiments. Chem Geol 277:70–77

Wachter EA, Hayes JM (1985) Exchange of oxygen isotopes in carbon dioxide-phosphoric acid systems. Chem Geol 52:365–374

Wang Z, Hu P, Gaetani G, Liu C, Saenger C, Cohen A, Hart S (2013b) Experimental calibration of Mg isotope fractionation between aragonite and seawater. Geochim Cosmochim Acta 102:113–123

Wang Y, Sessions AL, Nielsen JR, Goddard WA (2009a) Equilibrium ^{2}H/^{1}H fractionations in organic molecules. I. Calibration of ab initio calculations. Geochim Cosmochim Acta 73:7060–7075

Wang Y, Sessions AL, Nielsen RJ, Goddard WA (2009b) Equilibrium ^{2}H/^{1}H fractionations in organic molecules. II: Linear alkanes, alkenes, ketones, carboxylic acids, esters, alcohols and ethers. Geochim Cosmochim Acta 73:7076–7086

Wang Y, Sessions AL, Nielsen RJ, Goddard WA (2013a) Equilibrium ^{2}H/^{1}H fractionation in organic molecules. III Cyclic ketones and hydrocarbons. Geochim Cosmochim Acta 107:82–95

Wanner C, Sonnenthal EL, Liu XM (2014) Seawater δ^{7}Li: a direct proxy for global CO_2 consumption by continental silicate weathering? Chem Geol 381:154–167

Wasylenki LE, Swihart JW, Romaniello SJ (2014) Cadmium isotope fractionation during adsorption to Mn oxyhydroxide at low and high ionic strength. Geochim Cosmochim Acta 140:212–226

Wei G, Ma J, Liu Y, Xie L, Lu W, Deng W, Ren Z, Zeng T, Yang Y (2013) Seasonal changes in the radiogenic and stable strontium isotopic composition of Xijiang River: implications for chemical weathering. Chem Geol 343:67–75

Weinstein C, Moynier F, Wang K, Paniello R, Foriel J, Catalano J, Pichat S (2011) Isotopic fractionation of Cu in plants. Chem Geol 286:266–271

Weiss DJ, Mason TFD, Zhao FJ, Kirk GJD, Coles BJ, Horstwood MSA (2005) Isotopic discriminationof zinc in higher plants. New Phytol 165:703–710

Weiss DJ, Rausch N, Mason TFD, Coles BJ, Wilkinson JJ, Ukonmaanaho L, Arnold T, Nieminen TM (2007) Atmospheric deposition and isotope biogeochemistry of zinc in ombrotrophic peat. Geochim Cosmochim Acta 71:3498–3517

Welch SA, Beard BL, Johnson CM, Braterman PS (2003) Kinetic and equilibrium Fe isotope fractionation between aqueous Fe(II) and Fe(III). Geochim Cosmochim Acta 67:4231–4250

Wen H, Carignan J (2011) Selenium isotopes trace the source and redox processes in the black shale-hosted Se-rich deposits in China. Geochim Cosmochim Acta 75:1411–1427

Wenzel B, Lecuyer C, Joachimski MM (2000) Comparing oxygen isotope records of Silurian calcite and phosphate—δ^{18}O composition of brachiopods and conodonts. Geochim Cosmochim Acta 69:1859–1872

Weyer S, Anbar AD, Brey GP, Münker C, Mezger K (2005) Iron isotope fractionation during planetary differentiation. Earth Planet Sci Lett 240:251–264

Weyer S, Anbar AD, Gerdes A, Gordon GW, Algeo TJ, Boyle EA (2008) Natural fractionation of ^{238}U/^{235}U. Geochim Cosmochim Acta 72:345–3359

Weyer S, Ionov D (2007) Partial melting and melt percolation in the mantle: the message from Fe isotopes. Earth Planet Sci Lett 259:119–133

Weyer S, Schwieters JB (2003) High precision Fe isotope measurements with high mass resolution MC-ICPMS. Inter J Mass Spectr 226:355–368

Wiechert U, Fiebig J, Przybilla R, Xiao Y, Hoefs J (2002) Excimer laser isotope-ratio-monitoring mass spectrometry for in situ oxygen isotope analysis. Chem Geol 182:179–194

Wiechert U, Halliday AN (2007) Non-chondritic magnesium and the origin of the inner terrestrial planets. Earth Planet Sci Lett 256:360–371

Wiechert U, Hoefs J (1995) An excimer laser-based microanalytical preparation technique for in-situ oxygen isotope analysis of silicate and oxide minerals. Geochim Cosmochim Acta 59:4093–4101

Wiederhold JG, Kraemer SM, Teutsch N, Borer PM, Halliday AN, Kretzschmar R (2006) Iron isotope fractionation during proton-promoted, ligand-controlled and reductive dissolution of goethite. Environ Sci Tech 40:3787–3793

Wiegand BA, Chadwick OA, Vitousek PM, Wooden JH (2005) Ca cycling and isotopic fluxes in forested ecosystems in Hawaii. Geophys Res Lett 32:L11404

Wilkinson JJ, Weiss DJ, Mason TF, Coles BJ (2005) Zinc isotope variation in hydrothermal systems: preliminary evidence from the Irish Midlands ore field. Econ Geol 100:583–590

Wille M, Kramers JD, Nägler TF, Beukes NJ, Schroder S, Meiser T, Lacassie JP, Voegelin AR (2007) Evidence for a gradual rise of oxygen between 2.6 and 2.5 Ga from Mo isotopes and Re-PGE signatures in shales. Geochim Cosmochim Acta 71:2417–2435

Wille M, Sutton J, Ellwood MJ, Sambridge M, Maher W, Eggins S, Kelly M (2010) Silicon isotopic fractionation in marine sponges: a new model for understanding silicon isotope variations in sponges. Earth Planet Sci Lett 292:281–289

Williams LB, Ferrell RE, Hutcheon I, Bakel AJ, Walsh MM, Krouse HR (1995) Nitrogen isotope geochemistry of organic matter and minerals during diagenesis and hydrocarbon migration. Geochim Cosmochim Acta 59:765–779

Williams LB, Hervig RL (2004) Boron isotopic composition of coals: a potential tracer of organic contaminated fluids. Appl Geochem 19:1625–1636

Williams LB, Hervig RL, Holloway JR, Hutcheon I (2001) Boron isotope geochemistry during diagenesis. Part I. Experimental determination of fractionationduring illitization of smectite. Geochim Cosmochim Acta 65:1769–1782

Williams HM, Markowski A, Quitte G, Halliday AN, Teutsch N, Levasseur S (2006) Fe isotope fractionations in iron meteorites: new insight into metal-sulphide segregation and planetary accretion. Earth Planet Sci Lett 250:486–500

Williams HM, Peslier AH, McCammon C, Halliday AN, Levasseur S, Teutsch N, Burg JP (2005) Systematic iron isotope variations in mantle rocks and minerals: the effects of partial melting and oxygen fugacity. Earth Planet Sci Lett 235:435–452

Wimpenny J, Gislason SR, James RH, Gannoun A, Pogge von Strandmann P, Burton KW (2010) The behavior of Li and Mg isotopes during primary phase dissolution and secondary mineral formation in basalt. Geochim Cosmochim Acta 74:5259–5279

Wombacher F, Rehkämper M, Mezger K (2004) Dependence of the mass-dependence in cadmium isotope fractionation during evaporation. Geochim Cosmochim Acta 68:2349–2357

Wombacher F, Rehkämper M, Mezger K (2008) Cadmium stable isotope cosmochemistry. Geochim Cosmochim Acta 72:646–667

Wombacher F, Rehkämper M, Mezger K, Münker C (2003) Stable isotope compositions in geological materials and meteorites determined by multiple-collector ICPMS. Geochim Cosmochim Acta 67:4639–4654

Wortmann UG, Bernasconi SM, Böttcher ME (2001) Hypersulfidic deep biosphere indicates extreme sulfur isotope fractionation during single-step microbial sulfate reduction. Geology 29:647–650

Wu L, Beard BL, Roden EE, Johnson CM (2011) Stable iron isotope fractionation between aqueous Fe (II) and hydrous ferric oxide. Environ Sci Technol 45:1845–1852

Wunder B, Meixner A, Romer RL, Feenstra A, Schettler G, Heinrich W (2007) Lithium isotope fractionation between Li-bearing staurolite, Li-mica and aqueous fluids: an experimental study. Chem Geol 238:277–290

Wunder B, Meixner A, Romer R, Heinrich W (2006) Tempearature-dependent isotopic fractionation of lithium between clinopyroxene and high-pressure hydrous fluids. Contr Mineral Petrol 151:112–120

Wunder B, Meixner A, Romer R, Wirth R, Heinrich W (2005) The geochemical cycle of boron: constraints from boron isotope partitioning experiments between mica and fluid. Lithos 84:206–216

Xiao YK, Liu WG, Qi HP, Zhang CG (1993) A new method for the high-precision isotopic measurement of bromine by thermal ionization mass spectrometry. Int J Mass Spectrom Ion Proc 123:117–123

Xiao Y, Teng FZ, Zhang HF, Yang W (2013) Large magnesium isotope fractionation in peridotite xenoliths from eastern North China craton: product of melt-rock interaction. Geochim Cosmochim Acta 115:241–261

Xue Z, Rehkämper M, Horner TJ, Abouchami W, Middag R, van de Flierd T, de Baar HJ (2013) Cadmium isotope variations in the Southern Ocean. Earth Planet Sci Lett 382:161–172

Yamaguchi KE, Johnson CM, Beard BL, Ohmoto H (2005) Biogeochemical cycling of iron in the Archean-Paleoproterozoic Earth: constraints from iron isotope variations in sedimentary rocks from the Kapvaal and Pilbara cratons. Chem Geol 218:135–169

Yamazaki E, Nakai S, Yokoyama T, Ishihara S, Tang HF (2013) Tin isotopic analysis of cassiterites from southeastern and eastern Asia. Geochem J 47:21–35

Yang S-C, Lee D-C, Ho L-Y (2012b) The isotopic composition of cadmium in the water column of the South China Sea. Geochim Cosmochim Acta 98:66–77

Yang W, Teng FZ, Zhang HF (2009) Chondritic magnesium isotopic composition of the terrestrial mantle: a case study of peridotite xenoliths from the North China craton. Earth Planet Sci Lett 288:475–482

Yang W, Teng FZ, Zhang HF, Li SG (2012a) Magnesium isotopic systematics of continental basalts from the North China craton: implications for tracing subducted carbonate in the mantle. Chem Geol 328:185–194

Yesavage T, Fantle MS, Vervoort J, Mathur R, Jin L, Liermann LJ, Brantley SL (2012) Fe cycling in the Shale Hills Critical Zone Observatory, Pennsylvania: an analysis of biogeochemical weathering and Fe isotope fractionation. Geochim Cosmochim Acta 99:18–38

Yin R, Feng X, Shi W (2010) Application of the stable isotope system to the study of sources and fate of Hg in the environment: a review. Appl Geochem 25:1467–1477

Yin R, Feng X, Wang J, Li P, Liu J, Zhang Y, Chen J, Zheng L, Hu T (2013) Mercury speciation and mercury isotope fractionation during ore roasting process and their implication to source identification of downstream sediment in the Wanshan mercury mining area, SW China. Chem Geol 366:39–46

Yokochi R, Marty B, Chazot G, Burnard P (2009) Nitrogen in perigotite xenoliths: lithophile behaviour and magmatic isotope fractionation. Geochim Cosmochim Acta 73:4843–4861

Young ED, Galy A (2004) The isotope geochemistry and cosmochemistry of magnesium. Rev Mineral Geochem 55:197–230

Young ED, Galy A, Nagahara H (2002) Kinetic and equilibrium mass-dependent isotope fractionation laws in nature and their geochemical and cosmochemical significance. Geochim Cosmochim Acta 66:1095–1104

Young ED, Manning CE, Schauble EA, Shahar A, Macris CA, Lazar C, Jordan M (2015) High-temperature equilibrium isotope fractionation of non-traditional isotopes: experiments, theory and applications. Chem Geol 395:176–195

Young MB, McLaughlin K, Kendall C, Stringfellow W, Rollow M, Elsbury K, Donald E, Payton A (2009) Characterizing the oxygen isotopic composition of phosphate sources to aquatic ecosystems. Environ Sci Techn 43:5190–5196

Zambardi T, Poitrasson F, Corgne A, Meheut M, Quitte Anand M (2013) Silicon isotope variations in the inner solar system: implications for planetary formation, differentiation and composition. Geochim Cosmochim Acta 121:67–83

Zambardi T, Sonke JE, Toutain JP, Sortino F, Shinohara H (2009) Mercury emissions and stable isotope compositions at Vulcano Island (Italy). Earth Planet Sci let 277:236–243

Zeebe RE (2005) Stable boron isotope fractionation between dissolved $B(OH)_3$ and $B(OH)_4^-$. Geochim Cosmochim Acta 69:2753–2766

Zeebe RE (2007) An expression for the overall oxygen isotope fractionation between the sum of dissolved inorganic carbon and water. Geochem Geophys Geosys 8: 10.1029/2007GC001663

Zerkle AL, Schneiderich K, Maresca JA, Liermann LJ, Brantley SL (2011) Molybdenum isotope fractionation by cyanobacterial assimilation during nitrate utilization and N_2 fixation. Geobiology 9:94–106

Zhang L, Chan LH, Gieskes JM (1998) Lithium isotope geochemistry of pore waters from Ocean Drilling Program Sites 918 and 919, Irminger Basin. Geochim Cosmochim Acta 62:2437–2450

Zhang J, Quay PD, Wilbur DO (1995) Carbon isotope fractionation during gas-water exchange and dissoltion of CO2. Geochim Cosmochim Acta 59:107–114

Zheng W, Hintelmann H (2010) Nuclear field shift effects in isotope fractionation of mercury during abiotic reduction in the absence of light. J Phys Chem A 114:4238–4245

Zhou JX, Huang ZL, Zhou MF, Zhu XK, Muchez P (2014) Zinc, sulphur and lead isotopic variations in carbonate-hosted Pb-Zn sulfide deposits, southwest China. Ore Geol Rev 58:41–54

Zhu XK et al (2002) Mass fractionation processes of transition metal isotopes. Earth Planet Sci Lett 200:47–62

Zhu JM, Johnson TM, Clark SK, Zhu XK, Wang XL (2014) Selenium redox cycling during weathering of Se-rich shales: a selenium isotope study. Geochim Cosmochim Acta 126:228–249

Zhu P, MacDougall JD (1998) Calcium isotopes in the marine environment and the oceanic calcium cycle. Geochim Cosmochim Acta 62:1691–1698

Ziegler K, Chadwick OA, Brzezinski MA, Kelly EF (2005a) Natural variations of δ^{30}Si ratios during progressive basalt weathering. Geochim Cosmochim Acta 69:4597–4610

Ziegler K, Chadwick OA, White AF, Brzezinski MA (2005b) δ^{30}Si systematics in a granitic saprolite, Puerto Rico. Geology 33:817–820

Ziegler K, Young ED, Schauble E, Wasson JT (2010) Metal-silicate silicon isotope fractionationin enstatite meteorites and constraints on Earth's core formation. Earth Planet Sci Lett 295:487–496

Zink S, Schoenberg R, Staubwasser M (2010) Isotopic fractionation and reaction kinetics between Cr(III) and Cr(VI) in aqueous media. Geochim Cosmochim Acta 74:5729–5745

Variations of Stable Isotope Ratios in Nature

3

3.1 Extraterrestrial Materials

Extraterrestrial materials consist of samples from the moon, Mars and a variety of smaller bodies such as asteroids and comets. These planetary samples have been used to deduce the evolution of our solar system. A major difference between extraterrestrial and terrestrial materials is the existence of primordial isotopic heterogeneities in the early solar system. These heterogeneities are not observed on Earth, because they have become obliterated during high-temperature processes over geologic time. Nevertheless, isotopes have been used as a genetic link between meteorites and the Earth (i.e. Clayton 2004). Small differences in isotope composition between the Earth and meteorite groups may identify the type of meteorites that are representative of precursor material that formed the early Earth (Simon and de Paolo 2010; Valdes et al. 2014).

Heterogeneities in isotope composition indicate incomplete mixing of distinct presolar materials during formation of the solar system. Such isotope anomalies have been documented on all scales, from microscopic zoning in meteoritic minerals to bulk asteroids. The most extreme examples, however, have been documented from minute presolar grains extracted from primitive meteorites and measured with the ion microprobe. The abundance of presolar grains in meteorites is at the level of tens of ppm; the bulk isotope composition of meteorites remains more or less unaffected. These high-temperature grains of silicon carbide, graphite, diamond etc. have been formed by condensation in cooling gases and show isotope variations that may vary by several orders of magnitude, too large to be explained by chemical or physical fractionation, but pointing to nuclear reactions. They have acquired their isotope characteristics before the solar system has been formed. The implications of these variations for models of stellar formation have been summarized by Zinner (1998), Hoppe and Zinner (2000), Clayton and Nittler (2004) and others.

J. Hoefs, *Stable Isotope Geochemistry*, DOI 10.1007/978-3-319-19716-6_3

3.1.1 Chondrites

Primitive meteorites of chondritic composition are stony undifferentiated bodies that have formed from the primitive solar material during the formation of the solar system. Chondritic meteorites can be divided into different classes on the basis of their volatile contents and of their total iron content distributed between Fe in silicates and Fe in metal.

Most chondrites have experienced a complex history, which includes primary formation processes and secondary processes that include thermal metamorphism and aqueous alteration. It is generally very difficult to distinguish between the effects of primary and secondary processes on the basis of isotope composition.

3.1.1.1 Oxygen

It is generally agreed that variations in the oxygen isotope composition within the solar system result from mixing of two distinct reservoirs: an ^{16}O-rich and an ^{17}O,^{18}O-rich reservoir relative to Earth. The first observation, that clearly demonstrated isotopic inhomogeneities in the early solar system, was made by Clayton et al. (1973a). Previously, it had been thought that in a plot of ^{17}O/^{16}O versus ^{18}O/^{16}O, all physical and chemical processes must produce mass–dependent O-isotope fractionations yielding a straight line with a slope of 0.52. This line has been called the “Terrestrial Fractionation Line”. Figure 3.1 shows that O-isotope data from terrestrial and lunar samples fall along the predicted mass–dependent fractionation line. Bulk meteorites, the Moon and Mars lie within a few ‰ above or below the terrestrial fractionation line. However, selected anhydrous high-temperature minerals in carbonaceous chondrites, do not fall along the chemical fractionation trend, but instead define another trend with a slope of 1. The first evidence for oxygen isotope anomalies was found in Ca–Al-rich refractory inclusions (CAI) in the Allende carbonaceous chondrite, which are composed predominantly of melilite, pyroxene, and spinel.

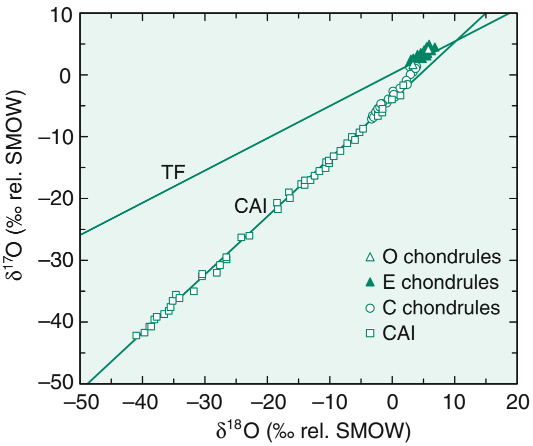

Fig. 3.1 ^{17}O versus ^{18}O isotopic composition of Ca–Al rich inclusions (CAI) from chondrites (Clayton 1993) (Fig. 3.1, 6th edition, p. 95)

The carbonaceous chondrites display the widest range in oxygen isotope composition of any meteorite group (Clayton and Mayeda 1999). The evolution of these meteorites can be interpreted as a progression of interactions between dust and gas components in the solar nebula followed by solid/fluid interactions within parent bodies. Young et al. (1999) have shown that reactions between rock and water inside a carbonaceous chondrite parent body could have produced groups of different carbonaceous chondrite types having different paragenesis of secondary minerals. The analysis of the isotope compositions of phyllosilicates, carbonates etc. provide evidence under which conditions aqueous alteration took place. Clumped isotope temperatures between 20 and 70 °C allow the reconstruction of aqueous alterations in carbonaceous chondrites (Guo and Eiler 2007).

Yurimoto et al. (2008) have summarized the oxygen isotope composition of the chondrite components (refractory inclusions, chondrules and matrix) and concluded that O isotope variations within a chondrite are typically larger than O isotope variations among bulk chondrites. The question remains as to where, when, and how the isotopic anomalies were originally produced (Thiemens 1988). Even without full understanding of the causes of isotope variations in meteorites, oxygen isotopes are very useful in classifying meteorites and in relating meteorites to their precursor asteroids and planets (Clayton 2004). Oxygen isotope signatures have confirmed that eucrites, diogenites, howardites and mesosiderites originate from one single parent body probably derived from the asteroid 4 Vesta, as shergottites, nakhlites and chassignites come from another parent body (Clayton and Mayeda 1996). The main group of pallasites represent intermixed core-mantle material from a single disrupted asteroid with no equivalent known (Greenwood et al. 2006).

In the past it had been assumed that the oxygen isotope composition of the Sun is the same as that of the Earth. This view has changed with the suggestion of Clayton (2002) that the Sun and the initial composition of the solar system is ^{16}O rich. By assuming the O-isotope composition of the Sun is reflected in the composition of the solar wind. McKeegan et al. (2011) measured the solar wind collected during the Genesis Discovery mission, which indeed is highly enriched in ^{16}O and they demonstrated that rocks from the inner solar system are enriched in ^{17}O and ^{18}O by about 70 ‰ relative to ^{16}O by mass-independent fractionation processes. According to this model, solar sytem rocks had become ^{16}O poor due to UV self shielding of CO, the most abundant oxygen containg molecule in the solar system. Oxygen released by the UV dissociation of CO then form together with other components of the solar system solid minerals with mass-independent oxygen isotope compositions.

In addition to oxygen isotopes, the volatile elements H, C, N and S show extremely large variations in isotope composition of bulk meteorites. Rather than analyzing bulk meteorite samples, investigations in recent years have concentrated on the analyses of individual components.

3.1.1.2 Hydrogen

The solar system consists of water containing reservoirs with very different D/H isotope compositions that can be used as fingerprints for the origin of water in planetary bodies (Saal et al. 2013; Sarafian et al. 2014). Hydrogen isotopes indicate a gradient through the solar system as a function of distance from the Sun: the protosolar nebula is very D-depleted whereas ice in the outer solar system is very D enriched. Similar ranges of D/H ratios among carbonaceous chondrites, Earth, Mars and Moon suggest a common source region for water in these planetary bodies. Alexander et al. (2012) compared D-isotope ratios of chondritic meteorites with those in comets and demonstrated that they are distinct from one another with comets being highly enriched in D relative to chondrites. Since the various types of chondrites have D-contents being similar to Earth, the dominant source of volatiles on Earth appear to be from asteroids (Sarafian et al. 2014).

In extraterrestrial material. hydrogen is bound in hydrated minerals and in organic matter. Hydrogen isotopes, thus, may provide insight not only into the origin of water in planetary material (Robert 2001; Alexander et al. 2012; Marty 2012; Saal et al. 2013), but also in the origin of organic molecules (Deloule and Robert 1995; Deloule et al. 1998).

Bulk D/H ratios of meteorites give a relatively homogeneous composition with a mean δD-value of −100 ‰ (Robert et al. 2000). This relatively homogeneous composition masks the very heterogeneous distribution of individual components. Considerable efforts have been undertaken to analyze D/H ratios of the different compounds (Robert et al. 1978; Kolodny et al. 1980; Robert and Epstein 1982; Becker and Epstein 1982; Yang and Epstein 1984; Kerridge 1983; Kerridge et al. 1987; Halbout et al. 1990; Krishnamurthy et al. 1992). Eiler and Kitchen (2004) have evaluated the hydrogen isotope composition of water-rich carbonaceous chondrites by stepped-heating analysis of very small amounts of separated water-rich material. They observed a decrease in δD with increasing extent of aqueous alteration from 0 ‰ (least altered, most volatile rich) to −200 ‰ (most altered, least volatile rich).

Hydrogen in organic matter reveals a δD-variation from −500 to +6000 ‰ whereas water in silicates gives a variation from −400 to +3700 ‰ (Deloule and Robert 1995; Deloule et al. 1998). Two mechanisms have been proposed to account for the deuterium enrichment: (i) for organic molecules, high D/H ratios can be explained by ion molecule reactions that occur in interstellar space and (ii) for the phyllosilicates the enrichment can be produced via isotope exchange between water and hydrogen (Robert et al. 2000).

Alexander et al. (2010) reported even larger D-enrichment up to almost +12,000 ‰ in insoluble organic material. These authors suggested that such large enrichments may be produced in the meteorite parent body through the loss of isotopically very light H_2 generated through Fe oxidation by water at temperatures below 200 °C.

3.1.1.3 Carbon

Besides the bulk carbon isotopic composition, the various carbon phases occurring in carbonaceous chondrites (kerogen, carbonates, graphite, diamond, silicon carbide) have been individually analyzed. The $\delta^{13}C$–values of the total carbon fall into a narrow range, whereas $\delta^{13}C$–values for different carbon compounds in single meteorites show extremely different ^{13}C-contents. Figure 3.2 shows one such example, the Murray meteorite after Ming et al. (1989).

Of special interest are the minute grains of silicon carbide and graphite in primitive carbonaceous chondrites, which obviously carry the chemical signature of the pre–solar environment (Ott 1993). The SiC grains, present at a level of a few ppm, have a wide range in silicon and carbon isotope composition, with accompanying nitrogen also being isotopically highly variable. The $^{12}C/^{13}C$ ratio ranges from 2 to 2500, whereas it is 89 for the bulk Earth. According to Ott (1993), the SiC grains can be regarded as “star dust”, probably from carbon stars that existed long before our solar system. Amari et al. (1993) presented ion microprobe data of individual micrometer sized graphite grains in the Murchison meteorite, that also deviate from values typical for the solar system. These authors interpreted the isotope variability as indicating at least three different types of stellar sources.

The analysis of meteoritic organic matter may provide information about the origin of prebiotic organic matter in the early solar system. Carbonaceous chondrites contain organic carbon in solvent-insoluble form (about 70 %) and a mixture of solvent-soluble organic compounds (about 30 %). The organic carbon is substantially enriched in ^{13}C and ^{15}N, indicating that the material is not a terrestrial contaminant.

Two hypotheses have dominated the debate over formation mechanisms for the organic matter: I. formation by a Fischer-Tropsch type process (the synthesis of hydrocarbons from carbon monoxide and hydrogen) promoted by catalytic mineral grains and II. formation by Miller–Urey type reactions (the production of organic compounds by radiation or electric discharge) in an atmosphere in contact with an

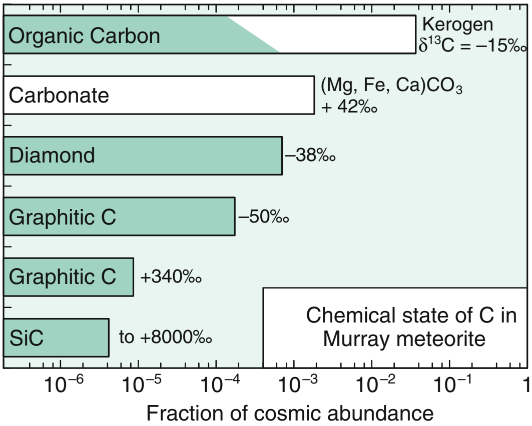

Fig. 3.2 Carbon compounds in primitive meteorites. Species classified as interstellar on the basis of C-isotopes are *coloured*. Only a minor fraction of organic carbon is interstellar (after Ming et al. 1989) (Fig. 3.2, 6th edition, p. 97)

aqueous phase. However, the isotopic variability exhibited by the volatile elements in different phases in carbonaceous chondrites is not readily compatible with abiotic syntheses. Either complex variants of these reactions must be invoked, or totally different types of reactions need to be considered. δ^{13}C-values reported for amino acids in the Murchison meteorite vary between +23 and +44 ‰ (Epstein et al. 1987). Engel et al. (1990) analyzed individual amino acids in the Murchison meteorite and also confirmed a strong ^{13}C enrichment. Of particular importance is the discovery of a distinct δ^{13}C difference between D- and L-alanine, which suggests that optically active forms of material were present in the early solar system.

Compound specific C- and D-isotope compositions of carboxylic acids, the most abundant class of soluble organic compounds in carbonaceous chondrites show a large range in δ^{13} C-values (from −31 to +32 ‰) and positive δD-values, that give evidence that these materials are not terrestrial contaminants (Huang et al. 2005).

In the insoluble macromolecular organic matter Alexander et al. (2007) observed very large variations within and between chondrite classes. These authors excluded Fischer-Tropsch type reactions being responsible for the large variations but instead argued that processes within parent bodies, such as different degrees of thermal alteration, may cause differences in δD-values.

3.1.1.4 Nitrogen

The extent and the origin of the nitrogen isotope composition in the solar system is unknown. Solar wind collected during the Genesis mission has a ^{15}N-content that is about 400 ‰ depleted relative to the terrestrial atmosphere (Marty et al. 2011). Thus, it can be expected that nitrogen should be isotopically heterogeneous in the solar system. What was considered by Kaplan (1975) to be a wide range of δ^{15}N values in meteorites has continuously expanded over the years (Kung and Clayton 1978; Robert and Epstein 1982; Lewis et al. 1983; Prombo and Clayton 1985; Grady and Pillinger 1990, 1993). In general, chondrites have whole rock nitrogen isotope values of 0 ± 50 ‰. However, some chondrites have δ-values up to 850 ‰ (Grady and Pillinger 1990). Nitrogen released during step-wise heating indicate two N-components: one at low temperatures has δ^{15}N-values between −20 and −40 ‰ and one at high temperatures has a δ^{15}N composition of +260 ‰ (Alexander et al. 1998). The large ^{15}N-enrichment in bulk meteorites relative to the protosolar gas requires the existence of especially enriched ^{15}N-compounds and cannot be explained by isotope fractionation processes in planetary environments.

3.1.1.5 Sulfur

There are many sulfur components in meteorites which may occur in all possible valence states (−2 to +6). Troilite is the most abundant sulfur compound of iron meteorites and has a relatively constant S-isotope composition (recall that troilite from the Canyon Diablo iron meteorite is the international sulfur standard). Carbonaceous chondrites contain sulfur in the form of sulfates, sulfides, elemental sulfur and complex organic sulfur-containing molecules. Monster et al. (1965), Kaplan and Hulston (1966) and Gao and Thiemens (1993a, b) separated the various sulfur components and demonstrated that sulfides are characterized by the highest δ^{34}S-values, whereas sulfates have the lowest δ^{34}S-values, just the opposite from what is generally observed in terrestrial samples. This is strong evidence against any microbiological activity and instead favors a kinetic isotope fractionation in a sulfur–water reaction (Monster et al. 1965). The largest internal isotope fractionation (7 ‰) is found in the Orgueil carbonaceous chondrite (Gao and Thiemens 1993a). Orgueil and Murchison have internal isotopic variations between different specimens, which may indicate that sulfur isotope heterogeneity existed in meteorite parent bodies.

Quadruple sulfur isotope measurements potentially may help in identifying genetic relationships between meteorites in a similar way to oxygen isotopes. Early measurements by Hulston and Thode (1965) and Kaplan and Hulston (1966), and those by Gao and Thiemens (1993a, b), did not indicate any nuclear isotope anomaly. However, more recent measurements by Rai et al. (2005) on achondrites and by Rai and Thiemens (2007) on chondrites did show the presence of mass independent sulfur isotope fractionations indicating photochemical reactions of gaseous sulfur species in the early solar nebula.

3.1.1.6 Metal Isotopes

Mass dependent metal isotope fractionations in meteorites may be due to (i) initial heterogeneities, (ii) fractionation processes during condensation and planetary accretion and (iii) differentiation processes after planet formation. Metal isotope studies of meteorites have been used to characterize the conditions of planetary accretion, including core formation and the loss of volatiles. Isotope variations in meteorites have been found for example for Fe (Weyer et al. 2005; Williams et al. 2006; Schoenberg and von Blanckenburg 2006), for Zn and for Cu (Luck et al. 2005; Moynier et al. 2007). Mass dependent Mg, Si and Fe isotope fractionations among different extraterrestrial objects may, in principle, result from loss of planetary material to space through vaporization or to loss to a planet's core.

Because of the high abundance and variable oxidation state, iron is the most studied metal element in the solar system. Differences in Fe isotope composition between chondrites, iron meteorites and terrestrial basalts may indicate isotope fractionations between metallic and ferrous Fe during segregation of planetary objects into a metallic core and a silicate mantle (Poitrasson et al. 2005; Weyer et al. 2005; Schoenberg and von Blanckenburg 2006; Williams et al. 2012; Craddock et al. 2013). Temperatures above 1000 °C necessary for core segregation were long considered too high to record any detectable isotope fractionation. Fe, Mg and Si isotope investigations have shown, however, that this is not the case (Georg et al. 2007; Weyer and Ionov 2007; Wiechert and Halliday 2007; Fitoussi et al. 2009; Ziegler et al. 2010). Whether core-mantle segregation fractionates Fe isotopes on Earth is a matter of debate. At temperatures between 1750 and 2000 °C, Poitrasson et al. (2009) observed no Fe isotope fractionation between Fe-Ni alloy and ultramafic melt (see also discussion on p. 211).

Of special interest are iron meteorites, generally used as analogues of planetary core formation. As shown by Williams et al. (2006) Fe isotope differences between metal and troilite in the range of 0.5 ‰—the metal phase being heavier than the sulfide phase troilite—may be interpreted as equilibrium fractionations. On the other hand, metal-sulfide fractionations for Cu isotopes are very variable, being one order of magnitude greater than for Fe isotopes and thus cannot represent equilibrium conditions (Williams and Archer 2011).

Calcium is a pure lithophile element which does not partition into planetary cores and is not affected by evaporation. Therefore, Ca isotopes may indicate genetic links between Earth and different classes of meteorites. Earth, Moon, Mars and differentiated asteroids are indistinguishable from primitive ordinary chondrites in Ca isotope composition (Simon and de Paolo 2010; Valdes et al. 2014). In contrast, enstatite chondrites are slightly enriched in heavy Ca isotopes, whereas carbonaceous chondrites are slightly depleted in heavy Ca isotopes, suggesting that ordinary chondrites can be regarded as Earth's building block.

Due to its high volatility, Zn isotopes may be used to explore variations in the impact history of planets. Large isotope variations (over 6 ‰) in δ^{66}Zn values have been explained by impact induced volatilization with preferential loss of the light isotopes in the gas phase (Moynier et al. 2007; Chen et al. 2013). In iron meteorites, δ^{66}Zn values are indistinguishable from the bulk silicate earth (Bridgestock et al. 2014). In the case of nickel, Ni isotope compositions have been measured for the search of extinct ^{60}Fe (Moynier et al. 2007; Steele et al. 2011).

Metal isotopes can be also used to investigate the formation of chondrules and calcium-aluminium inclusions (CAI). Chondrules have the same Mg and Si isotope composition as most other components of the solar system, but CAIs generally have higher Mg and Si isotope compositions. The systematic enrichment of heavy isotopes in CAIs has been interpreted as being due to evaporation of molten CAIs at low pressures (Shahar and Young 2007; Rumble et al. 2011). These authors argued that melting has occurred during a short interval of heating, perhaps as a result of shock waves. Why chondrules have not been fractionated during melting remains an open question.

Chondrules show a large variation in iron isotope compositions, whereas chondrites, samples from the Moon and Mars have nearly indistinguishable Fe isotope ratios (Craddock and Dauphas 2010).

3.1.2 The Moon

3.1.2.1 Oxygen

Since the early days of the Apollo missions it is well known that the oxygen isotope composition of the common lunar igneous minerals is very constant, with very little variation from one sampled locality to another (Onuma et al. 1970; Clayton et al. 1973b). Small ^{18}O differences between low-Ti and high Ti-basalts are obviously due to modal mineralogical differences (Spicuzza et al. 2007; Liu et al. 2010).

This constancy implies that the lunar interior should have a $\delta^{18}O$–value of about 5.5 ‰, essentially identical to terrestrial mantle rocks. The fractionations observed among coexisting minerals indicate temperatures of crystallization of about 1000 °C or higher, similar to values observed in terrestrial basalts (Onuma et al. 1970). By comparison with other terrestrial rocks, the range of observed $\delta^{18}O$–values is very narrow. For instance, terrestrial plagioclase exhibits an O-isotope variation which is at least ten times greater than that for all lunar rocks (Taylor 1968). This difference may be attributed to the much greater role of low–temperature processes in the evolution of the Earth's crust and to the high water contents on Earth.

Today, the Moon is generally viewed as the product of a collision between the early Earth and a Mars-sized protoplanet. Renewed interest in measuring the oxygen isotope composition of lunar basalts results from theoretical considerations that the moon forming material should mainly derive from the impacting body not from the proto-Earth. This means that even very small differences in ^{17}O and ^{18}O content between the impacting body and the Earth should leave a detectable difference in lunar rocks. However, precise ^{17}O and ^{18}O-isotope measurements by Wiechert et al. (2001), Liu et al. (2010) and Hallis et al. (2010) revealed no differences between the Earth and the Moon. Very recently, Herwarth et al. (2014) found a very small difference in $\Delta^{17}O$ between Earth and the Moon which supports the giant impact hypothesis of Moon formation. On the other hand, the Si and Fe isotope composition of the Earth's mantle and the Moon closely match indicating that the two bodies are very similar in Si and Fe isotope composition (Armytage et al. 2012; Liu et al. 2010).

3.1.2.2 Hydrogen

For years it was thought that the Moon is very dry and therefore very low in volatiles. Early studies of lunar samples (soils and breccia) reported variable H_2O concentrations and δD compositions, which were interpreted as hydrogen being implanted on the lunar surface due to the interaction with solar wind. Water extracted from basalts has been interpreted as being terrestrial water that has contaminated samples.

This picture has changed as recent progress in SIMS techniques has enabled measurement of very low OH concentrations in volcanic glass, olivine hosted melt inclusions and apatite. Hauri et al. (2011) demonstrated that some parts of the Moon contain as much water as the Earth's upper mantle. Greenwood et al. (2011) and Barnes et al. (2013) reported δD-values in apatite from +600 to +1100 ‰ and postulated that a significant portion of the water originated from comets. On the other hand, Saal et al. (2013) and Safarian et al. (2014) concluded that lunar water is indistinguishable from bulk water in carbonaceous chondrites and similar to terrestrial water implying a asteroidal origin for the Earth and the Moon.

By analysing chlorine isotopes, Sharp et al. (2010) observed a very large spread in $\delta^{37}Cl$ values in basalts and glasses, which they explained by volatilization of metal chlorides being stable only under very low hydrogen concentrations and implying an anhydrous lunar interior.

Enrichments of the heavy isotopes on the surfaces of the lunar fines are most probably due to the influence of the solar wind. Detailed interpretation of their isotopic variations is difficult due to both the lack of knowledge of the isotopic composition of the solar wind and uncertainties of the mechanisms for trapping. Kerridge (1983) demonstrated that nitrogen trapped in lunar surface rocks consists of at least two components differing in release characteristics during experimental heating and isotopic composition: the low-temperature component is consistent with solar wind nitrogen, whereas the high-temperature component consists of solar energetic particles.

3.1.3 Mars

In the late 1970s and early 1980s it was realized that differentiated meteorites referred to as the SNC (Shergottites, Nakhlites, Chassignites) group were samples from Mars (McSween et al. 1979; Bogard and Johnson 1983, besides others). This conclusion is based on young crystallization ages compared to that of other meteorites and compositions of trapped volatiles that match those of the martian atmosphere.

3.1.3.1 Oxygen

SNC-meteorites have an average δ^{18}O-value of 4.3 ‰, which is distinctly lower than the 5.5 ‰ value for the Earth–Moon system (Clayton and Mayeda 1996; Franchi et al. 1999). Small ^{18}O-variations among the different SNC-meteorites result primarily from different modal abundances of the major minerals. On a three-isotope plot the δ^{17}O offset between Mars and Earth is 0.3 ‰ (see Fig. 3.3). In this connection it is interesting to note that the so-called HED (howardites, eucrites and diogenites) meteorites, possibly reflecting material from the asteroid Vesta, have an oxygen isotope composition of 3.3 ‰ (Clayton and Mayeda 1996). The δ^{17}O-offset to the Earth is about −0.3 ‰ (Fig. 3.3). These differences in O-isotope composition among the terrestrial planets must reflect differences in the raw material from which the planets were formed.

3.1.3.2 Hydrogen

Volatiles, especially water, on Mars are of special relevance to reveal the geological and geochemical evolution of the planet. The hydrogen isotope composition of Mars can be estimated from two sources: (i) in situ measurements of the present day Martian atmosphere (Webster et al. 2013) and (ii) hydrogen containing compounds in Martian meteorites (Usui et al. 2012 and others). The D/H ratio of the atmosphere is enriched by a factor of 5 relative to terrestrial ocean water with a δD value of +4000 ‰. This enrichment is thought to result from preferential loss of H relative to D from the martian atmosphere over time (Owen et al. 1988). Ion microprobe

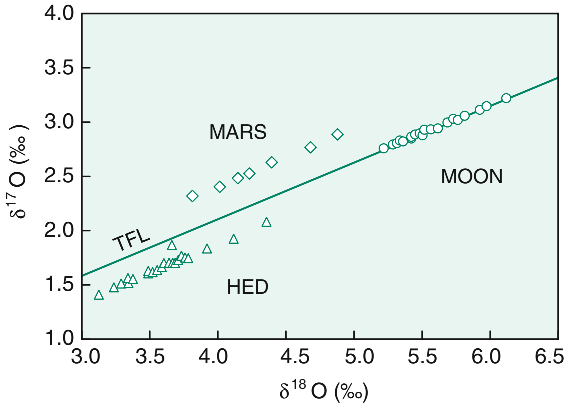

Fig. 3.3 Three oxygen isotope plot of lunar, Martian rocks and HED meteorites supposed to be fragments of asteroid Vesta (after Wiechert et al. 2001) (Fig. 3.3, 6th edition, p. 101)

studies of amphibole, biotite, and apatite in SNC meteorites by Watson et al. (1994) and stepwise heating studies by Leshin et al. (1996) reported large variations in δD-values. These authors observed that water in the samples originated from two sources: a terrestrial contaminant released largely at low temperatures and an extraterrestrial component at high temperatures showing extreme D-enrichments. Boctor et al. (2003) observed D-rich water in all minerals analyzed—including nominally anhydrous minerals—but also found low δD-values, consistent with a more Earth-like composition and concluded no single process can explain the large range in D/H ratios. Instead they suggested that the δD-values are affected by three reservoirs and mechanisms: a magmatic water component, devolatilization by impact melting and terrestrial contamination.

3.1.3.3 Carbon

As is the case for hydrogen, carbon isotope signatures in Martian meteorites present evidence for different carbon reservoirs. Wright et al. (1990) and Romanek et al. (1994) distinguished three carbon compounds: one component released at temperatures below ≈500 °C, mostly derived from terrestrial contamination, a second component, released between 400 and 700 °C in heating experiments or by reaction with acid, originates mostly from breakdown of carbonates and gives δ^{13}C-values up to +40 ‰ and the third component, released at temperatures above 700 °C, has δ^{13}C-values between −20 and −30 ‰ reflecting the isotope composition of magmatic carbon on Mars.

Carbonates in Martian meteorites have been especially well studied due to the hypothesis that they might indicate past life on Mars (McKay et al. 1996). Understanding the conditions of formation of the carbonates is thus crucial to the whole debate. Despite extensive chemical and mineralogical studies, the environment of carbonate formation has remained unclear. δ^{18}O-values of the carbonates are highly variable ranging from about 5–25 ‰ depending on different investigators and the carbonate investigated (Romanek et al. 1994; Valley et al. 1997; Leshin et al. 1998). In situ C isotope analysis by Niles et al. (2005) gave highly zoned

δ^{13}C-values from ≈+30 to +60 ‰ consistent with a derivation from the Martian atmosphere and suggesting abiotic formation.

Further evidence about a nonbiogenic origin of Martian carbonates have been presented by Farquhar et al. (1998) and Farquhar and Thiemens (2000). By measuring δ^{17}O and δ^{18}O-values Farquhar et al. (1998) observed an ^{17}O anomaly in carbonates relative to silicates which they interpreted as being produced by photochemical decomposition of ozone just as in the Earth's stratosphere.

McKay et al. (1996) furthermore suggested on the basis of morphology that tiny sulfide grains inside the carbonates may have formed by sulfate-reducing bacteria. δ^{34}S-values of sulfides range from 2.0 to 7.3 ‰ (Greenwood et al. 1997), which is similar to values from terrestrial basalts and probably not the result of bacterial reduction of sulfate.

The isotopic results are, therefore, not in favor of a microbiological activity on Mars, but the discussion will certainly continue on this exciting topic.

Finally, it should be mentioned that recent in situ isotope measurements of the Martian atmosphere from the Curiosity Rover indicate large enrichments in carbon and oxygen isotopes of CO_2, which might reflect substantial atmospheric loss (Webster et al. 2013; Mahaffy et al. 2013).

3.1.3.4 Sulfur

Mars seems to be rich in sulfur (King and McLennan 2009). Sulfur has been observed as primary igneous sulfides and most importantly as secondary sulfates near the surface of Mars. Mass-independent ^{33}S anomalies have been identified in both sulfides and sulfates (Farquhar et al. 2007; Franz et al. 2014), which obviously result from photochemical reactions in the Martian atmosphere favoring a surficial sulfur cycle for at least 3.5 billion years. Variations observed in Δ^{33}S, but the absence of Δ^{36}S anomalies implies MIF production by different pathways from those on Earth.

3.1.4 Venus

The mass spectrometer on the Pioneer mission in 1978 measured the atmospheric composition relative to CO_2, the dominant atmospheric constituent. The $^{13}C/^{12}C$ and $^{18}O/^{16}O$ ratios were observed to be close to the Earth value, whereas the $^{15}N/^{14}N$ ratio is within 20 % of that of the Earth (Hoffman et al. 1979). One of the major problems related to the origin and evolution of Venus is that of its "missing water". There is no liquid water on the surface of Venus today and the water vapor content in the atmosphere is probably not more than 220 ppm (Hoffman et al. 1979). This means that either Venus was formed from material very poor in water or whatever water was originally present has disappeared, possibly as the result of escape of hydrogen into space. And indeed Donahue et al. (1982) measured a

100-fold enrichment of deuterium relative to Earth, which is consistent with such an outgassing process. The magnitude of this process is, however, difficult to understand.

3.2 The Isotopic Composition of the Earth's Upper Mantle

Considerable geochemical and isotopic evidence has accumulated supporting the concept that many parts of the mantle have experienced a complex history of partial melting, melt emplacement, crystallization, recrystallization, deformation and metasomatism. A result of this complex history is that the mantle is chemically and isotopically heterogeneous with a complex pattern of depletion and fertilisation signatures. A major goal of isotope mantle geochemistry is the characterization of distinct mantle reservoirs and the processes for their evolution.

Heterogeneities in stable isotopes are difficult to detect, because stable isotope ratios are affected by various partial melting-crystal fractionation processes that are governed by temperature-dependent fractionation factors between residual crystals and partial melt and between cumulate crystals and residual liquid. Unlike radiogenic isotopes, stable isotopes are also fractionated by low temperature surface processes. Therefore, they offer a potentially important means by which recycled crustal material can be distinguished from intra-mantle fractionation processes.

O, H, C, S, and N isotope compositions of mantle derived rocks are substantially more variable than expected from the small fractionations at high temperatures. The most plausible process that may result in variable isotope ratios in the mantle is the input of subducted oceanic crust, and less frequent of continental crust, into some portions of the mantle. Because different parts of subducted slabs have different isotopic compositions, the released fluids may also differ in the O, H, C, N and S isotope composition. In this context, the process of mantle metasomatism is of special significance. Metasomatic fluids rich in Fe^{3+}, Ti, K, LREE, P and other LIL (Large Ion Lithophile) elements tend to react with peridotite mantle and form secondary micas, amphiboles and other accessory minerals. The origin of metasomatic fluids is likely to be either (i) exsolved fluids from an ascending magma or (ii) fluids or melts derived from subducted, hydrothermally altered crust and its overlying sediments.

With respect to the volatile behavior during partial melting, it should be noted that volatiles will be enriched in the melt and depleted in the parent material. During ascent of melts, volatiles will be degassed preferentially, and this degassing will be accompanied by isotopic fractionation (see discussion under "magmatic volatiles").

Sources of information about the isotopic composition of the upper portion of the lithospheric mantle come from the direct analysis of unaltered ultramafic xenoliths brought rapidly to the surface in explosive volcanic vents. Due to rapid transport, these peridotite nodules are in many cases chemically fresh and considered by most workers to be the best samples available from the mantle. The other primary source of information is from basalts, which represent partial melts of the mantle. The problem with basalts is that they do not necessarily represent the mantle composition because partial melting processes may have caused an isotopic fractionation relative to the precursor material. Partial melting of peridotites would result in the preferential melting of Ca–Al-rich minerals leaving behind refractory residues dominated by olivine and orthopyroxene which may differ slightly in the isotopic composition from the original materials. Also, basaltic melts may interact with the crustal lithosphere through which the magmas pass on their way to the Earth's surface. The following section will focus on ultramafic xenoliths, the isotopic characteristics of basalts is discussed under "magmatic rocks".

3.2.1 Oxygen

The δ^{18}O value of the bulk Earth is constrained by the composition of lunar basalts and bulk chondritic meteorites to be close to 6 ‰. Insight into the detailed oxygen isotope composition of the subcontinental lithospheric mantle has mostly come from the analysis of peridotitic xenoliths entrained in alkali basalts and kimberlites. The first oxygen isotope studies of such ultramafic nodules by Kyser et al. (1981, 1982) created much debate (e.g. Gregory and Taylor 1986; Kyser et al. 1986). The Kyser et al. data showed that clinopyroxene and orthopyroxene had similar and rather constant δ^{18}O-values around 5.5 ‰, whereas olivine exhibited a much broader variation with δ^{18}O-values extending from 4.5 to 7.2 ‰. Oxygen isotope fractionations between clinopyroxene and olivine ($\Delta_{\text{cpx-ol}}$) were suggested to vary from −1.4 to +1.2 ‰, implying that these phases are not in isotopic equilibrium at mantle temperatures. Gregory and Taylor (1986) suggested that the fractionations in the peridotite xenoliths analyzed by Kyser et al. (1981, 1982) arose through open-system exchange with fluids having variable oxygen isotope compositions and with olivine exchanging ^{18}O more rapidly than pyroxene.

It should be recognized, however, that olivine is a very refractory mineral and, as a result, quantitative reaction yields are generally not achieved, when analyzed by convential fluorination techniques. Mattey et al. (1994) analysed 76 samples of olivine in spinel-, garnet- and diamond-facies peridotites using laser fluorination techniques and observed an almost invariant O-isotope composition around 5.2 ‰. Assuming modal proportions of olivine, orthopyroxene and clinopyroxene of 50:40:10, the calculated bulk mantle δ^{18}O-value would be 5.5 ‰. Such a mantle source could generate liquids, depending on melting temperatures and degree of partial melting, with O-isotope ratios equivalent to those observed for MORB and many ocean island basalts.

Although the results of Mattey et al. (1994) have been confirmed by Chazot et al. (1997), it should be kept in mind that most of the mantle peridotites that have been analyzed for δ^{18}O originate from the continental lithospheric mantle and not from the mantle as a whole. More recently there have been several indications that the O-isotope composition of mantle xenoliths from certain exotic settings can be more variable than indicated by Mattey et al. (1994) and Chazot et al. (1997). Zhang et al. (2000) and Deines and Haggerty (2000) documented complex disequilibrium features among peridotitic minerals and intra-crystalline isotope zonations, which presumably result from metasomatic fluid/rock interactions.

Eclogite xenoliths from diamondiferous kimberlites constitute an important suite of xenoliths because they may represent the deepest samples of the continental lithospheric mantle. Eclogite xenoliths have the most diverse range in $\delta^{18}O$-values between 2.2 and 7.9 ‰ (McGregor and Manton 1986, Ongley et al. 1987). This large range of ^{18}O-variation indicates that the oxygen isotope composition of the continental lithosphere varies substantially, at least in any region where eclogite survives and is the most compelling evidence that some nodules represent metamorphic equivalents of hydrothermally altered oceanic crust.

3.2.2 Hydrogen

The origin of the water on Earth is a controversial topic with very different schools of thought. One view postulates that water was delivered to Earth from exogeneous sources such as comets and/or meteorites, the other holds that Earth's water has an indigeneous origin (Drake and Righter 2002). Delivery of water from comets and meteorites can be evaluated in the light of their D/H ratios, suggesting that comets cannot be the **major** source of water on Earth, but should be less than 10 % (Marty 2012). Estimates of the D/H ratio of the bulk Earth are uncertain, because volatiles derived from mantle-derived rocks may have been lost and fractionated during magma degassing.

In this connection the concept of "juvenile water" has to be introduced, which has influenced thinking in various fields of igneous petrology and ore genesis. Juvenile water is defined as water that originates from degassing of the mantle and that has never been part of the surficial hydrologic cycle. The analysis of OH-bearing minerals such as micas and amphiboles of deep-seated origin has been considered to be a source of information for juvenile water (e.g. Sheppard and Epstein 1970). Because knowledge about fractionation factors is limited and temperatures of final isotope equilibration between the minerals and water not known, calculations of the H-isotope composition of water in equilibrium with the mantle is rather crude.

Figure 3.4 gives δD-data on phlogopites and amphiboles, indicating that the hydrogen isotope composition of mantle water should lie in general between −80 and −50 ‰, the range first proposed by Sheppard and Epstein (1970) and subsequently supported by several other authors. Also shown in Fig. 3.4 are a considerable number of phlogopites and amphiboles which have δD-values higher than −50 ‰. Such elevated δD-values may indicate that water from subducted oceanic crust has played a role in the genesis of these minerals. Similar conclusions have been reached as a result of the analysis of water of submarine basalts from the

Fig. 3.4 Hydrogen isotope variations in mantle-derived minerals and rocks (modified after Bell and Ihinger 2000) (Fig. 3.4, 6th edition, p. 106)

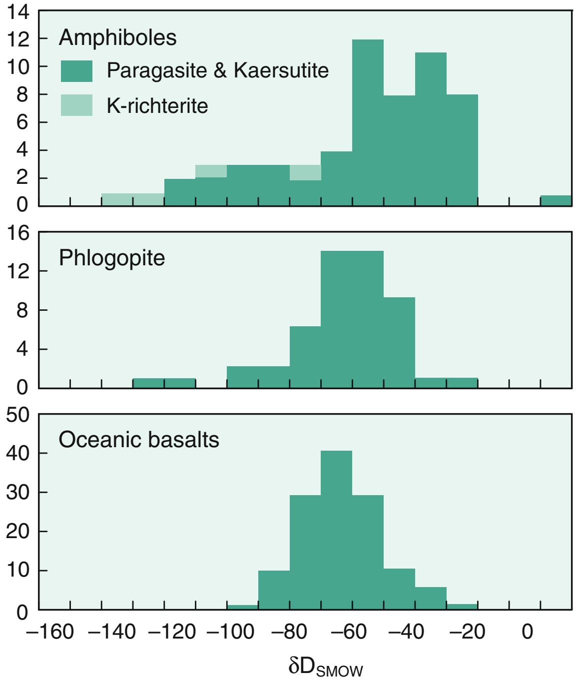

Mariana arc (Poreda 1985) and from estimates of the original δD-values in boninites from Bonin Island (Dobson and O'Neil 1987).

Water in the mantle is found in different states: as a fluid especially near subduction zones, as a hydrous phase and as a hydroxyl point defect in nominally anhydrous minerals. δD-values between −90 and −110 ‰ have been obtained by Bell and Ihinger (2000) analyzing nominally anhydrous mantle minerals (garnet, pyroxene) containing trace quantities of OH. Nominally anhydrous minerals from mantle xenoliths are the most D-depleted of all mantle materials with δD-values 50 ‰ lower than MORB (O'Leary et al. 2005). This difference may either imply that these minerals represent an isotopically distinct mantle reservoir or that the samples analyzed have exchanged hydrogen during or after their ascent from the mantle (meteoric-water interaction?).

Water is carried into the mantle at subduction zones. The average δD-composition of the oceanic crust is estimated to be −50 ‰ (Agrinier et al. 1995; Shaw et al. 2008). Experimentally determined fractionation factors between water and hydrous minerals indicate that the fluids released from the slab during its subduction path are D-rich. Analyzing olivine-hosted melt inclusions from a subduction zone-setting, Shaw et al. (2008) determined δD-values from −55 to −12 ‰. Continuous losses of D-enriched fluids leads to a depletion in remaining water containing phases Thus, slab-bound water will evolve to progressively lower D-values as D-enriched waters is released to the mantle wedge. This might explain the exceptionally low δD-values that have been found in mantle xenoliths (Deloule et al. 1991).

3.2.3 Carbon

The presence of carbon in the upper mantle has been well documented through several observations: CO_2 is a significant constituent in volcanic gases associated with basaltic eruptions with the dominant flux at mid-ocean ridges. The eruption of carbonatite and kimberlite rocks further testifies to the storage of CO_2 in the upper mantle. Additionally, the presence of diamond and graphite in kimberlites, peridotite and eclogite xenoliths reflects a wide range of mantle redox conditions, suggesting that carbon is related to a number of different processes in the mantle.

The isotopic composition of mantle carbon varies by more than 30 ‰ (see Fig. 3.5). To what extent this wide range is a result of mantle fractionation processes, the relict of accretional heterogeneities, or a product of recycling of crustal carbon is still unanswered. In 1953, Craig noted that diamonds exhibited a range of $\delta^{13}C$-values which clustered around −5 ‰. Subsequent investigations which included carbonatites (e.g. Deines 1989) and kimberlites (e.g. Deines and Gold 1973) indicated similar $\delta^{13}C$-values, which led to the concept that mantle carbon is relatively constant in C-isotopic composition, with $\delta^{13}C$-values between −7 and −5 ‰. During the formation of a carbonatite magma, carbon is concentrated in the melt and is almost quantitatively extracted from its source reservoir. Since the carbon content of the mantle is low, the high carbon concentration of carbonatite melts requires extraction over volumes up to 10,000 times higher than the volume

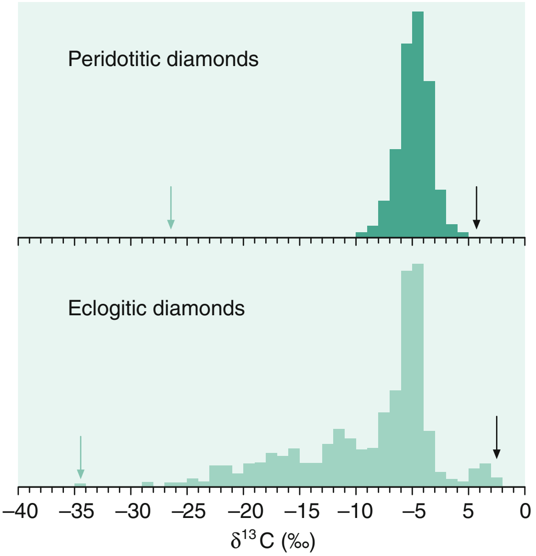

Fig. 3.5 Carbon isotope variations of diamonds (*arrows* indicate highest and lowest $\delta^{13}C$-values (modified after Cartigny 2005) (Fig. 3.5, 6th edition, p. 108)

of a carbonatite magma (Deines 1989). Thus, the mean δ^{13}C-value of a carbonatite magma should represent the average carbon isotope composition of a relatively large volume of the mantle.

The C-isotope distribution of diamonds is in contrast to that for carbonatites. As more and more data for diamonds became available (at present more than 4000 C-isotope data) (Deines et al. 1984; Galimov 1985b; Cartigny 2005; Cartigny et al. 2014), the range of C-isotope variation broadened to more than 40 ‰. (from −41 to +5 ‰ (Galimov 1991; Kirkley et al. 1991; Cartigny 2005; Stachel et al. 2009; Shirey et al. 2013). More than 70 % of the data vary in the narrower range from −8 to −2 ‰ with a mean of −5 ‰, being similar to the range of carbon in other mantle derived rocks. The large ^{13}C variability is not random but restricted to certain genetic classes: Common "peridotitic diamonds" (diamonds associated with peridotitic xenoliths) have less variable carbon isotope compositions than "eclogitic diamonds", which span the entire range of ^{13}C/^{12}C variations (see Fig. 3.5; Cartigny 2005). Diamond formed in metamorphic rocks subducted to ultrahigh pressures have δ^{13}C-values from −30 to −3 ‰, whereas carbonados, a unique type of polycrystalline diamond (Cartigny 2010) have C-isotope values around −25 ‰. Current debate centers on whether the more extreme values are characteristic of the mantle source regions or whether they have resulted from isotope fractionation processes linked to diamond formation. What appears to be obvious: the observed ranges cannot be assigned to a single process or to variations in the carbon source alone (Stachel et al. 2009). A combination of processes and multiple carbon sources are required.

Spatially resolved analyses of individual diamonds by SIMS measurements first described by Harte and Otter (1992) and later by others have been summarized by Hauri et al. (2002). The latter authors have shown δ^{13}C variations of about 10 ‰ and more than 20 ‰ in δ^{15}N which are associated with cathodoluminescence-imaged growth zones. Although the origin of these large variations is still unclear, they point to complex growth histories of diamonds.

3.2.4 Nitrogen

A large fraction of Earth's total nitrogen resides in the mantle, either being primordial or being recycled crustal nitrogen. In silicates nitrogen as NH_4^+ replaces K^+, in melts and fluids nitrogen speciation depends on redox conditions. Nitrogen trapped in MORB and OIB glasses has been analyzed by Marty and Humbert (1997) and Marty and Zimmermann (1999) (see Fig. 3.6). By analysing separate minerals in peridotite xenoliths Yokochi et al. (2009) observed large N-isotope disequilibria. δ^{15}N-values as low as −17.3 ‰ have been measured for phlogopite, whereas clinopyroxene and olivine show positive ^{15}N values. Positive δ-values of about +3 ‰ have been found also in deep mantle material sampled by mantle plumes which may suggest that recycling of oceanic crust may account for heavy nitrogen in the deep mantle (Dauphas and Marty 1999).

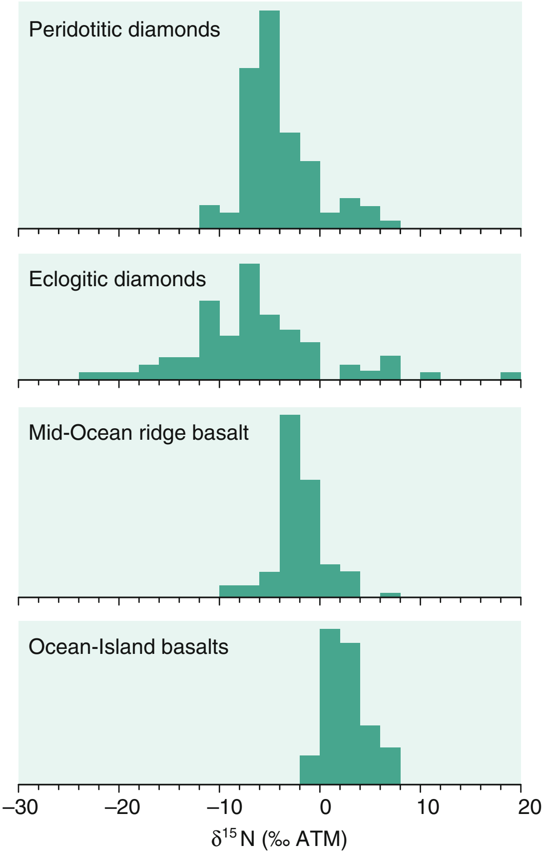

Fig. 3.6 Nitrogen isotope variations in mantle derived materials (modified after Marty and Zimmermann 1999) (Fig. 3.6, 6th edition, p. 109)

Nitrogen is the main trace component in diamonds. Nitrogen isotopes have been measured in over 700 diamond samples with δ^{15}N-values ranging from +13 to −23 ‰. Despite this broad distribution, the majority varies around −5 ‰ (Javoy et al. 1986; Boyd et al. 1992; Boyd and Pillinger 1994; Hauri et al. 2002; Cartigny 2005; Cartigny et al. 1997, 1998, 2014). Nitrogen in diamonds, thus, is depleted in ^{15}N compared to atmospheric nitrogen (0 ‰) and sedimentary nitrogen which is enriched in ^{15}N (Cartigny and Marty 2013). The negative δ-values in diamonds clearly indicate that the mantle contains non-atmospheric nitrogen.

3.2.5 Sulfur

Sulfur occurs in a variety of forms in the mantle, the major sulfur phase is monosulfide solid solution between Fe, Ni and Cu. Ion microprobe measurements on sulfide inclusions from megacrysts and pyroxenite xenoliths from alkali basalts

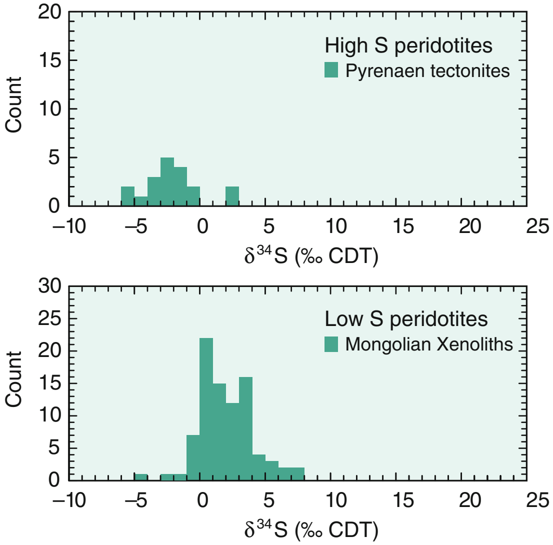

Fig. 3.7 Sulfur isotope compositions of high- and low-S peridotites (Fig. 3.7, 6th edition, p. 110)

and kimberlites and in diamonds gave δ^{34}S-values from −11 to +14 ‰ (Chaussidon et al. 1987, 1989; Eldridge et al. 1991).

Interesting differences in sulfur isotope compositions are observed when comparing high-S peridotitic tectonites with low-S peridotite xenoliths (Fig. 3.7). Tectonites from the Pyrenees predominantly have negative δ^{34}S-values of around −5 ‰, whereas low-S xenoliths from Mongolia have largely positive δ^{34}S-values of up to +7 ‰. Ionov et al. (1992) determined sulfur contents and isotopic compositions in some 90 garnet and spinel lherzolites from six regions in southern Siberia and Mongolia for which the range of δ^{34}S values is from −7 to +7 ‰. Ionov et al. (1992) concluded that low sulfur concentrations (<50 ppm) and largely positive δ^{34}S-values predominate in the lithospheric continental mantle worldwide.

Sulfur isotope variations within diamonds exhibit the same characteristics as previously described for carbon: i.e. eclogitic diamonds are much more variable than peridotitic diamonds. Furthermore, mass independent sulfur isotope fractionations have been preserved in some sulfide inclusions in eclogitic diamonds (Farquhar et al. 2002; Thomassot et al. 2009), implying that sulfide inclusions contain an Archean sedimentary component.

3.2.6 Lithium and Boron

Since lithium and boron isotope fractionations mainly occur during low temperature processes, Li and B isotopes may provide a robust tracer of surface material that is recycled to the mantle (Elliott et al. 2004). Heterogeneous distribution of subducted oceanic and continental crust in the mantle will thus result in variations in Li and B isotope ratios. Furthermore dehydration processes active in subduction zones appear to be of crucial importance in the control of Li and B isotope composition of different parts of the mantle. For the upper mantle as a whole, Jeffcoate et al. (2007) gave an average δ^7Li value of 3.5 ‰.

Seitz et al. (2004), Magna et al. (2006) and Jeffcoate et al. (2007) reported significant Li isotope fractionation among mantle minerals. Olivines are about 1.5 ‰ lighter than coexisting orthopyroxenes, clinopyroxenes and phlogopites are in contrast highly variable, which might indicate isotope disequilibrium. In situ SIMS analyses show Li isotope zonations in peridotite minerals. Jeffcoate et al. (2007) report a 40 ‰ variation in a single orthopyroxene crystal from San Carlos, which is attributed to diffusive fractionation during ascent and cooling.

Since boron concentrations in mantle minerals are exceedingly low, boron isotope analysis of mantle minerals are very restricted. On the basis of a boron budget between mantle and crust, Chaussidon and Marty (1995) concluded that the primitive mantle had a δ^{11}B value of −10 ± 2 ‰. For MORB Spivack and Edmond (1987) and Chaussidon and Marty (1995) reported a δ^{11}B-value of around—4 ‰. Higher and lower δ^{11}B-values observed in some ocean island basalts should be due to crustal assimilation (Tanaka and Nakamura 2005).

3.2.7 Stable Isotope Composition of the Core

Although the composition of the core remains largely unknown, cosmochemical and geophysical arguments indicate that the core must contain lighter elements other than Fe and Ni. One plausible candidate is silicon, because liquid iron reacts with silicate to form a iron-silicon alloy at the relevant pT conditions of the core. Because of the different bonding environments of the two phases, silicon in silicate should be enriched in ^{28}Si relative to the alloy phase (Schauble 2004; Georg et al. 2007). As shown experimentally by Shahar et al. (2009, 2011), at temperatures between 1800 and 2200 °C, silicates are distinctly enriched in ^{28}Si relative to metal. At the even higher temperatures of the core, a 1.2 ‰ depletion of the metal phase in the core relative to silicates in the mantle can be anticipated. Somewhat smaller Si isotope fractionations have been determined by Hin et al. (2014).

With respect to iron isotopes, an enrichment of the heavy Fe isotopes in the metal phase relative to Fe-oxides should be expected (Young et al. 2015). Experiments on the iron isotope distribution between metal and silicates have yielded, however, no iron isotope fractionation between the two phases (Poitrasson et al. 2009; Hin et al. 2012). To better simulate natural conditions, Shahar et al. (2014) added sulfur to their experimental runs and indeed observed a 0.4 ‰ fractionation between metal and Fe-oxides. More experimental studies are needed to solve this inconsistency.

3.2.8 Magmatic Rocks

On the basis of their high temperature of formation, it could be expected that magmatic rocks exhibit relatively small differences in isotopic composition. However, as a result of secondary alteration processes and the fact, that magmas can have a crustal and a mantle origin, the variation observed in isotopic composition of magmatic rocks can actually be quite large.

Provided an igneous rock has not been affected by subsolidus isotope exchange or hydrothermal alteration, its isotope composition will be determined by:

(i) the isotope composition of the source region in which the magma was generated,
(ii) the temperature of magma generation and crystallization,
(iii) the mineralogical composition of the rock, and
(iv) the evolutionary history of the magma including processes of isotope exchange, assimilation of country rocks, magma mixing, etc.

In the following sections, which concentrate on $^{18}O/^{16}O$ measurements, some of these points are discussed in more detail (see also Taylor 1968; 1986a, b; Taylor and Sheppard 1986). Isotope variations of metal isotopes reported for magmatic rocks are discussed briefly in Chap. 2 under the specific elements.

3.2.9 Fractional Crystallization

Because fractionation factors between melt and solid are small at magmatic temperatures, fractional crystallization is expected to play only a minor role in influencing the oxygen isotopic composition of magmatic rocks. Matsuhisa (1979), for example, reported that $\delta^{18}O$ values increased by approximately 1 ‰ from basalt to dacite within a lava sequence from Japan. Muehlenbachs and Byerly (1982) analyzed an extremely differentiated suite of volcanic rocks at the Galapagos spreading center and showed that 90 % fractionation only enriched the residual melt by about 1.2 ‰. On Ascension Island Sheppard and Harris (1985) measured a difference of nearly 1 ‰ in a volcanic suite ranging from basalt to obsidian. Furthermore, modelling closed-system crystal fractionation, an ^{18}O enrichment of about 0.4 ‰ per 10 wt% increase in SiO_2 content can be predicted.

3.2.10 Differences Between Volcanic and Plutonic Rocks

Systematic differences in O-isotope composition are observed between fine-grained, rapidly quenched volcanic rocks and their coarse-grained plutonic equivalents (Taylor 1968; Anderson et al. 1971). Fractionations among minerals in plutonic mafic rocks are on average about twice as great as for the corresponding fractionations observed in equivalent extrusive mafic rocks. This difference may result from retrograde exchange between minerals or post-crystallization exchange reactions of the plutonic rocks with a fluid phase. This interpretation is supported by the fact that basaltic and gabbroic rocks from the lunar surface yield the same "isotopic temperatures" corresponding to their initial temperatures of crystallization. Due to the low water concentration on the Moon, retrograde exchange is very limited.

3.2.11 Low Temperature Alteration Processes

Because of their high glass contents and very fine grain size, volcanic rocks are very susceptible to low-temperature processes such as hydration and weathering, which are characterized by large ^{18}O-enrichment effects in the altered rocks.

In general, it is probable that Tertiary and older volcanic rocks will exhibit O-isotope compositions that have been modified to higher $^{18}O/^{16}O$ ratios from their primary state (Taylor 1968; Muehlenbachs and Clayton 1972; Cerling et al. 1985; Harmon et al. 1987). Although there is no way to ascertain the magnitude of these ^{18}O-enrichments on a sample by sample basis, a crude estimate can be made by determining the water (and carbon dioxide) content and "correcting" to what are considered primary values of the suite of rocks to be analyzed (Taylor et al. 1984; Harmon et al. 1987). The primary water content of a magma is difficult to estimate, however, but it is generally accepted that primary basaltic magmas should not contain more than 1 wt % water. Thus, any water content >1 % could be of secondary origin and the δ^{18}O-value for such samples should be corrected before such ^{18}O-measurements are to be used for primary, magmatic interpretations.

3.2.12 Assimilation of Crustal Rocks

Because the various surface and crustal environments are characterized by different and distinctive isotope compositions, stable isotopes provide a powerful tool for discriminating between the relative role of mantle and crust in magma genesis. This is especially true when stable isotopes are considered together with radiogenic isotopes, because variations within these independent isotopic systems may arise from unrelated geologic causes. For instance, a mantle melt that has been affected by contamination processes within the upper crust will exhibit increases in $^{18}O/^{16}O$ and $^{87}Sr/^{86}Sr$ ratios that correlate with an increase in SiO_2 and decrease in Sr content. In contrast, a mantle melt, which evolves only through differentiation unaccompanied by interaction with crustal material, will have an O-isotope composition that mainly reflects that of its source region, independent of variations in chemical composition. In this latter case, correlated stable and radiogenic isotope variations would be an indication of variable crustal contamination of the source region, (i.e. crustal material that has been recycled into the mantle via subduction).

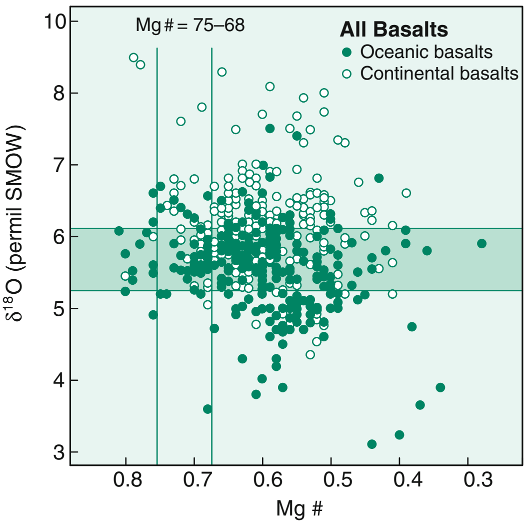

Fig. 3.8 Plot of δ^{18}O-values vs Mg numbers for oceanic basalts (*filled circles*) and continental basalts (*open circles*). The *shaded field* denotes the ±2 σ range of a MORB mean value of +5.7 ‰. the *clear vertical field* denotes the range for primary basaltic partial melts in equilibrium with a peridotitic source (Harmon and Hoefs 1995) (Fig. 3.8, 6th edition, p. 114)

Modelling by Taylor (1980) and James (1981) has demonstrated that it is possible to distinguish between the effects of source contamination as well as crustal contamination. Magma mixing and source contamination are two-component mixing processes which obey two-component hyperbolic mixing relations, whereas crustal contamination is a three-component mixing process, involving the magma, the crustal contaminant, and the cumulates, that results in more complex mixing trajectories on an oxygen—radiogenic isotope plot. Finally, it has to be mentioned, that in contrast to the radiogenic isotopes, oxygen is the major component in rocks, implying that modification of the δ^{18}O-value by several tenths of 1 ‰ requires uptake of volumetrically significant sediment masses, that may cause a space problem.

3.2.13 Glasses from Different Tectonic Settings

3.2.13.1 Oxygen

Early investigations of oxygen isotopes in igneous rocks relied on whole rock data analyzed by the classical reaction with fluorine compounds. Relatively large oxygen isotope variations can be due to secondary alteration effects. Correcting for these low-temperature effects, Harmon and Hoefs (1995) assembled a database consisting of 2855 O-isotope analyses of Neogene volcanic rocks worldwide. They observed a 5 ‰ variation in the δ^{18}O-values of fresh basalts and glasses, which they have taken as evidence of significant oxygen isotope heterogeneities in the mantle sources of the basalts. This is documented in Fig. 3.8, which plots δ^{18}O-values versus Mg-numbers (Harmon and Hoefs 1995).

The usage of whole rock data has, however, its ambiguities. Estimates of original magmatic δ^{18}O values are best achieved through analysis of unaltered phenocrysts within rocks in particular refractory phenocrysts such as olivine and zircon. Laser-based extraction methods on small amounts of separated mineral phases have documented subtle, but resolvable differences among different types of basaltic lavas (Eiler et al. 1996, 2000, 2011; Dorendorf et al. 2000; Cooper et al. 2004; Bindeman et al. 2004, 2005, 2008 and others).

MORB has a rather uniform O-isotope composition of all basalt types (5.5 ± 0.2 ‰) and can be used as a reference against which basalts erupted in other tectonic settings can be compared. By performing high precision laser isotope analyses on MORB glasses from the North Atlantic, Cooper et al. (2004) observed a δ^{18}O variation range of about 0.5 ‰, which is larger than originally thought by Harmon and Hoefs (1995). ^{18}O variations correlate with geochemical parameters of mantle enrichment such as high ^{87}Sr/^{86}Sr and low ^{143}Nd/^{144}Nd ratios. According to Cooper et al. (2004) the enriched material reflects subducted altered dehydrated oceanic crust.

The largest variability in oxygen isotope composition has been found in subduction related basalts. Bindeman et al. (2005) observed a δ^{18}O range in olivine phenocrysts between 4.9 to 6.8 ‰. Oxygen isotope variations in arc-related lavas can constrain the contributions of subducted sediments and fluids to the sub-arc mantle assuming the δ^{18}O of the subducted component is known (Eiler et al. 2000; Dorendorf et al. 2000). These authors demonstrated that crustal assimilation or a contribution of oceanic sediments is negligible (<1–2 %). Instead, the observed ^{18}O-enrichment in olivines and clinopyroxenes may result from exchange with high ^{18}O fluids derived from subducted altered oceanic crust.

Continental basalts tend to be enriched in ^{18}O relative to oceanic basalts and exhibit considerably more variability in O-isotope composition, a feature attributed to interaction with ^{18}O-enriched continental crust during magma ascent (Harmon and Hoefs 1995; Baker et al. 2000).

3.2.13.2 Hydrogen

Water dissolves in silicate melts and glasses in at least two distinct forms: water molecules and hydroxyl groups. Because the proportions of these two species change with total water content, temperature and chemical composition of the melt, the bulk partitioning of hydrogen isotopes between vapor and melt is a complex function of these variables. Dobson et al. (1989) determined the fractionation between water vapor and water dissolved in felsic glasses in the temperature range from 530 to 850 °C. Under these conditions, the total dissolved water content of the glasses were below 0.2 %, with all water present as hydroxyl groups. The measured hydrogen fractionation factors vary from 1.051 to 1.035 and are greater than those observed for most hydrous mineral—water systems, perhaps reflecting the strong hydrogen bonding of hydroxyl groups in glasses.

Hydrogen isotope and water content data for MORB, OIB and BAB glasses have been determined by Kyser and O'Neil (1984), Poreda (1985), and Poreda et al. (1986). The range of δD-values for MORB glasses is from −90 to −40 ‰ and is indistinguishable from that reported for phlogopites and amphiboles from kimberlites and peridotites (see Fig. 3.4). Kyser and O'Neil (1984) demonstrated that D/H ratios and water content in fresh submarine basalt glasses can be altered by (i) degassing, (ii) addition of seawater at magmatic temperature and (iii) low-temperature hydration. Extrapolations to possible unaltered D/H-ratios indicate that primary δD-values for most basalts are −80 ± 5 ‰.

Shaw et al. (2008) measured the hydrogen isotope composition of melt inclusions hosted in olivine crystals from the Mariana arc which should be little affected by degassing processes. δD-values range from −55 to −12 ‰, significantly heavier than MORB values and indicating enriched fluids in D released from the subducted plate.

The process of degassing has been documented best for rhyolitic magmas where water-rich magmas (about 2 %) have a δD-value of −50 ‰. At very late eruption stages with remaining water contents of around 0.1 % the δD-value is around −120 ‰ (Taylor et al. 1983; Taylor 1986a, b). For this process the decisive parameter is the isotopic fractionation between the vapor and the melt, which can be between 15 and 35 ‰ (Taylor 1986a, b) and the amount of water lost from the system (Rayleigh fractionation). The degassing process produces an opposite trend to a meteoric water hydrothermal alteration, showing decreasing δD-values with increasing water content. De Hoog et al. (2009) modeled hydrogen isotope fractionation during degassing taking the variation of water species with water content and temperature into account. Progressively increasing OH/H_2O ratios during degassing in melts lead to increasing H fractionation factors.

3.2.13.3 Carbon

Isotopic fractionation between CO_2 and dissolved carbon in melts has been estimated by various authors to vary between 2 and 4 ‰ (as summarized by Holloway and Blank 1994), the vapor being enriched in ^{13}C relative to the melt. This fractionation can be used to interpret the carbon isotope composition of glasses and CO_2 in volcanic gases and to estimate the initial carbon concentration of undegassed basaltic melts.

Reported $\delta^{13}C$-values for basaltic glass vary from −30 to about −3 ‰ that represent isotopically distinct carbon extracted at different temperatures by stepwise heating (Pineau et al. 1976; Pineau and Javoy 1983; Des Marais and Moore 1984; Mattey et al. 1984). A "low-temperature" component of carbon is extractable below 600 °C, whereas a "high-temperature" fraction of carbon is liberated above 600 °C. There are two different interpretations regarding the origins of these two different types of carbon. While Pineau et al. (1976) and Pineau and Javoy (1983) consider that the whole range of carbon isotope variation observed to represent primary dissolved carbon, which becomes increasingly ^{13}C depleted during multi-stage degassing of CO_2, Des Marais and Moore (1984) and Mattey et al. (1984) suggest that the "low-temperature" carbon originates from surface contamination. For MORB glasses, the "high-temperature" carbon has an isotopic composition typical for that of mantle values. Island arc glasses have lower $\delta^{13}C$-values, which might be explained by mixing two different carbon compounds in the source regions: a MORB—like carbon and an organic carbon component from subducted pelagic sediments (Mattey et al. 1984).

3.2.13.4 Nitrogen

The determination of nitrogen isotopes in basaltic glasses is severely complicated by its low concentration, which makes nitrogen sensitive to atmospheric contamination and to addition of surface-derived materials i.e. organic matter. Nitrogen in basaltic glasses has been determined by Exley et al. (1987), Marty and Humbert (1997) and Marty and Zimmermann (1999). Marty and coworkers reported that nitrogen in MORB and OIB glasses has an average $\delta^{15}N$-value of around -4 ± 1 ‰ (see Fig. 3.6). The major factors affecting its isotopic composition appear to be magma degassing and assimilation of surface-derived matter.

3.2.13.5 Sulfur

The behavior of sulfur in magmatic systems is particularly complex: sulfur can exist as both sulfate and sulfide species in four different forms: dissolved in the melt, as an immiscible sulfide melt, in a separate gas phase, and in various sulfide and sulfate minerals. To determine the source of sulfur in magmatic rocks requires knowledge of complex parameters such as oxygen fugacity, speciation of dissolved sulfur in melt and what is most important the degassing history. Mandeville et al. (2009) have demonstrated that magmatic degassing can modify the initial sulfur isotope composition by up to 14 ‰ On the other hand de Moor et al. (2010) demonstrated that degassing of a magma body resulted in a slight ^{34}S enrichment only.

Early measurements on MORB glasses and submarine Hawaiian basalts indicated a very narrow range in sulfur isotope composition, with $\delta^{34}S$-values clustering around zero (Sakai et al. 1982, 1984). More recent measurements by Labidi et al. (2012) showed that published MORB data are affected by incomplete sulfur recovery during analytical extraction. Labidi et al. (2012, 2014) argued that the sulfur isotope composition of the depleted mantle is more negative than previously thought and has a $\delta^{34}S$-values of -1.4 ‰. Negative $\delta^{34}S$-values for the mantle could result from a low-^{34}S oceanic crust recycled within the MORB mantle source (Cabral et al. 2013) or from sulfur isotope fractionation during core-mantle segregation leading to a ^{34}S enriched core and a ^{34}S depleted mantle (Labidi et al. 2013). The discovery of mass-independent sulfur isotope fractionations in young ocean island basalts indicates that Archean oceanic crust may survive in the mantle (Cabral et al. 2013).

In subaerial basalts, the variation of δ^{34}S-values is larger and generally shifted towards positive values. One reason for this larger variation is the loss of a sulfur-bearing phase during magmatic degassing. Isotopic shifts that accompany degassing depend on temperature and speciation, the latter is directly proportional to the fugacity of oxygen (Sakai et al. 1982) and on open-system conditions (immediate removal from the magma) or closed-system conditions (vapor exsolved remains in equilibrium with the magma) (Taylor 1986a, b).

3.2.13.6 Ocean Water/Basaltic Crust Interactions

Information about the O-isotope character of the oceanic crust comes from DSDP/ODP drilling sites and from studies of ophiolite complexes, which presumably represent pieces of ancient oceanic crust. Primary, unaltered oceanic crust has δ^{18}O-values close to MORB (δ^{18}O: 5.7 ‰). Two types of alteration can be distinguished within the oceanic lithosphere: at low temperatures weathering may markedly enrich the groundmass of basalts in ^{18}O, but not affect phenocrysts. The extent of this low temperature alteration correlates with the water content: the higher the water content, the higher the δ^{18}O-values (e.g. Alt et al. 1986). At temperatures in excess of about 300 °C hydrothermal circulation beneath the midocean ridges leads to a high-temperature water/rock interaction in which deeper parts of the oceanic crust become depleted in ^{18}O by 1–2 ‰. Similar findings have been reported from ophiolite complexes, the most cited example is that of Oman (Gregory and Taylor 1981). Maximum ^{18}O contents occur in the uppermost part of the pillow lava sequence and decrease through the sheeted dike complex. Below the base of the dike complex down to the Moho, δ^{18}O-values are lower than typical mantle values by about 1–2 ‰.

Thus, separate levels of the oceanic crust are simultaneously enriched and depleted in ^{18}O relative to “normal” mantle values because of reaction with sea water at different temperatures. Muehlenbachs and Clayton (1976) and Gregory and Taylor (1981) concluded that the ^{18}O enrichments are balanced by the ^{18}O depletions which acts like a buffer for the oxygen isotope composition of ocean water.

Gao et al. (2006) evaluated the existing data base and concluded that apparent differences in mass-weighed δ^{18}O-values exist among profiles through the recent and the fossil oceanic crust depending on differences in spreading rates. Oceanic crust formed under fast spreading ridges usually have depleted or balanced δ^{18}O-values, whereas oceanic crust formed under slow spreading ridges is characterized by enriched δ^{18}O-values. This difference might be due to different depths of seawater penetration in fast and slow spreading ridges.

Of special significance in the oceanic crust are serpentinites that are formed by the hydration of olivine-rich ultramafic rocks, because they play an important role in the recycling of water and other volatiles from the surface to the deep lithosphere and back to the surface via mantle wedges and arc magmas (Evans et al. 2013). Serpentinization, thus, may take place over a range of temperatures and in a variety of geologic settings. Experimentally determined H isotope fractionation factors (Saccocia et al. 2009) allow to constrain fluid sources. Serpentine from mid-ocean ridge environments, for instance, has been formed by interaction with hot ocean water.

3.2.14 Granitic Rocks

On the basis of $^{18}O/^{16}O$ ratios, Taylor (1977, 1978) subdivided granitic rocks into three groups: (i) normal ^{18}O-granitic rocks with $\delta^{18}O$-values between 6 and 10 ‰, (ii) high ^{18}O granitic rocks with $\delta^{18}O$-values >10 ‰ and (iii) low ^{18}O granitic rocks with $\delta^{18}O$-values <6 ‰. Although this is a somewhat arbitrary grouping it nevertheless turns out to be a useful geochemical classification.

Many granitic plutonic rocks throughout the world have relatively uniform ^{18}O-contents with $\delta^{18}O$-values between 6 and 10 ‰. Granitoids at the low ^{18}O end of the normal group have been described from oceanic island—arc areas where continental crust is absent (e.g., Chivas et al.1982). Such plutons are considered to be entirely mantle-derived. Granites at the high end of the normal ^{18}O-group may have formed by partial melting of crust that contained both a sedimentary and a magmatic fraction. It is interesting to note that many of the normal ^{18}O-granites are of Precambrian age and that metasediments of this age quite often have $\delta^{18}O$-values below 10 ‰ (Longstaffe and Schwarcz 1977).

Granitic rocks with $\delta^{18}O$-values higher than 10 ‰ require derivation from some type of ^{18}O-enriched sedimentary or metasedimentary protolith. For instance, such high $\delta^{18}O$-values are observed in many Hercynian granites of western Europe (Hoefs and Emmermann 1983), in Damaran granites of Africa (Haack et al. 1982) and in granites from the Himalayas of Central Asia (Blattner et al. 1983). All these granites are easily attributed to anatexis within a heterogeneous crustal source, containing a large metasedimentary component.

Granitic rocks with $\delta^{18}O$-values lower than 6 ‰ cannot be derived by any known differentiation process from basaltic magmas. Excluding those low ^{18}O granites which have exchanged with ^{18}O depleted meteoric-hydrothermal fluids under subsolidus conditions (see p. 87), a few primary low ^{18}O granitoids have been observed (Taylor 1987a, b). These granites obviously inherited their ^{18}O depletion while still predominantly liquid, prior to cooling and crystallization. Such low ^{18}O magmas may be formed by remelting of hydrothermally altered country rocks or by large-scale assimilation of such material in a rift-zone tectonic setting.

Si isotopes have been also used to distinguish among different granite types (Savage et al. 2012). Because weathering leads to the formation of ^{30}Si depleted clay minerals, granites derived from sedimentary rocks (S-type granites) are isotopically more variable and on average more depleted than I- and A-type granites. However, the relatively small variations indicate that Si-isotopes are less sensitive than O-isotopes.

3.2.14.1 Zircon

Recent advances in combining in situ measurements of radiogenic and stable isotopes in zircons allow a better understanding of the petrogenesis of granites and the evolution of the continental crust (Hawkesworth and Kemp 2006). Non-metamict zircons preserve their δ^{18}O-value from the time of crystallization because of their refractory and robust nature (Valley 2003). The δ^{18}O-value of zircons, thus, can be used to trace relative contributions of mantle-derived crust and of crust derived by reworking of pre-existing igneous or (meta)-sedimentary crust. Magmas in equilibrium with the mantle crystallize zircon that have a narrow range in δ^{18}O-values of 5.3 ± 0.3 ‰. Zircons from plutonic oceanic crust have average δ^{18}O-values of 5.2 ± 0.5 ‰, thus indicating that plagiogranites and differentiated gabbros do not carry a significant seawater signature (Grimes et al. 2011).

δ^{18}O-variations towards higher values result if the parental magma incorporates higher ^{18}O material (supracrustal rocks through melting or assimilation). Zircons with δ^{18}O-values lower than 5.3 ‰ indicate an origin of low ^{18}O magmas pointing to meteoric water-rock interaction.

Analyses of the oxygen isotope composition of zircons that have been dated may provide a record of growth and maturation of the crust. Valley et al. (2005) have analyzed 1200 dated zircons representing the whole spectrum of geologic ages. Uniformly low δ^{18}O-values are found in the first half of Earth history, but much more varied values are observed in younger rocks. In contrast to the Archean, ^{18}O-values during the Proterozoic gradually increase possibly indicating a maturation of the crust (see Fig. 3.9). After 1.5 Ga high δ^{18}O-values above 8 ‰ reflect gradual changes in the composition of sediments and the rate and style of recycling of surface-derived material into magmas (Valley et al. 2005).

3.3 Volatiles in Magmatic Systems

The isotope composition of magmatic volatiles and related isotope fractionation processes can be deduced by analyses of volcanic gases and hot springs. The main process that can cause isotope fractionation of volatile compounds is degassing. Informations can be also gained about the initial composition in the melt prior to gas loss. In addition the interaction of magmas with subducting slabs, oceanic and continental crust may also imprint their volatile characteristics onto those of the source (Hahm et al. 2012). The ultimate origin of volatiles in magmatic systems—whether juvenile in the sense that they originate from primary mantle degassing, or recycled by subduction processes—is difficult to assess, but may be deduced in some cases.

Because large differences exist in the isotope compositions of surface rocks relative to the mantle, the analysis of volatiles is important in assessing the extent of volatile transfer from the surface reservoirs to the mantle via subduction. Volatiles from arc related volcanic and hydrothermal systems may indicate an appreciable amount of surface derived materials and provide strong evidence of volatile recycling in subduction zones (Hauri 2002a; Snyder et al. 2001; Fischer et al. 2002).

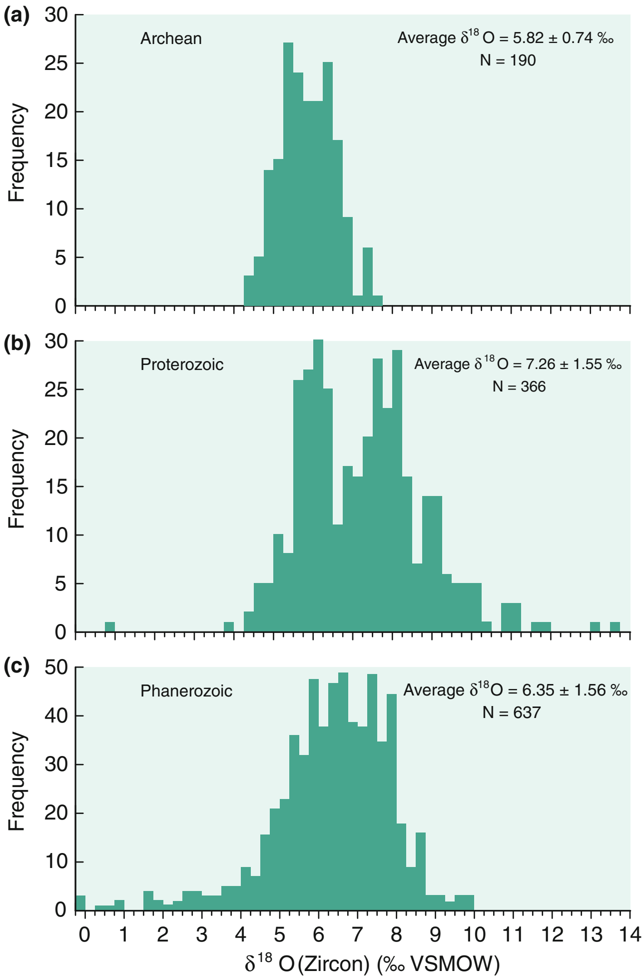

Fig. 3.9 Histogram of δ^{18}O-values for igneous zircons (**a** *Archean*, **b** *Proterozoic*, **c** *Phanerozoic*) (after Valley et al. 2005) (Fig. 3.9, 6th edition, p. 117)

3.3.1 Volcanic Gases and Hot Springs

The chemical composition of volcanic gases is naturally variable and can be modified significantly during sample collection, storage and handling. While it is relatively simple to recognize and correct for atmospheric contamination, the effects of natural contamination processes in the near-surface environment are much more difficult to address. Thus, the identification of truly mantle-derived gases except helium remains very problematic. In addition to assimilation/contamination processes, the degassing history can significantly alter the isotopic composition of magmatic volatiles.

3.3.1.1 Water

A long-standing geochemical problem is the source of water in volcanic eruptions and geothermal systems: how much is derived from the magma itself and how much is recycled meteoric water? One of the principal and unequivocal conclusions drawn from stable isotope studies of fluids in volcanic hydrothermal systems is that most hot spring waters are meteoric waters derived from local precipitation (Craig et al. 1956; Clayton et al. 1968; Clayton and Steiner 1975; Truesdell and Hulston 1980, and others).

Most hot spring waters have deuterium contents similar to those of local precipitation, but are usually enriched in ^{18}O as a result of isotopic exchange with the country rock at elevated temperatures. The magnitude of the oxygen isotope shift depends on the original O-isotope composition of both water and rock, the mineralogy of the rock, temperature, water/rock ratio, and the time of interaction.

There is increasing evidence, however, that a magmatic water component cannot be excluded in some volcanic systems. As more and more data have become available from volcanoes around the world, especially from those at very high latitudes, Giggenbach (1992) demonstrated that "horizontal" ^{18}O shifts are actually the exception rather than the rule: shifts in oxygen isotope composition are also accompanied by a change in the deuterium content (Fig. 3.10). Giggenbach (1992) argued that these waters all followed similar trends corresponding to mixing of local ground waters with a water having a rather uniform isotopic composition with a $\delta^{18}O$-value of about 10 ‰ and a δD-value of about −20 ‰. He postulated the existence of a common magmatic component in andesite volcanoes having a δD of

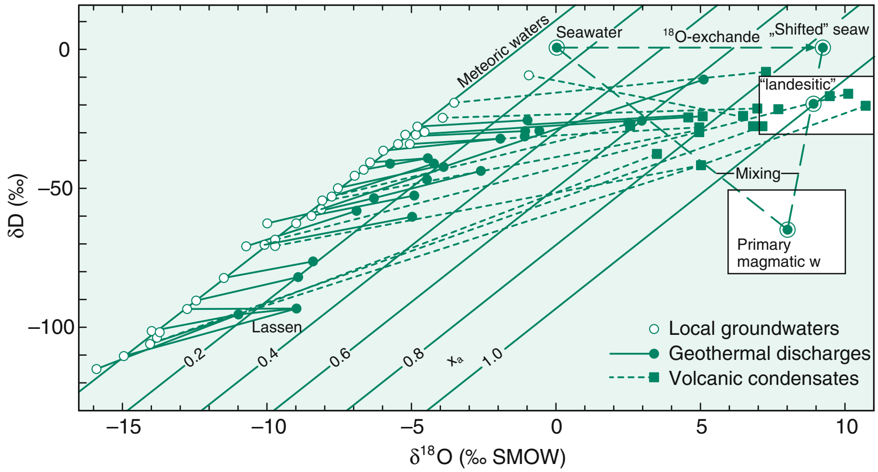

Fig. 3.10 Isotopic composition of thermal waters and associated local ground waters. Lines connect corresponding thermal waters to local groundwaters (Giggenbach 1992) (Fig. 3.10, 6th edition, p. 121)

−20 ‰ which is much higher than the generally assumed mantle water composition. The most likely source would be recycled seawater carried to zones of arc magma generation by the subducted slab.

What is sometimes neglected in the interpretation of isotope data in volcanic degassing products are the effects of boiling. Loss of steam from a geothermal fluid can cause isotopic fractionations. Quantitative estimates of the effects of boiling on the isotopic composition of water can be made using known temperature-dependent fractionation coefficients and estimates of the period of contact between the steam and liquid water during the boiling process (Truesdell and Hulston 1980).

3.3.1.2 Carbon

CO_2 is the second most abundant gas species in magmatic systems. In a survey of CO_2 emanations from tectonically active areas worldwide, Barnes et al. (1978) attributed $\delta^{13}C$-values between −8 and −4 ‰ to a mantle source. This is, however, problematic, because average crustal and mantle isotope compositions are more or less identical and surficial processes that can modify the carbon isotope composition are numerous. A more promising approach may be to analyze the ^{13}C-content of CO_2 collected directly from magmas at high temperatures.

The volcano where gases have been collected and analyzed for the longest time is Kilauea in Hawaii, the data base covering a period from about 1960 to 1985 (Gerlach and Thomas 1986; Gerlach and Taylor 1990). Gerlach and Taylor (1990) consider a $\delta^{13}C$-value of -3.4 ± 0.05 ‰ to be the best estimate of the mean for the total summit gas emission of Kilauea. A two-stage degassing model was developed to explain these values: (1) ascent and pressure equilibration in the summit magma chamber and (2) rapid, near surface decompression of summit-stored magma during ascent and eruption. The study demonstrated that the gas at the summit is a direct representation of the parental magma C-isotope ratio ($\delta^{13}C$: −3.4 ‰), whereas gases given off during East Rift Zone eruptions have a $\delta^{13}C$-value of −7.8 ‰, corresponding to a magma which had been affected by degassing in a shallow magmatic system.

It is well documented that carbon dioxide in vesicles of MORB is derived from the upper mantle. In island arcs and subduction-related volcanism major portions of carbon may derive from limestones and organic carbon. Sano and Marty (1995) demonstrated that the $CO_2/^3He$ ratio in combination with the $\delta^{13}C$-value can be used to distinguish between sedimentary organic, limestone and MORB carbon. Using this approach Nishio et al. (1998) and Fischer et al. (1998) concluded that about two-thirds of the carbon in a subduction zone originates from carbonates, whereas up to one third is derived from organic carbon. Even larger portions (>80 %) of CO_2 derived from marine carbonates have been found by Shaw et al. (2003) in volcanoes from the Central American arc. Carbon derived from a primary mantle source thus only plays a minor role in a subduction environment.

Besides CO_2, methane has been reported in high-temperature hydrothermal vent fluids (Welhan 1988, Ishibashi et al. 1995). The origin of this methane is somewhat unclear, even in systems which are associated with ^{3}He anomalies. Whereas a non-biogenic magmatic origin of methane has been assumed for the East Pacific Rise (Welhan 1988), a thermogenic origin has been proposed for the Okinawa trough (Ishibashi et al. 1995).

In recent years there is growing evidence that methane can be produced abiogenic during a Fischer-Tropsch type synthesis (reduction of CO or CO_2 by H_2 in the presence of a catalyst) (Sherwood-Lollar et al. 2006; McCollom and Seewald 2006 and others). Hydrocarbons (C_1–C_4) synthesized under abiogenic hydrothermal conditions are significantly depleted in ^{13}C relative to their CO_2 source. The magnitude of ^{13}C depletion may be similar to C isotope fractionations during biological processes making it impossible to distinguish between biogenic and abiogenic sources of reduced carbon. This finding has important implications for the discussion of the Earth earliest biosphere. Sherwood-Lollar et al. (2002) observed a trend of decreasing ^{13}C contents with increasing carbon numbers C_1–C_4 just opposite to gases derived from biologic sources. Experiments by Fu et al. (2007), however, could not confirm the trend observed by Sherwood-Lollar et al. (2002).

3.3.1.3 Nitrogen

Nitrogen in particular is a potential tracer of volatile recycling between the surface and the mantle, because of the large differences in N-isotope composition of MORB (δ^{15}N: −5 ‰), the atmosphere (0 ‰) and sediments (6−7 ‰). As demonstrated by Zimmer et al. (2004), Clor et al. (2005) and Elkins et al. (2006), nitrogen isotopes are very well suited for determining the fate of organic matter in subduction zones. These authors have demonstrated variable contributions of organic matter-derived nitrogen along arcs in Costa Rica, Nicaragua and Indonesia. For instance, Elkins et al. (2006) estimated that sediment contributions to volcanic and geothermal gases in the Nicaraguan volcanic front are around 70 %.

3.3.1.4 Sulfur

Elucidation of the origin of sulfur in volcanic systems is complicated by the fact that next to SO_2, significant amounts of H_2S, sulfate and elemental sulfur can also be present. The bulk sulfur isotope composition must be calculated using mass balance constraints. The principal sulfur gas in equilibrium with basaltic melts at low pressure and high temperature is SO_2. With decreasing temperature and/or increasing water fugacity, H_2S becomes more stable. δ^{34}S-values of SO_2 sampled at very high temperatures provide the best estimate of the ^{34}S-content of magmas (Taylor 1986a, b). Sakai et al. (1982) reported δ^{34}S-values of 0.7–1 ‰ in the solfataric gases of Kilauea which compare well with the δ^{34}S-values of 0.9–2.6 ‰ for Mount Etna gases, measured by Allard (1983) and Liotta et al. (2012). De Moor et al. (2013) investigated sulfur isotope systematics in gases and rocks from a relative reduced volcanic system (Erta Ale in Ethopia) and a relative oxidized

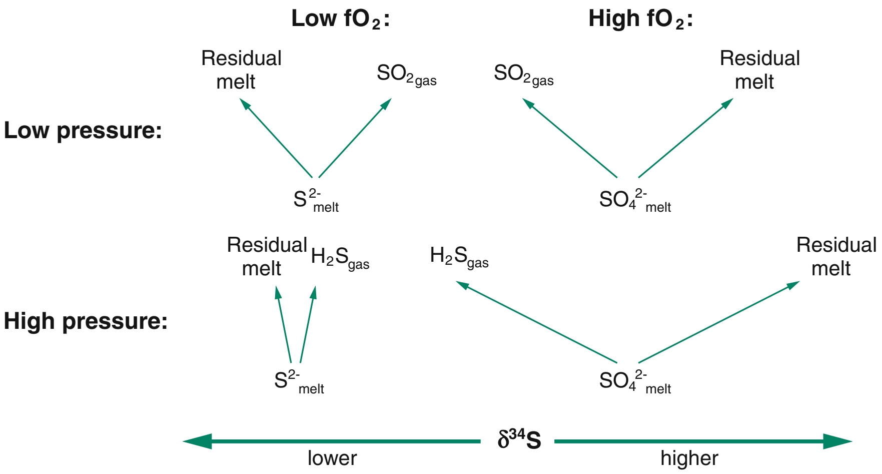

Fig. 3.11 S-isotope degassing scenarios at high and low pressures and at high and low oxygen fugacities (De Moor et al. 2013)

system (Masaya in Nicaragua). δ^{34}S-values in Erta Ale ($\delta^{34}S_{(gas)}$ −0.5 ‰, $\delta^{34}S_{(rock)}$ +0.9 ‰) are considerably more depleted than δ^{34}Svalues from the arc volcano Masaya ($\delta^{34}S_{(gas)}$ +4.8 ‰, $\delta^{34}S_{(rock)}$ +7.4 ‰). High values in Masaya obviously reflect recycling of subducted sulfate. Figure 3.11 shows schematically sulfur isotope degassing scenarios at high and low pressures one one hand and high and low oxygen fugacities.on the other.

Volcanic sulfur compounds play a key role for the monitoring of volcanoes, because SO_2 may convert to submicron particles of sulfate aerosol that may lead to a cooling of the atmosphere for months or even yerars. The injection of large quantities of volcanic SO_2 from explosive eruptions into the stratosphere, thus, may have a significant impact on global climate. Bindeman et al. (2007) and Martin and Bindeman (2009) investigated the sulfur and oxygen isotope composition of sulfate in volcanic ash. They observed a large range in δ^{34}S, δ^{18}O and Δ^{33}S- and Δ^{17}O-isotope values. The existence of mass-independent S-isotope fractionations demonstrates that the chemistry required for MIF generation occurs in parts of the modern oxygen rich atmosphere. MIF of oxygen occurs through oxidation of SO_2 in the upper atmosphere by interaction with mass-independent ozone.

In summary, stable isotope analysis (H, C, S) of volcanic gases and hot springs allow for estimates of the isotopic composition of the mantle source. However, it must be kept in mind that numerous possibilities for contamination, assimilation, and gas phase isotopic fractionation, especially in the surficial environment, make such deductions problematic at best. In cases where it may possible to "see through" these secondary effects, small differences in H, C, N and S isotope compositions of volcanic gases and hot springs might be characteristic of different geotectonic settings.

3.3.2 Isotope Thermometers in Geothermal Systems

Although there are many isotope exchange processes occurring within a geothermal fluid, many of which have the potential to provide thermometric information, only a few have generally been applied, because of suitable exchange rates for achieving isotope equilibrium (Hulston 1977; Truesdell and Hulston 1980; Giggenbach 1992). Temperatures are determined on the basis of calculated fractionation factors of Richet et al. (1977). Differences among geothermometers in the C–O–H–S system are generally ascribed to differences in exchange rates in the decreasing order CO_2–H_2O (oxygen) > H_2O–H_2 (hydrogen) > SO_2–H_2S (sulfur) > CO_2–CH_4 (carbon). Especially pronounced are the differences for the CO_2–CH_4 thermometer which are often higher than the actual measured temperatures. Investigations on Nisyros volcano, Greece, however, suggest that chemical and isotopic equilibrium between CO_2 and CH_4 may occur to temperatures as low as 320 °C (Fiebig et al. 2004).

3.4 Ore Deposits and Hydrothermal Systems

Stable isotopes have become an integral part of ore deposits studies. The determination of light isotopes of H, C, O and S can provide information about the diverse origins of ore fluids, about temperatures of mineralization and about physico-chemical conditions of mineral deposition. In contrast to early views, which assumed that almost all metal deposits owed their genesis to magmas, stable isotope investigations have convincingly demonstrated that ore formation has taken place in the Earths near-surface environment by recycling processes of fluids, metals, sulfur, and carbon. Reviews of the application of stable isotopes to the genesis of ore deposits have been given by Ohmoto (1986), Taylor (1987a, b) and Taylor (1997).

Inasmuch as water is the dominant constituent of ore-forming fluids, knowledge of its origin is fundamental to any theory of ore genesis. There are two ways for determining δD- and $\delta^{18}O$-values of ore fluids:

by direct measurement of fluid inclusions contained within hydrothermal minerals, or

by analysis of hydroxyl-bearing minerals and calculation of the isotopic composition of fluids from known temperature-dependent mineral-water fractionations, assuming that minerals were precipitated from solutions under conditions of isotope equilibrium.

There are two different methods through which fluids and gases may be extracted from rocks: (i) thermal decrepitation by heating in vacuum and (ii) crushing and grinding in vacuum. Serious analytical difficulties may be associated with both techniques. The major disadvantage of the thermal decrepitation technique is that, although the amount of gas liberated is higher than by crushing, compounds present in the inclusions may exchange isotopically with each other and with the host mineral at the high temperatures necessary for decrepitation. Crushing in vacuum largely avoids isotope exchange processes. However, during crushing large new surfaces are created which easily adsorb some of the liberated gases and that, in turn, might be associated with fractionation effects. Both techniques preclude separating the different generations of inclusions in a sample and, therefore, the results obtained represent an average isotopic composition of all generations of inclusions.

Numerous studies have used the δD-value of the extracted water to deduce the origin of the hydrothermal fluid. However, without knowledge of the internal distribution of hydrogen in quartz, such a deduction can be misleading (Simon 2001). Hydrogen in quartz mainly occurs in two reservoirs: (i) in trapped fluid inclusions and (ii) in small clusters of structurally bound molecular water. Because of hydrogen isotope fractionation between the hydrothermal fluid and the structurally bound water, the total hydrogen extracted from quartz does not necessarily reflect the original hydrogen isotope composition. This finding may explain why δD-values from fluid inclusions often tend to be lower than δD-values from associated minerals (Simon 2001).

Oxygen-bearing minerals crystallize during all stages of mineralization, whereas the occurrence of hydrogen-bearing minerals is restricted in most ore deposits. Examples of hydroxyl-bearing minerals include biotite and amphibole at high temperatures (in porphyry copper deposits), chlorite and sericite at temperatures around 300 °C, and kaolinite at around 200 °C.

The mineral alunite, and its iron equivalent jarosite, are a special case. Alunite ($KAl_3(SO_4)_2(OH)_6$) contains four sites where elements containing stable isotopes are found and both the sulfate and hydroxyl anionic groups may provide information on fluid source and condition of formation.

Alunite forms under highly acidic oxidizing conditions and is characterized by the assemblage alunite + kaolinite + quartz ± pyrite. Stable isotope data of alunite in combination with associated sulfides and kaolinite permit recognition of environments and temperatures of formation (Rye et al. 1992).

The indirect method of deducing the isotope composition of ore fluids is more frequently used, because it is technically easier. Uncertainties arise from several sources: uncertainty in the temperature of deposition, and uncertainty in the equations for isotope fractionation factors. Another source of error is an imprecise knowledge of the effects of fluid chemistry (“salt effect”) on mineral-water fractionation factors.

Several studies (e.g. Berndt et al. 1996; Driesner and Seward 2000; Horita et al. 1995; Shmulovich et al. 1999) have demonstrated that the approach of using mineral—pure water fractionation factors to deduce the origin of the water is incorrect. Isotope fractionations involving aqueous solutions depend not only on temperature and fluid composition, but also on the presence or absence of phase separation (“boiling”). Phase separation is an important process causing potentially isotope fractionation. Hydrogen isotope studies (Berndt et al. 1996; Shmulovich et al. 1999) indicate that high temperature phase separation produces D-enrichment in the vapor and D-depletion in the conjugate fluid. If the fractionation effect inherent in a boiling fluid system is disregarded, one may easily misinterpret the isotope composition of hydrothermal minerals, since boiling may mask the source of the parent fluids. In addition, for hydrogen isotope fractionations, pressure may have some control on mineral-water fractionations (Driesner 1997; Horita et al. 1999).

3.4.1 Origin of Ore Fluids

Ore fluids may be generated in a variety of ways. The principal types include (i) sea water, (ii) meteoric waters and (iii) juvenile water, all of which have a strictly defined isotopic composition. All other possible types of ore fluids such as formation, metamorphic and magmatic waters can be considered recycled derivatives or mixtures from one or more of the three reference waters (see Fig. 3.12).

(i) Sea water

The oxygen isotopic composition of present-day ocean water is more or less constant with δ-values close to zero permil. The isotopic composition of ancient ocean water, however, is less well constrained (see Sect. 3.7), but still should not be removed from zero by more than 1 or 2 ‰. Many volcanogenic massive sulfide deposits are formed in submarine environments from heated oceanic waters. This concept gains support from the recently observed hydrothermal systems at ocean ridges, where measured isotopic compositions of fluids are only slightly modified relative to 0 ‰. $\delta^{18}O$ and δD-values of vent fluids are best understood in terms of seawater interaction with the ocean crust (Shanks 2001).

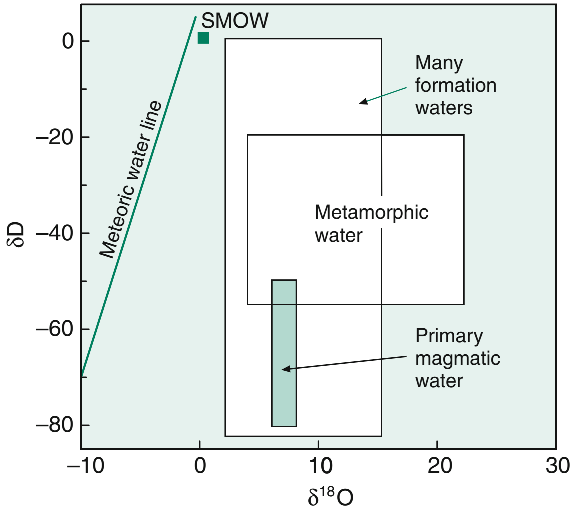

Fig. 3.12 Plot of δD versus $\delta^{18}O$ of waters of different origin (Fig. 3.11, 6th edition, p. 126)

Bowers and Taylor (1985) have modelled the isotopic composition of an evolving seawater hydrothermal system. At low temperatures, the δ^{18}O-value of the fluid decreases relative to ocean water because the alteration products in the oceanic crust are ^{18}O rich. At around 250 °C, the solution returns to its initial seawater isotopic composition. Further reaction with basalt at 350 °C increases the δ^{18}O value of modified seawater to ~2 ‰. The δD-value of the solution increases slightly at all temperatures because mineral-water fractionations are generally all less than zero. At 350 °C, the δD-value of the solution is 2.5 ‰. The best documented example for the role of ocean water during ore deposition is for the Kuroko-type deposits (see the extensive monograph by Ohmoto and Skinner (1983)).

(ii) Meteoric waters

Heated meteoric waters are a major constituent of ore-forming fluids in many ore deposits and may become dominant during the latest stages of ore deposition. The latter has been documented for many porphyry skarn-type deposits. The isotopic variations observed for several Tertiary North American deposits vary systematic with latitude and, hence, palaeo-meteoric water composition (Sheppard et al. 1971). The ore-forming fluid has commonly been shifted in O-isotope composition from its meteoric δ^{18}O-value to higher ^{18}O contents through water-rock interaction. Meteoric waters may become dominant in epithermal gold deposits and other vein and replacement deposits.

(iii) Juvenile water

The concept of juvenile water has influenced early discussions about ore genesis tremendously. The terms "juvenile water" and "magmatic water" have been used synonymously sometimes, but they are not exactly the same. Juvenile water originates from degassing of the mantle and has never existed as surface water. Magmatic water is a non-genetic term and simply means a water that has equilibrated with a magma.

It is difficult to prove that juvenile water has ever been sampled. One way to search for juvenile water is by analyzing hydroxyl-bearing minerals of mantle origin (Sheppard and Epstein 1970). The estimated isotopic composition of juvenile water from such an approach is δD: −60 ± 20 ‰ and δ^{18}O: +6 ± 1 ‰ (Ohmoto 1986).

3.4.1.1 Magmatic Water

Despite the close association of intrusions with many ore deposits, there is still debate about the extent to which magmas contribute water and metals to ore-forming fluids. Many early studies of the stable isotope composition of hydrothermal minerals indicated a dominance of meteoric water (Taylor 1974), more recent studies show that magmatic fluids are commonly present, but that their isotopic compositions may be masked or erased during later events such as the influx of meteoric waters (Rye 1993).

The δD-value of magmatic water changes progressively during degassing, resulting in a positive correlation between δD and the residual water content of an igneous body. Thus, late-formed hydroxyl-bearing minerals represent the isotopic composition of a degassed melt rather than that of the initial magmatic water. The δD values of most of the water exsolved from many felsic melts is in the range of −60 to −30 ‰, whereas the associated magmatic rocks may be significantly depleted in D.

The calculated range of isotopic composition for magmatic waters is commonly 6–10 ‰ for δ^{18}O-values and −50 to −80 ‰ for δD-values. Magmatic fluids may change their isotopic composition during cooling through isotope exchange with country rocks and mixing with fluids entrained within the country rocks. Thus, the participation of a magmatic water component during an ore-forming process is generally not easily detected.

3.4.1.2 Metamorphic Water

Metamorphic water is defined as water associated with metamorphic rocks during metamorphism. Thus, it is a descriptive, non-genetic term and may include waters of different ultimate origins. In a narrower sense, metamorphic water refers to the fluids generated by dehydration of minerals during metamorphism. The isotopic composition of metamorphic water may be highly variable, depending on the respective rock types and their history of fluid/rock interaction. A wide range of δ^{18}O-values (5–25 ‰) and δD-values (−70 to −20 ‰) is generally attributed to metamorphic waters (Taylor 1974).

3.4.1.3 Formation Waters

The changes in the D- and ^{18}O-contents of pore fluids depend on the origin of initial fluid (ocean water, meteoric water), temperature and the lithology of rocks with which the fluids are or have been associated. Generally, formation waters with the lowest temperature and salinity have the lowest δD- and δ^{18}O-values, approaching those of meteoric waters. Brines of the highest salinities are generally more restricted in isotopic composition. It is still an unanswered question though whether meteoric water was the only source of water to these brines. The final isotope composition of brines can be produced by reactions between meteoric water and sediments, or result from mixtures of fossil ocean water trapped in the sediments and meteoric water.

3.4.2 Wall-Rock Alteration

Information about the origin and genesis of ore deposits can also be obtained by analyzing the alteration products in wall-rocks. Hydrogen and oxygen isotope zonation in wall-rocks around hydrothermal systems can be used to define the size and the conduit zones of a hydrothermal system. The fossil conduit is a zone of large water fluxes, generally causing a strong alteration in the rocks and lowering the $\delta^{18}O$-values. Thus, fossil hydrothermal conduits can be outlined by following the zones of ^{18}O-depletion. Oxygen isotope data are especially valuable in rock types that do not show diagnostic alteration mineral assemblages as well as those in which the assemblages have been obliterated by subsequent metamorphism (e.g. Beaty and Taylor 1982; Green et al. 1983). Criss et al. (1985, 1991) found excellent spatial correlations between low $\delta^{18}O$-values and economic mineralization in siliceous rocks. Similar zonation around ore deposits in carbonate rocks have also been observed (e.g. Vazquez et al. 1998). Thus, zones having anomalously low ^{18}O-contents may be a useful guide for exploration of hydrothermal ore deposits.

3.4.3 Fossil Hydrothermal Systems

Mainly through the work of H.P.Taylor and coworkers, it has become well established that many epizonal igneous intrusions have interacted with meteoric groundwaters on a very large scale. The interaction and transport of large amounts of meteoric water through hot igneous rocks produces a depletion in ^{18}O in the igneous rocks by up to 10–15 ‰ and a corresponding shift in the ^{18}O content of the water. About 60 of such systems have been observed to date (Criss and Taylor 1986). They exhibit great variations in size from relatively small intrusions (<100 km^2) to large plutonic complexes (>1000 km^2). Amongst the best documented examples are the Skaergaard intrusion in Greenland, the Tertiary intrusions of the Scottish Hebrides, and the Tertiary epizonal intrusions of the northwestern United States and southern British Columbia, where 5 % of the land surface has been altered by meteoric hydrothermal water (Criss et al. 1991).

The best-studied example of a hydrothermal system associated with a gabbro is the Skaergaard intrusion (Taylor and Forester 1979; Norton and Taylor 1979). The latter authors carried out a computer simulation of the Skaergaard hydrothermal system and found a good match between calculated and measured $\delta^{18}O$-values. They further demonstrated that most of the sub-solidus hydrothermal exchange took place at very high temperatures (400–800 °C), which is compatible with the general absence of hydrous alteration products in the mineral assemblages and with the presence of clinopyroxene.

In granitic hydrothermal systems, temperatures of alteration are significantly lower because of differences in the intrusion temperatures. The most conspicious petrographic changes are chloritization of mafic minerals, particularly of biotite, and a major increase in the turbidity of feldspars. Large non-equilibrium quartz—feldspar oxygen isotope fractionations are typical. Steep linear trajectories on plots of $\delta^{18}O_{(feldspar)}$ versus $\delta^{18}O_{(quartz)}$ are a characteristic feature of these hydrothermally altered rocks (see Fig. 2.17). The trajectories result from the fact that feldspar exchanges ^{18}O with hydrothermal fluids much faster than coexisting quartz and from the fact that the fluids entering the rock system have $\delta^{18}O$-values which are out of equilibrium with the mineral assemblage. The process seldom goes to completion, so the final mineral assemblage is in isotope disequilibrium, which is the most obvious fingerprint of the hydrothermal event.

Taylor (1988) distinguished three types of fossil hydrothermal systems on the basis of varying water/rock ratios, temperatures, and the length of time that fluid/rock interaction proceeds:

Epizonal systems with a wide variation in whole rock ^{18}O-contents and extreme oxygen isotope disequilibrium among coexisting minerals. These systems typically have temperatures between 200 and 600 °C and life-times $<10^6$y.

Deeper-seated and/or longer-lived systems, also with a wide spectrum of whole rock $^{18}O/^{16}O$ ratios, but with equilibrated $^{18}O/^{16}O$ ratios among coexisting minerals. Temperatures are between 400 and 700 °C and life-times $>10^6$ y.

Equilibrated systems with a relatively uniform oxygen isotope composition in all lithologies. These systems require a large water/rock ratio, temperatures between 500 and 800 °C, and life times around 5×10^6 y.

These types are not mutually exclusive, Type III systems for example may have been subjected to Type I or Type II conditions at an earlier stage of their hydrothermal history.

3.4.4 Hydrothermal Carbonates

The measured $\delta^{13}C$- and $\delta^{18}O$-values of carbonates can be used to estimate the carbon and oxygen isotope composition of the fluid in the same way as has been discussed before for oxygen and hydrogen. The isotopic composition of carbon and oxygen in any carbonate precipitated in isotopic equilibrium with a fluid depends on the isotopic composition of carbon and oxygen in the fluid, the temperature of formation, and the relative proportions of dissolved carbon species (CO_2, H_2CO_3, HCO_3^-, and/or CO_3^{2-}). To determine carbonate speciation, pH and temperature must be known; however, in most geologic fluids with temperatures above about 100 °C, the content of HCO_3^- and CO_3^{2-} is negligible compared to CO_2 and H_2CO_3.

Experimental investigations have shown that the solubility of carbonate increases with decreasing temperature. Thus, carbonate cannot be precipitated from a hydrothermal fluid due to simple cooling in a closed system. Instead, an open system is required in which processes such as CO_2 degassing, fluid-rock interaction or fluid mixing can cause the precipitation of carbonate. These processes result in correlation trends in $\delta^{13}C$ vs $\delta^{18}O$ space for hydrothermal carbonates as often observed in nature and theoretically modeled by Zheng and Hoefs (1993).

Figure 3.13 presents $\delta^{13}C$ and $\delta^{18}O$-values of hydrothermal carbonates from the Pb–Zn deposits of Bad Grund and Lautenthal, Germany. The positive correlation between $^{13}C/^{12}C$- and $^{18}O/^{16}O$-ratios can be explained either by calcite precipitation due to the mixing of two fluids with different NaCl concentrations or by calcite precipitation from a H_2CO_3-dominant fluid due to a temperature effect coupled with either CO_2 degassing or with fluid-rock interaction.

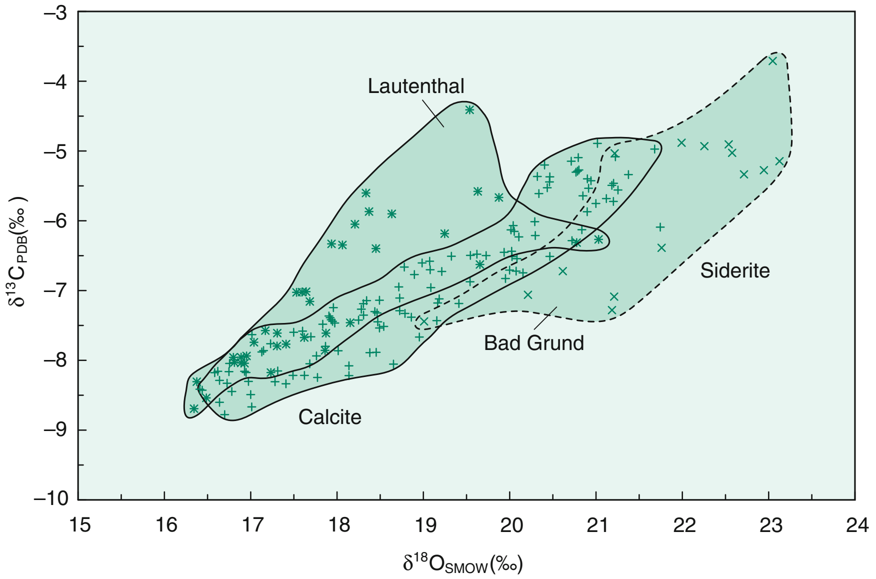

Fig. 3.13 C- and O-isotope compositions of calcites and siderites from the Bad Grund and Lautenthal deposits, Harz (after Zheng and Hoefs 1993) (Fig. 3.12, 6th edition, p. 130)

3.4.5 Sulfur Isotope Composition of Ore Deposits

A huge amount of literature exists about the sulfur isotope composition in hydrothermal ore deposits. Some of this information has been discussed in earlier editions and, therefore, is not repeated here. Out of the numerous papers on the subject the reader is referred to comprehensive reviews by Ohmoto and Rye (1979), Ohmoto (1986), Taylor (1987a, b) and Ohmoto and Goldhaber (1997). The basic principles to be followed in the interpretation of $\delta^{34}S$ values in sulfidic ores were elucidated by Sakai (1968), and subsequently, were extended by Ohmoto (1972).

The isotopic composition of a hydrothermal sulfide is determined by a number of factors such as (1) isotopic composition of the hydrothermal fluid from which the mineral is deposited, (2) temperature of deposition, (3) chemical composition of the dissolved element species including pH and fO_2 at the time of mineralization, and (4) relative amount of the mineral deposited from the fluid. The first parameter is characteristic of the source of sulfur, the three others relate to the conditions of deposition.

3.4.5.1 The Importance of FO_2 and pH

First, consider the effect of p_H-increase due to the reaction of an acidic fluid with a carbonate-bearing host rocks. At pH = 5, practically all of the dissolved sulfur is undissociated H_2S, whereas at pH = 9 the dissolved sulfide is almost entirely

Fig. 3.14 Influence of fO_2 and pH on the sulfur isotope composition of sphalerite and barite at 250 °C and $\delta^{34}S_{\Sigma S}$ = 0 ‰ (modified after Ohmoto 1972) (Fig. 3.13. 6th edition, p. 131)

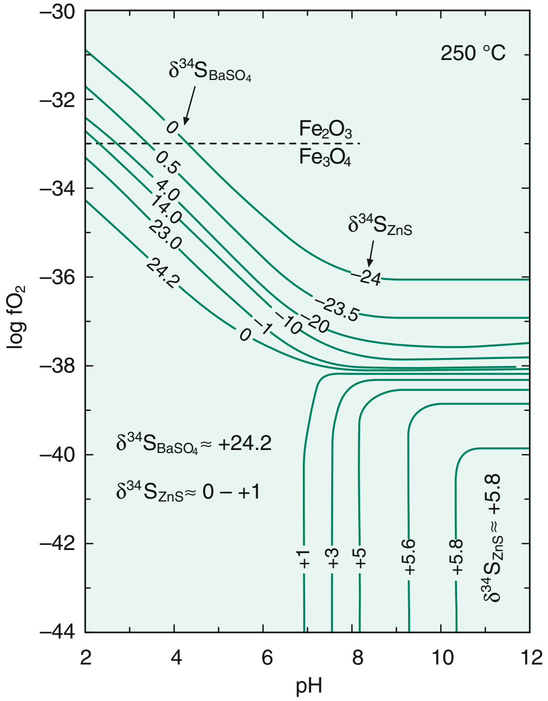

dissociated. Since H_2S concentrates ^{34}S relative to dissolved sulfide ion, an increase in pH leads directly to an increase in the $\delta^{34}S$ of precipitated sulfides.

An increase in oxygen fugacities has a much stronger effect on the $\delta^{34}S$-values than a pH change, because of the large isotope fractionation between sulfate and sulfide. Figure 3.14 shows an example of the effect of pH and fO_2 variation on the sulfur isotope compositions of sphalerite and barite in a closed system at 250 °C with $\delta^{34}S_{\Sigma S}$ = O ‰. The curves are $\delta^{34}S$ contours, which indicate the sulfur isotope compositions of the minerals in equilibrium with the solution. Sphalerite $\delta^{34}S$-values can range from −24 to +5.8 ‰ and those for barite from about 0–24.2 ‰ within geologically reasonable limits of pH and fO_2. In the low fO_2 and pH region, sulfide ^{34}S contents can be similar to $\delta^{34}S_{\Sigma S}$ and can be rather insensitive to pH and fO_2 changes. In the region of high fO_2 values where the proportion of sulfate species becomes significant, mineral $\delta^{34}S$ values can be greatly different from $\delta^{34}S_{\Sigma S}$ and small changes in pH or fO_2 may result in large changes in the sulfur isotope composition of either sulfide or sulfate. Such a change must, however, be balanced by a significant change in the ratio of sulfate to sulfide.

In summary, interpretation of the distribution of $\delta^{34}S$-values relies on information about the source of sulfur and on a knowledge of the mineral parageneses that constrain the ambient temperature, Eh and pH. If the oxidation state of the fluid is below the sulfate/H_2S boundary, then the $^{34}S/^{32}S$ ratios of sulfides will be insensitive to redox shifts.

In the following section different classes of ore deposits are discussed.

3.4.5.2 Magmatic Ore Deposits

Magmatic deposits are characterized by sulfides which precipitate from mafic silicate melts rather than hydrothermal fluids. They can be divided into S-poor (deposits of platinum group elements) and S-rich magmatic sulfide systems (Ni–Cu deposits) (Ripley and Li 2003) The majority of this type of deposits are hosted within sedimentary country rocks in which the sulfur is assimilated or volatized during magma emplacement.Typical examples are the deposits of Duluth, Stillwater, Bushveld, Sudbury and Norils'k. In many of these deposits relatively large deviations in $\delta^{34}S$-values from the presumed mantle melt value near zero are observed, indicating magma contamination by interactions with country rocks. The large spread in $\delta^{34}S$ is generally attributed to assimilation of sulfur from the wall rocks, provided that the sulfur isotope composition of the country rocks is significantly different from the magma.

3.4.5.3 Magmatic Hydrothermal Deposits

This group of deposits is closely associated in space and time with magmatic intrusions that were emplaced at relatively shallow depths. They have been developed in hydrothermal systems driven by the cooling of magma (e.g. porphyry-type deposits and skarns). From δD- and $\delta^{18}O$-measurements, it has been concluded that porphyry copper deposits show the clearest affinity of a magmatic water imprint (Taylor 1974) with variable involvement of meteoric water generally at late stages of ore formation.

The majority of $\delta^{34}S$-values of sulfides fall between −3 and 1 ‰ and of sulfates between 8 and 15 ‰ (Field and Gustafson 1976; Shelton and Rye 1982; Rye 2005). Sulfate-sulfide isotope date suggest a general approach to isotope equilibrium. Calculated sulfate-sulfide temperatures, for conditions of complete isotope equilibrium, are typically between 450 and 600 °C and agree well with temperatures estimated from other methods. Thus, the sulfur isotope data and temperatures support the magmatic origin of the sulfur in porphyry deposits.

3.4.5.4 Epithermal Deposits

Epithermal ore deposits are hydrothermal deposits that form at shallow crustal levels. A wide spectrum of ore deposits of a different nature occurs in this category. Typical temperatures of mineralization range from 150 to 350 °C with variable salinities. Individual deposits often reveal that more than one type of fluid was involved in the formation of a single ore deposit. One of the fluids involved often appears to be of meteoric origin. In many deposits different fluids were alternatively discharged into the vein system and promoted the precipitation of a specific suite of minerals, such as one fluid precipitating sulfides and another precipitating carbonates (Ohmoto 1986).

Compared to porphyry copper deposits δ^{34}S-values in epithermal deposits are more variable due to lower temperatures of formation and significant amounts of both sulfide and sulfate in the hydrothermal fluid.

3.4.5.5 Recent and Fossil Sulfide Deposits at Mid-Ocean Ridges

Numerous sulfide deposits have been discovered on the seafloor along the East Pacific Rise, Juan de Fuca Ridge, Explorer Ridge and Mid-Atlantic Ridge (Shanks 2001). These deposits are formed from hydrothermal solutions which result from the interaction of circulating hot seawater with oceanic crust. Sulfides are derived mainly from two sources: (i) leaching from igneous and sedimentary wall rocks and (ii) thermochemical sulfate reduction due to interaction with ferrous silicates and oxides or with organic matter.

The role of sulfur in these vents is complex and often obscured by its multiple redox states and by uncertainties in the degree of equilibration. Studies by Styrt et al. (1981), Arnold and Sheppard (1981), Skirrow and Coleman (1982), Kerridge et al. (1983), Zierenberg et al. (1984), and others have shown that the sulfur in these deposits is enriched in ^{34}S relative to a mantle source (typical δ^{34}S ranges are between 1 and 5 ‰), implying small additions of sulfide derived from seawater.

Vent sulfides at sediment covered hydrothermal systems may carry, in addition, signatures of sulfides derived from bacterial reduction. δ^{34}S-values alone may be unable to distinguish between the different sulfur sources. High precision measurements of δ^{33}S, δ^{34}S and δ^{36}S allow, however, the distinction of biological isotope fractionation from abiological fractionation (Ono et al. 2007; Rouxel et al. 2008a, b). Biogenic sulfides are characterized by relatively high Δ^{33}S values compared to hydrothermal sulfides. Sulfides from the East Pacific Rise and the Mid-Atlantic Ridge, analyzed by Ono et al. (2007), gave low Δ^{33}S values compared to biogenic sulfides suggesting no contribution of biogenic sulfides. In altered oceanic basalts at ODP Site 801, however, Rouxel et al. (2008a, b) provided evidence for secondary biogenic pyrite. These authors estimated that at least 17 % of pyrite sulfur was derived from bacterial reduction.

For ancient seafloor sulfide deposits an alternative model has been discussed by Ohmoto et al. (1983), in which H_2S and sulfides are buffered by precipitated anhydrite and where δ^{34}S-values reflect temperature dependent equilibrium fractionations between SO_4 and H_2S.

To the category of ancient hydrothermal seafloor ore deposits belong volcanic associated massive sulfide deposits. They are characterized by massive Cu–Pb–Zn–Fe sulfide ores associated with submarine volcanic rocks. They appear to have been formed near the seafloor by submarine hot springs at temperatures of 150–350 °C. Massive sulfide deposits have δ^{34}S-values typically between zero and the δ-value of contemporaneous oceanic sulfate, whereas the sulfate has δ-values similar to or higher than contemporaneous seawater. According to Ohmoto et al. (1983) the ore-forming fluid is evolved seawater fixed as disseminated anhydrite and then reduced by ferrous iron and organic carbon in the rocks.

Another group belonging to this category of ore deposits are sedimentary-exhalative (sedex) massive sulfide deposits Just as volcanic massive sulfide deposits, this group has formed on the seafloor or in unconsolidated marine sediments. Its members differ from volcanogenic massive deposits in that the dominant host-rock lithologies are marine shales and carbonates, the associated igneous activity is minor or negligible, and water depths seem to be considerably less than the >2000 m proposed for most volcanogenic deposits. The total range of sulfide δ^{34}S-values is much larger than the range observed in volcanogenic massive sulfide deposits.

Sulfides are fine-grained and texturally complex containing multiple generations of minerals. Two different origins of sulfur can be envisaged: biogenic and hydrothermal. Mineral separation methods cannot insure that mineral separates contain only one type of sulfur. Therefore, conventional techniques cannot answer questions such as: is most of the sulfur produced by bacterial reduction of seawater or is it inorganically acquired and hydrothermally introduced together with the metals? In situ ion microprobe techniques allow isotope analysis on a scale as small as 20 µm. Studies by Eldridge et al. (1988, 1993) have revealed extremely large variations on distances of millimeters with gross disequilibrium between base metal sulfides and overgrown pyrites. Thus, the mean δ^{34}S-values of these deposits are not particularly diagnostic of its origin, but additional measurements of Δ^{33}S might be able to distinguish between different sulfur sources.

Like sulfur, Fe isotope investigations show complex patterns (Severmann et al. 2004; Rouxel et al. 2004a, b, 2008a, b; Bennett et al. 2009). High temperature vent fluids are depleted in ^{56}Fe relative to their source rocks. Precipitating marcasite and pyrite from various mid-ocean ridge vents are isotopically lighter than chalcopyrite. When vent fluids enter oxygen-rich ocean water, polymetallic sulfide and Fe hydoxides precipitate causing a 0.6 ‰ isotope fractionation with the sulfides being depleted in ^{56}Fe (Bennett et al. 2009).

3.4.5.6 Mississippi-Valley-Type (MVT) Deposits

The Mississippi-Valley-Type deposits are epigenetic Zn–Pb deposits which mainly occur in carbonates from continental settings (Ohmoto 1986).

Characteristics often ascribed to MVT deposits include temperatures generally <200 °C and deposition from externally derived fluids, possibly basinal brines. Sulfur isotope values from MVT deposits suggest two major sulfide reservoirs, one between −5 and +15 ‰ and one greater than +20 ‰ (Seal 2006). Both sulfide reservoirs can be related, however, to a common seawater sulfate source that has undergone different sulfur fractionation processes. Reduction of sulfate occurs either bacterially or by abiotic thermochemical reduction. High δ^{34}S-values should reflect minimal fractionations associated with thermochemical reduction of seawater sulfate (Jones et al. 1996).

3.4.5.7 Biogenic Deposits

The discrimination between bacterial sulfate and thermal sulfate reduction in ore deposits on the basis of δ^{34}S-values is rather complex. The best criterion to distinguish between both types is the internal spread of δ-values. If individual sulfide grains at a distance of only a few millimeters exhibit large and nonsystematic differences in δ^{34}S-values, then it seems reasonable to assume an origin involving bacterial sulfate reduction. Irregular variations in ^{34}S-contents are attributed to bacteria growing in reducing microenvironments around individual particles of organic matter. In contrast, thermal sulfate reduction requires higher temperatures supplied by external fluids, which is not consistent with the closed system environment of bacterial reduction.

Two types of deposits, where the internal S-isotope variations fit the expected scheme of bacterial reduction, but where the biogenic nature was already known from other geological observations, are the "sandstone-type" uranium mineralization in the Colorado Plateau (Warren 1972) and the Kupferschiefer in Central Europe (Marowsky 1969), although thermal sulfate reduction may have occurred at the base of the Kupferschiefer (Bechtel et al. 2001).

3.4.5.8 Metamorphosed Deposits

It is generally assumed that metamorphism reduces the isotopic variations in a sulfide ore deposit. Recrystallization, liberation of sulfur from fluid and vapor phases, such as the breakdown of pyrite into pyrrhotite and sulfur, and diffusion at elevated temperatures should tend to reduce initial isotopic heterogeneities.

Studies of regionally metamorphosed sulfide deposits (Seccombe et al. 1985; Skauli et al. 1992) indicate, however, little evidence of homogenisation on the deposit scale. Significant changes may take place in certain restricted parts of the deposit as a result of special local conditions, controlled by factors such as fluid flow regimes and tectonics. Thus, a very limited degree of homogenisation takes place during metamorphism (Cook and Hoefs 1997). The extent of this is obscured by primary distribution and zonation patterns.

3.4.6 Metal Isotopes

One of the most important questions in the genesis of ore deposits is the origin of the metals. Recent analytical developments have provided a new tool for the analysis of metal isotopes (Fe, Cu, Zn, Mo). Since the bulk silicate earth (crust + mantle) shows a uniform mean isotope composition of the metals, different metal reservoirs with distinct isotopic compositions are not easily recognizable. It is therefore necessary to determine the ranges of metal isotopes in different ore deposit types and to investigate the mechanism that fractionate metal isotopes. Variations in metal isotope ratios depend on various parameters such as formation temperatures, abiotic or biotic processes and redox state during ore formation making interpretation of metal isotope ratios in ore deposits complex.

Like sulfur, mass balance among reduced and oxidized species controls the isotopic composition of metal sulfides (Asael et al. 2009). Thus far, Cu has received the greatest attention in applying metal stable isotopes to ore deposits (see the summary of Li et al. (2010a, b). Cu isotope studies have been performed in a wide spectrum of ore deposits, including black smokers (Zhu et al. 2000a, b; Rouxel et al. 2004a, b), massive sulfide deposits (Mason et al. 2005; Ikehate et al. 2011), porphyry deposits (Graham et al. 2004; Mathur et al. 2010; Li et al. 2010a), skarn (Maher and Larson 2007) and other hydrothermal deposits (Markl et al. 2006a, b). A common feature of these investigations is that Cu-mineralizations influenced by low temperature redox processes show larger variations than high temperature Cu-mineralizations

Since Fe is also sensitive to redox processes, it might be expected that Cu and Fe isotope variations in a specific ore deposit are coupled, which, however seems to be not the case. One reason for a decoupling might be that the redox potential of Cu^{2+}/Cu^{+} is much lower than for Fe^{3+}/Fe^{2+} making Cu isotopes more sensitive to redox processes.

A range of more than 5 ‰ in $\delta^{65}Cu$ has been interpreted by Markl et al. (2006a) as being due to redox processes among dissolved Cu-species and to fractionations during precipitation of Cu minerals. A 2.5 ‰ variation of iron minerals in $\delta^{56}Fe$ has been explained by mixing models either through mixing with oxygen-rich surface waters resulting in ^{56}Fe depleted hematite or through mixing with CO_2-rich fluids leading to precipitation of isotopically depleted siderite (Markl et al. 2006b).

Thus an important reserch field is the identifaction of low-temperature alteration processes in hydrothermal ore deposits, where biogenic and abiogenic redox processes potentially lead to significant isotope fractionations as already has been demonstrated in Sect. 2.13, 2.14 and 2.18, for Fe, Cu and Mo isotopes.

3.5 Hydrosphere

First, some definitions concerning water of different origin are given. The term **"meteoric"** applies to water that has been part of the meteorological cycle, and participated in processes such as evaporation, condensation, and precipitation. All continental surface waters, such as rivers, lakes, and glaciers, fall into this general category. Because meteoric water may seep into the underlying rock strata, it will also be found at various depths within the lithosphere dominating all types of continental ground waters. The **ocean**, although it continuously receives the continental run-off of meteoric waters as well as rain, is not regarded as being meteoric in nature. **Connate** water is water, which has been trapped in sediments at the time of burial. **Formation** water is present in sedimentary rocks and may be a useful nongenetic term for waters of unknown origin and age within these rocks.

3.5.1 Meteoric Water—General Considerations

When water evaporates from the surface of the ocean, the water vapor is enriched in H and ^{16}O because $H_2^{16}O$ has a higher vapor pressure than HDO and $H_2^{18}O$ (Table 1.1). Under equilibrium conditions at 25 °C, the fractionation factors for evaporating water

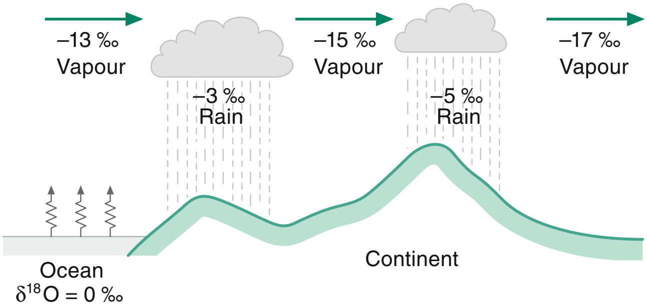

Fig. 3.15 Schematic O-isotope fractionation of water in the atmosphere (Fig. 3.14, 6th edition, p. 137)

are 1.0092 for ^{18}O and 1.074 for D (Craig and Gordon 1965). However, under natural conditions, the actual isotopic composition of water is more negative than the predicted equilibrium values due to kinetic effects (Craig and Gordon 1965). Vapor leaving the surface of the ocean cools as it rises and rain forms when the dew point is reached. During removal of rain from a moist air mass, the residual vapor is continuously depleted in the heavy isotopes, because the rain leaving the system is enriched in ^{18}O and D. If the air mass moves poleward and becomes cooler, additional rain formed will contain less ^{18}O than the initial rain. This relationship is schematically shown in Fig. 3.15. The isotope composition of mean world-wide precipitation is estimated to be δD = −22 and δ^{18}O = −4 ‰ (Craig and Gordon 1965).

The theoretical approaches to explain isotope variations in meteoric waters evolved from the "isolated air mass" models, which are based on Rayleigh condensation, with immediate removal of precipitation and with a part of the condensate being kept in the cloud during the rain-out process. Isotope studies of individual rain events have revealed that successive portions of single events may vary drastically (Rindsberger et al. 1990). Quite often the pattern is "V-shaped", a sharp decrease of δ-values is usually observed at the beginning of a storm with a minimum somewhere in the middle of the event. The most depleted isotope values usually correspond to the period of most intense rain with little evaporation experienced by individual rain drops. It has also been observed that convective clouds produce precipitation with higher δ-values than stratiform clouds. Thus, the isotope composition of precipitation from a given rain event depends on meteorological history of the air mass in which the precipitation is produced and the type of cloud through which it falls. Liquid precipitation (rain) and solid precipitation (snow, hail) may differ in their isotope composition insofar as rain drops may undergo evaporation and isotope exchange with atmospheric vapor on their descent to the surface. By analyzing hailstones, discrete meteorological events can be studied because hailstones keep a record on the internal structure of a cloud. Jouzel et al. (1975) concluded that hailstones grow during a succession of upward and downward movements in a cloud.

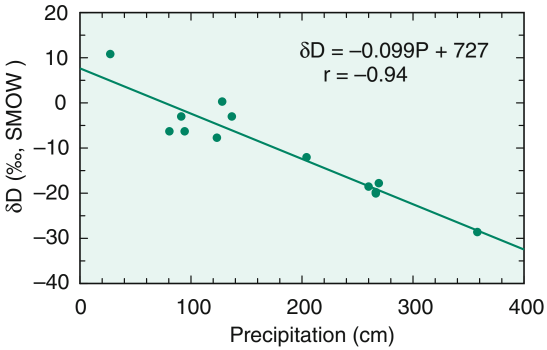

Fig. 3.16 Average δD-values of the annual precipitation from oceanic islands as a function of the amount of annual rainfall. The island stations are distant from continents, within 30° of the equator and at elevations less than 120 m (after Lawrence and White 1991) (Fig. 3.15 6th edition, p. 138)

The International Atomic Energy Agency (IAEA) conducts a world-wide survey of the isotope composition of monthly precipitation for more than 50 years. The global distribution of D and ^{18}O in rain has been monitored since 1961 through a network of stations (Yurtsever 1975). From this extensive data base it can be deduced how geographic and meteorological factors (rainout, temperature, humidity) influence the isotopic composition of precipitation.

The first detailed evaluation of the equilibrium and non-equilibrium factors that determine the isotopic composition of precipitation was published by Dansgaard (1964). He demonstrated that the observed geographic distribution in isotope composition is related to a number of environmental parameters that characterize a given sampling site, such as latitude, altitude, distance to the coast, amount of precipitation, and surface air temperature. Out of these, two factors are of special significance: temperature and the amount of precipitation. As shown in Fig. 3.16, the best temperature correlation is observed in continental regions nearer to the poles, whereas the correlation with amount of rainfall is most pronouced in tropical regions (Lawrence and White 1991). The apparent link between local surface air temperature and the isotope composition of precipitation is of special interest mainly because of the potential importance of stable isotopes as palaeoclimatic indicators. The amount effect is ascribed to gradual saturation of air below the cloud, which diminishes any shift to higher δ^{18}O-values caused by evaporation during precipitation (Fricke and O'Neil 1999)

A compilation of studies throughout the world's mountain belts has revealed a consistent and linear relationship between change in the isotopic composition of precipitation and change in elevation (Poage and Chamberlain 2001). The isotopic composition of precipitation decreases linearly with increasing elevation by about 0.28 ‰/100 m in most regions of the world except in the Himalayas and at elevations above 5000 m.

3.5.1.1 δD - δ^{18}O Relationship, Deuterium (D) - Excess

In all processes concerning evaporation and condensation, hydrogen isotopes are fractionated in proportion to oxygen isotopes, because a corresponding difference in vapor pressures exists between H_2O and HDO in one case and $H_2^{16}O$ and $H_2^{18}O$, in the other. Therefore, hydrogen and oxygen isotope distributions are correlated in meteoric waters. Craig (1961a) first defined the following relationship:

$$\delta D = 8\ d^{18}O + 10$$

which is generally known as the "Global Meteoric Water Line".

Dansgaard (1964) introduced the concept of "deuterium excess", d defined as $d = \Delta d - 8\ \delta^{18}O$. Neither the numerical coefficient, 8, nor the deuterium excess, d, are really constant, both depend on local climatic processes. The long term arithmetic mean for all analyzed stations of the IAEA network (Rozanski et al. 1993) is:

$$\delta D = (8.17 \pm 0.06)\ \delta^{18}O + (10.35 \pm 0.65) \quad r^2 = 0.99, \quad n = 206$$

Relatively large deviations from the general equation are evident when monthly data for individual stations are considered (Table 3.1). In an extreme situation, represented by the St. Helena station, a very poor correlation between δD and $\delta^{18}O$ exists. At this station, it appears that all precipitation comes from nearby sources and represents the first stage of the rain-out process. Thus, the generally weaker correlations for the marine stations (Table 3.1) may reflect varying contributions of air masses with different source characteristics and a low degree of rain-out.

Table 3.1 Variations in the numerical constant and the deuterium excess for selected stations of the IAEA global network (Rozanski et al. 1993)

Station	Numerical constant	Deuterium excess	r^2
Continental and coastal stations			
Vienna	7.07	−1.38	0.961
Ottawa	7.44	+5.01	0.973
Addis Ababa	6.95	+11.51	0.918
Bet Dagan,Israel	5.48	+6.87	0.695
Izobamba(Ecuador)	8.01	+10.09	0.984
Tokyo	6.87	+4.70	0.835
Marine Stations			
Weathership E (N.Atlantic)	5.96	+2.99	0.738
Weathership V (N.Pacific)	5.51	−1.10	0.737
St.Helena (S.Atlantic)	2.80	+6.61	0.158
Diego Garcia Isl.(Indian Oc.)	6.93	+4.66	0.880
Midway Isl. (N.Pacific)	6.80	+6.15	0.840
Truk Isl.(N.Pacific)	7.07	+5.05	0.940

The imprint of local conditions can also be seen at other coastal and continental stations. The examples in Table 3.1 demonstrate that varying influences of different sources of vapor with different isotope characteristics, different air mass trajectories, or evaporation and isotope exchange processes below the cloud base, may often lead to much more complex relationships at the local level between δD and $\delta^{18}O$ than suggested for the regional or continental scale by the global "Meteoric Water Line" equation.

Knowledge about the isotopic variations in precipitation is increased when single rain events are analyzed from local stations. Especially under mid-latitude weather conditions, such short-term variations arise from varying contributions of tropical, polar, marine, and continental air masses.

The d-excess in oceanic water vapour is determined by evaporative conditions (surface temperature, relative humidity, wind speed) (e.g. Merlivat and Jouzel 1979). Deuterium excess over the oceans increases when humidity over the ocean decreases. Thus, reduced d-excess values in Antartic ice cores have been interpreted as indicators of higher relative humidity in the oceanic source area providing the moisture for Antarctic precipitation (Jouzel et al. 1982). Later Johnsen et al. (1989), followed by others, showed that besides humidity temperatures in the source regions also have an effect on the size of the d-excess.

Deuterium excess profiles from Greenland and Antarctic ice cores show well defined climatic changes being negatively correlated with $\delta^{18}O$-values. Combining $\delta^{18}O$-values with deuterium excess values, temperature estimates at the site of precipitation and at the source region of the moisture can be achieved (Masson-Delmotte et al. 2005).

3.5.1.2 $\delta^{17}O$-$\delta^{18}O$ Relationships, ^{17}O Excess

It has been common belief for many years that the ^{17}O abundance in meteoric waters carries no additional information to that of ^{18}O. Although mass-independent fractionations are not known to occur in water, $H_2^{17}O$ is a useful tracer within the hydrologic cycle (Angert et al. 2004). As already demonstrated the isotopic composition of water is controlled by two mass-dependent processes. (i) the equilibrium fractionation that is caused by the different vapour pressures of $H_2^{17}O$ and $H_2^{18}O$ and (ii) the kinetic fractionation that is caused by the different diffusivities of $H_2^{17}O$ and $H_2^{18}O$ during transport in air. Angert et al. (2004) have demonstrated that for kinetic water transport in air, the slope in a $\delta^{17}O$-$\delta^{18}O$ diagram is 0.511, whereas it is 0.526 for equilibrium effects. Similar values have been given by Barkan and Luz (2007).

Improvements in analytical techniques allow to measure $\delta^{17}O$ and $\delta^{18}O$ with a precision of a few 0.01 ‰ which permits calculation of $\Delta^{17}O$ with similar precision and thus the detection of very small $\delta^{17}O$ variations.

Similar to the deuterium excess, the deviation from an expected $^{17}O/^{16}O$ – $^{18}O/^{16}O$ relationship has been defined as ^{17}O excess (Barkan and Luz 2007)

$$^{17}\text{O excess} = \ln(\delta^{17}\text{O} + 1) - 0.528\ \ln(\delta^{18}\text{O} + 1)$$

Atmospheric vapor collected above the ocean shows the existence of a small ^{17}O excess and a negative correlation between ^{17}O excess and relative humidity. The ^{17}O excess originates from evaporation of sea water into marine air that is undersaturated in water vapor and from the transfer of vapor to liquid water or snow (Luz and Barkan 2010).

^{17}O-excess is thus a unique tracer, which is, in contrast to the deuterium excess, temperature independent and which may give additional informations on humidity relations. Glacial-interglacial ^{17}O records from ice cores in Antarctica (Landais et al. 2008; Uemura et al. 2010) reveal small shifts in ^{17}O excess from low values in glacial periods to high values in interglacial periods.

Last not least, it should be noted that d-excess and ^{17}O excess have different definitions: while d-excess is defined in a linear scale, ^{17}O excess is in a logarithm scale.

3.5.1.3 Meteoric Waters in the Past

Assuming that the H- and O-isotope compositions and temperatures of ancient ocean waters are comparable to present-day values, the isotopic composition of ancient meteoric waters may have been governed by relations similar to those existing presently. However, given the local complexities, the application of this relationship back through time should be treated with caution. To date, however, there is no compelling evidence that the overall systematics of ancient meteoric waters were very different from the present meteoric water relationship (Sheppard 1986). If the isotope composition of ocean water has changed with time, but global circulation patterns were like today, the "meteoric water line" at a specific time would be parallel to the modern meteoric water line, that is the slope would remain at a value of 8, but the intercept would be different.

The systematic behavior of stable isotopes in precipitation as a function of altitude can be used to provide estimates of paleoaltitude. For paleoelevation reconstruction the isotope relationship between precipitation and elevation must be quantitatively known or assumed. In this approach the isotopic composition of paleoprecipitation is determined from the analysis of in situ formed authigenic minerals (Chamberlain and Poage 2000; Blisnink and Stern 2005 and others). The effect of topography on the isotopic composition of precipitation is most straightforward in temperate mid-latitude regions and in topographically and climatically simple settings and varies generally between 2 and 5 ‰ per 1 km. Paleoelevation can be also reconstructed by using clumped isotope thermometry (Huntington et al. 2010; Quade et al. 2011).

3.5.2 Ice Cores

The isotopic composition of snow and ice deposited in polar regions and at high elevations in mountains depend primarily on temperature. Snow deposited during the summer has less negative δ^{18}O and δD-values than snow deposited during the winter. A good example of the seasonal dependence has been given by Deutsch et al. (1966) on an Austrian glacier, where the mean δD-difference between winter and summer snow was observed to be −14 ‰. This seasonal cycle has been used to determine the annual stratigraphy of glaciers and to provide short-term climatic records. However, alteration of the snow and ice by seasonal meltwater can result in changes of the isotopic composition of the ice, thus biasing the historical climate record. Systematic isotope studies also have been used to study the flow patterns of glaciers. Profiles through a glacier should exhibit lower isotope ratios at depth than nearer the surface, because deep ice may have originated from locations upstream of the ice-core site, where temperatures should be colder.

In the last decades, several ice cores over 1000 m depth have been recovered from Greenland and Antarctica. In these cores, seasonal variations are generally observed only for the uppermost portions. After a certain depth, which depends on accumulation rates, seasonal variations disappear completely and isotopic changes reflect long-term climatic variations. No matter how thin a sample one cuts from the ice core, its isotope composition will represent a mean value of several years of snow deposition.

The most recent ice cores—investigated in great detail by large groups of researchers—are the Vostok core from East Antarctica (Lorius et al. 1985; Jouzel et al. 1987) and the GRIP and GISP 2 cores from Greenland (Dansgaard et al. 1993; Grootes et al. 1993). In the Vostok core, the low accumulation rate of snow in Antarctica results in very thin annual layers, which means that climate changes of a century or less are difficult to resolve. The newer Greenland ice cores GRIP and GISP 2 were drilled in regions with high snow accumulation near the centre of the Greenland ice sheet. In these cores it is possible to resolve climate changes on the timescale of decades or less, even though they occurred a hundred thousand years ago. The GRIP and GISP 2 data indicate a dramatic difference between our present climate and the climate of the last interglacial period. Whereas the present interglacial climate seems to have been very stable over the last 10,000 years, the early and late parts of the last interglacial (c.135,000 and c.115,000 years before present, respectively) were characterized by rapid fluctuations between temperatures, both warmer and very much colder than the present. It apparently took only a decade or two to shift between these very different climatic regimes.

Figure 3.17 compares $\delta^{18}O$ profiles from Antarctica and Greenland. The dramatic δ-shifts observed in Greenland cores are less pronounced in the δ-record along the Vostok core, probably because the shifts in Greenland are connected to rapid ocean/atmosphere circulation changes in the North Atlantic (for more details, see 3.12.1).

3.5.3 Groundwater

In temperate and humid climates the isotopic composition of groundwater is similar to that of the precipitation in the area of recharge (Gat 1971). This is strong evidence for direct meteoric recharge to an aquifer. The seasonal variation of all

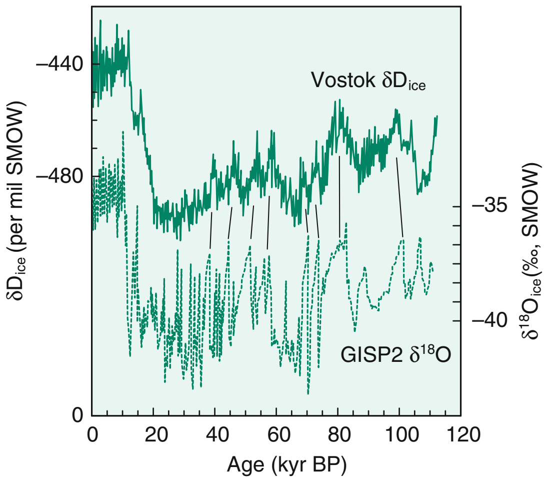

Fig. 3.17 Correlations of δD and δ^{18}O values of Greenland (GISP-2) and Antarctic (Vostok) ice cores covering the last glacial-interglacial cycles (http://www.gisp2.sr.unh.edu/GISP2/DATA/Bender.html) (Fig. 3.16, 6th edition, p. 142)

meteoric water is strongly attenuated during transit and storage in the ground. The degree of attenuation varies with depth and with surface and bedrock geologic characteristics, but in general deep groundwaters show no seasonal variation in δD and δ^{18}O values and have an isotopic composition close to amount-weighted mean annual precipitation values.

The characteristic isotope fingerprint of precipitation provides an effective means for identifying possible groundwater recharge areas and hence subsurface flow paths. For example, in areas close to rivers fed from high altitudes, groundwaters represent a mixture of local precipitation and high-altitude low-^{18}O waters. In suitable cases, quantitative estimates about the fraction of low-^{18}O river water in the groundwater can be carried out as a function of the distance from the river.

The main mechanisms that can cause variations between precipitation and recharged groundwater are (Gat 1971):

(1) recharge from partially evaporated surface water bodies,

(2) recharge that occurred in past periods of different climate when the isotopic composition of precipitation was different from that at present,

(3) isotope fractionation processes resulting from differential water movement through the soil or the aquifer or due to kinetic or exchange reactions within geologic formations.

In semi-arid or arid regions, evaporative losses before and during recharge shift the isotopic composition of groundwater towards higher δ-values. Furthermore, transpiration of shallow groundwater through plant leaves, may also be an important evaporation process. Detailed studies of soil moisture evaporation have shown that evaporation loss and isotopic enrichment are greatest in the upper part of the soil profile and are most pronounced in unvegetated soils (Welhan 1987). In some arid regions, groundwater may be classified as paleowaters, which were recharged under different meteorological conditions than present in a region today and which imply ages of water of several thousand years. Gat and Issar (1974) have demonstrated that the isotopic composition of such paleowaters can be distinguished from more recently recharged groundwaters, which have been experienced some evaporation.

In summary, the application of stable isotopes to groundwater studies is based on the fact that the isotopic composition of water behaves conservatively in low-temperature environments where water-rock contact times are short relative to the kinetics of mineral-water isotope exchange reactions.

3.5.4 Isotope Fractionations During Evaporation

In an evaporative environment, one could expect to find extreme enrichments in the heavy isotopes D and^{18}O. However, this is generally not the case. Taking the Dead Sea as the typical example of an evaporative system, Fig. 3.18 shows only moderately enriched δ^{18}O-values and even to an even lesser degree δD-values (Gat 1984). Isotope fractionations accompanying evaporation are rather complex and can be best described by subdividing the evaporation process into several steps (Craig and Gordon 1965):

(a) the presence of a saturated sublayer of water vapor at the water-atmosphere interface, which is depleted in the heavy isotopes,

(b) the migration of vapor away from the boundary layer, which results in further depletion of heavy isotopes in the vapor due to different diffusion rates,

(c) the vapor reaching a turbulent region where mixing with vapor from other sources occurs, and

(d) the vapor of the turbulent zone then condensing and back-reacting with the water surface.

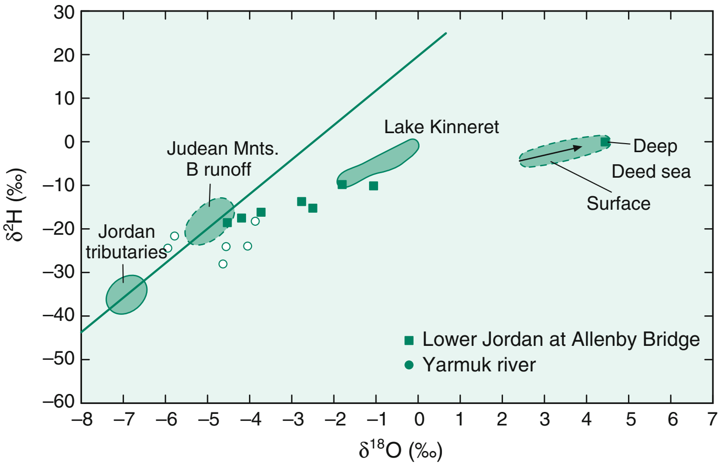

Fig. 3.18 δD versus δ^{18}O values of the Dead Sea and its water sources as an example of an evaporative environment (after GAT 1984) (Fig. 3.17, 6th edition, p. 144)

This model qualitatively explains the deviation of isotopic compositions away from the "Meteoric Water Line" because molecular diffusion adds a non-equilibrium fractionation term and the limited isotopic enrichment occurs as a consequence of molecular exchange with atmospheric vapor. It is mainly the humidity which controls the degree of isotope enrichment. Only under very arid conditions, and only in small water bodies, really large enrichments in D and ^{18}O are observed. For example, Gonfiantini (1986) reported a δ^{18}O-value of +31.3 ‰ and a δD-value of +129 ‰ for a small, shallow lake in the western Sahara.

3.5.5 Ocean Water

The isotopic composition of ocean water has been discussed in detail by Craig and Gordon (1965), and Broecker (1974). It is governed by fractionation during evaporation and sea-ice formation and by the isotope content of precipitation and runoff entering the ocean.

Ocean water with 3.5 % salinity exhibits a very narrow range in isotopic composition. There is, however, a strong correlation with salinity because evaporation, which increases salinity, also concentrates ^{18}O and D. Low salinities, which are caused by freshwater and meltwater dilution, correlate with low D and ^{18}O concentrations. As a consequence modern ocean waters plot along two trends that meet at an inflection point where salinity is 3.55 % and δ^{18}O is 0.5 ‰ (Fig. 3.19).

The high-salinity trend represents areas where evaporation exceeds precipitation and its slope is determined by the volume and isotopic composition of the local precipitation and the evaporating water vapor. However, isotope enrichments due to evaporation are limited in extent, because of back-exchange of atmospheric moisture with the evaporating fluid. The slope of the low salinity trend (see

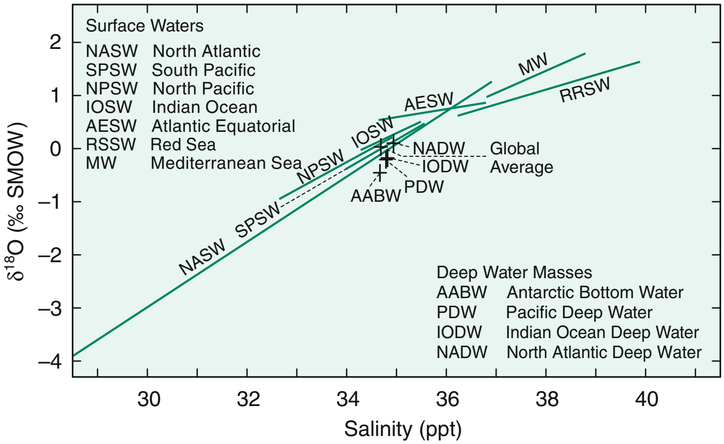

Fig. 3.19 Salinity versus δ^{18}O relationships in modern ocean surface and deep waters (after Railsback et al. 1989) (Fig. 3.18, 6th edition, p. 145)

Fig. 3.19) extrapolates to a freshwater input of about −21 ‰ for $\delta^{18}O$ at zero salinity, reflecting the influx of high-latitude precipitation and glacial meltwater. This δ-value is, in all probability, not typical of freshwater influx in non-glacial periods. Thus, the slope of the low salinity trend may have changed through geologic time.

Delaygue et al. (2000) have modeled the present day ^{18}O distribution in the Atlantic and Pacific Ocean and its relationship with salinity (see Fig. 3.20). A good agreement is found between observed and simulated $\delta^{18}O$ values using an oceanic circulation model. As shown in Fig. 3.20 the Atlantic Ocean is enriched by more than 0.5 ‰ relative to the Pacific Ocean, but both ocean basins show the same general patterns with high ^{18}O-values in the sub-tropics and lower values at high latitudes.

Another important question concerning the isotopic composition of ocean water is how constant its isotopic composition has been throughout geological history. This remains an area of ongoing controversy in stable isotope geochemistry (see sect. 3.8). Short-term fluctuations in the isotope composition of sea water must arise during glacial periods. If all the present ice sheets in the world were melted, the $\delta^{18}O$-value of the ocean would be lowered by about 1 ‰. By contrast, Fairbanks (1989) has calculated an ^{18}O-enrichment of 1.25 ‰ for ocean water during the last maximum glaciation.

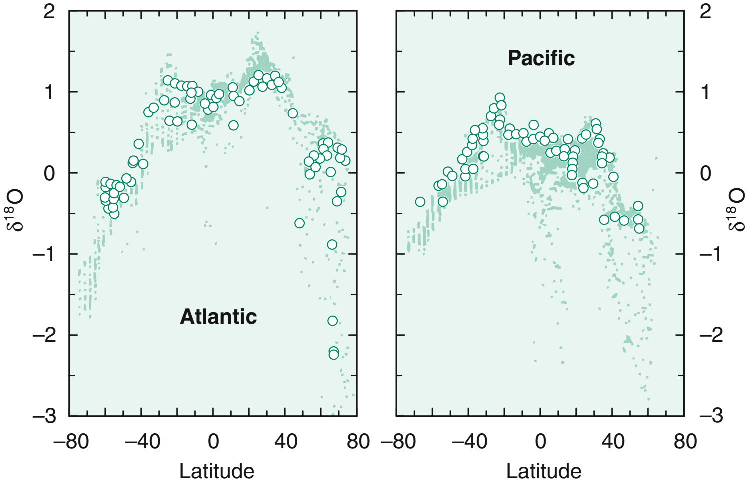

Fig. 3.20 Comparison of measured and modeled $\delta^{18}O$ values of surface ocean waters. Characteristic features are: tropical maxima, equatorial low- and high-latitude minima, enrichment of the Atlantic relative to the Pacific (after Delaygue et al. 2000) (Fig. 3.19, 6th edition, p. 146)

3.5.6 Pore Waters

In the marine environment oxygen and hydrogen isotope compositions of pore waters may be inherited from ocean water or influenced by diagenetic reactions in the sediment or underlying basement. Knowledge of the chemical composition of sedimentary pore waters has increased considerably since the beginning of the Deep-Sea-Drilling-Project. From numerous drill sites, similar depth-dependent trends in the isotopic composition have been observed.

For oxygen this means a decrease in ^{18}O from an initial δ-value very near 0 ‰ (ocean water) to about −2 ‰ at depths around 200 m (Perry et al. 1976; Lawrence and Gieskes 1981; Brumsack et al. 1992). Even lower $\delta^{18}O$-values of about −4 ‰ at depths of around 400 m have been observed by Matsumoto (1992). This decrease in ^{18}O is mainly due to the formation of authigenic ^{18}O-enriched clay minerals such as smectite from alteration of basaltic material and volcanic ash. Other diagenetic reactions include recrystallization of biogenic carbonates, precipitation of authigenic carbonates and transformation of biogenic silica (opal-A) through opal-CT to quartz. The latter process, however, tends to increase $\delta^{18}O$-values of the water. Material balance calculations by Matsumoto (1992) have indicated that the ^{18}O-shift towards negative δ-values is primarily controlled by low-temperature alteration of basement basalts, which is slightly compensated by the transformation of biogenic opal to quartz.

D/H ratios may also serve as tracers of alteration reactions. Alteration of basaltic material and volcanic ash should increase δD-values of pore waters because the hydroxyl groups in clay minerals incorporate the light hydrogen isotope relative to water. However, measured δD-values of pore waters generally decrease from seawater values around 0 ‰ at the core tops to values that are 15–25 ‰ lower, with a good correlation between δD and $\delta^{18}O$. This strong covariation suggests that the same process is responsible for the D and ^{18}O depletion observed in many cores recovered during DSDP/ODP drilling. Quite a different process has been suggested by Lawrence and Taviani (1988) to explain the depth-dependent decrease in porewater δD-values. They proposed oxidation of local organic matter or oxidation of biogenic or mantle methane. Lawrence and Taviani (1988) favored the oxidation of mantle methane, or even hydrogen, noting that oxidation of locally-derived organic compounds may not be feasible because of the excessive quantity of organic material required. In conclusion, the depletion of D in porewaters is not clearly understood.

3.5.7 Formation Water

Formation waters are saline with salt contents ranging from ocean water to very dense Ca–Na–Cl brines. Their origin and evolution are still controversial, because the processes involved in the development of saline formation waters are complicated by the extensive changes that have taken place in the brines after sediment deposition.

Oxygen and hydrogen isotopes are a powerful tool in the study of the origin of subsurface waters. Prior to the use of isotopes, it was generally assumed that most of the formation waters in marine sedimentary rocks were of connate marine origin. This widely held view was challenged by Clayton et al. (1966), who demonstrated that waters from several sedimentary basins were predominantly of local meteoric origin.

Although formation waters show a wide range in isotopic composition, waters within a sedimentary basin are usually isotopically distinct. As is the case with surface meteoric waters, there is a general decrease in isotopic composition from low to high latitude settings (Fig. 3.21). Displacements of δD and δ^{18}O-values from the Meteoric Water Line (MWL) are very often correlated with salinity: the most depleted waters in D and^{18}O are usually the least saline, fluids most distant from the MWL tend to be the most saline.

Presently, in the view of numerous subsequent studies, (i.e. Hitchon and Friedman 1969; Kharaka et al. 1974; Banner et al. 1989; Connolly et al. 1990; Stueber and Walter 1991), it is obvious that basin subsurface waters have complicated histories and frequently are mixtures of waters with different origins. As was proposed by Knauth and Beeunas (1986) and Knauth (1988), formation waters in sedimentary basins may not require complete flushing by meteoric water, but

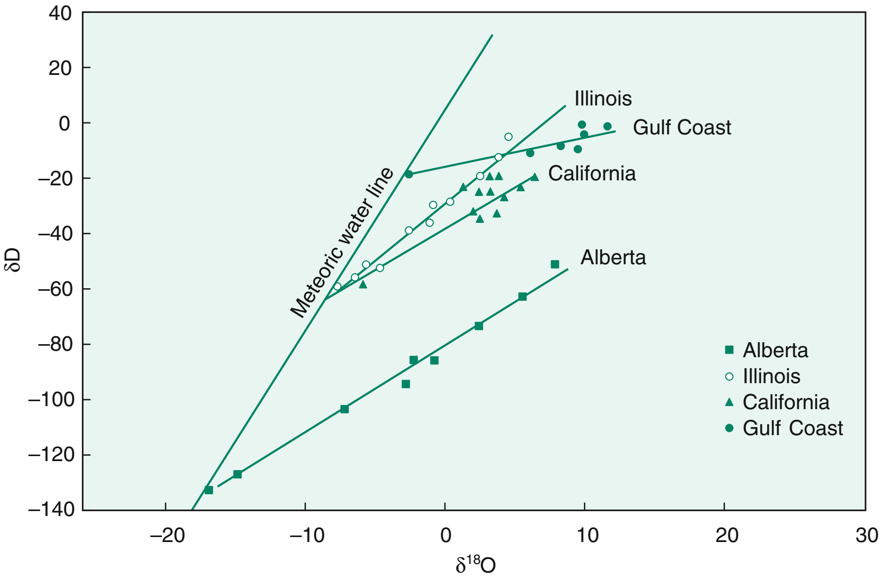

Fig. 3.21 δD versus δ^{18}O values for formation waters from the midcontinental region of the United States (after Taylor 1974) (Fig. 3.20, 6th edition, p. 148)

instead can result from mixing between meteoric water and the remnants of original connate waters.

The characteristic $\delta^{18}O$ shift observed in formation waters may be due to isotopic exchange with ^{18}O-rich sedimentary minerals, particularly carbonates. The δD-shift is less well understood, possible mechanisms for D-enrichment are (i) fractionation during membrane filtration, and/or (ii) exchange with H_2S, hydrocarbons and hydrous minerals. (i) It is well known that shales and compacted clays can act as semipermeable membranes which prevent passage of ions in solution while allowing passage of water (ultrafiltration). Coplen and Hanshaw (1973) have shown experimentally that ultrafiltration may be accompanied by hydrogen and oxygen isotope fractionation. However, the mechanism responsible for isotopic fractionation is poorly understood. Phillips and Bentley (1987) proposed that fractionation may result from increased activity of the heavy isotopes in the membrane solution, because high cation concentrations increase hydration sphere fractionation effects. (ii) Hydrogen isotope exchange between H_2S and water will occur in nature, but probably will not be quantitatively important. Due to the large fractionation factor between H_2S and H_2O, this process might be significant on a local scale. Isotope exchange with methane or higher hydrocarbons will probably not be important, because exchange rates are extremely low at sedimentary temperatures.

Somewhat unusual isotopic compositions have been observed in highly saline deep waters from Precambrian crystalline rocks as well as in deep drill holes, which plot above or to the left of the Meteoric Water Line (Frape et al. 1984; Kelly et al. 1986; Frape and Fritz 1987). There are two major theories about the origin of these Ca-rich brines.

(a) the brines represent modified Paleozoic seawater or basinal brines (Kelly et al. 1986),

(b) the brines are produced by leaching of saline fluid inclusions in crystalline rocks or by intense water/rock interactions (Frape and Fritz 1987).

Since then quite a number of studies have indicated that the unusual composition is a wide-spread phenomenon in low-permeability fractured rocks with slow water movement and not too high temperatures. Kloppman et al. (2002) summarized the existing data base of 1300 oxygen and hydrogen isotope analyses from crystalline rocks and suggested that the isotope shift to the left side can be explained by seawater which has dissolved and precipitated fracture minerals and subsequently been diluted by meteoric waters. Bottomley et al. (1999) argued that the extremely high concentrations of chloride and bromide in the brines make crystalline host rocks a less likely source for the high salinities. By measuring Li-isotopes these authors postulated that the brines in crystalline rocks share a common marine origin.

Table 3.2 Experimentally determined fractionation factors of salt minerals and their corrections using "salt effect" coefficients (after Horita 1989)

Mineral	Chemical formula	T° C	αD	$αD_{(corr)}$	$α^{18}O$	$α^{18}O_{(corr)}$
Borax	$Na_2B_4O_7 \times 10\ H_2O$	25	1.005	1.005	–	–
Epsomite	$MgSO_4 \times 7\ H_2O$	25	0.999	0.982	–	–
Gaylussite	$Na_2CO_3 \times CaCO_3 \times 5\ H_2O$	25	0.987	0.966	–	–
Gypsum	$CaSO_4 \times 2\ H_2O$	25	0.980	0.980	1.0041	1.0041
Mirabilite	$Na_2SO_4 \times 10\ H_2O$	25	1.017	1.018	1.0014	1.0014
Natron	$Na_2CO_3 \times 10\ H_2O$	10	1.017	1.012	–	–
Trona	$Na_2CO_3 \times NaHCO_3 \times 2\ H_2O$	25	0.921	0.905	–	–

3.5.8 Water in Hydrated Salt Minerals

Many salt minerals have water of crystallization in their crystal structure. Such water of hydration can provide information on the isotope compositions and/or temperatures of brines from which the minerals were deposited. To interpret such isotope data, it is necessary to know the fractionation factors between the hydration water and the solution from which they are deposited. Several experimental studies have been made to determine these fractionation factors (Matsuo et al. 1972; Matsubaya and Sakai 1973; Stewart 1974; Horita 1989). Because most saline minerals equilibrate only with highly saline solutions, the isotopic activity and isotopic concentration ratio of water in the solution are not the same (Sofer and Gat 1972). Most studies determined the isotopic concentration ratios of the source solution and as Horita (1989) demonstrated, these fractionation factors have to be corrected using the "salt effect" coefficients when applied to natural settings (Table 3.2).

3.6 The Isotopic Composition of Dissolved and Particulate Compounds in Ocean and Fresh Waters

The following chapter will discuss the carbon, nitrogen, oxygen and sulfur isotope composition of dissolved and particulate compounds in ocean and fresh waters. Investigations of non-traditional isotope systems in recent years have demonstrated that chemical weathering is a complex process that may induce large isotope fractionations. The weathering of silicates rarely result in the dissolution of the initial mineral, but instead in the formation of secondary minerals with isotopic compositions that differ from the initial mineral. The isotopic compositions of released components in waters of different origins depend on a variety of processes such as the composition of the minerals which have been weathered, the inorganic or organic nature of the precipitation process, and exchange with atmospheric gases. Of special importance are biological processes acting mainly in surface waters, which tend to deplete certain elements such as carbon, nitrogen and silicon in surface waters by biological uptake, and which subsequently are returned at depth by oxidation and dissolution processes.

3.6.1 Carbon Species in Water

3.6.1.1 Bicarbonate in Ocean Water

In addition to organic carbon, four other carbon species exist in natural water: dissolved CO_2, H_2CO_3, HCO_3^- and CO_3^{2-}, all of which tend to equilibrate as a function of temperature and p_H. HCO_3^- is the dominant C-bearing species in ocean water. The first global $\delta^{13}C$ measurements of dissolved inorganic carbon (DIC) were published by Kroopnick et al. (1972) and Kroopnick (1985) within the geochemical ocean sections study (GEOSECS). These studies have yielded a global average $\delta^{13}C$-value of 1.5 ‰ with a variation range of ±0.8 ‰ with the least variations at equatorial regions and greater variability at higher latitudes.

The distribution of $\delta^{13}C$-values with water depth is mainly controlled by biological processes: Conversion of CO_2 into organic matter removes ^{12}C resulting in a ^{13}C enrichment of the residual DIC. In turn, the oxidation of organic matter releases

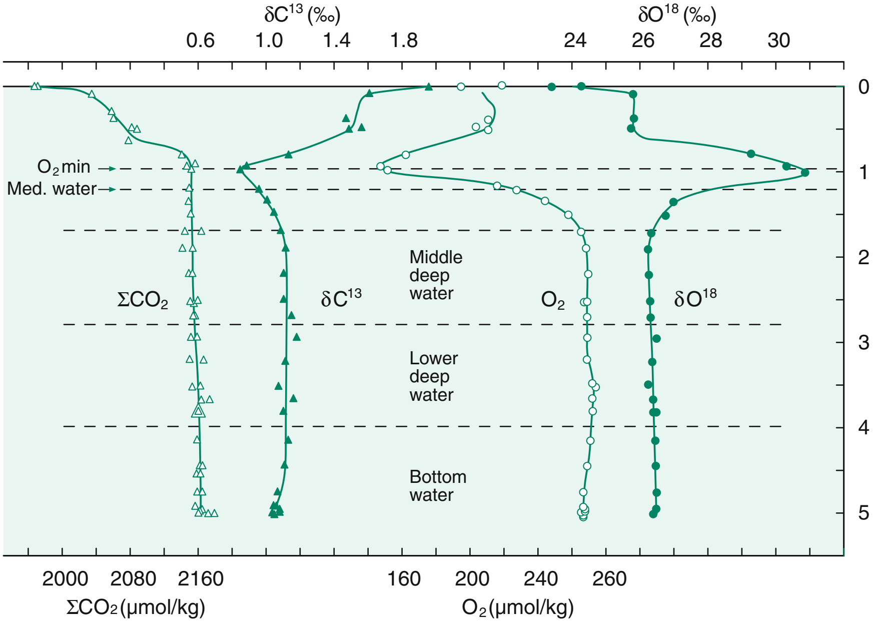

Fig. 3.22 Vertical profiles of dissolved CO_2, $\delta^{13}C$, dissolved O_2 and $\delta^{18}O$ in the North Atlantic (Kroopnick et al. 1972) (Fig. 3.21, 6th edition, p. 151)

^{12}C-enriched carbon back into the inorganic reservoir, which results into a depth-dependent isotope profile. A typical example is shown in Fig. 3.22.

North Atlantic Deep Water (NADW), which is formed with an initial δ^{13}C-value between 1.0 and 1.5 ‰, becomes gradually depleted in ^{13}C as it travels southward and mixes with Antarctic bottom water, which has an average δ^{13}C-value of 0.3 ‰ (Kroopnick 1985). As this deep water travels to the Pacific Ocean, its ^{13}C/^{12}C ratio is further reduced by 0.5 ‰ by the continuous flux and oxidation of organic matter in the water column. This is the basis for using δ^{13}C-values as a tracer of paleo-oceanographic changes in deep water circulation (e.g. Curry et al.1988).

The uptake of anthropogenic CO_2 by the ocean is a crucial process for the carbon cycle, resulting in changes of the δ^{13}C-value of dissolved oceanic bicarbonate (Quay et al. 1992; Bacastow et al. 1996; Gruber 1998; Gruber et al. 1999; Sonnerup et al. 1999). Quay et al. (1992) first demonstrated that the δ^{13}C-value of dissolved bicarbonate in the surface waters of the Pacific has decreased by about 0.4 ‰ between 1970 and 1990. If this number is valid for the ocean as a whole, it would allow a quantitative estimate for the net sink of anthropogenically produced CO_2. Recent studies estimate that the Earth's ocean has absorbed around 50 % of the CO_2 emitted over the industrial period (Mikaloff-Fletcher et al. 2006).

3.6.1.2 Particulate Organic Matter (POM)

POM in the ocean originates largely from plankton in the euphotic zone and reflects living plankton populations. Between 40°N and 40°S δ^{13}C of POM varies between −18.5 and −22 ‰. In cold Arctic waters δ^{13}C-values are on average −23.4 ‰ and in high latitude southern ocean δ^{13}C are even lower with values between −24 and −36 ‰ (Goericke and Fry 1994). As POM sinks, biological reworking changes its chemical composition, the extent of this reworking depends on the residence time in the water column. Most POM profiles described in the literature exhibit a general trend of surface isotopic values comparable to those for living plankton, with δ^{13}C-values becoming increasingly lower with depth. Jeffrey et al. (1983) interpreted this trend as the loss of labile, ^{13}C-enriched amino acids and sugars through biological reworking which leaves behind the more refractory, isotopically light lipid components.

C/N ratios of POM increase with depth of the water column consistent with preferential loss of amino acids. This implies that nitrogen is more rapidly lost than carbon during degradation of POM, which is the reason for the much greater variation in δ^{15}N-values than in δ^{13}C-values (Saino and Hattori 1980; Altabet and McCarthy 1985).

3.6.1.3 Carbon Isotope Composition of Pore Waters

Initially the pore water at the sediment/water interface has a δ^{13}C-value near that of sea water. In sediments, the decomposition of organic matter consumes oxygen and releases isotopically light CO_2 to the pore water, while the dissolution of $CaCO_3$ adds CO_2 that is isotopically heavy. The carbon isotope composition of pore waters at a given locality and depth should reflect modification by the interplay of these

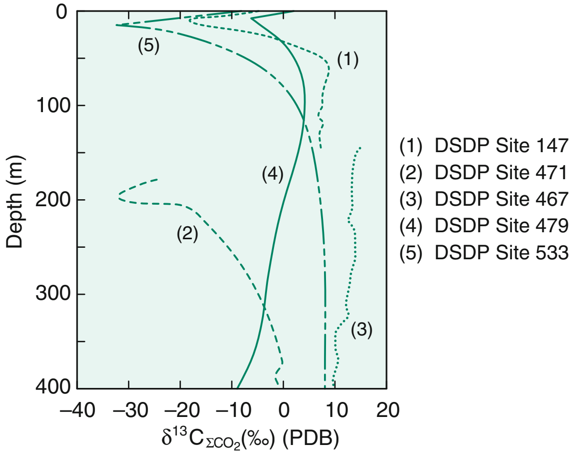

Fig. 3.23 δ^{13}C records of total dissolved carbon from pore waters of anoxic sediments recovered in various DSDP sites (after Anderson and Arthus 1983) (Fig. 3.22, 6th edition, p. 152)

two processes. The net result is to make porewaters isotopically lighter than the overlying bottom water (Grossman 1984). McCorkle et al. (1985) and McCorkle and Emerson (1988) have shown that steep gradients in porewater δ^{13}C-values exist in the first few centimeters below the sediment-water interface. The observed δ^{13}C-profiles vary systematically with the "rain" of organic matter to the sea floor, with higher carbon rain rates resulting in isotopically lower δ^{13}C-values (Fig. 3.23).

One would expect that pore waters would have ^{13}C/^{12}C ratios no lower than organic matter. However, a more complex situation is actually observed due to bacterial methanogenesis. Bacterial methane production generally follows sulfate reduction in anaerobic carbon-rich sediments, the two microbiological environments being distinct from one another, except for substrate-rich sections. Since methane-producing bacteria produce very ^{12}C-rich methane, the residual pore water can become significantly enriched in ^{13}C as shown in some profiles in Fig. 3.23.

3.6.1.4 Carbon in Fresh Waters

Chemical weathering consumes atmospheric CO_2 through two pathways. (I) atmospheric CO_2 dissolves in rain and surface waters and reacts with rock forming minerals generating HCO_3^- and (2) atmospheric CO_2 is converted to plant organic matter and subsequently released as soil CO_2 The mixing proportion from the two different sources determine the carbon isotope composition of fresh waters resulting in extremely variable isotopic composition, because varying mixtures of carbonate species derived from weathering of carbonates and of CO_2 originating from biogenic sources in soils are isotopically different (Hitchon and Krouse 1972; Longinelli and Edmond 1983; Pawellek and Veizer 1994; Cameron et al. 1995).

Although the CO_2 partial pressures in rivers vary widely, studies of major rivers often show that CO_2 concentrations are about 10–15 times greater than expected for equilibrium conditions with the atmosphere. Rivers thus are actively degassing CO_2 into the atmosphere, affecting the natural carbon cycle. This explains an increased interest in analyzing river systems for their carbon isotope composition. Despite the

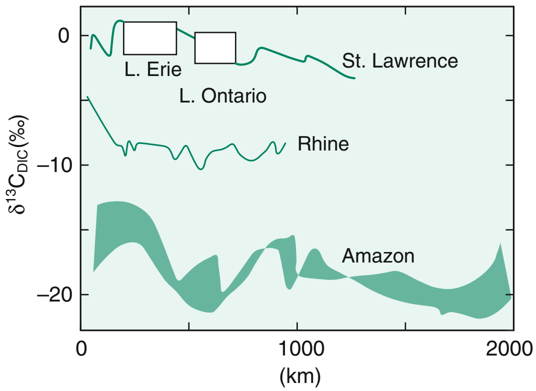

Fig. 3.24 Carbon isotopic composition of total dissolved carbon in large river systems. Data source: Amazon: Longinelli and Edmond (1983), Rhine: Buhl et al. (1991), St.Lawrence: Yang et al. (1996) (Fig. 3.23, 6th edition, p. 153)

fact that the carbon isotopic composition of carbonate minerals and of soil-CO_2 are distinctive, the observed $\delta^{13}C$-variations of dissolved inorganic carbon are often not easy to interpret, because riverine respiration and exchange processes with atmospheric CO_2 play a role. Figure 3.24 gives some examples where carbon sources can be clearly identified. In the Amazon dissolved CO_2 originates from decomposition of organic matter (Longinelli and Edmond 1983), whereas in the St. Lawrence river system CO_2 originates from the dissolution of carbonates and equilibration with the atmosphere (Yang et al. 1996). The Rhine represents a mixture of both sources (Buhl et al. 1991).

In river systems often a ^{13}C enrichment is observed from upstream to downstream due to enhanced isotopic exchange with atmospheric CO_2 and/or in situ photosynthetic activity (Telmer and Veizer 1999). Variable seasonal signals can be explained by changes in the oxidation rate of ^{13}C-depleted organic matter from the soils in watersheds. Rivers that are characterized by the presence of large lakes at their head—like the Rhone and St. Lawrence—show heavy ^{13}C-values at their head (Ancour et al. 1999; Yang et al. 1996). Due to the long residence time of dissolved carbon in lakes, the bicarbonate is in near equilibrium with atmospheric CO_2.

3.6.2 Silicon

Silicon isotope variations in the ocean are caused by biological Si-uptake through siliceous organisms like diatoms. Insofar strong similarities exist with C-isotope variations. Diatoms preferentially incorporate ^{28}Si as they form biogenic silica. Thus high $\delta^{30}Si$ values in surface waters go parallel with low Si-concentrations and depend on differences in silicon surface water productivity. In deeper waters dissolution of sinking silica particles causes an increase in Si concentration and a decrease of $\delta^{30}Si$-values. Therefore, in ocean water distinct ^{30}Si gradients with depth exist (Georg et al. 2006; Beucher et al. 2008). Surface waters may show a large variation from +2.2 to +4.4 ‰ (Grasse et al. 2013). Deep water masses have on the other hand more ^{30}Si depleted values with regional variations indicating mixing of different water masses (Ehlert et al. 2013).

Vertical and horizontal gradients of Si isotopes have been observed in ocean water profiles, preferentially in the Southern Ocean having higher Si concentrations than the Northern Ocean (Beucher et al. 2008; de Souza et al. 2012a, b; Fripiat et al. 2012). Dissolved silica in North Atlantic Deep Water has a δ^{30}Si-value being 0.5 ‰ higher than deep water of the Southern Ocean which suggests export of Si from surface waters of the Southern Ocean (de Souza et al. 2012a).

3.6.3 Nitrogen

Nitrogen is one of the limiting nutrients in the ocean. Apparently, the rate of nitrate formation is so slow, and marine denitrification so rapid, that nitrate is in short supply. Dissolved nitrogen is subject to isotope fractionation during microbial processes and during biological uptake. Nitrate dissolved in oceanic deep waters has a δ^{15}N-value of 6–8 ‰ (Cline and Kaplan 1975; Wada and Hattori 1976). Denitrification seems to be the principal mechanism that keeps marine nitrogen at higher δ^{15}N-values than atmospheric nitrogen.

The δ^{15}N-value of particulate material was originally thought to be determined by the relative quantities of marine and terrestrial organic matter. However, temporal variations in the ^{15}N-content of particulate matter predominate and obscure N-isotopic differences previously used to distinguish terrestrial from marine organic matter. Altabet and Deuser (1985) observed seasonal variations in particles sinking to the ocean bottom and suggested that δ^{15}N-values of sinking particles represent a monitor for nitrate flux in the euphotic zone. Natural ^{15}N-variations can thus provide information about the vertical structure of nitrogen cycling in the ocean.

Saino and Hattori (1980) first observed distinct vertical changes in the ^{15}N content of suspended particulate nitrogen and related these changes to particle diagenesis. A sharp increase in ^{15}N below the base of the euphotic zone has been ubiquitously observed (Altabet and McCarthy 1985; Saino and Hattori 1987; Altabet 1988). These findings imply that the vertical transport of organic matter is mediated primarily by rapidly sinking particles and that most of the decomposition of organic matter takes place in the shallow layer beneath the bottom of the euphotic zone.

3.6.4 Oxygen

As early as 1951, Rakestraw et al. demonstrated that dissolved O_2 in the oceans is enriched in ^{18}O relative to atmospheric oxygen. Like its concentration, the δ^{18}O of dissolved oxygen is affected by three processes: air-water gas exchange, respiration and photosynthesis. When gas exchange dominates over photosynthesis and respiration as in the surface ocean dissolved oxygen is close to saturation and the $\delta^{18}O$ is $\sim$24.2 ‰, because there is a 0.7 ‰ equilibrium fractionation during gas dissolution (Quay et al. 1993). Extreme enrichments up to 14 ‰ (Kroopnick and Craig 1972) occur in the oxygen minimum region of the deep ocean due to preferential consumption of ^{16}O by bacteria in abyssal ocean waters, which is evidence for a deep metabolism (see Fig. 3.22).

Precise measurements of the ^{17}O content of dissolved oxygen in seawater indicate a small ^{17}O anomaly that can be used to estimate overall photosynthetic oxygen production in seawater (Luz and Barkan 2000, 2005; Juranek and Quay 2010).

Quay et al. (1995) measured $^{18}O/^{16}O$ ratios of dissolved oxygen in rivers and lakes of the Amazon Basin. They observed a large $\delta^{18}O$ range from 15 to 30 ‰. When respiration dominates over photosynthesis in fresh waters, dissolved O_2 will be undersaturated and $\delta^{18}O$ is >24.2 ‰; when photosynthesis exceeds respiration, dissolved O_2 will be supersaturated and $\delta^{18}O$ will be <24.2 ‰.

3.6.5 Sulfate

Modern ocean water sulfate has a fairly constant $\delta^{34}S$-value of 21 ‰ (Rees et al. 1978) and a $\delta^{18}O$-value of 9.3 ‰ (Lloyd 1967, 1968; Longinelli and Craig 1967). From theoretical calculations of Urey (1947), it is quite clear that the $\delta^{18}O$-value of dissolved sulfate does not represent equilibrium with $\delta^{18}O$-value of the water, because under surface conditions oxygen isotope exchange of sulfate with ambient water is extremely slow (Chiba and Sakai 1985). By using quantum-chemical calculations Zeebe (2010) estimated the equilibrium fractionation between dissolved sulfate and water to be 23 ‰ at 25 °C.

Lloyd (1967, 1968) proposed a model in which the fast bacterial turnover of sulfate at the sea bottom determines the oxygen isotope composition of dissolved sulfate. Böttcher et al. (2001), Aharon and Fu (2000, 2003) and others demonstrated that the $\delta^{18}O$ of sulfate is not only influenced by microbial sulfate reduction, but also by disproportionation and reoxidation of reduced sulfur compounds. In marine pore waters, ^{18}O enrichments up to 30 ‰ have been observed, generally associated with strong ^{34}S enrichments. By plotting $\delta^{18}O_{(SO4)}$ vs $\delta^{34}S_{(SO4)}$ two different slopes can be distinguished: in some cases $\delta^{18}O$ increases linearly with $\delta^{34}S$ in residual sulfate (slope 1), whereas in most cases the $\delta^{18}O$ increases initially until it reaches a constant value with no further increase while $\delta^{34}S$ may continue to increase (slope 2). Böttcher et al. (1998), Brunner et al. (2005) and Antler et al. (2013) discussed models to explain the different slopes of $\delta^{18}O$-$\delta^{34}S$ plots: (i) a model that postulates the predominance of kinetic oxygen isotope fractionation steps linked to different sulfate reduction steps and (ii) a model postulating a predominance of oxygen isotope exchange between cell-internal sulfur compounds and ambient water (Brunner et al. 2005; Wortmann et al. 2007).

In freshwater environments the sulfur and oxygen isotope composition of dissolved sulfate is much more variable and potentially the isotope ratios can be used

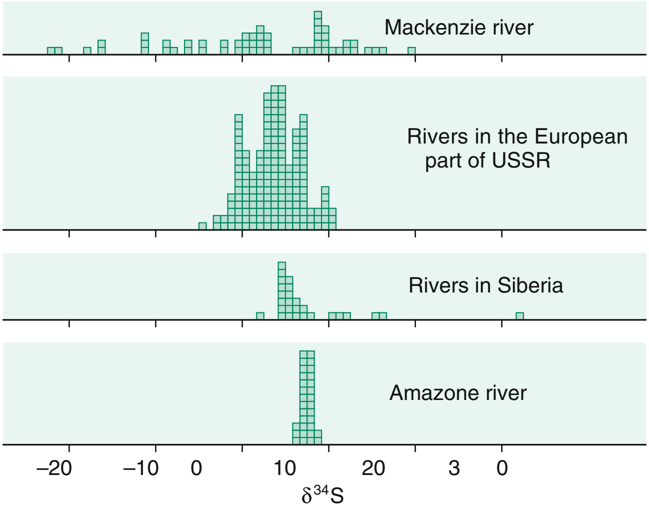

Fig. 3.25 Frequency distribution of $\delta^{34}S$-values in river sulfate (Fig. 3.24 6th edition, p. 156)

to identify the sources: (i) oxidation of sedimentary and magmatic sulfides, (ii) dissolution of evaporates, (iii) atmospheric aerosols, (iv) anthropogenic input. However, such attempts have been only partially successful because of the variable composition of the different sources. $\delta^{34}S$-values of dissolved sulfate of different rivers and lakes show a rather large spread as is demonstrated in Fig. 3.25. The data of Hitchon and Krouse (1972) for water samples from the MacKenzie River drainage system exhibit a wide range of $\delta^{34}S$-values reflecting contributions from marine evaporites and shales. Calmels et al. (2007) argue that around 85 % of the sulfate in the MacKenzie river is derived from pyrite oxidation and not from sedimentary sulfate. For the Amazon River, Longinelli and Edmond (1983) found a very narrow range in $\delta^{34}S$-values which they interpreted as representing a dominant Andean source for sulfate from the dissolution of Permian evaporites with a lesser admixture of sulfide sulfur. Rabinovich and Grinenko (1979) reported time-series measurements for the large European and Asian rivers in Russia. The sulfur in the European river systems should be dominated by anthropogenically derived sources, which in general have $\delta^{34}S$-values between 2 and 6 ‰. Burke et al. (2013) estimated a mean $\delta^{34}S$-value of 4.3 ‰ for anthropogenic sulphur; excluding the most polluted rivers, the mean value shifts to 5.4 ‰.

A special case represent acid sulfate waters released from mines where metal sulfide ores and lignite have been exploited. S- and O-isotope data may define the conditions and processes of pyrite oxidation, such as the presence or absence of dissolved oxygen and the role of sulfur-oxidizing bacteria (i.e. Taylor and Wheeler 1994).

The oxygen isotope composition of freshwater sulfate can be highly variable too. Cortecci and Longinelli (1970) and Longinelli and Bartelloni (1978) observed a range in δ^{18}O values from 5 to 19 ‰ in rainwater samples from Italy and postulated that most of the sulfate is not oceanic in origin, but rather produced by oxidation of sulfur during the burning of fossil fuels. The oxidation of reduced sulfur to sulfate is a complex process which involves chemical and microbiological aspects. Two general pathways of oxidation have been suggested: (i) oxidation by molecular oxygen and (ii) oxidation by ferric iron plus surface water.

3.6.6 Phosphate

As is well known phosphorus is essential for all living matter. Because P has only one stable isotope, stable P-isotope ratios cannot be used to study sources of P in the environment as is the case for C, N and S. But since P is strongly bound to oxygen, O isotope investigations can be used instead.

Oxygen isotope exchange between phosphate and water under purely abiotic conditions is negligible (Tudge 1960; Blake et al. 1997 and others), but is fast in biologically mediated systems (Luz and Kolodny 1985; Blake et al. 1997, 2005). Experiments with microbiological cultures as well as with enzymes indicate that oxygen isotope fractionations depend on growth conditions, phosphate concentrations and sources (Blake et al. 2005). Thus the δ^{18}O-value of phosphate in fresh and ocean water can be used to distinguish different P sources and biological pathways.

Phosphate depth profiles in the Atlantic and Pacific showed that ^{18}O is near equilibrium with water (Colman et al. 2005), whereas it is not in near coastal shallow waters (McLaughlin et al. (2006). In a 2 years time series experiment these authors observed seasonal ^{18}O variations up to 6 ‰ in the Monterey Bay. Isotope equilibrium is approached during episodic upwelling events when phosphate is extensively cycled by the biological community, lower values have been observed when phosphate is not extensively used. Even larger ^{18}O variations have been observed in pore waters (Goldhammer et al. 2011).

Identification of phosphate sources is important to reduce anthropogenic inputs of phosphorus to the environment. Young et al. (2009a, b) measured the δ^{18}O-value of different phosphate sources such as fertilizers, detergents, animal feces and observed a large range in δ^{18}O-values from 8 to 25 ‰. Although δ^{18}O-values overlap, Young et al. (2009a, b) concluded that in suitable cases some phosphate sources are distinct and can be identified.

3.7 Isotopic Composition of the Ocean During Geologic History

The growing concern with respect to “global change” brings with it the obvious need to document and understand the geologic history of sea water. From paleoecological studies it can be deduced that ocean water should not have changed its chemical composition very drastically, since marine organisms can only tolerate relatively small chemical changes in their marine environment. The similarity of the mineralogy and to some extent paleontology of sedimentary rocks during the Earth's history strengthens the conclusion that the chemical composition of ocean water has not varied substantially. This was the general view for many years. More recently, however, fluid inclusions in evaporite minerals have indicated that the chemical concentrations of major ions in ocean water such as Ca, Mg and SO_4 have changed substantially over the Phanerozoic (Horita et al. 2002a, b and others). It is thus likely that steady state conditions of input fluxes to and output fluxes from the oceans are not always equal during earth's history. The rate of these changes in ocean chemistry is dictated by the residence time of ions in the ocean.

One of the most sensitive tracers recording the composition of ancient sea water is the isotopic composition of chemical sediments precipitated from sea water. The following discussion concentrates on the stable isotope composition of oxygen, carbon, and sulphur. More recently, other isotope systems have been investigated such as Ca (De La Rocha and DePaolo 2000b; Schmitt et al. 2003; Fantle and DePaolo 2005; Farkas et al. 2007), B (Lemarchand et al. 2000, 2002; Joachimski et al. 2005) and Li (Hoefs and Sywall 1997; Misra and Froelich 2012; Wanner et al. 2014). One of the fundamental questions in all these approaches is which kind of sample provides the necessary information, in the sense that it represents the coexisting ocean water composition during the time of sediment formation and has not been modified subsequently by diagenetic reactions. Furthermore, since most chemical sediments are deposited close to the continental margins, they are not necessarily representative for the whole ocean.

3.7.1 Oxygen

It is generally agreed that continental glaciation and deglaciation induce changes in the δ^{18}O-value of the ocean on short time scales. There is, however, considerable debate about long-term changes.

The present ocean is depleted in ^{18}O by at least 6 ‰ relative to the total reservoir of oxygen in the crust and mantle. Muehlenbachs and Clayton (1976) presented a model in which the isotopic composition of ocean water is held constant by two different processes: (i) low temperature weathering of oceanic crust which depletes ocean water in ^{18}O, because ^{18}O is preferentially bound in weathering products and (ii) high-temperature hydrothermal alteration of ocean ridge basalts which enriches ocean water in ^{18}O, because ^{16}O is preferentially incorporated into the solid phase during the hydrothermal alteration of oceanic crust. If sea floor-spreading ceased, or its rate were to decline, the δ^{18}O-value of the oceans would slowly change to lower values because of continued continental and submarine weathering. Gregory and Taylor (1981) presented further evidence for this rock/water buffering and argued that the δ^{18}O of sea water should be invariant within about ±1 ‰, as long as sea-floor spreading was operating at a rate of at least 50 % of its modern value.

The sedimentary record, however, is not in accord with this model for constant oxygen isotope compositions because in a general way carbonates, cherts, and phosphates show a decrease in $\delta^{18}O$ in progressively older samples (Veizer and Hoefs 1976; Knauth and Lowe 1978; Shemesh et al. 1983). The prime issue arising from these trends is whether they are of primary or secondary (post-depositional) origin. Veizer et al. (1997, 1999) presented strong evidence that they are, at least partly, of primary origin. Based on well-selected Phanerozoic low-Mg calcite shells (mostly brachiopods), they observed a 5 ‰ decline from the Quaternary to the Cambrian. Because well preserved textures and trace element contents are comparable to modern low-Mg calcitic shells, Veizer and coworkers argued that the shells preserved the primary oxygen isotope composition and can be used to deduce the past ocean composition. Prokoph et al. (2008) provided on updated compilation of 39,000 $\delta^{18}O$ and $\delta^{13}C$ isotope data for the entire earth history confirming earlier observation of Veizer and coworkers.

Jaffrés et al. (2007) reviewed models about the potential influence of varying chemical weathering and hydrothermal circulation rates. These authors argued that seawater $\delta^{18}O$ values increased from −13.3 to −0.3 ‰ over a period of 3.4 Ga (see Fig. 3.26) with ocean surface temperatures fluctuating between 10 and 33 °C. The most likely explanation for the long-term trend in seawater $\delta^{18}O$ involves stepwise increases in the ratio of high- to low-temperature fluid/rock interactions.

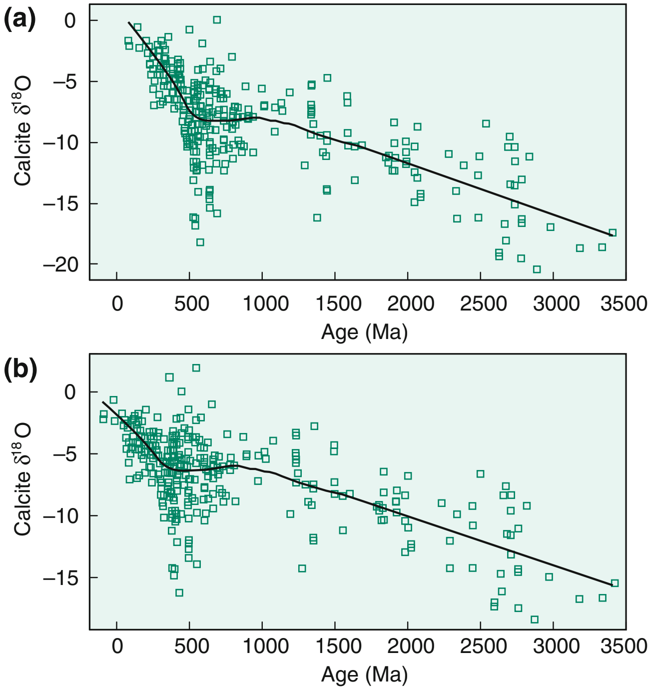

Fig. 3.26 $\delta^{18}O$ data of bulk rock calcite and brachiopods over time for **a** measured and **b** shifted values (upward shift of 2 ‰ for all bulk rock data (Jaffres et al. 2007) (Fig. 3.25. 6th edition, p. 159)

Presumably, global changes in spreading rate will affect δ^{18}O of the oceans, albeit by a smaller amount. Model calculations on the geological water cycle by Wallman (2001) support the idea that seawater δ^{18}O-values were not constant through time, but evolved from an ^{18}O depleted state to the current value. Kasting et al. (2006) argue that the low δ^{18}O-values during the Precambrian might be a consequence of changes in midocean ridge-crest depth associated with higher heat flow. However, the processes responsible for the ^{18}O changes during earth's earliest history are presently not fully understood.

3.7.2 Carbon

The ^{13}C content of a marine carbonate is closely related to that of the dissolved marine bicarbonate from which the carbonate precipitated. For a long time the δ^{13}C-value of ancient oceans was regarded as essentially constant around 0 ‰. It was in the 1980s when it was first realized that the observed fluctuations represent regular secular variations. Shifts in the carbon isotopic composition of marine carbonates may be interpreted as representing shifts in the amount of organic carbon being buried. An increase in the amount of buried organic carbon means that ^{12}C would be preferentially removed from seawater, so that the ocean reservoir would become isotopically heavier. Negative δ^{13}C-shifts accordingly may indicate a decrease in the rate of carbon burial and/or enhanced oxidative weathering of once buried organic matter.

δ^{13}C-values of limestones vary mostly within a band of 0 ± 3 ‰ since at least 3.5 Ga (Veizer and Hoefs 1976). The longer term C-isotope trend for carbonates has been punctuated by sudden shifts over short time intervals named "carbon isotope events", which are considered to represent characteristic features, and have been used as time markers for stratigraphic correlations. Characteristic carbon isotope events are the Paleocene-Eocene Thermal Maximum (Cohen et al. 2007), the Jurassic-Cretaceous Oceanic Anoxic events (Jenkyns 2010) and the Permian-Triassic extinction (Payne and Kump 2007).

Especially noteworthy are very high δ^{13}C-values of up to 10 ‰ and higher for 2.2–2.0 Ga old carbonates and at the end of the Proterozoic with both periods representing periods of increased burial of organic carbon (Knoll et al. 1986, Baker and Fallick 1989; Derry et al. 1992 and others). By compiling the data base for the Proterozoic, Shields and Veizer (2002) (Fig. 3.27) demonstrated ^{13}C fluctuations of at least 15 ‰, coincident with wide spread glaciations (see also Special Issue of Chemical Geology 237, 2007). Highly ^{13}C enriched intervals are related to interglacial times, where the ^{13}C enrichment appears to be the result of unusually efficient burial of organic carbon. Hayes and Waldbauer (2006), on the other hand, interpreted the unusual ^{13}C-enrichment as indication for the importance of methanogenic bacteria in sediments.

Negative δ^{13}C intervals are generally associated with glaciations (Kaufmann and Knoll 1995). The most negative ^{13}C-values have been found in massive carbonates

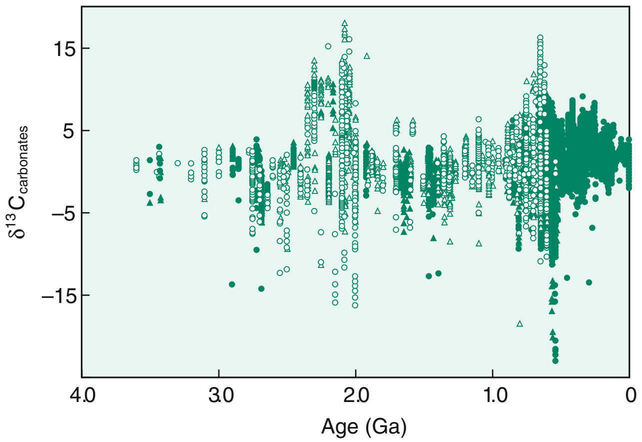

Fig. 3.27 δ^{13}C-values for marine carbonates over time. Note persistent values of 0–3 ‰ for the last 600 Ma, anomaleous variability at 0.6–0.8 Ga and 2.0–2.3 Ga correlative with snowball earth episodes (Shields and Veizer 2002) (Fig. 3.26, 6th edition, p. 160)

that cap glaciogenic sequences (“cap” carbonates), which record the most profound carbon isotope variations on Earth. The change from very heavy to very light δ^{13}C-values has been interpreted as a collapse of biological productivity for millions of years due to global glaciations (Hoffmann et al. 1998) representing one the central arguments of the “snowball Earth” hypothesis. Glaciations ended abruptly when subaerial volcanic outgassing raised atmospheric CO_2 to very high levels shifting the ^{13}C of carbonates to values around −5 ‰.

Because of the relationship between carbonate and organic carbon, a parallel shift in the isotope composition of both carbon reservoirs should be observed. Unfortunately, very often carbonate-carbon and organic carbon have not been investigated together. Hayes et al. (1999) have compiled the existing data base on both reservoirs. In contrast to previous assumptions, the long term fractionation is invariant and its average close to 30 ‰ rather than 25 ‰. Variations in the fractionations between the two reservoirs can, in principle, be interpreted as reflecting variations in the pCO2 content of the atmosphere (Kump and Arthur 1999). By employing a simple model which is subjected to different perturbations each lasting 500,000 years, Kump and Arthur (1999) demonstrated that increased burial of organic carbon leads to a fall in atmospheric pCO_2 and to positive ^{13}C-shifts in both carbonate and organic carbon. Lately, shifts in ^{13}C have been correlated to variations in the O_2/CO_2 ratio of the ambient atmosphere (Strauß and Peters-Kottig 2003).

3.7.3 Sulfur

Because isotope fractionation between dissolved sulfate in ocean water and gypsum/anhydrite is small (Raab and Spiro 1991), evaporite sulfates should closely reflect the sulfur isotope composition of marine sulfate through time. The first S-isotope "age curves" were published by Nielsen and Ricke (1964) and Thode and Monster (1964). Since then, this curve has been updated by many more analyses (Holser and Kaplan 1966; Holser 1977; Claypool et al. 1980). The sulfur isotope curve varies from a maximum of $\delta^{34}S$ = +30 ‰ in early Paleozoic time, to a minimumm of +10 ‰ in Permian time. These shifts are considered to reflect net fluxes of isotopically light sulfur generated during bacterial reduction of oceanic sulfate to the reservoir of reduced sulfide in sediments, thus increasing the ^{34}S-content in the remaining oceanic sulfate reservoir. Conversely, a net return flux of the light sulfide to the ocean during weathering or enhanced hydrothermal sulfide input lead to a decrease of marine sulfate $\delta^{34}S$-values. Modeling by Kump (1989) has indicated that pyrite burial was twice as large as today during most of the early Paleozoic followed by a decrease to values that are about half of today's rate during the Carboniferous and Permian and by approximately constant rates for the last 180 Ma (Kump 1989).

Since evaporites through geologic time contain large gaps and considerable scatter in sulfur isotope composition, two alternative approaches for the reconstruction of seawater $\delta^{34}S$ values through time have been utilized: (I) Structurally substituted sulfate in marine carbonates (Burdett et al. 1989, Kampschulte and Strauss 2004). This approach avoids apparent disadvantages of the evaporite record namely that evaporites are discontinuous with a poor age resolution representing continental margin formations with potential influence from nearby continents. Hence, a much better temporal resolution from structural sulfate records has been obtained. (II) Marine barite in pelagic sediments. Paytan et al. (1998, 2004) generated a seawater sulfur curve for the Cenozoic and for the Cretaceous with a resolution of ~1 million years. Barite has advantages over the other two sulfate proxies, because of its resistance to diagenesis as long as dissolved pore water is present to prevent barite dissolution (see Fig. 3.28). Since pelagic sediments are restricted to the modern ocean, the barite record lasts for the last 150 million years only.

The oxygen isotope composition of marine barite might be also a useful tracer for the sulfate cycle in the past. Turchin and Schrag (2004, 2006) observed a 5 ‰ variability in $\delta^{18}O$ over the past 10 million years. Oxygen is incorporated into sulfate through sulfide oxidation and released through sulfate reduction. Turchin and Schrag (2004) suggested that sea level fluctuations reducing the area of continental shelves and increasing sulfide weathering may be responsible for the observed variations.

It might be expected that a parallel age curve to that for sulfates should exist for sedimentary sulfides. However, the available S-isotope data for sulfides range widely and seem to depend strongly on the degree to which the reduction system is

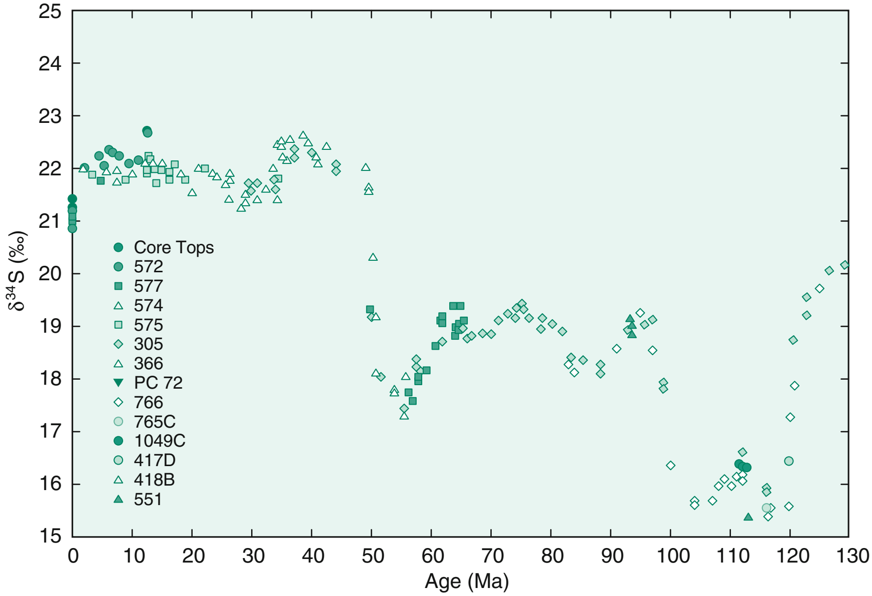

Fig. 3.28 Marine sulfate δ^{34}S curve of marine barite for 130 Ma to present (Paytan et al. 2004)

"open" and on the sedimentation rate so that age trends are obscured (Strauß 1997, 1999). Changes in the maximum sulphur isotope fractionation between sulphides and coexisting sulfates were used to propose changes in the complexity of the sulphur cycle (Canfield and Teske 1996). The large variability in $\delta^{34}S_{\text{sulfide}}$ values within age-equivalent strata might be best explained by time-dependent steps of pyrite formation during progressive diagnesis.

Considering a difference in δ^{34}S-values of 40–60 ‰ between bacteriogenic sulfide and marine sulfate in present-day sedimentary environments, similar fractionations in ancient sedimentary rocks may be interpreted as evidence for the activity of sulfate-reducing bacteria. The presence or absence of such fractionations in sedimentary rocks thus may constrain the time of emergence of sulfate-reducing bacteria. In early Archean sedimentary rocks most sulfides and the rare sulfates have δ^{34}S-values near 0 ‰ (Monster et al. 1979; Cameron 1982). The lack of substantial isotope fractionation between sulfate and sulfide has been interpreted initially as indicating an absence of bacterial reduction in the Archean, but could also indicate complete sulfate reduction. Ohmoto et al. (1993) employed a laser microprobe approach to analyze single pyrite grains from the ca 3.4 Ga Barberton greenstone belt and observed a variation of up to 10 ‰ among pyrites from a single rock specimen, which could imply that bacterial reduction has occurred since at least 3.4 Ga. Shen and Buick (2004) argued that the large spread in δ^{34}S values of microscopic pyrites aligned along growth faces of former gypsum in the 3.47 Ga North Pole barite deposit, Australia represents the oldest evidence for microbial sulfate reduction.

3.7.4 Lithium

The two major sources of Li to the ocean are rivers and hydrothermal input at spreading centers, major sinks are Li-incorporation into marine sediment and low temperature oceanic crust. By analyzing well-dated planktonic foraminifera, Misra and Froelich (2012) presented a Li-isotope curve for the last 68 Ma. They observed a Li isotope increase of 9 ‰ over the past 50 million years, which they interpreted to reflect a general increase in continental weathering rates. Since Li–in contrast to Ca and Sr—is preferentially incorporated in silicate minerals, the Li isotope record is sensitive to changes in the weathering of silicate rocks. Modelling by Wanner et al. (2014) revealed a correlation between δ^7Li-values and CO_2 consumption rates by silicate weathering. Thus, the Li isotope record may quantify atmospheric CO_2 consumption.

3.7.5 Boron

Geochemical modelling has indicated significant variations in the boron isotope composition of sea water with geologic time (Lemarchand et al. 2002; Simon et al. 2006). δ^{11}B-values of past seawater depend, like Li and other elements, on continental erosion rates and rates of chemical exchange at oceanic ridges. What makes B unique is its dependence on the pH of ocean water (see p. 61). Studies on foraminifera to reconstruct the δ^{11}B-value of past ocean water have been used either to determine the pH-value (Pearson and Palmer 2000; Pearson et al. 2009), or to determine changes in the boron isotope composition of ocean water (Raitzsch and Hönisch 2014). By using independent estimates of past deep-ocean pH, benthic foraminifera, being less pH affected than planktonic foraminifera, demonstrate oscillations of 2 ‰ in ^{11}B-values with a striking ^{11}B increase of about 3 ‰ since the Eocene (Raitzsch and Hönisch 2014), also indicating similarities with the Li isotope record of Misra and Froelich (2012).

3.7.6 Calcium

Several studies have documented secular changes in the Ca isotope composition of the ocean (De La Rocha and De Paolo 2000; Griffith et al. 2008a, b, c; Steuber and Buhl 2006; Farkas et al. 2007; Fantle 2010), that indicate a dynamic Ca cycle during earth's history and suggest feedbacks between the Ca and the C-cycle to buffer the oceanic carbon reservoir. A large drop in δ^{44}Ca-values at the Eocene-Oligocene boundary observed by Fantle (2010) might suggest a substantial increase in weathering relative to sedimentation. Besides changes in the input and output fluxes to the ocean, other processes might also change the Ca isotope composition such as a shift from Early Paleozoic calcitic oceans to late Paleozoic aragonitic oceans or changes in the magnitude of dolomite formation.

3.8 Atmosphere

The basic chemical composition of the atmosphere is quite simple, being made up almost entirely of three elements: nitrogen, oxygen and argon. Other elements and compounds are present in amounts that although small are nevertheless significant. A mixture of gases with different molecular weights should partially segregate and fractionate in a gravity field. However the lower atmosphere—the troposphere—is much too turbulent for gravitational fractionation to be observed. While it appears possible that certain gases in the upper atmosphere—the stratosphere—could be affected by this process, isotopic evidence for this has not been found so far (Thiemens et al. 1995). (Gravitational fractionation can however be observed in air trapped in ice cores and in sand dunes (Sowers et al. 1992) see p. 18).

In recent years, tremendous progress has been achieved in the analysis of the isotope composition of important trace compounds in the atmosphere, mainly through the introduction of the GC-IRMS technique allowing the precise analysis of nanomole quantities of O_3, CH_4, N_2O, CO, H_2 and also sulfate and nitrate, Of special importance is the isotope composition of ozone having a unique composition that affects other trace components.

Trace gases continually break apart and recombine in a multitude of photochemical reactions, which may produce isotope fractionations (Kaye 1987; Brenninkmeijer et al. 2003). Isotope analysis is increasingly employed in studies of the cycles of atmospheric trace gases e.g. CH_4 and N_2O, giving insights into sources and sinks and transport processes of these compounds. The rationale is that various sources have characteristic isotope ratios and that sink processes are accompanied by isotope fractionation.

Many of the processes responsible for isotope fractionations in the Earth's atmosphere may also occur in the atmospheres of other planetary systems, such as the atmospheric escape of atoms and molecules to outer space. Likely unique to Earth are isotope fractionations related to biological processes or to interactions with the ocean. One aspect of atmospheric reserach which has great potential for the application of stable isotope investigations is the study of anthropogenic pollution.

Compared to the troposphere very different fractionation effects and reactions can be observed in the stratosphere. Of special importance is the isotope composition of stratospheric ozone. In situ mass-spectrometric measurements by Mauersberger (1981, 1987) demonstrated that an equal enrichment in ^{17}O and ^{18}O of about 40 % exists in the stratosphere, with a maximum at about 32 km. The rate of formation of isotopically partially substituted ozone (mass 50) is obviously faster than that of unsubstituted ozone (mass 48). Later measurements by Krankowsky et al. (2000) did not confirm the very large enrichments orginally reported by Mauersberger, but gave enrichments of 7–11 %. CO_2 samples collected between 26 and 35 km altitude show a mass—independent enrichment in both^{17}O and ^{18}O of up to about 15 ‰ above tropospheric values (Thiemens et al. 1995). The enrichment of stratospheric CO_2 relative to tropospheric CO_2 should make it possible to study mixing processes across the tropopause.

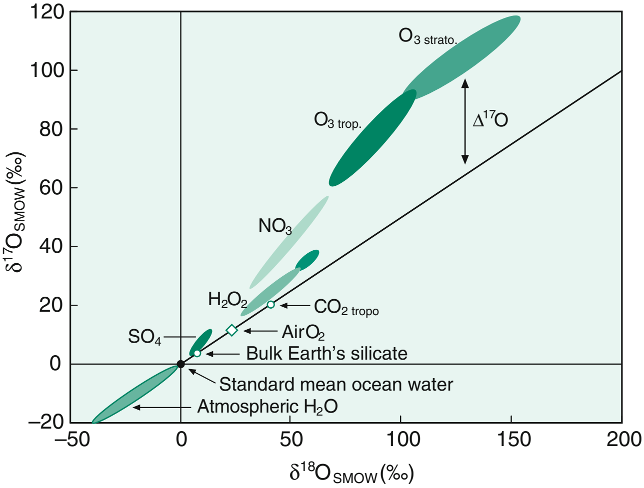

Fig. 3.29 $\delta^{17}O$ versus $\delta^{18}O$ plot of atmospheric oxygen species (Thiemens 2006) (Fig. 3.35, 6th edition, p. 176)

Similar effects have also been observed in stratospheric nitrous oxide. $\delta^{17}O$ and $\delta^{18}O$ measurements by Cliff and Thiemens (1997) reveal that stratospheric N_2O possesses a large variable mass-independent isotope composition, which also requires a mass-independent process (Thiemens 1999).

Figure 3.29 summarizes mass independent isotope compositions of a number of atmospheric molecules such as ozone, CO_2, N_2O, and CO (Thiemens 1999, 2006).

3.8.1 Atmospheric Water Vapour

While the major compounds nitrogen, oxygen and argon have a constant concentration in the lower part of the atmosphere, water vapour concentrations are highly variable: Craig and Gordon (1965) first measured the isotopic composition of atmospheric water vapour over the North Pacific. Later Rozanski and Sonntag (1982) and Johnson et al. (2001) observed in vertical profiles of troposheric and stratospheric water vapour a gradual depletion of δD (and $\delta^{18}O$) with increasing altitude up to the tropopause with a reversal in the stratosphere. The depletion trend in the troposphere can be explained by isotope fractionation associated with cloud formation and rainout processes leading to preferential removal of heavy isotopes from water vapour. In the stratosphere photochemical oxidation of methane might be responsible for the observed increase in δD.

3.8.2 Nitrogen

Nearly 80 % of the atmosphere consists of elemental nitrogen. This nitrogen, collected from different altitudes, exhibits a constant isotopic composition (Dole et al. 1954; Sweeney et al. 1978) and represents the "zero-point" of the naturally occuring isotope variations. Besides the overwhelming predominance of elemental nitrogen, there are various other nitrogen compounds in the atmosphere, which play a key role in atmospheric pollution and determining the acidity of precipitation.

Combustion of fossil fuels and biomass converts inert N_2 into the reactive form NO_x ($NO + NO_2$). Other sources of NO_x include microbial processes in soils, but anthropogenic activities currently dominate NOx production.

Fractionations during the conversion of NO_x to nitrate appear to be small, therefore $\delta^{15}N$-values should reflect sources of NO_x. Heaton (1986) has discussed the possibility of isotopically differentiating between naturally produced and anthropogenic NO_x. Since very little isotope fractionation is expected at the high temperatures of combustion in power plants and vehicles, the $\delta^{15}N$-value of pollution nitrate is expected to be similar to that of the nitrogen which is oxidized.

In soils, NO_x is produced by nitrification and denitrification processes which are kinetically controlled. This, in principle, should lead to more negative $\delta^{15}N$-values in natural nitrate compared to anthropogenic nitrate. However, Heaton (1986) concluded that this distinction cannot be made on the basis of ^{15}N-contents, which has been confirmed by Durka et al. (1994).

^{18}O variations in atmospheric nitrate are very large (ranging from +25 to +115 ‰, Morin et al. 2008; Michalski et al. 2011), and vary during a yearly cycle. Higher $\delta^{18}O$-values are found in wintertime, lower values in summer time. High latitude nitrate has higher ^{18}O-values than mid-latitude nitrate. Similar trends are observed in $\Delta^{17}O$-values, which indicate a strong mass-independent anomaly derived from exchange with ozone.

3.8.2.1 Nitrous Oxide

Besides NO_x oxides, there is nitrous oxide (N_2O), which is of special interest in isotope geochemistry. N_2O is present in air at around 300 ppb and increases by about 0.2 % per year. Nitrous oxide is an important greenhouse gas that is, on a molecular basis, a much more effective contributor to global warming than CO_2 and has also a major chemical control on stratospheric ozone budgets.

N_2O forms during microbial nitrification and denitrifaction processes in soils and water, the global budget is, however poorly constrained. The first $\delta^{15}N$-values for N_2O were determined by Yoshida et al. (1984), the first $\delta^{18}O$-values were published by Kim and Craig (1990) and the first dual isotope determinations have been presented by Kim and Craig (1993). $\delta^{15}N$ and $\delta^{18}O$ values of atmospheric N_2O today range from 6.4 to 7.0 ‰ and 43 to 45.5 ‰ (Sowers 2001). First isotope measurements of N_2O from the Vostok ice core by Sowers (2001) indicate large ^{15}N and ^{18}O variations with time ($\delta^{15}N$ from 10 to 25 ‰ and $\delta^{18}O$ from 30 to

50 ‰), which have been interpreted to result from in situ N_2O production via nitrification.

Terrestrial emissions, mainly from soils, have generally lower δ-values than marine sources. As shown by Kool et al. (2009), $\delta^{18}O$ signatures in N_2O are determined by oxygen isotope exchange with ambient water. Due to kinetic effects, production of N_2O from both nitrification and denitrification yields N_2O which is isotopically light relative to its precursors whereas reduction during denitrification results in an ^{15}N and ^{18}O enrichment in the residual N_2O (Well and Flessa 2009).

Atmospheric nitrous oxide exhibits a small mass-independent ^{17}O component (Cliff and Thiemens 1997; Cliff et al. 1999), providing a characteristic isotope signature from ^{17}O enriched ozone. $\delta^{15}N$ and $\delta^{18}O$-values of stratospheric N_2O gradually increase with altitude due to preferential photodissociation of the lighter isotopes (Rahn and Wahlen 1997).

There is another aspect that makes N_2O a very interesting compound for isotope geochemists. N_2O is a linear molecule in which one nitrogen atom is at the centre and one at the end. The center site is called α-position, the end site β-position. Yoshida and Toyoda (2000) and Röckmann et al. (2003) showed that the ^{15}N content in the two N-positions varies and can be used as an fingerprint. In contrast to ^{18}O and mean ^{15}N-values, the difference between the N^{α} and the N^{β} position is independent of the isotope composition of the precursor (Popp et al. 2002). The uneven intramolecular distribution, thus, may help to identify the sources and sinks of N_2O (see p. 17 on site specific isotope composition).

3.8.3 Oxygen

Atmospheric oxygen has a rather constant isotopic composition (Dole et al. 1954; Kroopnick and Craig 1972; Bender et al. 1994) with a $\delta^{18}O$-value of 23.5 ‰, which, more recently, has been re-determined to be 23.88 ‰ (Barkan and Luz 2005). Oxygen is produced by photosynthesis without fractionation with respect to the substrate water (Helman et al. 2005). Because the ocean is the largest water reservoir on Earth, the $\delta^{18}O$-value of atmospheric oxygen, therefore, is linked to the seawater composition.

Urey (1947) calculated that under equilibrium conditions atmospheric oxygen should be enriched in ^{18}O relative to water by 6 ‰ at 25 °C. This means atmospheric oxygen cannot be in equilibrium with the hydrosphere and thus the ^{18}O-enrichment of atmospheric oxygen, the so-called "Dole" effect, must have another explanation. It is generally agreed that the ^{18}O-enrichment is of biological origin and results from the fact that during respiration most species preferentially use ^{16}O (Lane and Dole 1956). Oxygen consumed during respiration has a ^{18}O-content that is about 20 ‰ lower than the intake of O_2 (Guy et al. 1993).

The Dole effect can be separated into terrestrial and oceanic contributions. Bender et al. (1994) estimated that the terrestrial contribution should be 22.4 ‰ whereas the marine contribution should be 18.9 ‰. The δ-value should be thus very sensitive to changes in the ratio of marine to terrestrial photosynthesis when the climate shifted from glacial to interglacial periods. As has been shown by the analysis of molecular oxygen trapped in ice cores, the δ^{18}O-value of atmospheric oxygen has indeed varied with geologic time. Sowers et al. (1991), Bender et al. (1994) and Severinghaus et al. (2009) have pioneered the analysis of δ^{18}O of O_2 in air bubbles trapped in ice cores by measuring the difference between the δ^{18}O-value of atmospheric oxygen and ocean water. δ^{18}O-values within glacial-interglacial cycles vary within 1.5 ‰ and follow the δ^{18}O value of sea water (Severinhaus et al. 2009).

Further insight into the isotopic composition of atmospheric oxygen comes from the measurement of the ^{17}O content having a δ^{17}O-value of 12.03 ‰ (Luz et al. 1999; Luz and Barkan 2000, 2005; Barkan and Luz 2011). These studies revealed that atmospheric oxygen carries a mass-independent ^{17}O signature due to photochemical reactions in the stratosphere. Photosynthesis and respiration fractionate ^{17}O and ^{18}O in a mass dependent way, whereas photochemical stratospheric reactions among O_3, O_2 and CO_2 (Thiemens et al. 1995) lead to a mass independent isotope fractionation of tropospheric oxygen. As a result, troposheric oxygen is depleted in ^{17}O by about 0.2 ‰ relative to oxygen affected by photosynthesis and respiration alone. The magnitude of the ^{17}O depletion depends on the relative proportions of biological productivity and stratospheric mixing. As proposed by Luz et al. (1999) and Luz and Barkan (2000) the ^{17}O anomaly can be used as a tracer of global biosphere production rates.

The ^{17}O signal of atmospheric oxygen may be transferred to crustal minerals such as gypsum and barite through oxidative weathering of continental sulfides. Thus by analysing terrestrial sulfates, a record of ^{17}O anomalies through geological history may be obtained (Bao et al. 2000, 2001; Bao 2015).

3.8.3.1 Evolution of Atmospheric Oxygen

Geological, mineralogical and geochemical indicators have been used to deduce oxygen levels of past atmospheres. For half of Earth history, oxygen contents probably have been less than 0.001 % of the present atmospheric level (PAL). Stable isotope proxies document the oxygenation of the Earth's atmosphere and oceans. The increase in oxygen concentration seems to have occurred in several steps. The first major step occurred at about 2.4 Ga (Farquhar et al. 2000; Farquhar and Wing 2003 and others), the socalled "Great Oxidation Event (GOE)", which is characterized by oxidative weathering. The most convincing argument for the existence of the GOE are mass-independent sulfur isotope fractionations that have persisted until the onset of the GOE. Recent studies have indicated that the evolution of atmospheric oxygen is more complex than a single stage transition from anoxic in the Archean to oxic in the Paleoproterozoic (Anbar and Rouxel 2007; Wille et al. 2007, 2013; Frei et al. 2009; Voegelin et al. 2010). On the basis of Mo isotope and Cr isotope data, these authors argued there is evidence for significant amounts of oxygen prior to 2.4 Ga.

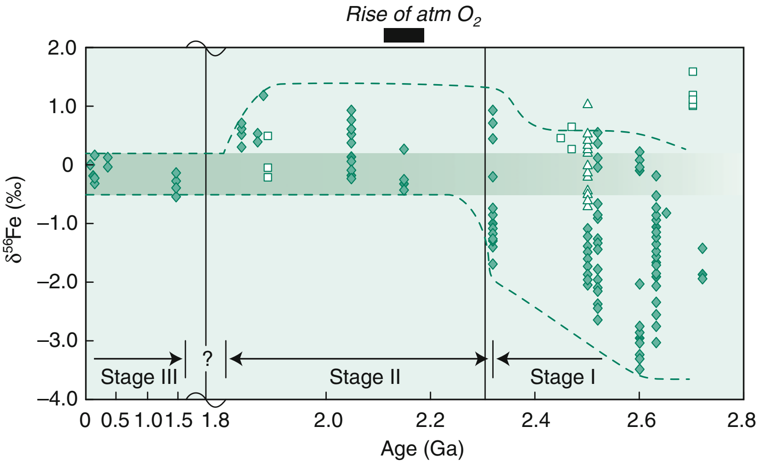

Fig. 3.30 δ^{56}Fe values of pyrite and iron oxides versus time showing three evolutionary stages of the ocean (Anbar and Rouxel 2007) (Fig. 3.28, 6th edition, p. 163)

The evolution of atmospheric oxygen can be also deduced from iron isotopes. Besides carbon and sulfur, iron as a third element controls the redox chemistry of the ocean. Rouxel et al. (2005) demonstrated a progressive change in iron cycling from 3.5 to 0.5 Ga that was associated with the oxygenation of the ocean (see Fig. 3.30). According to Rouxel et al. (2005) the iron isotope distribution during earth's history can be divided into 3 stages: stage I (2.8–2.3 Ga) is characterized by highly variable and negative δ^{56}Fe values of pyrite, stage II (2.3–1.6 Ga) is characterized by unusually high δ-values and stage III (from 1.6 Ga till today) is characterized by pyrite having a small δ^{56}Fe range from about 0 to −1 ‰. These different stages might reflect changes in the redox state of the earth. In stage I (older than 2.3 Ga), iron was removed from the ocean as iron oxides and as pyrite. Iron oxides enriched in ^{56}Fe were precipitated by anaerobic oxidation, which drove the ocean toward lower δ^{56}Fe-values (Kump 2005). In stage II from 2.3 to 1.8 Ga the atmosphere became oxidized, but the ocean remained more or less anoxic. In stage III atmosphere and ocean were oxygenated, ensuring that iron did not accumulate in the ocean, but was removed as insoluble Fe^{3+} that retained the iron isotope composition of the iron inputs to the ocean which are close to the crustal average.

3.8.4 Carbon Dioxide

3.8.4.1 Carbon

The increasing CO_2-content of the atmosphere is a problem of world-wide concern. By measuring both the concentration and isotope composition of CO_2 on the same samples of air, it is possible to determine whether variations are of anthropogenic,

Fig. 3.31 Relationship between atmospheric CO_2 concentration and $\delta^{13}C_{(CO2)}$ (after Keeling 1958)
(Fig. 3.30, 6th edition, p. 168)

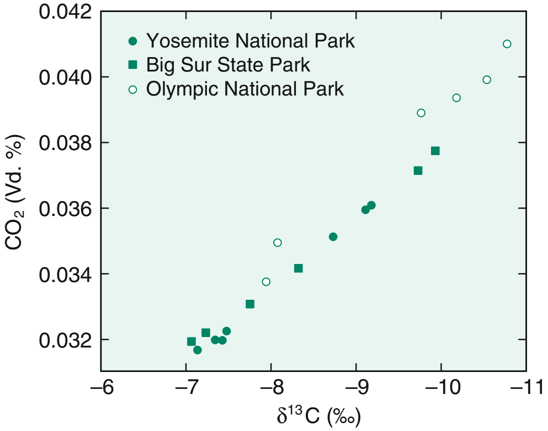

oceanic or biologic origin. Carbon dioxide sequestration is considered an important option to reduce greenhouse-gas emissions. Sedimentary basins in general and deep saline aquifers are regarded as possible repositories for anthropogenic CO_2 and the isotopic composition of injected CO_2 may provide an ideal tracer for the fate of injected CO_2 in the reservoir (Kharaka et al. 2006 and others).

The first extensive measurements of the carbon isotope ratio of CO_2 were made in 1955/56 by Keeling (1958, 1961). He noted daily, seasonal, secular, local and regional variations as regular fluctuations. Daily variations exist over continents, which depend on plant respiration and reach a distinct maximum around midnight or in the early morning hours. At night there is a measurable contribution of respiratory CO_2, which shifts $\delta^{13}C$-values towards lower values (see Fig. 3.31). Seasonal variations in ^{13}C are very similar to CO_2-concentrations and result from terrestrial plant activity. As shown in Fig. 3.32 the seasonal cycle diminishes from north to south, as expected from the greater seasonality of plant activity at high latitude and the larger amount of land area in the northern hemisphere. This effect is hardly discernible in the southern hemisphere (Keeling et al. 1989).

Long-term measurements of atmospheric CO_2 are available for a few clean-air locations on an almost continuous basis since 1978 (Keeling et al. 1979; Mook et al. 1983; Keeling et al. 1984, 1989, 1995; Ciais et al. 1995). These measurements clearly demonstrate that on average atmospheric CO_2 increases by about 1.5 ppm per year while the isotope ratio shifts towards lower $^{13}C/^{12}C$ ratios. The annual combustion of 10^{15}g of fossil fuel with an average $\delta^{13}C$-value of −27 ‰ would change the ^{13}C-content of atmospheric CO_2 by −0.02 ‰ per year. The observed change is, however, much smaller. Of the CO_2 emitted into the atmosphere roughly half remains in the atmosphere and the other half is absorbed into the oceans and the terrestrial biosphere. The partitioning between these two sinks is a matter of debate. Whereas most oceanographers argue that the oceanic sink is not large enough to account for the entire absorption, terrestrial ecologists doubt that the terrestrial biosphere can be a large carbon sink.

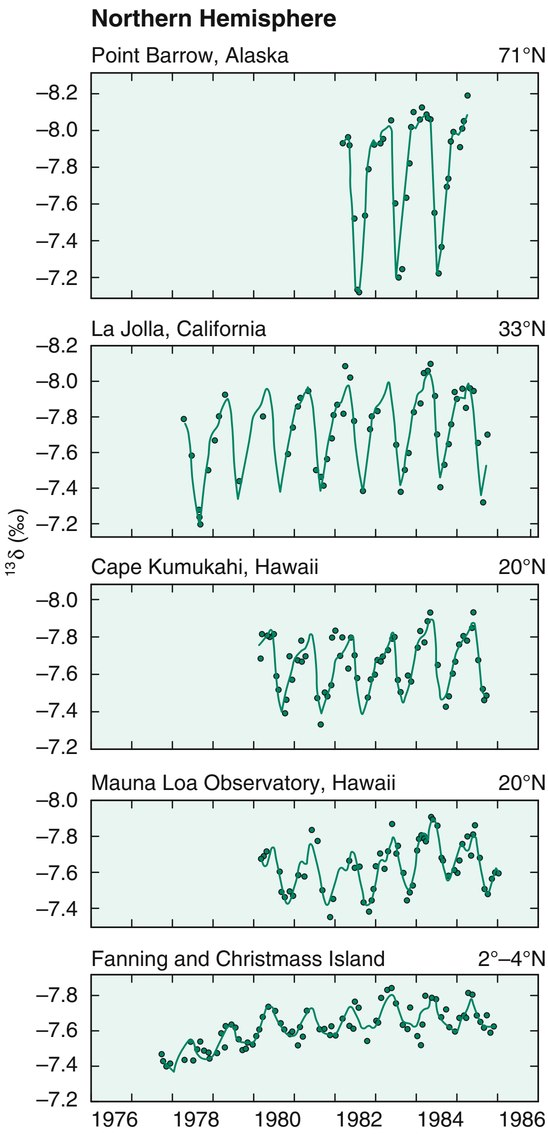

Fig. 3.32 Seasonal $\delta^{13}C$ variations of atmospheric CO_2 from five stations in the Northern Hemisphere. *Dots* denote monthly averages, *oscillating curves* are fits of daily averages (after Keeling et al. 1989) (Fig. 3.31, 6th edition, p. 169)

3.8.4.2 Oxygen

Atmospheric CO_2 has a $\delta^{18}O$-value of about +41 ‰, which means that atmospheric CO_2 is in approximate isotope equilibrium with ocean water, but not with atmospheric oxygen (Keeling 1961; Bottinga and Craig 1969). Measurements by Mook et al. (1983) and Francey and Tans (1987) have revealed large-scale seasonal and regional variations. There is a North–South shift in ^{18}O-contents of almost 2 ‰ increasing towards the south, about ten times larger than for ^{13}C. Seasonal cycles

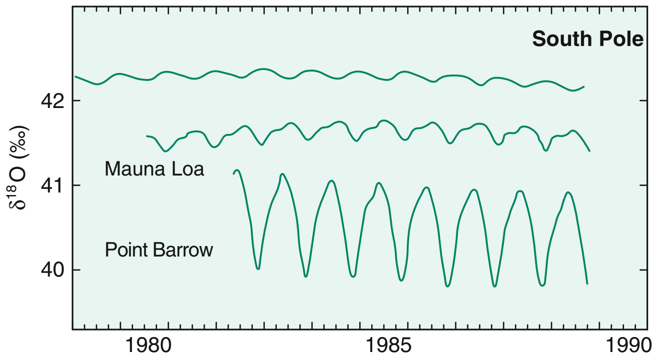

Fig. 3.33 $\delta^{18}O$ seasonal record of atmospheric CO_2 from three stations: Point Barrow 71.3°N, Mauna Loa 19.5°S, South Pole 90.0°S (after Ciais et al. 1998) (Fig. 3.32, 6th edition, p. 170)

are similar in magnitude to those of $\delta^{13}C$ (see Fig. 3.33). This north–south gradient is caused by the unequal distribution of ocean and land between the two hemispheres and by the very different oxygen isotope composition of ocean and meteoric water.

Farquhar et al. (1993) demonstrated that much more CO_2 comes into contact with leaf water than is actually taken up by plants during photosynthesis. For every CO_2 molecule that is taken up by photosynthesis, two others enter the leaf through the stomata. They rapidly equilibrate with the leaf water and then diffuse back to the atmosphere without having been incorporated by the plant. This large flux therefore only influences the ^{18}O content of atmospheric CO_2, but has no influence on the $\delta^{13}C$-value.

Additional insight into the cycling of atmospheric CO_2 can be gained by the analysis of triple oxygen isotopes. Hoag et al. (2005) suggested that the determination of the ^{17}O content besides the ^{18}O content of tropospheric CO_2 might be a tracer for CO_2 interactions with the biosphere and the hydrophere. As CO_2 in the stratosphere is anomaleouly enriched in ^{17}O and ^{18}O through exchange with ozone, the influx of stratospheric CO_2 enriches tropospheric CO_2 in ^{17}O and ^{18}O which is resetted by exchange with the oxygen isotope composition of surface water. A precise determination of the $^{17}O/^{16}O$ and $^{18}O/^{16}O$ equilibrium fractionation between CO_2 and water has been carried out by Hofmann et al. (2012). They demonstrated that the $\Delta^{17}O$ signal of tropospheric CO_2 varies temporally but does not simply follow the $\delta^{18}O$ seasonal variations.

Horvath et al. (2012) determined the triple oxygen isotope composition of CO_2 from combustion processes and from human breath. High-temperature combustion CO_2 inherits its oxygen isotope composition from ambient air O_2, wheras the O-isotope composition of human breath is controlled by isotope exchange with body water. Thus, the triple oxygen isotope composition of anthropogenic CO_2 can be clearly distinguished from natural CO_2 sources.

3.8.4.3 Long Term Variations in the CO_2 Concentration

There is increasing awareness that the CO_2 content of the Earth's atmosphere has varied considerably over the last 500 Ma. The clearest evidence comes from measurements of CO_2 from ice cores, which have yielded an impressive record of CO_2 variations over the past 420,000 years (Petit et al. 1999a, b).

In a much broader context, Berner (1990) has modeled how long-term changes in CO_2 concentrations can result from the shifting balance of processes that deliver CO_2 to the atmosphere (such as volcanic activity) and processes that extract CO_2 (such as weathering and the deposition of organic material). The theoretical carbon dioxide curve calculated for the past 500 Ma matches the climate record at several key points: it is low during the ice age of the Carboniferous and Permian and rises to a maximum in the Cretaceous. Although the exact curve is far from being known, it is clear that fluctuations in the CO_2 content of the ancient atmosphere may have played a critical role in determining global surface paleotemperatures. To elucidate these short- and long-term CO_2-fluctuations, several promising "CO_2-paleobarometers" use variations of carbon isotopes in different materials.

Short-term carbon isotope variations in tree rings have been interpreted as indicators of anthropogenic CO_2 combustion (Freyer 1979; Freyer and Belacy 1983). While different trees show wide variability in their isotope records due to climatic and physiological factors, many tree-ring records indicate a 1.5 ‰ decrease in $\delta^{13}C$-values from 1750 to 1980. Freyer and Belacy (1983) reported C-isotope data for the past 500 years on two sets of European oak trees: forest trees exhibit large non-systematic ^{13}C variations over the 500 years, whereas free-standing trees show smaller ^{13}C fluctuations, which can be correlated to climatic changes. Since industrialization of these areas in 1850, the ^{13}C record for the free-standing trees has been dominated by a systematic decrease of about 2 ‰.

The most convincing evidence for changes in atmospheric CO_2-concentrations and $\delta^{13}C$-values comes from air trapped in ice cores in Antarctica. Figure 3.34 shows a high time-resolution record for the last 1000 years from analysis of the Law Dome, Antarctica ice core (Trudinger et al. 1999). Changes in CO_2 concentration and in $\delta^{13}C$ values during the last 150 years are clearly related to the increase of anthropogenic fossil fuel burning. During the last ice age with low CO_2-concentrations, atmospheric CO_2 was isotopically lighter by about 0.3 ‰ relative to interglacial periods (Leuenberger et al. 1992). Schmitt et al. (2012) presented $\delta^{13}C$-data for the past 24,000 years from two Antarctic ice cores and observed a 0.3 ‰ decrease from about 17,500–14,000, a time where CO_2 concentrations rose, which they interpreted as being due to upwelling of CO_2 enriched waters in the Southern ocean.

Two different classes of approaches have been used in the study of long-term atmospheric CO_2 change: one utilizing deep-sea sediments, the other studying continental sediments. Cerling (1991) has been reconstructing the CO_2 content of the ancient atmosphere by analyzing fossil soil carbonate that formed from CO_2 diffusion from the atmosphere or plant roots. This method relies on certain assumptions and prerequisites. One, for instance, is the necessity of differentiating

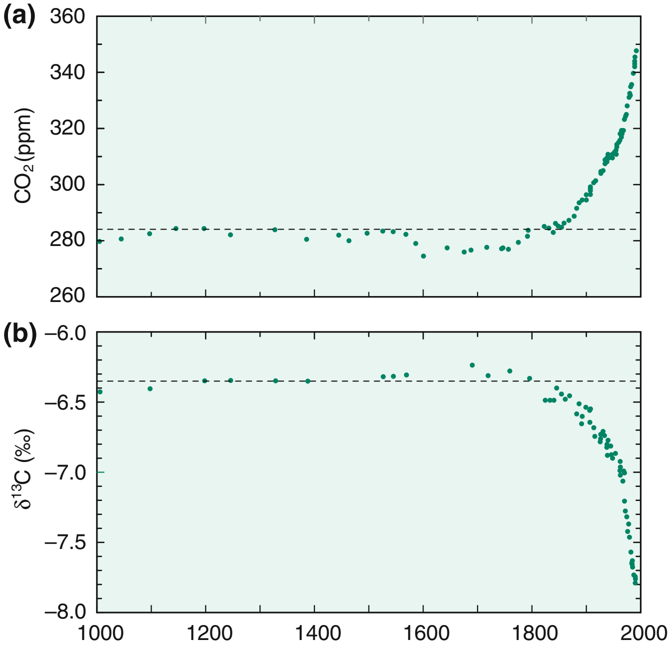

Fig. 3.34 Law Dome ice core CO_2 and $\delta^{13}C$ record for the last 1000 years (after Trudinger et al. 1999) (Fig. 3.33, 6th edition, p. 171)

pedogenic calcretes from those formed in equilibrium with groundwater, which can not be used for p_{CO2} determinations (Quast et al. 2006).

Another approach uses the relationship between the concentration of molecular CO_2 and the $\delta^{13}C$-value of marine organic plankton (Rau et al. 1992). Attempts to quantify the relationship between $CO_{2(aq)}$ and $\delta^{13}C_{org}$ have resulted in several empirically derived calibrations (Jasper and Hayes 1990; Jasper et al. 1994; Freeman and Hayes 1992 and others). Theoretical considerations and experimental work demonstrated that cellular growth rate (Laws et al. 1995; Bidigare et al. 1997) and cell geometry (Popp et al. 1998) also exert considerable control on $\delta^{13}C_{org}$, insofar as they influence the intracellular CO_2 concentration. Other complicating factors are potential contamination of terrestrial organic matter and marine photosynthesizers with varying carbon fixation pathways that are integrated in bulk organic matter. Therefore it is preferable to use specific biomarkers, such as alkenones. Alkenones are long-chain (C_{36}–C_{39}) unsaturated ketones, produced by a few taxa of phytoplankton such as the common *Emiliani huxleyi*, in which the number of double bonds is correlated with the water temperature at the time of synthesis. Palaeo-CO_2 levels can be estimated from the carbon isotope composition of alkenones and coeval carbonates (Jasper and Hayes 1990; Pagani et al. 1999a, b).

The boron isotope approach (see Sect. 2.3.2) to estimate pCO_2 relies on the fact that a rise in the atmospheric CO_2 concentration will increase pCO_2 of the surface ocean which in turn causes a reduction of pH. By measuring the boron isotope composition of planktonic foraminifera Palmer et al. (1998) and Pearson and Palmer (2000) have reconstructed the pH-profile of Eocene seawater and estimated past atmospheric CO_2 concentrations. However, Lemarchand et al. (2000) argued that $\delta^{11}B$ records of planktonic foraminifera partly reflect changes in the marine boron isotope budget rather than changes in ocean pH.

3.8.5 Carbon Monoxide

Carbon monoxide is an important trace gas, which has a mean residence time of about 2 months and a mean concentration of the order of 0.1 ppm. The principal sources of CO are (i) oxidation of methane and other higher hydrocarbons, (ii) biomass burning, (iii) traffic, industry and domestic heating, (iv) oceans and (v) vegetation. The dominant sinks are (i) in situ oxidation by hydroxyl radical (OH), which is responsible for the removal of contaminant gases from the troposphere and (ii) uptake by soils. The first isotope data on CO have been presented by Stevens et al. (1972), which have later been confirmed by Brenninkmeijer (1993) and Brenninkmeijer et al. (1995). Seasonal variations in $\delta^{13}C$ values appear to reflect a shift in the relative contributions from two major sources, biomass burning and atmospheric oxidation of methane. $\delta^{18}O$-values are even more variable than $\delta^{13}C$ due to a kinetic isotope effect accompanying the removal of CO from the atmosphere. Oxygen in CO also exhibits a mass independent fractionation with a pronounced ^{17}O excess of up to 7.5 ‰, which must be related to the removal reaction with OH (Röckmann et al. 1998).

Röckmann et al. (2002) measured the complete isotope composition of CO from high northern latitude stations. $\delta^{13}C$, $\delta^{17}O$ and $\delta^{18}O$ values show strong seasonal variations and indicate mixing between mid and high northern latitude CO. In winter high amounts of combustion CO from industrial regions are transported to high latitudes. Large variations in C- and O- isotope compositions have been observed in CO from ice cores, which have been interpreted as being due to changes in biomass burning (Wang et al. (2011).

3.8.6 Methane

Methane enters the atmosphere from biological and anthropogenic sources and is destroyed by reaction with the hydroxyl radical. Thus, a mass-weighted average composition of all CH_4 sources is equal to the mean $\delta^{13}C$-value of atmospheric methane, corrected for any isotope fractionation effects in CH_4 sink reactions. Based on the concentration measured in air contained in polar ice cores, methane concentrations have doubled over the past several hundred years (Stevens 1988). Concentrations were increasing at almost 1 % per year in the late 70s and early 80s, the growth rate has slowed down since then for unknown reasons.

Methane is produced by bacteria under anaerobic conditions in wet environments such as wetlands, swamps and rice fields. It is also produced in the stomachs of cattle and by termites. Typical anthropogenic sources are from fossil fuels such as coal mining and as a byproduct in biomass burning. The latter sources are considerably heavier in ^{13}C than the former. Methane may be also formed in terrestrial plants under oxic conditions Keppler et al. (2006). The size of this methane source is still unknown but it might play a important role for the methane cycle.

Atmospheric methane has a mean $\delta^{13}C$-value of around −47 ‰ (Stevens 1988). Quay et al. (1999) presented global time series records between 1988 and 1995 on the carbon and hydrogen isotope composition of atmospheric methane. They measured spatial and temporal variation in ^{13}C and D with a slight enrichment observed for the southern hemisphere (−47.2 ‰) relative to the northern hemisphere (−47.4 ‰). The mean δD was −86 ± 3 ‰ with a 10 ‰ depletion in the northern relative to the southern hemisphere.

Methane extracted from air bubbles in polar ice up to 350 years in age has a $\delta^{13}C$-value which is 2 ‰ lower than at present (Craig et al. 1988). This may indicate that anthropogenic burning of the Earth's biomass may be the principal cause of the recent ^{13}C enrichment in methane.

Stratospheric methane collected over Japan gave a $\delta^{13}C$-value of −47.5 ‰ at the tropopause and increased to −38.9 ‰ at around 35 km (Sugawara et al. 1998). These authors suggested that reaction with Cl in the stratosphere might be responsible for the ^{13}C-enrichment.

3.8.7 Hydrogen

Molecular hydrogen (H_2) is after methane the second most abundant reduced gas in the atmosphere with an average concentration of 0.53 ppm (Ehhalt and Rohrer 2009). Although hydrogen distribution is rather uniform, the concentration in the southern hemisphere is around 3 % higher than in the northern hemisphere. The isotope geochemistry of hydrogen in the atmosphere is very complex, because there are numerous hydrogen-containing compounds undergoing continuous chemical and physical transformations. Early studies of the isotope composition of H_2 have been performed in conjunction with the measurement of atmospheric tritium. An early estimate of the average hydrogen isotope composition of atmospheric H_2 (Friedman and Scholz 1974) was +70 ± 30 ‰. The major result from these studies is that there is a large seasonal and latitudinal variability in deuterium content with higher δD-values in the southern hemisphere than in the northern hemisphere (Batenburg et al. 2011).

The largest hydrogen sources are the oxidation of methane and other hydrocarbons and combustion processes (biomass and fossil fuel burning), the largest sink is soil uptake which explains the 3 % higher concentration in the southern hemisphere (less landmass). Due to the large mass difference between H and D, large isotope fractionations occur in the processes that produce or remove hydrogen. Of special importance are kinetic isotope effects during soil uptake of atmospheric hydrogen (Rice et al. 2011).

Considering low δD-values of H_2 sources during bacterial processes, fossil fuel combustion and biomass burning (−250 ‰ and lower), the D-enrichment of atmospheric hydrogen is difficult to explain. One way is to attribute the enrichment with a kinetic fractionation during reaction with OH, the other is photochemical production of H_2 from methane and higher hydrocarbons.

Extreme D enrichments in H_2 have been found in stratospheric air samples (Rahn et al. 2002b). δD-values vary up to +440 ‰, representing the most D-enriched natural material on Earth.

3.8.8 Sulfur

Sulfur is found in trace compounds in the atmosphere, where it occurs in aerosols as sulfate and in the gaseous state as H_2S and SO_2. Sulfur can orginate naturally (volcanic, sea spray, aeolian weathering, biogenic) or anthropogenically (combustion and refining of fossil fuels, ore smelting, gypsum processing). These different sources differ greatly in their isotopic composition as shown in Fig. 3.35. The complexities involved in the isotopic composition of atmospheric sulfur have been discussed in the SCOPE 43 report, edited by Krouse and Grinenko (1991).

In brief, the isotopic compositions of the industrial sulfur sources are generally so variable, that the assessment of anthropogenic contributions to the atmosphere is extremely difficult. Krouse and Case (1983) were able to give semiquantitative estimates for a unique situation in Alberta where the industrial SO_2 had a constant

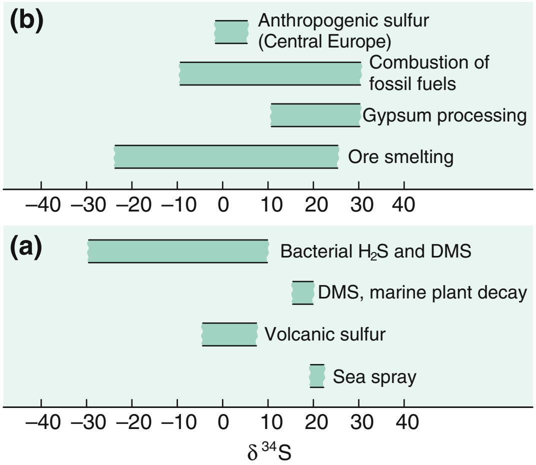

Fig. 3.35 S-isotope composition of **a** natural and **b** anthropogenic sulfur sources in the atmosphere. *DMS* Dimethylsulfide (Fig. 3.34, 6th edition, p. 174)

δ^{34}S-value near 20 ‰. Generally, situations are much more complicated which limits the "fingerprint" character of the sulfur isotope composition of atmospheric sulfur to such rare cases.

Very interesting seasonal dependencies for sulfur in precipitation and in aerosol samples have been observed by Nriagu et al. (1991). δ^{34}S-data for aerosol samples of the Canadian arctic show pronounced seasonal differences, with the sulfur being more ^{34}S enriched in summer than in winter. This situation is quite different from that observed for airborne sulfur in southern Canada. In rural and remote areas of southern Canada, the δ^{34}S-values of atmospheric samples are higher in winter and lower in summer. While during the winter sulfur is mainly derived from sources used for heating and industrial sources, in summer the large emission of ^{34}S-depleted biogenic sulfur from soils, vegetation, marshes, and wetlands results in the lowering of the δ^{34}S-values of airborne sulfur. The opposite trend observed for aerosol sulfur in the Arctic suggests a different origin of the sulfur in these high latitude areas.

3.8.9 Sulfate and Nitrate in Ice Cores

Upon oxidation of SO_2 and NO_2 to sulfate and nitrate, the mass independent composition of ozone is transferred to sulfate and nitrate. Measurements of the oxygen isotope composition of ice core sulfate and nitrate can thus provide a historical record of natural variations in sulfur and nitrogen pathways (Alexander et al. 2002, 2004; Thiemens 2006). Such a record is of importance in understanding global climate change particularly through glacial and volcanic events. Alexander et al. (2002) showed that the mass independent fractionation of sulfate is significantly greater during the warmer interglacials than during the colder glacials. However, as discussed by Alexander et al. (2002) it is not a record of temperatures, but a measure of the oxidative efficiency of the atmosphere. During colder periods the oxidation of SO_2 to sulfate in clouds is obviously suppressed. In a later study Alexander et al. (2004) demonstrated that a combined approach of sulfate and nitrate measurements in ice cores may give additional evidence for changes in the oxidative capacity of the atmosphere over different time periods.

Additional informations can be gained by measurements of the different sulfur isotopes in stratospheric sulfate aerosols (Baroni et al. 2007). During large explosive eruptions that release large amounts of SO_2 (Pinatubo, Agung, Tambora), sulfur gases rise to the stratosphere where they form small sulfuric acid aerosols that can remain in the stratosphere for several years before they settle to the ground. By extracting sulfate from the Antartic ice sheet, Baroni et al. (2007) demonstrated that sulfate from the Agung and Pinatubo eruptions exhibit large mass-independent sulfur isotope fractionations. The sign of the Δ^{33}S changed over time from an initial positive component to a negative component, which indicates a fast process during photochemical oxidation of SO_2 to sulfuric acid on a time scale of months.

3.8.10 Perchlorate

Perchlorate has been detected in soils, waters, plants and food in concentrations that may cause health problems. δ^{37}Cl-, δ^{18}O- and Δ^{17}O-values may indicate chlorate sources (Bao and Gu 2004; Böhlke et al. 2005). Perchlorate in the environment is either of man-made or of natural origin. Synthetic perchlorate is used as a constituent of explosives, missiles and rockets or in car airbags. Natural perchlorate is a minor component in hyperarid salt deposit, such as the Atacama dersert. Synthetic perchlorate is produced by electrolytic reactions from aqueous chloride. Its δ^{37}Cl-values vary around zero ‰ like natural Cl-sources. δ^{18}O-values range from about −25 to −12 ‰ and are much lower than presumed water sources indicating isotope fractionations during synthesis. Δ^{17}O-values show no variations.

In contrast, natural perchlorate show the lowest δ^{37}Cl-values reported so far (Bao and Gu 2004; Böhlke et al. 2005), indicating fractionations during formation in the atmosphere. δ^{18}O-values vary too, but the most prominent property are large positive ^{17}O-anomalies reflecting photochemical reactions of atmospheric Cl-species with ozone.

3.9 Biosphere

As used here, the term "biosphere" includes the total sum of living matter—plants, animals, and microbial biomass and the residues of the living matter in the geological environment such as coal and petroleum. A fairly close balance exists between photosynthesis and respiration, although over the whole of geological time respiration has been exceeded by photosynthesis, and the energy derived from this is stored mostly in disseminated organic matter, and, of course, in coal and petroleum.

Photosynthesis is responsible for isotope fractionations in the biosphere, not only for carbon, but also for hydrogen and oxygen. Nevertheless, as will be shown, the transformation of biogenic matter to organic matter in sediments also involves isotope fractionations, occurring in two stages: a biochemical and a geochemical stage. During the biochemical stage microorganisms play the major role in reconstituting the organic matter. During the geochemical stage, increasing temperature and to a much lesser extent pressure are responsible for the further transformation of organic matter (see review of Galimov 2006).

3.9.1 Living Organic Matter

3.9.1.1 Bulk Carbon

Wickman (1952) and Craig (1953) were the first to demonstrate that marine plants are about 10 ‰ enriched in ^{13}C relative to terrestrial plants. Since that time numerous studies have broadened this view and provided a much more detailed account of isotope variations in the biosphere. The reason for the large C-isotope differences found in plants were only satisfactorily explained after the discovery of new photosynthetic pathways in the 1960s. The majority of land plants (80–90 %) employ the C3 (or Calvin) photosynthetic pathway which results in organic carbon approximately 18 ‰ depleted in ^{13}C with respect to atmospheric CO_2. Around 10–20 % of carbon uptake by modern land plants is via C4 (or Hatch-Slack) photosynthesis with a carbon isotope fractionation of only 6 ‰ on average. The C4 pathway is thought to represent an adaptation to CO_2 limited photosynthesis, which developed relatively late in the Earth᾽s history. It is advantageous under warm, dry and saline environmental conditions. Differences in the isotope composition of C3 and C4 plants are widely used as a palaeoenvironmental indicator to trace climatic changes or changes in the diet of animals and humans.

One of the most important groups of all living matter is marine phytoplankton. Natural oceanic phytoplankton populations vary in $\delta^{13}C$-value by about 15 ‰ (Sackett et al. 1973; Wong and Sackett 1978). Rau et al. (1982) demonstrated that different latitudinal trends in the carbon isotope composition of plankton exist between the northern and the southern oceans: south of the equator the correlation between latitude and plankton ^{13}C-content is significant, whereas a much weaker relationship exists in the northern oceans.

The unusual ^{13}C depletion in high latitude Southern Ocean plankton has been puzzling for years. Rau et al. (1989, 1992) found a significant inverse relationship between high-latitude ^{13}C-depletion in plankton and the concentration of molecular CO_2 in surface waters. Thus, it has been assumed that the major factor controlling the C isotope composition of phytoplankton is the availability of aqueous dissolved CO_2. However, as has been shown in culture experiments with marine microalgae (Laws et al.1995; Bidigare et al. 1997; Popp et al. 1998) the carbon isotope composition of phytoplankton depends on many more factors including cell wall permeability, growth rate, cell size, the ability of the cell to actively assimilate inorganic carbon and the influence of nutrients on cell growth. Therefore, estimates of paleo-CO_2 concentrations based on the C-isotope composition of marine organic matter need to consider the paleoenvironmental conditions at the time of phytoplankton production, which are difficult to constrain for the geologic past.

Organic material that comprises living matter consists of carbohydrates (saccharides, “Sacc”)—the first product of carbon fixation—and proteins (“Prot”), nucleic acids (“NA”) and lipids (“Lip”) with prevailing regularities within these compound classes:

$\delta NA \sim \delta Prot$,
$\delta Prot - \delta Sacc \sim -1$ ‰ and
$\delta Lip - \delta Sacc \sim -6$ ‰ (Hayes 2001).

What is known for a long time is that lipids are depleted in ^{13}C by 5–8 ‰ relative to the bulk biomass. On the other hand, the carbohydrate fraction of various organisms is on average enriched in ^{13}C by 4.6 ‰ relative to the bulk (Teece and Fogel 2007). Even larger variations are observed for individual amino acids (Abelson and Hoering 1961) and individual carbohydrates (Teece and Fogel 2007), where variations are probably associated with different metabolic pathways during their synthesis.

The δ^{13}C-value of the total marine organic matter represents a mixed isotope signal derived from land plant detritus, primary production by aquatic organisms and microbial biomass. The possibility of analyzing individual components has refined the interpretation of bulk δ^{13}C-data. Compound-specific isotope analyses allow the resolution of the isotopic composition of material derived from primary sources from that of secondary inputs. These source-specific molecules have become known as biomarkers, which are complex organic compounds derived from living organisms, showing little structural difference from their parent biomolecules, being not affected by diagenesis as long as the basic biological structure is preserved. Due to the specificity of their origin, biomarkers allow for an investigation of the extent to which various organisms contribute organic materials to complex mixtures. In the Messel Shale, Freeman et al. (1990) observed C-isotope variations of individual compounds between −73.4 and −20.9 ‰ (see Table 3.3). This large range can be interpreted as representing a mixture of secondary, bacterially mediated processes and primary producers. While the major portion of the analyzed hydrocarbons reflect the primary biological source material, some hydrocarbons having low concentrations are extremely ^{13}C depleted indicating their secondary microbial origin in a methane-rich environment. Later studies by Summons et al. (1994), Thiel et al. (1999), Hinrichs et al. (1999) and Peckmann and Thiel (2005) clearly suggested that fermentative and chemoautotrophic organisms must have made significant contributions to total sedimentary organic matter. For example, extremely depleted δ^{13}C-values as low as −120 ‰ of specific biomarkers indicate that ^{13}C-depleted methane must be the carbon source for the respective archaea rather than the metabolic product. In another example Schoell et al. (1994) demonstrated that steranes and hopanes can be used as a monitor of water depth. These authors showed that δ^{13}C-values of C_{35} hopanes and the Δ-difference between steranes and hopanes follow the climatic evolution of the Miocene in the Pacific Ocean.

Table 3.3 δ^{13}C-values of separated individual hydrocarbons from the Messel shale (Freeman et al.1990)

Peak	δ^{13}C	Compound
1	−22.7	Norpristane
2	−30.2	C19 acyclic isoprenoid
3	−25.4	Pristane
4	−31.8	Phytane
5	−29.1	C23 acyclic isoprenoid
8	−73.4	C32 acyclic isoprenoid
9	−24.2	Isoprenoid alkane
10	−49.9	22,29,30-trisnorhopane
11	−60.4	Isoprenoid alkane
15	−65.3	30-norhopane
19	−20.9	Lycophane

3.9.1.2 Position Specific Isotope Composition of Organic Constituents

Generally the isotopic composition of the bulk organic matter is measured. However, each distinctive site in an organic compound has not necessarily the same isotopic composition (Galimov 2006; Eiler 2013, Eiler et al. 2014). For example, as is known for some time (Blair et al.1985), acetate has two different carbon groups, the methyl (CH_3 group) and the carboxyl group (COO) that differ in $\delta^{13}C$ values by up to 20 ‰. In recent years it has become possible to measure the C and H isotope composition at the site specific level (Eiler 2013; Eiler et al. 2014) that undoubtedly will provide new insights in the formation and transformation of organic molecules.

3.9.1.3 Hydrogen

During photosynthesis plants remove hydrogen from water and transfer it to organic compounds. Because plants utilize environmental water during photosynthesis, δD-values of plants are primarily determined by the δD-value of the water available for plant growth. Hydrogen enters the plant as water from roots in the case of terrestrial plants or via diffusion in the case of aquatic plants. In both cases, the water enters the organisms without any apparent fractionation. In higher terrestrial plants water transpires from the leaf due to evaporation, which is associated with a H-isotope fractionation of up to 40–50 ‰ (White 1989).

Large negative isotope fractionations occur in biochemical reactions during the synthesis of organic compounds (Schiegl and Vogel 1970). A generalized picture of the hydrogen isotope fractionations in the metabolic pathway of plants is shown in Fig. 3.36 (after Sachse et al. 2012).

There are systematic differences in the D/H ratios among classes of compounds in plants: lipids usually contain less deuterium than the protein and the carbohydrate fractions (Hoering 1975; Estep and Hoering 1980). Lipids can be divided into two

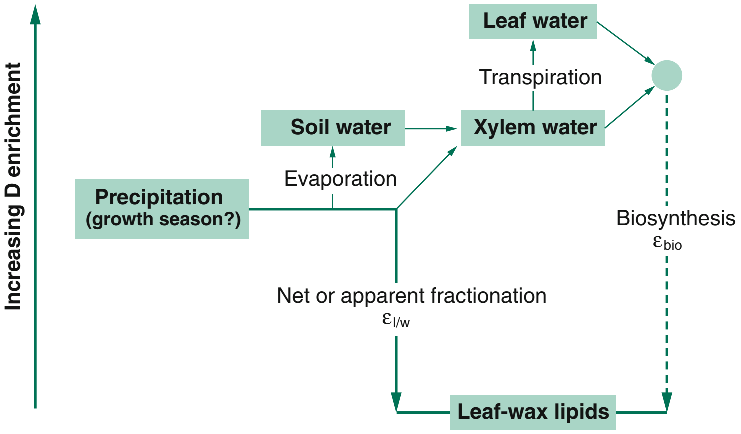

Fig. 3.36 Generalized scheme of hydrogen isotope changes in plants (Sachse et al. 2012)

groups: straight-chain lipids are depleted in D by 150–200 ‰ relative to water whereas isoprenoid lipids are depleted by about 200–300 ‰.

The component typically analyzed in plants is cellulose, which is the major structural carbohydrate in plants (Epstein et al. 1976, 1977). Cellulose contains 70 % carbon-bound hydrogen, which is isotopically non-exchangeable and 30 % of exchangeable hydrogen in the form of hydroxyl groups (Epstein et al. 1976; Yapp and Epstein 1982). The hydroxyl-hydrogen readily exchanges with the environmental water and its D/H ratio is not a useful indicator of the D/H ratio of the water used by the plants.

Compound-specific analysis of individual lipids have revealed a large range of δD-values from about –400 to +200 ‰ (Sachse et al. 2012 besides others) that can be related to isotope fractionations associated with different biosynthetic pathways and secondary hydrogenation and dehydrogenation exchange reactions. These effects have to be known when interpreting δD-values of lipid biomarkers as paleoclimate indicators.

Hydrogen and carbon in organic matter, although both of biological origin, undergo very different changes during diagenesis and maturation. Whereas carbon tends to be preserved, hydrogen is exchanged during various diagenetic reactions with environmental water. The timescale for H-isotope exchange depends on the structure of the organic molecule and can reach millions of years. Schimmelmann et al. (2006) demonstrated as thermal maturation increases δD-values of individual hydrocarbons steadily increase while the 100 ‰ biosynthetic difference between linear and isoprenoid structures disappear, which, as shown by Wang et al. (2009b), can be attributed to hydrogen isotope exchange towards an equilibrium state. The endpoint of isotope exchange results in fractionations between hydrocarbons and pore water to be in the range of −80 to −110 ‰.

3.9.1.4 Oxygen

The experimental difficulties in determining the oxygen isotope composition of biological materials is due to the rapid exchange between organically bound oxygen, in particular the oxygen of carbonyl and carboxyl functional groups, with water. This explains why studies on the oxygen isotope fractionation within living systems have concentrated on cellulose, the oxygen of which is only very slowly exchangeable (Epstein et al. 1977; DeNiro and Epstein 1979, 1981).

Oxygen potentially may enter organic matter from three different sources: CO_2, H_2O and O_2. DeNiro and Epstein (1979) have shown that ^{18}O-contents of cellulose for two sets of plants grown with water having similar oxygen isotope ratios, but with CO_2 initially having different oxygen isotope ratios, did not differ significantly. This means that CO_2 is in oxygen isotope equilibrium with the water. Therefore, the isotopic composition of water determines the oxygen isotope composition of organically bound oxygen. Similar to hydrogen, oxygen isotope fractionation does not occur during uptake of soil water through the root, but rather in the leaf because of evapotranspiration causing isotope enrichment, the extent depends on the ratio of external to internal water vapor pressures. A high $\delta^{18}O$-value in cellulose can thus reflect an increase in temperature or a decrease in relative humidity, making the interpretation of $\delta^{18}O$-values ambiguous (Sternberg et al. 2002).

Current methods of ^{18}O analysis give a mean value of the individual positions in the cellulose molecule. Waterhouse et al. (2013) describe a method for the measurement of different oxygen positions in cellulose by demonstrating that different oxygen positions undergo variable degrees of O-isotope exchange. The method potentially enables a separate determination of temperatures and humidities of the past.

3.9.1.5 Nitrogen

There are various pathways by which inorganic nitrogen can be fixed into organic matter during photosynthesis. N-autotrophs can utilize a variety of materials and thus can have a wide range of $\delta^{15}N$-values depending on environmental conditions. However, most plants have $\delta^{15}N$-values between −5 and +2 ‰. Plants fixing atmospheric nitrogen have δ-values between 0 and +2 ‰. Isotope fractionation will occur when the inorganic nitrogen source is in excess (Fogel and Cifuentes 1993). Isotope fractionations during assimilation of NH_4 by algae varied extensively from −27 to 0 ‰ (Fogel and Cifuentes 1993). A similar range of fractionations has been observed with algae grown on nitrate as the source of nitrogen.

A large fraction of organic nitrogen is comprised by amino acids. As shown by McClelland and Montoya (2002) and others internal differences in ^{15}N contents among different amino acids are due to differences in metabolic pathways. McClelland and Montoya (2002) distinguished two groups of amino acids: a "source" group reflecting the ^{15}N composition of the system and a "trophic level" group showing ^{15}N enrichments relative to the source.

3.9.1.6 Sulfur

The processes responsible for the direct primary production of organically bound sulfur are the direct assimilation of sulfate by living plants and microbiological assimilatory processes in which organic sulfur compounds are synthesized. Generally inorganic sulfate and atmospheric SO_2 serve as the major sulfur sources in plants. Typically plants have $\delta^{34}S$-values that are about 1 ‰ depleted relative to environmental sulfate (Trust and Fry 1992).

Since biosynthetic organic sulphur occurs in chemically labile forms, such as amino acids, sulphur contents in organic matter should decrease during diagenesis. However, this is not the case, generally S-contents increase. Most organic sulfur contained in humic and fulvic acids results from secondary sulfuruzation during early diagenesis being generally considerably depleted in ^{34}S relative to the original plant material. This indicates the addition of isotopically depleted sulfides from bacterially reduced sulfate.

3.9.1.7 Metal Isotopes

Metals play an essential role in plant nutrition. For example, Fe plays a vital role in various redox reactions and the biosynthesis of chlorophyll. Zn is important for carbohydrate and protein metabolism. Mo and Cu are important micronutrient, excesses of these elements can lead to toxic effects.

Bioessential metals are extracted from soils and cycled through living organic matter. During these cycling processes various fractionation processes do occur and metal isotopes, thus, can be used to study the transfer processes from soils to plants and within plants.

The range of isotope variations of metal isotopes in plants and animals is of similar magnitude as those reported for geological materials (Jaouen et al. 2013). In plants, the metal isotope compositions vary between seeds, stem and leaves, all being isotopically different from the growth media. In animals metal isotope compositions vary among organs. Thus metal isotopes are potential tracers to reconstruct paleodiet.

Metal isotope fractionation in plants has been investigated for Fe (Guelke and von Blanckenburg 2007; Kiczka et al. 2010). These studies demonstrated that the uptake of Fe by plants at the plasma membrane creates an Fe pool that is depleted in heavy isotopes. Studies on Zn and Mg isotopes (Moynier et al. 2008; Viers et al. 2007; Black et al. 2008) have demonstrated the complex chemistry in plants For Ca, Page et al. (2008) and Cobert et al. (2011) identified 3 isotope fractionation steps in higher plants that may allow the study of Ca transfer mechanisms within plants.

In summary, the extent and direction of isotope fractionations are metal dependent and in many cases unknown till today. Potentially like the light elements, metals may create isotope signatures characteristic for life.

3.9.2 Indicators of Diet and Metabolism

A similarity in $\delta^{13}C$-values between animals and plants from the same environment was already noted by Harmon Craig in 1953. Later, many field and laboratory studies have documented small shifts of 1–2 ‰ in ^{13}C and even smaller shifts in ^{34}S between an organism and its food source (DeNiro and Epstein 1978; Peterson and Fry 1987; Fry 1988).

This technique has been widely used in tracing the origin of carbon, sulfur and nitrogen in modern and prehistoric food webs (e.g. DeNiro and Epstein 1978) and culminates in the classic statement “You are what you eat plus/minus a few permil”. The precise magnitude of the isotopic difference between diet and a particular tissue depends on the extent to which the heavy isotope is incorporated or lost during synthesis. In contrast to carbon and sulfur, nitrogen shows a 3 to 4 ‰ enrichment in ^{15}N in the muscle tissue, bone collagen or whole organism relative to the food source (Minigawa and Wada 1984; Schoeninger and DeNiro 1984). When this fractionation is taken into account, nitrogen isotopes are also a good indicator of dietary source. Due to the preferential excretion of ^{14}N, the 3 to 4 ‰ shift in $\delta^{15}N$ values occurs with each trophic level along the food chain and thus provides a basis for establishing trophic structure.

Multi-element isotope analysis on the origin of organic compounds has lead to new applications of stable isotope investigations termed stable isotope forensics (e.g. Meier-Augustein 2010). In this fast growing branch of research not only the origin of food such as honey or whisky are traced, but also successful attempts have been carried out distinguishing sources for drugs and elucidating explosives.

Archaeological studies have used the stable isotope analysis of collagen extracted from fossil bones to reconstruct the diet of prehistoric human populations (e.g. Schwarcz et al. 1985).

Carbon isotopes have been used successfully to explore changes in the vegetation on Earth. Ecosystems with abundant C4 biomass have been documented only from the late Neogene to the present (Cerling et al. 1993, 1997). In South Asia, isotopic records from soil carbonates and tooth enamel reveal a dramatic increase in the abundance of C4 plants at 7 ± 1 million years ago (Quade et al. 1992; Quade and Cerling 1995 and others).

3.9.3 Tracing Anthropogenic Organic Contaminant Sources

The identification of organic compounds polluting the environment is a problem of worldwide concern. Compound-specific stable isotope analysis has become a powerful tool to study the sources of organic contaminants and their transformation reactions in the environment. The first studies on degradation of groundwater pollutants were published in the late 1990. Since then the field has rapidly grown resulting in many articles that monitor natural attenuation of contaminated sites (i.e. Schmidt et al. 2004; Philp 2007; Hofstetter et al. 2008 and others).

Types of contaminants in the environment are manifold and include natural seepage of crude oils, leaking tanks and pipelines, polychlorinated biphenyls, and other types of chemicals. The ultimate goal of many of these studies is the question who was responsible for the contamination and will have to pay for the cleanup.

Temporal and spatial isotope variations of individual organic contaminants may reveal by which pathway contaminants may degrade or even in some cases to which degree a reaction has progressed. When a biotic or abiotic transfer reaction process takes place, a kinetic isotope effect usually occurs making the reaction products initially lighter than their parent products.

Natural attenuation processes may preclude easy application of the isotope ratios as a tracer of pollution. Besides bacterial degradation, isotope fractionations during evaporation and migration of chlorinated hydrocarbons may also affect the isotope composition.

Of special concern for the environment are chlorinated hydrocarbons which are extensively used in many industries and which are, therefore, a potential source of environmental pollution. Coupling the study of C- with Cl-isotopes represents a powerful tool to trace sources, pathways and degradation of chlorinated hydrocarbons (Heraty et al. 1999; Huang et al. 1999; Jendrzejewski et al. 2001). The use of C- and Cl-isotopes as tracers of pollution requires the isotope ratios of the polluting product to be significantly different from the natural abundance. Jendrzejewski et al. (2001) demonstrated on a set of chlorinated hydrocarbons from various manufacturers that both carbon (δ^{13}C from –24 to –51 ‰) and chlorine (δ^{37}Cl from –2.7 to +3.4 ‰) had a large compositional range. The range for chlorine is especially significant, because it is much larger than that of inorganic chlorine.

3.9.4 Marine Versus Terrestrial Organic Matter

The commonly observed difference in δ^{13}C of about 7 ‰ between organic matter of marine primary producers and land plants has been successfully used to trace the origin of recent organic matter in coastal oceanic sediments (e.g. Westerhausen et al. 1993). Samples collected along riverine-offshore transects reveal very consistent and similar patterns of isotopic change from terrestrial to marine values (for instance Sackett and Thompson 1963; Kennicutt et al. 1987 and others). It is evident that the decreasing contribution of terrestrial organic matter to distal marine sediments is reflected in the C-isotope composition of the marine sedimentary organic matter. But even deep-sea sediments deposited in areas remote from continents may contain a mixture of marine and continental organic matter.

The C-isotope difference between terrestrial and marine organic matter cannot, however, be used as a facies indicator as originally thought. Carbon isotope fractionation associated with the production of marine organic matter has changed with geologic time, while that associated with the production of terrestrial organic matter has been nearly constant (Arthur et al. 1985; Hayes et al. 1989; Popp et al. 1989; Whittacker and Kyser 1990). Particularly intriguing has been the unusually ^{13}C-depleted organic matter in Cretaceous marine sediments, which has been interpreted as resulting from elevated aqueous CO_2 concentrations allowing for greater discrimination during algal photosynthesis.

Hayes et al. (1999) systematically evaluated the carbon isotope fractionation between carbonates and coeval organic matter for the past 800 Ma. They concluded that earlier assumptions of a constant fractionation between carbonate and organic matter is untenable and that fractionations may vary by about 10 ‰ depending on the dominant biogeochemical pathway as well on environmental conditions.

Not only carbon, but the nitrogen isotope composition of sediments also is primarely determined by the source organic matter. Source studies have been undertaken to trace the contribution of terrestrial organic matter to ocean water and to sediments (i.e. Sweeney et al. 1978; Sweeney and Kaplan 1980). Such studies are based, however, on the assumption that the ^{15}N content remains unchanged in the water column. Investigations by Cifuentes et al. (1989), Altabet et al. (1991), and Montoya et al. (1991) have demonstrated that there may be rapid temporal (even on a time scale of days) and spatial changes in the nitrogen isotope composition of the water column due to biogeochemical processes. This complicates a clear distinction between terrestrial and marine organic matter, although marine organic matter generally has a higher 15 N/14 N ratio than terrestrial organic matter.

3.9.5 Fossil Organic Matter

Similar to living organisms, organic matter in the geosphere is a complex mixture of particulate organic remains and living bacterial organisms. This complexity results from the multitude of source organisms, variable biosynthetic pathways, and transformations that occur during diagenesis and catagenesis. Of special importance are different stabilities of organic compounds in biological and inorganic degradation processes during diagenesis and subsequent metamorphism.

Immediately after burial of the biological organic material into sediments, complex diagenetic changes occur. Two processes have been proposed to explain the observed changes in carbon isotope composition: (i) preferential degradation of organic compounds which have different isotope composition compared to the preserved organic compounds. Since easily degradable organic compounds like amino acids are enriched in ^{13}C compared to the more resistant compounds like lipids, this causes a shift to slightly more negative δ-values. (ii) Isotope fractionations due to metabolism of microorganisms. Early diagenesis does not only encompass degradation of organic matter, but also production of new compounds that potentially have different isotopic compositions than the original source material. A classic example has been presented by Freeman et al. (1990) analyzing hydrocarbons from the Messel shale in Germany (see Table 3.3). Considered as a whole, recent marine sediments show a mean $\delta^{13}C$-value of −25 ‰ (Deines 1980). Some ^{13}C loss occurs with transformation to kerogen, leading to an average $\delta^{13}C$-value of −27.5 ‰ (Hayes et al. 1983). This ^{13}C depletion might be best explained by the large losses of CO_2 that occur during the transformation to kerogen and which are especially pronounced during the decarboxylation of some ^{13}C-rich carboxyl groups. With further thermal maturation the opposite effect (a^{13}C enrichment) is observed. Experimental studies of Peters et al. (1981) and Lewan (1983) indicate that thermal alteration produces a maximum ^{13}C change of about +2 ‰ in kerogens. Changes of more than 2 ‰ are most probably not due to isotope fractionation during thermal degradation of kerogen, but rather to isotope exchange reactions between kerogen and carbonates.

Whereas carbon tends to be preserved during diagenesis and maturation, hydrogen is exchanged during various diagenetic reactions with environmental water. δD-values of organic compounds, therefore, can be regarded as a continuously evolving system that can provide information about processes during burial of sedimentary rocks (Sessions et al. 2004). Radke et al. (2005) examined how maturation processes alter the δD-value of individual compounds. They demonstrated that aliphatic hydrocarbons are most favourable to record the primary composition because they resist hydrogen exchange. Pedentschouk et al. (2006) argued that n-alkanes and isoprenoids have the potential to preserve the original biological signal till the onset of oil generation.

The isotopic compositions of the end products of organic matter diagenesis - carbon dioxide, methane and insoluble complex kerogen- may record the primary depositional environment. Boehme et al. (1996) determined the C-isotope budget in a well defined coastal site. These authors demonstrated that the degradation of biogenic carbon proceeds via sulfate reduction and methanogenesis. The dominant carbon isotope effect during diagenesis is associated with methanogenesis, which shifts the carbon isotope value of the carbon being buried towards higher ^{13}C-contents.

3.9.6 Oil

Questions concerning the origins of coal and petroleum center on three topics: the nature and composition of the parent organisms, the mode of accumulation of the organic material, and the reactions whereby this material was transformed into the end products.

Petroleum or crude oil is a naturally occurring complex mixture, composed mainly of hydrocarbons. Although there are, without any doubt, numerous compounds that have been formed directly from biologically produced molecules, the majority of petroleum components are of secondary origin, either decomposition products or products of condensation and polymerization reactions.

Combined stable isotope analysis (^{13}C, D, $^{!5}$N, ^{34}S) has been used successfully in petroleum exploration (Stahl 1977; Schoell 1984; Sofer 1984). The isotopic composition of crude oil is mainly determined by the isotopic composition of its source material, more specifically, the type of kerogen and the sedimentary environment in which it has been formed and by its degree of thermal alteration (Tang et al. 2005). Other secondary effects like biodegradation, water washing, and migration distances appear to have only minor effects on its isotopic composition.

Variations in ^{13}C have been the most widely used parameter. Generally, oils are depleted by 1–3 ‰ compared to the carbon in their source rocks. The various chemical compounds within crude oils show small, but characteristic δ^{13}C-differences. With increasing polarity the ^{13}C-content increases from the saturated to aromatic hydrocarbons to the heterocomponents (N, S, O compounds) and to the asphaltene fraction. These characteristic differences in ^{13}C have been used for correlation purposes. Sofer (1984) plotted the ^{13}C-contents of the saturated and aromatic fractions against each other. Oils and suspected source rock extracts that are derived from similar types of source materials will plot together in such a graph whereas those derived from different types of source material will plot in other regions of the graph. The approach of Stahl (1977) and Schoell (1984) is somewhat different: the ^{13}C-contents of the different fractions are plotted as shown in Fig. 3.37. In this situation, oils derived from the same source rock will define a near linear relationship in the plot. Figure 3.37 illustrates a positive oil-oil correlation and a negative oil-source rock correlation.

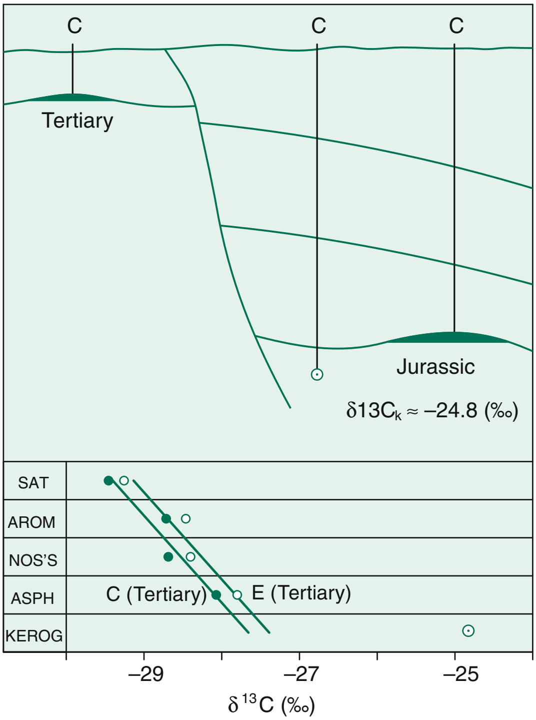

Fig. 3.37 Petroleum-type curves of different oil components from the North Sea showing a positive oil-oil correlation and a negative source rock—oil correlation (*SAT* saturated hydrocarbons, *AROM* aromatic hydrocarbons, *NOS'S* heterocompounds, *ASPH* asphaltenes (Stahl 1977) (Fig. 3.37, 6th edition, p. 186)

Combined compound specific ^{13}C and D-analyses have been applied in a number of areas of petroleum geochemistry. Tang et al. 2005 demonstrated that variation in δD-values of long chain hydrocarbons provide a sensitive measure of the extent of thermal maturation. Such studies have demonstrated that thermal maturation processes tend to alter the shape of the curves, particularly the curves for the saturate fraction, making correlations more difficult. Furthermore oil migration might affect the isotope composition. Generally a slight ^{13}C depletion is observed with migration distance, which is caused by a relative increase in the saturate fraction and a loss in the more ^{13}C-enriched aromatic and asphaltene fraction.

Compound-specific analyses also indicate that ^{13}C differences between the isoprenoid-hydrocarbons, pristane, and phytane, for which a common origin from chlorophyll is generally assumed, point to different origins of these two components (Freeman et al. 1990). Other classes of biomarkers, such as the hopanes, are also not always derived from a common precursor. Schoell et al. (1992) have demonstrated that hopanes from an immature oil can be divided into two groups: one that is ^{13}C depleted by 2–4 ‰ relative to the whole oil, whereas the other is depleted by 9 ‰, which suggests that the latter group is derived from chemoautotrophic bacteria which utilize a ^{13}C-depleted source. These results indicate that the origin and fate of organic compounds are far more complicated than was previously assumed.

Individual organosulfur compounds may reveal ^{34}S-variations of up to 50 ‰ in oils from the same source rock (Amrani et al. 2012; Amrani 2014). ^{34}S-variations between individual sulphur compounds reflect different stages of thermal sulphate reductions and thus can be used as an indicator of different stages of thermal sulphate alteration.

3.9.7 Coal

Carbon and hydrogen isotope compositions of coals are rather variable (Schiegl and Vogel 1970; Redding et al. 1980; Smith et al. 1982; Schimmelmann et al. 1999; Mastalerz and Schimmelmann 2002). Different plant communities and climates may account for these variations. Due to the fact that during coalification, the amount of methane and other higher hydrocarbons liberated is small compared to the total carbon reservoir, very little change in the carbon isotope composition seems to occur with increasing grade of coalification.

The D/H ratio in coals is usually measured on total hydrogen, although it consists of two portions: exchangeable and non-exchangeable hydrogen. In lignite up to 20 % of hydrogen consists of isotopically labile hydrogen that exchanges fast and reversibly with ambient water. With increasing temperature (maturity) the exchangeable portion decreases to about 2 % (Schimmelmann et al. 1999; Mastalerz and Schimmelmann 2002). Non-exchangeable organic hydrogen may have preserved original biochemical D/H ratios. δD-values in coals typically become isotopically heavier with increasing maturity, which suggests that exchange between organic hydrogen and formation water occurs during thermal maturation.

The origin and distribution of sulfur in coals is of special significance, because of the problems associated with the combustion of coals. Sulfur in coals usually occurs in different forms, as pyrite, organic sulfur, sulfates, and elemental sulfur. Pyrite and organic sulfur are the most abundant forms. Organic sulfur is primarily derived from two sources: the originally assimilated organically- bound plant sulfur preserved during the coalification process, and biogenic sulfides which reacted with organic compounds during the biochemical alteration of plant debris.

Studies by Smith and Batts (1974), Smith et al. (1982), Price and Shieh (1979) and Hackley and Anderson (1986) have shown that organic sulfur exhibits rather characteristic S-isotope variations, which correlate with sulfur contents. In low-sulfur coals δ^{34}S-values of organic sulfur are rather homogeneous and reflect the primary plant sulfur. By contrast, high-sulfur coals are isotopically more variable and typically have more negative δ^{34}S-values, suggesting a significant contribution of sulfur formed during bacterial processes.

3.9.7.1 Black Carbon

The combustion of organic material under restricted oxygen concentration produces carbon-rich materials such as charcoal and soot. This black carbon is a common minor component in many recent and palaeoenvironments, because it is resistant to decay and thus the carbon isotope composition may allow deductions about its origin (Bird and Ascough 2012 and others). However, what has to be taken into account is the fact, that charcoal and other forms of black carbon may change its isotope composition during pyrolysis by up to 2 ‰ with pyrolysis temperature and conditions (vacuum or open fire conditions).

3.9.8 Natural Gas

Natural gases are dominated by a few simple hydrocarbons, which may form in a wide variety of environments. While methane is always a major constituent of the gas, other components may be higher hydrocarbons (ethane, propane, butane), CO_2, H_2S, N_2 and rare gases. Two different types of gas occurrences can be distinguished—biogenic and thermogenic gas—the most useful parameters in distinguishing both types are their $^{13}C/^{12}C$ and D/H ratios. Complications in assessing sources of natural gases are introduced by mixing, migration and oxidative alteration processes. For practical application an accurate assessment of the origin of a gas, the maturity of the source rock and the timing of gas formation would be desirable. A variety of models has been published that describes the carbon and hydrogen isotope variations of natural gases (Berner et al. 1995; Galimov 1988; James 1983, 1990; Rooney et al. 1995; Schoell 1983, 1988).

Rather than using the isotopic composition of methane alone James (1983, 1990) and others have demonstrated that carbon isotope fractionations between the hydrocarbon components (particularly propane, iso-butane and normal butane) within a natural gas can be used with distinct advantages to determine maturity, gas-source rock and gas-gas correlations. With increasing molecular weight, from C_1 to C_4, a ^{13}C enrichment is observed which approaches the carbon isotope composition of the source.

Genetic models for natural gases were based in the past primarily on field data and on empirical models. More recently, mathematical modeling based on Rayleigh distillation theory and kinetic isotopic theory (Rooney et al. 1995; Tang et al. 2000) may explain why, in a single gas $\delta^{13}C$ values increase from C_1 to C_4 and why in different gases $\delta^{13}C$ values of a given hydrocarbon increase with increasing thermal maturity. Such models may provide information on the isotope composition of each gas at any stage of generation.

Although most natural gas occurences yield the sequence $\delta^{13}C_1$ (methane) $\leq \delta^{13}C_2$(ethane) $\leq \delta^{13}C_3$(propane), an increasing number of studies (Jenden et al. 1993; Burruss and Laughrey 2010; Tilley and Muehlenbachs 2013; Xia et al. 2013 and others) have described reversed isotope trends with $\delta^{13}C_1 \geq \delta^{13}C_2 \geq \delta^{13}C_3$. Gases with reversed trends can be explained by mixing of primary gas (methane from kerogen cracking) and secondary gas ("wetter" gas from intermediate products of kerogen with a higher proportion of higher alkanes).

Apart from gas sources and formation mechanisms, isotope effects during migration might affect the isotope composition of natural gas. Early experimental work has indicated that migrating methane could be enriched in ^{12}C or ^{13}C depending on the mechanism of migration and on the properties of the medium through which the gas is moving. Experiments by Zhang and Kroos (2001) on natural shales with different organic matter contents demonstrate variable ^{13}C depletions (1–3 ‰) during migration, which depend on the amount of organic matter in shales.

Of special interest in recent years has been the analysis of natural gas hydrates that form in marine sediments and polar rocks when saline pore waters are saturated with gas at high pressure and low temperature. Large $\delta^{13}C$ and δD-variations of hydrate bound methane, summarized by Kvenvolden (1995) and Milkov (2005), suggest that gas hydrates represent complex mixtures of gases of both microbial and thermogenic origin. The proportions of both gas types can vary significantly even between proximal sites.

As has been proposed by numerous studies (e.g. Röhl et al. 2000; Dickens 2003) the massive release of gas hydrates could modify climate. The best example for this hypothesis are sedimentary rocks deposited at around 55 Ma during the Paleocene-Eocene thermal maximum, where a $\delta^{13}C$ decrease of 2–3 ‰ in carbonate-carbon is interpreted as a consequence of an abrupt thermal release of gas-hydrate methane and its subsequent incorporation into the carbonate pool.

3.9.8.1 Biogenic Gas

According to Rice and Claypool (1981), over 20 % of the world's natural gas accumulations are of biogenic origin. Biogenic methane commonly occurs in recent anoxic sediments and is well documented in both freshwater environments, such as lakes and swamps, and in marine environments, such as estuaries and shelf regions. Two primary metabolic pathways are generally recognized for methanogenesis: fermentation of acetate and reduction of CO_2. Although both pathways may occur in marine and freshwater environments, CO_2-reduction is dominant in the sulfate-free zone of marine sediments, while acetate fermentation is dominant in freshwater sediments.

During microbial action, kinetic isotope fractionations on the organic material by methanogenic bacteria result in methane that is highly depleted in ^{13}C, typically with $\delta^{13}C$-values between −110 to −50 ‰ (Schoell 1984, 1988; Rice and Claypool 1981; Whiticar et al. 1986). In marine sediments, methane formed by CO_2 reduction is often more depleted in ^{13}C than methane formed by acetate fermentation in freshwater sediments. Thus, typical $\delta^{13}C$ ranges for marine sediments are between −110 and −60 ‰, while those for methane from freshwater sediments are from −65 to −50 ‰ (Whiticar et al. 1986; Whiticar 1999).

The difference in composition between methane of freshwater and of marine origin is even more pronounced on the basis of hydrogen isotopes. Marine bacterial methane has δD-values between −250 to −170 ‰ while biogenic methane in freshwater sediments is strongly depleted in D with δD-values between −400 to −250 ‰ (Whiticar et al. 1986; Whiticar 1999). Different hydrogen sources may account for these large differences: formation waters supply the hydrogen during CO_2 reduction, whereas during fermentation up to three quarters of the hydrogen come directly from the methyl group, which is extremely depleted in D.

3.9.8.2 Thermogenic Gas

Thermogenic gas is produced when organic matter is deeply buried and—as a consequence—temperature rises. Thereby, increasing temperatures modify the organic matter due to various chemical reactions, such as cracking and hydrogen disproportionation in the kerogen. ^{12}C–^{12}C bonds are preferentially broken during the first stages of organic matter maturation. As this results in a ^{13}C-enrichment of the residue, more ^{13}C–^{12}C bonds are broken with increasing temperatures which produces higher $\delta^{13}C$-values. Thermal cracking experiments carried out by Sackett (1988) have confirmed this process and demonstrated that the resulting methane is depleted in ^{13}C by some 4–25 ‰ relative to the parent material. Thus, thermogenic gas typically has $\delta^{13}C$-values between −50 and −20 ‰ (Schoell 1980, 1988). Gases generated from non-marine (humic) source rocks are isotopically enriched relative to those generated from marine (sapropelic) source rocks at equivalent levels of maturity. In contrast to $\delta^{13}C$-values, δD-values are independent of the composition of the precursor material, but solely depend on the maturity of kerogen.

In conclusion, the combination of carbon and hydrogen isotope analysis of natural gases is a powerful tool to discriminate different origins of gases. In a plot of $\delta^{13}C$ versus δD (see Fig. 3.38) not only is a distinction of biogenic and thermogenic gases from different environments clear, but it is also possible to delineate mixtures between the different types.

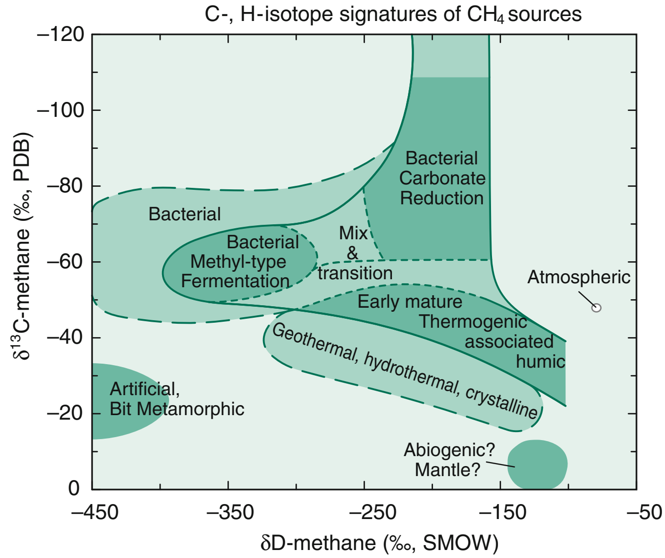

Fig. 3.38 $\delta^{13}C$ and δD variations of natural gases of different origins (after Whiticar 1999) Fig. 3.38, 6th edition, p. 190)

3.9.8.3 Isotope Clumping in Methane

Ten isotopologues of methane contribute to the generally given $\delta^{13}C$ and δD-values. If methane forms in internal equilibrium, excesses of clumped isotopologues yield informations about temperatures of methane formation (Eiler et al. 2014). With conventional mass spectrometers, the relative contribution of each isotopologue cannot be measured. Using a high resolution multi-collector mass spectrometer, Stolper et al. (2014) were able to measure clumped isotope distributions of methane. They demonstrated that precise measurements of the abundance of $^{13}CH_3D$ and $^{12}CH_2D_2$ can be used as a geothermometer allowing the distinction of biogenic from thermogenic methane.

3.9.8.4 Abiogenic Methane

Abiogenic methane is defined as methane that does not involve biogenic organic precursors (Welhan 1988). Methane emanating in mid-ocean ridge hydrothermal systems is one of the occurrences for which an abiogenic formation can be postulated with confidence. Considerably higher $\delta^{13}C$-values than biogenic methanes (up to −7 ‰; Abrajano et al. 1988) were thought to be the characteristic feature of abiogenic methane. Horita and Berndt (1999) demonstrated that abiogenic methane can be formed under hydrothermal conditions in the presence of a nickel-iron catalyst. Isotope fractionations induced by the catalyst, however, result in very low $\delta^{13}C$-values. In serpentinites, the circulation of water induces mineral reactions, which may release hydrogen (H_2) that under Fischer-Tropsch type reactions form methane. Another important source of abiogenic methanogenesis has been found in crystalline rocks from the Canadian and Ferroscandian shield areas (Sherwood Lollar et al. 1993; Sherwood Lollar et al. (2002).

Etiope and Sherwood-Lollar (2013) and Etiope and Schoell (2014) demonstrated that abiotic methane is more common than previously thought. These authors listed nine specific mechanisms of CH_4 production in two main environments: (i) high-temperature magmatic processes and (ii) low-temperature (below 150 °C) serpentinization processes of ultramafic rocks. The isotopic composition may be divided into two groups: ^{13}C and D enriched ($\delta^{13}C$-values ≥ -20 and $\delta D \geq -200$) and ^{13}C and D depleted ($\delta^{13}C \leq -30$ and $\delta D \leq -200$). Clumped isotope data of abiogenic methane yields a large range of high temperatures of formation (Stolper et al. 2014).

The two groups may reflect variable mantle or crustal sources and/or variable degrees of CO_2 and CH_4 isotope exchange. Nevertheless, it remains problematic to distinguish abiogenic from biogenic organic compounds on the basis of their $\delta^{13}C$ and δD signatures (Taran et al. 2007; Bradley and Summons 2010; Etiope and Sherwood-Lollar 2013).

3.9.8.5 Nitrogen in Natural Gas

Nitrogen is sometimes a major constituent of natural gases, but the origin of this nitrogen is still enigmatic. While a certain fraction is released from degrading sedimentary organic matter during burial, several non-sedimentary sources of nitrogen may also contribute to the natural gas. By analyzing nitrogen-rich natural gases from California's Great Valley, Jenden et al. (1988) demonstrated, however, that these gases had a complex origin involving mixing of multiple sources. These authors interpreted relatively constant $\delta^{15}N$-values between 0.9 and 3.5 ‰ as indicating a deep-crustal metasedimentary origin. Hydrocarbon-rich and nitrogen-rich gases can thus be genetically unrelated.

3.10 Sedimentary Rocks

Sediments are the weathering products and residues of magmatic, metamorphic, and sedimentary rocks and reflect weathering, erosion, transport and accumulation in water and air. As a result, sediments may be complex mixtures of material that has been derived from multiple sources. It is convenient to consider sedimentary rocks, and the components of sedimentary rocks, in two categories: clastic and chemical. Transported fragmental debris of all kinds makes up the clastic component of the rock. Inorganic and organic precipitates from water belong to the chemical constituents. According to their very different constituents and low temperatures of formation, sedimentary rocks may be extremely variable in isotopic composition. For example, the $\delta^{18}O$-values of sedimentary rocks span a large range from about +10 (certain sandstones) to about +44 ‰ (certain cherts).

3.10.1 Clay Minerals

Savin and Epstein (1970a and b) and Lawrence and Taylor (1971) established the general isotope systematics of clay minerals from continental and oceanic environments. Subsequent reviews by Savin and Lee (1988) and Sheppard and Gilg (1996) have summarized the isotope studies of clay minerals applied to a wide range of geological problems. All applications depend on the knowledge of isotope fractionation factors between clay minerals and water, the temperature, and the time when isotopic exchange with the clay ceased. Because clay minerals may be composed of a mixture of detrital and authigenic components, and because particles of different ages may have exchanged to varying degrees, the interpretation of isotopic variations of clay minerals requires a firm understanding of the clay mineralogy of a given sediment.

By comparison with many other silicate minerals, isotope studies of natural clays are complicated by a number of special problems related to their small particle size and, hence, much larger specific surface area and the presence of interlayer water in certain clays. Surfaces of clays are characterized by 1 or 2 layers of adsorbed water. Savin and Epstein (1970a) demonstrated that adsorbed and interlayer water can exchange its isotopes with atmospheric water vapour in hours. Complete removal of interlayer water for analysis with the total absence of isotopic exchange between it and the hydroxyl group, may not be possible in all instances (Lawrence and Taylor 1971).

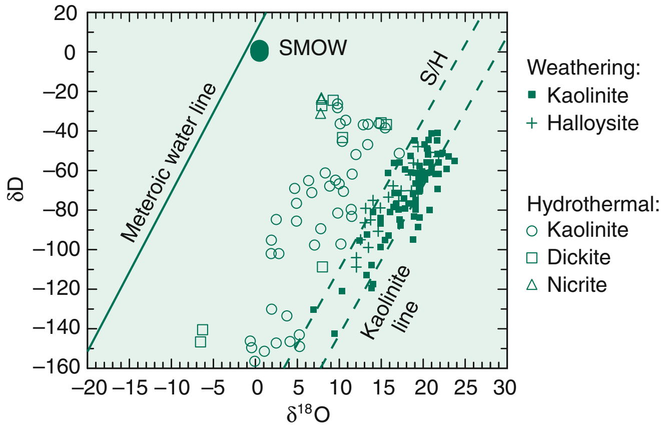

Fig. 3.39 δD and $\delta^{18}O$ values of kaolinites and related minerals from weathering and hydrothermal environments. The Meteoric Water Line, kaolinite weathering and supergene/hypogene (S/H) lines are given for reference (after Sheppard and Gilg 1996) (Fig. 3.39, 6th edition, p. 192)

One portion of the oxygen in clay minerals occurs as the hydroxyl ion. Hamza and Epstein (1980), Bechtel and Hoernes (1990) and Girard and Savin (1996) have attempted to separate the hydroxyl and non-hydoxyl bonded oxygen for separate isotope analysis. Techniques include thermal dehydroxylation and incomplete fluorination, both of which indicate that hydroxyl oxygen is considerably depleted in ^{18}O relative to non-hydroxyl oxygen.

Do natural clay minerals retain their initial isotopic compositions? Evidence concerning the extent of isotopic exchange for natural systems is contradictory (Sheppard and Gilg 1996). Many clay minerals such as kaolinite, smectite and illite are often out of equilibrium with present-day local waters. This is not to imply that these clay minerals never underwent any post-formational or retrograde exchange. Sheppard and Gilg (1996) concluded that convincing evidence for complete O- and/or H-isotope exchange without recrystallization is usually lacking, unless the clay has been subjected to either higher temperatures or an unusual set of geological circumstances. Thus, isotopic compositions of clay minerals that formed in contact with meteoric waters should have isotopic compositions that plot on sub-parallel lines to the Meteoric Water Line, the offset being related to their respective fractionation factor (see Fig. 3.39). This implies that some information of past environments is usually recorded in clay minerals and in suitable cases can be used as a paleoclimate indicator (Stern et al. 1997; Chamberlain and Poage 2000; Gilg 2000). By analysing a large number of smectites from the Basin and Range Province and the Great Plains in North America, Mix and Chamberlain (2014) concluded that in some localities temperature change is the decisive factor in controlling the D and ^{18}O isotope composition, while in other localities the change in meteoric water composition is responsible for the variations in isotope composition.

3.10.2 Clastic Sedimentary Rocks

Clastic sedimentary rocks are composed of detrital grains that normally retain the oxygen isotope composition of their source and of authigenic minerals formed during weathering and diagenesis, whose isotopic composition is determined by the physicochemical environment in which they formed. This means authigenic minerals formed at low temperatures will be enriched in ^{18}O compared to detrital minerals of igneous origin (Savin and Epstein 1970b). Due to the difficulty of separating authigenic overgrowths from detrital cores, few studies of this kind have been reported in the literature. However, recent improvements in the precision of ion microbe analysis with high spatial resolution (1–10 µm) both types of quartz can be clearly distinguished (see Fig. 3.40, Kelly et al. 2007). These authors suggested that the homogeneous $\delta^{18}O$ values of quartz overgrowth formed from meteoric waters at low temperatures (10–30 °C).

^{18}O enrichments of authigenic minerals are controlled by fluid composition, temperature, and the effective mineral/water ratio. Is the fluid a low-^{18}O meteoric water, the oxygen isotope composition of the precipitating mineral will have a low-^{18}O signature, assuming no change in temperature (Longstaffe 1989). Thus, the changes that occur in sedimentary rocks during diagenesis are largely a function of fluid composition, fluid/rock ratio and temperature.

One way to estimate temperatures employs the oxygen isotope composition of diagenetic assemblages. For example, using quartz–illite pairs from the Precambrian Belt Supergroup, Eslinger and Savin (1973) calculated temperatures that range from 225 to 310 °C, with increasing depth. In this case the $\delta^{18}O$-values were consistent with the observed mineralogy and fractionations between minerals are reasonable for the grade of burial metamorphism. This approach assumes that the diagenetic minerals used have equilibrated their O-isotopes with each other and that no retrograde re-equilibration occurred following maximum burial.

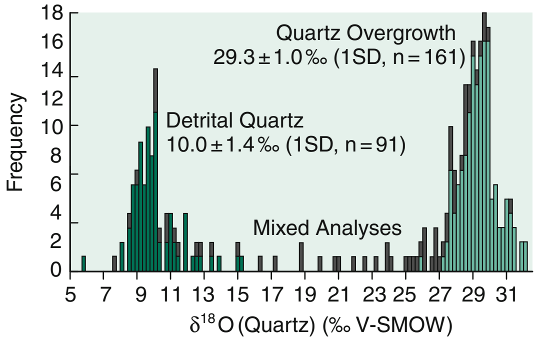

Fig. 3.40 Histogram of $\delta^{18}O$-values of quartz in sandstone from 6–10 µm spots by ion microprobe. Mixed analyses are on the boundary of detrital quartz and quartz overgrowth (Kelly et al. 2007) (Fig. 3.40, 6th edition, p. 193)

Another application of stable isotopes in clastic rocks is the analysis of weathering profiles, which can potentially provide insight into the continental climate during their formation. Despite this potential, only few studies (Bird and Chivas 1989; Bird et al. 1992) have used this approach because of the (i) imprecise knowledge of mineral-water fractionations at surficial temperatures and (ii) the difficulty of obtaining pure phases from complex, very fine grained rocks. Bird et al. (1992) developed partial dissolution techniques and used this methodology to separate nine pure minerals from a lateritic soil in Haiti (see Fig. 3.41). The measured δ^{18}O-values for some minerals agree with ^{18}O/^{16}O ratios predicted from available fractionation factors, whereas other do not. Discrepancies might be due to incorrect fractionation factors for the respective minerals or to processes that may have influenced the formation of particular minerals (e.g. evaporation) (Bird et al. 1992).

Lastly, detrital minerals in clastic sediments can be used for provenance studies. If not recrystallized, many common rock-forming minerals, such as quartz, muscovite, garnets etc. can retain their original source rock compositions up to medium-grade metamorphic conditions. Hence, they can potentially be used as tracers of provenance to the sediments. Applications of this type of approach are useful, particularly for siliciclastic sediments that may lack other indicator minerals of provenance. Examples of such applications have been given by Vennemann et al. (1992) and (1996) for the provenance of Archean Au- and U-bearing conglomerates of South Africa and Canada. δ^{18}O-values of well dated zircons may be used to document changes with time in the composition of sediments (Valley et al. 2005) (see discussion on p. 219)

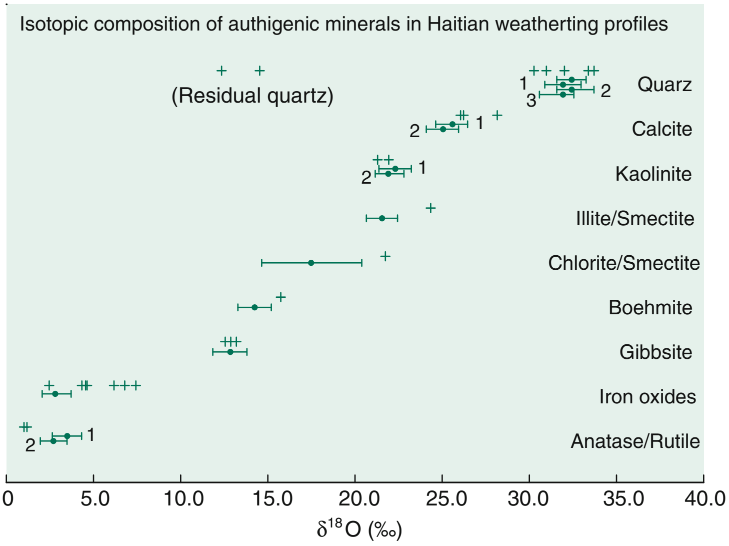

Fig. 3.41 Predicted (*bars*) and measured (*crosses*) oxygen isotope composition of separated minerals from Haitian weathering profiles. The range of predicted δ^{18}O-values are calculated assuming a temperature of 25 °C and a meteoric water δ^{18}O-value of −3.1 ‰ (after Bird et al. 1992) (Fig. 3.41, 6th edition, p. 194)

3.10.3 Biogenic Silica and Cherts

3.10.3.1 Biogenic Silica

Due to the large oxygen isotope fractionation between SiO_2 and water at low temperatures, biogenic silica and cherts represent the "heaviest" oxygen isotope components in nature. Just as is the case for carbonates, the oxygen isotope composition of biogenic silica such as diatoms and radiolarians is potentially a paleoclimate indicator, which would enable the extension of climate records into oceanic regions depleted in $CaCO_3$ such as high latitude regions. Thus a variety of techniques have been developed for the extraction of biogenic silica oxygen. The presence of loosely bound water within cherts and biogenic silica precipitates complicates measurements of the O-isotope composition of biogenic silica. Biogenic silica has an amorphous structure containing not only Si–O–Si bonds, but Si–OH bonds and crystallization water which easily can exchange with environmental water and making it imperative to be removed before isotope analysis. At present 3 techniques exist (Chapligin et al. 2011):

(i) Controlled isotope exchange. Using controlled exchange with waters of different isotope composition, Labeyrie and Juillet (1982) and Leclerc and Labeyrie (1987) were able to estimate the isotope ratio of both exchanged and unexchanged silica-bound oxygen.

(ii) Stepwise fluorination

Haimson and Knauth (1983), Matheney and Knauth (1989) and Dodd and Sharp (2010) noted that the first fractions of oxygen were ^{18}O depleted compared with oxygen recovered in later fractions, suggesting that the water-rich components of hydrous silica react preferentially in the early steps of fluorination.

(iii) High temperature carbon reduction (Lücke et al. 2005).

The technique is based on inductive high temperature heating (>1500 °C) leading to carbon monoxide. It enables complete dehydration and decomposition in a single continuous process.

Silica-water oxygen isotope fractionation factors differ considerably: Diatoms from sediment cores (Matheney and Knauth 1989) are up to 8 ‰ higher than living fresh water diatoms (Brandriss et al. 1998; Dodd and Sharp 2010) or diatoms from sediment traps (Moschen et al. 2006; Schmidt et al. 2001).

Schmidt et al. (2001) demonstrated that the enrichment in sedimentary diatoms can be correlated with structural and compositional changes arising from the in situ condensation of Si-OH groups during silica maturation in surface sediments. Dodd et al. (2013) argued that the ^{18}O enrichment in sedimentary diatoms is due to post-mortem alteration. They demonstrated that diatoms can reach near equilibrium silica water compositions within half a year after diatom death.

3.10.3.2 Cherts

In sediments, opaline skeletons are dissolved and transform to different forms of silica. Microquartz (crystal size between 2–20 µm) and chalcedonic quartz represent the first forms of silica precipitated during chert formation. As was shown from the early studies of Degens and Epstein (1962), cherts exhibit temporal isotopic variations like carbonates: the older cherts having lower ^{18}O contents. Thus, cherts of different geological ages may contain a record of temperature, isotopic composition of ocean water, and diagenetic history. However, because cherts may have formed by sedimentary, hydrothermal and volcanic silification and may have been altered by metamorphic fluids, the reconstruction of ocean water temperatures on the basis of ^{18}O-values remain a matter of debate.

High resolution in situ O- and Si-isotope analysis of cherts (Marin et al. 2010; Marin-Carbonne et al. 2011, 2012; Steinhoefel et al. 2010; Chakrabarti et al. 2012) reveal very large O- and Si-isotope variations on the micrometer-scale that complicate a temperature determination indicating oxygen isotope exchange during burial diagenesis and the formation of microquartz from diagenetic or metamorphic fluids.

Low δ^{30}Si-values in Archean cherts favor a hydrothermal source of silica, increasing δ^{30}Si-values during the Proterozoic may reflect an increase in continental Si-sources relative to hydrothermal ones (Chakrabarti et al. 2012).

3.10.4 Marine Carbonates

3.10.4.1 Oxygen

In 1947, Urey discussed the thermodynamics of isotopic systems and suggested that variations in the temperature of precipitation of calcium carbonate from water should lead to measurable variations in the ^{18}O/^{16}O ratio of the calcium carbonate. He postulated that the determination of temperatures of the ancient oceans should be possible, in principle, by measuring the ^{18}O content of fossil shell calcite. The first paleotemperature "scale" was introduced by Mc Crea (1950). Subsequently this scale has been refined several times. Through experiments which compare the actual growth temperatures of foraminifera with calculated isotope temperatures Erez and Luz (1983) determined the following temperature equation

$$T^\circ C = 17.0 - 4.52\,(\delta^{18}O_c - \delta^{18}O_w) + 0.03\,(\delta^{18}O_c - \delta^{18}O_w)^2$$

where $\delta^{18}O_c$ is the O-isotope composition of CO_2 derived from carbonate and $\delta^{18}O_w$ is the O-isotope composition of CO_2 in equilibrium with water at 25 °C.

According to this equation an ^{18}O increase of 0.26 ‰ in carbonate represents a 1 °C temperature decrease. Bemis et al. (1998) have re-evaluated the different temperature equations and demonstrated that they can differ as much as 2 °C in the temperature range between 5 and 25 °C. The reason for these differences is that in addition to temperature and water isotopic composition, the δ^{18}O of a shell may be affected by the carbonate ion concentration in seawater and by photosynthetic activity of algal symbionts.

Laboratory experiments and field studies on biogenic and inorganic $CaCO_3$ have demonstrated that nonequilibrium effects such as carbonate concentration, pH and precipitation rates may also affect measured $CaCO_3$ compositions. As Dietzel et al. (2009) argued there is no definite proof that spontaneously precipitated calcite from aqueous solution is in true oxygen isotope equilibrium and it can well be that currently adapted equilibrium values for calcite-water fractionations are actually too low (Coplen 2007).

Before a meaningful temperature calculation of a fossil organism can be carried out several assumptions have to be fulfilled. The isotopic composition of an aragonite or calcite shell will remain unchanged until the shell material dissolves and recrystallizes during diagenesis. In most shallow depositional systems, C- and O-isotope ratios of calcitic shells are fairly resistant to diagenetic changes, but many organisms have a hollow structure allowing diagenetic carbonate to be added. With increasing depths of burial and time the chances of diagenetic effects generally increase. Because fluids contain much less carbon than oxygen, $\delta^{13}C$-values are thought to be less affected by diagenesis than $\delta^{18}O$-values. Criteria of how to prove primary preservation are not always clearly resolved (see discussion "diagenesis of limestones"). Schrag (1999) argued that carbonates formed in warm tropical surface oceans are particularly sensitive to the effects of diagenesis, because pore waters—having much lower temperatures than tropical surface waters—could shift the primary composition to higher δ-values. This is not the case for high latitude carbonates, where surface and pore fluids are quite similar in their average temperature.

Shell-secreting organisms to be used for paleotemperature studies must have been precipitated in isotope equilibrium with ocean water. As was shown by studies of Weber and Raup (1966a, b), some organisms precipitate their skeletal carbonate in equilibrium with the water in which they live, but others do not. Wefer and Berger (1991) summarized the importance of the so-called "vital effect" on a broad range of organisms (see Fig. 3.42). For oxygen isotopes, most organisms precipitate $CaCO_3$ with isotope compositions close to predicted equilibrium values; if disequilibrium prevails, the isotopic difference from equilibrium is rather small (Fig. 3.42). For carbon, disequilibrium is the rule, with $\delta^{13}C$-values being more negative than expected at equilibrium. As discussed below, this does not preclude the reconstruction of the $^{13}C/^{12}C$ ratio of the palaeo-ocean waters.

Isotopic disequilibria effects can be classified as either metabolic or kinetic (McConnaughey 1989a, b). Metabolic isotope effects apparently result from changes in the isotopic composition of dissolved inorganic carbon in the neighborhood of the precipitating carbonate caused by photosynthesis and respiration. Kinetic isotope effects result from discrimination against ^{13}C and ^{18}O during hydration and hydroxylation of CO_2. Strong kinetic disequilibrium fractionation often is associated with high calcification rates (McConnaughey McConnaughey 1989a, b).

Besides temperature, a variable isotopic composition of the ocean is another factor responsible for ^{18}O variations in foraminifera. A crucial control is salinity: ocean waters with salinities greater than 3.5 % have a higher ^{18}O content, because ^{18}O is preferentially depleted in the vapor phase during evaporation, whereas waters with salinities lower than 3.5 % have a lower ^{18}O content due to dilution by fresh

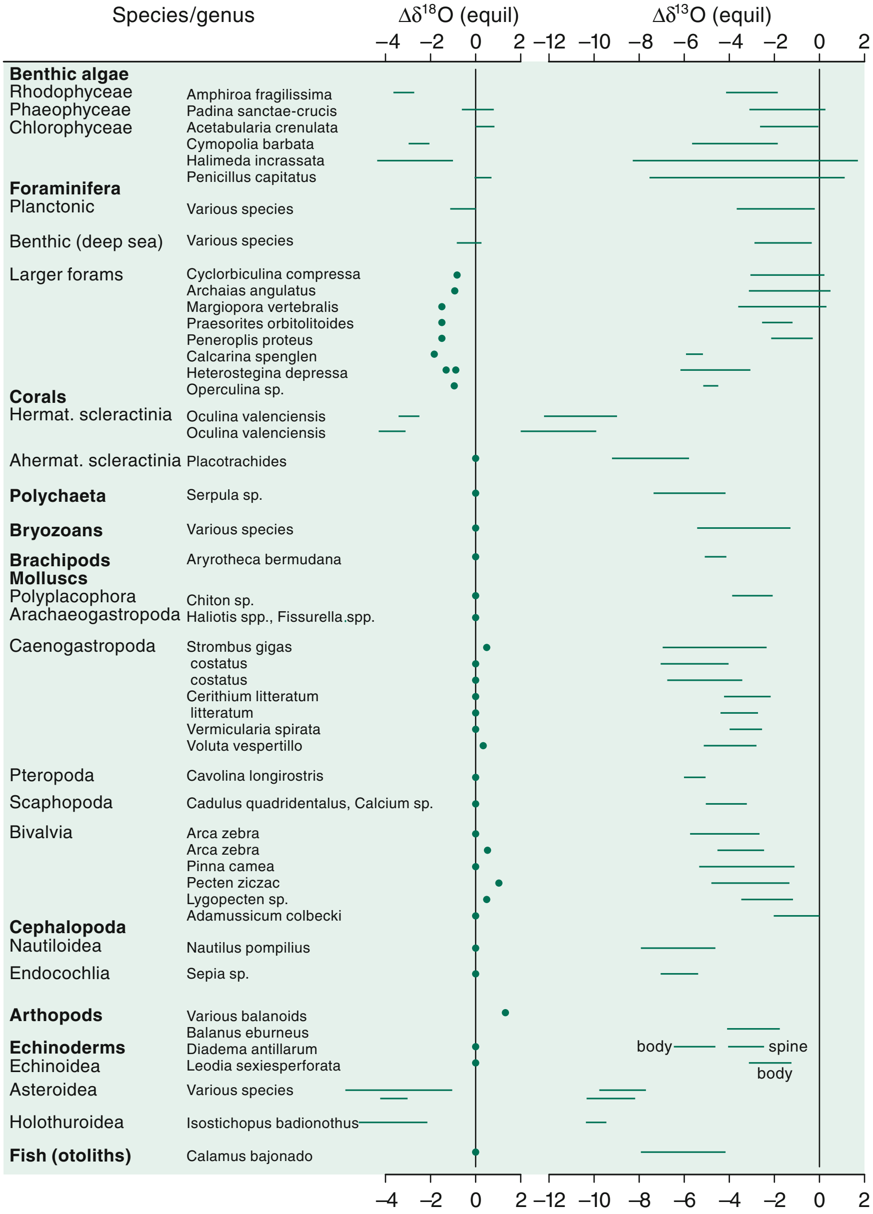

Fig. 3.42 $\Delta^{18}O$ and $\Delta^{13}C$ differences from equilibrium isotope composition of extant calcareous species (after Wefer and Berger 1991) (Fig. 3.42, 6th edition, p. 197)

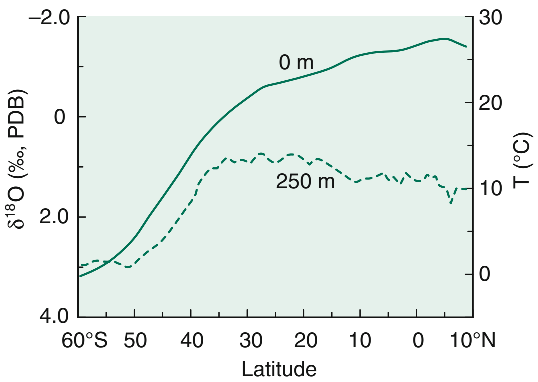

Fig. 3.43 Latitudinal distribution of O-isotope composition of planktonic foraminifera and yearly averaged temperatures at sea surface and 250 m water depth (after Mulitza et al. 1997) (Fig. 3.43, 6th edition, p. 198)

waters, especially meltwaters. The other factor which causes variations in the isotopic composition of ocean water is the volume of low-^{18}O ice present on the continents. As water is removed from the ocean during glacial periods, and temporarily stored on the continents as ^{18}O-depleted ice, the ^{18}O/^{16}O ratio of the global ocean increases in direct proportion to the volume of continental and polar glaciers. The magnitude of the temperature effect versus the ice volume effect can be largely resolved by separately analyzing planktonic and benthic foraminifera. Planktonic foraminifera live vertically dispersed in the upper water column of the ocean recording the temperature and the isotopic composition of the water. Figure 3.43 shows a latitudinal plot of annually averaged temperature distribution at the sea surface and 250 m depth together with the δ^{18}O-values of different foraminifera species. The ^{18}O difference between shallow and deep-living planktonic foraminifera increases from nearly 0 ‰ in subpolar regions to ~3 ‰ in the tropics. The difference between shallow and deep-calcifying taxa can be used to calculate the vertical temperature gradient in the upper 250 m of the oceans.

It is expected that the temperature of deep-water masses is more or less constant, as long as ice caps exist at the poles. Thus, the oxygen isotope composition of benthic organisms should preferentially reflect the change in the isotopic composition of the water (ice-volume effect), while the δ^{18}O-values of planktonic foraminifera are affected by both temperature and isotopic water composition.

The best approach to disentangle the effect of ice volume and temperature is to study shell material from areas where constant temperatures have prevailed for long periods of time, such as the western tropical Pacific Ocean or the tropical Indian Ocean. On the other end of the temperature spectrum is the Norwegian Sea, where deep water temperatures are near the freezing point today and, therefore, cannot have been significantly lower during glacial time, particularly as the salinities are also already high in this sea. Within the framework of this set of limited assumptions, a reference record of the ^{18}O variations of a water mass which has experienced no temperature variations during the last climatic cycle can be obtained (Labeyrie et al. 1987).

A direct approach to measuring the δ^{18}O-value of seawater during the Last Glacial Maximum (LGM) is based on the isotopic composition of pore fluids (Schrag et al. 1996). Variations in deep water δ^{18}O caused by changes in continental ice volume diffuse down from the seafloor leaving a profile of δ^{18}O versus depth in the pore fluid. Using this approach Schrag et al. (1996) estimated that the global δ^{18}O change of ocean water during LGM is 1.0 ± 0.1 ‰.

In addition to these variables the interpretation of ^{18}O-values in carbonate shells is complicated by the seawater carbonate chemistry. In culture experiments with living foraminifera Spero et al. (1997) demonstrated that higher pH-values or increasing CO_3^{2-} concentrations result in isotopically lighter shells, which is due to changing sea water chemistry. As shown by Zeebe (1999) an increase of seawater pH by 0.2–0.3 units causes a decrease in ^{18}O of about 0.2–0.3 ‰ in the shell. This effect has to be considered for instance when samples from the last glacial maximum are analyzed.

Another approach to distinguish between the temperature effect and the unknown water composition is the clumped isotope thermometer (Eiler 2007; Ghosh et al. 2006; Tripati et al. 2010; Thiagarajan et al. 2011) that has the potential to circumvent the ambiguities of the classic carbonate thermometer of Urey (1947). Most species that exhibit non-equilibrium δ^{18}O- and δ^{13}C-values (vital effects) are characterized by ^{13}C-^{18}O bond abundances that are generally indistinguishable from equilibrium (Tripati et al. 2010).

Furthermore, clumping of ^{13}C and ^{18}O into carbonate structures is independent of the δ^{18}O of the water from which the mineral is formed. Calibrations of Δ_{47} for inorganic and biogenic calcite give a sensitivity of about 0.004–0.005 ‰/°C (Huntington et al. 2010; Tripati et al. 2010; Dennis and Schrag 2010; Wacker et al. 2014 and others) (see Fig. 1.5).

3.10.4.2 Carbon

A large number of studies have investigated the use of ^{13}C-contents of foraminifera as a paleo-oceanographic tracer. As previously noted, δ^{13}C-values are not in equilibrium with sea water. However, by assuming that disequilibrium ^{13}C/^{12}C ratios are, on average, invariant with time, then systematic variations in C-isotope composition may reflect variations in ^{13}C content of ocean water. The first record of carbon isotope compositions in Cenozoic deep-sea carbonates was given by Shackleton and Kennett (1975). They clearly demonstrated that planktonic and benthic foraminifera yield consistent differences in δ^{13}C-values, the former being enriched in ^{13}C by about 1 ‰ relative to the latter. This ^{13}C-enrichment in planktonic foraminifera is due to photosynthesis which preferentially incorporates ^{12}C in organic carbon thereby depleting surface waters in ^{12}C. A portion of the organic matter is transferred to deep waters, where it is reoxidized, which causes a ^{12}C enrichment in the deeper water masses. Figure 3.44 presents δ^{13}C-values of benthic foraminifera ranked according to their relative tendency to concentrate ^{13}C.

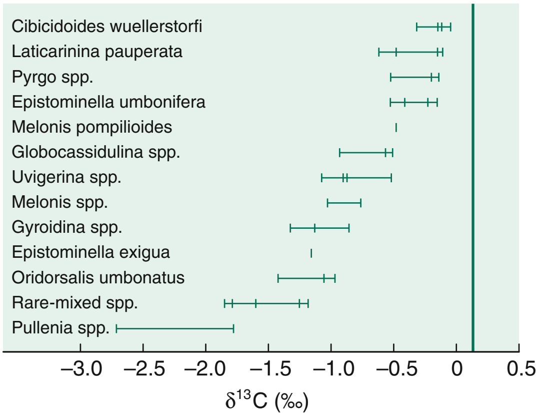

Fig. 3.44 δ^{13}C-values of benthic foraminifera species. The δ^{13}C-value for the dissolved bicarbonate in deep equatorial water is shown by the vertical line (after Wefer and Berger 1991) (Fig. 3.44, 6th edition, p. 200)

δ^{13}C-values in planktonic and benthic foraminifera can be used to monitor CO_2 variations in the atmosphere by measuring the vertical carbon isotope gradient, which is a function of the biological carbon pump. This approach was pioneered by Shackleton et al. (1983), who showed that enhanced contrast between surface waters and deeper waters was correlated with intervals of reduced atmospheric CO_2 contents. Increased organic carbon production in surface waters (possibly caused by enhanced nutrient availabilty) leads to removal of carbon from surface waters, which in turn draws down CO_2 from the atmospheric reservoir through re-equilibration.

Another application of carbon isotopes in foraminifera is to distinguish distinct water masses and to trace deep water circulation (Bender and Keigwin 1979; Duplessy et al. 1988). Since dissolved carbonate in the deeper waters becomes isotopically lighter with time and depths in the area of their formation due to the increasing oxidation of organic material, comparison of sites of similar paleodepth in different areas can be used to trace the circulation of deep waters as they move from their sources. Such a reconstruction can be carried out by analyzing δ^{13}C-values of well-dated foraminifera.

Reconstructions of pathways of deep-water masses in the North Atlantic during the last 60,000 years have been performed by analyzing high resolution records of benthic foraminifera *Cibicides wuellerstorfi*, as this species best reflects changes in the chemistry of bottom waters (Duplessy et al. 1988; Sarntheim et al. 2001). The initial δ^{13}C-signature of North Atlantic Deep Water (NADW) is ~1.3–1.5 ‰. As NADW flows southward the ongoing oxidation of organic matter results in a progressive ^{13}C-depletion down to less than 0.4 ‰ in the Southern Ocean. Reductions in ^{13}C observed in many cores from the North-Atlantic (Sarntheim et al. 2001; Elliot et al. 2002) have been interpreted as meltwater input to the surface ocean (Heinrich events), which caused changes in deep water circulation.

3.10.5 Diagenesis

Diagenetic modification of carbonates may begin immediately after the formation of primary carbonates. Two processes may change the isotope composition of carbonate shells: (i) cementation and (ii) dissolution and reprecipitation. (i) Cementation means the addition of abiogenic carbonate from ambient pore waters. Cements added early after primary formation may be in equilibrium with ocean water, whereas late cements depend on the isotope composition of pore waters and temperature. (ii) Dissolution and reprecipitation occurs in the presence of a bicarbonate containing pore fluid and represents the solution of an unstable carbonate phase such as aragonite and the reprecipitation of a stable carbonate phase, mostly low Mg-calcite. Diagenetic modification may occur in two subsequent pathways, often termed as burial and meteoric diagenesis.

3.10.5.1 Burial Pathway

This type of diagenetic stabilization is best documented in deep sea environments. Entrapped pore waters are of marine origin and in equilibrium with the assemblage of carbonate minerals. The conversion of sediment into limestone is not achieved by a chemical potential gradient, but rather through a rise in pressure and temperature due to deposition of additional sediments. In contrast to the meteoric pathway, fluid flow is confined to squeezing off pore waters upwards into the overlying sedimentary column. Theoretically, O-isotope ratios should not change appreciably with burial, because the $\delta^{18}O$ is of sea water origin. Yet, with increasing depth, the deep-sea sediments and often also the pore waters exhibit ^{18}O depletions by several permil (Lawrence 1989). The major reason for this ^{18}O depletion seems to be a low-temperature exchange with the oceanic crust in the underlying rock sequence. The ^{18}O shift in the solid phases is mostly due to an increase in temperature with increasing burial. Independent estimates of diagenetic temperatures may be obtained by clumped isotope thermometry (Huntington et al. 2011; Ferry et al. 2011).

The other important diagenetic process is the oxidation of organic matter. With increasing burial, organic matter in sediments passes successively through different zones which are characterized by distinct redox reactions that are mediated by assemblages of specific bacteria. The usual isotopic changes of these processes will result in a shift towards lighter C-isotope values, the degree of ^{13}C-depletion being proportional to the relative contribution of carbon from the oxidation of organic matter. Under special conditions of fermentation, the CO_2 released may be isotopically heavy, which may cause a shift in the opposite direction.

3.10.5.2 Meteoric Pathway

Carbonate sediments deposited in shallow marine environments are often exposed to the influence of meteoric waters during their diagenetic history. Meteoric diagenesis lowers $\delta^{18}O$- and $\delta^{13}C$-values, because meteoric waters have lower $\delta^{18}O$-values than seawater. For example, Hays and Grossman (1991) demonstrated that oxygen isotope compositions of carbonate cements depend on the magnitude of ^{18}O depletion of respective meteoric waters. δ^{13}C-values are lowered because soil bicarbonate is ^{13}C-depleted relative to ocean water bicarbonate.

A more unusual effect of diagenesis is the formation of carbonate concretions in argillaceous sediments. Isotope studies by Hoefs (1970), Sass and Kolodny (1972), and Irwin et al. (1977) suggest that micobiological activity created localized supersaturation of calcite in which dissolved carbonate species were produced more rapidly than they could be dispersed by diffusion. Extremely variable δ^{13}C-values in these concretions indicate that different microbiological processes participated in concretionary growth. Irwin et al. (1977) presented a model in which organic matter is diagenetically modified in a sequence by (a) sulfate reduction, (b) fermentation and (c) thermally induced abiotic CO_2 formation which can be distinguished on the basis of their δ^{13}C-values, (a) −25 ‰, (b) +15 ‰ and (c) −20 ‰.

3.10.6 Limestones

Early limestone studies utilized whole-rock samples. In later studies, individual components, such as different generations of cements, have been analyzed (Hudson 1977; Dickson and Coleman 1980; Moldovany and Lohmann 1984; Given and Lohmann 1985; Dickson et al. 1990). These studies suggest that early cements exhibit higher δ^{18}O and δ^{13}C values with successive cements becoming progressively depleted in both ^{13}C and ^{18}O. The ^{18}O trend may be due to increasing temperatures and to isotopic evolution of pore waters. Employing a laser ablation technique, Dickson et al. (1990) identified a very fine-scale O-isotope zonation in calcite cements, which they interpreted as indicating changes in the isotope composition of the pore fluids.

3.10.7 Dolomites

Dolomite is found abundantly in Paleozoic and older strata, but is rare in younger rocks. Two reqirements are necessary for dolomite formation: (i) the presence of a high Mg/Ca fluid and (ii) large volumes of fluid that are pumped through limestones. There are only few locations where dolomite is forming today. In laboratory experiments, researchers have struggled to produce dolomite at temperatures and pressures realistic for its sedimentary formation (Horita 2014). This is the crux of the “dolomite problem”.

Since dolomitization takes place in the presence of water, oxygen isotope compositions are controlled by the pore fluid composition, the temperature of formation and to a lesser extent by the salt content. Carbon isotope compositions, in contrast, are determined by the precursor carbonate composition, because pore fluids generally have low carbon contents, so that the δ^{13}C-value of the precursor is generally retained. Two problems complicate the interpretation of isotope data to delineate the origin and diagenesis of dolomites: (i) extrapolations of high-temperature experimental dolomite-water fractionations to low temperatures suggest that at 25 °C dolomite should be enriched in ^{18}O relative to calcite by 4–7 ‰ (e.g. Sheppard and Schwarcz 1970). On the hand, the oxygen isotope fractionation observed between Holocene calcite and dolomite is somewhat lower, namely in the range between 2 and 4 ‰ (Land 1980; McKenzie 1984), in agreement with recent theoretical predictions (Zheng and Böttcher 2015). The fractionation also may depend partly on the crystal structure, more specifically on the composition and the degree of crystalline order. (ii) For many years it has not been possible to determine the equilibrium oxygen isotope fractionations between dolomite and water at sedimentary temperatures directly, because the synthesis of dolomite at these low temperatures is problematic. With the discovery, that bacteria mediate the precipitation of dolomite, Vasconcelos et al. (2005) presented however, a new paleothermometer enabling the reconstruction of temperature conditions of ancient dolomite deposits. Horita (2014) determined experimentally C- and O-isotope fractionations by precipitation of dolomite at 80 °C and by dolomitization of $CaCO_3$ in the temperature range 100–350 °C. In this temperature range dolomite is enriched relative to calcite by 0.7–2.6 ‰. As postulated by Horita (2014) fractionations can be extrapolated to lower temperatures. To elucidate temperatures of formation and the oxygen isotope composition of the dolomitizing fluid, Ferry et al. (2011), for instance, demonstrated that dolomite in the Italian dolomites formed at temperatures between 40 and 80 °C.

Figure 3.45 summarizes oxygen and carbon isotope compositions of some recent and Pleistocene dolomite occurences (after Tucker and Wright 1990). Variations in oxygen isotope composition reflect the involvement of different types of waters (from marine to fresh waters) and varying ranges of temperatures. With respect to carbon, $\delta^{13}C$-values between 0 and 3 ‰ are typical of marine compositions. In the presence of abundant organic matter, negative $\delta^{13}C$-values in excess of −20 ‰ indicate that carbon is derived from the decomposition of organic matter. Very positive $\delta^{13}C$-values up to +15 ‰ result from fermentation of organic matter (Kelts and McKenzie 1982). Such isotopically heavy dolomites have been described, for example, from the Guaymas Basin, where dolomite formation has taken place in the zone of active methanogenesis.

Besides C- and O-isotope compositions, Ca isotopes (Holmden 2009) and Mg isotopes (Geske et al. 2015) have been investigated in a wide range of dolomite types. Geske et al. (2015) argued that Mg isotope ratios of dolomites are affected by various factors including Mg sources and precipitation/dissolution processes complicating its application as a proxy for dolomite formation models.

3.10.8 Freshwater Carbonates

Carbonates deposited in freshwater lakes exhibit a wide range in isotopic composition, depending upon the isotopic composition of the rainfall in the catchment area, its amount and seasonality, the temperature, the rate of evaporation, the

Fig. 3.45 Carbon and oxygen isotope composition of some recent and Pleistocene dolomite occurences (after Tucker and Wright 1990) (Fig. 3.45, 6th edition, p. 204)

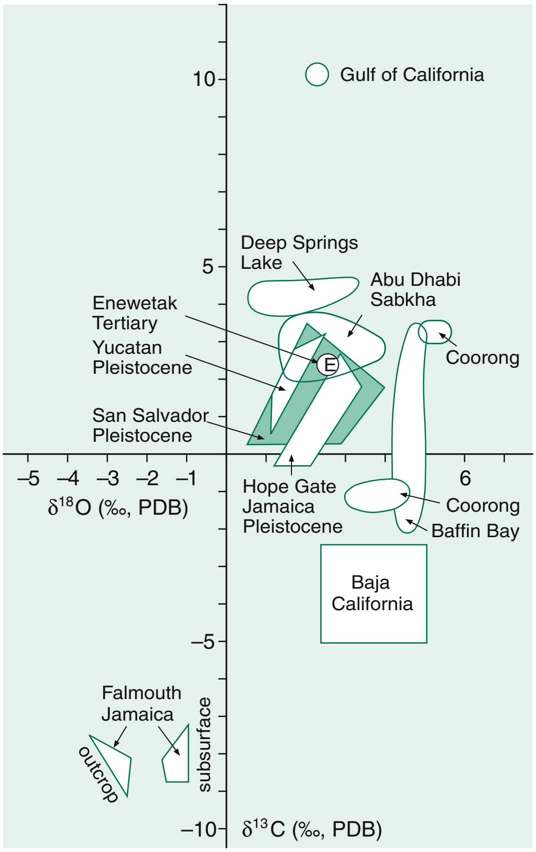

relative humidity, and the biological productivity. Lake carbonates typically consist of a matrix of discrete components, such as detrital components, authigenic precipitates, neritic and benthic organisms. The separate analysis of such components has the potential to permit investigation of the entire water column. For example, the oxygen isotopic composition of authigenic carbonates and diatoms can be used to obtain a surface water signal of changes in temperature and meteoric conditions, while the composition of bottom dwellers can be used as a monitor of the water composition, assuming that the bottom water temperatures remained constant.

The carbon and oxygen isotope compositions of carbonate precipitated from many lakes show a strong covariance with time, typically in those lakes which represent closed systems or water bodies with long residence times (Talbot 1990). In contrast, weak or no temporal covariance is typical of lakes which represent open systems with short residence times. Figure 3.46 gives examples of such covariant trends. Each closed lake appears to have a unique isotopic identity defined by its covariant trend, which depends on the geographical and climatic setting of a basin, its hydrology and the history of the water body (Talbot 1990).

3.10.9 Phosphates

The stable isotope composition of biogenic phosphates record a combination of environmental parameters and biological processes. Biogenic phosphate, $Ca_5(PO_4, CO_3)_3(F,OH)$, for paleoenvironmental reconstructions were first used by Longinelli (e.g. Longinelli 1966, 1984; Longinelli and Nuti 1973), and later by Kolodny and his coworkers (Kolodny et al. 1983; Luz and Kolodny 1985). However, the use was rather limited for many years, because of analytical difficulties. More recently these problems have been overcome by refinements in analytical techniques (Crowson et al. 1991; O'Neil et al. 1994; Cerling and Sharp 1996; Vennemann et al. 2002; Lecuyer et al. 2002), so the isotope analyses of phosphates for paleoenvironmental reconstruction has been used much more widely

Under abiotic surface conditions phosphate is resistant to oxygen isotope exchange. During biological reactions, however, phosphate-water oxygen isotope exchange is rapid due to enzymatic catalysis (Kolodny et al. 1996; Blake et al. 1997; Paytan et al. 2002; Blake et al. 2005). O'Neil et al. (1994) have shown the importance of phosphate speciation in determining O isotope fractionation among different PO_4(aq) species and between PO_4(aq) species and water.

Phosphate materials that may be analyzed are bone, dentine, enamel, fish scales and invertebrate shells. In contrast to bone and dentine, enamel is extremely dense, so it is least likely to be affected diagenetically and the prime candidate for paleoevironmental reconstructions. Biogenic apatites contain besides the PO_4 group $CO_3{}^{2-}$ that substitutes for $PO_4{}^{3-}$ and OH^- as well as "labile" $CO_3{}^{2-}$ (Kohn and Cerling 2002), the latter is removed by pretreatment with a weak acid. The remaining $CO_3{}^{2-}$ component in bioapatites is then analyzed similar to the analysis of carbonates (McCrea 1950). Early results of the carbonate-carbon seemed to imply diagenetic overprint and it was not until the 1990s that it became accepted

Fig. 3.46 Carbon and oxygen isotope compositions of freshwater carbonates from recently closed lakes (after Talbot 1990) (Fig. 3.46, 6th edition, p. 205)

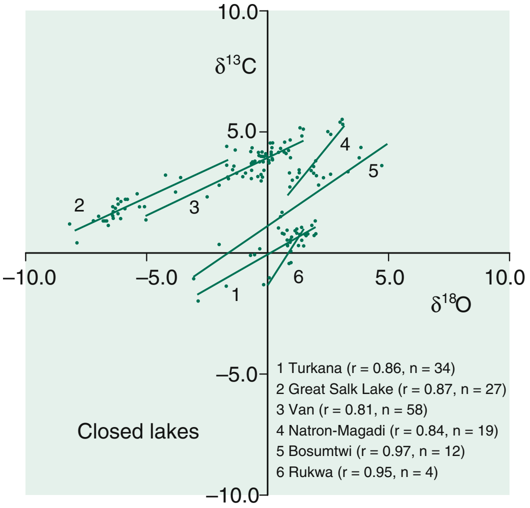

that the carbon isotope composition of tooth enamel carbonate is a recorder of diet (Cerling et al. 1993, 1997).

Of special geological interest is the isotopic analyses of coeval carbonate-phosphate pairs (Wenzel et al. 2000), which helps to distinguish primary marine signals from secondary alteration effects and sheds light on the causes for $\delta^{18}O$ variations of fossil ocean water. Wenzel et al. (2000) compared Silurian calcitic brachiopods with phosphatic brachiopods and conodonts from identical stratigraphic horizons. They showed that primary marine oxygen isotope compositions are better preserved in conodonts than in brachiopod shell apatite and suggested that conodonts record paleotemperature and $^{18}O/^{16}O$ ratios of Silurian sea water. Joachimski et al. (2004) reached similar conclusions for Devonian seawater.

Studies on mammals, invertebrates and fishes clearly indicate that the oxygen isotope composition of biogenic apatite varies systematically with the isotope composition of the body water that depends on local drinking water (Longinelli 1984; Luz et al. 1984; Luz and Kolodny; 1985). For mammals, there is a constant offset between the $\delta^{18}O$ of body water and PO_4 ($\sim$18 ‰, Kohn and Cerling 2002) and between PO_4 and CO_3 components of bioapatite of $\sim$8 ‰ (Bryant et al. 1996; Iacumin et al. 1996). Studies by Luz et al. (1990), and Ayliffe and Chivas (1990) demonstrated that $\delta^{18}O$ of biogenic apatite can also depend on humidity and on diet.

A different approach to get informations about the earth's climate has been used by Pack et al. (2013) by measuring the triple oxygen isotope composition of small mammals. The approach relies on the fact that atmospheric oxygen along with drinking water and water in food is one of the oxygen sources for mammals. By measuring the triple oxygen isotope composition of bone and teeth apatite Pack et al. (2013) used the relation between the ^{17}O anomaly of air oxygen and atmospheric CO_2, which is transferred to bone apatite thereby giving hints to atmospheric CO_2 concentrations during the animal's lifetime.

3.10.10 Iron Oxides

3.10.10.1 Oxygen

Iron oxides/hydroxides are ubiquitous in soils and sediments and are common precursors to goethite and hematite. The initial precipitates in natural settings are water-rich ferric oxide gels and poorly ordered ferrihydrite, which are later slowly aged to goethite and hematite.The determination of oxygen isotope fractionations in the iron oxide—water system has led to controversial results (Yapp 1983, 1987, 2007; Bao and Koch 1999), yet oxygen isotope fractionations are small and relatively insensitive to changes in temperatures. This seems to make iron oxides ideal recorders of the isotope composition of ambient waters. Bao and Koch (1999) argued that the isotopic composition of original ferric oxide gels and ferrihydrite are erased by later exchange with ambient water during the ageing process. Thus,

δ^{18}O-values of natural crystalline iron oxides may monitor the long-term average δ^{18}O-value of soil waters.

During conversion of goethite to hematite only small fractionation effects seem to occur, because most of the oxygen remains in the solid (Yapp 1987). Thus, in principle it should be possible to reconstruct the sedimentary environment of iron oxides from Precambrian Banded Iron Formations (BIF). By analyzing the least metamorphosed BIFs, Hoefs (1992) concluded, however, that the situation is not so simple. Infiltration of external fluids during diagenesis and/or low temperature metamorphism appears to have erased the primary isotope record in these ancient sediments.

3.10.10.2 Iron

Due to the poorly crystalline state of ferric hydrous oxides and due to their fast transformations to stable minerals, Fe isotope fractionations between iron hydroxides and other Fe phases are not well known. Approaches to determine the equilibrium fractionation factor between $\mathrm{FeII_{(aq)}}$ and Fe hydroxides yield Fe fractionations around −3.2 ‰, making Fe(III) minerals the most enriched in ^{56}Fe (Johnson et al. 2002; Welch et al. 2003; Wu et al. 2011). Since fractionations between $\mathrm{FeII_{aq}}$ and Fe hydroxides are similar to fractionations between $\mathrm{FeII_{aq}}$ and $\mathrm{FeIII_{aq}}$ (Johnson et al. 2002; Welch et al. 2003), Fe isotope fractionations between $\mathrm{Fe(III)_{aq}}$ and Fe-hydroxides should close to zero.

Special attention has been given to banded iron formations (BIFs), in which the largest range of Fe-isotope compositions on Earth are observed (Johnson et al. 2003, 2008; Steinhöfel et al. 2009, 2010; Halverson et al. 2011). Although models of BIF formation are still under debate, there is however general agreement, that the large Fe-isotope variations result from reduction and oxidation of iron in the sedimentary environment and during diagenetic overprint (Steinhöfel et al. 2009, 2010). It is noteworthy that small-scale heterogeneities in iron oxides remain preserved to very high metamorphic stages (Frost et al. 2007).

3.10.11 Sedimentary Sulfur and Pyrite

3.10.11.1 Sulfur

Analysis of the sulfur and iron isotope composition of sediments may yield important information about the origin and further transformations of sulfur and iron compounds. Pyrite is the end product of sedimentary S- and Fe-cycling and their stable isotopes record variations of redox changes. Bacterial sulfate reduction is accomplished by the oxidation of organic matter:

$$2\,\mathrm{CH_2O} + \mathrm{SO_4^{2-}} \rightarrow \mathrm{H_2S} + 2\,\mathrm{HCO_3^-}$$

the resulting $\mathrm{H_2S}$ reacting with available iron, which is in the reactive non-silicate bound form (oxy-hydroxides). Thus, the amount of pyrite formed in sediments may be limited by (i) the amount of sulfate, (ii) the amount of organic matter and (iii) the amount of reactive iron. Based upon the relationships between these three reservoirs different scenarios for pyrite formation in anoxic environments can be envisaged (Raiswell and Berner 1985). In normal marine sediments, where oxygen is present in the overlying water body, the formation of pyrite appears to be limited by the supply of organic matter.

Due to the activity of anaerobic sulfate reducing bacteria, most sulfur isotope fractionation takes place in the uppermost mud layers in shallow seas and tidal flats. As a result, sedimentary sulfides are depleted in ^{34}S relative to ocean water sulfate. The depletion is usually in the order of 20–60 ‰ (Hartmann and Nielsen 1969; Goldhaber and Kaplan 1974), although bacteria in pure cultures have been observed to produce fractionations up to a maximum reported value of 47 ‰ (Kaplan and Rittenberg 1964; Bolliger et al. 2001). Therefore, sedimentary sulfides depleted in ^{34}S by more than the apparent limit of 47 ‰ suggest additional fractionations that probably accompany sulfide oxidation and formation of sulfur intermediates and further metabolism. To explain the discrepancy between culture experiments and natural environments the bacterial disproportionation of intermediate sulfur compounds has been proposed (Canfield and Thamdrup, 1994; Cypionka et al. 1998; Böttcher et al. 2001).

Sulfur isotope variations in sediments reflect a record of primary syngenetic as well as secondary diagenetic processes (Jorgenson et al. 2004). For a given range of sulfur isotope values the most negative value should represent the least affected, most primary signal or the one that is most affected by the oxidative part of the sulfur cycle. In a few cases pyrite sulfur with higher $\delta^{34}S$-values than coexisting seawater has been found in the fossil record, which has been attributed to post-depositional diagenetic overprint by anaerobic methane oxidation (Jorgensen et al. 2004).

There has been much progress to identify and measure the isotopic composition of different forms of sulfur in sediments (e.g. Mossmann et al. 1991; Zaback and Pratt 1992; Brüchert and Pratt 1996; Neretin et al. 2004). Pyrite is generally considered to be the end product of sulfur diagenesis in anoxic marine sediments. Acid-volatile sulfides (AVS), which include "amorphous" FeS, mackinawite, greigite and pyrrhotite, are considered to be transient early species, but investigations by Mossmann et al. (1991) have demonstrated that AVS can form before, during and after precipitation of pyrite within the upper tens of centimeters of sediment.

Up to six or even seven sulfur species have been separated and analyzed for their isotope composition by Zaback and Pratt (1992), Brüchert and Pratt (1996) and Neretin et al. (2004). Their data provides information regarding the relative timing of sulfur incorporation and the sources of the individual sulfur species. Pyrite exhibits the greatest ^{34}S depletion relative to sea water. Acid-volatile sulfur and sulfur in organic compounds are generally enriched in ^{34}S relative to pyrite. This indicates that pyrite is precipitated nearest to the sediment-water interface under mildly reducing conditions, while AVS and kerogen sulfur resulted from formation at greater depth under more reducing conditions with low concentrations of pore water sulfate. Elemental sulfur is most abundant in surface sediments and, probably, formed by oxidation of sulfide diffusing across the sediment-water interface.

By using a GC-MC-ICP-MS technique, Raven et al. (2015) were able to measure the compound-specific S isotope composition of organic sulfur compounds. In contrast to earlier findings, extractable organic S-compounds are ^{34}S depleted relative to kerogen and porewater sulfide proviiding additional informations about organic matter sulfurization.

3.10.11.2 Pyrite

The analyses of pyrite in sediments yields the average of bulk pyrite. δ^{34}S-values of bulk pyrite integrate over the time, in which pyrite has formed by different processes and in different environments. Microanalytical techniques open the possibility to determine intra-grain and inter-grain variability of bulk pyrite. Investigating pyrites from Devonian carbonates with the ionprobe, Riciputi et al. (1996) observed a bimodal distribution of sulfides that are very heterogeneous on a thin section scale varying by as much as 25 ‰. The predominantly low δ-values indicate bacterial sulfate reduction, whereas the higher values reflect formation at much greater depths by thermochemical sulfate reduction. Correlations between pyrite morphology and isotope values suggest that sulfate reduction was a very localized process, which varied considerably on a small scale. Similar large ^{34}S-variations within and among individual pyrite grains have been reported by Kohn et al. (1998d). McKibben and Riciputi (1998) reported δ^{34}S-variations of about 105 ‰ over 200 µm in single pyrite grains. Generally pyrite grains become enriched in ^{34}S towards the margin of grains which these authors interpreted as evidence for microbial sulfate reduction in closed systems.

In summary intra-grain and intergrain S-isotope compositions of pyrite vary enormously reflecting different pyrite formation processes over a long time span. Thus bulk analyses of pyrite δ^{34}S-values that integrate over all diagenetic processes may lead to misinterpretations.

Besides bacterial sulfate reduction, thermochemical sulfate reduction in the presence of organic matter is another process which can produce large quantities of H_2S. The crucial question is whether abiological sulfate reduction can occur at temperatures as low as 100 °C, which is just above the limit of microbiological reduction. Trudinger et al. (1985) concluded that abiological reduction below 200 °C had not been unequivocally demonstrated, although they did not dismiss its possible significance. As shown by Krouse et al. (1988) and others, the evidence for thermochemical sulfate reduction, even at temperatures near 100 °C or lower, has increased. Thus, it is likely that this process is much more prevalent than originally thought.

By summarizing the isotope record of sedimentary sulfides throughout the Phanerozoic, Strauss (1997, 1999) argued that the long term trend for the entire Phanerozoic broadly parallels the sulfate curve with maximum values in the early Paleozoic, minimum values in the Permian and a shift back to higher values in the Cenozoic. The isotopic difference between sulfate sulfur and minimum sulfide sulfur varies within −51 ± 8 ‰.

Precise MC-ICP-MS investigations of Fe isotopes in pyrite may reflect the isotope composition of the reactive iron source and/or may reflect Fe isotope fractionation during pyrite formation. SIMS techniques allow the determination of highly resolved Fe isotope profiles in individual pyrite grains (Virtasalo et al. 2013).

In modern anoxic basins pyrite shows δ^{56}Fe isotope values between −0.4 and −1.3 ‰ (Severmann et al. 2006); pyrite in Proterozoic and Archean formations is even lighter (see discussion on p. 274). Mackinawite (FeS_x) is often regarded as a precursor mineral for pyrite formation and Fe isotope fractionations in the Fe^{2+}(aq)—FeS system have been taken as decisive for pyrite Fe isotope signatures. Butler et al. (2005) and Guilbaud et al. (2011) demonstrated experimentally that FeS is depleted in ^{56}Fe relative to Fe^{2+}. Johnson et al. (2008) argued that δ^{56}Fe values of pyrite reflect a mixture of FeS compounds formed during bacterial reduction and Fe that is produced by dissimilatory iron reduction. According to Marin-Carbonne et al. (2014) coupled Fe and S isotope variations in pyrite indicate different mineral precursors: (i) mackinawite that is precipitated in the water column and (ii) greigite that is formed in the sediment.

In summary, detailed investigations on sedimentary pyrite have revealed large variations in sulfur and iron isotope compositions that should be investigated by a combined use of S- and Fe-isotopes (i.e. Archer and Vance 2006, Marin-Carbonne et al. 2014).

3.11 Palaeoclimatology

Past climates leave their imprint in the geologic record in many ways. For temperature reconstructions the most widely used geochemical method is the measurement of stable isotope ratios. Samples for climate reconstruction have in common that their isotope composition depends in a sensitive way on the temperature at the time of their formation.

Climatic records can be divided into (i) marine and (ii) continental records. Because the ocean system is very large and well-mixed, the oceanic record carries a global signal, while continental records are affected by regional factors. One restriction in reconstructing climates is the temporal resolution. This is especially true for marine sediments. Sedimentation rates in the deep-ocean generally are between 1–5 cm/10^3 y, highly productive areas have 20 cm/10^3y, which limits the temporal resolution to 50 years for productive areas and to 200 years for the other areas. Furthermore, benthic organisms can mix the top 20 cm of marine sediments, which further reduces temporal resolutions.

3.11.1 Continental Records

Isotopic reconstruction of climatic conditions on the continents is difficult, because land ecosystems and climates exhibit great spatial and temporal heterogeneity. The most readily determined terrestrial climatic parameter is the isotopic composition of precipitation, which is in turn dependent largely but not exclusively on temperature.

Relevant climatic information from meteoric precipitation is preserved in a variety of natural archives, such as (i) tree rings, (ii) organic matter and (iii) hydroxyl-bearing minerals.

3.11.1.1 Tree Rings

Tree rings offer an absolute chronology with annual resolution, but the scarcity of suitable old material and uncertainties about the preservation of original isotope ratios are major restrictions in the application of tree rings. The cellulose component of plant material is generally used for isotope studies because of its stability and its well-defined composition. Numerous studies have investigated the stable isotope composition of tree rings. However, in many respects climatic applications are limited. Although there are strong correlations of δD and δ^{18}O with source water, there are variable fractionations between water and cellulose. An increasing number of studies have investigated the complex processes that transfer the climatic signal in the meteoric water to tree cellulose (for instance White et al. 1994; Tang et al. 2000). The complexities result from the interplay of various factors such as humidity, amount of precipitation, topography, biological isotope fractionation, root structure, ageing of late-wood. Tang et al. (2000) assessed both systematic (variations of temperature, humidity, precipitation etc.) and random isotopic variations in tree rings from a well characterized area in the northwestern United States, and demonstrated for instance that temperature only explains up to 26 % of the total variance of δD values of cellulose nitrate.

3.11.1.2 Organic Matter

The utility of D/H ratios in organic matter as paleoclimatic proxies relies on the preservation of its primary biosynthetic signal. In recent years the D/H analysis of compound-specific sedimentary biomarkers have been increasingly used. δD-values of lipid biomarkers from aquatic organism and terrestrial plants, for instance, can be used as palaeohydological proxies (Sachse et al. 2012 and others)

The question arises at what point paleoclimatic information is lost during diagenesis and thermal maturation. Schimmelmann et al. (2006) argued that in the earliest stages of diagenesis δD-values of most lipid biomarkers are unaffected. With the onset of catagenesis quantitative information diminishes, but qualitative information may be still preserved. At the highest levels of maturity, biomarkers become thermally unstable and can undergo degradation leading to extensive hydrogen isotope exchange (Sessions et al. 2004) and therefore limiting paleoclimate information.

3.11.1.3 Hydroxyl-Bearing Minerals

Hydoxyl bearing minerals might be regarded as another tool to reconstruct climatic changes. Again there are major difficulties that restrict a general application. Fractionation factors of clay minerals and hydroxides are not well constrained, especially at low temperatures and meaningful δD and δ^{18}O measurements require pure mineral separates, which are extremely difficult to achieve due to their small particle size and because these phases are often intergrown. Furthermore, there is a concern that some clays are detrital, whereas others are authigenic; thus, mixtures may be difficult to interpret.

3.11.1.4 Lake Sediments

The isotope composition of biogenic and authigenic mineral precipitates from lake sediments can be used to infer changes in either temperature or the isotope composition of lake water. Knowledge of the factors that may have influenced the isotope composition of the lake water is essential for the interpretation of the precipitated phases (Leng and Marshall 2004). In many lakes the combined analysis of different types of authigenic components (precipitated calcite, ostracodes, bivalves, diatoms etc.) may offer the possibility of obtaining seasonally specific informations.

One of the most useful components for estimating past climate variations are non-marine ostracodes (small bivalved crustaceans), which can live in most types of fresh-water and can be regarded as the “foraminifera of the continent”. In recent years, an increasing number of studies have demonstrated the potentials of ostracodes to reconstruct changes in temperatures of mean annual precipitation, changes in paleohydrology and evaporation histories (Lister et al. 1991; Xia et al. 1997a, b; von Grafenstein et al. 1999; Schwalb et al. 1999). A number of authors have demonstrated systematic differences in $\delta^{18}O$ of up to 2 ‰ between ostracodes and calcite precipitated under equilibrium conditions and even larger differences for $\delta^{13}C$. These differences have not been explained satisfactorily, because the knowledge about life cycles, habitat preferences and valve formation mechanisms of ostracodes is still limited.

3.11.1.5 Speleothems

Two features in caves facilitate the use of stable isotopes as a palaeoarchive: (i) cave air temperatures remain relatively constant throughout the year and are similar to the mean annual temperature above the cave. (ii) In cool temperate climate regions, cave air is characterized by very high humidity that minimizes evaporation effects. Interest in speleothems as recorders of continental palaeo-environments has increased considerable in recent years. The potential of speleothems as climate indicators was first discussed by Hendy and Wilson (1968) followed by Thompson et al. (1974). These early investigators already recognized the complexity of cave carbonate isotope compositions. An early goal was to reconstruct absolute changes in mean annual temperatures, but this appears to be rather unrealistic because various effects can influence the isotope composition of drip water, and thus the precipitated cave carbonate (see reviews by McDermott 2004 and Lachniet 2009).

Most isotope studies on speleothems have concentrated on $\delta^{18}O_{calcite}$ as the principlal paleoclimatic indicator. Some studies have discussed the potential of using δD and $\delta^{18}O$ of fluid inclusions in speleothems (Dennis et al. 2001; McGarry et al. 2004; Zhang et al. 2008). With respect to oxygen, isotope exchange may occur between calcite and water, which may lead to a shift of the original drip water composition, but for hydrogen no isotope exchange can take place. With an improved crushing technique for the liberation of the fluid inclusion water, Zhang et al. (2008) were able to recover the water without isotopic fractionation. They demonstrated that it is possible to obtain accurate paleotemperatures.

Complications with respect to paleoclimate reconstructions may arise from kinetic isotope effects during rapid degassing of CO_2. As shown by Affek et al. (2008), Daeron et al. (2011) and others, clumped isotopes may provide a sensitive indicator for disequilibrium effects. In such cases decreased Δ_{47} values correlate with increased δ^{18}O-values corresponding to higher apparent temperatures

3.11.1.6 Phosphates

Oxygen isotope compositions of phosphates have also been used as a paleotemperature indicator. Since the body temperature of mammals is constant at around 37 °C, δ^{18}O values in either bones or teeth depend only on the δ^{18}O value of the body water, which in turn depends on drinking water (Kohn 1996). Thus phosphates from continental environments are an indirect proxy of ancient meteoric waters.

The best proxy appears to be mammalian tooth enamel (Ayliffe et al. 1994; Fricke et al. 1998a, b), which forms incrementally from the crown to the base of the tooth. Enamel, therefore, preserves a time series of δ^{18}O values of precipitation along the direction of growth that reflect only ^{18}O-changes of ingested water. Oxygen isotope data for teeth of mammal herbivores that lived over a wide range of climatic conditions demonstrate that intra tooth δ^{18}O-values mirror both seasonal and mean annual differences in the ^{18}O content of local precipitation (Fricke et al. 1998a). Records going back to glacial-interglacial transitions have been described by Ayliffe et al. (1992). Fricke et al. (1998b) even postulated that tooth enamel may provide a temperature record as far back as the Early Cenozoic.

3.11.2 Ice Cores

Ice cores from polar regions represent prime recorders of past climates. They have revolutionized our understanding of Quaternary climates by providing high resolution records of changing isotope compositions of snow or ice and of changing air compositions from air bubbles occluded in the ice. The best documented ice-core record from Greenland is a pair of 3 km long ice cores from the summit of Greenland. These cores provide a record of climate as far back as 110,000 years ago. Precise counting of individual summer and winter layers extends back to at least 45,000 years ago.

The Antarctic ice sheet also has provided numerous ice cores for paleoclimate research. Antarctica is colder and its ice sheet is larger and thicker than that on Greenland. It accumulates more slowly than at the Greeenland sites, such that its temporal resolution is not as good. The Vostok ice core has provided strong evidence of the nature of climate changes over the past 420 ky. More recently, a core from Dome C, Antarctica has almost doubled the age range to the past 740 ky (Epica 2004). A good agreement with the Vostok core was observed for the 4 most recent glacial cycles, the Dome C core extends back to 8 glacial cycles.

High elevation ice cores from low latitudes, that have been drilled in Africa (Kilimanjaro), South America and Asian Himalayas (e.g. Thompson et al. 2006) represent an important addition to the polar region ice cores. Some of these high altitude, low latitude ice cores span the last 25,000 years, representing a high resolution record of the late glacial stage and the Holocene (Thompson et al. 2000). The interpretation of δ-values is, however, challenging, because of large seasonal differences in precipitation regimes (amount effect) in the tropics.

Oxygen and hydrogen isotope ratios and various atmospheric constituents in ice cores have revealed a detailed climatic record for the past 700 ky. To convert isotopic changes to temperatures, temperature—δ^{18}O correlations must be known. In early work, Dansgaard et al. (1993) proposed a relationship of 0.63 ‰ per 1 °C, whereas Johnsen et al. 1995) have used 0.33 ‰ per 1 °C (but see the remarks of caution by Allen and Cuffey 2001). The δ-T relationship varies with climatic conditions, especially between interglacial and glacial periods, because a more extensive sea-ice cover increases the distance to moisture sources and the isotopic composition of oceans changed during glacial periods.

Figure 3.47 compares δ^{18}O ice core data from GRIP and NGRIP in Greenland for the time period 50,000–30,000 years with significantly colder temperatures during the Last Glacial Maximum (LGM) than the time period for the last 10,000 years. Characteristic features of Fig. 3.47 are fast changes in δ^{18}O-values fluctuating between −37 and −45 ‰. These socalled Dansgaard-Oeschger events (Dansgaard et al. 1993; Grootes et al. 1993) are characterized by rapid warming episodes within decades followed by gradual cooling over a longer period. 23 Dansgaard-Oeschger events have been identified between 110,000 and 23,000 years before present, the causes for these sawtooth patterns are still unclear.

3.11.2.1 Correlations of Ice-Core Records

Ice-core isotope stratigraphy represents a major advance in paleoclimatology because it enables the correlation of climate records from the two poles with each other and with the high-resolution deep-sea marine climate records over the past 100 ka (Bender et al. 1994), allowing the study of phasing between the ocean and the atmosphere. One of the most difficult problems in correlating ice-cores is determining the age-depth relationship. If accumulation rates are high enough, accurate timescales have been achieved for the last 10,000 years. Prior to that there is increasing uncertainty, but in recent years new approaches have been developed, improving age determinations and allowing age correlations between different ice cores (see Fig. 3.47).

A very promising method for correlation purposes relies on changes in atmospheric gas composition. As the mixing time of the atmosphere is on the order of 1–2 years, changes in gas composition should be synchronous. Bender et al. (1994)

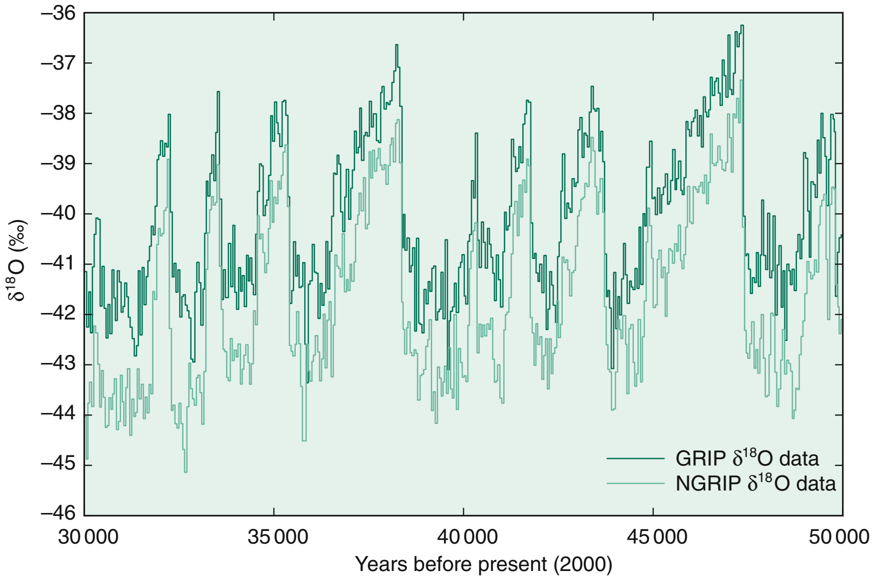

Fig. 3.47 Dansgaard-Oeschger events in the time period from 45,000 to 30,000 years before present from GRIP and NGRIP ice core data (http://en.wikipedia.org/wiki/Image:Grip-ngrip-do18-closeup.png) (Fig. 3.47, 6th edition, p. 213)

have used variations of $\delta^{18}O$ in gas inclusions from ice-cores correlating the Vostok and GISP-2 ice cores. Similar ^{18}O-variations in both cores makes an aligment of the two records possible (Bender et al. 1985; Sowers et al. 1991, 1993), which then allows the comparison of other parameters such as CO_2 and CH_4 with temperature changes as deduced from the isotopic composition of the ice.

3.11.2.2 Gas-Inclusions in Ice Cores

Atmospheric trace gas chemistry is a rapidly growing field of paleo-atmospheric research, because the radiative properties of CO_2, CH_4 and N_2O make them potential indicators of climate change. A fundamental problem in constructing a record of trace gas concentrations from ice-cores is the fact that the air in bubbles is always younger than the age of the surrounding ice. This is because as snow is buried by later snowfalls and slowly becomes transformed to firn and ice, the air between the snow crystals remains in contact with the atmosphere until the air bubbles become sealed at the firn/ice transition, when density increases to about 0.83 g/cm^3. The trapped air is thus younger than the matrix, with the age difference depending mainly on accumulation rate and temperature. In Greenland, for instance the age difference varies between 200 and 900 years.

Sowers et al. (1993) and Bender et al. (1994) showed that it is possible to construct an oxygen isotope curve similar to that derived from deep-sea foraminifera from molecular O_2 trapped in ice. These authors argued that $\delta^{18}O$(atm) can serve as a proxy for ice volume just as $\delta^{18}O$ values in foraminifera. The isotope signal of atmospheric oxygen can be converted from seawater via photosynthetic marine organisms according to the following scheme

$$\delta^{18}\mathrm{O(seawater)}^{\rightarrow}\mathrm{photosynthesis} \rightarrow \delta^{18}\mathrm{O(atm)}^{\rightarrow}\mathrm{polar\ ice} \rightarrow \delta^{18}\mathrm{O(ice)}$$

This conversion scheme is, however, complex and several hydrological and ecological factors have to be considered. Sowers et al. (1993) argued that these factors remained near constant over the last glacial-interglacial cycle, so that the dominant signal in the atmospheric oxygen isotope record represents an ice-volume signal.

Air composition in ice cores is slightly modified by physical processes, such as gravitational and thermal fractionation. A gas mixture in ice cores with different molecular weights will partially segregate due to thermal diffusion and gravitational fractionation. Generally, the species with greater mass will migrate towards the bottom and/or the cold end of a column of air. By slow diffusion, air trapped in ice-cores can develop slight changes in atmospheric ratios such as the Ar/N_2 ratio as well as fractionate the nitrogen and oxygen isotope composition of air molecules. This approach was pioneered by Severinghaus et al. (1996), who first showed that thermal diffusion can be observed in sand dunes. Later Severinghaus et al. (1998), Severinghaus and Brook (1999) and Grachev and Severinghaus (2003) demonstrated that thermally driven isotopic anomalies are detectable in ice core air bubbles. Since gases diffuse about 50 times faster than heat, rapid climatic temperature changes will cause an isotope anomaly. Nitrogen in bubbles in snow thus may serve as a tracer for palaeoclimatic reconstructions because the $^{29}N/^{28}N$ ratio of atmospheric N_2 has stayed constant in the atmosphere. The measurement of nitrogen isotope ratios can, therefore, supplement the oxygen isotope record and can be used to determine the rapidity and scale of climate change. By measuring the thickness of ice separating nitrogen and oxygen isotope anomalies at the end of Younger Dryas 11,500 years ago, Severinghaus et al. (1998) estimated that the rate of temperature change to be less than 50–100 years and suggested that the Younger Dryas was about 15 °C colder than today which is about twice as large as estimated from Dansgaard-Oeschger events.

3.11.3 Marine Records

Most oceanic paleoclimate studies have concentrated on foraminifera. In many cases analyses have been made both of planktonic and benthonic species. Since the first pioneering paper of Emiliani (1955), numerous cores from various sites of the DSDP and ODP program have been analyzed and, when correlated accurately, have produced a well-established oxygen isotope curve for the Pleistocene and Tertiary. These core studies have demonstrated that similar $\delta^{18}O$-variations are observed in all areas. With independently dated time scales on hand, these systematic $\delta^{18}O$ variations result in synchronous isotope signals in the sedimentary record because the mixing time of the oceans is relatively short (10^3 years). These signals provide stratigraphic markers enabling correlations between cores which may be thousands of kilometers apart. Several Pleistocene biostratigraphic data have been calibrated with oxygen isotope stratigraphy, which helps to confirm their synchrony. This correlation has greatly facilitated the recognition of both short and long time periods of characteristic isotopic compositions, and times of rapid change from one period with characteristic composition to another, thus, making oxygen isotope stratigraphy a practical tool in modern paleoceanographic studies. Figure 3.48 shows the oxygen isotope curve for the Pleistocene. This diagram exhibits several striking features: the most obvious one is the cyclicity, furthermore fluctuations never go beyond a certain maximum value on either side of the range. This seems to imply that very effective feedback mechanisms are at work stopping the cooling and warming trends at some maximum level. The "sawtooth"-like curve in Fig. 3.48 is characterized by very steep gradients: maximum cold periods are immediately followed by maximum warm periods.

Emiliani (1955) introduced the concept of "isotopic stages" by designating stage numbers for identifiable events in the marine foraminiferal oxygen isotope record for the Pleistocene. Odd numbers identify interglacial or interstadial (warm) stages, whereas even numbers define ^{18}O enriched glacial (cold) stages. A second terminology used for subdividing isotope records is the concept of terminations labeled with Roman numbers I, II, III etc. which describe rapid transitions from peak glacial to peak interglacial values. This approach was used by Martinson et al. (1987) to produce a high-resolution chronology, called the Specmap time scale which is used when plotting different isotope records on a common time scale. With these different techniques a rather detailed chronology can be worked out.

A careful examination of the curve shown in Fig. 3.48 shows a periodicity of approximately 100,000 years. Hays et al. (1976) argued that the main structure of the oxygen isotope record is caused by variations in solar insolation, promoted by variations in the Earth's orbital parameters. Thus, isotope data have played a capital role in the confirmation of the "Milankovitch Theory" which argues that the isotope and paleoclimate record is a response to the forcing of the orbital parameters operating at specific frequencies.

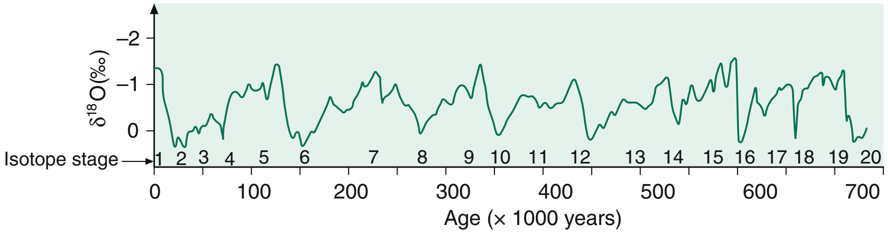

Fig. 3.48 Composite δ^{18}O fluctuation in the foraminifera species G saculifer from Caribbean cores (Emiliani 1978) (Fig. 3.48, 6th edition, p. 215)

3.11.3.1 Corals

Reef-building corals provide high-resolution records up to several centuries that potentially are ideal tools for the reconstruction of tropical climate. Annual banding provides chronological control and high year-round growth rates allows annual to subannual resolution. Coral skeletons are well known for strong vital effects, their oxygen isotope composition is generally depleted relative to equilibrium by 1–6 ‰. Because of this strong non-equilibrium fractionation early workers were highly skeptical about the usefulness of δ^{18}O-values as climate indicators. Later workers, however, realized that the δ^{18}O records reveal subseasonal variations in seawater temperature and salinity. Most climate studies circumvent the problem of equilibrium offsets by assuming a time independent constant offset and interpret relative changes only. Thus δ^{18}O values of corals generally are not interpreted as temperature records, but as records reflecting combinations of temperature and salinity changes. δ^{18}O values in corals may record anomalies associated with El Nino (Cole et al. 1993; Dunbar et al. 1994), including the dilution effect on δ^{18}O by high amounts of precipitation (Cole and Fairbanks 1990).

Coral growth rates vary over the course of a year, which is expressed in an annual banding. Leder et al. (1996) demonstrated that a special microsampling technique (fifty samples a year) is necessary to accurately reproduce annual sea surface conditions. Generally, δ^{18}O records show a long-term warming and/or decrease in salinity throughout the tropical oceans (Gagan et al. 2000; Grottoli and Eakin 2007). Fossil coral samples imply an additional problem. Since corals dominantly are composed of aragonite, subaereal exposure of fossil corals will easily change oxygen isotope values due to diagenetic recrystallization to calcite.

3.11.3.2 Conodonts

Conodonts are tooth-like phosphatic microfossils that are widespread in both space and time.

Since the early work of Longinelli (1966), Longinelli and Nuti (1973) and Kolodny et al. (1983) phosphates have been used to reconstruct temperatures, Although being more difficult to analyze, they are advantageous over carbonates because they are more resistant towards isotope exchange. Puceat et al. (2010) redetermined the phosphate-water oxygen isotope fractionation on fish raised under controlled conditions and observed a similar slope to earlier equations, but an offset of about +2 ‰, shifting calculated temperatures to 4 to 8 °C higher temperatures. With this temperature calibration, reasonable temperatures can be obtained for the Devonian (Joachimski et al. 2009); at the Permian/Triassic boundary a large temperature increase has been observed (Joachimski et al. 2012)

3.11.3.3 Characteristic Climatic Events

During the last two decades a rapid growth of high-resolution isotope records across the Cenozoic has taken place. Zachos et al. (2001) have summarized 40 DSDP and ODP sites representing various intervals in the Cenozoic. Their compilation of benthic foraminifera shows a range of 5.4 ‰ over the course of the Cenozoic. This variation provides constraints on the evolution of deep-sea temperature and continental ice volume. Because deep ocean waters are derived primarily from cooling and sinking of water in polar regions, the deep-sea temperature data also reflect high-latitude sea-surface temperatures.

One of the most dramatic climatic events during the Cenozoic is the Paleocene-Eocene-Thermal-Maximum (PETM) at about 56 Ma lasting less than 200,000 years (McInerney and Wing 2011). The PETM is characterized by an abrupt temperature increase of about 5 °C or even up to 8 °C in conjunction with a large negative carbon isotope anomaly.

For the period prior to the first onset of Antarctic glaciation (around 33 Ma), oxygen isotope variations in global benthic foraminifera records reflect temperature changes only. Oxygen isotope data suggest the deep oceans of Cretaceous and Paleocene age may have been as warm as 10–15 °C, which is very different from today's conditions, when deep waters vary from about +4 to −1 °C. The compilation of Zachos et al. (2001) indicates a bottom water temperature increase of about 5 °C over 5 million years during the Paleocene to the early Eocene.

Variations in the benthic foraminifera record after 33 Ma indicate fluctuations in global ice volume in addition to temperature changes. Since then the majority of the $\delta^{18}O$ variations can be attributed to fluctuations in the global ice volume. Thus, Tiedemann et al. (1994) demonstrated the presence of at least 45 glacial-interglacial cycles over the last 2.5 Ma.

Zachos et al. (2001) discussed the Cenozoic climatic history in respect to three different time frames: (i) long-term variations driven mainly by tectonic processes on time scales of 10^5–10^7 years, (ii) rhythmic and periodic cycles driven by orbital processes with characteristic frequencies of roughly 100, 40 and 23 kyr. (These orbitally driven variations in the spatial and seasonal distribution of solar radiation are thought to be the fundamental drivers of glacial and interglacial oscillations), (iii) brief, aberrant events with durations of 10^3–10^5 years. These events are usually accompanied by a major perturbation in the global carbon cycle; the 3 largest occurred at 55, 34 and 23 Ma.

Figure 3.49 summarizes the oxygen isotope curve for the last 65 Ma. The most pronounced warming trend is expressed by a 1.5 ‰ decrease in $\delta^{18}O$ and occurred early in the Cenozoic from 59 to 52 Ma, with a peak in Early Eocene. Coinciding with this event is a brief negative carbon isotope excursion, explained as a massive release of methane into the atmosphere (Norris and Röhl 1999). These authors used high resolution analysis of sedimentary cores to show that two thirds of the carbon shift occured just in a few thousand years, indicating a catastrophic release of carbon from methane clathrates into the ocean and atmosphere.

A 17 Ma trend toward cooler conditions followed, as expressed by a 3 ‰ rise in $\delta^{18}O$, which can be attributed to a 7 °C decline in deep-sea temperatures. All subsequent changes reflect a combined effect of ice-volume and temperature.

To investigate the rhythmic scales, Zachos et al. (2001) looked in detail to 4 time intervals (0–4.0; 12.5–16.5; 20.5–24.5; 31–35 Ma) each representing an interval of major continental ice-sheet growth or decay. These intervals demonstrate that climate varies in a quasi-periodic fashion. In terms of frequency, Zachos et al. (2001)

concluded that much of the power in the climate spectrum appears to be related with changes in the obliquity (40 ky). This inference of a 40 ky periodicity contrasts with the obvious 100 Ky periodicity indicated by isotope curves for the last 1–2 Ma.

3.12 Metamorphic Rocks

The isotope composition of metamorphic rocks is mainly controlled by three factors, besides the temperature of exchange (i) the composition of the pre-metamorphic protolith, (ii) the effects of volatilization with increasing temperatures and (iii) an exchange with infiltrating fluids or melts. The relative importance of these three factors can vary extremely from area to area and from rock type to rock type; and the accurate interpretation of the causes of isotope variations in metamorphic rocks requires knowledge of the reaction history of the respective metamorphic rocks.

(i) The isotope composition of the precursor rock—either sedimentary or magmatic—is usually difficult to estimate. Only in relatively dry non-volatile-bearing precursor rocks do retain metamorphic rocks their original composition.

(ii) Prograde metamorphism of sediments causes the liberation of volatiles, which can be described by two end-member processes (Valley 1986):

(a) Batch volatilization, where all fluid is evolved before any is permitted to escape and (b) Rayleigh volatilization, which requires that once fluid is generated it is isolated immediately from the rock. Natural processes seem to fall between both end-member processes, nevertheless they describe useful limits. Metamorphic volatilization reactions generally reduce the δ^{18}O-value of a rock because CO_2 and, in most cases, H_2O lost are enriched in ^{18}O compared to the bulk rock. The magnitude of ^{18}O depletion can be estimated by considering the relevant fractionations at the respective temperatures. In most cases the effect on the δ^{18}O-value should be small (around 1 ‰), because the amount of oxygen liberated is small compared to the remaining oxygen in the rock and isotope fractionations at these rather high temperatures are small and, in some cases, may even reverse sign.

(iii) The infiltration of externally derived fluids is a controversal idea, but has gained much support in recent years. Many studies have convincingly demonstrated that a fluid phase plays a far more active role than was previously envisaged, although it is often not clear that the isotopic shifts observed are metamorphic rather than diagenetic (see also Kohn and Valley 1994).

A critical issue is the extent to which the isotope composition of a metamorphic rock is modified by a fluid phase. Volatilization reactions leave an isotope signature greatly different from that produced when fluid-rock interaction accompanies mineral-fluid reaction. Changes of 5–10 ‰ are a strong indication that fluid-rock interaction rather than volatilization reactions occurred during the metamorphic event. Coupled O–C depletions are seen in many metamorphic systems involving carbonate rocks. Figure 3.50 summarizes results from 28 studies of marble mostly in contact metamorphic settings. In each of the localities shown in Fig. 3.50, the

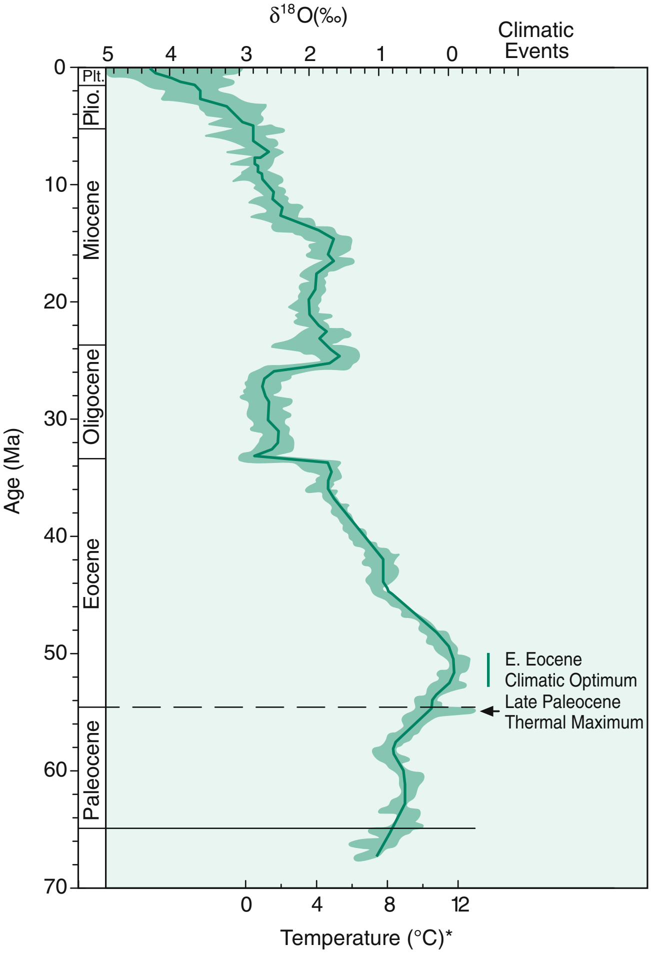

Fig. 3.49 Global deep-sea isotope record from numerous DSDP and ODP cores (Zachos et al. 2001) (Fig. 3.49, 6th edition, p. 218)

O–C trend has a negative slope, qualitatively similar to the effects of devolatilization. However, in each area the magnitude of depletions is too large to be explained by closed-system devolatilization processes, but fluid infiltration and exchange with low ^{18}O and ^{13}C fluids is indicated (Valley 1986; Baumgartner and Valley 2001).

Two end-member situations can be postulated in which coexisting minerals would change their isotopic composition during fluid-rock interaction (Kohn and Valley 1994): (i) A pervasive fluid moves independently of structural and lithologic control through a rock and leads to a homogenization of whatever differences in isotopic composition may have existed prior to metamorphism.

(ii) A channelized fluid leads to local equilibration on the scale of individual beds or units, but does not result in isotopic homogenization of all rocks or units. Channelized flow favors chemical heterogeneity, allowing some rocks to remain unaffected. Although both types of fluid flow appear to be manifest in nature, the latter type appears to be more common.

Numerical modeling of isotope exchange amongst minerals has provided a detailed view of how fluid flow occurs during metamorphism. Stable isotope fronts similar to chromatographic fronts will develop when fluids infiltrate rocks that are not in equilibrium with the infiltrating fluid composition. Isotope ratios increase or decrease abruptly at the front depending on the initial ratio in the rock and infiltrating fluid. Taylor and Bucher-Nurminen (1986), for instance, report sharp isotopic gradients of up to 17 ‰ in δ^{18}O and 7 ‰ in δ^{13}C over distances of a few mm in calcite around veins in the contact aureole of the Bergell granite. Similar sharp gradients have been also observed in other metasomatic zones but are often unrecognized because an unusually detailed mm-scale sampling is required.

Well defined stable isotope profiles may be used to provide quantitative information on fluid fluxes such as the direction of fluid flow and the duration of infiltration events (Baumgartner and Rumble 1988; Bickle and Baker 1990; Cartwright and Valley 1991; Dipple and Ferry 1992; Baumgartner and Valley 2001). In well constrained situations, fluid flow modeling permits estimation of fluid fluxes that are far more realistic than fluid/rock ratios calculated from a zero-dimensional model.

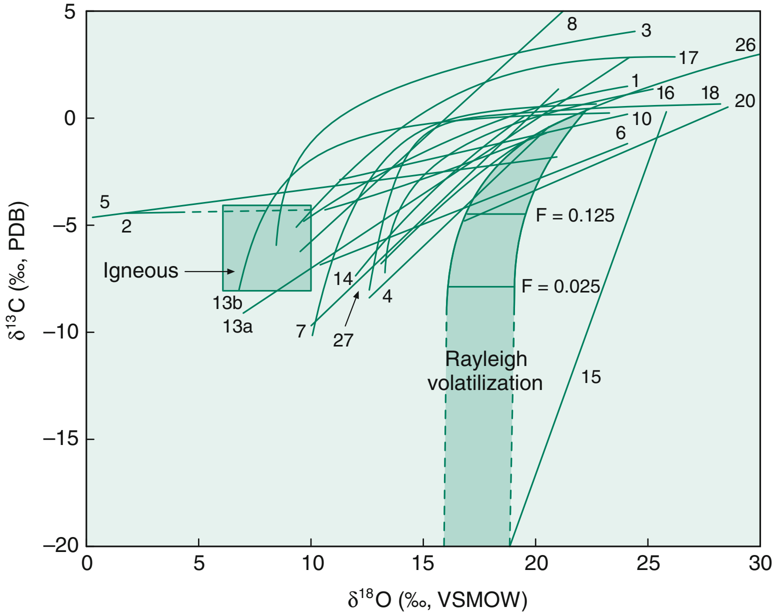

Fig. 3.50 Coupled C-O trends showing decreasing values of δ^{13}C and δ^{18}O with increasing metamorphic grade from contact metamorphic localities (Baumgartner and Valley 2001) (Fig. 3.50, 6th edition, p. 219)

Due to the invention of new micro-analytical techniques (laser sampling and ion microprobe), it has become possible to document small-scale isotope gradients within single mineral grains. Oxygen isotope zoning may develop at a variety of scales, from outcrop scale to the grain scale. Patterns of zoning may reflect multiple processes including diffusive oxygen isotope exchange and infiltration of external fluids. For garnets, zoning has been observed in several cases with increases or decreases from core to rim (Kohn et al. 1993; Young and Rumble 1993; Xiao et al. 2002; Errico et al. 2012; Russell et al. 2013). The shape of the isotopic gradient across a grain will allow distinction among processes controlled by open-system fluid migration or closed-system diffusion.

In a detailed ion microprobe study, Ferry et al. (2014) observed in a large number of different minerals large intercrystalline and intracrystalline ^{18}O variability. Regional metamorphic rocks are more variable in ^{18}O than contact metamorphic rocks. Ferry et al. (2014) explained the difference in ^{18}O variability by the longer duration and slower reaction rates of regional metamorphism rather than to differences in temperature.

3.12.1 Contact Metamorphism

Because the isotopic composition of igneous rocks is quite different from those of sedimentary rocks, studies of the isotope variations in the vicinity of an intrusive contact offer the possibility of investigating the role of fluids interacting with rocks around cooling plutons. Two types of aureole can be distinguished (Nabelek 1991): (a) “closed” aureoles where fluids are derived from the pluton or the wall-rock and (b) “open” aureoles that for at least part of their metamorphic history have been infiltrated by fluids of external origin. Some aureoles will be dominated by magmatic or metamorphic fluids, whereas others by surface-derived fluids. The occurrence of meteoric-hydrothermal systems around many plutonic complexes has been documented by H.P.Taylor and his coworkers and has been described in more detail on p. . The depth to which surface-derived fluids can penetrate is still under debate, but most meteoric-hydrothermal systems appear to have developed at depths less than ~6 km (Criss and Taylor 1986). However, Wickham and Taylor (1985) suggested that seawater infiltration has been observed to a depth of 12 km in the Trois Seigneur Massif, Pyrenees.

In many contact aureoles combined petrologic and isotope studies have provided evidence that fluids were primarily locally derived. Oxygen isotope compositions of calc-silicates from many contact aureoles have revealed that the ^{18}O-contents of the calc-silicate hornfelses approach those of the respective intrusions. This, together with characteristic hydrogen and carbon isotope ratios, has led many workers to conclude that magmatic fluids were dominant during contact metamorphism with meteoric fluids becoming important during subsequent cooling only (Taylor and O’Neil 1977; Nabelek et al. 1984; Bowman et al. 1985; Valley 1986). Ferry and Dipple (1992) developed different models to simulate fluid-rock interaction on the

Notch Peak aureole, Utah. Their preferred model assumes fluid flow in the direction of increasing temperature, thus arguing against magmatic fluids, but instead proposing fluids derived from volatilization reactions. Nabelek (1991) calculated model δ^{18}O-profiles which should result from both "down-temperature" and "up-temperature" flow in a contact aureole. He demonstrated that the presence of complex isotopic profiles can be used to get information about fluid fluxes. Gerdes et al. (1995) have examined meter-scale ^{13}C and ^{18}O transport in a thin marble layer near a dike in the Adamello contact aureole, Southern Alps. They observed systematic stable isotope changes in the marble over <1 m as the dike is approached with δ^{13}C-values ranging from 0 to −7 ‰ and δ^{18}O values from 22.5 to 12.5 ‰. These authors have compared the isotope profiles to one- and two-dimensional models of advective-dispersive isotope transport. Best agreement is obtained using a two-dimensional model that specifies (i) a high permeability zone flow and (ii) a lower permeability zone in marble away from the dike.

3.12.2 Regional Metamorphism

It is a general observation that low-grade metamorphic pelites have δ^{18}O-values between 15 and 18 ‰ whereas high-grade gneisses have δ^{18}O-values between 6 and 10 ‰ (Garlick and Epstein 1967; Shieh and Schwarcz 1974; Longstaffe and Schwarcz 1977; Rye et al. 1976; Wickham and Taylor 1985; Peters and Wickham 1995). In the absence of infiltration of a fluid phase, isotopic shifts resulting from net transfer reactions in typical amphibolite or lower granulite facies metapelites and metabasites are about 1 ‰ or less for about 150 °C of heating (Kohn et al. 1993, Young 1993). Thus, the processes responsible for this decrease in ^{18}O must be linked to large-scale fluid transport in the crust.

There are several factors which control fluid transport. One is the lithology of a metamorphic sequence. Marbles, in particular, are relatively impermeable during metamorphism (Nabelek et al. 1984) and, therefore, may act as barriers to fluid flow, limiting the scale of homogenization and preferentially channeling fluids through silicate layers. Marbles may act as local high—^{18}O reservoirs and may even increase the ^{18}O content of adjacent lithologies (Peters and Wickham 1995). Therefore, massive marbles generally preserve their sedimentary isotope signatures, even up to the highest metamorphic grades (Valley et al. 1990).

Sedimentary sequences undergoing a low-grade metamorphism initially may contain abundant connate pore fluids which provide a substantial low-^{18}O reservoir and a medium for isotopic homogenization. An additional important fluid source is provided by metamorphic dehydration reactions at higher grades of metamorphism (e.g. Ferry 1992). In some areas, petrological and stable isotope studies suggest that metamorphic fluid compositions were predominantly internally buffered by devolatilization reactions and that large amounts of fluid did not interact with the rocks during regional metamorphism (e.g. Valley et al. 1990). In a high-grade polymetamorphic terrane, later metamorphic events are likely to be dominated by magmatic fluid sources since previous events would have caused extensive dehydration, thereby limiting potential fluid sources (Peters and Wickham 1995). A detailed study of the O-isotope composition of pelites, amphibolites and marbles from the island of Naxos, Greece demonstrates that the isotopic pattern observed today is the result of at least three processes: two fluid flow events and a pre-existing isotopic gradient (Baker and Matthews 1995).

Shear zones are particularly good environments to investigate fluid flow at various depths within the crust (Kerrich et al. 1984; Kerrich and Rehrig 1987; McCaig et al. 1990; Fricke et al. 1992). During retrograde metamorphism aqueous fluids react with dehydrated rocks and fluid flow is concentrated within relatively narrow zones. By analyzing quartzite mylonites in Nevada, Fricke et al. (1992) demonstrated that significant amounts of meteoric waters must have infiltrated the shear zone during mylonitization to depths of at least 5–10 km. Similarly, McCaig et al. (1990) showed that formation waters were involved in shear zones in the Pyrenees and that the mylonitization process occurred at a depth of about 10 km.

Unusually low δ^{18}O-values—as light as −5 to −10 ‰—have been observed in ultra-high pressure (UHP)-rocks from Dabie Shan and Sulu, China (Rumble and Yui 1998; Zheng et al. 1998; Xiao et al. 2006 besides others). UHP-rocks are characterized by coesite and microdiamond in eclogite and other crustal rocks, which is strong evidence that a sizable segment of ancient continental crust was subducted to mantle depths. The extremely low δ^{18}O-values result from meteoric water interaction prior to UHP metamorphism. Surprisingly, these rocks have preserved their extremely low δ^{18}O-values indicating a short residence time at mantle depth followed by a rapid uplift. Quartz-garnet oxygen isotope temperatures in the range 700–900 °C are consistent with an approach to grain-scale oxygen isotope equilibrium under UHP conditions (Rumble and Yui 1998; Xiao et al. 2006). Figure 84 shows an 5000 m oxygen isotope profile through the CCSD (Chinese Continental Scientific Drilling) UHP drill hole, which indicates meteoric water interaction till a depth of 3300 m. Mineral δ^{18}O compositions are homogeneous on a mm to cm scale, but heterogeneous on a meter scale.

The Dabie-Sulu terrain is the largest among the UHP belts worldwide and covers an area of 5000 km^2 in Dabie and >10,000 km^2 in Sulu. The huge amounts of meteoric water necessary to cause the ^{18}O-depletions probably originate from the deglaciation of the Neoproterozoic snowball earth.

3.12.3 Lower Crustal Rocks

Granulites constitute the dominant rock type in the lower crust. Granulites may be found at the Earth's surface in two different settings: (i) exposed in high grade regional metamorphic belts and (ii) found as small xenoliths in basaltic pipes. Both types of granulites suggest a compositionally diverse lower crust ranging in composition from mafic to felsic.

Stable isotope studies of granulite terranes (Sri Lanka—Fiorentini et al. 1990; South India—Jiang et al. 1988; Limpopo Belt—Hoernes and Van Reenen 1992; Venneman and Smith 1992, Adirondacks—Valley and coworkers) have shown that terranes are isotopically heterogeneous and are characterized by δ^{18}O-values that range from "mantle-like" values to typical metasedimentary values above 10 ‰. Investigations of amphibolite/granulite transitions have shown little evidence for a pervasive fluid flux as a major factor in granulite facies metamorphism (Valley et al. 1990; Cartwright and Valley 1991; Todd and Evans 1993).

Similar results have been obtained from lower crustal granulite xenoliths, which also exhibit a large range in δ^{18}O-values from 5.4 to 13.5 ‰ (Mengel and Hoefs 1990; Kempton and Harmon 1992). Mafic granulites are characterized by the lowest δ^{18}O-values and range of ^{18}O-contents. By contrast, silicic meta-igneous and meta-sedimentary granulites are significantly enriched in ^{18}O with an average δ^{18}O-value around 10 ‰. The overall variation of 8 ‰ emphasizes the O-isotope heterogeneity of the lower crust and demonstrates that pervasive deep crustal fluid flow and isotopic homogenization is not a major process.

3.12.4 Thermometry

Oxygen isotope thermometry is widely used to determine temperatures of metamorphic rocks. The principal concern in isotope thermometry continues to be the preservation of peak metamorphic temperatures during cooling. It has long been recognized that oxygen isotope thermometers often record discordant temperatures in slowly cooled metamorphic rocks. Figure 3.51 gives a compilation of literature data (Kohn 1999) showing δ^{18}O values and calculated temperature ranges for quartz-magnetite and muscovite-biotite. Muscovite-biotite pairs from rocks whose metamorphic conditions range from greenschist to granulite facies cluster around an apparent temperature of ~300 °C, whereas quartz-magnetite pairs have an apparent temperature of ~540 °C. These data demonstrate substantial diffusional resetting, which is consistent with relatively high water fugacities during cooling (Kohn 1999).

Assuming that a rock behaves as a closed system and consists of the three mineral assemblage quartz, feldspar and horblende, then hornblende will be the slowest diffusing phase and feldspar the fastest diffusing phase. Using the formulation of Dodson (1973) for closure temperature and a given set of parameters (diffusion constants, cooling rate and grain size), Giletti (1986) calculated apparent temperatures that would be obtained in rocks with different modal proportions of the three minerals once all isotope exchange had ceased in the rock. In the Giletti model, the apparent quartz—hornblende temperature is dependent only on the quartz/feldspar ratio and is independent of the amount of hornblende in the rock, since hornblende is the first phase to reach its closure temperature. Eiler et al. (1992, 1993), however, demonstrated that the abundance of the slow diffusing phase (e.g. hornblende) can

Fig. 3.51 Plot of $\delta^{18}O$ of quartz versus $\delta^{18}O$ magnetite (*solid squares*) and of biotite versus muscovite (*open squares*) from rocks whose peak metamorphic conditions range from greenschist through granulite facies (after Kohn 1999) (Fig. 3.52, 6th edition, p. 225)

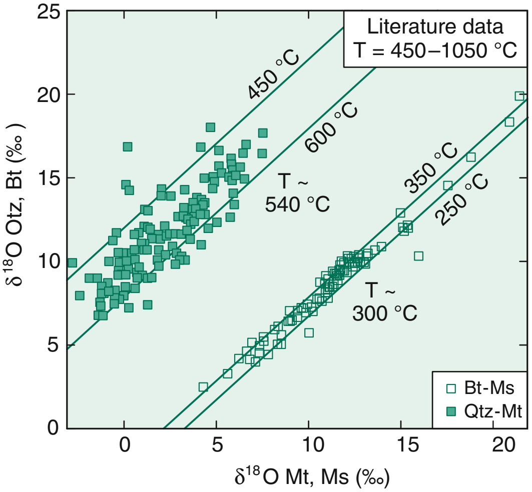

affect apparent equilibrium temperatures because of continued exchange between the grain boundaries of this phase and fast diffusing phases. Thus, retrograde diffusion related oxygen isotope exchange makes the calculation of peak metamorphic temperatures impossible, but can be used to estimate cooling rates.

Diffusion modelling, on the other hand, also predicts that accurate temperatures can be obtained from refractory accessory minerals, if they occur in a rock that is modally dominated by a readily exchangeable mineral (Valley 2001). The basis of this approach is that the accessory mineral preserves the isotope composition from crystallization because of slow diffusion while the dominant mineral preserves its isotope composition by mass balance because there are no other sufficiently abundant exchangeable phases.

Several refractory accessory mineral thermometers have been applied, including aluminosilicate, magnetite, garnet and rutile in quartz-rich rocks and magnetite, titanite or diopside in marble. Refractory minerals are defined based on their relative diffusion rates relative to the matrix of the total rock. Thus plagioclase—magnetite or plagioclase—rutile may be good thermometers in amphibolite or eclogite-facies basic rocks, but fail in the granulite facies.

Other suitable phases for the preservation of peak metamorphic temperatures are the Al_2SiO_5 polymorphs kyanite and sillimanite, having both slow oxygen diffusion rates. By analyzing the alumosilicate polymorphs from a variety of rocks with different temperature histories, Sharp (1995) could derive empirical equilibrium fractionation factors for kyanite and sillimanite. In some rocks oxygen isotope temperatures are far higher than the regional metamorphic temperatures, possibly reflecting early high-temperature contact metamorphic effects that are preserved only in the most refractory phases.

Despite extensive diffusional resetting under water-buffered conditions, some rocks clearly retain oxygen isotope fractionations that are not reset by diffusion during cooling. Farquhar et al. (1996) have investigated two granulite terrains from NW Canada and Antarctica. Quartz-garnet temperatures of around 1000 °C are in good agreement with a variety of independent temperature estimations. Quartz-pyroxene temperatures are significantly lower and still lower quartz-magnetite temperatures of around 670 °C are attributed to a combination of faster oxygen diffusion in quartz and magnetite and recrystallization during late-stage deformation. The "dry" nature of granulites is obviously critical for preservation of high-temperature records. Cooler and more hydrous rocks seem to be less capable of retaining a record of peak temperatures.

Carbon isotope partitioning between calcite and graphite is another example of a favorable thermometer to record peak metamorphic temperatures in marbles because calcite is the abundant phase with relatively high carbon diffusivities whereas graphite is of minor abundance and has a very slow diffusion rate. Figure 3.52 shows the decrease of fractionation of calcite and graphite (Δ) with increasing metamorphic grade. The narrow range of graphite δ-values associated with granulite facies rocks indicates isotope equilibrium between carbonate and graphite at high temperatures. Figure 3.52 also indicates that under granulite-facies conditions the original carbon isotope composition has been obliterated due to exchange between carbonate and reduced carbon.

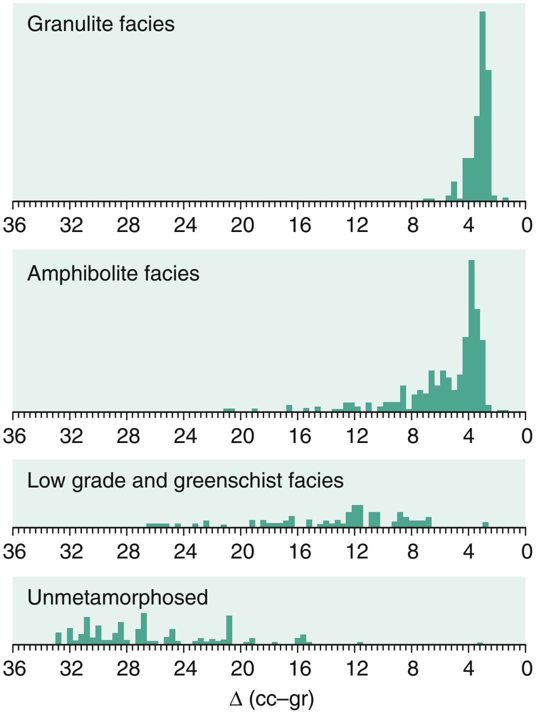

Fig. 3.52 Frequency distribution of calcite-graphite fractionations (Δ) with increasing metamorphic grade (after Des Marais 2001) (Fig. 3.53, 6th edition, p. 226)

References

Abelson PH, Hoering TC (1961) Carbon isotope fractionation in formation of amino acids by photosynthetic organisms. Proc Natl Acad Sci USA 47:623

Abrajano TA, Sturchio NB, Bohlke JH, Lyon GJ, Poreda RJ, Stevens MJ (1988) Methane—hydrogen gas seeps Zambales ophiolite, Phillippines: deep or shallow origin. Chem Geol 71:211–222

Affek HP, Bar-Matthews M, Ayalon A, Matthews A, Eiler JM (2008) Glacial/interglacial temperature variations in Soreq cave speleothems as recorded by "clumped isotope" thermometry. Geochim Cosmochim Acta 72:5351–5360

Agrinier P, Hekinian R, Bideau D, Javoy M (1995) O and H stable isotope compositions of oceanic crust and upper mantle rocks exposed in the Hess Deep near the Galapagos Triple Junction. Earth Planet Sci Lett 136:183–196

Aharon P, Fu B (2000) Microbial sulfate reduction rates and sulfur and oxygen isotope fractionation at oil and gas seeps in deepwater Gulf of Mexico. Geochim Cosmochim Acta 64:233–246

Aharon P, Fu B (2003) Sulfur and oxygen isotopes of coeval sulphate-sulfide in pore fluids of cold seep sediments with sharp redox gradients. Chem Geol 195:201–218

Alexander CM, Russell SS, Arden JW, Ash RD, Grady MM, Pillinger CT (1998) The origin of chondritic macromolecular organic matter: a carbon and nitrogen isotope study. Meteorit Planet Sci 33:603–622

Alexander B, Savarino J, Barkov N, Delmas RJ, Thiemens MH (2002) Climate driven changes in the oxidation pathways of atmospheric sulfur. Geophys Res Lett 29(14):30–31

Alexander B, Savarino J, Kreutz KJ, Thiemens MH (2004) Impact of preindustrial biomass-burning emissions on the oxidation pathways of troposheric sulfur and nitrogen. J Geophys Res 109:8030–8038

Alexander CM, Fogel M, Yabuta H, Cody GD (2007) The origin and evolution of chondrites recorded in the elemental and isotopic compositions of their macromolecular organic matter. Geochim Cosmochim Acta 71:4380–4403

Alexander CM, Newsome SD, Fogel ML, Nittler LR, Busemann H, Cody GR (2010) Deuterium enrichments in chondritic macromolecular material—implications for the origin and evolution of organics, water and asteroids. Geochim Cosmochim Acta 74:4417–4437

Alexander CM, Bowden R, Fogel ML, Howard KT, Herd CD, Nittler LR (2012) The provenances of asteroids and their contributions to the volatile inventories of the terrestrila planets. Science 337:721–723

Allard P (1983) The origin of hydrogen, carbon, sulphur, nitrogen and rare gases in volcanic exhalations: evidence from isotope geochemistry. In: Tazieff H, Sabroux JC (eds) Forecasting volcanic events. Elsevier Publlishing Co., pp 337–386

Allen RB, Cuffey KM (2001) Oxygen- and hydrogen-isotopic ratios of water in precipitation: beyond paleothermometry. Rev Mineral Geochem 43:527–553

Alt JC, Muehlenbachs K, Honnorez J (1986) An oxygen isotopic profile through the upper kilometer of the oceanic crust, DSDP hole 504 B. Earth Planet Sci Lett 80:217–229

Altabet MA, Deuser WC (1985) Seasonal variations in natural abundance of ^{15}N in particles sinking to the deep Sargasso Sea. Nature 315:218–219

Altabet MA, McCarthy JJ (1985) Temporal and spatial variations in the natural abundance of ^{15}N in POM from a warm-core ring. Deep Sea Res 32:755–772

Altabet MA, Deuser WG, Honjo S, Stienen C (1991) Seasonal and depth related changes in the source of sinking particles in the North Atlantic. Nature 354:136–139

Amari S, Hoppe P, Zinner E, Lewis RS (1993) The isotopic compositions of stellar sources of meteoritic graphite grains. Nature 365:806–809

Amrani A (2014) Organosulfur compounds: molecular and isotopic evolution from biota to oil and gas. Ann Rev Earth Planet Sci 42:733–768

Amrani A, Deev A, Sessions AL, Tang Y, Adkins JF, Hill RL, Moldowan JM, Wei Z (2012) The sulfur-isotopic comppositions of benzothiophenes and dibenzothiophenes as a proxy for thermochemical sulfate reduction. Geochim Cosmochim Acta (in press)

Anbar AD, Rouxel O (2007) Metal stable isotopes in paleoceanography. Ann Rev Earth Planet Sci 35:717–746

Ancour AM, Sheppard SMF, Guyomar O, Wattelet J (1999) Use of ^{13}C to trace origin and cycling of inorganic carbon in the Rhone river system. Chem Geol 159:87–105

Anderson AT, Clayton RN, Mayeda TK (1971) Oxygen isotope thermometry of mafic igneous rocks. J Geol 79:715–729

Angert A, Cappa CD, DePaolo DJ (2004) Kinetic O-17 effects in the hydrologic cycle: indirect evidence and implications. Geochim Cosmochim Acta 68:3487–3495

Antler G, Turchyn AV, Rennie V, Herut B, Sivan O (2013) Coupled sulphur and oxygen isotope insight into bacterial sulphate reduction in the natural environment. Geochim Cosmochim Acta 118:98–117

Archer C, Vance D (2006) Coupled Fe and S isotope evidence for Archean microbial Fe(III) and sulphate reduction. Geology 34:153–156

Armytage RMG, Georg RB, Williams HM, Halliday AN (2012) Silicon isotopes in lunar rocks: implications for the Moon, s formation and the early history of the Earth. Geochim Cosmochim Acta 77:504–514

Arnold M, Sheppard SMF (1981) East Pacific Rise at 21°N: isotopic composition and origin of the hydrothermal sulfur. Earth Planet Sci Lett 56:148–156

Arthur MA, Dean WE, Claypool CE (1985) Anomalous ^{13}C enrichment in modern marine organic carbon. Nature 315:216–218

Asael D, Matthews A, Oszczepalski S, Bar-Matthews M, Halicz L (2009) Fluid speciation controls of low temperature copper isotope fractionation applied to the Kupferschiefer and Timna ore deposits. Chem Geol 262:147–158

Ayliffe LK, Chivas AR (1990) Oxyen isotope composition of the bone phosphate of Australian kangaroos: potential as a palaeoenvironmental recorder. Geochim Cosmochim Acta 54:2603–2609

Ayliffe LK, Lister AM, Chivas AR (1992) The preservation of glacial-interglacial climatic signatures in the oxygen isotopes of elephant skeletal phosphate. Palaeo, Palaeo, Palaeo 99:179–191

Ayliffe LK, Chivas AR, Leakey MG (1994) The retention of primary oxygen isotope compositions of fossil elephant skeletal phosphate. Geochim Cosmochim Acta 58:5291–5298

Bacastow RB, Keeling CD, Lueker TJ, Wahlen M, Mook WG (1996) The $\delta\ ^{13}$C Suess effect in the world surface oceans and its implications for oceanic uptake of CO_2: analysis of observations at Bermuda. Global Biochem Cycles 10:335–346

Baker AJ, Fallick AE (1989) Heavy carbon in two-billion-year-old marbles from Lofoten-Vesteralen, Norway: implications for the Precambrian carbon cycle. Geochim Cosmochim Acta 53:1111–1115

Baker J, Matthews A (1995) The stable isotope evolution of a metamorphic complex, Naxos, Greece. Contr Mineral Petrol 120:391–403

Baker JA, Macpherson CG, Menzies MA, Thirlwall MF, Al-Kadasi M, Mattey DP (2000) Resolving crustal and mantle contributions to continental flood volcanism, Yemen: constraints from mineral oxygen isotope data. J Petrol 41:1805–1820

Banner JL, Wasserburg GJ, Dobson PF, Carpenter AB, Moore CH (1989) Isotopic and trace element constraints on the orgin and evolution of saline groundwaters from central Missouri. Geochim Cosmochim Acta 53:383–398

Bao H (2015) Sulfate: a time capsule for Earth's O_2, O_3 and H_2O. Chem Geol 395:108–118

Bao H, Gu B (2004) Natural perchlorate has a unique oxygen isotope signature. Environ Sci Tech 38:5073–5077

Bao H, Koch PL (1999) Oxygen isotope fractionation in ferric oxide-water systems: low temperature synthesis. Geochim Cosmochim Acta 63:599–613

Bao H, Thiemens MH, Farquahar J, Campbell DA, Lee CC, Heine K, Loope DB (2000) Anomalous ^{17}O compositions in massive sulphate deposits on the Earth. Nature 406:176–178

Bao H, Thiemens MH, Heine K (2001) Oxygen-17 excesses of the Central Namib gypcretes: spatial distribution. Earth Planet Sci Lett 192:125–135

Barkan E, Luz B (2005) High precision measurements of $^{17}O/^{16}O$ and $^{18}O/^{16}O$ ratios in H_2O. Rapid Commun Mass Spectr 19:3737–3742

Barkan E, Luz B (2007) Diffusivity fractionations of $H_2^{16}O/H_2^{17}O$ and $H_2^{16}O/H_2^{18}O$ in air and their implications for isotope hydrology. Rapid Commun Mass Spectrom 21:2999–3005

Barkan E, Luz B (2011) The relationship among the three stable isotopes of oxygen in air, seawater and marine photosynthesis. Rapid Commun Mass Spectrom 25:2367–2369

Barnes I, Irwin WP, White DE (1978) Global distribution of carbon dioxide discharges and major zones of seismicity. US Geol Survey, Water-Resources Investigation 78–39, Open File Report

Barnes JJ, Franchi IA, Anand M, Tartese R, Starkey NA, Koike M, Sano Y, Russell SS (2013) Accurate and precise measurements of the D/H ratio and hydroxyl content in lunar apaites using NanoSIMS. Chem Geol 337–338:48–55

Baroni M, Thiemens MH, Delmas RJ, Savarino J (2007) Mass-independent sulfur isotopic composition in stratospheric volcanic eruptions. Science 315:84–87

Batenburg AM, Walter S et al (2011) Temporal and spatial variability of the stable isotope composition of atmospheric molecular hydrogen. Atm Chem Phys Discuss 11:10087–10120

Baumgartner LP, Rumble D (1988) Transport of stable isotopes. I. Development of a kinetic continuum theory for stable isotope transport. Contr Mineral Petrol 98:417–430

Baumgartner LP, Valley JW (2001) Stable isotope transport and contact metamorphic fluid flow. In: Stable Isotope Geochemistry. Rev Mineral Geochem 43:415–467

Beaty DW, Taylor HP (1982) Some petrologic and oxygen isotopic relationships in the Amulet Mine, Noranda, Quebec, and their bearing on the origin of Archaean massive sulfide deposits. Econ Geol 77:95–108

Bechtel A, Hoernes S (1990) Oxygen isotope fractionation between oxygen of different sites in illite minerals: a potential geothermometer. Contrib Mineral Petrol 104:463–470

Bechtel A, Sun Y, Püttmann W, Hoernes S, Hoefs J (2001) Isotopic evidence for multi-stage base metal enrichment in the Kupferschiefer from the Sangershausen Basin, Germany. Chem Geol 176:31–49

Becker RH, Epstein S (1982) Carbon, hydrogen and nitrogen isotopes in solvent-extractable organic matter from carbonaceous chondrites. Geochim Cosmochim Acta 46:97–103

Bell DR, Ihinger PD (2000) The isotopic composition of hydrogen in nominally anhydrous mantle minerals. Geochim Cosmochim Acta 64:2109–2118

Bemis BE, Spero HJ, Bijma J, Lea DW (1998) Reevaluation of the oxygen isotopic composition of planktonic foraminifera: experimental results and revised paleotemperature equations. Paleoceanography 13:150–160

Bender ML, Keigwin LD (1979) Speculations about upper Miocene changes in abyssal Pacific dissolved bicarbonate $\delta^{13}C$. Earth Planet Sci Lett 45:383–393

Bender M, Sowers T, Labeyrie L (1994) The Dole effect and its variations during the last 130000 years as measured in the Vostok ice core. Global Biogeochem Cycles 8:363–376

Bennett SA, Rouxel O, Schmidt K, Garbe-Schönberg D, Statham PJ, German CR (2009) Iron isotope fractionation in a buyant hydrothermal plume, 5°S Mid-Atlantic Ridge. Geochim Cosmochim Acta 73:5619–5634

Berndt ME, Seal RR, Shanks WC, Seyfried WE (1996) Hydrogen isotope systematics of phase separation in submarine hydrothermal systems: experimental calibration and theoretical models. Geochim Cosmochim Acta 60:1595–1604

Berner RA (1990) Atmospheric carbon dioxide levels over Phanerozoic time. Science 249:1382–1386

Berner U, Faber E, Scheeder G, Panten D (1995) Primary cracking of algal and landplant kerogens: kinetic models of isotope variations in methane, ethane and propane. Chem Geol 126:233–245

Beucher CP, Brzezinski MA, Jones JL (2008) Sources and biological fractionation of silicon isotopes in the Eastern Equatorial Pacific. Geochim Cosmochim Acata 72:3063–3073

Bickle MJ, Baker J (1990) Migration of reaction and isotopic fronts in infiltration zones: assessments of fluid flux in metamorphic terrains. Earth Planet Sci Lett 98:1–13

Bidigare RR et al (1997) Consistent fractionation of ^{13}C in nature and in the laboratory: growth-rate effects in some haptophyte algae. Global Biogeochem Cycles 11:279–292

Bindeman IN, Eiler JN et al (2005) Oxygen isotope evidence for slab melting in modern and ancient subduction zones. Earth Planet Sci Lett 235:480–496

Bindeman IN, Ponomareva VV, Bailey JC, Valley JW (2004) Volcanic arc of Kamchatka: a province with high-δ^{18}O magma sources and large scale ^{18}O/^{16}O depletion of the upper crust. Geochim Cosmochim Acta 68:841–865

Bindeman IN, Eiler JM, Wing BA, Farquhar J (2007) Rare sulfur and triple oxygen isotope geochemistry of volcanogenic sulfate aerosols. Geochim Cosmochim Acta 71:2326–2343

Bindeman IN, Gurenko A, Sigmarsson O, Chaussidon M (2008) Oxygen isotope heterogeneity and disequilibria of olivine crystals in large volume Holocene basalts from Iceland: evidence for magmatic digestion and erosion of Pleistocene hyaloclastites. Geochim Cosmochim Acta 72:4397–4420

Bird MI, Ascoughz PL (2012) Isotopes in pyrogenic carbon: a review. Org Geochem 42:1529–1539

Bird MI, Chivas AR (1989) Stable-isotope geochronology of the Australian regolith. Geochim Cosmochim Acta 53:3239–3256

Bird MI, Longstaffe FJ, Fyfe WS, Bildgen P (1992) Oxygen isotope systematics in a multiphase weathering system in Haiti. Geochim Cosmochim Acta 56:2831–2838

Black JR, Epstein E, Rains WD, Yin Q-Z, Casey WD (2008) Magnesium isotope fractionation during plant growth. Environ Sci Technol 42:7831–7836

Blair N, Leu A, Munoz E, Olsen J, Kwong E, Desmarais D (1985) Carbon isotopic fractionation in heterotrophic microbial metabolism. Appl Environ Microbiol 50:996–1001

Blake RE, O'Neil JR, Garcia GA (1997) Oxygen isotope systematics of biologically mediated reactions of phosphate: I Microbial degradation of organophosphorus compounds. Geochim Cosmochim Acta 61:441–4422

Blake RE, O'Neil JR, Surkov A (2005) Biogeochemical cycling of phosphorus: insights from oxygen isotope effects of phosphoenzymes. Am J Sci 305:596–620

Blattner P, Dietrich V, Gansser A (1983) Contrasting ^{18}O enrichment and origins of High Himalayan and Transhimalayan intrusives. Earth Planet Sci Lett 65:276–286

Blisnink PM, Stern LA (2005) Stable isotope altimetry: a critical review. Am J Sci 305:1033–1074

Boctor NZ, Alexander CM, Wang J, Hauri E (2003) The sources of water in Martian meteorites: clues from hydrogen isotopes. Geochim Cosmochim Acta 67:3971–3989

Boehme SE, Blair NE, Chanton JP, Martens CS (1996) A mass balance of ^{13}C and ^{12}C in an organic-rich methane-producing marine sediment. Geochim Cosmochim Acta 60:3835–3848

Bogard DD, Johnson P (1983) Martian gases in an Antarctic meteorite. Science 221:651–654

Böhlke JK, Sturchio NC, Gu B, Horita J, Brown GM, Jackson WA, Batista Jr, Hatzinger PB (2005) Perchlorate isotope forensics. Anal Chem 77:7838–7842

Bolliger C, Schroth MH, Bernasconi SM, Kleikemper J, Zeyer J (2001) Sulfur isotope fractionation during microbial reduction by toluene-degrading bacteria. Geochim Cosmochim Acta 65:3289–3299

Böttcher ME, Brumsack HJ, Lange GJ (1998) Sulfate reduction and related stable isotope (^{34}S, ^{18}O) variations in interstitial waters from the eastern Mediterranean. Proc Ocean Drill Program, Sci Res 160:365–373

Böttcher ME, Thamdrup B, Vennemann TW (2001) Oxygen and sulfur isotope fractionation during anaerobic bacterial disproportionation of elemental sulfur. Geochim Cosmochim Acta 65:1601–1609

Bottinga Y, Craig H (1969) Oxygen isotope fractionation between CO_2 and water and the isotopic composition of marine atmospheric CO_2. Earth Planet Sci Lett 5:285–295

Bottomley DJ, Katz A, Chan LH, Starinsky A, Douglas M, Clark ID, Raven KG (1999) The origin and evolution of Canadian Shield brines: evaporation or freezing of seawater? New lithium isotope and geochemical evidence from the Slave craton. Chem Geol 155:295–320

Bowers TS, Taylor HP (1985) An integrated chemical and isotope model of the origin of midocean ridge hot spring systems. J Geophys Res 90:12583–12606

Bowman JR, O'Neil JR, Essene EJ (1985) Contact skarn formation at Elkhorn, Montana. II. Origin and evolution of C-O-H skarn fluids. Am J Sci 285:621–660

Boyd SR, Pillinger CT (1994) A preliminary study of $^{15}N/^{14}N$ in octahedral growth from diamonds. Chem Geol 116:43–59

Boyd SR, Pillinger CT, Milledge HJ, Mendelssohn MJ, Seal M (1992) C and N isotopic composition and the infrared absorption spectra of coated diamonds: evidence for the regional uniformity of CO_2-H_2O rich fluids in lithospheric mantle. Earth Planet Sci Lett 109:633–644

Bradley AS, Summons RE (2010) Multiple origins of methane at the Lost City hydrothermal field. Earth Planet Sci Lett 297:34–41

Brandriss ME, O'Neil JR, Edlund MB, Stoermer EF (1998) Oxygen isotope fractionation between diatomaceous silica and water. Geochim Cosmochim Acta 62:1119–1125

Brenninkmeijer CAM (1993) Measurement of the abundance of ^{14}CO in the atmosphere and the $^{13}C/^{12}C$ and $^{18}O/^{16}O$ ratio of atmospheric CO with applications in New Zealand and Australia. J Geophys Res 98:10595–10614

Brenninkmeijer CAM, Lowe DC, Manning MR, Sparks RJ, van Velthoven PFJ (1995) The ^{13}C, ^{14}C and ^{18}O isotopic composition of CO, CH_4 and CO_2 in the higher southern latitudes and lower stratosphere. J Geophys Res 100:26163–26172

Brenninkmeijer CAM, Janssen C, Kaiser J, Röckmann T, Rhee TS, Assonov SS (2003) Isotope effects in the chemistry of atmospheric trace compounds. Chem Rev 103:5125–5161

Bridgestock LJ, Williams H et al (2014) Unlocking the zinc isotope systematics of iron meteorites. Earth Planet Sci Lett 400:153–164

Broecker WS (1974) Chemical oceanography. Harcourt Brace Jovanovich, New York

Brüchert V, Pratt LM (1996) Contemporaneous early diagenetic formation of organic and inorganic sulfur in estuarine sediments from the St Andrew Bay, Florida, USA. Geochim Cosmochim Acta 60:2325–2332

Brumsack HJ, Zuleger E, Gohn E, Murray RW (1992) Stable and radiogenic isotopes in pore waters from Leg 1217, Japan Sea. Proc Ocean Drill Program 127(128):635–649

Brunner B, Bernasconi SM, Kleikemper J, Schroth MH (2005) A model of oxygen and sulfur isotope fractionation in sulfate during bacterial sulfate reduction. Geochim Cosmochim Acta 69:4773–4785

Bryant JD, Koch PL, Froelich PN, Showers WJ, Genna BJ (1996) Oxygen isotope partitioning between phosphate and carbonate in mammalian apatite. Geochim Cosmochim Acta 60:5145–5148

Buhl D, Neuser RD, Richter DK, Riedel D, Roberts B, Strauss H, Veizer J (1991) Nature and nurture: environmental isotope story of the river Rhine. Naturwissenschaften 78:337–346

Burdett JW, Arthur MA, Richardson A (1989) A Neogene seawater sulfate isotope age curve from calcareous pelagic microfossils. Earth Planet Sci Lett 94:189–198

Burke A, Adkins JF et al (2013) Constraining the modern riverine sulphur isotope budget. Abstr VM Goldschmidt Conf

Burruss RC, Laughrey CD (2010) Carbon and hydrogen isotope reversal in deep basin gas: evidence for limits to the stability of hydrocarbons. Org Geochem 41:1285–1296

Butler IB, Archer C, Vance D, Oldroyd A, Rickard D (2005) Fe isotope fractionation on FeS formation in ambient aqueous solution. Earth Planet Sci Lett 236:430–442

Cabral RA, Jackson MG, Rose-Koga EF, Koga KT, Whitehouse MJ, Antonelli MA, Farquhar J, Day JM, Hauri EH (2013) Anomaleous sulphur isotopes in plume lavas reveal deep mantle storage of Archaean crust. Nature 496:490–493

Calmels D, Gaillerdet J, Brenot A, France-Lanord C (2007) Sustained sulfide oxidation by physical erosion processes in the Mackenzie River basin: climatic perspectives. Geology 35:1003–1006

Cameron EM (1982) Sulphate and sulphate reduction in early Precambrian oceans. Nature 296:145–148

Cameron EM, Hall GEM, Veizer J, Krouse HR (1995) Isotopic and elemental hydrogeochemistry of a major river system: Fraser River, British Columbia, Canada. Chem Geol 122:149–169

Canfield DE, Teske A (1996) Late Proterozoic rise in atmospheric oxygen concentration inferred from phylogenetic and sulphur-isotope studies. Nature 382:127–132

Canfield DE, Thamdrup B (1994) The production of ^{34}S depleted sulfide during bacterial disproportion to elemental sulfur. Science 266:1973–1975

Cartigny P (2005) Stable isotopes and the origin of diamond. Elements 1:79–84

Cartigny P (2010) Mantle-related carbonados? Geochemical insights from diamonds from the Dachine komatiite (French Guiana). Earth Planet Sci Lett 296:329–339

Cartigny P, Marty B (2013) Nitrogen isotopes and mantle geodynamics: the emergence of life and the atmosphere-crust-mantle connection. Elements 9:359–366

Cartigny P, Boyd SR, Harris JW, Javoy M (1997) Nitrogen isotopes in peridotitic diamonds from Fuxian, China: the mantle signature. Terra Nova 9:175–179

Cartigny P, Harris JW, Javoy M (1998) Subduction related diamonds? The evidence for a mantle-derived origin from coupled delta ^{13}C - delta ^{15}N determinations. Chem Geol 147:147–159

Cartigny P, Palot M, Thomassot E, Harris JW (2014) Diamond formation: a stable isotope perspective. Ann Rev Earth Planet Sci 42:699–732

Cartwright I, Valley JW (1991) Steep oxygen isotope gradients at marble-metagranite contacts in the NW Adirondacks Mountains, N.Y. Earth Planet Sci Lett 107:148–163

Cerling TE (1991) Carbon dioxide in the atmosphere: evidence from Cenozoic and Mesozoic paleosols. Am J Sci 291:377–400

Cerling TE, Sharp ZD (1996) Stable carbon and oxygen isotope analyses of fossil tooth enamel using laser ablation. Palaeo Palaeo Palaeoecol 126:173–186

Cerling TE, Brown FH, Bowman JR (1985) Low-temperature alteration of volcanic glass: hydration, Na, K, ^{18}O and Ar mobility. Chem Geol 52:281–293

Cerling TE, Wang Y, Quade J (1993) Expansion of C4 ecosystems as an indicator of global ecological change in the late Miocene. Nature 361:344–345

Cerling TE, Harris JM, MacFadden BJ, Leakey MG, Quade J, Eisenmann V, Ehleringer JR (1997) Global vegetation change through the Miocene/Pliocene boundary. Nature 389:153–158

Chakrabarti R, Knoll AH, Jacobsen SB, Fischer WW (2012) Si isotope variability in Proterozoic cherts. Geochim Cosmochim Acta (in press)

Chamberlain CP, Poage MA (2000) Reconstructing the paleotopography of mountain belts from the isotopic composition of authigenic minerals. Geology 28:115–118

Chapligin B, Leng MJ et al (2011) Inter-laboratory comparison of oxygen isotope compositions from biogenic silica. Geochim Cosmochim Acta 75:7242–7256

Chaussidon M, Marty B (1995) Primitive boron isotope composition of the mantle. Science 269:383–386

Chaussidon M, Albarede F, Sheppard SMF (1987) Sulphur isotope heterogeneity in the mantle from ion microprobe measurements of sulphide inclusions in diamonds. Nature 330:242–244

Chaussidon M, Albarede F, Sheppard SMF (1989) Sulphur isotope variations in the mantle from ion microprobe analysis of microsulphide inclusions. Earth Planet Sci Lett 92:144–156

Chazot G, Lowry D, Menzies M, Mattey D (1997) Oxygen isotope compositions of hydrous and anhydrous mantle peridotites. Geochim Cosmochim Acta 61:161–169

Chen H, Savage PS, Teng FZ, Helz RT, Moynier F (2013) Zinc isotopic fractionation during magmatic differentiation and the isotopic composition of bulk Earth. Earth Planet Sci Lett 369–370:34–42

Chiba H, Sakai H (1985) Oxygen isotope exchange rate between dissolved sulphate and water at hydrothermal temperatures. Geochim Cosmochim Acta 49:993–1000

Chivas AR, Andrew AS, Sinha AK, O'Neil JR (1982) Geochemistry of Pliocene-Pleistocene oceanic arc plutonic complex, Guadalcanal. Nature 300:139–143

Ciais P, Tans PP, Trolier M, White JWC, Francey RJ (1995) A large northern hemisphere terrestrial CO_2 sink indicated by the $^{13}C/^{12}C$ ratio of atmospheric CO_2. Science 269:1098–1102

Cifuentes LA, Fogel ML, Pennock JR, Sharp JR (1989) Biogeochemical factors that influence the stable nitrogen isotope ratio of dissolved ammonium in the Delaware Estuary. Geochim Cosmochim Acta 53:2713–2721

Claypool GE, Holser WT, Kaplan IR, Sakai H, Zak I (1980) The age curves of sulfur and oxygen isotopes in marine sulfate and their mutual interpretation. Chem Geol 28:199–260

Clayton RN (2002) Self-shielding in the solar nebula. Nature 451:860–861

Clayton RN (2004) Oxygen isotopes in meteorites. In: Treatise on geochemistry, vol 1. Elsevier, Amsterdam, pp 129–142

Clayton RN, Mayeda TK (1996) Oxygen isotope studies of achondrites. Geochim Cosmochim Acta 60:1999–2017

Clayton RN, Mayeda TK (1999) Oxygen isotope studies of carbonaceous chondrites. Geochim Cosmochim Acta 63:2089–2104

Clayton DD, Nittler LR (2004) Astrophysics with presolar stardust. Ann Rev Astron Astrophys 42:39–78

Clayton RN, Steiner A (1975) Oxygen isotope studies of the geothermal system at Warakei, New Zealand. Geochim Cosmochim Acta 39:1179–1186

Clayton RN, Friedman I, Graf DL, Mayeda TK, Meents WF, Shimp NF (1966) The origin of saline formation waters. 1. Isotopic composition. J Geophys Res 71:3869–3882

Clayton RN, Muffler LJP, White (1968) Oxygen isotope study of calcite and silicates of the River Branch No. I well, Salton Sea Geothermal Field, California. Am J Sci 266:968–979

Clayton RN, Grossman L, Mayeda TK (1973a) A component of primitive nuclear composition in carbonaceous meteorites. Science 182:485–488

Clayton RN, Hurd JM, Mayeda TK (1973b) Oxygen isotopic compositions of Apollo 15, 16 and 17 samples and their bearing on lunar origin and petrogenesis. In: Proceedings of 4th lunar Science Conference, Geochimica Cosmochimica Acta Supplement, vol 2, pp 1535–1542

Cliff SS, Thiemens MH (1997) The $^{18}O/^{16}O$ and $^{17}O/^{16}O$ ratios in atmospheric nitrous oxide: a mass independent anomaly. Science 278:1774–1776

Cliff SS, Brenninkmeijer CAM, Thiemens MH (1999) First measurement of the $^{18}O/^{16}O$ and $^{17}O/^{16}O$ ratios in stratospheric nitrous oxide: a mass-independent anomaly. J Geophys Res 104:16171–16175

Cline JD, Kaplan IR (1975) Isotopic fractionation of dissolved nitrate during denitrification in the eastern tropical North Pacific Ocean. Mar Chem 3:271–299

Clor LE, Fischer TP, Hilton DR, Sharp ZD, Hartono U (2005) Volatile and N isotope chemistry of the Molucca Sea collision zone: tracing source components along the Sangihe arc, Indonesia. Geochem Geophys Geosys 6:Q03J14. doi:10.1029/2004GC00825

Cobert F, Schmitt AD, Bourgeade P, Labolle F, Badot PM, Chabaux F, Stille P (2011) Experimental identification of Ca isotopic fractionations in higher plants. Geochim Cosmochim Acta 75:5467–5482

Cohen AS, Al Coe, Kemp DB (2007) The Late-Paleocene-Early Eocene and Toarcian (Early Jurassic) carbon isotope excursions: a comparison of their time scales, associated environmental changes, causes and consequences. J Geol Soc 164:1093–1108

Cole JE, Fairbanks RG (1990) The southern oscillation recorded in the $\delta^{18}O$ of corals from Tarawa atoll. Paleoceanography 5:669–683

Cole JE, Fairbanks RG, Shen GT (1993) The spectrum of recent variability in the southern oscillation: results from a Tarawa atoll. Science 260:1790–1793

Colman AS, Blake RE, Karl DM, Fogel ML, Turekian KK (2005) Marine phosphate oxygen isotopes and organic matter remineralization in the oceans. PNAS 102:13023–13028

Connolly CA, Walter LM, Baadsgaard H, Longstaffe F (1990) Origin and evolution of formation fluids, Alberta Basin, western Canada sedimentary basin: II. Isotope systematics and fluid mixing. Appl Geochem 5:397–414

Cook N, Hoefs J (1997) Sulphur isotope characteristics of metamorphosed Cu-(Zn) volcanogenic massive sulphide deposits in the Norwegian Caledonides. Chem Geol 135:307–324

Cooper KM, Eiler JM, Asimov PD, Langmuir CH (2004) Oxygen isotope evidence for the origin of enriched mantle beneath the mid-Atlantic ridge. Earth Planet Sci Lett 220:297–316

Coplen TB (2007) Calibration of the calcite-water oxygen-isotope geothermometer at Devils Hole, Nevada, a natural laboratory. Geochim Cosmochim Acta 71:3948–3957

Coplen TB, Hanshaw BB (1973) Ultrafiltration by a compacted clay membrane. I. Oxygen and hydrogen isotopic fractionation. Geochim Cosmochim Acta 37:2295–2310

Cortecci G, Longinelli A (1970) Isotopic composition of sulfate in rain water, Pisa, Italy. Earth Planet Sci Lett 8:36–40

Craddock PR, Dauphas N (2010) Iron isotopic compositions of geological reference materials and chondrites. Geostand Geoanal Res 35:101–123

Craddock PR, Warren JM, Dauphas N (2013) Abyssal peridotites reveal the near-chondritic Fe isotope composition of the Earth. Earth Planet Sci Lett 365:63–76

Craig H (1953) The geochemistry of the stable carbon isotopes. Geochim Cosmochim Acta 3:53–92

Craig H (1961) Isotopic variations in meteoric waters. Science 133:1702–1703

Craig H, Gordon L (1965) Deuterium and oxygen-18 variations in the ocean and the marine atmosphere. In: Symposium on marine geochemistry. Graduate School of Oceanography, vol 3. University of Rhode Island, OCC Publications, p 277

Craig H, Boato G, White DE (1956) Isotopic geochemistry of thermal waters. In: Proceedings of 2nd Conference on Nuclear Process Geological Settings, p 29

Craig H, Chou CC, Welhan JA, Stevens CM, Engelkemeier A (1988) The isotopic composition of methane in polar ice cores. Science 242:1535–1539

Criss RE, Taylor HP (1986) Meteoric-hydrothermal systems. Stable isotopes in high temperature geological processes. Rev Mineral 16:373–424

Criss RE, Champion DE, McIntyre DH (1985) Oxygen isotope, aeromagnetic and gravity anomalies associated with hydrothermally altered zones in the Yankee Fork Mining District, Custer County, Idaho. Econ Geol 80:1277–1296

Criss RE, Fleck RJ, Taylor HP (1991) Tertiary meteoric hydrothermal systems and their relation to ore deposition, Northwestern United States and Southern British Columbia. J Geophys Res 96:133335–13356

Crowson RA, Showers WJ, Wright EK, Hoering TC (1991) Preparation of phosphate samples for oxygen isotope analysis. Anal Chem 63:2397–2400

Curry WB, Duplessy JC, Labeyrie LD, Shackleton NJ (1988) Quaternary deep-water circulation changes in the distribution of $\delta^{13}C$ of deep water ΣCO_2 between the last glaciation and the Holocene. Paleoceanography 3:317–342

Cypionka H, Smock A, Böttcher MA (1998) A combined pathway of sulfur compound disproportionation in Desulfovibrio desulfuricans. FEMS Microbiol Lett 166:181–186

D'Errico ME, Lackey JS, Surpless BE, Loewy SL, Wooden JL, Barnes JD, Strickland A, Valley JW (2012) A detailed record of shallow hydrothermal fluid flow in the Sierra Nevada magmatic arc from low-$d^{18}O$ skarn garnets. Geology 40:763–766

Daeron M, Guo W et al (2011) $^{13}C^{18}O$ clumping in speleothems: observations from natural caves and precipitation experiments. Geochim Cosmochim Acta 75:3303–3317

Dansgaard W (1964) Stable isotope in precipitation. Tellus 16:436–468

Dansgaard W et al (1993) Evidence for general instability of past climate from a 250 kyr ice-core record. Nature 364:218–220

Dauphas N, Marty B (1999) Heavy nitrogen in carbonatites of the Kola peninsula: a possible signature of the deep mantle. Science 286:2488–2490

De Hoog JCM, Taylor BE, Van Bergen MJ (2009) Hydrogen-isotope systematics in degassing basaltic magma and application to Indonesian arc basalts. Chem Geol 266:256–266

De La Rocha CL, De Paolo DJ (2000) Isotopic evidence for variations in the marine calcium cycle over the Cenozoic. Science 289:1176–1178

De Moor JM, Fischer TP et al (2013) Sulfur degassing at Erta Ale (Ethiopia) and Masaya (Nicaragua) volcanoes: implications for degassing processes and oxygen fugacities of basaltic systems. Geochem Geophys Geosys 14(10). doi:10.102/ggge.20255

De Moor JM, Fischer TP, Sharp ZD, Hauri EH, Hilton DR, Atudorei V (2010) Sulfur isotope fractionation during the May 2003 eruption of Anatahan volcano, Mariana Islands: implications for sulfur sources and plume processes. Geochim Cosmochim Acta 74:5382–5397

De Souza GF, Reynolds BC, Johnson GC, Bullister JL, Bourdon B (2012a) Southern Ocean control of silicon stable isotope distribution in the deep Atlantic Ocean. Global Biogeochem Cycl 26:GB2035. doi:10.1029/2011GB004141

Degens ET, Epstein S (1962) Relationship between $^{18}O/^{16}O$ ratios in coexisting carbonates, cherts and diatomites. Bull Am Assoc Pet Geol 46:534–535

Deines P (1980) The isotopic composition of reduced organic carbon. In: Fritz P, Fontes JC (eds) Handbook of environmental geochemistry, Vol 1. Elsevier, New York Amsterdam, pp 239–406

Deines P (1989) Stable isotope variations in carbonatites. In: Carbonatites, genesis and evolution, K.Bell (ed) Unwin Hyman, London 619p

Deines P, Gold DP (1973) The isotopic composition of carbonatite and kimberlite carbonates and their bearing on the isotopic composition of deep-seated carbon. Geochim Cosmochim Acta 37:1709–1733

Deines P, Haggerty SE (2000) Small-scale oxygen isotope variations and petrochemistry of ultradeep (>300 km) and transition zone xenoliths. Geochim Cosmochim Acta 64:117–131

Deines P, Gurney JJ, Harris JW (1984) Associated chemical and carbon isotopic composition variations in diamonds from Finsch and Premier Kimberlite, South Africa. Geochim Cosmochim Acta 48:325–342

Delaygue G, Jouzel J, Dutay JC (2000) Oxygen-18 - salinity relationship simulated by an oceanic general simulation model. Earth Planet Sci Lett 178:113–123

Deloule E, Robert F (1995) Interstellar water in meteorites? Geochim Cosmochim Acta 59:4695–4706

Deloule E, Albarede F, Sheppard SMF (1991) Hydrogen isotope heterogeneities in the mantle from ionprobe analysis of amphiboles from ultramafic rocks. Earth Planet Sci Lett 105:543–553

Deloule E, Robert F, Doukhan JC (1998) Interstellar hydroxyl in meteoritic chondrules: implications for the origin of water in the inner solar system. Geochim Cosmochim Acta 62:3367–3378

DeNiro MJ, Epstein S (1978) Influence of diet on the distribution of carbon isotopes in animals. Geochim Cosmochim Acta 42:495–506

DeNiro MJ, Epstein S (1979) Relationship between the oxygen isotope ratios of terrestrial plant cellulose, carbon dioxide and water. Science 204:51–53

DeNiro MJ, Epstein S (1981) Isotopic composition of cellulose from aquatic organisms. Geochim Cosmochim Acta 45:1885–1894

Dennis KJ, Schrag DP (2010) Clumped isotope thermometry of carbonatites as an indicator of diagenetic alteration. Geochim Cosmochim Acta 74:4110–4122

Dennis PF, Rowe PJ, Atkinson TC (2001) The recovery and isotopic measurement of water from fluid inclusions in speleothems. Geochim Cosmochim Acta 65:871–884

Derry LA, Kaufmann AJ, Jacobsen SB (1992) Sedimentary cycling and environmental change in the Late Proterozoic: evidence from stable and radiogenic isotopes. Geochim Cosmochim Acta 56:1317–1329

Des Marais DJ (2001) Isotopic evolution of the biogeochemical carbon cycle during the Precambrian. In: Valley J, Cole D (eds) Stable isotope geochemistry. Rev Mineralogy 43:555–578

Des Marais DJ, Moore JG (1984) Carbon and its isotopes in mid-oceanic basaltic glasses. Earth Planet Sci Lett 69:43–57

Deutsch S, Ambach W, Eisner H (1966) Oxygen isotope study of snow and firn of an Alpine glacier. Earth Planet Sci Lett 1:197–201

Dickens GR (2003) Rethinking the global carbon cycle with a large dynamic and micrmediated gas hydrate capacitor. Earth Planet Sci Lett 213:169–182

Dickson JAD, Coleman ML (1980) Changes in carbon and oxygen isotope composition during limestone diagenesis. Sedimentology 27:107–118

Dickson JAD, Smalley PC, Raheim A, Stijfhoorn DE (1990) Intracrystalline carbon and oxygen isotope variations in calcite revealed by laser micro-sampling. Geology 18:809–811

Dietzel M, Tang J, Leis A, Köhler SJ (2009) Oxygen isotopic fractionation during inorganic calcite precipitation—effects of temperature, precipitation rate and pH. Chem Geol 268:107–115

Dipple GM, Ferry JM (1992) Fluid flow and stable isotope alteration in rocks at elevated temperatures with applications to metamorphism. Geochim Cosmochim Acta 56:3539–3550

Dobson PF, O'Neil JR (1987) Stable isotope composition and water contents of boninite series volcanic rocks from Chichi-jima, Bonin Islands, Japan. Earth Planet Sci Lett 82:75–86

Dobson PF, Epstein S, Stolper EM (1989) Hydrogen isotope fractionation between coexisting vapor and silicate glasses and melts at low pressure. Geochim Cosmochim Acta 53:2723–2730

Dodd JP, Sharp ZD (2010) A laser fluorination method for oxygen isotope analysis of biogenic silica and a new oxygen isotope calibration of modern diatoms in freshwater environments. Geochim Cosmochim Acta 74:1381–1390

Dodd JP, Sharp ZD, Fawcett PJ, Brearley AJ, McCubbin FM (2013) Rapid post-mortem maturation of diatom silica oxygen isotope values. Geochem Geophys Geosys 13(9). doi:10.1029/2011GC004019

Dodson MH (1973) Closure temperature in cooling geochronological and petrological systems. Contr Mineral Petrol 40:259–274

Dole M, Lange GA, Rudd DP, Zaukelies DA (1954) Isotopic composition of atmospheric oxygen and nitrogen. Geochim Cosmochim Acta 6:65–78

Donahue TM, Hoffman JH, Hodges RD, Watson AJ (1982) Venus was wet: a measurement of the ratio of deuterium to hydrogen. Science 216:630–633

Dorendorf F, Wiechert U, Wörner G (2000) Hydrated sub-arc mantle: a source for the Kluchevskoy volcano, Kamchatka, Russia. Earth Planet Sci Lett 175:69–86

Drake MJ, Righter K (2002) Determining the composition of the Earth. Nature 416:39–44

Driesner T (1997) The effect of pressure on deuterium-hydrogen fractionation in high-temperature water. Science 277:791–794

Driesner T, Seward TM (2000) Experimental and simulation study of salt effects and pressure/density effects on oxygen and hydrogen stable isotope liquid-vapor fractionation for 4–5 molal aqueous NaCl and KCl solutions to 400 °C. Geochim Cosmochim Acta 64:1773–1784

Dunbar RB, Wellington GM, Colgan MW, Glynn PW (1994) Eastern sea surface temperature since 1600 A.D.: The $\delta^{18}O$ record of climate variability in Galapagos corals. Paleoceanography 9:291–315

Duplessy JC, Shackleton NJ, Fairbanks RG, Labeyrie L, Oppo D, Kallel N (1988) Deepwater source variations during the last climatic cycle and their impact on the global circulation. Paleoceanography 3:343–360

Durka W, Schulze ED, Gebauer G, Voerkelius S (1994) Effects of forest decline on uptake and leaching of deposited nitrate determined from ^{15}N and ^{18}O measurements. Nature 372:765–767

Ehhalt D, Rohrer F (2009) The tropospheric cycle of H_2: a critical review. Tellus 61:500–535

Eiler JM (2007) The study of naturally-occuring multiply-substituted isotopologues. Earth Planet Sci Lett 262:309–327

Eiler JM (2013) The isotopic anatomies of molecules and minerals. Ann Rev Earth Planet Sci 41:411–441

Eiler JM, Kitchen N (2004) Hydrogen isotope evidence for the origin and evolution of the carbonaceous chondrites. Geochim Cosmochim Acta 68:1395–1411

Eiler JM, Baumgartner LP, Valley JW (1992) Intercrystalline stable isotope diffusion: a fast grain boundary model. Contr Mineral Petrol 112:543–557

Eiler JM, Valley JW, Baumgartner LP (1993) A new look at stable isotope thermometry. Geochim Cosmochim Acta 57:2571–2583

Eiler JM, Farley KA, Valley JW, Hofmann A, Stolper EM (1996) Oxygen isotope constraints on the sources of Hawaiian volcanism. Earth Planet Sci Lett 144:453–468

Eiler JM, Crawford A, Elliott T, Farley KA, Valley JW, Stolper EM (2000) Oxygen isotope geochemistry of oceanic-arc lavas. J Petrol 41:229–256

Eiler JM, Stolper EM, McCanta M (2011) Intra- and interc rystalline oxygen isotope variations in minerals from basalts and peridotites. J Petrol 52:1393–1413

Eiler JM et al (2014) Frontiers of stable isotope geoscience. Chem Geol 372:119–143

Eldridge CS, Compston W, Williams IS, Both RA, Walshe JL, Ohmoto H (1988) Sulfur isotope variability in sediment hosted massive sulfide deposits as determined using the ion microprobe SHRIMP. I. An example from the Rammelsberg ore body. Econ Geol 83:443–449

Eldridge CS, Compston W, Williams IS, Harris JW, Bristow JW (1991) Isotopic evidence for the involvement of recycled sediments in diamond formation. Nature 353:649–653

Eldridge CS, Williams IS, Walshe JL (1993) Sulfur isotope variability in sediment hosted massive sulfide deposits as determined using the ion microprobe SHRIMP. II. A study of the H.Y.C. deposit at McArthur River, Northern Territory, Australia. Econ Geol 88:1–26

Elkins LJ, Fischer TP, Hilton DR, Sharp ZD, McKnight S, Walker J (2006) Tracing nitrogen in volcanic and geothermal volatiles from the Nicaraguan volcanic front. Geochim Cosmochim Acta 70:5215–5235

Elliot M, Labeyrie L, Duplessy JC (2002) Changes in North Atlantic deep-water formation associated with the Dansgaard-Oeschger temperature oscillations (60–10 ka). Quat Sci Rev 21:1153–1165

Elliott T, Jeffcoate AB, Bouman C (2004) The terrestrial Li isotope cycle: light-weight constraints on mantle convection. Earth Planet Sci Lett 220:231–245

Emiliani C (1955) Pleistocene temperatures. J Geol 63:538–578

Emiliani C (1978) The cause of the ice ages. Earth Planet Sci Lett 37:349–354

Engel MH, Macko SA, Silfer JA (1990) Carbon isotope composition of individual amino acids in the Murchison meteorite. Nature 348:47–49

Epica community members (2004) Eight glacial cycles from an Antarctic ice core. Nature 429:623–628

Epstein S, Yapp CJ, Hall JH (1976) The determination of the D/H ratio of non-exchangeable hydrogen in cellulose extracted from aquatic and land plants. Earth Planet Sci Lett 30:241–251

Epstein S, Thompson P, Yapp CJ (1977) Oxygen and hydrogen isotopic ratios in plant cellulose. Science 198:1209–1215

Epstein S, Krishnamurthy RV, Cronin JR, Pizzarello S, Yuen GU (1987) Unusual stable isotope ratios in amino acid and carboxylic acid extracts from the Murchison meteorite. Nature 326:477–479

Erez J, Luz B (1983) Experimental paleotemperature equation for planktonic foraminifera. Geochim Cosmochim Acta 47:1025–1031

Eslinger EV, Savin SM (1973) Oxygen isotope geothermometry of the burial metamorphic rocks of the Precambrian Belt Supergroup, Glacier National Park, Montana. Bull Geol Soc Am 84:2549–2560

Estep MF, Hoering TC (1980) Biogeochemistry of the stable hydrogen isotopes. Geochim Cosmochim Acta 44:1197–1206

Etiope G, Schoell M (2014) Abiotic gas: atypical, but not rare. Elements 10:291–296

Etiope G, Sherwood-Lollar B (2013) Abiotic methane on Earth. Rev Geophys 51:276–299

Evans BW, Hattori K, Baronnet A (2013) Serpentinite: what, why where? Elements 9:99–106

Exley RA, Mattey DP, Boyd SR, Pillinger CT (1987) Nitrogen isotope geochemistry of basaltic glasses: implications for mantle degassing and structure. Earth Planet Sci Lett 81:163–174

Fairbanks RG (1989) A 17000 year glacio-eustatic sea level record: influence of glacial melting rates on the Younger Dryas event and deep ocean circulation. Nature 342:637–642

Fantle MS (2010) Evaluating the Ca isotope proxy. Am J Sci 310:194–210

Fantle MS, De Paolo DJ (2005) Variations in the marine Ca cycle over the past 20 million years. Earth Planet Sci Lett 237:102–117

Farkas J, Buhl D, Blenkinsop J, Veizer J (2007) Evolution of the oceanic calcium cycle during the late Mesozoic: evidence from $\delta^{44/40}$ Ca of marine skeletal carbonates. Earth Planet Sci Lett 253:96–111

Farquhar J, Thiemens MH (2000) The oxygen cycle of the Martian atmosphere-regolith system: Δ^{17}O of secondary phases in Nakhla and Lafayette. J Geophys Res 105:11991–11998

Farquhar GD et al (1993) Vegetation effects on the isotope composition of oxygen in atmospheric CO_2. Nature 363:439–443

Farquhar J, Chacko T, Ellis DJ (1996) Preservation of oxygen isotopic compositions in granulites from Northwestern Canada and Enderby Land, Antarctica: implications for high-temperature isotopic thermometry. Contr Mineral Petrol 125:213–224

Farquhar J, Thiemens MH, Jackson T (1998) Atmosphere-surface interactions on Mars: Δ^{17}O measurements of carbonate from ALH 84001. Science 280:1580–1582

Farquhar J, Bao H, Thiemens M (2000) Atmospheric influence of Earth's earliest sulfur cycle. Science 289:756–759

Farquhar J, Wing B, McKeegan KD, Harris JW (2002) Insight into crust-mantle coupling from anomalous Δ^{33}S of sulfide inclusions in diamonds. Geochim Cosmochim Acta Spec Suppl 66: A225

Farquhar J, Johnston DT, Wing BA, Habicht KS, Canfield DE, Airieau S, Thiemens MH (2003) Multiple sulphur isotope interpretations for biosynthetic pathways: implications for biological signatures in the sulphur isotope record. Geobiology 1:27–36

Farquhar J, Kim ST, Masterson A (2007) Implications from sulfur isotopes of the Nakhla meteorite for the origin of sulfate on Mars. Earth Planet Sci Lett 264:1–8

Ferry JM (1992) Regional metamorphism of the Waits River Formation: delineation of a new type of giant hydrothermal system. J Petrol 33:45–94

Ferry JM, Dipple GM (1992) Models for coupled fluid flow, mineral reaction and isotopic alteration during contact metamorphism: the Notch Peak aureole, Utah. Am Mineral 77:577–591

Ferry JM, Passey BH, Vasconcelos C, Eiler JM (2011) Formation of dolomite at 40–80 °C in the Latemar carbonate buildup, Dolomites, Italy from clumped isotope thermometry. Geology 39:571–574

Ferry JM, Kitajima K, Strickland A, Valley JW (2014) Ion microprobe survey of the grain-scale oxygen isotope geochemistry of minerals in metamorphic rocks. Geochim Cosmochim Acta (in press)

Fiebig J, Chiodini G, Caliro S, Rizzo A, Spangenberg J, Hunziker JC (2004) Chemical and isotopic equilibrium between CO_2 and CH_4 in fumarolic gas discharges: generation of CH_4 in arc magmatic-hydrothermal systems. Geochim Cosmochim Acta 68:2321–2334

Field CW, Gustafson LB (1976) Sulfur isotopes in the porphyry copper deposit at El Salvador, Chile. Econ Geol 71:1533–1548

Fiorentini E, Hoernes S, Hoffbauer R, Vitanage PW (1990) Nature and scale of fluid-rock exchange in granulite-grade rocks of Sri Lanka: a stable isotope study. In: Vielzeuf D, Vidal Ph (eds) Granulites and crustal evolution. Kluwer Dordrecht, pp 311–338

Fischer TP, Giggenbach WF, Sano Y, Williams SN (1998) Fluxes and sources of volatiles discharged from Kudryavy, a subduction zone volcano, Kurile Islands. Earth Planet Sci Lett 160:81–96

Fischer TP, Hilton DR, Zimmer MM, Shaw AM, Sharp ZD, Walker JA (2002) Subduction and recycling of nitrogen along the Central American margin. Science 297:1154–1157

Fittoussi C, Bourdon B, Kleine T, Oberli F, Reynolds BC (2009) Si isotope systematics of meteorites and terrestrial peridotites: implications for Mg/Si fractionation in the solar nebula and for Si in the Earth's core. Earth Planet Sci Lett 287:77–85

Fogel ML, Cifuentes LA (1993) Isotope fractionation during primary production. In: Engel MH, Macko SA (eds) Organic Geochemistry, Plenum Press, pp 73–98

Francey RJ, Tans PP (1987) Latitudinal variation in oxygen-18 of atmospheric CO_2. Nature 327:495–497

Franchi IA, Wright IP, Sexton AS, Pillinger T (1999) The oxygen isotopic composition of Earth and Mars. Meteorit Planet Sci 34:657–661

Franz HB et al (2014) Isotopic links between atmospheric chemistry and the deep sulphur cycle on Mars. Nature 508:364–368

Frape SK, Fritz P (1987) Geochemical trends from groundwaters from the Canadian Shield. In: Fritz P, Frape SK (eds) Saline water and gases in crystalline rocks, Geological Association of Canada, Special Paper, vol 33. pp 19–38

Frape SK, Fritz P, McNutt RH (1984) Water-rock interaction and chemistry of groundwaters from the Canadian Shield. Geochim Cosmochim Acta 48:1617–1627

Freeman KH, Hayes JM (1992) Fractionation of carbon isotopes by phytoplankton and estimates of ancient CO_2 levels. Global Biogeochem Cycles 6:185–198

Freeman KH, Hayes JM, Trendel JM, Albrecht P (1990) Evidence from carbon isotope measurements for diverse origins of sedimentary hydrocarbons. Nature 343:254–256

Frei R, Gaucher C, Poulton SW, Canfield DE (2009) Fluctuations in Precambrian atmospheric oxygenation recorded by chromium isotopes. Nature 461:250–253

Freyer HD (1979) On the ^{13}C-record in tree rings. I. ^{13}C variations in northern hemisphere trees during the last 150 years. Tellus 31:124–137

Freyer HD, Belacy N (1983) $^{13}C/^{12}C$ records in northern hemispheric trees during the past 500 years—anthropogenic impact and climatic superpositions. J Geophys Res 88:6844–6852

Fricke HC, O'Neil JR (1999) The correlation between $^{18}O/^{16}O$ ratios of meteoric water and surface temperature: its use in investigating terrestrial climate change over geologic time. Earth Planet Sci Lett 170:181–196

Fricke HC, Wickham SM, O'Neil JR (1992) Oxygen and hydrogen isotope evidence for meteoric water infiltration during mylonitization and uplift in the Ruby Mountains—East Humboldt Range core complex, Nevada. Contr Mineral Petrol 111:203–221

Fricke HC, Clyde WC, O'Neil JR (1998a) Intra-tooth variations in $\delta^{18}O$ (PO_4) of mammalian tooth enamel as a record of seasonal variations in continental climate variables. Geochim Cosmochim Acta 62:1839–1850

Fricke HC, Clyde WC, O'Neil JR, Gingerich PD (1998b) Evidence for rapid climate change in North America during the latest Paleocene thermal maximum: oxygen isotope compositions of biogenic phosphate from the Bighorn Basin (Wyoming). Earth Planet Sci Lett 160:193–208

Friedman I, Scholz TG (1974) Isotopic composition of atmospheric hydrogen (1967–1969). J Geophys Res 79:785–788

Fripiat F, Cavagna AJ, Delairs F, de Brauwere A, Andre L, Cardinal D (2012) Processes controlling the Si isotopic composition in the Southern Ocean and application for paleoceanography. Biogeosciences 9:2443–2457

Frost CD, von Blanckenburg F, Schoenberg R, Frost BR, Swapp SM (2007) Preservation of Fe isotope heterogeneities during diagenesis and metamorphism of banded iron formation. Contr Mineral Petrol 153:211–235

Fry B (1988) Food web structure on Georges Bank from stable C, N and S isotopic compositions. Limnol Oceanogr 3:1182–1190

Fu Q, Sherwood Lollar B, horita J, Lacrampe-Couloume G, Seyfried WE (2007) Abiotic formation of hydrocarbons under hydrothermal conditions: constraints from chemical and isotope data. Geochim Cosmochim Acta 71:1982–1998

Gagan MK, Ayliffe LK, Beck JW, Cole JE, Druffel ER, Schrag DP (2000) New views of tropical paleoclimates from corals. Quat Sci Rev 19:45–64

Galimov EM (1985) The relation between formation conditions and variations in isotope compositions of diamonds. Geochem Int 22(1):118–141

Galimov EM (1988) Sources and mechanisms of formation of gaseous hydrocarbons in sedimentary rocks. Chem Geol 71:77–95

Galimov EM (1991) Isotopic fractionation related to kimberlite magmatism and diamond formation. Geochim Cosmochim Acta 55:1697–1708

Galimov EM (2006) Isotope organic geochemistry. Org Geochem 37:1200–1262

Gao X, Thiemens MH (1993a) Isotopic composition and concentration of sulfur in carbonaceous chondrites. Geochim Cosmochim Acta 57:3159–3169

Gao X, Thiemens MH (1993b) Variations of the isotopic composition of sulfur in enstatite and ordinary chondrites. Geochim Cosmochim Acta 57:3171–3176

Gao Y, Hoefs J, Przybilla R, Snow JE (2006) A complete oxygen isotope profile through the lower oceanic crust, ODP hole 735B. Chem Geol 233:217–234

Garlick GD, Epstein S (1967) Oxygen isotope ratios in coexisting minerals of regionally metamorphosed rocks. Geochim Cosmochim Acta 31:181

Gat JR (1971) Comments on the stable isotope method in regional groundwater investigation. Water Resour Res 7:980

Gat JR (1984) The stable isotope composition of Dead Sea waters. Earth Planet Sci Lett 71:361–376

Gat JR, Issar A (1974) Desert isotope hydrology: water sources of the Sinai desert. Geochim Cosmochim Acta 38:1117–11131

Georg RB, Reynolds BC, Frank M, Halliday AN (2006) Mechanisms controlling the silicon isotopic compositions of river water. Earth Planet Sci Lett 249:290–306

Georg RB, Halliday AN, Schauble EA, Reynolds BC (2007) Silicon in the Earth's core. Nature 447:1102–1106

Gerdes ML, Baumgartner LP, Person M, Rumble D (1995) One- and two-dimensional models of fluid flow and stable isotope exchange at an outcrop in the Adamello contact aureole, Southern Alps, Italy. Am Mineral 80:1004–1019

Gerlach TM, Taylor BE (1990) Carbon isotope constraints on degassing of carbon dioxide from Kilauea volcano. Geochim Cosmochim Acta 54:2051–2058

Gerlach TM, Thomas DM (1986) Carbon and sulphur isotopic composition of Kilauea parental magma. Nature 319:480–483

Geske A, Goldstein RH, Mavromatis V, Richter DK, Buhl D, Kluge T, John CM, Immenhauser A (2015) The magnesium isotope (δ^{26}Mg) signature of dolomites. Geochim Cosmochim Acta 149:131–151

Ghosh P et al (2006) ^{13}C-^{18}O bonds in carbonate minerals: a new kind of paleothermometer. Geochim Cosmochim Acta 70:1439–1456

Giggenbach WF (1992) Isotopic shifts in waters from geothermal and volcanic systems along convergent plate boundaries and their origin. Earth Planet Sci Lett 113:495–510

Giletti BJ (1986) Diffusion effect on oxygen isotope temperatures of slowly cooled igneous and metamorphic rocks. Earth Planet Sci Lett 77:218–228

Gilg HA (2000) D/H evidence for the timing of kaolinization in Northeast Bavaria, Germany. Chem Geol 170:5–18

Girard JP, Savin S (1996) Intercrystalline fractionation of oxygen isotopes between hydroxyl and non-hydroxyl sites in kaolinite measured by thermal dehydroxylation and partial fluorination. Geochim Cosmochim Acta 60:469–487

Given RK, Lohmann KC (1985) Derivation of the original isotopic composition of Permian marine cements. J Sediment Petrol 55:430–439

Goericke R, Fry B (1994) Variations of marine plankton δ^{13}C with latitude, temperature and dissolved CO_2 in the world ocean. Global Geochem Cycles 8:85–90

Goldhaber MB, Kaplan IR (1974) The sedimentary sulfur cycle. In: Goldberg EB (ed) The sea, vol IV. Wiley, New York

Goldhammer T, Brunner B, Bernasconi SM, Ferdelman TG, Zabel M (2011) Phosphate oxygen isotopes: insights into sedimentary phosphorus cycling from the Benguela upwelling system. Geochim Cosmochim Acta 75:3741–3756

Gonfiantini R (1986) Environmental isotopes in lake studies. In: Fritz P, Fontes J (eds) Handbook of environmental isotope geochemistry, vol 2. Elsevier Publ Co, pp 112–168

Grachev AM, Severinghaus JP (2003) Laboratory determination of thermal diffusion constants for $^{29}N/^{28}N_2$ in air at temperatures from -60 to 0°C for reconstruction of magnitudes of abrupt climate changes using the ice core fossil-air paleothermometer. Geochim Cosmochim Acta 67:345–360

Grady MM, Pillinger CT (1990) ALH 85085: nitrogen isotope analysis of a highly unusual primitive chondrite. Earth Planet Sci Lett 97:29–40

Grady MM, Pillinger CT (1993) Acfer 182: search for the location of ^{15}N-enriched nitrogen. Earth Planet Sci Lett 116:165–180

Graham S, Pearson N, Jackson S, Griffin W, O‘ Reilly SY (2004) Tracing Cu and Fe from source to porphyry: in situ determination of Cu and Fe isotope ratios in sulfides from the Grasberg Cu-Au deposit. Chem Geol 207:147–169

Grasse P, Ehlert C, Frank M (2013) The influence of water mass mixing on the dissolved Si isotope composition in the eastern Equatorial Pacific. Earth Planet Sci Lett 380:60–71

Green GR, Ohmoto D, Date J, Takahashi T (1983) Whole-rock oxygen isotope distribution in the Fukazawa-Kosaka Area, Hokuroko District, Japan and its potential application to mineral exploration. Econ Geol Monogr 5:395–411

Greenwood JP, Riciputi LR, McSween HY (1997) Sulfide isotopic compositions in shergottites and ALH 84001, and possible implications for life on Mars. Geochim Cosmochim Acta 61:4449–4453

Greenwood RC, Franchi IA, Jambon A, Barrat JA, Burbine TH (2006) Oxygen isotope variation in stony-iron meteorites. Science 313:1763–1765

Greenwood JP, Itoh S, Sakamoto N, Warren P, Taylor L, Yurimoto H (2011) Hydrogen isotope ratios in lunar rocks indicate delivery of cometary water to the Moon. Nat Geosci 4:79–82

Gregory RT, Taylor HP (1981) An oxygen isotope profile in a section of Cretaceous oceanic crust, Samail Ophiolite, Oman: evidence for $\delta^{18}O$ buffering of the oceans by deep (>5 km) seawater-hydrothermal circulation at Mid-Ocean Ridges. J Geophys Res 86:2737–2755

Gregory RT, Taylor HP (1986) Possible non-equilibrium oxygen isotope effects in mantle nodules, an alternative to the Kyser-O, Neil-Carmichael $^{18}O/^{16}O$ geothermometer. Contr Mineral Petrol 93:114–119

Griffith EM, Paytan A, Kozdon R, Eisenhauer A, Ravelo AC (2008a) Influences on the fractionation of calcium isotopes in planktonic foraminifera. Earth Planet Sci Lett 268:124–136

Griffith EM, Schauble EA, Bullen TD, Paytan A (2008b) Characterization of calcium isotopes in natural and synthetic barite. Geochim Cosmochim Acta 72:5641–5658

Griffith EM, Payton A, Caldeira K, Bullen TD, Thomas E (2008c) A dynamic marine calcium cycle during the past 28 million years. Science 322:1671–1674

Grimes CB, Ushikubo T, John BE, Valley JW (2011) Uniformly mantle-like $\delta^{18}O$ in zircons from oceanic plagiogranite and gabbros. Contr Mineral Petrol 161:13–33

Grootes PM, Stuiver M, White JWC, Johnsen S, Jouzel J (1993) Comparison of oxygen isotope records from the GISP-2 and GRIP Greenland ice cores. Nature 366:552–554

Grossman EL (1984) Carbon isotopic fractionation in live benthic foraminifera—comparison with inorganic precipitate studies. Geochim Cosmochim Acta 48:1505–1512

Grottoli AG, Eakin CM (2007) A review of modern coral $\delta^{18}O$ and $\Delta^{14}C$ proxy records. Earth Sci Rev 81:67–91

Gruber N (1998) Anthropogenic CO_2 in the Atlantic Ocean. Global Biogeochem Cycles 12:165–191

Gruber N et al (1999) Spatiotemporal patterns of carbon-13 in the global surface oceans and the oceanic Suess effect: Global Biogeochem Cycles 13: 307–335

Guelke M, von Blanckenburg F (2007) Fractionation of stable iron isotopes in higher plants. Environ Sci Tech 41:1896–1901

Guilbaud R, Butler IB, Ellam RM (2011) Abiotic pyrite formation produces a large Fe isotope fractionation. Science 332:1548–1551

Guo W, Eiler JM (2007) Temperatures of aqueous alteration and evidence for methane generation on the parent bodies of the CM chondrites. Geochim Cosmochim Acta 71:5565–5575

Guy RD, Fogel ML, Berry JA (1993) Photosynthetic fractionation of the stable isotopes of oxygen and carbon. Plant Phys 101:37–47

Haack U, Hoefs J, Gohn E (1982) Constraints on the origin of Damaran granites by Rb/Sr and δ^{18}O data. Contrib Mineral Petrol 79:279–289

Hackley KC, Anderson TF (1986) Sulfur isotopic variations in low-sulfur coals from the Rocky Mountain region. Geochim Cosmochim Acta 50:703–1713

Hahm D, Hilton DR, Castillo PR, Hawkins JW, Hanan BB, Hauri EH (2012) An overview of the volatile systematics of the Lau Basin—resolving the effects of source variation, magmatic degassing and crustal contamination. Geochim Cosmochim Acta 85:88–113

Haimson M, Knauth LP (1983) Stepwise fluorination-a useful approach for the isotopic analysis of hydrous minerals. Geochim Cosmochim Acta 47:1589–1595

Halbout J, Robert F, Javoy M (1990) Hydrogen and oxygen isotope compositions in kerogen from the Orgueil meteorite: clues to a solar origin. Geochim Cosmochim Acta 54:1453–1462

Hallis LJ, Anand M, Greenwood RC, Miller MF, Franchi IA, Russell SS (2010) The oxygen isotope composition, petrology and geochemistry of mare basalts: evidence for large-scale compositional variation in the lunar mantle. Geochim Cosmochim Acta 74:6885–6899

Halverson GP, Poitrasson F, Hoffman PE, Nedelec A, Montel JM, Kirby J (2011) Fe isotope and trace element geochemistry of the Neoproterozoic syn-glacial Rapitan iron formation. Earth Planet Sci Lett 309:100–112

Hamza MS, Epstein S (1980) Oxygen isotope fractionation between oxygen of different sites in hydroxyl-bearing silicate minerals. Geochim Cosmochim Acta 44:173–182

Harmon RS, Hoefs J (1995) Oxygen isotope heterogeneity of the mantle deduced from global ^{18}O systematics of basalts from different geotectonic settings. Contr Mineral Petrol 120:95–114

Harmon RS, Hoefs J, Wedepohl KH (1987) Stable isotope (O, H, S) relationships in Tertiary basalts and their mantle xenoliths from the Northern Hessian Depression, W.Germany. Contr Mineral Petrol 95:350–369

Harte B, Otter M (1992) Carbon isotope measurements on diamonds. Chem Geol 101:177–183

Hartmann M, Nielsen H (1969) δ^{34}S-Werte in rezenten Meeressedimenten und ihre Deutung am Beispiel einiger Sedimentprofile aus der westlichen Ostsee. Geol Rundsch 58:621–655

Hauri EH, Wang J, Pearson DG, Bulanova GP (2002) Microanalysis of δ^{13}C, δ^{15}N and N abundances in diamonds by secondary ion mass spectrometry. Chem Geol 185:149–163

Hauri EH, Weinreich T, Saal AE, Rutherford MC, Van Orman JA (2011) High pre-eruptive water contents preserved in melrt inclusions. Science 333:213–215

Hawkesworth CJ, Kemp AIS (2006) Using hafnium and oxygen isotopes in zircons to unravel the record of crustal evolution. Chem Geol 226:144–162

Hayes JM (2001) Fractionation of carbon and hydrogen isotopes in biosynthetic processes. In: Valley JW, Cole DR (eds) Stable isotope geochemistry. Reviews in mineralogy and geochemistry, vol 43. pp 225–277

Hayes JM, Waldbauer JR (2006) The carbon cycle and associated redox processes through time. Phil Trans R Soc B 361:931–950

Hayes JM, Kaplan IR, Wedeking KW (1983) Precambrian organic chemistry, preservation of the record. In: Schopf JW (ed) Earth's earliest biosphere: its origin and evolution, chap 5. Princeton University Press, pp 93–132

Hayes JM, Popp BN, Takigiku R, Johnson MW (1989) An isotopic study of biogeochemical relationships between carbonates and organic carbon in the Greenhorn Formation. Geochim Cosmochim Acta 53:2961–2972

Hayes JM, Strauss H, Kaufman AJ (1999) The abundance of ^{13}C in marine organic matter and isotopic fractionation in the global biogeochemical cycle of carbon during the past 800 Ma. Chem Geol 161:103–125

Hays PD, Grossman EL (1991) Oxygen isotopes in meteoric calcite cements as indicators of continental paleoclimate. Geology 19:441–444

Hays JD, Imbrie J, Shackleton NJ (1976) Variations in the earth's orbit: pacemaker of the ice ages. Science 194:943–954

Heaton THE (1986) Isotopic studies of nitrogen pollution in the hydrosphere and atmosphere: a review. Chem Geol 59:87–102

Helman Y, Barkan E, Eisenstadt D, Luz B, Kaplan A (2005) Fractionation of the three stable oxygen isotopes by oxygen producing and consuming reactions in photosynthetic organisms. Plant Phys 2005:2292–2298

Hendy CH, Wilson AT (1968) Paleoclimatic data from speleothems. Nature 219:48–51

Heraty LJ, Fuller ME, Huang L, Abrajano T, Sturchio NC (1999) Isotopic fractionation of carbon and chlorine by microbial degradation of dichlormethane. Org Geochem 30:793–799

Herwarth D, Pack A, Friedrichs B, Bischoff A (2014) Identification of the giant impactor Theia in lunar rocks. Science 344:1146–1150

Hin RC, Schmidt MW, Bourdon B (2012) Experimental evidence for the absence of iron isotope fractionation between metal and silicate liquids at 1GPA and 1250-1300°C and its cosmochemical consequences. Geochim Cosmochim Acta 93:164–181

Hin RC, Fitoussi C, Schmidt MW, Bourdon B (2014) Experimental determination of the Si isotope fractionation factor between liquid metal and liquid silicate. Earth Planet Sci Lett 387:55–66

Hinrichs KU, Hayes JM, Sylva SP, Brewer PG, DeLong EF (1999) Methane-consuming archaebacteria in marine sediments. Nature 398:802–805

Hitchon B, Friedman I (1969) Geochemistry and origin of formation waters in the western Canada sedimentary basin. 1. Stable isotopes of hydrogen and oxygen. Geochim Cosmochim Acta 33:1321–1349

Hitchon B, Krouse HR (1972) Hydrogeochemistry of the surface waters of the Mackenzie River drainage basin, Canada. III. Stable isotopes of oxygen, carbon and sulfur. Geochim Cosmochim Acta 36:1337–1357

Hoag KJ, Still CJ, Fung IY, Boering KA (2005) Triple oxygen isotope composition of tropospheric carbon dioxide as a tracer of terrestrial gross carbon fluxes. Geophys Res Lett 32: L02802

Hoefs J (1970) Kohlenstoff-und Sauerstoff-Isotopenuntersuchungen an Karbonatkonkretionen und umgebendem Gestein. Contrib Mineral Petrol 27:66–79

Hoefs J (1992) The stable isotope composition of sedimentary iron oxides with special reference to Banded Iron Formations. In: Isotopic signatures and sedimentary records. Lecture Notes in Earth Science, vol 43. Springer Verlag, pp 199–213

Hoefs J, Emmermann R (1983) The oxygen isotope composition of Hercynian granites and pre-Hercynian gneisses from the Schwarzwald, SW Germany. Contrib Mineral Petrol 83:320–329

Hoefs J, Sywall M (1997) Lithium isotope composition of quaternary and Tertiary biogene carbonates and a global lithium isotope balance. Geochim Cosmochim Acta 61:2679–2690

Hoering T (1975) The biochemistry of the stable hydrogen isotopes. Carnegie Inst Washington Yearb 74:598

Hoernes S, Van Reenen DC (1992) The oxygen isotopic composition of granulites and retrogressed granulites from the Limpopo Belt as a monitor of fluid-rock interaction. Precambrian Res 55:353–364

Hoffman JH, Hodges RR, McElroy MB, Donahue TM, Kolpin M (1979) Composition and structure of the Venus atmosphere: results from Pioneer Venus. Science 205:49–52

Hoffman PE, Kaufman AJ, Halverson GP, Schrag DP (1998) Neoproterozoic snowball earth. Science 281:1342–1346

Hofmann ME, Horvath B, Pack A (2012) Triple oxygen isotope equilibrium fractionation between carbon dioxide and water. Earth Planet Sci Lett 319–320:159–164

Hofstetter TB, Scharzenbach RP, Bernasconi SM (2008) Assessing transformation processes of organic compounds using stable isotope fractionation. Environ Sci Technol 42:7737–7743

Holloway JR, Blank JG (1994) Application of experimental results to C-O-H species in natural melts. In: Carroll MR, Holloway JR (eds) Volatiles in magmas. Review on Mineral, vol 30, pp 187–230

Holmden C (2009) Ca isotope study of Ordovician dolomite, limestone, and anhydrite in the Williston basin: Implications for subsurface dolomitization and local Ca cycling. Chem Geol 268:180–188

Holser WT (1977) Catastrophic chemical events in the history of the ocean. Nature 267:403–408

Holser WT, Kaplan IR (1966) Isotope geochemistry of sedimentary sulfates. Chem Geol 1:93–135

Hoppe P, Zinner E (2000) Presolar dust grains from meteorites and their stellar sources. J Geophys Res Space Phys 105:10371–10385

Horita J (1989) Stable isotope fractionation factors of water in hydrated salt minerals. Earth Planet Sci Lett 95:173–179

Horita J (2014) Oxygen and carbon isotope fractionation in the system dolomite-water-CO_2 to elevated temperatures. Geochim Cosmochim Acta (in press)

Horita J, Berndt ME (1999) Abiogenic methane formation and isotope fractionation under hydrothermal conditions. Science 285:1055–1057

Horita J, Cole DR, Wesolowski DJ (1995) The activity-composition relationship of oxygen and hydrogen isotopes in aqueous salt solutions: III. Vapor-liquid water equilibration of NaCl solutions to 350 °C. Geochim Cosmochim Acta 59:1139–1151

Horita J, Driesner T, Cole DR (1999) Pressure effect on hydrogen isotope fractionation between brucite and water at elevated temperatures. Science 286:1545–1547

Horita J, Cole DR, Polyakov VB, Driesner T (2002a) Experimental and theoretical study of pressure effects on hydrous isotope fractionation in the system brucite-water at elevated temperatures. Geochim Cosmochim Acta 66:3769–3788

Horita J, Zimmermann H, Holland HD (2002b) Chemical evolution of seawater during the Phanerozoic: implications from the record of marine evaporates. Geochim Cosmochim Acta 66:3733–3756

Horvath B, Hofmann M, Pack A (2012) On the triple oxygen isotope composition of carbon dioxide from some combustion processes. Geochim Cosmochim Acta 95:160–168

Huang L, Sturchio NC, Abrajano T, Heraty LJ, Holt BD (1999) Carbon and chlorine isotope fractionation of chlorinated aliphatic hydrocarbons by evaporation. Org Geochem 30:777–785

Huang Y, Wang Y, Alexandre M, Lee T, Rose-Petruck C, Fuller M, Pizzarello S (2005) Molecular and compound-specific isotopic characterization of monocarboxylic acids in carbonaceous chondrites. Geochim Cosmochim Acta 69:1073–1084

Hudson JD (1977) Stable isotopes and limestone lithification. J Geol Soc London 133:637–660

Hulston JR (1977) Isotope work applied to geothermal systems at the Institute of Nuclear Sciences, New Zealand. Geothermics 5:89–96

Hulston JR, Thode HG (1965) Variations in the ^{33}S, ^{34}S and ^{36}S contents of meteorites and their relations to chemical and nuclear effects. J Geophys Res 70:3475–3484

Huntington KW, Wernicke BP, Eiler JM (2010) Influence of climate change and uplift on Colorado Plateau paleotemperatures from carbonate clumped isotope thermometry. Tectonics 29:TC3005. doi:101.1029/2009TC002449

Huntington KW, Budd DA, Wernicke BP, Eiler JM (2011) Use of clumped-isotope thermometry to constrain the crystallization temperature of diagenetic calcite. J Sediment Res 81:656–669

Iacumin P, Bocherens H, Marriotti A, Longinelli A (1996) Oxygen isotope analysis of coexisting carbonate and phosphate in biogenic apatite; a way to monitor diagenetic alteration of bone phosphate? Earth Planet Sci Lett 142:1–6

Ikehata K, Notsu K, Hirata T (2011) Copper isotope characteristics of copper-rich minerals from Besshi-type volcanogenic massive sulfide deposits, Japan, determined using a Femtosecond La-MC-ICP-MS. Econ Geol 106:307–316

Ionov DA, Hoefs J, Wedepohl KH, Wiechert U (1992) Contents and isotopic composition of sulfur in ultramafic xenoliths from Central Asia. Earth Planet Sci Lett 111:269–286

Irwin H, Curtis C, Coleman M (1977) Isotopic evidence for the source of diagenetic carbonate during burial of organic-rich sediments. Nature 269:209–213

Ishibashi J, Sano Y, Wakita H, Gamo T, Tsutsumi M, Sakai H (1995) Helium and carbon geochemistry of hydrothermal fluids from the Mid-Okinawa trough back arc basin, southwest of Japan. Chem Geology 123:1–15

Jaffrés JB, Shields GA, Wallmann K (2007) The oxygen isotope evolution of seawater: a critical review of a long-standing controversy and an improved geological water cycle model for the past 3.4 billion years. Earth Sci Rev 83:83–122

James DE (1981) The combined use of oxygen and radiogenic isotopes as indicators of crustal contamination. Ann Rev Earth Planet Sci 9:311–344

James AT (1983) Correlation of natural gas by use of carbon isotopic distribution between hydrocarbon components. Am Assoc Petrol Geol Bull 67:1167–1191

James AT (1990) Correlation of reservoired gases using the carbon isotopic compositions of wet gas components. Am Assoc Petrol Geol Bull 74:1441–1458

Jaouen K, Pons ML, Balter V (2013) Iron, copper and zinc isotopic fractionation up mammal trophic chains. Earth Planet Sci Lett (in press)

Jasper JP, Hayes JM (1990) A carbon isotope record of CO_2 levels during the late Quaternary. Nature 347:462–464

Jasper JP, Hayes JM, Mix AC, Prahl FG (1994) Photosynthetic fractionation of C-13 and concentrations of dissolved CO_2 in the central equatorial Pacific. Paleoceanography 9:781–798

Javoy M, Pineau F, Delorme H (1986) Carbon and nitrogen isotopes in the mantle. Chem Geology 57:41–62

Jeffcoate AB, Elliott T, Kasemann SA, Ionov D, Cooper K, Brooker R (2007) Li isotope fractionation in peridotites and mafic melts. Geochim Cosmochim Acta 71:202–218

Jeffrey AW, Pflaum RC, Brooks JM, Sackett WM (1983) Vertical trends in particulate organic carbon $^{13}C/^{12}C$ ratios in the upper water column. Deep Sea Res 30:971–983

Jenden PD, Kaplan IR, Poreda RJ, Craig H (1988) Origin of nitrogen-rich natural gases in the California Great Valley: evidence from helium, carbon and nitrogen isotope ratios. Geochim Cosmochim Acta 52:851–861

Jenden PD, Drazan DJ, Kapan IR (1993) Mixing of thermogenic natural gases in northern Appalachian Basin. Am Assoc Petrol Geol Bull 77:980–998

Jendrzejewski N, Eggenkamp HGM, Coleman ML (2001) Characterisation of chlorinated hydrocarbons from chlorine and carbon isotopic compositions: scope of application to environmental problems. Appl Geochem 16:1021–1031

Jenkyns HC (2010) Geochemistry of oceanic anoxic events. Geochem Geophys Geosys 11: Q03004

Jiang J, Clayton RN, Newton RC (1988) Fluids in granulite facies metamorphism: a comparative oxygen isotope study on the South India and Adirondack high grade terrains. J Geol 96:517–533

Joachimski M, van Geldern R, Breisig S, Buggisch W, Day J (2004) Oxygen isotope evolution of biogenic calcite and apatite during the Middle and Late Devonian. Int J Earth Sci 93:542–553

Joachimski M, Simon L, van Geldern R, Lecuyer C (2005) Boron isotope geochemistry of Paleozoic brachiopod calcite: implications for a secular change in the boron isotope geochemistry of seawater over the Phanerozoic. Geochim Cosmochim Acta 69:4035–4044

Joachimski MM, Breisig S, Buggisch W, Talent JA, Mawson R, Gereke M, Morrow JR, Day J, Weddige K (2009) Devonian climate and reef evolution: insights from oxygen isotopes in apatite. Earth Planet Sci Lett 284:599–609

Joachimski MM, Lai X, Shen S, Jiang H, Luo G, Chen J, Sun Y (2012) Climate warming in the latest Permian and the Permian-Triassic mass extinction. Geology 40:195–198

Johnsen SJ, Dansgaard W, White JW (1989) The origin of Arctic precipitation under present and glacial conditions. Tellus 41B:452–468

Johnsen SJ, Clausen HB, Dansgaard W, Gundestrup N, Hammer CU, Tauber H (1995) The Eem stable isotope record along the GRIP ice core and ist interpretation. Quat Res 43:117–124

Johnson DG, Jucks KW, Traub WA, Chance KV (2001) Isotopic composition of stratospheric water vapour: measurements and photochemistry. J Geophys Res 106D:12211–12217

Johnson CM, Skulan JL, Beard BL, Sun H, Nealson KH, Braterman PS (2002) Isotopic fraction between Fe(III) and Fe(II) in aqueous solutions. Earth Planet Sci Lett 195:141–153

Johnson CM, Beard BL, Beukes NJ, Klein C, O‘ Leary JM (2003) Ancient geochemical cycling in the Earth as inferred from Fe-isotope studies of banded iron formations from the Transvaal craton. Contr Mineral Petrol 114:523–547

Johnson CM, Beard BL, Roden EE (2008) The iron isotope fingerprints of redox and biogeochemical cycling in modern and ancient Earth. Ann Rev Earth Planet Sci 36:457–493

Jones HD, Kesler SE, Furman FC, Kyle JR (1996) Sulfur isotope geochemistry of southern Appalachian Mississippi Valley-type depopsits. Econ Geol 91:355–367

Jǿrgensen BB, Böttcher MA, Lüschen H, Neretin LN, Volkov II (2004) Anaerobic methane oxidation and a deep H_2S sink generate isotopically heavy sulfides in Black Sea sediments. Geochim Cosmochim Acta 68:2095–2118

Jouzel J, Merlivat L, Roth E (1975) Isotopic study of hail. J Geophys Res 80:5015–5030

Jouzel J, Merlivat L, Lorius C (1982) Deuterium excess in an East Antarctic ice core suggests higher relative humidity at the oceanic surface during the last glacial maximum. Nature 299:688–691

Jouzel J, Lorius C, Petit JR, Barkov NI, Kotlyakov VM, Petrow VM (1987) Vostok ice core: a continuous isotopic temperature record over the last climatic cycle (160000 years). Nature 329:403–408

Juranek LW, Quay PD (2010) Basin-wide photosynthetic production rates in the subtropical and tropical Pacific Ocean determined from dissolved oxygen isotope ratio measurements. Global Biogeochem Cycles 24:GB2006. doi:10.1029/2009GB003492

Kampschulte A, Strauss H (2004) The sulfur isotope evolution of Phanerozoic seawater based on the analyses of sructurally substituted sulfate in carbonates. Chem Geol 204:255–280

Kaplan IR (1975) Stable isotopes as a guide to biogeochemical processes. Proc R Soc London Ser B 189:183–211

Kaplan IR, Hulston JR (1966) The isotopic abundance and content of sulfur in meteorites. Geochim Cosmochim Acta 30:479–496

Kaplan IR, Rittenberg SC (1964) Microbiological fractionation of sulphur isotopes. J Gen Microbiol 34:195–212

Kasting JF, Howard MT, Wallmann K, Veizer J, Shields G, Jaffrés J (2006) Paleoclimates, ocean depth and the oxygen isotopic composition of the ocean. Earth Planet Sci Lett 252:82–93

Kaufman AJ, Knoll GM (1995) Neoproterozoic variations in the C-isotopic composition of seawater: stratigraphic and biogeochemical implications. Precambrian Res 73:27–49

Kaye J (1987) Mechanisms and observations for isotope fractionation of molecular species in planetary atmospheres. Rev Geophysics 25:1609–1658

Keeling CD (1958) The concentration and isotopic abundance of atmospheric carbon dioxide in rural areas. Geochim Cosmochim Acta 13:322–334

Keeling CD (1961) The concentration and isotopic abundances of carbon dioxide in rural and marine air. Geochim Cosmochim Acta 24:277–298

Keeling CD, Mook WG, Tans P (1979) Recent trends in the $^{13}C/^{12}C$ ratio of atmospheric carbon dioxide. Nature 277:121–123

Keeling CD, Carter AF, Mook WG (1984) Seasonal, latitudinal and secular variations in the abundance and isotopic ratio of atmospheric carbon dioxide. II. Results from oceanographic cruises in the tropical Pacific Ocean. J Geophys Res 89:4615–4628

Keeling CD, Bacastow RB, Carter AF, Piper SC, Whorf TR, Heimann M, Mook WG, Roeloffzen H (1989) A three dimensional model of atmospheric CO_2 transport based on observed winds. 1. Analysis of observational data. Geophys Monogr 55:165–236

Keeling CD, Whorf TP, Wahlen M, van der Plicht J (1995) Interannual extremes in the rate of rise of atmospheric carbon dioxide since 1980. Nature 375:666–670

Kelly WC, Rye RO, Livnat A (1986) Saline minewaters of the Keweenaw Peninsula, Northern Michigan: their nature, origin and relation to similar deep waters in Precambrian crystalline rocks of the Canadian Shield. Am J Sci 286:281–308

Kelly J, Fu B, Kita N, Valley J (2007) Optically continuous silcrete quartz cements in the St. Peter sandstone. Geochim Cosmochim Acta 71:3812–3832

Kelts K, McKenzie JA (1982) Diagenetic dolomite formation in quaternary anoxic diatomaceous muds of DSDP Leg 64, Gulf of California. Initial Rep DSDP 64:553–569

Kempton PD, Harmon RS (1992) Oxygen isotope evidence for large-scale hybridization of the lower crust during magmatic underplating. Geochim Cosmochim Acta 56:971–986

Kennicutt MC, Barker C, Brooks JM, De Freitaas DA, Zhu GH (1987) Selected organic matter indicators in the Orinoco, Nile and Changjiang deltas. Org Geochem 11:41–51

Keppler F, Hamilton JTG, Braß M, Röckmann (2006) Methane emissions from terrestrial plants under aerobic conditions. Nature 439:187–191

Kerrich R, Rehrig W (1987) Fluid motion associated with Tertiary mylonitization and detachment faulting: $^{18}O/^{16}O$ evidence from the Picacho metamorphic core complex, Arizona. Geology 15:58–62

Kerrich R, Latour TE, Willmore L (1984) Fluid participation in deep fault zones: evidence from geological, geochemical and to $^{18}O/^{16}O$ relations. J Geophys Res 89:4331–4343

Kerridge JF (1983) Isotopic composition of carbonaceous-chondrite kerogen: evidence for an interstellar origin of organic matter in meteorites. Earth Planet Sci Lett 64:186–200

Kerridge JF, Haymon RM, Kastner M (1983) Sulfur isotope systematics at the 21°N site, East Pacific Rise. Earth Planet Sci Lett 66:91–100

Kerridge JF, Chang S, Shipp R (1987) Isotopic characterization of kerogen-like material in the Murchison carbonaceous chondrite. Geochim Cosmochim Acta 51:2527–2540

Kharaka YK, Berry FAF, Friedman I (1974) Isotopic composition of oil-field brines from Kettleman North Dome, California and their geologic implications. Geochim Cosmochim Acta 37:1899–1908

Kharaka YK, Cole DR, Hovorka SD, Gunter WD, Knauss KG, Freifeld BM (2006) Gas-water-rock interactions in Frio formation following CO_2 injection: implications to the storage of greenhouse gases in sedimentary basins. Geology 34:577–580

Kiczka M, Wiederhold JG, Kraemer SM, Bourdon B, Kretzschmar R (2010) Iron isotope fractionation during Fe uptake and translocation in Alpine plants. Environ Sci Technol 44:6144–6150

Kim KR, Craig H (1990) Two isotope characterization of N_2O in the Pacific Ocean and constraints on its origin in deep water. Nature 347:58–61

Kim KR, Craig H (1993) Nitrogen-15 and oxygen-18 characteristics of nitrous oxide. Science 262:1855–1858

King PL, McLennan SM (2009) Sulfur on Mars. Elements 6:107–112

Kirkley MB, Gurney JJ, Otter ML, Hill SJ, Daniels LR (1991) The application of C-isotope measurements to the identification of the sources of C in diamonds. Appl Geochemistry 6:477–494

Kloppmann W, Girard JP, Négrel P (2002) Exotic stable isotope composition of saline waters and brines from the crystalline basement. Chem Geol 184:49–70

Knauth LP (1988) Origin and mixing history of brines, Palo Duro Basin, Texas, USA. Appl Geochem 3:455–474

Knauth LP, Beeunas MA (1986) Isotope geochemistry of fluid inclusions in Permian halite with implications for the isotopic history of ocean water and the origin of saline formation waters. Geochim Cosmochim Acta 50:419–433

Knauth LP, Lowe DR (1978) Oxygen isotope geochemistry of cherts from the Onverwacht group (3.4 billion years), Transvaal, South Africa, with implications for secular variations in the isotopic composition of chert. Earth Planet Sci Lett 41:209–222

Knoll AH, Hayes JM, Kaufman AJ, Swett K, Lambert IB (1986) Secular variation in carbon isotope ratios from Upper Proterozoic successions of Svalbard and East Greenland. Nature 321:832–838

Kohn MJ (1996) Predicting animal $\delta^{18}O$: accounting for diet and physiological adaptation. Geochim Cosmochim Acta 60:4811–4829

Kohn MJ (1999) Why most “dry” rocks should cool “wet”. Am Mineral 84:570–580

Kohn MJ, Cerling TE (2002) Stable isotope compositions of biological apatite. Rev Mineral Geochem 48:455–488

Kohn MJ, Valley JW (1994) Oxygen isotope constraints on metamorphic fluid flow, Townshend Dam, Vermont, USA. Geochim Cosmochim Acta 58:5551–5566

Kohn MJ, Valley JW, Elsenheimer D, Spicuzza M (1993) Oxygen isotope zoning in garnet and staurolite: evidence for closed system mineral growth during regional metamorphism. Am Mineral 78:988–1001

Kohn MJ, Riciputi LR, Stakes D, Orange DL (1998) Sulfur isotope variability in biogenic pyrite: reflections of heterogeneous bacterial colonzation? Am Mineral 83:1454–1486

Kolodny Y, Kerridge JF, Kaplan IR (1980) Deuterium in carbonaceous chondrites. Earth Planet Sci Lett 46:149–153

Kolodny Y, Luz B, Navon O (1983) Oxygen isotope variations in phosphate of biogenic apatites, I. Fish bone apatite—rechecking the rules of the game. Earth Planet Sci Lett 64:393–404

Kolodny Y, Luz B, Sander M, Clemens WA (1996) Dinosaur bones: fossils or pseudomorphs? The pitfalls of physiology reconstruction from apatitic fossils. Palaeo, Palaeo, Palaeoecol 126:161–171

Kool DM, Wrage N, Oenema O, Harris D, Van Groenigen JW (2009) The ^{18}O signature of biogenic nitrous oxide is determined by O exchange with water. Rapid Commun Mass Spectrom 23:104–108

Krankowsky D, Lämmerzahl P, Mauersberger K (2000) Isotopic measurements of stratospheric ozone. Geophys Res Lett 27:2593–2595

Krishnamurthy RV, Epstein S, Cronin JR, Pizzarello S, Yuen GU (1992) Isotopic and molecular analyses of hydrocarbons and monocarboxylic acids of the Murchison meteorite. Geochim Cosmochim Acta 56:4045–4058

Kroopnick P (1985) The distribution of ^{13}C of ΣCO2 in the world oceans. Deep Sea Res 32:57–84

Kroopnick P, Craig H (1972) Atmospheric oxygen: isotopic composition and solubility fractionation. Science 175:54–55

Kroopnick P, Weiss RF, Craig H (1972) Total CO_2, ^{13}C and dissolved oxygen-^{18}O at Geosecs II in the North Atlantic. Earth Planet Sci Lett 16:103–110

Krouse HR, Case JW (1983) Sulphur isotope abundances in the environment and their relation to long term sour gas flaring, near Valleyview, Alberta. Final report, Research Management Division, University Alberta RMD Rep 83/18

Krouse HR, Viau CA, Eliuk LS, Ueda A, Halas S (1988) Chemical and isotopic evidence of thermochemical sulfate reduction by light hydrocarbon gases in deep carbonate reservoirs. Nature 333:415–419

Kump LR (1989) Alternative modeling approaches to the geochemical cycles of carbon, sulfur and strontium isotopes. Am J Sci 289:390–410

Kump LR (2005) Ironing out biosphere oxidation. Science 307:1058–1059

Kump LR, Arthur MA (1999) Interpreting carbon-isotope excursions: carbonates and organic matter. Chem Geol 161:181–198

Kung CC, Clayton RN (1978) Nitrogen abundances and isotopic compositions in stony meteorites. Earth Planet Sci Lett 38:421–435

Kvenvolden KA (1995) A review of the geochemistry of methane in natural gas hydrate. Org Geochem 23:997–1008

Kyser TK, O'Neil JR (1984) Hydrogen isotope systematics of submarine basalts. Geochim Cosmochim Acta 48:2123–2134

Kyser TK, O'Neil JR, Carmichael ISE (1981) Oxygen isotope thermometry of basic lavas and mantle nodules. Contrib Mineral Petrol 77:11–23

Kyser TK, O'Neil JR, Carmichael ISE (1982) Genetic relations among basic lavas and mantle nodules. Contrib Mineral Petrol 81:88–102

Kyser TK, O' Neil JR, Carmichael ISE (1986) Reply to "Possible non-equilibrium oxygen isotope effects in mantle nodules, an alternative to the Kyser-O' Neil-Carmichael geothermometer. Contr Mineral Petrol 93:120–123

Labeyrie LD, Juillet A (1982) Oxygen isotope exchangeability of diatom valve silica; interpretation and consequences for paleoclimatic studies. Geochim Cosmochim Acta 46:967–975

Labeyrie LD, Duplessy JC, Blanc PL (1987) Deep water formation and temperature variations over the last 125000 years. Nature 327:477–482

Labidi J, Catigny P, Birck JL, Assayag N, Bourrand JJ (2012) Determination of multiple sulphur isotopes in glasses: a reappraisal of the MORB δ^{34}S. Chem Geol 334:189–198

Labidi J, Cartigny P, Moreira M (2013) Non-chondritic sulphur isotope composition of the terrestrial mantle. Nature 501:208–211

Labidi J, Cartigny P, Hamelin C, Moreira M, Dosso L (2014) Sulfur isotope budget (^{32}S, ^{33}S, ^{34}S, ^{36}S) in Pacific-Antarctic ridge basalts: a record of mantle source heterogeneity and hydrothermal sulfide assimilation. Geochim Cosmochim Acta 133:47–67

Lachniet MS (2009) Climatic and environmental controls on speleothem oxygen-isotope values. Quat Sci Rev 28:412–432

Land LS (1980) The isotopic and trace element geochemistry of dolomite: the state of the art. In: Concepts and models of dolomitization. Soc Econ Paleontol Min Spec Publ 28:87–110

Landais A, Barkan E, Luz B (2008) Record of δ^{18}O and ^{17}O excess in ice from Vostok, Antarctica during the last 150000 years. Geophys Res Lett 35:L02709

Lane GA, Dole M (1956) Fractionation of oxygen isotopes during respiration. Science 123:574–576

Lawrence JR (1989) The stable isotope geochemistry of deep-sea pore water. In: Handbook of environmental isotope geochemistry, vol 3. Elsevier Publ Co, pp 317–356

Lawrence JR, Gieskes JM (1981) Constraints on water transport and alteration in the oceanic crust from the isotopic composition of the pore water. J Geophys Res 86:7924–7934

Lawrence JR, Taviani M (1988) Extreme hydrogen, oxygen and carbon isotope anomalies in the pore waters and carbonates of the sediments and basalts from the Norwegian Sea: methane and hydrogen from the mantle? Geochim Cosmochim Acta 52:2077–2083

Lawrence JR, Taylor HP (1971) Deuterium and oxygen-18 correlation: clay minerals and hydroxides in quaternary soils compared to meteoric waters. Geochim Cosmochim Acta 35:993–1003

Lawrence JR, White JWC (1991) The elusive climate signal in the isotopic composition of precipitation. In: Stable isotope geochemistry: a tribute to Samuel Epstein. Special Publication, The Geochemical Society vol 3, pp 169–185

Laws EA, Popp BN, Bidigare RR, Kennicutt MC, Macko SA (1995) Dependence of phytoplankton carbon isotopic composition on growth rate and CO_{2aq}: theoretical considerations and experimental results. Geochim Cosmochim Acta 59:1131–1138

Leclerc AJ, Labeyrie LC (1987) Temperature dependence of oxygen isotopic fractionation between diatom silica and water. Earth Planet Sci Lett 84:69–74

Lécuyer C, Grandjean P, Reynard B, Albarede F, Telouk P (2002) ^{11}B/^{10}B analysis of geological materials by ICP-MS Plasma 54: application to bron fractionation between brachiopod calcite and seawater. Chem Geol 186:45–55

Leder JL, Swart PK, Szmant AM, Dodge RE (1996) The origin of variations in the isotopic record of scleractinian corals: I. Oxygen. Geochim Cosmochim Acta 60:2857–2870

Lemarchand D, Gaillardet J, Lewin E, Allegre CJ (2000) The influence of rivers on marine boron isotopes and implications for reconstructing past ocean pH. Nature 408:951–954

Lemarchand D, Gaillardet J, Lewin E, Allègre CJ (2002) Boron isotope systematics in large rivers: implications for the marine boron budget and paleo-pH reconstruction over the Cenozoic. Chem Geol 190:123–140

Leng MJ, Marshall JD (2004) Palaeoclimate interpretation of stable isotope data from lake sediment archives. Quaternary Sci Rev 23:811–831

Leshin LA, Epstein S, Stolper EM (1996) Hydrogen isotope geochemistry of SNC meteorites. Geochim Cosmochim Acta 60:2635–2650

Leshin LA, McKeegan KD, Carpenter PK, Harvey RP (1998) Oxygen isotopic constraints on the genesis of carbonates from Martian meteorite ALH 84001. Geochim Cosmochim Acta 62:3–13

Leuenberger M, Siegenthaler U, Langway CC (1992) Carbon isotope composition of atmospheric CO_2 during the last ice age from an Antarctic ice core. Nature 357:488–490

Lewan MD (1983) Effects of thermal maturation on stable carbon isotopes as determined by hydrous pyrolysis of Woodford shale. Geochim Cosmochim Acta 47:1471–1480

Lewis RS, Anders E, Wright IP, Norris SJ, Pillinger CT (1983) Isotopically anomalous nitrogen in primitive meteorites. Nature 305:767–771

Li W, Jackson SE, Pearson NJ, Graham S (2010a) Copper isotope zonation in the Northparkes porphyry Cu-Au deposit, SE Australia. Geochim Cosmochim Acta 74:4078–4096

Li W-Y, Teng F-Z, Ke S, Rudnick R, Gao S, Wu F-Y, Chappell B (2010b) Heterogeneous magnesium isotopic composition of the upper continental crust. Geochim Cosmochim Acta 74:6867–6884

Liotta M, Rizzo A, Paonita A, Caracausi A, Martelli M (2012) Sulfur isotopic compositions of fumarolic and plume gases at Mount Etna (Italy) and inferences on their magmatic source. Geochem Geophys Geosys 13(5). doi:1029/2012GC0042118

Lister GS, Kelts K, Chen KZ, Yu JQ, Niessen F (1991) Lake Qinghai, China: closed-basin lake levels and the oxygen isotope record for ostracoda since the latest Pleistocene. Palaeo, Palaeo, Palaeoecology 84:141–162

Liu Y, Spicuzza MJ, Craddock PR, Day JM, Valley JW, Dauphas N, Taylor LA (2010) Oxygen and iron isotope constraints on near-surface fractionation effects and the composition of lunar mare basalt source regions. Geochim Cosmochim Acta 74:6249–6262

Lloyd MR (1967) Oxygen-18 composition of oceanic sulfate. Science 156:1228–1231

Lloyd MR (1968) Oxygen isotope behavior in the sulfate-water system. J Geophys Res 73:6099–6110

Longinelli A (1966) Ratios of oxygen-18: oxygen-16 in phosphate and carbonate from living and fossil marine organisms. Nature 211:923–926

Longinelli A (1984) Oxygen isotopes in mammal bone phosphate: a new tool for paleohydrological and paleoclimatological research? Geochim Cosmochim Acta 48:385–390

Longinelli A, Bartelloni M (1978) Atmospheric pollution in Venice, Italy, as indicated by isotopic analyses. Water Air Soil Poll 10:335–341

Longinelli A, Craig H (1967) Oxygen-18 variations in sulfate ions in sea-water and saline lakes. Science 156:56–59

Longinelli A, Edmond JM (1983) Isotope geochemistry of the Amazon basin. A reconnaissance. J Geophys Res 88:3703–3717

Longinelli A, Nuti S (1973) Revised phosphate-water isotopic temperature scale. Earth Planet Sci Lett 19:373–376

Longstaffe FJ (1989) Stable isotopes as tracers in clastic diagenesis. In: Hutcheon IE (ed) Short course in burial diagenesis, Mineralogical Association of Canada short course series, vol 15, pp 201–277

Longstaffe FJ, Schwarcz HP (1977) $^{18}O/^{16}O$ of Archean clastic metasedimentary rocks: a petrogenetic indicator for Archean gneisses? Geochim Cosmochim Acta 41:1303–1312

Lorius C, Jouzel J, Ritz C, Merlivat L, Barkov NI, Korotkevich YS, Kotlyakov VM (1985) A 150000 year climatic record from Antarctic ice. Nature 316:591–596

Luck JM, Ben Othman D, Albarede F (2005) Zn and Cu isotopic variations in chondrites and iron meteorites: early solar nebula reservoirs and parent-body processes. Geochim Cosmochim Acta 69:5351–5363

Lücke A, Moschen R, Schleser G (2005) High-temperature carbon reduction of silica: a novel approach for oxygen isotope analysis of biogenic opal. Geochim Cosmochim Acta 69:1423–1433

Luz B, Barkan E (2000) Assessment of oceanic productivity with the triple-isotope composition of dissolved oxygen. Science 288:2028–2031

Luz B, Barkan E (2005) The isotopic ratios $^{17}O/^{16}O$ and $^{18}O/^{16}O$ in molecular oxygen and their significance in biogeochemistry. Geochim Cosmochim Acta 69:1099–1110

Luz B, Barkan E (2010) Variations of $^{17}O/^{16}O$ and $^{18}O/^{16}O$ in meteoric waters. Geochim Cosmochim Acta 74:6276–6286

Luz B, Kolodny Y (1985) Oxygen isotope variations in phosphate of biogenic apatites, IV: mammal teeth and bones. Earth Planet Sci Lett 75:29–36

Luz B, Kolodny Y, Horowitz M (1984) Fractionation of oxygen isotopes between mammalian bone-phosphate and environmental drinking water. Geochim Cosmochim Acta 48:1689–1693

Luz B, Cormie AB, Schwarcz HP (1990) Oxygen isotope variations in phosphate of deer bones. Geochim Cosmochim Acta 54:1723–1728

Luz B, Barkan E, Bender ML, Thiemens MH, Boering KA (1999) Triple-isotope composition of atmospheric oxygen as a tracer of biosphere productivity. Nature 400:547–550

Magna T, Wiechert U, Halliday AN (2006) New constraints on the lithium isotope composition of the Moon and terrestrial planets. Earth Planet Sci Lett 243:336–353

Mahaffy PR, Webster CR et al (2013) Abundance and isotopic composition of gases in the Martian atmosphere from the Curiosity Rover. Science 341:263–266

Maher K, Larson P (2007) Variation in copper isotope ratios and controls on fractionation in hypogene skarn mineralization at Coroccohuayco and Tintaya, Peru. Econ Geol 102:225–237

Mandeville CW, Webster JD, Tappen C, Taylor BE, Timbal A, Sasaki A, Hauri E, Bacon CR (2009) Stable isotope and petrologic evidence for open-system degassing during the climactic and pre-climactic eruptions of Mt. Mazama, Crater Lake, Oregon. Geochim Cosmochim Acta 73:2978–3012

Marin J, Chaussidon M, Robert F (2010) Microscale oxygen isotope variations in 1.9 Ga Gunflint cherts: assessments of diagenetic effects and implications for oceanic paleotemperature reconstructions. Geochim Cosmochim Acta 74:116–130

Marin-Carbonne J, Chaussidon M, Boiron MC, Robert F (2011) A combined in situ oxygen, silicon and fluid inclusion study of a chert sample from Onverwacht Group (3.35 Ga, South Africa): new constraints on fluid circulation. Chem Geol 286:59–71

Marin-Carbonne J, Chaussidon M, Robert F (2012) Micrometer-scale chemical and isotopic criteria (O and Si) on the origin and history of Precambrian cherts: implications for paleo-temperature reconstructions. Geochim Cosmochim Acta 92:129–147

Marin-Carbonne J et al (2014) CoupleFe and WS isotope variatiions in pyrite nodules from Archaen shale. Earth Planet Sci Lett 392:67–79

Markl G, Lahaye Y, Schwinn G (2006a) Copper isotopes as monitors of redox processes in hydrothermal mineralization. Geochim Cosmochim Acta 70:4215–4228

Markl G, von Blanckenburg F, Wagner T (2006b) Iron isotope fractionation during hydrothermal ore deposition and alteration. Geochim Cosmochim Acta 70:3011–3030

Marowsky G (1969) Schwefel-, Kohlenstoff-und Sauerstoffisotopenuntersuchungen am Kupferschiefer als Beitrag zur genetischen Deutung. Contrib Mineral Petrol 22:290–334

Martin E, Bindeman I (2009) Mass-independent isotopic signatures of volcanic sulfate from three supereuption ash deposits in Lake Tecopa, California. Earth Planet Sci Lett 282:102–114

Martinson DG, Pisias NG, Hays JD, Imbrie J, Moore TC, Shackleton NJ (1987) Age dating and the orbital theory of the ice ages: development of a high resolution 0 to 300000 year chronostratigraphy. Quat Res 27:1–29

Marty B (2012) The origins and concentrations of water, carbon, nitrogen and noble gases on Earth. Earth Planet Sci Lett 313–314:56–66

Marty B, Humbert F (1997) Nitrogen and argon isotopes in oceanic basalts. Earth Planet Sci Lett 152:101–112

Marty B, Zimmermann L (1999) Volatiles (He, C, N, Ar)in mid-ocean ridge basalts: assesment of shallow-level fractionation and characterization of source composition. Geochim Cosmochim Acta 63:3619–3633

Marty B, Chaussidon M, Wiens RC, Jurewicz Burnett DS (2011) A ^{15}N-poor isotopic composition for the solar system as shown by Genesis solar wind samples. Science 332:1533–1536

Mason TFD et al (2005) Zn and Cu isotopic variability in the Alexandrinka volcanic-hosted massive sulphide (VHMS) ore deposit, Urals, Russia. Chem Geol 221:170–187

Masson-Delmotte V, Jouzel J et al (2005) GRIP deuterium excess reveals rapid and orbital-scale changes in Greenland moisture origin. Science 309:118–121

Mastalerz M, Schimmelmann A (2002) Isotopically exchangeable organic hydrogen in coal relates to thermal maturity and maceral composition. Org Geochem 33:921–931

Matheney RK, Knauth LP (1989) Oxygen isotope fractionation between marine biogenic silica and seawater. Geochim Cosmochim Acta 53:3207–3214

Mathur R, Dendas M, Titley S, Phillips A (2010) Patterns in the copper isotope composition of minerals in porphyry copper deposits in southwestern United States. Econ Geol 105:1457–1467

Matsubaya O, Sakai H (1973) Oxygen and hydrogen isotopic study on the water of crystallization of gypsum from the Kuroko-type mineralization. Geochem J 7:153–165

Matsuhisa Y (1979) Oxygen isotopic compositions of volcanic rocks from the east Japan island arcs and their bearing on petrogenesis. J Volcanic Geotherm Res 5:271–296

Matsumoto R (1992) Causes of the oxygen isotopic depletion of interstitial waters from sites 798 and 799, Japan Sea, Leg 128. Proc Ocean Drill Program, Sci Results 127(128):697–703

Matsuo S, Friedman I, Smith GI (1972) Studies of quaternary saline lakes. I. Hydrogen isotope fractionation in saline minerals. Geochim Cosmochim Acta 36:427–435

Mattey DP, Carr RH, Wright IP, Pillinger CT (1984) Carbon isotopes in submarine basalts. Earth Planet Sci Lett 70:196–206

Mattey DP, Lowry D, MacPherson C (1994) Oxygen isotope composition of mantle peridotites. Earth Planet Sci Lett 128:231–241

Mauersberger K (1981) Measurement of heavy ozone in the stratosphere. Geophys Res Lett 8:935–937

Mauersberger K (1987) Ozone isotope measurements in the stratosphere. Geophys Res Letter 14:80–83

McCaig AM, Wickham SM, Taylor HP (1990) Deep fluid circulation in Alpine shear zones, Pyrenees, France: field and oxygen isotope studies. Contr Mineral Petrol 106:41–60

McClelland JW, Montoya JP (2002) Trophic relationships and the nitrogen isotope composition of amino acids in plankton. Ecology 83:2173–2180

McCollom TM, Seewald JS (2006) Carbon isotope composition of organic compounds produced by abiotic synthesis under hydrothermal conditions. Earth Planet Sci Lett 243:74–84

McConnaughey T (1989a) ^{13}C and ^{18}O disequilibrium in biological carbonates. II. In vitro simulation of kinetic isotope effects. Geochim Cosmochim Acta 53:163–171

McConnaughey T (1989b) °) ^{13}C and $^{18\circ}$ disequilibrium in biological carbonates.I. Patterns. Geochim Cosmochim Acta 53:151–162

McCorkle DC, Emerson SR (1988) The relationship between pore water isotopic composition and bottom water oxygen concentration. Geochim Cosmochim Acta 52:1169–1178

McCorkle DC, Emerson SR, Quay P (1985) Carbon isotopes in marine porewaters. Earth Planet Sci Lett 74:13–26

McCrea JM (1950) On the isotopic chemistry of carbonates and a paleotemperature scale. J Chem Phys 18:849–857

McDermott F (2004) Palaeo-climate reconstruction from stable isotope variations in speleothems: a review. Quaternary Sci Rev 23:901–918

McGarry S, Bar-Matthews M, Matthews A, Vaks A, Schilman B, Ayalon A (2004) Constraints on hydrological and paleotemperature variations in the eastern Mediterranean region in the last 140 ka given by the δD values of speleothem fluid inclusions. Quat Sci Rev 23:919–934

McGregor ID, Manton SR (1986) Roberts Victor eclogites: ancient oceanic crust. J Geophys Res 91:14063–14079

McInerney FA, Wing SL (2011) The Paleocene-Eocene thermal maximum: a perturbation of carbon cycle, climate and biosphere with implications for the future. Ann Rev Earth Planet Sci 39:489–516

McKay DS et al (1996) Search for past life on Mars: possible relic biogenic activity in martian meteorite ALH 84001. Science 273:924–930

McKeegan KD, Kallio AP, Heber VS et al (2011) The oxygen isotopic composition of the Sun inferred from captured solar wind. Science 332:1528–1532

McKenzie J (1984) Holocene dolomitization of calcium carbonate sediments from the coastal sabkhas of Abu Dhabi, U.A.E.: A stable isotope study. J Geol 89:185–198

McKibben MA, Riciputi LR (1998) Sulfur isotopes by ion microprobe. In: Applications of microanalytical techniques to understanding mineralizing processes. Rev Econ Geol 7:121–140

McLaughlin K, Chavez F, Pennington JT, Paytan A (2006) A time series investigation of the oxygen isotope composition of dissolved inorganic phosphate in Monterey Bay, California. Limnol Oceanogr 51:2370–2379

McSween HY, Taylor LA, Stolper EM (1979) Allan Hills 77005: a new meteorite type found in Antarctica. Science 204:1201–1203

Meier-Augustein W (2010) Stable isotope forensics. Wiley-Blackwell, Chichester

Mengel K, Hoefs J (1990) Li - $\delta^{18}O$ - SiO_2 systematics in volcanic rocks and mafic lower crustal xenoliths. Earth Planet Sci Lett 101:42–53

Merlivat L, Jouzel J (1979) Global climatic interpretation of the deuterium-oxygen 18 relationship for precipitation. J Geophys Res 84:5029–5033

Michalski G, Bhattacharya SK, Mase DF (2011) Oxygen isotope dynamics of atmospheric nitrate and its precursor molecules. In: Baskaran M (ed) Handbook of environmental isotope geochemistry, Springer, pp 613–635

Mikaloff-Fletcher SE et al (2006) Inverse estimates of anthropogenic CO_2 uptake, transport and storage by the ocean. Global Biogeochem Cycles 20:GB2002. doi:10/10292005GB002532

Milkov AV (2005) Molecular and stable isotope compositions of natural gas hydrates: a revised global dataset and basic interpretations in the context of geological settings. Org Geochem 36:681–702

Ming T, Anders E, Hoppe P, Zinner E (1989) Meteoritic silicon carbide and its stellar sources, implications for galactic chemical evolution. Nature 339:351–354

Minigawa M, Wada E (1984) Stepwise enrichments of ^{15}N along food chains: further evidence and the relation between $\delta^{15}N$ and animal age. Geochim Cosmochim Acta 48:1135–1140

Misra S, Froelich PN (2012) Lithium isotope history of Cenozoic seawater: changes in silicate weathering and reverse weathering. Science 335:818–823

Mix HT, Chamberlain CP (2014) Stable isotope records of hydrologic change and paleotemperature from smectite in Cenozoic western North America. Geochim Cosmochim Acta 141:532–546

Moldovanyi EP, Lohmann KC (1984) Isotopic and petrographic record of phreatic diagenesis: Lower Cretaceous Sligo and Cupido Formations. J Sediment Petrol 54:972–985

Monster J, Anders E, Thode HG (1965) $^{34}S/^{32}S$ ratios for the different forms of sulphur in the Orgueil meteorite and their mode of formation. Geochim Cosmochim Acta 29:773–779

Monster J, Appel PW, Thode HG, Schidlowski M, Carmichael CW, Bridgwater D (1979) Sulphur isotope studies in early Archean sediments from Isua, West Greenland: implications for the antiquity of bacterial sulfate reduction. Geochim Cosmochim Acta 43:405–413

Montoya JP, Horrigan SG, McCarthy JJ (1991) Rapid, storm-induced changes in the natural abundance of ^{15}N in a planktonic ecosystem, Chesapeake Bay, USA. Geochim Cosmochim Acta 55:3627–3638

Mook WG, Koopman M, Carter AF, Keeling CD (1983) Seasonal, latitudinal and secular variations in the abundance and isotopic ratios of atmospheric carbon dioxide. I. Results from land stations. J Geophys Res 88:10915–10933

Morin S, Savarino J, Frey MF, Yan N, Bekki S, Bottenheim JW, Martins JM (2008) Tracing the origin and fate of NO_x in the arctic atmosphere using stable isotopes in nitrate. Science 322:730–732

Moschen R, Lücke A, Parplies U, Radtke B, Schleser GH (2006) Transfer and early diagenesis of biogenic silica oxygen isotope signals during settling and sedimentation of diatoms in a temperate freshwater lake (Lake Holzmaar, Germany). Geochim Cosmochim Acta 70:4367–4379

Mossmann JR, Aplin AC, Curtis CD, Coleman ML (1991) Geochemistry of inorganic and organic sulfur in organic-rich sediments from the Peru Margin. Geochim Cosmochim Acta 55:3581–3595

Moynier F, Blichert-Toft J, Telouk P, Luck JM, Albarede F (2007) Comparative stable isotope geochemistry of Ni, Cu, Zn and Fe in chondrites and iron meteorites. Geochim Cosmochim Acta 71:4365–4379

Moynier F, Pichat S, Pons ML, Fike D, Balter V, Albarède F (2008) Isotope fractionation and transport mechanisms of Zn in plants. Chem Geol 267:125–130

Muehlenbachs K, Byerly G (1982) ^{18}O enrichment of silicic magmas caused by crystal fractionation at the Galapagos Spreading Center. Contr Mineral Petrol 79:76–79

Muehlenbachs K, Clayton RN (1972) Oxygen isotope studies of fresh and weathered submarine basalts. Can J Earth Sci 9:471–479

Muehlenbachs K, Clayton RN (1976) Oxygen isotope composition of the oceanic crust and its bearing on seawater. J Geophys Res 81:4365–4369

Mulitza S, Duerkoop A, Hale S, Wefer S, Niebler HS (1997) Planktonic foraminifera as recorders of past surface water stratification. Geology 25: 335–338

Nabelek PI (1991) Stable isotope monitors. In: Contact metamorphism. Rev Mineral 26:395–435

Nabelek PI, Labotka TC, O'Neil JR, Papike JJ (1984) Contrasting fluid/rock interaction between the Notch Peak granitic intrusion and argillites and limestones in western Utah: evidence from stable isotopes and phase assemblages. Contr Mineral Petrol 86:25–43

Neretin LN, Böttcher ME, Jǿrgensen BB, Volkov II, Lüschen H, Hilgenfeldt K (2004) Pyritization processes and greigite formation in the advancing sulfidization front in the Upper Pleistone sediments of the Black Sea. Geochim Cosmochim Acta 68:2081–2094

Nielsen H, Ricke W (1964) S-Isotopenverhaltnisse von Evaporiten aus Deutschland. Ein Beitrag zur Kenntnis von δ^{34}S im Meerwasser Sulfat. Geochim Cosmochim Acta 28:577–591

Niles PB, Leshin LA, Guan Y (2005) Microscale carbon isotope variability in ALH84001 carbonates and a discussion of possible formation environments. Geochim Cosmochim Acta 69:2931–2944

Nishio Y, Sasaki S, Gamo T, Hiyagon H, Sano Y (1998) Carbon and helium isotope systematics of North Fiji basin basalt glasses: carbon geochemical cycle in the subduction zone. Earth Planet Sci Lett 154:127–138

Norris RD, Röhl U (1999) Carbon cycling and chronology of climate warming during the Paleocene/Eocene transition. Nature 401:775–778

Norton D, Taylor HP (1979) Quantitative simulation of the hydrothermal systems of crystallizing magmas on the basis of transport theory and oxygen isotope data: an analysis of the Skaergaard intrusion. J Petrol 20:421–486

Nriagu JO, Coker RD, Barrie LA (1991) Origin of sulphur in Canadian Arctic haze from isotope measurements. Nature 349:142–145

O'Leary JA, Eiler JM, Rossman GR (2005) Hydrogen isotope geochemistry of nominally anhydrous minerals. Geochim Cosmochim Acta 69:A745

O'Neil JR, Roe LJ, Reinhard E, Blake RE (1994) A rapid and precise method of oxygen isotope analysis of biogenic phosphate. Israel J Earth Sci 43:203–212

Ohmoto H (1972) Systematics of sulfur and carbon isotopes in hydrothermal ore deposits. Econ Geol 67:551–578

Ohmoto H (1986) Stable isotope geochemistry of ore deposits. Rev Mineral 16:491–559

Ohmoto H, Goldhaber MB (1997) Sulfur and carbon isotopes. In: Barnes HL (ed) Geochemistry of hydrothermal ore deposits, 3rd edn. Wiley Interscience, New York, pp 435–486

Ohmoto H, Rye RO (1979) Isotopes of sulfur and carbon. In: Geochemistry of hydrothermal ore deposits, 2nd edn. Holt Rinehart and Winston, New York

Ohmoto H, Mizukani M, Drummond SE, Eldridge CS, Pisutha-Arnond V, Lenagh TC (1983) Chemical processes of Kuroko formation. Econ Geol Monogr 5:570–604

Ohmoto H, Kakegawa T, Lowe DR (1993) 3.4 billion year old biogenic pyrites from Barberton, South Africa: sulfur isotope evidence. Science 262:555

Ongley JS, Basu AR, Kyser TK (1987) Oxygen isotopes in coexisting garnets, clinopyroxenes and phlogopites of Roberts Victor eclogites: implications for petrogenesis and mantle metasomatism. Earth Planet Sci Lett 83:80–84

Ono S, Shanks WC, Rouxel OJ, Rumble D (2007) S-33 constraints on the seawater sulphate contribution in modern seafloor hydrothermal vent sulfides. Geochim Cosmochim Acta 71:1170–1182

Onuma N, Clayton RN, Mayeda TK (1970) Oxygen isotope fractionation between minerals and an estimate of the temperature of formation. Science 167:536–538

Ott U (1993) Interstellar grains in meteorites. Nature 364:25–33

Owen T, Maillard JP, DeBergh C, Lutz BL (1988) Deuterium on Mars: the abundance of HDO and the value of D/H. Science 240:1767–1770

Pack A, Gehler A, Süssenberger A (2013) Exploring the usability of isotopically anomaleous oxygen in bones and teeth as palaeo-CO_2-barometer. Geochim Cosmochim Acta 102:306–317

Pagani M, Arthur MA, Freeman KH (1999a) Miocene evolution of atmospheric carbon dioxide. Paleoceanography 14:273–292

Pagani M, Freeman KH, Arthur MA (1999b) Late Miocene atmospheric CO_2 concentrations and the expansion of C_4 grasses. Science 285:876–879

Page B, Bullen T, Mitchell M (2008) Influences of calcium availability and tree species on Ca isotope fractionation in soil and vegetation. Biogeochemistry 88:1–13

Palmer MR, Pearson PN, Conbb SJ (1998) Reconstructing past ocean pH-depth profiles. Science 282:1468–1471

Pawellek F, Veizer J (1994) Carbon cycle in the upper Danube and its tributaries: $\delta^{13}C_{DIC}$ constraints. Israel J Earth Sci 43:187–194

Payne JL, Kump LR (2007) Evidence for recurrent early triassic massive volcanism from quantitative interpretation of carbon isotope fluctuations. Earth Planet Sci Lett 256:264–277

Paytan A, Kastner M, Campbell D, Thiemens MH (1998) Sulfur isotope composition of Cenozoic seawater sulfate. Science 282:1459–1462

Paytan A, Luz B, Kolodny Y, Neori A (2002) Biologically mediated oxygen isotope exchange between water and phosphorus. Global Biogeochem Cycles 16–13:1–7

Paytan A, Kastner M, Campbell D, Thiemens M (2004) Seawater sulfur isotope fluctuations in the Cretaceous. Science 304:1663–1665

Pearson PN, Palmer MR (2000) Atmospheric carbon dioxide concentrations over the past 60 million years. Nature 406:695–699

Pearson PN, Foster GI, Wade BS (2009) Atmospheric carbon dioxide through the Eocene-Oligocene climate transition. Nature 461:1110–1113

Peckmann J, Thiel V (2005) Carbon cycling at ancient methane-seeps. Chem Geol 205:443–467

Pedentchouk N, Freeman KH, Harris NB (2006) Different response of δD-values of n-alkanes, isoprenoids and kerogen during thermal maturation. Geochim Cosmochim Acta 70:2063–2072

Perry EA, Gieskes JM, Lawrence JR (1976) Mg, Ca and $^{18}O/^{16}O$ exchange in the sediment-pore water system, Hole 149, DSDP. Geochim Cosmochim Acta 40:413–423

Peters MT, Wickham SM (1995) On the causes of ^{18}O depletion and ^{18}O/^{16}O homogenization during regional metamorphism, the east Humboldt Range core complex, Nevada. Contr Mineral Petrol 119:68–82

Peters KE, Rohrbach BG, Kaplan IR (1981) Carbon and hydrogen stable isotope variations in kerogen during laboratory-simulated thermal maturation. Am Assoc Petrol Geol Bull 65:501–508

Peterson BJ, Fry B (1987) Stable isotopes in ecosystem studies. Ann Rev Ecol Syst 18:293–320

Petit JR et al (1999a) Climate and atmospheric history of the past 420000 years from the Vostok ice core, Antarctica. Nature 399:429–436

Petit JR et al (1999b) Climate and atmospheric history of the past 420000 years from the Vostok ice core, Antarctica. Nature 399:429–436

Phillips FM, Bentley HW (1987) Isotopic fractionation during ion filtration: I. Theory. Geochim Cosmochim Acta 51:683–695

Philp RP (2007) The emergence of stable isotopes in environmental and forensic geochemistry studies: a review. Eviron Chem Lett 5:57–66

Pineau F, Javoy M (1983) Carbon isotopes and concentrations in mid-ocean ridge basalts. Earth Planet Sci Lett 62:239–257

Pineau F, Javoy M, Bottinga Y (1976) ^{13}C/^{12}C ratios of rocks and inclusions in popping rocks of the Mid-Atlantic Ridge and their bearing on the problem of isotopic composition of deep-seated carbon. Earth Planet Sci Lett 29:413–421

Poage MA, Chamberlain CP (2001) Empirical relationships between elevation and the stable isotope composition of precipitation and surface waters: considerations for studies of paleoelevation change. Am J Sci 301:1–15

Poitrasson F, Levasseur S, Teutsch N (2005) Significance of iron isotope mineral fractionation in pallasites and iron meteorites for the core-mantle differentiation of terrestrial planets. Earth Planet Sci Lett 234:151–164

Poitrasson F, Roskosz M, Corgne A (2009) No iron isotope fractionation between molten alloys and silicate melt to 2000°C and 7.7 GPa: experimental evidence and implications for planery differentiation and accretion. Earth Planet Sci Lett 278:376–385

Popp BN, Takigiku R, Hayes JM, Louda JW, Baker EW (1989) The post Paleozoic chronology and mechanism of ^{13}C depletion in primary organic matter. Am J Sci 289:436–454

Popp BN, Laws EA, Bidigare RR, Dore JE, Hanson KL, Wakeham SG (1998) Effect of phytoplankton cell geometry on carbon isotope fractionation. Geochim Cosmochim Acta 62:69–77

Popp BN et al (2002) Global Biogeochemical Cycles 16. doi:10.1029/2001GB001806

Poreda R (1985) Helium-3 and deuterium in back arc basalts: Lau Basin and the Mariana trough. Earth Planet Sci Lett 73:244–254

Poreda R, Schilling JG, Craig H (1986) Helium and hydrogen isotopes in ocean-ridge basalts north and south of Iceland. Earth Planet Sci Lett 78:1–17

Price FT, Shieh YN (1979) The distribution and isotopic composition of sulfur in coals from the Illinois Basin. Econ Geol 74:1445–1461

Prokoph A, Shields GA, Veizer J (2008) Compilation and time-series analysis of a marine carbonate δ^{18}O, δ^{13}C, ^{87}Sr/^{86}Sr and δ^{34}S database through Earth history. Earth Sci Rev 87:113–133

Prombo CA, Clayton RN (1985) A striking nitrogen isotope anomaly in the Bencubbin and Weatherford meteorites. Science 230:935–937

Puceat E, Joachimski MM et al (2010) Revised phosphate-water fractionation equation reassessing paleotemperatures derived from biogenic apatite. Earth Planet Sci Lett 298:135–142

Quade J et al (1992) A 16-Ma record of paleodiet using carbon and oxygen isotopes in fossil teeth from Pakistan. Chem Geol 94:183–192

Quade J, Cerling TE (1995) Expansion of C4 grasses in the late Miocene of northern Pakistan: evidence from stable isotopes in paleosols. Palaeo, Palaeo, Palaeo 115:91–116

Quade J, Breecker DO, Daeron M, Eiler J (2011) The paleoaltimetry of Tibet: an isotopic perspective. Am J Sci 311:77–115

Quast A, Hoefs J, Paul J (2006) Pedogenic carbonates as a proxy for palaeo-CO_2 in the Paleozoic atmosphere. Palaeo, Palaeo, Palaeo 242:110–125

Quay PD, Tilbrook B, Wong CS (1992) Oceanic uptake of fossil fuel CO_2: carbon-13 evidence. Science 256:74–79

Quay PD, Emerson S, Wilbur DO, Stump S (1993) The $\delta^{18}O$ of dissolved O_2 in the surface waters of the subarctic Pacific: a tracer of biological productivity. J Geophys Res 98:8447–8458

Quay PD, Wilbur DO, Richey JE, Devol AH, Benner R, Forsberg BR (1995) The $^{18}O/^{16}O$ of dissolved oxygen in rivers and lakes in the Amazon Basin: determining the ratio of respiration to photosynthesis in freshwaters. Limnol Oceanogr 40:718–729

Quay PD, Stutsman J, Wibur D, Snover A, Dlugokencky E, Brown T (1999) The isotopic composition of atmospheric methane. Global Geochemical Cycles 13:445–461

Raab M, Spiro B (1991) Sulfur isotopic variations during seawater evaporation with fractional crystallization. Chem Geol 86:323–333

Rabinovich AL, Grinenko VA (1979) Sulfate sulfur isotope ratios for USSR river water. Geochemistry 16(2):68–79

Radke J, Bechtel A, Gaupp R, Püttmann W, Schwark L, Sachse D, Gleixner D (2005) Correlation between hydrogen isotope ratios of lipid biomarkers and sediment maturity. Geochim Cosmochim Acta 69:5517–5530

Rahn T, Wahlen M (1997) Stable isotope enrichment in stratospheric nitrous oxide. Science 278:1776–1778

Rahn T et al (2002) The deuterium anomaly in stratospheric molecular hydrogen. Geochim Cosmochim Acta 66:A622 (special supplement)

Rai VK, Thiemens MH (2007) Mass independently fractionated sulphur components in chondrites. Geochim Cosmochim Acta 71:1341–1354

Rai VK, Jackson TL, Thiemens MH (2005) Photochemical mass-independent sulphur isotopes in achondritic meteorites. Science 309:1062–1065

Raiswell R, Berner RA (1985) Pyrite formation in euxinic and semi-euxinic sediments. Am J Sci 285:710–724

Raitzsch M, Hönisch B (2014) Cenozoic boron isotope variations in benthic foraminifera. Geology 41:591–594

Rau GH, Sweeney RE, Kaplan IR (1982) Plankton $^{13}C/^{12}C$ ratio changes with latitude: differences between northern and southern oceans. Deep Sea Res 29:1035–1039

Rau GH, Takahashi T, DesMarais DJ (1989) Latitudinal variations in plankton ^{13}C: implications for CO_2 and productivity in past ocean. Nature 341:516–518

Rau GH, Takahashi T, DesMarais DJ, Repeta DJ, Martin JH (1992) The relationship between $\delta^{13}C$ of organic matter and $\Sigma CO_2(aq)$ in ocean surface water: data from a JGOFS site in the northeast Atlantic Ocean and a model. Geochim Cosmochim Acta 56:1413–1419

Raven MR, Adkins JF, Werne JP, Lyons TW, Sessions AL (2015) Sulfur isotopic composition of individual organic compounds from Cariaco Basin sediments. Org Geochem (in press)

Redding CE, Schoell M, Monin JC, Durand B (1980) Hydrogen and carbon isotopic composition of coals and kerogen. In: Douglas AG, Maxwell JR (eds) Phys Chem Earth 12:711–723

Rees CE, Jenkins WJ, Monster J (1978) The sulphur isotopic composition of ocean water sulphate. Geochim Cosmochim Acta 42:377–381

Rice DD, Claypool GE (1981) Generation, accumulation and resource potential of biogenic gas. Am Assoc Petrol Geol Bull 65:5–25

Rice A, Dayalu A, Quay P, Gammon R (2011) Isotopic fractionation during soil uptake of atmospheric hydrogen. Biogeosciences 8:763–769

Richet P, Bottinga Y, Javoy M (1977) A review of H, C, N, O, S, and Cl stable isotope fractionation among gaseous molecules. Ann Rev Earth Planet Sci 5:65–110

Riciputi LR, Cole DR, Machel HG (1996) Sulfide formation in reservoir carbonates of the Devonian Nishu Formation, Alberta, Canada: an ion microprobe study. Geochim Cosmochim Acta 60:325–336

Rindsberger MS, Jaffe S, Rahamin S, Gat JR (1990) Patterns of the isotopic composition of precipitation in time and space; data from the Israeli storm water collection program. Tellus 42B:263–271

Ripley EM, Li C (2003) Sulfur isotope exchange and metal enrichment in the formation of magmatic Cu-Ni-(PGE)-deposits. Econ Geol 98:635–641

Robert F (2001) The origin of water on Earth. Science 293:1056–1058

Robert F, Epstein S (1982) The concentration and isotopic composition of hydrogen, carbon and nitrogen carbonaceous meteorites. Geochim Cosmochim Acta 46(8):1–95

Robert F, Merlivat L, Javoy M (1978) Water and deuterium content in ordinary chondrites. Meteoritics 12:349–354

Robert F, Gautier D, Dubrulle B (2000) The solar system D/H ratio: observations and theories. Space Sci Rev 92:201–224

Röckmann T et al (1998) Mass independent oxygen isotope fractionation in atmospheric CO as a result of the reaction CO + OH. Science 281:544–546

Röckmann T, Jöckel P, Gros V, Bräunlich M, Possnert G, Brenninkmeijer CAM (2002) Using ^{14}C, ^{13}C, ^{18}O and ^{17}O isotopic variations to provide insights into the high northern latitude surface CO inventory. Atmos Chem Phys 2:147–159

Röckmann T, Kaiser J, Brenninkmeijer CAM, Brand WA (2003) Gas chromatography/isotope ratio mass spectrometry method for high-precision position-dependent ^{15}N and ^{18}O measurements of atmospheric nitrous oxide. Rapid Commun Mass Spectrom 17:1897–1908

Röhl U, Norris RD, Bralower TJ, Wefer G (2000) New chronology for the late Paleocene thermal maximum and its environmental implications. Geology 28:927–930

Romanek CS et al (1994) Record of fluid-rock interaction on Mars from the meteorite ALH 84001. Nature 372:655–657

Rooney MA, Claypool GE, Chung HM (1995) Modeling thermogenic gas generation using carbon isotope ratios of natural gas hydrocarbons. Chem Geol 126:219–232

Rouxel O, Fouquet Y, Ludden JN (2004a) Copper isotope systematics of the Lucky Strike, Rainbow and Logatschev seafloor hydrothermal fields on the Mi-Atlantic Ridge. Econ Geol 99:585–600

Rouxel O, Fouquet Y, Ludden JN (2004b) Subsurface processes at the Lucky Strike hydrothermal field, Mid-Atlantic Ridge: evidence from sulfur, selenium and iron isotopes. Geochim Cosmochim Acta 68:2295–2311

Rouxel O, Bekker A, Edwards KJ (2005) Iron isotope constraints on the Archean and Proterozoic ocean redox state. Science 307:1088–1091

Rouxel O, Ono S, Alt J, Rumble D, Ludden J (2008a) Sulfur isotope evidence for microbial sulfate reduction in altered oceanic basalts at ODP Site 801. Earth Planet Sci Lett 268:110–123

Rouxel O, Shanks WC, Bach W, Edwards KJ (2008b) Integrated Fe- and S-isotope study of seafloor hydrothermal vents at East Pacific Rise 9-10°N.Chem Geol 252:214–227

Rozanski K, Sonntag C (1982) Vertical distribution of deuterium in atmospheric water vapour. Tellus 34:135–141

Rozanski K, Araguas-Araguas L, Gonfiantini R (1993) Isotopic patterns in modern global precipitation. In: Climate change in continental isotopic records. Geophys Monograph 78:1–36

Rumble D, Yui TF (1998) The Qinglongshan oxygen and hydrogen isotope anomaly near Donghai in Jiangsu Province, China. Geochim Cosmochim Acta 62:3307–3321

Rumble D, Young ED, Shahar A, Guo W (2011) Stable isotope cosmochemistry and the evolution of planetary systems. Elements 7:23–28

Russell AK, Kitajima K, Strickland A, Medaris LG, Schulze DJ, Valley JW (2013) Eclogite-facies fluid infiltration: constraints from δ^{18}O zoning in garnet. Contr Mineral Petrol 165:103–116

Rye RO (1993) The evolution of magmatic fluids in the epithermal environment: the stable isotope perspective. Econ Geol 88:733–753

Rye RO (2005) A review of stable isotope geochemistry of sulfate minerals in selected igneous environments and related hydrothermal systems. Chem Geol 215:5–36

Rye RO, Schuiling RD, Rye DM, Jansen JBH (1976) Carbon, hydrogen and oxygen isotope studies of the regional metamorphic complex at Naxos, Greece. Geochim Cosmochim Acta 40:1031–1049

Rye RO, Bethke PM, Wasserman MD (1992) The stable isotope geochemistry of acid sulfate. Econ Geol 87:227–262

Saal AE, Hauri EH, Van Orman JA, Rutherford MJ (2013) Hydrogen isotopes in lunar volcanic glasses and melt inclusions reveal a carbonaceous chondrite heritage. Science 340:1317–1320

Saccocia PJ, Seewald JS, Shanks WC (2009) Oxygen and hydrogen isotope fractionation in serpentine-water and talc-water systems from 250 to 450°C, 50 MPa. Geochim Cosmochim Acta 73:6789–6804

Sachse D, Billault I et al (2012) Molecular paleohydrology: interpreting the hydrogen-isotopic composition of lipid biomarkers from photosynthesizing organisms. Ann Rev Earth Planet Sci 40:221–249

Sackett WM (1988) Carbon and hydrogen isotope effects during the thermocatalytic production of hydrocarbons in laboratory simulation experiments. Geochim Cosmochim Acta 42:571–580

Sackett WM, Thompson RR (1963) Isotopic organic carbon composition of recent continental derived clastic sediments of Eastern Gulf Coast, Gulf of Mexico. Bull Am Assoc Petrol Geol 47:525

Sackett WM, Eadie BJ, Exner ME (1973) Stable isotope composition of organic carbon in recent Antarctic sediments. Adv Org Geochem 1973:661

Safarian AR, Nielsen SG, Marschall HR, McCubbin FM, Monteleone BD (2014) Early accretion of water in the inner solar system from a carbonaceous-like source. Science 346:623–626

Saino T, Hattori A (1980) ^{15}N natural abundance in oceanic suspended particulate organic matter. Nature 283:752–754

Saino T, Hattori A (1987) Geophysical variation of the water column distribution of suspended particulate organic nitrogen and its ^{15}N natural abundance in the Pacific and its marginal seas. Deep Sea Res 34:807–827

Sakai H (1968) Isotopic properties of sulfur compounds in hydrothermal processes. Geochem J 2:29–49

Sakai H, Casadevall TJ, Moore JG (1982) Chemistry and isotope ratios of sulfur in basalts and volcanic gases at Kilauea volcano, Hawaii. Geochim Cosmochim Acta 46:729–738

Sakai H, DesMarais DJ, Ueda A, Moore JG (1984) Concentrations and isotope ratios of carbon, nitrogen and sulfur in ocean-floor basalts. Geochim Cosmochim Acta 48:2433–2441

Sano Y, Marty B (1995) Origin of carbon in fumarolic gas from island arcs. Chem Geol 119:265–274

Sarntheim M et al (2001) Fundamental modes and abrupt changes in North Atlantic circulation and climate over the last 60 ky—concepts, reconstruction and numerical modeling. In: Schäfer P, Ritzau W, Schlüter M, Thiede J (eds) The northern North Atlantic, Springer Verlag, Heidelberg, pp 365–410

Sass E, Kolodny Y (1972) Stable isotopes, chemistry and petrology of carbonate concretions (Mishash formation, Israel). Chem Geol 10:261–286

Savage PS, Georg RB, Williams HM, Turner S, Halliday AN, Chappell BW (2012) The silicon isotope composition of granites. Geochim Cosmochim Acta 92:184–202

Savin SM, Epstein S (1970a) The oxygen and hydrogen isotope geochemistry of clay minerals. Geochim Cosmochim Acta 34:25–42

Savin SM, Epstein S (1970b) The oxygen and hydrogen isotope geochemistry of ocean sediments and shales. Geochim Cosmochim Acta 34:43–63

Savin SM, Lee M (1988) Isotopic studies of phyllosilicates. Rev Mineral 19:189–223

Schauble EA (2004) Applying stable isotope fractionation theory to new systems. Rev Mineral Geochem 55: 65-111

Schiegl WE, Vogel JV (1970) Deuterium content of organic matter. Earth Planet Sci Lett 7: 307–313

Schimmelmann A, Lewan MD, Wintsch RP (1999) D/H ratios of kerogen, bitumen, oil and water in hydrous pyrolysis of source rocks containing kerogen types I, II, IIS and III. Geochim Cosmochim Acta 63: 3751–3766

Schimmelmann A, Sessions AL, Mastalerz M (2006) Hydrogen isotopic (D/H) composition of organic matter during diagenesis and thermal maturation. Ann.Rev Earth Planet Sci 34: 501–533

Schmidt M, Botz R, Rickert D, Bohrmann G, Hall SR, Mann S (2001) Oxygen isotopes of marine diatoms and relations to opal-A maturation. Geochim Cosmochim Acta 65: 201–211

Schmidt TC, Zwank L, Elsner M, Berg M, Meckenstock RU, Haderlein SB (2004) Compound-specific stable isotope analysis of organic contaminants in natural environments: a critical review of the state of the art, prospects and future challenges. Anal Bioanal Chem 378:283–300

Schmitt J, Schneider R et al (2012) Carbon isotope constraints on the deglacial CO_2 rise from ice cores. Science 336:711–714

Schmitt AD, Stille P, Vennemann T (2003) Variations of the $^{44}Ca/^{40}Ca$ ratio in seawater during the past 24 million years: evidence from $\delta^{44}Ca$ and $\delta^{18}O$ values of Miocene phosphates. Geochim Cosmochim Acta 67:2607–2614

Schoell M (1980) The hydrogen and carbon isotopic composition of methane from natural gases of various origins. Geochim Cosmochim Acta 44:649–661

Schoell M (1983) Genetic characterization of natural gases. Bull Am Assoc Petrol Geol 67:2225–2238

Schoell M (1984) Recent advances in petroleum isotope geochemistry. Org Geochem 6:645–663

Schoell M (1988) Multiple origins of methane in the Earth. Chem Geol 71:1–10

Schoell M, McCaffrey MA, Fago FJ, Moldovan JM (1992) Carbon isotope compositions of 28,30-bisnorhopanes and other biological markers in a Monterey crude oil. Geochim Cosmochim Acta 56:1391–1399

Schoell M, Schouten S, Sinninghe Damste JS, de Leeuw JW, Summons RE (1994) A molecular organic carbon isotope record of Miocene climatic changes. Science 263:1122–1125

Schoenberg R, von Blanckenburg F (2006) Modes of planetary-scale Fe isotope fractionation. Earth Planet Sci Lett 252:342–359

Schoeninger MJ, DeNiro MJ (1984) Nitrogen and carbon isotopic composition of bone collagen from marine and terrestrial animals. Geochim Cosmochim Acta 48:625–639

Schrag DP (1999) Effects of diagenesis on the isotopic record of late Paleogene tropical sea surface temperature. Chem Geol 161:2265–2278

Schrag DP, Hampt G, Murry DW (1996) Pore fluid constraints on the temperature and oxygen isotopic composition of the Glacial ocean. Science 272:1930–1932

Schwalb A, Burns SJ, Kelts k (1999) Holocene environments from stable isotope stratigraphy of ostracods and authigenic carbonate in Chilean Altiplano lakes. Palaeo, Palaeo, Palaeo 148:153–168

Schwarcz HP, Melbye J, Katzenberg MA, Knyf M (1985) Stable isotopes in human skeletons of southern Ontario: reconstruction of palaeodiet. J Archaeol Sci 12:187–206

Seal RR (2006) Sulfur isotope geochemistry of sulfide minerals. Rev Mineral Geochem 61: 633–677

Seccombe PK, Spry PG, Ra Both, Jones MT, Schiller JC (1985) Base metal mineralization in the Kaumantoo Group, South Australia: a regional sulfur isotope study. Econ Geol 80:1824–1841

Seitz HM, Brey GP, Lahaye Y, Durali S, Weyer S (2004) Lithium isotope signatures of peridotite xenoliths and isotope fractionation at high temperature between olivine and pyroxene. Chem Geol 212:163–177

Sessions AL, Sylva SP, Summons RE, Hayes JM (2004) Isotopic exchange of carbon-bound hydrogen over geologic time scales. Geochim Cosmochim Acta 68:1545–1559

Severinghaus JP, Brook EJ (1999) Abrupt climate change at the end of the last glacial period inferred from trapped air in polar ice. Science 286:930–934

Severinghaus JP, Bender ML, Keeling RF, Broecker WS (1996) Fractionation of soil gases by diffusion of water vapor, gravitational settling and thermal diffusion. Geochim Cosmochim Acta 60:1005–1018

Severinghaus JP, Sowers T, Brook EJ, Alley RB, Bender ML (1998) Timing of abrupt climate change at the end of the Younger Dryas interval from thermally fractionated gases in polar ice. Nature 391:141–146

Severinghaus JP, Beaudette R, Headly MA, Taylor K, Brook EJ (2009) Oxygen-18 of O_2 records the impact of abrupt climate change on terrestrial biosphere. Science 324:1431–1434

Severmann S, Johnson CM, Beard BL, German CR, Edmonds HN, Chiba H, Green DRH (2004) The effect of plume processes on the Fe isotope composition of hydrothermally derived Fe in the deep ocean as inferred from the Rainbow vent site, Mid-Atlantic Ridge, 36° !4 N. Earth Planet Sci Lett 225:63–76

Severmann S, Johnson CM, Beard BL, McManus J (2006) The effect of early diagenesis on the Fe isotope composition of porewaters and authigenic minerals in continental margin sediments. Geochim Cosmochim Acta 70:2006–2022

Shackleton NJ, Kennett JP (1975) Paleotemperature history of the Cenozoic and initiation of Antarctic glaciation: oxygen and carbon isotope analyses in DSDP sites 277, 279 and 281. Initial Rep DSDP 29:743–755

Shackleton NJ, Hall MA, Line J, Cang S (1983) Carbon isotope data in core V19-30 confirm reduced carbon dioxide concentration in the ice age atmosphere. Nature 306:319–322

Shahar A, Young ED (2007) Astrophysics of CAI formation as revealed by silicon isotope LA-MC-ICPMS of an igneous CAI. Earth Planet Sci Lett 257:497–510

Shahar A, Ziegler K, Young ED, Ricollaeu A, Schauble E, Fei Y (2009) Experimentally determined Si isotope fractionation between silcate and Fe metal and implications for the Earth's core formation. Earth Planet Sci Lett 288:228–234

Shahar A, Hillgren VJ, Young ED, Fei Y, Macris CA, Deng L (2011) High-temperature Si isotope fractionation between iron metal and silicate. Geochim Cosmochim Acta 75:7688–7697

Shahar A, Hillgren VJ, Horan MF, Mesa-Garcia J, Kaufman LA, Mock TD (2014) Sulfur-controlled iron isotope fractionation experiments of core formation in planetary bodies. Geochim Cosmochim Acta (in press)

Shanks WC (2001) Stable isotopes in seafloor hydrothermal systems: vent fluids, hydrothermal deposits, hydrothermal alteration, and microbial processes. Rev Mineral Geochem 43:469–525

Sharp ZD (1995) Oxygen isotope geochemistry of the Al_2SiO_5 polymorphs. Am J Sci 295:1058–1076

Sharp ZD, Shearer CK, McKeegan KD, Barnes JD, Wang YQ (2010) The chlorine isotope composition of the Moon and implications for an anhydrous mantle. Science 329:10501053

Shaw AM, Hilton DR, Fischer TP, Walker JA, Alvarado GE (2003) Contrasting He-C relationshipsin Nicaragua and Costa Rica: insights into C cycling through subduction zones. Earth Planet Sci Lett 214:499–513

Shaw AM, Hauri EH, Fischer TP, Hilton DR, Kelley KA (2008) Hydrogen isotopes in Mariana arc melt inclusions: implications for subduction dehydration and the deep-earth water cycle. Earth Planet Sci Lett 275:138–145

Shelton KL, Rye DM (1982) Sulfur isotopic compositions of ores from Mines Gaspe, Quebec: An example of sulfate-sulfide isotopic disequilibria in ore forming fluids with applications to other porphyry type deposits. Econ Geol 77:1688–1709

Shemesh A, Kolodny Y, Luz B (1983) Oxygen isotope variations in phosphate of biogenic apatites, II. Phosphorite rocks. Earth Planet Sci Lett 64:405–441

Shen Y, Buick R (2004) The antiquity of microbial sulfate reduction. Earth Sci Rev 64:243–272

Sheppard SMF (1986) Characterization and isotopic variations in natural waters. In: Stable isotopes in high temperature geological processes. Rev Mineral 16:165–183

Sheppard SMF, Epstein S (1970) D/H and O^{18}/O^{16} ratios of minerals of possible mantle or lower crustal origin. Earth Planet Sci Lett 9:232–239

Sheppard SMF, Gilg HA (1996) Stable isotope geochemistry of clay minerals. Clay Mineral 31:1–24

Sheppard SMF, Harris C (1985) Hydrogen and oxygen isotope geochemistry of Ascension Island lavas and granites: variation with crystal fractionation and interaction with sea water. Contrib Mineral Petrol 91:74–81

Sheppard SMF, Schwarcz HP (1970) Fractionation of carbon and oxygen isotopes and magnesium between coexisting metamorphic calcite and dolomite. Contr Mineral Petrol 26:161–198

Sheppard SMF, Nielsen RL, Taylor HP (1971) Hydrogen and oxygen isotope ratios in minerals from Porphyry Copper deposits. Econ Geol 66:515–542

Sherwood Lollar B, Frape SK, Weise SM, Fritz P, Macko SA, Welhan JA (1993) Abiogenic methanogenesis in crystalline rocks. Geochim Cosmochim Acta 57:5087–5097

Sherwood Lollar B, Westgate TD, Ward JA, Slater GF, Lacrampe-Couloume G (2002) Abiogenic formation of alkanes in the Earth's crust as a minor source for global hydrocarbons reservoirs. Nature 416:522–524

Sherwood Lollar B et al (2006) Unravelling abiogenic and biogenic sources of methane in the earth,s deep subsurface. Chem Geol 226:328–339

Shieh YN, Schwarcz HP (1974) Oxygen isotope studies of granite and migmatite, Grenville province of Ontario, Canada. Geochim Cosmochim Acta 38:21–45

Shields G, Veizer J (2002) Precambrian marine carbonate isotope database: version 1.1. Geochem Geophys Geosyst 300. doi:10.1029/2001GC000266

Shirey et al (2013) RIMG

Shmulovich KI, Landwehr D, Simon K, Heinrich W (1999) Stable isotope fractionation between liquid and vapour in water-salt systems up to 600 °C. Chem Geol 157:343–354

Simon K (2001) Does δD from fluid inclusions in quartz reflect the original hydrothermal fluid? Chem Geol 177:483–495

Simon JI, dePaolo DJ (2010) Stable calcium isotopic composition of meteorites and rocky planets. Earth Planet Sci Lett 289:457–466

Simon L, Lecuyer C, Marechal C, Coltice N (2006) Modelling the geochemical cycle of boron: implications for the long-term $d^{11}B$ evolution of seawater and oceanic crust. Chem Geol 225:61–76

Skauli H, Boyce AJ, Fallick AE (1992) A sulphur isotope study of the Bleikvassli Zn-Pb-Cu deposit, Nordland, northern Norway. Mineral Deposita 27:284–292

Skirrow R, Coleman ML (1982) Origin of sulfur and geothermometry of hydrothermal sulfides from the Galapagos Rift, 86°W. Nature 249:142–144

Smith JW, Batts BD (1974) The distribution and isotopic composition of sulfur in coal. Geochim Cosmochim Acta 38:121–123

Smith JW, Gould KW, Rigby D (1982) The stable isotope geochemistry of Australian coals. Org Geochem 3:111–131

Snyder G, Poreda R, Hunt A, Fehn U (2001) Regional variations in volatile composition: isotopic evidence for carbonate recycling in the Central American volcanic arc. Geochem Geophys Geosystems 2:U1–U32

Sofer Z (1984) Stable carbon isotope compositions of crude oils: application to source depositional environments and petroleum alteration. Am Assoc Petrol Geol Bull 68:31–49

Sofer Z, Gat JR (1972) Activities and concentrations of oxygen-18 in concentrated aqueous salt solutions: analytical and geophysical implications. Earth Planet Sci Lett 15:232–238

Sonnerup RE, Quay PD, McNichol AP, BullisterJL Westby TA, Anderson HL (1999) Reconstructing the oceanic ^{13}C Suess effect. Global Biogeochem Cycles 13:857–872

Sowers T (2001) The N_2O record spanning the penultimate deglaciation from the Vostok ice core. J Geophys Res 106:31903–31914

Sowers T, Bender M, Raynaud D, Korotkevich YS, Orchardo J (1991) The $\delta^{18}O$ of atmospheric O_2 from air inclusions in the Vostok ice core: timing of CO_2 and ice volume changes during the Penultimate deglaciation. Paleoceanography 6:679–696

Sowers T, Bender M, Raynaud D, Korotkevich YS (1992) $\delta^{15}N$ of N_2 in air trapped in polar ice: a tracer of gas transport in the firn and a possible constraint on ice age-gas age differences. J Geophys Res 97:15683–15697

Sowers T et al (1993) A 135000 year Vostock-SPECMAP common temporal framework. Paleoceanography 8:737–766

Spero HJ, Bijma J, Lea DW, Bemis BE (1997) Effect of seawater carbonate concentration on foraminiferal carbon and oxygen isotopes. Nature 390:497–500

Spicuzza M, Day J, Taylor L, Valley JW (2007) Oxygen isotope constraints on the origin and differentiation of the Moon. Earth Planet Sci Lett 253:254–265

Spivack AJ, Edmond JM (1987) Boron isotope exchange between seawater and the oceanic crust. Geochim Cosmochim Acta 51:1033–1043

Stachel T, Harris JW, Muehlenbachs K (2009) Sources of carbon in inclusion bearing diamonds. Lithos 112S:625–637

Stahl W (1977) Carbon and nitrogen isotopes in hydrocarbon research and exploration. Chem Geol 20:121–149

Steele RC, Elliott T, Coath CD, Regelous M (2011) Confirmation of mass-independent Ni isotopic variability in iron meteorites. Geochim Cosmochim Acta 75:7906–7925

Steinhoefel G, Horn I, von Blanckenburg F (2009) Micro-scale tracing of Fe and Si isotope signatues in banded iron formation using femtosecond laser ablation. Geochim Cosmochim Acta 73:5343–5360

Steinhoefel G, von Blanckenburg F, Horn I, Konhauser KO, Beukes NJ, Gutzmer J (2010) Deciphering formation processes of banded iron formations from the Transvaal and Hamersley successions by combined Si and Fe isotope analysis using UV femtosecond laser ablation. Geochim Cosmochim Acta 74:2677–2696

Stern LA, Chamberlain CP, Reynolds RC, Johnson GD (1997) Oxygen isotope evidence of climate change from pedogenic clay minerals in the Himalayan molasse. Geochim Cosmochim Acta 61:731–744

Sternberg LS, Anderson WT, Morrison K (2002) Separating soil and leaf water ^{18}O isotope signals in plant stem cellulose. Geochim Cosmochim Acta 67:2561–2566

Steuber T, Buhl D (2006) Calcium-isotope fractionation in selected modern and ancient marine carbonates. Geochim Cosmochim Acta 70:5507–5521

Stevens CM (1988) Atmospheric methane. Chem Geol 71:11–21

Stevens CM, Krout L, Walling D, Venters A, Engelkemeier A, Ross LE (1972) The isotopic composition of atmospheric carbon monoxide. Earth Planet Sci Lett 16:1457–165

Stewart MK (1974) Hydrogen and oxygen isotope fractionation during crystallization of mirabilite and ice. Geochim Cosmochim Acta 38:167–172

Stolper DA, Sessions AL, Ferreira AA, Santos Neto EV, Schimmelmann A, Shusta SS, Valentine DL, Eiler JM (2014) Combined ^{13}C-D and D-D clumping in methane: methods and preliminary results. Geochim Cosmochim Acta 126:169–191

Strauß H (1997) The isotopic composition of sedimentary sulfur through time. Palaeo, Palaeo, Palaeo 132:97–118

Strauß H (1999) Geological evolution from isotope proxy signals—sulfur. Chem Geol 161:89–101

Strauß H, Peters-Kottig W (2003) The Phanerozoic carbon cycle revisited: the carbon isotope composition of terrestrial organic matter. Geochem Geophys Geosys 4:1083. doc:10.1029/2003GC000555

Stueber AM, Walter LM (1991) Origin and chemical evolution of formation waters from Silurian—Devonian strata in the Illinois basin. Geochim Cosmochim Acta 55:309–325

Styrt MM, Brackmann AJ, Holland HD, Clark BC, Pisutha-Arnold U, Eldridge CS, Ohmoto H (1981) The mineralogy and the isotopic composition of sulfur in hydrothermal sulfide/sulfate deposits on the East Pacific Rise, 21°N latitude. Earth Planet Sci Lett 53:382–390

Sugawara S, Nakazawa T, Shirakawa Y, Kawamura K, Aoki S, Machida T, Honda H (1998) Vertical profile of the carbon isotope ratio of stratospheric methane over Japan. Geophys Res Lett 24:2989–2992

Summons RE, Jahnke LL, Roksandic Z (1994) Carbon isotopic fractionation in lipids from methanotrophic bacteria: relevance for interpretation of the geochemical record of biomarkers. Geochim Cosmochim Acta 58:2853–2863

Sweeney RE, Kaplan IR (1980) Natural abundance of ^{15}N as a source indicator for near-shore marine sedimentary and dissolved nitrogen. Mar Chem 9:81–94

Sweeney RE, Liu KK, Kaplan IR (1978) Oceanic nitrogen isotopes and their use in determining the source of sedimentary nitrogen. In: Robinson BW (ed) DSIR Bull 220:9–26

Talbot MR (1990) A review of the palaeohydrological interpretation of carbon and oxygen isotopic ratios in primary lacustrine carbonates. Chem Geol 80:261–279

Tanaka R, Nakamura E (2005) Boron isotopic constraints on the source of Hawaiian shield lavas. Geochim Cosmochim Acta 69:3385–3399

Tang Y, Perry JK, Jenden PD, Schoell M (2000) Mathematical modeling of stable carbon isotope ratios in natural gases. Geochim Cosmochim Acta 64:2673–2687

Tang Y, Huang Y, Ellis GS, Wang Y, Kralert PG, Gillaizeau B, Ma Q, Hwang R (2005) A kinetic model for thermally induced hydrogen and carbon isotope fractionation of individual n-alkanes in crude oil. Geochim Cosmochim Acta 69:4505–4520

Taran YA, Kliger GA, Sevastianov VS (2007) Carbon isotope effect in the open system Fischer Trosch synthesis. Geochim Cosmochim Acta 71:4474–4487

Taylor HP (1968) The oxygen isotope geochemistry of igneous rocks. Contr Mineral Petrol 19:1–71

Taylor HP (1974) The application of oxygen and hydrogen isotope studies to problems of hydrothermal alteration and ore deposition. Econ Geol 69:843–883

Taylor HP (1977) Water/rock interactions and the origin of H_2O in granite batholiths. J Geol Soc 133:509

Taylor HP (1978) Oxygen and hydrogen isotope studies of plutonic granitic rocks. Earth Planet Sci Lett 38:177–210

Taylor HP (1980) The effects of assimilation of country rocks by magmas on $^{18}O/^{16}O$ and $^{87}Sr/^{86}Sr$ systematics in igneous rocks. Earth Planet Sci Lett 47:243–254

Taylor HP (1986a) Igneous rocks: II. Isotopic case studies of circumpacific magmatism. In: Stable isotopes in high temperature geological processes. Review in Mineralogy, vol 16. pp 273–317

Taylor BE (1986b) Magmatic volatiles: isotopic variation of C, H and S. Rev Mineral 16:185–225

Taylor BE (1987a) Stable isotope geochemistry of ore-forming fluids. In: Stable isotope geochemistry of low-temperature fluids. Short Course Mineralogical Association Canada, vol 13, pp 337–445

Taylor HP (1987b) Comparison of hydrothermal systems in layered gabbros and granites, and the origin of low-$\delta^{18}O$ magmas. In: Magmatic processes: physicochemical principles. The Geochemical Society Special Publication, vol 1. pp 337–357

Taylor HP (1988) Oxygen, hydrogen and strontium isotope constraints on the origin of granites. Trans Royal Soc Edinburgh: Earth Sci 79:317–338

Taylor HP (1997) Oxygen and hydrogen isotope relationships in hydrothermal mineral deposits. In: Barnes HL (ed) Geochemistry of hydrothermal ore deposits, 3rd edn. Wiley-Interscience p, New York, pp 229–302

Taylor BE, Bucher-Nurminen K (1986) Oxygen and carbon isotope and cation geochemistry of metasomatic carbonates and fluids - Bergell aureole, Northern Italy. Geochim Cosmochim Acta 50:1267–1279

Taylor HP, Forester RW (1979) An oxygen and hydrogen isotope study of the Skaergaard intrusion and its country rocks: a description of a 55 M.Y. old fossil hydrothermal system. J Petrol 20:355–419

Taylor BE, O'Neil JR (1977) Stable isotope studies of metasomatic Ca-Fe-Al-Si skarns and associated metamorphic and igneous rocks, Osgood Mountains, Nevada. Contr Mineral Petrol 63:1–49

Taylor HP, Sheppard SMF (1986b) Igneous rocks: I.Processes of isotopic fractionation and isotope systematics. In: Stable isotopes in high temperature geological processes. Review in Mineralogy, vol 16. pp 227–271

Taylor BE, Wheeler MC (1994) Sulfur- and oxygen isotope geochemistry of acid mine drainage in the Western United States. In: Environmental geochemistry of sulphide oxidation. American Chemical Society Symposium Series, vol 550. American Chemical Society, Washington, DC, pp 481–514

Taylor BE, Eichelberger JC, Westrich HR (1983) Hydrogen isotopic evidence of rhyolitic magma degassing during shallow intrusion and eruption. Nature 306:541–545

Taylor HP, Turi B, Cundari A (1984) $^{18}O/^{16}O$ and chemical relationships in K-rich volcanic rocks from Australia, East Africa, Antarctica and San Venanzo Cupaello, Italy. Earth Planet Sci Lett 69:263–276

Teece MA, Fogel ML (2007) Stable carbon isotope biogeochemistry of monosaccharides in aquatic organisms and terrestrial plants. Org Geochem 38:458–473

Telmer KH, Veizer J (1999) Carbon fluxes, pCO2 and substrate weathering in a large northern river basin, Canada: carbon isotope perspective. Chem Geol 159:61–86

Thiagarajan N, Adkins J, Eiler J (2011) Carbonate clumped isotope thermometry of deep-sea corals and implications for vital effects. Geochim Cosmochim Acta 75:4416–4425

Thiel V, Peckmann J, Seifert R, Wehrung P, Reitner J, Michaelis W (1999) Highly isotopically depleted isoprenoids: molecular markers for ancient methane venting. Geochim Cosmochim Acta 63:3959–3966

Thiemens MH (1988) Heterogeneity in the nebula: evidence from stable isotopes. In: Kerridge JF, Matthews MS (eds) Meteorites and the early solar system, University of Arizona Press, pp 899–923

Thiemens MH (1999) Mass-independent isotope effects in planetary atmospheres and the early solar system. Science 283:341–345

Thiemens MH (2006) History and applications of mass-independent isotope effects. Annu Rev Earth Planet Sci 34:217–262

Thiemens MH, Jackson T, Zipf EC, Erdman PW, van Egmond C (1995) Carbon dioxide and oxygen isotope anomalies in the mesophere and stratosphere. Science 270:969–972

Thode HG, Monster J (1964) The sulfur isotope abundances in evaporites and in ancient oceans. In: Vinogradov AP (ed) Proceedings of geochemistry conference commemorating the centenary of V I Vernadskii's birth, vol 2, 630 p

Thomassot E, Cartigny P, Harris JW, Lorand JP, Rollion-Bard C, Chaussidon M (2009) Metasomatic diamond growth: a multi-isotope study (^{13}C, ^{15}N, ^{33}S, ^{34}S) of sulphide inclusions and their host diamonds from Jwaneng (Botswana). Earth Planet Sci Lett 282:79–90

Thompson P, Schwarcz HP, Ford DE (1974) Continental Pleistocene climatic variationa from speleothem age and isotopic data. Science 184:893–895

Thompson LG, Mosley-Thompson E, Henderson KA (2000) Ice-core palaeoclimate records in tropical South America since the last glacial maximum. J Quat Sci 15:377–394

Thompson LG et al (2006) Abrupt tropical climate change: past and present. Proc Nat Acad Sci 103:10536–10543

Tiedemann R, Sarntheim M, Shackleton NJ (1994) Astronomic timescale for the Pliocene Atlantic $\delta^{18}O$ and dust flux records of Ocean Drilling Program site 659. Paleoceanography 9:619–638

Tilley B, Muehlenbachs K (2013) Isotope reversals and universal stages and trends of gas maturation in sealed self-contained petroleum systems. Chem Geol (in press)

Todd CS, Evans BW (1993) Limited fluid-rock interaction at marble-gneiss contacts during Cretaceous granulite-facies metamorphism, Seward Peninsula, Alaska. Contr Mineral Petrol 114:27–41

Tripati AK, Eagle RA, Thiagarajan N, Gagnon AC, Bauch H, Halloran PR, Eiler JM (2010) 13C-18O isotope signaturesand "clumped isotope" thermometry in foraminifera and coccoliths. Geochim Cosmochim Acta 74:5697–5717

Trudinger PA, Chambers LA, Smith JW (1985) Low temperature sulphate reduction: biological versus abiological. Can J Earth Sci 22:1910–1918

Trudinger CM, Enting IG, Francey RJ, Etheridge DM, Rayner PJ (1999) Long-term variability in the global carbon cycle inferred from a high-precision CO_2 and $\delta^{13}C$ ice-core record. Tellus 51B:233–248

Truesdell AH, Hulston JR (1980) Isotopic evidence on environments of geothermal systems. In: Fritz P, Fontes J (eds) Handbook of environmental isotope geochemistry, vol I. Elsevier, New York Amsterdam, pp 179–226

Trust BA, Fry B (1992) Stable sulphur isotopes in plants: a review. Plant Cell Environ 15:1105–1110

Tucker ME, Wright PV (1990) Carbonate sedimentology. Blackwell Scientific Publishing, London, pp 365–400

Tudge AP (1960) A method of analysis of oxygen isotopes in orthophosphate—its use in the measurement of paleotemperatures. Geochim Cosmochim Acta 18:81–93

Turchin AV, Schrag DP (2006) Cenozoic evolution of the sulphur cycle: insight from oxygen isotopes in marine sulphate. Earth Planet Sci Lett 241:763–779

Turchyn AV, Schrag DP (2004) Oxygen isotope constraints on the sulfur cycle over the past 10 million years. Science 303:2004–2007

Uemura R, Abe O, Motoyama H (2010) Determining the $^{17}O/^{16}O$ ratio of water using a water–CO_2 equilibration method: application to glacial-interglacial changes in ^{17}O excess from the Dome Fuji ice core Antarctica. Geochim Cosmochim Acta 74:4919–4936

Urey HC (1947) The thermodynamic properties of isotopic substances. J Chem Soc 1947:562

Usui T, Alexander CM, Wang J, Simon JI, Jones JH (2012) Origin of water and mantle-crust interactions on Mars inferred from hydrogen isotopes and volatile element abundances of olivine-hosted melt inclusions of primitive shergottites. Earth Planet Sci Lett 357–358:119–129

Valdes MC, Moreira M, Foriel J, Moynier F (2014) The nature of Earth's building blocks as revealed by calcium isotopes. Earth Planet Sci Lett 394:135–145

Valley JW (1986) Stable isotope geochemistry of metamorphic rocks. Rev Mineral 16:445–489

Valley JW (2001) Stable isotope thermometry at high temperatures. Rev Mineral Geochem 43:365–413

Valley JW (2003) Oxygen isotopes in zircon. Rev Mineral Geochem 53:343–385

Valley JW, Bohlen SR, Essene EJ, Lamb W (1990) Metamorphism in the Adirondacks. II. J Petrol 31:555–596

Valley JW, Eiler JM, Graham CM, Gibson EK, Romanek CS, Stolper EM (1997) Low temperature carbonate concretions in the martian meteorite ALH 84001: evidence from stable isotopes and mineralogy. Science 275:1633–1637

Valley JW et al (2005) 4.4 billion years of crustal maturation: oxygen isotope ratios in magmatic zircon. Contr Mineral Petrol 150:561–580

Vasconcelos C, Mackenzie JA, Warthmann R, Bernasconi S (2005) Calibration of the $\delta^{18}O$ paleothermometer for dolomite precipitated in microbial cultures and natural environments. Geology 33:317–320

Vazquez R, Vennemann TW, Kesler SE, Russell N (1998) Carbon and oxygen isotope halos in the host limestone, El Mochito Zn, Pb (Ag) skarn massive sulfide/oxide deposit, Honduras. Econ Geol 93:15–31

Veizer J, Hoefs J (1976) The nature of $^{18}O/^{16}O$ and $^{13}C/^{12}C$ secular trends in sedimentary carbonate rocks. Geochim Cosmochim Acta 40:1387–1395

Veizer J et al (1997) Oxygen isotope evolution of Phanerozoic seawater. Palaeo, Palaeo, Palaeo 132:159–172

Veizer J et al (1999) $^{87}Sr/^{86}Sr$, $\delta^{13}C$ and $\delta^{18}O$ evolution of Phanerozoic seawater. Chem Geol 161:37–57

Vennemann TW, Kesler SE, O'Neil JR (1992) Stable isotope composition of quartz pebbles and their fluid inclusions as tracers of sediment provenance: implications for gold- and uranium-bearing quartz pebble conglomerates. Geology 20:837–840

Vennemann TW, Kesler SE, Frederickson GC, Minter WEL, Heine RR (1996) Oxygen isotope sedimentology of gold and uranium-bearing Witwatersrand and Huronian Supergroup quartz pebble conglomerates. Econ Geol 91:322–342

Vennemann TW, Fricke HC, Blake RE, O'Neil JR, Colman A (2002) Oxygen isotope analysis of phosphates: a comparison of techniques for analysis of Ag_3PO_4. Chem Geol 185:321–336

VennemannTW Smith HS (1992) Stable isotope profile across the orthoamphibole isograd in the Southern Marginal Zone of the Limpopo Belt, S Africa. Precambrian Res 55:365–397

Viers J et al (2007) Evidence of Zn isotope fractionation in a soil-plant system of a pristine tropical watershed (Nsimi, Cameroon). Chem Geol 239:124–137

Virtasalo JJ, Whitehouse MJ, Kotilainen AT (2013) Iron isotope heterogeneity in pyrite fillings of Holocene worm burrows. Geology 41:39–42

Voegelin AR, Nägler TF, Beukes NJ, Lacassie JP (2010) Molybdenum isotopes in late Archean carbonate rocks: implications for early Earth oxygenation. Precambr Res 182:70–82

Von Grafenstein U, Erlenkeuser H, Trimborn P (1999) Oxygen and carbon isotopes in fresh-water ostracod valves: assessing vital offsets and autoecological effects of interest for paleoclimate studies. Palaeo, Palaeo, Palaeo 148:133–152

Wacker U, Fiebig J, Tödter J, Schöne BR, Bahr A, Friedrich O, Tütken T, Gischler E, Joachimski MM (2014) Emperical calibration of the clumped isotope paleothermometer using calcites of various origins. Geochim Cosmochim Acta 141:127–144

Wada E, Hattori A (1976) Natural abundance of ^{15}N in particulate organic matter in North Pacific Ocean. Geochim Cosmochim Acta 40:249–251

Wallmann K (2001) The geological water cycle and the evolution of marine $\delta^{18}O$ values. Geochim Cosmochim Acta 65:2469–2485

Wang Y, Sessions AL, Nielsen RJ, Goddard WA (2009) Equilibrium $^{2}H/^{1}H$ fractionations in organic molecules. II: Linear alkanes, alkenes, ketones, carboxylic acids, esters, alcohols and ethers. Geochim Cosmochim Acta 73:7076–7086

Wang Z, Chapellaz J, Park K, Mak JE (2011) Large variations in southern biomass burning during the last 650 years. Science 330:1663–1666

Wanner C, Sonnenthal EL, Liu XM (2014) Seawater $\delta^{7}Li$: a direct proxy for global CO_2 consumption by continental silicate weathering? Chem Geol 381:154–167

Warren CG (1972) Sulfur isotopes as a clue to the genetic geochemistry of a roll-type uranium deposit. Econ Geol 67:759–767

Waterhouse JS, Cheng S, Juchelka D, Loader NJ, McCarroll D, Switsur R, Gautam L (2013) Position-specific measurement of oxygen isotope ratios in cellulose: isotope exchange during heterotrophic cellulose synthesis. Geochim Cosmochim Acta 112:178–192

Watson LL, Hutcheon ID, Epstein S, Stolper EM (1994) Water on Mars: clues from deuterium/hydrogen and water contents of hydrous phases in SNC meteorites. Science 265:86–90

Weber JN, Raup DM (1966a) Fractionation of the stable isotopes of carbon and oxygen in marine calcareous organisms-the Echinoidea. I. Variation of ^{13}C and ^{18}O content within individuals. Geochim Cosmochim Acta 30:681–703

Weber JN, Raup DM (1966b) Fractionation of the stable isotopes of carbon and oxygen in marine calcareous organisms-the Echinoidea. II. Environmental and genetic factors. Geochim Cosmochim Acta 30:705–736

Webster CR, Mahaffy PR et al (2013) Isotope ratios of H, C, and O in CO_2 and H_2O of the Martian atmosphere. Science 341:260–263

Wefer G, Berger WH (1991) Isotope paleontology: growth and composition of extant calcareous species. Mar Geol 100:207–248

Welch SA, Beard BL, Johnson CM, Braterman PS (2003) Kinetic and equilibrium Fe isotope fractionation between aqueous Fe(II) and Fe(III). Geochim Cosmochim Acta 67:4231–4250

Welhan JA (1987) Stable isotope hydrology. In: Short course in stable isotope geochemistry of low-temperature fluids. Mineral Assoc Canada, vol 13, pp 129–161

Welhan JA (1988) Origins of methane in hydrothermal systems. Chem Geol 71:183–198

Well R, Flessa H (2009) Isotopogue enrichment factors of N_2O reduction in soils. Rapid Commum Mass Spectrom 23:2996–3002

Wenzel B, Lecuyer C, Joachimski MM (2000) Comparing oxygen isotope records of Silurian calcite and phosphate—$\delta^{18}O$ composition of brachiopods and conodonts. Geochim Cosmochim Acta 69:1859–1872

Westerhausen L, Poynter J, Eglinton G, Erlenkeuser H, Sarntheim M (1993) Marine and terrigenous origin of organic matter in modern sediments of the equatorial East Atlantic: the $\delta^{13}C$ and molecular record. Deep Sea Res 40:1087–1121

Weyer S, Ionov D (2007) Partial melting and melt percolation in the mantle: the message from Fe isotopes. Earth Planet Sci Lett 259:119–133

Weyer S, Anbar AD, Brey GP, Münker C, Mezger K (2005) Iron isotope fractionation during planetary differentiation. Earth Planet Sci Lett 240:251–264

White JWC (1989) Stable hydrogen isotope ratios in plants: a review of current theory and some potential applications. In: Stable isotopes in ecological research, Ecological Studies, vol 68. Springer, New York, pp 142–162

White JWC, Lawrence JR, Broecker WS (1994) Modeling and interpreting D/H ratios in tree rings: a test case of white pine in the northeastern United States. Geochim Cosmochim Acta 58:851–862

Whiticar MJ (1999) Carbon and hydrogen isotope systematics of bacterial formation and oxidation of methane. Chem Geol 161:291–314

Whiticar MJ, Faber E, Schoell M (1986) Biogenic methane formation in marine and freshwater environments: CO_2 reduction vs. acetate fermentation-Isotopic evidence. Geochim Cosmochim Acta 50:693–709

Whittacker SG, Kyser TK (1990) Effects of sources and diagenesis on the isotopic and chemical composition of carbon and sulfur in Cretaceous shales. Geochim Cosmochim Acta 54:2799–2810

Wickham SM, Taylor HR (1985) Stable isotope evidence for large-scale seawater infiltration in a regional metamorphic terrane; the Trois Seigneurs Massif, Pyrenees, France. Contrib Mineral Petrol 91:122–137

Wickman FE (1952) Variation in the relative abundance of carbon isotopes in plants. Geochim Cosmochim Acta 2:243–254

Wiechert U, Halliday AN (2007) Non-chondritic magnesium and the origin of the inner terrestrial planets. Earth Planet Sci Lett 256:360–371

Wiechert U, Halliday AN, Lee D-C, Snyder GA, Taylor LA, Rumble D (2001) Oxygen isotopes and the moon forming giant impact. Science 294:345–348

Wille M, Kramers JD, Nägler TF, Beukes NJ, Schroder S, Meiser T, Lacassie JP, Voegelin AR (2007) Evidence for a gradual rise of oxygen between 2.6 and 2.5 Ga from Mo isotopes and Re-PGE signatures in shales. Geochim Cosmochim Acta 71:2417–2435

Wille M, Nebel O, Van Kranendonk MJ, Schoenberg R, Kleinhans IC, Ellwood MJ (2013) Mo-Cr evidence for a reducing Archean atmosphere in 3.46–2.76 Ga black shales from the Pilbara, western Australia. Chem Geol 340:68–76

Williams HM, Archer C (2011) Copper stable isotopes as tracers of metal-sulphide segregation and fractional crystallization processeson iron meteorite parent bodies. Geochim Cosmochim Acta 75:3166–3178

Williams HM, Markowski A, Quitte G, Halliday AN, Teutsch N, Levasseur S (2006) Fe isotope fractionations in iron meteorites: new insight into metal-sulphide segregation and planetary accretion. Earth Planet Sci Lett 250:486–500

Williams HM, Wood BJ, Wade J, Frost DJ, Tuff J (2012) Isotopic evidence for internal oxidation of the Earth's mantle during accretion. Earth Planet Sci Lett 321–322:54–63

Wong WW, Sackett WM (1978) Fractionation of stable carbon isotopes by marine phytoplankton. Geochim Cosmochim Acta 42:1809–1815

Wortmann UG, Chernyavsky B, Bernasconi SM, Brunner B, Böttcher ME, Swart PK (2007) Oxygen isotope biogeochemistry of pore water sulfate in the deep biosphere: dominance of isotope exchange reactions with ambient water during microbial sulfate reduction (ODP Site 1130). Geochim Cosmochim Acta 71:4221–4232

Wright I, Grady MM, Pillinger CT (1990) The evolution of atmospheric CO_2 on Mars: the perspective from carbon isotope measurements. J Geophys Res 95:14789–14794

Wu L, Beard BL, Roden EE, Johnson CM (2011) Stable iron isotope fractionation between aqueous Fe (II) and hydrous ferric oxide. Environ Sci Technol 45:1845–1852

Xia J, Ito E, Engstrom DE (1997a) Geochemistry of ostracode calcite: part I. An experimental determination of oxygen isotope fractionation. Geochim Cosmochim Acta 61:377–382

Xia J, Engstrom DE, Ito E (1997b) Geochemistry of ostracode calcite: part 2. The effects of water chemistry and seasonal temperature variation on *Candona rawsoni*. Geochim Cosmochim Acta 61:383–391

Xia X, Chen J, Braun R, Tang Y (2013) Isotopic reversals with respect to maturity trends due to mixing of primary and secondary products in source rocks. Chem Geol (in press)

Xiao Y, Hoefs J, van den Kerkhof AM, Simon K, Fiebig J, Zheng YF (2002) Fluid evolution during HP and UHP metamorphism in Dabie Shan, China: constraints from mineral chemistry, fluid inclusions and stable isotopes. J Petrol 43:1505–1527

Xiao Y, Zhang Z, Hoefs J, van den Kerkhof A (2006) Ultrahigh pressure rocks from the Chinese Continental Scientific Drilling Project: II Oxygen isotope and fluid inclusion distributions through vertical sections. Contr Mineral Petrol 152:443–458

Yang J, Epstein S (1984) Relic interstellar grains in Murchison meteorite. Nature 311:544–547

Yang C, Telmer K, Veizer J (1996) Chemical dynamics of the “St Lawrence” riverine system: $\delta D_{H2}O$, $\delta^{18}OH_2O$, $\delta^{13}C_{DIC}$, $\delta^{34}SSO_4$ and dissolved $^{87}Sr/^{86}Sr$. Geochim Cosmochim Acta 60:851–866

Yapp CJ (1983) Stable hydrogen isotopes in iron oxides—isotope effects associated with the dehydration of a natural goethite. Geochim Cosmochim Acta 47:1277–1287

Yapp CJ (1987) Oxygen and hydrogen isotope variations among goethites (α-FeOOH) and the determination of paleotemperatures. Geochim Cosmochim Acta 51:355–364

Yapp CJ (2007) Oxygen isotopes in synthetic goethite and a model for the apparent pH dependence of goethite-water $^{18}O/^{16}O$ fractionation. Geochim Cosmochim Acta 71:1115–1129

Yapp CJ, Epstein S (1982) Reexamination of cellulose carbon-bound hydrogen δD measurements and some factors affecting plant-water D/H relationships. Geochim Cosmochim Acta 46:955–965

Yokochi R, Marty B, Chazot G, Burnard P (2009) Nitrogen in perigotite xenoliths: lithophile behaviour and magmatic isotope fractionation. Geochim Cosmochim Acta 73:4843–4861

Yoshida N, Toyoda S (2000) Constraining the atmospheric N_2O budget from intramolecular site preference in N_2O isotopomers. Nature 405:330–334

Yoshida N, Hattori A, Saino T, Matsuo S, Wada E (1984) $^{15}N/^{14}N$ ratio of dissolved N_2O in the eastern tropical Pacific Ocean. Nature 307:442–444

Young ED (1993) On the $^{18}O/^{16}O$ record of reaction progress in open and closed metamorphic systems. Earth Planet Sci Lett 117:147–167

Young ED, Rumble D (1993) The origin of correlated variations in in-situ $^{18}O/^{16}O$ and elemental concentrations in metamorphic garnet from southeastern Vermont, USA. Geochim Cosmochim Acta 57:2585–2597

Young ED, Ash RD, England P, Rumble D (1999) Fluid flow in chondritic parent bodies: deciphering the compositions of planetesimals. Science 286:1331–1335

Young ED, Tonui E, Manning CE, Schauble E, Macris CA (2009a) Spinel-olivine magnesium isotope thermometry in the mantle and implications for the Mg isotopic composition of Earth. Earth Planet Sci Lett 288:524–533

Young MB, McLaughlin K, Kendall C, Stringfellow W, Rollow M, Elsbury K, Donald E, Payton A (2009b) Characterizing the oxygen isotopic composition of phosphate sources to aquatic ecosystems. Environ Sci Techn 43:5190–5196

Young ED, Manning CE, Schauble EA, Shahar A, Macris CA, Lazar C, Jordan M (2015) High-temperature equilibrium isotope fractionation of non-traditional isotopes: experiments, theory and applications. Chem Geol 395:176–195

Yurimoto A, Krot A, Choi BG, Aléon J, Kunihiro T, Brearly AJ (2008) Oxygen isotopes in chondritic components. Rev Mineral Geochem 68:141–186

Yurtsever Y (1975) Worldwide survey of stable isotopes in precipitation. Rep Sect Isotope Hydrol IAEA, November 1975, 40 pp

Zaback DA, Pratt LM (1992) Isotopic composition and speciation of sulfur in the Miocene Monterey Formation: reevaluation of sulfur reactions during early diagenesis in marine environments. Geochim Cosmochim Acta 56:763–774

Zachos J, Pagani M, Sloan L, Thomas E, Billups K (2001) Trends, rhythms and aberrations in global climate 65 Ma to present. Science 292:686–693

Zeebe RE (1999) An explanation of the effect of seawater carbonate concentration on foraminiferal oxygen isotopes. Geochim Cosmochim Acta 63:2001–2007

Zeebe RE (2010) A new value for the stable oxygen isotope fractionation between dissolved sulfate ion and water. Geochim Cosmochim Acta 74:818–828

Zhang T, Krooss BM (2001) Experimental investigation on the carbon isotope fractionation of methane during gas migration by diffusion through sedimentary rocks at elevated temperature and pressure. Geochim Cosmochim Acta 65:2723–2742

Zhang HF et al (2000) Recent fluid processes in the Kapvaal craton, South Africa: coupled oxygen isotope and trace element disequilibrium in polymict peridotites. Earth Planet Sci Lett 176:57–72

Zhang R, Schwarcz HP, Ford DC, Schroeder FS, Beddows PA (2008) An absolute paleotemperature record from 10 to 6 ka inferred from fluid inclusion D/H ratios of a stalagmite from Vancouver Island, British Columbia, Canada. Geochim Cosmochim Acta 72:1014–1026

Zheng YF, Böttcher ME (2015) Oxygen isotope fractionation in double carbonates. Isotopes Environmental Health Studies (in press)

Zheng YF, Hoefs J (1993) Carbon and oxygen isotopic vovariations in hydrothermal calcites. Theoretical modeling on mixing processes and application to Pb-Zn deposits in the Harz Mountains, Germany. Mineral Deposita 28:79–89

Zheng YF, Fu B, Li Y, Xiao Y, Li S (1998) Oxygen and hydrogen isotope geochemistry of ultra-high pressure eclogites from the Dabie mountains and the Sulu terrane. Earth Planet Sci Lett 155:113–129

Zhu XK, O'Nions RK, Guo Y, Belshaw NS, Rickard D (2000a) Determination of natural Cu-isotope variations by plasma-source mass spectrometry: implications for use as geochemical tracers. Chem Geol 163:139–149

Zhu XK, O'Nions K, Guo Y, Reynolds BC (2000b) Secular variations of iron isotopes in North Atlantic Deep Water. Science 287:2000–2002

Ziegler K, Young ED, Schauble E, Wasson JT (2010) Metal-silicate silicon isotope fractionationin enstatite meteorites and constraints on Earth's core formation. Earth Planet Sci Lett 295:487–496

Zierenberg RA, Shanks WC, Bischoff JL (1984) Massive sulfide deposit at 21°N, East Pacific Rise: chemical composition, stable isotopes, and phase equilibria. Bull Geol Soc Am 95:922–929

Zimmer MM, Fischer TP, Hilton DR, Alvaredo GE, Sharp ZD, Walker JA (2004) Nitrogen systematics and gas fluxes of subduction zones: insights from Costa Rica arc volatiles. Geochem Geophys Geosys 5:Q05J11. doi:10.1029/2003GC000651

Zinner E (1998) Stellar nucleosynthesis and the isotopic composition of presolar grains from primitive meteorites. Ann Rev Earth Planet Sci 26:147–188

Index

A
Abiogenic methane, 300
Achondrite, 94, 197
Acid mine water, 125
Adsorption, 58, 62, 92, 115, 118, 122, 124, 128, 147, 148, 150
Aerosol, 38, 144, 282, 283
Alkenone, 279
Alunite, 227
Amino acid, 71, 196, 255, 285, 289, 293
Amphibole, 84, 201, 203, 205, 216, 227
Anoxic environment, 99, 137, 319
Anthropogenic contaminant, 127
Anthropogenic pollution, 64, 269
Antimony isotope, 141
Aragonite, 66, 78, 91, 111, 112, 307, 312, 329
Asteroid, 109, 191, 193, 194, 198
Atmosphere, 13, 31, 50, 70, 71, 73, 115, 135, 143, 144, 146, 195, 200, 202, 224, 225, 245, 256, 257, 265, 269–271, 274, 275, 277, 278, 280–284, 311, 325, 326, 330

B
Bacterial sulfate reduction, 99, 103, 238, 318, 320
Barite, 142, 234, 266, 273
Barium isotopes, 142
Barometer, 68
Basalt, 56, 89, 90, 94, 110, 119, 129, 139, 199, 204, 212, 214, 215, 218, 229
Benthic foraminifera, 268, 309, 310, 329, 330
Biogenic gas, 298
Biomass burning, 280–282
Biosphere, 284, 285
Biotite, 50, 74, 94, 227, 231
Black carbon, 296, 297
Black shales, 132, 137, 150
Boiling, 50, 146, 223, 227
Bond strength, 21, 24, 98
Bone, 108, 112, 290, 316, 317, 324
Boron isotopes
  pH-dependence, 61
Brachiopod, 134, 263, 317
Brine, 60, 99, 106, 125, 230, 251–253
Bromine isotopes, 132

C
C_3plant, 67
C_4plant, 68, 285, 291
Calcite, 16, 17, 27, 66, 78, 84, 111, 134, 232, 233, 263, 307, 313, 314, 323, 324, 329, 333, 339
Calcium isotopes, 108
Calibration curve, 84
Ca metabolism, 39
Cap carbonate, 265
Carbohydrate, 67, 68, 285, 287, 288, 290
Carbon dioxide, 213, 223, 274, 275
Carbon isotopes, 64
Carbon monoxide, 195, 280, 305
Carbonaceous chondrite, 110, 133, 139, 192–196, 199
Carbonate species, 82, 126, 256, 313
Carbonate thermometry, 15
Catagenesis, 293, 322
Cation mass, 21
Cave carbonate, 92, 323
Cavity ring spectroscopy, 49
Cellulose, 288, 289, 322
Channelized fluid, 333
Chert, 94, 262, 301, 305
Chlorinated hydrocarbon, 291, 292
Chlorine isotopes, 105
Chondrite, 90, 109, 192, 193
Chromium isotopes, 113
Clay minerals, 55, 59, 75, 90, 94, 95, 110, 219, 301, 302, 322
Clumped isotopes, 17, 324
Coal, 60, 130, 140, 146, 147, 284, 296
Comet, 191, 194, 199, 205
Compound-specific analysis, 32, 71, 286, 288, 295
Connate water, 239
Conodont, 317, 329

J. Hoefs, *Stable Isotope Geochemistry*, DOI 10.1007/978-3-319-19716-6

Contact metamorphism, 334
Continuous flow, 30, 49, 71, 79
Coordination number, 22, 39, 89, 118
Copper isotopes, 123
Coral, 61, 143, 329
Core, 94, 119, 122, 211, 324
Crustal contamination, 213, 214

D
Dansgaard-Oeschger event, 325–327
Decarboxylation, 293
Degassing, 32, 52, 127, 147, 148, 203, 205, 216, 217, 220, 223, 229, 230, 324
Dehydration, 63, 106, 210, 230, 305
Delta-delta plot, 87
Delta value, definition, 8
Denitrification, 71, 72, 74, 75, 258, 271, 272
Dentine, 316
Deuterium excess, 51, 242, 243
Diagenesis, 288, 289, 293, 303, 307, 312, 313, 318, 322
Diamond, 21, 73, 78, 191, 195, 207, 208
Diatom, 95, 96, 257, 305, 315, 323
Diet, 112, 285, 290, 317
Diffusion, 10, 12, 18, 54, 56, 86, 119, 238, 287, 313
Dissimilatory iron reduction, 120, 121, 321
Dissimilatory sulfate reduction, 98, 99
Dole effect, 272
Dolomite, 16, 17, 89, 91, 111, 268, 313, 314
Dual inlet, 28, 31

E
Eclogite, 336
Epsilon value, 8
Equilibrium fractionation, 23, 25, 38, 39, 54, 62, 85, 92, 198, 236, 243, 259, 318
Evaporation, 10, 37, 50, 51, 127, 139, 140, 198, 239, 241–243, 247, 248, 287, 291, 304, 307
Evaporite, 262, 97, 132, 266
Extraterrestrial material, 139, 191, 194

F
Fe–Mn oxide, 39, 125, 149, 150
Fertilizer, 59, 75, 261
Fick's law, 18
Fischer-Tropsch synthesis, 224
Fluid inclusion, 99, 106, 226, 227, 262, 323
Fluid-rock interaction, 58, 86, 87, 232, 331, 332, 334
Food chain, 290
Foraminifera, 16, 61, 62, 111, 268, 306, 307, 311, 323, 327
Formation water, 230, 239, 250, 251, 296, 299, 336
Fractional crystallization, 110, 119, 134, 212
Fractionation factor, 7–9, 23, 26, 48, 57, 61, 78, 80, 102, 205, 212, 226, 252, 302, 304, 322

H
Hailstone, 240
Heavy elements, 14
Heinrich event, 311
Hopane, 286, 295
Hot spring, 220, 221, 225
Humidity indicator, 243
Hydration sphere, 55, 81
Hydrogen isotopes, 48, 50, 51, 194, 215, 242, 251, 298
Hydrosphere, 75, 90, 106, 239, 272
Hydrothermal alteration, 58, 119, 147, 212, 262
Hydrothermal fluids, 91, 95, 111, 146, 231, 235
Hydrothermal system, 220, 226, 230, 231, 235, 236
Hydroxyl group, 54, 61, 215, 216, 250, 288, 301

I
Ice core, 18, 75, 244, 245, 269, 273, 278, 283, 324–326
Ice volume, 309, 327, 330
Illite, 302
Interplanetary dust, 193
Ion filtration, 106
Ion probe, 54
Iron isotopes, 116
Iron meteorites, 119, 131, 196–198
Iron oxides, 78, 117, 131, 274, 317, 318
Iron sulfide, 118
Isotope clumping, 300
Isotope effect
  mass dependence, 12
  mass independence, 13
Isotope fractionation
  adsorption, 62
  chemical composition, 99
  crystal structure, 21, 24, 253, 314
  pH dependence, 61
  sorption, 22, 39, 126
  speciation, 39, 62

Isotope salt effect, 82
Isotopologue, 14, 300

J
Jarosite, 227
Juvenile water, 205, 228, 229

K
Kaolinite, 227, 302
Kerogen, 195, 293, 294, 297, 299, 320
Kimberlite, 204, 207
Kinetic effect, 10, 47, 69, 111, 240, 272

L
Lakes, 239, 257, 259, 260, 298, 314, 315, 323
Laser probe, 76
Limestone, 111, 223, 264, 312, 313
Lipids, 54, 68, 285, 287, 288
Lithium isotopes, 55
Lower crust, 336, 337

M
Magmatic differentiation, 94, 119
Magmatic water, 201, 222, 228–230, 235
Magnesium isotopes, 88, 92, 290, 314
Magnetic isotope effect, 14, 144
Marble, 17, 331, 335, 336, 338
Marine organic matter, 258, 285, 286, 292, 293
Mars, 13, 109, 133, 191, 192, 194, 198, 199, 200–202
Mass spectrometer, 15, 27–30, 32, 37, 47, 98, 202, 300
Membrane filtration, 252
Mercury isotopes, 143–147
Metabolic isotope effect, 307
Metal isotopes, 22, 35, 38, 39, 197, 198, 212, 238, 289, 290
Metamorphic rocks, 73, 94, 97, 208, 230, 331, 334, 337
Metamorphic water, 230
Meteoric water, 51, 206, 216, 220, 222, 229, 230, 235, 239, 243, 244, 248, 251, 252, 277, 302, 312, 322, 336
Meteoric Water Line, 51, 53, 85, 242, 244, 251
Meteorites, 13, 94, 109, 113, 114, 118, 122, 127, 143, 191–193, 195, 197, 204
Methane, 17, 64, 223, 224, 250, 256, 270, 280, 294, 297, 298, 300, 319, 330
Methanogenesis, 256, 294, 298, 300, 314
Miller–Urey reactions, 195
Molybdenum isotope, 135–137, 239, 273
Moon, 90, 94, 107, 109, 119, 127, 133, 139, 192, 198, 199, 213
MORB, 57, 58, 73, 107, 119, 148, 204, 206, 208, 211, 214, 215, 217, 223, 224
Multicollector ICP mass spectrometry, 38
Muscovite, 63, 94, 304, 337

N
Nickel isotopes, 122, 123, 198
Nitrate, 71, 72, 74, 76, 79, 150, 258, 269, 271, 283, 289, 322
Nitrification, 71, 72, 271, 272
Nitrogen cycle, 70, 71, 73, 75
Nitrogen fixation, 72, 74
Nitrogen isotopes, 31, 70–75, 196, 209, 217, 224, 290, 292, 327
Nitrous oxide, 270–272
Non-traditional isotopes, 253
Nuclear volume, 14, 144

O
Oceanic crust, 58, 63, 90, 91, 147, 148, 203, 205, 206, 208, 215, 217, 218, 229, 236, 262, 268, 312
Ocean water, 34, 55, 59, 60, 73, 84, 87, 91, 95, 107, 112, 115, 123, 125, 135, 137, 139, 150, 200, 218, 228, 230, 244, 248–250, 254, 257, 259, 262, 266, 273, 276, 292, 306, 307, 310, 313, 317, 319, 330
Oil, 293–295
Olivine, 57, 58, 73, 78, 89, 94, 118, 119, 199, 204, 206, 208, 215, 216, 218
Ophiolite, 218
Ore deposits, 97, 106, 125, 128, 135, 140, 142, 145, 226, 227, 229–231, 233, 235, 238, 239
Ore fluids, 226–228
Organic matter, 54, 65, 68, 69, 75, 113, 124, 126, 128, 136, 142, 145, 146, 194, 195, 217, 224, 236, 250, 254, 255, 257, 284, 288, 292, 298, 300, 310, 312–314, 318, 320, 322
Organic sulfur, 196, 289, 296, 320
Ostracode, 323
Oxygen fugacity, 217
Oxygen isotopes, 10, 13, 21, 23, 26, 36, 37, 51, 77, 79, 80, 82, 85, 87, 102, 103, 192, 197, 198, 204, 214, 218, 222, 230, 232, 252, 259, 263, 266, 277, 288, 303, 305, 313–317, 324, 327, 329, 330, 334, 336, 338
Ozone, 13, 108, 132, 202, 225, 269–272, 277, 283, 284

P
Palaeoclimatology, 16, 321
Palaeo-CO_2, 68, 279

Paleoaltitude, 244
Partial-exchange, 25
Partial melting, 94, 110, 115, 119, 203, 204, 219
Particulate compounds, 253
Particulate organic matter, 255
Partition function, 6, 7, 11, 24, 98
Perchlorate, 108, 284
Peridotite, 57, 89, 110, 119, 125, 203, 204, 207, 208, 210, 211
Pervasive fluid, 332, 337
Petroleum, 113, 284, 294, 295
Phase separation, 227
Phlogopite, 73, 90, 205, 208, 211, 216
Phosphates, 61, 78, 79, 126, 139, 261, 263, 316, 324, 329
Phosphoric acid, 65, 77
Photochemical reaction, 146, 197, 202, 269, 284
Photolysis, 14, 104
Photosynthesis, 47, 54, 65, 66, 88, 92, 258, 259, 272, 273, 277, 284, 285, 289, 307, 310
Phytane, 54, 295
Phytoplankton, 68, 74, 92, 121, 128, 139, 279, 285
Planktonic foraminifera, 92, 134, 268, 280, 309
Pore water, 91, 106, 107, 121, 151, 250, 255, 256, 259, 266, 288, 298, 307, 312, 319
Porphyry copper deposits, 125, 147, 227, 235, 236
Position specific fractionation, 287
Presolar grain, 191
Pristane, 54, 295
Protein, 68, 285, 287, 290
Provenance, 141, 304
Pyrite, 98, 99, 117, 120, 149, 227, 236, 260, 266, 267, 274, 296, 318–321
Pyrolysis, 65, 79, 297

Q
Quadruple Sulfur Isotopes, 103

R
Radiolaria, 95, 305
Rain water, 64
Rayleigh fractionation, 216
Redox change, 114, 120, 124, 141, 150, 318
Regional metamorphism, 334, 335
Respiration, 257–259, 272, 273, 275, 284, 307
River water, 58, 90, 91, 110, 121, 128, 148, 246
Rubisco, 67

S
Sample preparation, 30–32, 34, 50, 97, 130
Sandstone, 94, 151, 238, 303
Sea water, 96, 134, 218, 228, 244, 249, 255, 261, 262, 268, 273, 310, 312, 317, 319
Secondary ion mass spectrometry (SIMS), 19, 37, 60, 78, 93, 107, 109, 116, 199, 208, 211, 321
Sedimentary rocks, 90, 104, 120, 135, 219, 251, 262, 267, 293, 298, 301, 303, 334
Selenium isotopes, 130
Silicon isotopes, 93, 94, 257
Site-specific isotope fractionations, 17, 18
Skaergaard intrusion, 231
SNC meteorites, 200, 201
Snow, 146, 240, 244, 245, 324, 326, 327
Snowball Earth, 265, 336
Soil, 18, 39, 58, 72, 90, 96, 112, 121, 122, 125, 131, 134, 139, 140, 146, 199, 246, 256, 271, 278, 280, 282–284, 288, 304, 313, 318
Sorption, 22, 58, 120, 126, 131
Speleothem, 16, 92, 134, 323
Sphalerite, 38, 99, 128, 234
Sponge, 96, 130
Standards, 33–35, 38, 50, 65, 79, 109, 135, 143, 149
Star dust, 195
Stochastic abundance, 15
Stratosphere, 13, 132, 202, 225, 269, 270, 273, 277, 281
Strontium isotopes, 133, 134, 142, 143
Sugar, 255
Sulfate, 13, 14, 79, 97, 98, 100–102, 104, 120, 131, 196, 197, 202, 217, 225, 234–236, 237, 256, 259–261, 266, 267, 282, 289, 313, 319, 320
Sulfate reduction, 99–103, 121, 237, 259, 266, 267, 294, 320
Sulfide, 13, 14, 21, 97–99, 101, 102, 104, 119, 120, 123, 125, 128, 129, 131, 136, 140, 141, 145, 196, 202, 210, 217, 227, 233–235, 237, 239, 260, 266, 267, 289, 296, 319, 320
Sulfide deposit, 228, 236, 238
Sulfur isotopes, 14, 97–99, 101–103, 197, 210, 217, 224, 233–235, 237, 253, 266, 273, 283, 319
Symmetry rule, 1

T
Tellurium isotopes, 141, 142
Terrestrial fractionation line, 85, 192

Terrestrial organic matter, 258, 279, 292, 293
Thallium isotopes, 147, 148
Thermochemical sulfate reduction, 103, 236, 320
Thermogenic gas, 297, 299
Thermometry, 16, 22, 23, 84, 244, 312, 337
Three isotope plot, 12, 200
Tin isotopes, 140, 141
Tooth, 291, 317, 324, 329
Tourmaline, 60, 63, 64
Transition metal, 39
Transition state, 11, 12
Transpiration, 246
Tree ring, 278, 322
Triple oxygen isotopes, 85, 277, 317
Troilite, 97, 119, 196, 198
Troposphere, 269, 270, 280
Two-direction approach, 25

U
Ultrafiltration, 55, 252
Ultra high pressure rock, 208
Ultramafic rock, 94, 113, 115, 218, 300
Upper mantle, 7, 57, 60, 110, 199, 203, 207, 211, 223
Uranium isotopes, 149, 150

V
Vanadium isotopes, 113
Vapour pressure, 243
Vent fluid, 128, 141, 223, 228, 237
Venus, 202
Vesta, 193, 200
Vital effect, 62, 66, 92, 137, 307, 310, 329
Volatile element, 73, 196
Volatiles, 127, 141, 146, 147, 192–194, 197, 199, 200, 203, 205, 218, 220, 221, 224
Volatilization, 73, 131, 198, 199, 331, 335
Volcanic gas, 107, 207, 216, 221, 225

W
Wall rock alteration, 230
Water-rock interaction, 220, 229
Water-rock ratio, 58, 222, 232
Water fractionation, 50, 51, 226–229
Weathering, 51, 58, 59, 90, 91, 94, 95, 110, 115, 120, 123, 134, 139, 148, 213, 219, 253, 256, 262, 264, 266, 268, 273, 278, 301, 303

X
Xenolith, 73, 110, 114, 115, 204–206, 208–210, 336, 337

Z
Zero point energy, 4, 5
Zinc isotopes, 126, 128
Zircon, 149, 215, 219, 220, 304